Defining the Mechanism of *VPS35* and *LRRK2* Parkinson's Disease *in vivo*

PhD Biomedical Science

School of Biological Sciences

Rachael Joan Chandler

PhD Thesis. May 2022.

Abstract

Mutation of *Vacuolar Protein Sorting 35* (*VPS35*) [D620N] was first identified in a small number of families with late onset, autosomal dominant Parkinson's disease (PD). VPS35 is an integral cargo component of the retromer complex, implicated in the retrograde transport of proteins from the endosomes to the trans-Golgi Network. The mechanism of mutation consequent neurodegeneration and resulting PD pathology is unclear, however recent studies have linked VPS35 mutation to increased kinase activity of Leucine Rich Repeat Kinase 2 (LRRK2), gain of function mutations of which are the most common cause of familial PD. The well characterised nematode model, *Caenorhabditis elegans*, shows great promise as a novel model for VPS35 function and potentially, the proposed LRRK2 interplay. Utilising a plethora of novel CRISPR/Cas9 modified *C. elegans* lines, encompassing orthologous PD relevant point mutations in VPS35 and LRRK2 orthologues, *vps-35* and *lrk-1* respectively, the mechanisms of *vps-35* mutation and LRK-1 interplay have been examined. The novel *vps-35[D638N]* PD *C. elegans* model shows age-dependent impairments in dopaminergic behaviour, increased dopaminergic degeneration and cellular aberrations relevant to PD modelling, while studies of the genetics of this model suggest a more complex mechanism of mutation action than loss of function alone. Assessment of the functional conservation extent between human LRRK2 and *C. elegans* LRK-1, through characterisation of novel PD and catalytic point mutants suggest there are kinase activity dependent phenotypes and therefore it is suitable for dissecting the VPS35/LRRK2 interplay. Subsequent pharmacological and genetic models suggest that in *C. elegans*, LRK-1 kinase hyperactivation is implicated in *vps-35[D638N]* pathology, with proposed LRK-1 inhibition or genetic kinase ablation resulting in *vps-35[D638N]* phenotypic rescue. This study is the first to utilise CRISPR/Cas9 modified *C. elegans* for modelling PD gene function, has demonstrated this novel model could share sufficient conservation for this and has developed understanding of the VPS35/LRRK2 interplay.

Original Authorship Declaration

I confirm that this is my own work and the use of all material from other sources has been properly and fully acknowledged.

Sections of text and figures within Chapter I: Introduction are adapted from recent publication "Chandler RJ, Cogo S, Lewis PA, Kevei E. Modelling the functional genomics of Parkinson's disease in *Caenorhabditis elegans: LRRK2* and beyond. Biosci Rep. 2021;41(9):20203672." (1).

I was the lead author in this publication, with responsibility for manuscript preparation, writing, figures and background research, with additional concepts, figures, edits and additions contributed by my co-authors.

Rachael Joan Chandler

12/01/22

Acknowledgements

I would like to thank Parkinson's UK for the funding of this research and studentship and inspiration through co-operation with the Research Support Network. Without the Parkinson's UK financial support, this project would not have been possible. My greatest thanks also go to my supervisors, Dr Eva Kevei and Dr Patrick Lewis, for their guidance, support and advice, along with their invaluable insights and ideas. I would also like to thank my thesis supervisory committee, Dr Nandini Vasudevan and Dr Mark Dallas, for their insightful feedback and research direction perspectives. Many thanks also go to the Kevei and Lewis laboratory teams, members past and present, for their support, discussions, and camaraderie. I would also like to thank the School of Biological Sciences community at the University of Reading and laboratory technical services. Thanks additionally go to the wider neurodegenerative disease, Parkinson's disease and *C. elegans* research communities and the Parkinson's UK Research Support Network, for their inspiration, productive feedback and new insights. Furthermore, I would like to thank my family and friends for their support, along with my grandparents, who were my inspirations to enter the field of neurodegenerative disease research.

Funded by

PARKINSON'S UK
CHANGE ATTITUDES.
FIND A CURE.
JOIN US.

Contents

Table of Figures

Table of Frequently Used Abbreviations

Neurodegenerative Condition		Retromer Components/Interactors	
PD	Parkinson's Disease	**CSC**	Cargo-Selective Complex
AD	Alzheimer's Disease	**SNX**	Sortin-Nexin
MND	Motor Neurone Disease	**WASH Complex**	Wiscott-Aldrich Syndrome Protein and SCAR homologue complex
FTLD	Fronto-Temporal Lobular Dementia	**Organelles/Cellular Processes**	
PD Relevant Genes		**CMA**	Chaperone Mediated Autophagy
VPS35	Vacuolar Protein Sorting 35	**TGN**	Trans-Golgi Network
LRRK2	Leucine Rich Repeat Kinase 2	**UPS**	Ubiquitin-Proteasome System
GBA1	Glucoceribrosidase 1	**PPI**	Protein-Protein Interaction
Therapeutics		**CME**	Chaperone Mediated Endocytosis
L-DOPA	Levodopa	**Retromer Cargo**	
ASO	Anti-Sense Oligonucleotide	**MFN1/2**	Mitofusin1/2
Reagents/Methodologies		**MUL1**	Mitochondrial E3 Ubiquitin Protein Ligase 1
TMRE	Tetramethylrhodamine, ethyl ester	**LAMP2A**	Lysosome-associated membrane protein 2
DiI	1,1'-Dioctadecyl-3,3,3',3'-Tetramethylindocarbocyanine Perchlorate	**CIMPR**	Cation-Independnet Mannose 6-Phosphate Receptor
ARS	Area Restricted Searching	**CTSD**	Cathepsin D
PCR	Polymerase Chain Reaction	**APP**	Amyloid-Precursor Protein

Chapter I: Introduction

1.1 Clinical Perspectives of Parkinson's Disease

1.1.1 Symptoms and Neuropathology

Parkinson's disease (PD) (2) is a common, progressive, and multi-system neurodegenerative disorder, for which there is currently no disease modifying therapeutic. Affecting 2% of the population over 65 (3), PD is clinically characterised by the development of a progressive resting tremor, bradykinesia and rigidity, responsive to dopamine pathway therapeutics (4–6). Although predominantly considered a movement disorder, non-motor symptoms of PD are debilitating and heterogeneous in their presence and extent between the affected individuals (4,6–8). These can include hyposmia, sleep disturbances and autonomic dysfunction, leading to postural hypotension, constipation and urinary incontinence (9). Psychological conditions such as anxiety and depression have a high incidence throughout PD progression (7–9), along with cognitive impairment. In fact, dementia affects approximately 60% of individuals 12 years post diagnosis (10), causing further debilitation, concurrent with declining motor function.

Neuropathologically, PD is characterised by the accumulation of Lewy bodies, intracellular protein inclusions composed of fibrillar α-synuclein, leading to the death of dopaminergic neurons in the substantia nigra (11,12). Lewy body pathology is widespread, with α-synuclein deposits found in non-neuronal tissues prior to diagnosis, within the gastrointestinal tract (13) and submandibular glands (14), further suggesting PD is a multisystem disorder, with origins in the periphery and autonomic nervous system. At clinical presentation, dopaminergic neurodegeneration has been induced in the substantia nigra of the midbrain and is widespread, leading to reduced dopamine concentrations in the caudate putamen, integral in the initiation of movement (15). Hence, this results in the cardinal motor symptoms of PD, with the function of surviving dopaminergic neurons throughout the brain increasingly impeded by the presence of Lewy bodies.

According to the Braak staging system, in sporadic PD α-synuclein pathology begins in the dorsal IX/X motor nucleus (11), which regulates parasympathetic, vagal nerves to the gastrointestinal tract. Retrospective studies of individuals affected by PD have illustrated that parasympathetic symptoms, such as constipation, have emerged up to 20 years prior to motor symptoms and clinical PD diagnosis (9), consistent with this neuropathological observation. Stage 2 indicates α-synuclein pathology in the raphe nuclei and the coeruleus/sub coreleus complex,

respectively implicated in serotonergic balance and maintaining muscle dystonia during rapid eye movement (REM) sleep. Coherently, instances of clinical depression have been commonly reported up to 10 years prior to PD diagnosis (16), while 80% of individuals with REM sleep behaviour disorder during middle age, later develop a neurodegenerative condition, predominantly PD (17). At the point of clinical PD diagnosis and onset of cardinal motor symptoms, individuals are likely to exhibit stage 3-4 Braak pathology, with an estimated 80% of dopaminergic neurons in the substantia nigra already lost (9). As PD progresses, α-synuclein pathology spreads to the dopaminergic neurons of the neocortex and prefrontal cortex, leading to cognitive impairment and dementia. From diagnosis, PD duration is heterogeneous between individuals, ranging between 10-15 years on average (8).

1.1.2 Current Therapeutics and Limitations

PD is commonly treated through oral administration of Levo-DOPA (L-DOPA), first used clinically in 1967 (18). In dopamine synthesis, tyrosine is metabolised to L-DOPA by tyrosine hydroxylases; L-DOPA, endogenously produced or exogenously supplemented, is converted to dopamine by DOPA-decarboxylases. Hence, the administration of L-DOPA targets the dopamine deficit induced by PD neuropathology. The epithelia of the small intestine can metabolise 90% of L-DOPA dosage, thus in conjunction, a peripheral DOPA decarboxylase inhibitor is administered, commonly carbidopa or benserazide (19), ensuring a sufficient, therapeutic concentration reaches the brain. Dopamine agonists can also be utilised, alone in the early stages of PD, or in conjunction with L-DOPA, along with inhibitors for monoamine oxidase B, the enzyme responsible for dopamine catabolism (20). These therapeutics are initially beneficial, in tackling the dopamine deficit induced by early PD, providing symptomatic relief in the years following diagnosis. However, through PD progression, efficacy is reduced due to the subsequent and continuous loss of dopaminergic neurons (19).

Currently, there is no disease modifying therapeutic for PD. A novel, pharmacological intervention for PD, in which the rate of neurodegeneration is slowed, or halted, is of great scientific and medical interest. Contemporaneously, there is much investigation into early PD biomarkers, which may be present with prodromal symptoms previously discussed. Therapeutics applied within this window would be most efficacious, prior to PD motor symptoms, in which Braak neuropathology is advanced. In order to identify new drug targets for disease modifying therapeutics, the perturbed molecular mechanisms of neurodegeneration leading to PD pathology must be thoroughly understood. This can be achieved through employing diverse functional models, *in vitro*, *in vivo* and *in silico*, to establish the fundamental science through identifying commonalities between models.

1.2 The Genetic Aetiology of Parkinson's disease

1.2.1 Mendelian Parkinson's disease

Approximately 90% of late adulthood-onset PD cases are idiopathic, defined by the absence of an evident monogenic determinant, while the remainder are familial, showing Mendelian patterns of inheritance and caused by mutations in single genes (21). In most cases, Mendelian PD is symptomatically indistinguishable from the idiopathic disease (21–23), suggesting a potentially shared pathophysiology. PD causative mutations have been identified in a plethora of genes summarised in Figure 1, many of which converge on common pathways including endosomal sorting, vesicle trafficking, lysosomal and mitochondrial function (24). There is increasing evidence that familial PD can follow an oligogenic pattern of inheritance, in which variants in a number of key genes result in an increased risk of PD onset. 30% of individuals with PD linked to a pathogenic mutation in a Mendelian PD gene, also have a concurrent variant in one or more known PD associated genes (25), potentially accounting for variance in disease progression and penetrance between affected individuals. Additionally in post-mortem studies of individuals whom had idiopathic PD with dementia, 23% had more than 1 genetic variant in known PD associated genes, compared to 10% in an unaffected control population without PD (26). Substantial progress has been made in elucidating the molecular mechanisms of neurodegeneration in PD, through functional studies of Mendelian PD genes in a diverse range of *in vitro*, *in vivo* and *in silico* models (27,28).

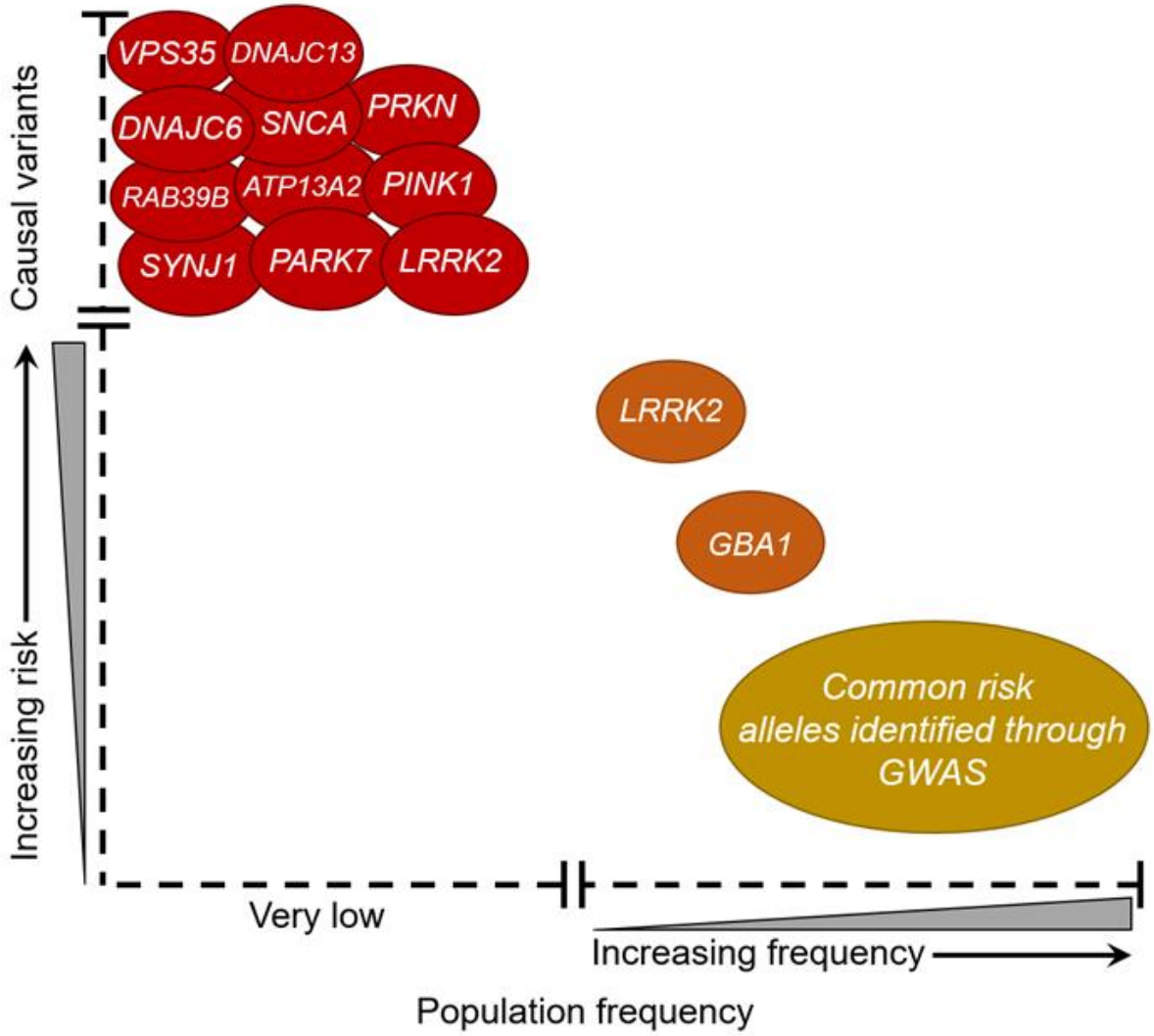

Figure 1- The emerging genetic architecture of Parkinson's disease

Mutations and variants in several genes have been identified to be causal or increase susceptibility to PD. Genes indicated in red, which have a very high or causal link with PD development, show Mendelian inheritance and are rare in the population. Genes indicated in orange confer a greater risk of PD development, but with incomplete penetrance. These genes have been identified through both Mendelian and GWAS studies. The expansion of GWAS targeting idiopathic PD has highlighted a plethora of common alleles, illustrated in yellow. These are very common in the population and confer a heightened susceptibility to PD development. Different PD linked mutations in LRRK2 confer varying risk of PD development and penetrance. There are protective variants in LRRK2, which significantly reduce the risk of PD development, highlighting the central role LRRK2 may play in PD pathogenesis. Taken from Chandler *et al*, 2021.

1.2.2 Oligogenic and Polygenic Inheritance

The complex aetiology of idiopathic PD is a rapidly expanding area of research, with a plethora of genetic and environmental factors associated with the lifetime risk of PD development (3,12,29,30). In terms of genetics, it is clear that there is a substantial contribution of common genetic variants to the increased risk of developing idiopathic PD, the type of PD where there is no family history of segregating disease (31). A multitude of these genetic risk factors have been identified through extensive and expanding Genome Wide Association Studies (GWAS),

comparing idiopathic PD and unaffected control populations (32). The development of GWAS in recent years, coupled to the expanding availability of genetic data, has further improved our understanding of the genetic architecture of PD (32–35). These studies have identified a large number of novel candidate genomic risk loci, with genetic variants observed in idiopathic PD populations compared to control groups. A recent, comprehensive meta-analysis of PD GWAS studies, utilising data from 37,700 idiopathic PD patients and 1.4 million unaffected controls, undertaken by Nalls and colleagues in 2019, identified 90 genomic risk signals at 78 genomic loci associated with increased lifetime risk of PD. These loci may explain up to 36% of heritable risk for PD (32,36). Although a great deal of further research is required to conclusively identify the causative variants of these loci, many of the candidate genes converge upon similar cellular pathways shown to be perturbed in functional studies of Mendelian PD genes, notably endocytic vesicle trafficking (24), lysosomal and mitochondrial function (37).

The burden of multiple, common variants of risk loci identified through GWAS, which may be present in a single individual, contribute to a polygenic risk score of lifetime PD development (32). Importantly, a polygenic risk score does not account for environmental factors, which also have an impact on PD risk and may therefore not be clinically useful in diagnosis, if considered alone (31). However, when taken in conjunction with prodromal PD symptoms, polygenic risk score may stratify groups for clinical trials with enhanced genetic precision for targeting, as novel drugs are developed (31). Identified genes vary in their effect size upon polygenic risk score depending on their functionality, with common variants in known PD associated genes driving larger effect sizes (31,32). An additional challenge of determining the effect size of novel GWAS loci upon polygenic risk score is that functional modelling for these genes in the context of PD are yet to be undertaken, as our understanding of their mechanism of action and impact upon risk of PD development is incomplete.

However, since the discovery of the first Parkinson's disease associated gene, SNCA in 1997, there has been substantial research in the PD community to develop and characterise functional models for Mendelian disease-causing genes. These have shed great insights into the mechanisms of action of key PD genes and even enabled the development of novel drugs targeting LRRK2, which are currently under early phase clinical trial. The development of diverse functional models *in vivo* and *in vitro* is integral to this understanding and fundamental research, in order to address key questions from different angles. Each model has strengths and limitations and as such, comparative study is necessary for a complete picture of the fundamental disease mechanisms.

1.3 *C. elegans* as a Parkinson's disease model

1.3.1 Introduction to *C. elegans* in neurodegenerative disease modelling

The nematode worm, *Caenorhabditis elegans* (*C. elegans*), provides an excellent model system for developing understanding of underlying disease biology in neurodegenerative conditions, including Alzheimer's disease (AD), polyglutamine disorders and prion diseases (28,38–40), and is a promising candidate for functional modelling of the complex genetic architecture of PD. Between 60-80% of human genes have orthologues in *C. elegans* (41) and its genome was the first of any multicellular organism to be completely sequenced (42,43). Thus, along with the extensive experimental tools available in this system, it facilitates the generation of simple, *in vivo* gene function models.

C. elegans have been widely used as a model for ageing (44), with their short lifespan and rapid reproduction rate facilitating straightforward and fast study of this process. *C. elegans* are highly amenable to neurobiology, as they have a fully mapped neural connectome (45,46), in which each neuron is characterised in its neurochemistry, connectivity and functionality, often with attributable behavioural phenotypes to each neural circuit to test (47,48). Furthermore, the majority of neurotransmitters utilised in neuronal signalling in the human brain, are also produced and utilised in the *C. elegans* neuronal system (42,49,50). The majority of Mendelian PD genes have orthologues in *C. elegans* and multiple models have been developed to study the functional effects of these genes in C. elegans, which have demonstrated substantial functional conservation with their human counterparts and yielded important insights into gene function (27,28) as described in figure 2.

Furthermore, developments in CRISPR/Cas9 genome engineering technology have been extended to *C. elegans* (51), facilitating study into the functional effect of specific, PD relevant mutations. Following review of the published literature, the study of PD genes through direct CRISPR/Cas9 modification of *C. elegans* orthologues to incorporate PD relevant point mutations has never been undertaken as a functional modelling approach, until this research project. CRISPR/Cas9 modification in *C. elegans* is more economical than development of murine models, enables rapid study due to their short lifespan and allows dissection of research questions from multiple angles, from the organismal, to the cellular to the molecular. The combination of well-established research methods applicable to *C. elegans* models and the novelty of CRISPR/Cas9 modification for PD modelling, opens an expansive window for this research in further understanding the Mendelian PD genes *VPS35* and *LRRK2*.

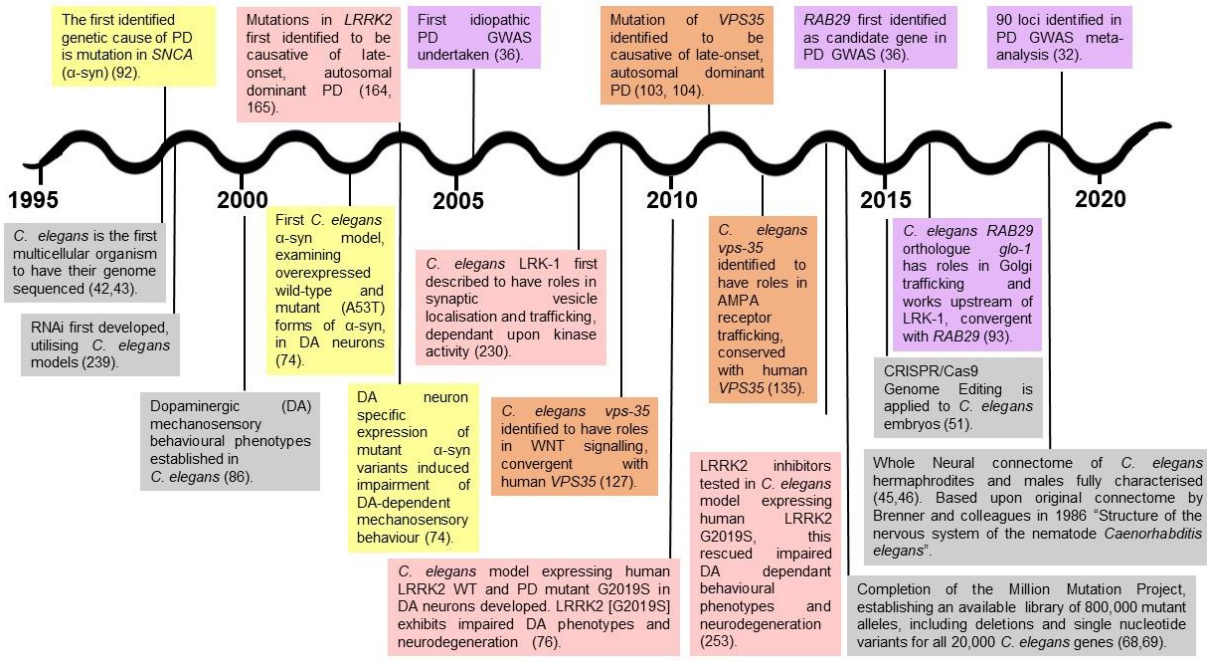

Figure 2- A Quarter Century of advances in human PD genetics, C. elegans technologies and functional modelling of Mendelian PD in C. elegans

Timeline of advancements in our understanding of PD genetics, from the identification of the first mendelian PD gene encoding for α-synuclein in 1997, to the novel and expanding insights recently gleaned through GWAS. Human PD genes are indicated above the timeline and have individual colours assigned to them, with the milestones in *C. elegans* research of this gene or orthologues beneath the timeline indicated with the same colour. Concurrent with the growth of human genetic data in PD, there has been much advancement in *C. elegans* technologies relevant to PD research, illustrated with grey boxes. As a model, *C. elegans* has been pivotal in the development of RNAi technology, whole organism genome sequencing and recently, CRISPR/Cas9 genome editing. Many of the Mendelian PD genes presented have been studied in *C. elegans* functional models, with promising conservation demonstrated. Adapted from Chandler, *et al*. 2021

1.3.2 *C. elegans* orthologues of PD relevant genes

Most Mendelian PD genes have orthologues in *C. elegans*, as described in Table 1 and multiple models for PD have been developed. These have demonstrated substantial functional conservation with their human counterparts and yielded important insights into gene function (27,28). This highlights the relevance of *C. elegans* for the application of CRISPR/Cas9 modification for the development of novel models. Through an Ortholist2 search, which identifies *C. elegans* orthologues of human genes of interest, 64 of the 90 risk loci for PD, have a direct orthologue in *C. elegans*, as shown in figure 3. These 90 loci have been identified through advanced meta-analysis and account for 36% of idiopathic PD heritability. This highlights the potential relevance of *C. elegans* for not only understanding Mendelian PD, but genes identified in idiopathic PD which often converge upon similar pathways to the Mendelian genes, or interplay with them in an oligogenic manner, are broadly conserved. This illustrates that PD relevant molecular pathways may be maintained in *C. elegans* and that study of Mendelian genes such as VPS35 and LRRK2 may shed broader insights.

PD Patient Phenotype	Mendelian PD Gene	Average Age of PD Onset	Number of Confirmed Pathogenic Mutations	Inheritance	GO Biological Functions Disrupted in PD Gene Functional Models	*C. elegans* Orthologue	*C. elegans* Model Availability (+/-) and Phenotypes		
							Deletion	**Transgenic Expression**	**RNAi**
Typical PD	***LRRK2***	58	8	Dominant	Endosomal Network, Endocytosis, Vesicle trafficking, Microtubules, Lysosomal Function, Macroautophagy	***lrk-1***	+ Synaptic Vesicle Mislocalisation, Axon Termination Impairment	+ Dopaminergic Behaviour	+ Oxidative Stress Response variant
	VPS35	50	1		Endosomal Network, Endocytosis, Vesicle trafficking, Lysosomal Function	***vps-35***	+ Neuronal Development and Migration variant, Cell Fate, Division & Polarity variant, Egg Laying Impairment	-	+ Embryonic Lethal, Locomotion Variant, Endocytosis Impairment
	SNCA	45	4		Lysosomal stressor	**-**	-	+ Dopaminergic Behaviour	-
	PINK-1	35	143	Recessive	Mitophagy	***pink-1***	+ Reduced Metabolism, Mitochondrial Alignment and Morphology Variant	-	+ Mitochondrial Repair Variant, Protein Aggregation
	PARKIN	31	14		Mitophagy	***pdr-1***	+ Mitochondria Morphology Variant, Manganese Hypersensitivity	-	+ Embryonic Lethal, Oxidative Stess Response
	DJ-1	58	5		Oxidative Stress Response	***djr-1.1***	+ Manganese Response Variant,	-	+ Oxidative Stress Response

							Mitochondrial Morphology Variant		
						djr-1.2	+ Reduced Lifespan, Impaired Dauer Metabolism	-	-
Parkinsonism	***DNAJC13***	67	0	Dominant		***rme-8***	+ Impaired Phagosome Maturation, Cell Corpse Clearance Defective, Protein Aggregation	-	+ Apoptosis variant, Cell Membrane Organisation Variant, Embryonic/Larval Lethality, Reduced Egg-count, Receptor Mediated Endocytosis Impairment
	DNAJC6	Juvenile	1	Recessive	Endocytosis	***dnj-25***	+	-	+ Lysosomal Related Organelle Variant, Larval Arrest, Slow Growth
	ATP13A2	Juvenile	6		Lysosomal Function	***catp-5***	+ Norspermidine Resistant	-	+ Lysosome Morphology Variant
						catp-6	+	-	+

							Mitochondrial Morphology Variant		Lysosome Morphology Variant, Nicotine Hypersensitivity, Protein Aggregation
						catp-7	-	-	-
	SYNJ1	Early-onset	3		Endosomal Network, Endocytosis	***unc-26***	+ Locomotion Variant, Muscle Variant, Stress Response Variant, Endosome Biogenesis, Synaptic Vesicle Organisation and Development	-	+ Locomotion Variant, Mitochondrial Morphology Variant
	RAB39B	Early-onset	3	X-linked recessive	Vesicle Trafficking	***rab-39***	-	-	+ Neuronal Migration Variant, Oxidative Stress Sensitivity

Table 1- Mendelian Parkinson's disease genes and their *C. elegans* orthologues

Mendelian PD genes with clinical data regarding PD patient phenotype, mode of inheritance and average age of onset are shown with the corresponding orthologue in *C. elegans* genes. Data has been obtained from Mendelian PD clinical studies (3,22,52–59). The number of confirmed pathogenic mutations has been obtained from NCBI ClinVar database (60), using the filtered by mis-sense and pathogenic mutations filters. *C. elegans* orthologues have been determined using Ortholist2 search of Mendelian PD genes (41). Existing *C. elegans* models and their reported phenotypes were obtained from 'phenotype' data on each orthologue's Wormbase entry (61,62). Existence of C. elegans model is denoted in the table with a + and absence with a -, with the most reported phenotypes, grouped by functionality beneath. GO Biological Functions have been identified utilising G:profiler (309). Most Mendelian PD genes have an orthologue in *C. elegans*, the gene function of which has been previously studied through either, or a combination of gene deletion, RNAi silencing, or transgenic overexpression. Adapted from Chandler *et al*. 2021

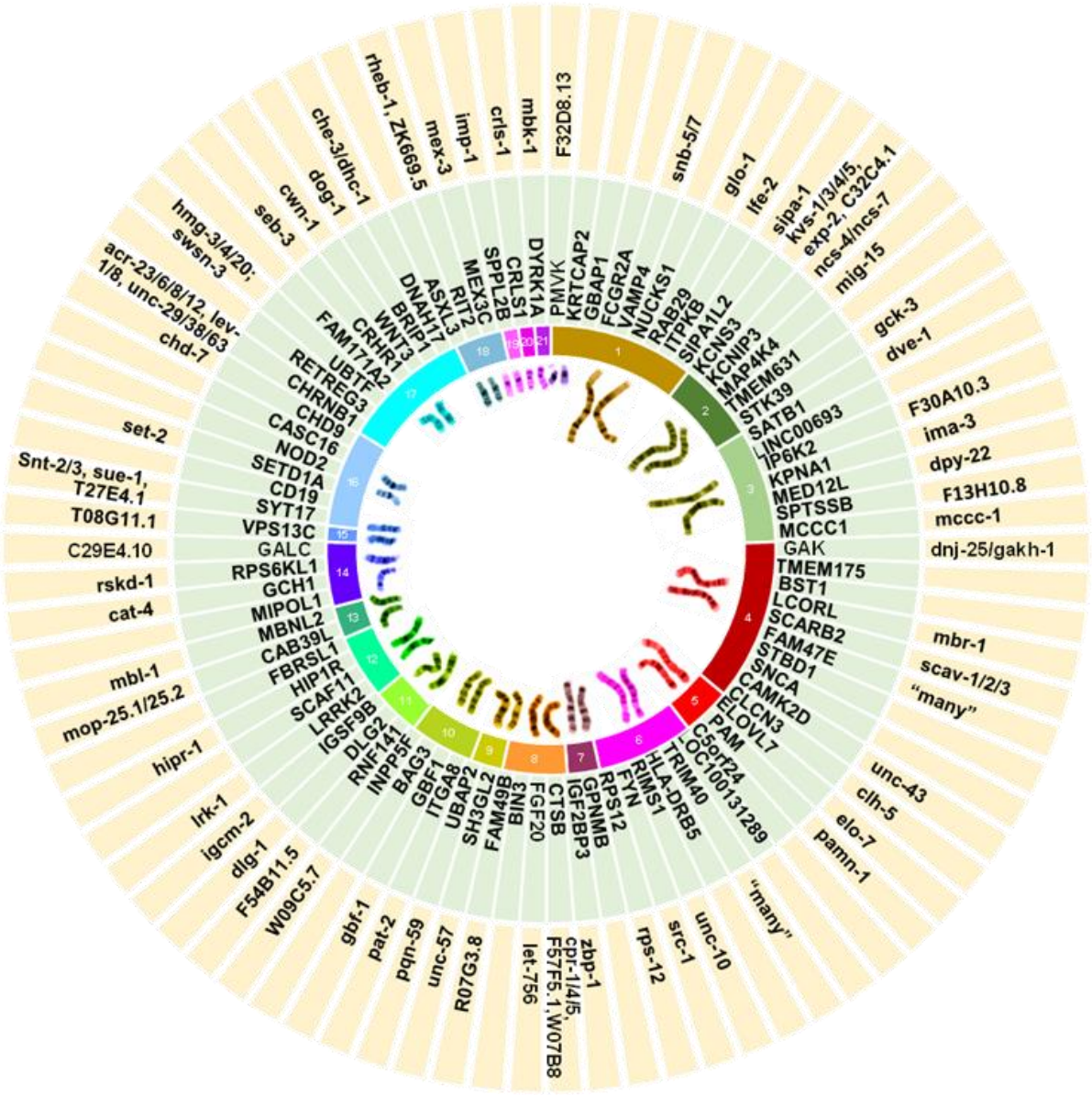

Figure 3-The conservation of PD GWAS Loci and potential for functional modelling

The most recent PD GWAS meta-analysis by Nalls et aland colleagues in 2019 (30) highlighted 90 genome-wide significant risk signals at 78 genomic regions, implicated in idiopathic PD. Search of the *C. elegans* orthologues of the nearest, or most relevant candidate genes suggested by the IPDGC GWAS locus browser (50), using Ortholist2 (39), demonstrated that 64 of the 86 listed candidate risk genes have orthologues in *C. elegans*, yet to be characterised in the context of PD modelling. Adapted from Chandler *et al*. 2021

1.3.3 The application of *C. elegans* genetics to PD modelling

C. elegans are hermaphrodites, with a low abundance of males in the population, however males can be generated through heat shock, leading to chromosomal non-disjunction and aneuploid oocytes or sperm *in utero* (63). This enables the use of forward genetics, to develop crosses to create progeny with multiple known gene mutations, for epistatic analysis of progeny phenotypes. Likewise, reverse genetics can be readily utilised, by sequencing the genome of nematodes exhibiting specific phenotypes, in order to determine responsible genes. In conjunction with reverse genetics, Ethyl methanesulfonate (EMS) and other chemicals can be employed to

mutagenize wildtype worms, which generate random mutations in the oocyte/sperm, with a high efficiency and low toxicity (64). The mutant progeny can then be utilised in large screens to find phenotypes of interest and in the instance of PD, may be used in tandem with environmental stressors, to investigate genetic modulators of survival, lethality, or alternate attributable phenotypes. Large scale RNAi screens have been deployed in a similar manner in order to identify modifiers of α-synuclein toxicity, through gene silencing in nematodes overexpressing humanised proteins (65–67). Notably, such screens have demonstrated that silencing the expression of Mendelian PD gene orthologues, such as *Parkin/pdr-1*, *DJ-1/djr-1.1*, *PINK1/pink-1* and *ATP13A2/catp-6* can act to modify α-synuclein pathology in the worm (67). This suggests promising pathway conservation, illustrating the great potential to dissect the mechanisms of PD relevant genes, in conjunction with transgenically expressed α-synuclein in *C. elegans*.

Deletion studies using a library of deletion mutants, generated by the *C. elegans* deletion mutant consortium and widely available through the CGC (68,69), have shed substantial insight into overall gene function in the organism. However, this does not enable the dissection of subtle alterations in protein function, caused by protein coding variants (70). In terms of PD modelling, as an example, many of the inherited mutations observed in the Mendelian gene *LRRK2*, lead to a gain of function in the LRRK2 protein through increasing kinase activity (71–73). Furthermore, amino-acid changes caused by point mutations in PD genes, could have various impacts on protein functions. Therefore, in many cases using a gene deletion, a loss of function, may not be relevant for modelling the PD gene of interest and might not give an exact insight to the timeline and the molecular pathology of the disease. Alternatively, transgenic expression or overexpression of the human or nematode disease gene of interest has been widely used, developed and the relevant strains distributed (27). This provides experimental tools to investigate for instance the impact of α-synuclein overexpression in muscle cells or in the PD relevant dopaminergic neurons of the worm (74,75), or to study the effect of dopaminergic neuronal expression of PD mutated human LRRK2 (76). This approach has many advantages, however if a wildtype *C. elegans* background is utilised, the studies do not account for potential overlapping activity of the endogenous *C. elegans* orthologue. This is the case in multiple human LRRK2 overexpression models (76–80), especially as the endogenous worm orthologue is less well characterised than the human protein of interest (81). This can be overcome by transgene expression in an orthologue deletion mutant background (28).

The development of CRISPR/Cas9 technologies has enabled the rapid generation of endogenous, knock-in point mutations for *C. elegans* orthologues of human genes (51,82–84), although this is not yet as widely used as deletion, RNAi silencing and transgenic expression studies. Endogenous CRISPR/Cas9 engineered mutations can be studied in homozygous or heterozygous form in *C.*

elegans, or in conjunction with a loss of function deletion allele and enables the investigation of gain of function and dominant negative effects. This is particularly relevant in the context of PD orthologue modelling and will be applied to *VPS35* and *LRRK2*.

1.3.4 The *C. elegans* Toolkit for Functional Modelling

Functional studies of PD in *C. elegans* have, to date, been undertaken using gene deletions, RNAi silencing and transgenic overexpression of the human protein of interest (Table 1). Over 20,000 *C. elegans* mutant strains are available from the Caenorhabditis elegans Genetics Centre (CGC) and the National Bioresource Project (Japan), facilitating easy procurement of multiple mutants to study and contrast their phenotypes in the laboratory. Furthermore, WormBase is a curated online database for *C. elegans* research, in which all current information on organism genes, strains and observed phenotypes are available for open community access (61,62). Similarly, WormBook is a comprehensive, open access collection of chapters on *C. elegans* biology and established protocols. Protocols can be nematode specific, however many are translated and applied to *C. elegans* from *in vitro* methods, such as staining with and detection of fluorescent dyes to determine assorted cellular functions. These can be studied through *in vivo* microscopy in *C. elegans*, as their bodies are transparent (85). Accessible resources and sharing of insights through these platforms enable collaborative, efficient research when establishing novel functional models. Additionally, transgenic proteins can be tagged with fluorescent reporters, as detailed in figure 3 and due to *C. elegans* ready application to *in vivo* microscopy, localisation studies can be undertaken (85). As such, *C. elegans* can be readily studied at organismal, cellular and molecular level.

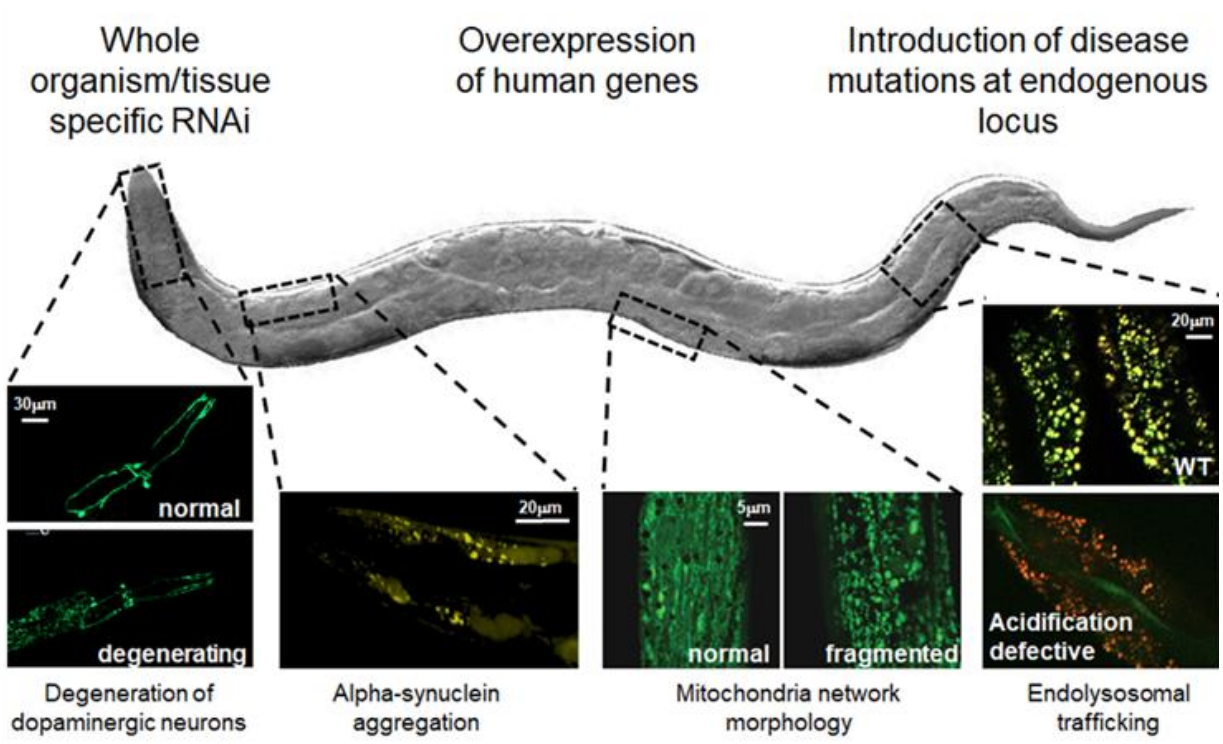

Figure 4- Selected Examples of the extensive C. elegans toolbox for PD gene modelling

Multiple genetic approaches can be utilised to investigate gene function in *C. elegans*. PD pathology can be investigated in *C. elegans* through *in vivo* microscopy, using established cellular reporters of dopaminergic neuron degeneration, α-synuclein aggregation, mitochondria network and lysosomal function. Microscopy images utilised in this figure were obtained within the Kevei laboratoy, through epifluorescent and brightfield confocal-like microscopy. Taken from Chandler *et al*. 2021

Organismal studies of *C. elegans* are frequently well established and global markers of health such as lifespan and fitness through motility can be readily studied. These can be easily studied in conjunction with environmental modifiers, such as bacterial colonies, oxidative stress inducers and pharmacological treatments. As *C. elegans* have a fully mapped neural connectome, each neuronal population has been understood in terms of functionality (46) and frequently, there are simple behavioural outputs to assay and test, as markers of neuronal function. For example, the 8 dopaminergic neurons present in *C. elegans* are responsible for modulating a nutrient sensing behaviour and nutrient searching chemotaxis (86,87).

At a cellular level, multiple models have been well established in which transgenic fluorescent proteins are expressed in specific cells for visualisation (85). In the context of PD modelling, there are established strains encompassing a dopaminergic specific transgene, for visualisation of dopaminergic neurons *in vivo* (88) as shown in figure 3. Furthermore, a vast range of dyes developed for investigating cellular processes *in vitro* can be utilised for *C. elegans* research in conjunction with confocal-like microscopy (85,89,90). This enables a dissection of phenotypes shown at the organismal level at a deeper, cellular level to understand more broadly what the underlying pathophysiology's could be. Moreover, this can be studied with greater acuity at a

molecular level, as individual proteins can be tagged with fluorescent proteins for visualisation and localisation studies (51,84). Moreover, some antibodies are amenable to *C. elegans* with some epitopes showing sufficient specificity for orthologous *C. elegans* proteins, enabling semi-quantitative immunoblotting, immunohistochemistry studies and protein pull-down for interactome analysis (91). With a wealth of methods applicable to this rapid, robust and economical model, key questions to probe novel functional models of PD genes can be undertaken from multiple angles.

1.3.5 The limitations of *C. elegans* in PD modelling

As with all models of gene function, *C. elegans* hold their own limitations, furthering the need to contrast them with alternative *in vitro* and in vivo systems. Due to their evolutionary divergence with humans, 20-40% of human genes do not have a direct orthologue in *C. elegans*, there are genes specific for *C. elegans* only, or *C. elegans* have just one orthologue for multiple closely related human genes. The nuances surrounding specific gene conservation, in the instance of *VPS35, LRRK2* and other PD relevant intermediates will be discussed in depth throughout this study. Pertinently in the context of PD modelling, *C. elegans* lack an orthologue for *SNCA* gene, the first gene identified in familial PD in 1997 (92) and a consistent GWAS loci (32), encoding the PD neuropathology hallmark α-synuclein. Multiple *C. elegans* models have been generated expressing wildtype or mutant human *SNCA* as a transgene, in muscles, neurons or dopaminergic neurons (74,93). These have been illustrated to recapitulate PD hallmarks of dopaminergic neurodegeneration (74,80,93) and have been employed to study a diverse range of PD relevant pathways, shedding insights into PD pathology.

Furthermore, due to *C. elegans* evolutionary distance from humans and their simplicity, they lack many of the key organs and tissues relevant for PD research (94). *C. elegans* possess a well-understood intestine, relevant for investigating microbiome interplay with neuronal health as a model of the gut/brain axis (95,96), however *C. elegans* do not poses a defined brain. A key question in PD research is the selective vulnerability of dopaminergic neurons in specific brain regions, such as the *substantia nigra pars compacta* and the midbrain (97,98), hence this is impossible to model in *C. elegans*. Even *Drosophila melanogaster*, the alternative invertebrate model possesses a simplistic brain-like structure, while mammalian *in vivo* models are evolutionarily closer to humans to further understand this. *C. elegans* do possess simplistic glial cells, however their neurons are unmyelinated due to their short length and the glia are not in an environment orthologous to the mammalian brain (99). In addition, there is no *in vitro* cell culture model derived from *C. elegans* to contrast the *in vivo* model with. In mammalian studies, *in vitro* cortical neurons, glia or embryonic fibroblasts can be studied in parallel (100), enabling greater

resolution, while the alternative invertebrate model, *D. melanogaster* has S2 cells grown in culture for study (101). Furthermore, due to their small size of 1mm biochemical studies, such as immunoblotting for proteins of interest, in specific tissues can be challenging. Molecular approaches are frequently undertaken utilising whole worm lysates, which limits the understanding of neuronal specific outputs in the context of PD modelling.

Despite these pertinent drawbacks, novel CRISPR/Cas9 modified *C. elegans* could pose as insightful novel models of gene function. Considering the increasing speed in dissecting the genetic component of PD and the requirement for rapid and robust functional validation, new models are required. Such a scenario is difficult to achieve in rodents, while *C. elegans* possess the optimal feasibility in terms of genetic manipulation. Endogenous CRISPR/Cas9 engineered mutations enable precise modelling of human genetic mutations, proven to be pathogenic in causing Mendelian disease and may open up a window to model subtle, common variants that increase the risk of PD, following validation of CRISPR/Cas9 *C. elegans* as a PD model (102). As *C. elegans* is one of the easiest and cheapest multicellular eukaryotic organism to apply precise genome editing to, the choice of this simple nematode for studying PD biology provides fast, cheap *in vivo* modelling with great translational potential (28,41,85),

1.4.VPS35[D620N] mutation consequent Parkinson's disease

1.4.1 Clinical Presentation and Neuropathology of VPS35[D620N] Parkinson's disease

A mutation in Vacuolar Protein Sorting 35, VPS35[D620N] (c.1858 G>A) , was identified in 2011 in a small number of families with late onset, autosomal dominant PD, showing similar symptomatic presentation to idiopathic PD (103–105). The median age of PD onset for affected individuals is 49 years, exhibiting classical clinical symptoms, responsive to L-DOPA therapeutics (106)(22). VPS35 is an integral subunit of the retromer complex, implicated in retrograde transport between the endosomes and the trans-Golgi network (TGN) (107). VPS35 and its link with the retromer was fist described in the unicellular *Saccharomyces cerevisiae,* with which the human retromer shows substantial conservation (107–109), while *C. elegans* have a well conserved, direct *VPS35* orthologue, *vps-35* (110). Interestingly, $VPS35^{D620N}$ has also been shown to enhance LRRK2 kinase activity 6-fold in *in vitro* CRISPR engineered murine fibroblasts and neutrophils isolated from PD patients carrying VPS35[D620N] (111). This suggests an interplay between LRRK2 and the retromer in PD, a plausible hypothesis for the molecular mechanism of VPS35[D620N] PD and further highlights the roles of LRRK2 and the endosomal network in neurodegeneration.

It is currently unclear whether individuals with VPS35[D620N] PD exhibit typical α-synuclein pathology, as due to the mutation's rarity autopsy studies so far have been very limited (112). In 2008, a post mortem study was undertaken with one individual from a Swiss family with multi-generational PD, which was later identified in 2011 as VPS35[D620N] consequent (10). However, only limited tissue from the cortex and basal ganglia were taken for analysis, with key PD relevant brain areas missed ; α-synuclein pathology was not shown(10). Hence, additional studies to obtain further insight into α-synuclein and tau pathology are required. *In vivo* murine models with VPS35[D620N] endogenously knocked in exhibit progressive neurodegeneration, driven by tauopathy (113), while retromer has been shown to modulate the lysosomal clearance of tau *in vitro* (114). The proposed mechanism of VPS35[D620N] resulting in enhanced LRRK2 kinase activity (111), further suggests that tau pathology could be present in VPS35[D620N] PD, as tauopathy is a hallmark of *LRRK2* PD (115).

1.4.2 The role of the retromer

VPS35 is an integral subunit of the retromer complex, implicated in retrograde transport of cargo between the late endosomes and the TGN, endosome to plasma membrane transport and recycling of transmembrane protein cargo (112), as shown in figure 5. It is a heteropentameric complex composed of a cargo selective complex (CSC) trimer (in which VPS35 is the core subunit) and a

sortin-nexin (SNX) dimer. The CSC is responsible for the binding to and sorting of protein cargo, while the SNX dimer facilitates association between the retromer and endosomal membrane. However, VPS35 forms an association with the Wiskott-Aldrich Syndrome Protein and SCAR Homolog (WASH) complex, which enables the formation actin patches for vesicular budding (116). SNX binds with the endosomal small GTPases Rab7 and 5 for endosomal retromer stabilisation (117). Within the CSC, there is a great diversity of interactions, suggesting cargo selectivity between and within subunits, facilitating specificity in delivery of cargo to distinct vesicular compartments (118). The 'apex' of the retromer complex arch, is formed by the α-solenoid, horseshoe shaped VPS35 subunit (119). This apical region of VPS35, homodimerizes, forming a retromer 'coat', integral for interaction with the late endosomes (120). The VPS35^{D620N} mutation implicated in PD is located adjacent to this apex, within the central interior of the CSC, hence it has been hypothesised that this mutation may impair retromer coat formation (120). Alternatively, this could have implications in cargo specificity, leading to selective defective cargo trafficking (118), or alter interactions with currently unknown effectors in regulating downstream signalling pathways (111).

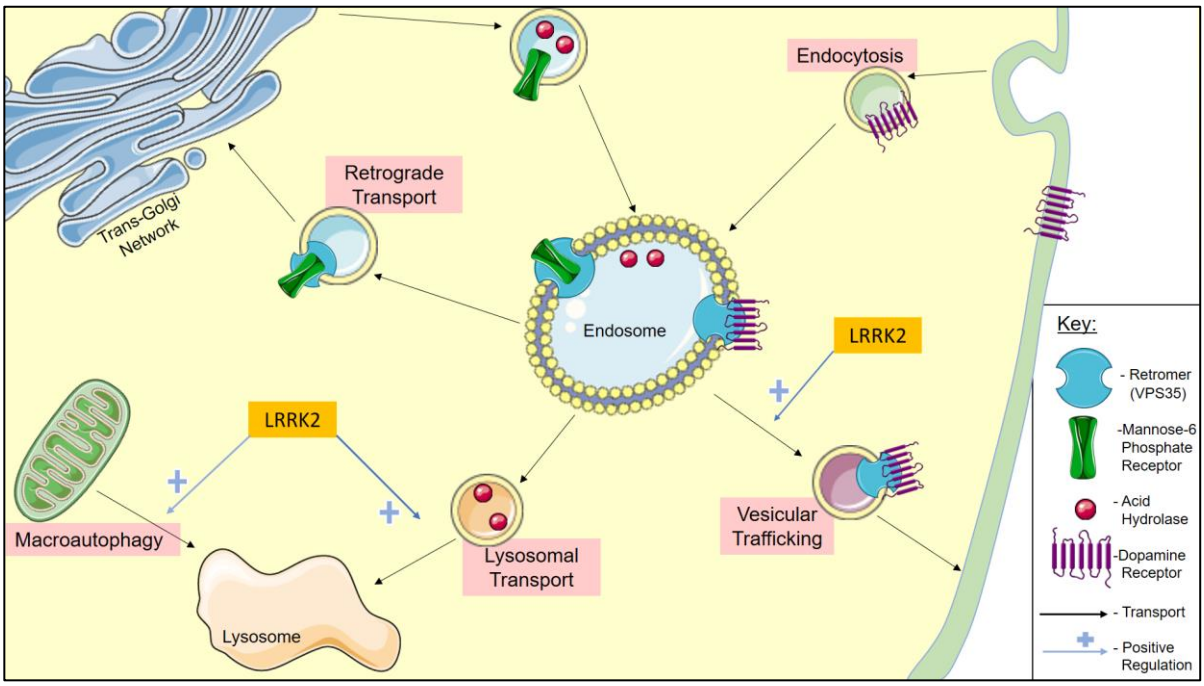

Figure 5- Key Functions of the Retromer in Cell Biology

Summary of cellular pathways implicated in VPS35 and potential convergences in LRRK2 functionality. VPS35 is an integral component of the retromer complex indicated in blue. LRRK2 has some proposed shared functions, highlighted in orange, the regulation indicated in blue arrows with +. The retromer has many cargoes, dopamine receptor (purple) and mannose-6-phosphate receptor (green) utilized as an example. Adapted from: Williams, Chen and Moore. 2017

1.4.3 Emergence of the Retromer and Endosomal Network in Neurodegenerative Conditions

Apart from PD, retromer dysfunction has been implicated in multiple neurodegenerative conditions, suggesting potential common perturbed pathways and the importance of retromer in neuronal function. In AD autopsy studies, microarrays have illustrated that retromer is depleted in the hippocampus, within the dentate gyrus and entorhinal cortex, a region in which AD pathology is initiated (121). Further mechanistic studies have illustrated that retromer facilitates the trafficking of amyloid precursor protein (APP) through sortilin binding within the retromer, thus retromer deficiency leads to APP accumulation and cleavage to pathogenic ß-amyloid (122), a driver of AD pathogenesis (123).

Furthermore, sortilin is a key gene implicated in AD, as well as Fronto-Temporal Lobular Dementia (FTLD), while mutations of the sortilin receptor have been implicated in familial PD (109,124). Sortilin is transported by the retromer, through interaction with VPS35 (125). In FTLD, sortilin binds to the causative protein aggregate progranulin, promoting its delivery to the lysosomes for degradation, thus in retromer dysfunction, this pathway is disturbed, leading to progranulin aggregate pathology (124). Progranulin is also implicated in FTLD with Motor Neurone Disease (MND) (124), further suggesting a potential role for the retromer. Additionally, mutations of RAB7, a key component in facilitating retromer-endosome binding are the cause of hereditary Charcot-Marie Tooth neuropathies (126).

Evidently, the retromer is integral in the maintenance of neuronal health, however the molecular mechanisms of neurodegeneration in the case of PD with VPS35[D620N] mutation is currently unclear, thus further investigation is required. Further study of this mutation in a novel *C. elegans* model could shed further insight into retromer biology, function and its impact upon a wide range of neurodegenerative diseases.

1.4.4 *C. elegans* as a model for VPS35[D620N]

As mentioned previously, the retromer, of which VPS35 is the core subunit, is well conserved in all eukaryotes, from *Saccharomyces cerevisiae*, to murine *in vivo* models, to humans. The extent of functional conservation between human VPS35 and *C. elegans* VPS-35 and its relevance to modelling PD will be discussed in Results chapters 3 and 5.

Thus far, *VPS35* has been studied in *C. elegans* through deletion models and RNAi silencing, to dissect the overall gene function. These may not be so useful for understanding precise point mutations with pathogenic consequences, such as the VPS35[D620N]. However, when findings from these studies are contrasted with retromer investigations in *in vitro*, *in vivo* and patient studies, observations in *C. elegans* are often consistent, suggesting high functional conservation. Studies conducted in *C. elegans* so far have demonstrated that VPS-35 and the retromer have a role in modulating WNT signalling, determining neuronal migration during development (127–131). The role of *VPS35* in WNT signalling is conserved in other invertebrate models, such as *D. melanogaster*, but also in mammals as observed in cell culture studies (131,132), suggesting maintained functional conservation through evolution. Recently, heterozygous VPS35[D620N] mouse models have been reported to display WNT/ß-catenin signalling dysfunction (133). This highlights the potential pathogenic perturbation of the WNT signalling pathway (133), converging with its impairments illustrated in the *LRRK2* PD models, discussed in 1.5 (134) and implicates WNT signalling as a core process with relevance to PD pathogenesis. Additionally, in *C. elegans*, VPS-35 has been implicated in trafficking of the nematode orthologue of the excitatory AMPA glutamate receptor, GLR-1 (135). Deletion of *vps-35* leads to a significant reduction in the number of GLR-1 puncta on the post-synaptic surface of ventral nervous cord dendrites and suggests a role for the retromer in GLR-1 recycling (135). Coherently, in iPSC neuronal cultures derived from people with VPS35[D620N] PD, APMA receptor trafficking was dysregulated and receptors were mislocalised (136), suggesting partial loss of function. This shared role between *C. elegans* VPS-35 and its human orthologue, suggest retained functional conservation through evolution.

Furthermore, pan-neuronal deletion of *VPS35* in recent novel mouse models have illustrated rapid motor deficits and early lethality, caused by degeneration of motor neurons, preceded by the formation of protein aggregate inclusions positive for the ubiquitin binding protein p62/SQSTM1(137) . This phenotype exhibited is closest to MND and further highlights the importance of *VPS35* and the retromers' pleiotropic effects in neurodegenerative disease. Developing further insights from *C. elegans* VPS-35 may have broader implications for furthering neurodegenerative disease research, than developing knowledge of PD alone.

In this study, a novel *C. elegans* model has been developed through CRISPR/Cas9 modification, incorporating an orthologous point mutation of human VPS35[D620N] in to the endogenous *C.*

elegans VPS-35, [D638N] in nematodes. Findings from characterisation and establishment of this model will be discussed extensively in chapter 3 and its proposed interplay with LRRK2 (LRK-1 in *C. elegans*), will be covered in chapter 5.

1.4.5 Proposed Mechanism of Action for VPS35[D620N]

Currently, the mechanisms of action of VPS35[D620N] PD are unclear. This research project is the first time VPS35[D620N] has been studied in *C. elegans,* however review of the literature has highlighted an assortment of functional studies, shedding great insight into cellular perturbations implicated (138). It is currently unclear whether VPS35[D620N] causes neurodegeneration due to a loss of function, dominant negative toxicity, haploinsufficiency, or a toxic gain of function mechanism. Notably interaction with LRRK2 has been illustrated in several models (111,139–141). Understanding of alternative model systems findings in terms of VPS35[D620N] mechanisms are integral in establishing the novel model and assessing functional conservation, as research findings can be contrasted with existing *in vitro, in vivo* and *in silico* models.

1.4.5.1 Reduction in Lysosomal Function

VPS35[D620N] has been shown to disrupt binding to the WASH complex, impairing the endosomal sorting of cation independent mannose-6-phosphate receptors (CIMPR) (116), which have an integral role in the transport of the protease cathepsin D (CTSD) to the lysosomes. Depletion of retromer, via RNAi knockdown of *VPS35* in transgenic human α-synuclein expressing *Drosophila* has been shown to reduce lysosomal CTSD content, resulting in accumulation of α-synuclein and impaired locomotor activity (142). Defective retromer binding to the WASH complex, caused by VPS35[D620N] mutation, may similarly perturb this mechanism through the loss of function of CIMPR sorting and consequent reduced lysosomal CTSD content, leading to α-synuclein accumulation.

Additionally, VPS35[D620N] has been implicated in defective chaperone mediated autophagy (CMA), in which cytosolic proteins are targeted to the lysosomes for degradation and translocated across the membrane, through binding to the lysosome associated membrane protein 2 (LAMP2a) CMA receptor in mice (143,144). Transgenic mouse studies have illustrated that *VPS35* knock out in the vulnerable dopaminergic neurons of the substantia nigra and thalamus, leads to a reduction in lysosomal LAMP2a levels, due to impaired endosome to Golgi retrieval, resulting in α-synuclein accumulation and a PD phenotype. VPS35[D620N] heterozygous mutants had the same phenotype, suggesting a mutation consequent loss of function in Golgi retrieval of LAMP2a, resulting in defective CMA and α-synuclein accumulation (143,144).

Aggregation of α-synuclein leads to proteotoxic stress and the production of aminoacyl tRNA synthetase complex-interacting multifunctional protein 2 (AIMP-2), which cannot be degraded by the E3 ubiquitin ligase Parkin in transgenic mice and *in vitro* human derived SH-SY5Y cells (145). Pertinently, mutations in Parkin lead to autosomal-recessive, juvenile PD (146). AIMP-2 is an activator of polyADP-ribose polymerase 1 (PARP-1), which initiates caspase independent cell death through parthanatos, leading to neurodegeneration (147). Retromer has been synchronistically implicated in defective lysosomal clearance of AIMP-2 *in vitro*, further exacerbating the impaired Parkin degradation; like α-synuclein, CMA of AIMP-2 is orchestrated through binding to LAMP2a (148). SH-SY5Y cells transfected with human VPS35[D620N] showed a twofold increase in AIMP-2 compared to cells transfected with wildtype VPS35. Parkin expression was unaffected, suggesting that VPS35 has a downstream role in the degradation of AIMP-2 (148). VPS35[D620N] leads to reduced lysosomal LAMP2a levels, resulting in impaired degradation. Concurrent accumulation of α-synuclein and AIMP-2 exacerbate the protein aggregate induced cell death pathway implicated in PD pathogenesis.

1.4.5.2 Impaired Retromer Cargo selectivity

VPS35 has been demonstrated to have implications in receptor trafficking from the endosome to the neuronal plasma membrane, with a pertinent loss of function mechanism shown in the case of D620N mutation. Studies undertaken by Munsie *et al*, in mouse cortical neurons and human dopamine-like neurons derived from PD affected VPS35[D620N] mutation carrier iPSC samples, have demonstrated that VPS35 is involved in the trafficking of excitatory AMPA-like glutamate receptors (AMPAR) (136). As described previously, in neuronal culture, VPS35[D620N] showed reduced motility in neuronal AMPAR transport, suggesting defective synaptic cargo trafficking(136). This dysregulation was supported studies undertaken by Zhang et al in the *C. elegans*, which demonstrated that expression of wildtype VPS35 sustained immobile GLR-1 on the cell surface, while in retromer silencing, GLR-1 were mislocalised in the ventral nervous cord and motor neurons (135). Similar effects were also implicated in human $VPS35^{D620N}$ dopamine-like neurons, in which GluR-1 were mislocalised with greater cluster intensity (136). This suggests a loss of function with regards to the regulation of receptor trafficking, with potential implications in impaired synaptic plasticity through long term potentiation(149). Notably, in the multigenerational Swiss family in which VPS35[D620N] was first identified, 3 of the 11 PD affected members had a learning disability (10). Alternatively, through this perturbed mechanism of AMPA-R transport, there is potential for a toxic gain of function through excitotoxicity, due to the dysregulation of GluR-1.

PD associated genes have also been implicated in the proposed, but controversial mechanism of α-synuclein propagation between affected neurons (150), thus defective receptor trafficking and cellular transport may be implicated. It is currently unclear how α-synuclein enters neurons, but recent screens have shown promise in identifying novel, previously unidentified receptors facilitating uptake (151). A *C. elegans* model, in which α-synuclein was expressed in individual neurons has been generated by Tyson et al, in which *vps-35* RNAi knockdown organisms showed an increase in α-synuclein propagation in aged *C. elegans,* while knockdown of other retromer components did not affect this (152). This suggests VPS35 might have a role in the transport of an unknown α-synuclein receptor, or clearance of transported α-synuclein within the cell. From this, it could be speculated that proposed the proposed VPS35 loss of function in D620N mutation may have implications in exacerbating the transport of α-synuclein.

In transgenic murine studies, it has been demonstrated that homozygous VPS35[D620N] mutants show impaired striatal dopamine release in the caudate putamen (153). However, these studies demonstrated that this may not be the underpinning cause of pathology. Homozygous *VPS35* deletion mutants showed embryonic lethality (153), while in dopamine receptor 1 and 2 knockout mice, this did not occur, suggesting dopamine independent roles for VPS35 are more pertinent in both neurodegeneration and development. Murine studies can be inconsistent in reflecting human neurodegenerative diseases, as their short lifespan may not facilitate an accurate representation of multi-decade pathology progression. Mice were sacrificed in 'middle age', the age of onset of VPS35[D620N] PD, at 20 weeks- contrary to other, established studies this indicated no alterations in lysosomal CTSD, LAMP2a or α-synuclein (153), suggesting that this timepoint may have been too premature and unrepresentative of VPS35[D620N] PD pathology. Impaired dopamine release has also been demonstrated in the *D. melanogaster* model, inducing defective dopamine dependent sleep and locomotor activity (141). Knockout of endogenous *Vps35* impaired endocytosis at the synaptic boutons in the adult fly brain and reduced the volume of synaptic vesicles- this was rescued by the expression of wildtype human VPS35, but not D620N(141). This further supports the partial loss of function mechanism of *VPS35* mutation.

Despite this, disrupted dopamine signalling may be implicated in VPS35 mutation through receptor trafficking. Wildtype VPS35 promotes the recycling and steady state levels of dopamine receptor D1 (DRD1), while downregulation of VPS35 causes an ablation of the downstream D1 activation pathway (154) in HEK293T cells. DRD1 is a G_s protein coupled receptor, which upon activation generates the production of cyclic AMP (cAMP), via adenylate cyclase (155). Following a signal transduction pathway, the transcription factor CREB is activated through phosphorylation. VPS35[D620N] mutants do not maintain DRD1 recycling and steady state and like the *VPS35* downregulation, show ablated CREB phosphorylation, further suggesting a loss of

function mechanism. Although dopaminergic dysfunction is integral in PD pathogenesis, the diverse role of the retromer in receptor trafficking implicates a greater number of potential effectors for development of pathology.

1.4.5.3 Altered Mitochondrial dynamics

Mitochondria have diverse physiological functions in the cell, from ATP generation through oxidative phosphorylation, to production of reactive oxygen species, calcium homeostasis and cell fate determination (156). Dopaminergic neurons, particularly in the *substantia nigra pars compacta*, are extremely sensitive to impairments in cellular bioenergetics, as they have high levels of connectivity and neural activity, leading to a high ATP demand (97), furthermore it has been hypothesised that vulnerability is increased due to their large size (97), because energy needs to be transmitted across long distances. This transmission is enabled through the mitochondrial network, a dynamic mechanism of mitochondrial transport, modulated and quality controlled by a delicate balance of mitochondrial fission and fusion. Fusion can be protective in preventing cellular damage from individual dysfunctional mitochondria and is regulated by mitofusin 1 and 2 (MFN1/2), while fission enables the segregation of defective mitochondria for autophagy and is regulated by dynamin like protein 1 (DLP1) (157). In the case of VPS35[D620N], both processes have been implicated in a loss of function mechanism (136,143,144,158).

In studies undertaken by Tang *et al*, *VPS35* depletion has been shown to cause dopaminergic neurodegeneration, α-synuclein accumulation and mitochondrial fragmentation in mice, which can be rescued by the expression of wildtype VPS35, but not VPS35[D620N], suggesting a loss of function (143). Depletion of retromer caused an accumulation of MUL1, an E3 ubiquitin ligase, which promotes the degradation of MFN2 (158), thus inhibiting mitochondrial fusion, leading to dysfunction and fragmentation. This increase in MUL1 was shown in both VPS35 depletion and VPS35[D620N] mice, further suggesting a loss of function for the PD linked *VPS35* mutation (158). This phenotype could be rescued by the suppression of MUL1 (158), but α-synuclein accumulation remained, implicating the retromer in diverse, integral cellular processes independent of the mitochondria.

VPS35 has similar implications in mitochondrial fission, leading to mitochondrial fragmentation, notably in *in vitro* fibroblasts from an individual carrying VPS35[D620N], cultured neurons and *in vivo* in transgenic mice (159). VPS35 has been shown to facilitate the clearance of mitochondrial DLP1, in order to enable the recruitment of fission competent DLP1. This is regulated through the mitochondrial derived vesicles, which interact with VPS35 and regulate the turnover of DLP1 and its inhibitory complexes (159). In the instance of VPS35[D620N], this process is dysregulated, promoting the turnover of inhibitory complexes, thus enhancing DLP1 interaction (160). This is

facilitated by a conserved sorting motif for DLP1, which may be disrupted in VPS35 mutation, further weighting the hypothesis of loss of function in cargo selectivity in retromer dysfunction.

1.4.5.4 VPS35[D620N] leads to a Gain of Function

In all cases of VPS35[D620N] PD, individuals are heterozygous and the mutation is dominant (3), eliminating the likelihood of a full loss of function mutation, which are inherited in a homozygous, autosomal recessive manner. For example, loss of function and truncation mutations in RAB39B lead to an early onset, atypical Parkinsonism, inherited in an autosomal recessive X-linked manner (161,162), with symptomatic presentation occurring in males. The fact that VPS35[D620N] is so penetrant in PD pathogenesis, despite affected individuals carrying a wildtype *VPS35* allele, suggests that there may be either a partial loss of function, dominant negative effects of the mutation impacting the function of the wildtype protein, haploinsufficiency, or a toxic gain of function implicated. There are no known individuals homozygous for VPS35[D620N], however the mutation is exceptionally rare and therefore an incredibly low likelihood of two parents carrying the mutation.

In 2014, Tsika et al proposed that VPS35[D620N] induces dopaminergic neurodegeneration through a gain of function mechanism. Retromer is conserved in all eukaryotes, and was first identified in the baker's yeast *saccharomyces cerevisiae* (107). A complementation study in yeast demonstrated that the incorporation of D620N caused no loss of function in growth and sensitivity to metal ions, suggesting mutation may act through a gain of function mechanism (109). Additionally, fibroblast cultures derived from PD affected VPS35[D620N] carriers showed no alteration in CIMPR localisation to the endosomes, suggesting retromer functionality was maintained, with no loss or function. However, functional effects of VPS35[D620N] are likely to be neuron specific and therefore loss may not be conserved in yeast, or as applicable in non-neuronal cultures.

This gain of function theory was supported by rat models, in which human wildtype *VPS35* and *VPS35[D620N]* was transfected and overexpressed, following adeno-associated viral (AAV) vector injection into the *substantia nigra*. Compared to the AAV control, expression of VPS35[D620N] caused a significant loss of dopaminergic neurons in the substantia nigra of 32.2%. However, dopaminergic neurodegeneration was also induced in rats expressing wildtype VPS35 with a loss of 24.6% and there were no significant differences in motor impairment (109). Findings from this model may not be as robust as a gene knock-in, as an exogenous human protein is transiently expressed in a vulnerable neuron population, with the potential to cause unforeseen cellular outcomes. Furthermore, other cardinal hallmarks of PD neuropathology and VPS35[D620N] linked cellular aberrations were not exhibited, with no change in CTSD, α-

synuclein or autophagy marker p62/SQSTM1 (109). However, in VPS35[D620N] expressing rats, there was significantly increased axonal and terminal degeneration. This implicates a toxic gain of function for VPS35[D620N], as the expression of endogenous, wildtype rat VPS35 was maintained.

An increasing body of evidence has linked *VPS35* mutation with dysfunctional LRRK2 interaction, through common pathways (111,139–141,163). Mutations of *LRRK2* are the most common cause of inherited PD (22) and act through a toxic gain of function mechanism, due to enhanced kinase activity (72). Although studies have been inconclusive with regards to VPS35 gain of function (109), this study hypothesises that mutation of VPS35 may lead to a gain of function linked to LRRK2. Coupled with the loss of retromer function likely to be implicated in *VPS35* mutation, a gain of function mechanism in LRRK2 toxicity may further exacerbate neurodegeneration through a shared pathway. This is poorly understood; thus this investigation aims to address and dissect this interaction, along with further contributing to the molecular mechanisms of neurodegeneration implicated in VPS35[D620N] through characterisation studies. The literature surrounding the VPS35/LRRK2 interplay will be discussed extensively, in section 1.6 and investigated in the novel models in Chapter 5. Prior to this, a thorough understanding of LRRK2 and its potential conservation with the *C. elegans* orthologue LRK-1 from existing studies, is required.

1.5 LRRK2 mutation consequent Parkinson's disease

1.5.1 The role of LRRK2 in PD and Pleiotropy in Neurodegenerative Disease

Through candidate gene sequencing and recombination mapping in 46 families with autosomal dominant, late-onset PD, seven coding variants in *LRRK2* have been identified to be causative for PD since the first description of mutations in 2004 (Figure 4) (164–167). Mutations in *LRRK2* are the most common cause of monogenic PD (21), with potential emerging roles of the protein in idiopathic PD (168–170) therefore it has been intensively investigated for the development of therapeutics (170).

LRRK2 incorporates a Ras-like GTP-ase domain, with an adjacent C-terminal of Roc, known as ROC and COR domains respectively. These are the defining feature of the ROCO protein family, of which LRRK2 is the most studied member. Adjacent to the ROC-COR is a kinase domain (171–173), as shown in Figure 4. LRRK2 also encompasses scaffold armadillo, ankyrin and the eponymous Leucine Rich Repeat (LRR) domains that facilitate protein-protein interactions (PPI's) at the N-terminus and at the C-terminus a WD40 terminal domain (174). Notably, PD pathogenic mutations are clustered in the catalytic ROC-COR and kinase domain and lead to enhanced kinase activity (71–73,175–177), a key molecular hallmark of *LRRK2* PD (134), which has attracted great attention from a therapeutic perspective (Clinical Trial ID:NCT03710707(178), NCT04056689 (179)). Several mutations are located in the ROC domain and disrupt GTP hydrolysis (180–182), thereby increasing the proportion of LRRK2 molecules bound to GTP rather than GDP, enhancing auto and substrate phosphorylation (176,182–187). The interdependence between GTPase and kinase activities is further supported by evidence that synthetically engineered GTP binding ablation mutations in LRRK2, significantly impair kinase activity *in vitro* (188,189), although this isn't reflected in all models (190,191) . LRRK2 acts as a homodimer (192,193), suggesting that the enzymatic core function via an interdependent mechanism, with the ROC domain activating the kinase domain when in its GTP bound state (171,185). This is contentious, as in alternative, well conserved bacterial models, LRRK2 monomerization occurs following GTP binding, but is found as a dimer when GTP bound or nucleotide free (194). In addition, LRRK2 is likely in equilibrium between a monomeric, cytosolic and dimeric, membrane bound form (195). Intriguingly, PD associated mutations in the ROC-COR domain were proposed to alter LRRK2 dimerization and cellular localisation (190,191), however the detailed mechanisms as to how the GTPase and kinase domain reciprocally cross regulate activity remains elusive (177,185).

The most common LRRK2 mutation associated with PD, G2019S, is located in the kinase domain and causes a modest 2 fold increase in kinase activity and phosphorylation of substrates *in vitro*

(71) and *in vivo* (196) , while increasing the LRRK2[G2019S] autophosphorylation activity 4-fold (197). The LRRK2[R1441C] mutation, located in the ROC domain, disrupts GTP hydrolysis, enhancing both substrate phosphorylation and autophosphorylation activity by approximately 3-4 fold (111,188,196). These differences in kinase activity might explain the lifetime risk of PD in *LRRK2* mutation carriers, with higher penetrance observed for LRRK2[R1441C] carriers (3,29), although with a later age of onset when compared to LRRK2[G2019S] carriers (3),illustrating that more complex mechanisms may be in action. In addition, while the impact of the LRRK2[G2019S] substitution is restricted to the kinase pocket of LRRK2, any alteration in the GTPase domain is likely to exert broader biochemical and cellular effects on protein function (189).

The majority of individuals with *LRRK2* PD present with classical PD symptoms and exhibit variable Lewy body pathology upon post mortem examination (29,164). Interestingly, all *LRRK2* PD cases exhibit significant tau accumulation (115,164,165,198,199), a pathology observed in some idiopathic PD cases (200), particularly PD with dementia (201), however this is not a diagnostic hallmark of PD upon autopsy (6,11). Moreover, the tau gene *MAPT* is within a consistent idiopathic PD GWAS locus (32,200), illustrating its potential relevance in idiopathic PD. Lewy bodies and tau have a pleomorphic role in neurodegenerative disease pathology (202,203), the former are pathognomonic for dementia with Lewy bodies (204), with α-synuclein found in glial cytoplasmic inclusions in Multiple System Atrophy (MSA) (205) and are found as a secondary protein aggregate pathology in up to half of AD cases (206). Meanwhile, tau is a prominent player in multiple neurodegenerative conditions including AD(207), Progressive supranuclear palsy (PSP) (208) and FTD (209), hence study of LRRK2, with its associated tauopathy and Lewy body aggregation, may be applicable to a range of neurodegenerative conditions.

LRRK2 is notable for exhibiting pleiomorphic pathology in neurodegeneration and in the peripheral immune system (210). In terms of neurodegeneration, variants in the *LRRK2* locus have recently been identified through GWAS as a candidate for increased survival in the tauopathy PSP (211). Additionally, LRRK2 is highly expressed in many cell types of the immune system (212) and expression is increased in the B cells, T cells and CD16+ monocytes of idiopathic PD patients, compared to an unaffected control population (213). This suggests there may be a mechanistic role for LRRK2 in PD relevant inflammation. Notably, variants in *LRRK2* have been observed to increase susceptibility to *Mycobacterium leprae* infection (214), the microbe causative of leprosy, characterised by peripheral neuron damage. Meanwhile, alternative variants in *LRRK2* have been shown to increase the risk of Crohn's disease (215), an inflammatory condition of the gastrointestinal tract. This further illustrates that studies of LRRK2 may shed additional insights into wider disease pathophysiology. In recent years, LRRK2 kinase hyperactivation has been

implicated in idiopathic PD, while *LRRK2* has remained a consistent candidate emerging from idiopathic PD GWAS (22,128–130) suggesting that *LRRK2* functional modelling will provide insights into idiopathic disease, a current challenge in PD research.

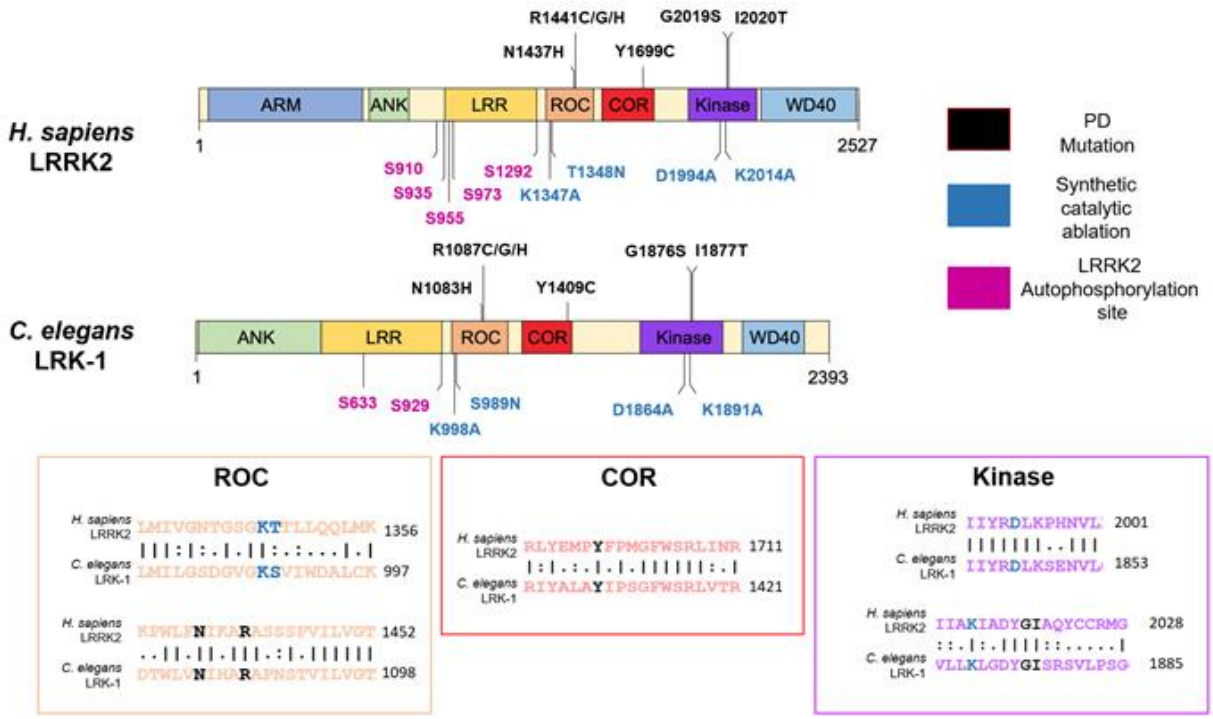

Figure 6- Conservation of Domain Organisation and Amino Acid Residues between H. sapiens LRRK2 and C. elegans LRK-

Human *LRRK2* and *C. elegans* LRK-1 share substantial conservation in terms of domain structure, particularly within the catalytic core incorporating ROC-COR and Kinase domains. The Armadillo domain (ARM), Ankyrin domain (ANK) Leucine Rich Repeats (LRR) and WD40 domain are scaffold regions, facilitating PPI's. Domain information has been obtained from ProSite and Interpro sites, domain visualisation generated in DOG1.0 (321). Sequence alignment obtained through analysis of full-length protein sequences with Emboss_001_Needle, pairwise sequence alignment online tool, Matrix: EBLOSUM62, Gap penalty:12, Extend penalty:2 (233,406,407). Key residues, that are mutated and pathogenic in PD (labelled with black), and residues, the synthetic mutation of which causes catalytic ablation with demonstrated functional consequences (highlighted in blue), are conserved in *C. elegans*, with high or similar sequence identity in surrounding residues. 2 of the 5 key autophosphorylation sites found in *LRRK2* are also present in LRK-1 (shown with pink labels). Taken from Chandler et al, 2021.

1.5.2 Potential of LRRK2 as a therapeutic target

LRRK2 is a promising, druggable target for developing a disease modifying therapeutic for PD, with the potential to be applicable in some cases of idiopathic disease presented with LRRK2 hyperactivation (170). However, upon the onset of diagnostic PD symptoms, disease pathology is already well established. Concurrent with the development of novel therapeutics, early biomarkers for PD and LRRK2 hyperactivation are under extensive investigation, with the aim to enable targeted pharmacological therapies early in disease pathogenesis or at a prodromal stage (216,217).

For over a decade, it has been known that LRRK2 inhibitors targeting kinase activity, can protect against PD associated phenotypes driven by LRRK2 phosphorylation, in *in vitro* and *in vivo*

models (218). Inhibitors have been under extensive development, and in pre-clinical models they have abated α-synuclein mediated neurodegeneration (219,220). Currently, LRRK2 kinase inhibitors are undergoing early stage clinical trials for safety and efficacy (Clinical Trial ID:NCT03710707 (178), NCT04056689 (179)). Furthermore, splice-switching antisense oligonucleotides (ASO's) targeting *LRRK2* have demonstrated, that in human patient-derived cells and murine humanised models, LRRK2 levels can be stably reduced, leading to reduced LRRK2 mediated phosphorylation activity (221). Reduced α-synuclein inclusions and dopaminergic neuron loss have been observed in the brain of *LRRK2*-ASO treated mice exposed to α-synuclein, while peripheral, off target effects of loss of LRRK2 expression were avoided through direct CNS injection of the ASO (222). ASO's targeting *LRRK2* are also entering early stage clinical trials (Clinical trial ID:NCT03976349 (223)), with promising potential. . Indeed, ASO's are approved for clinical use in the treatment of spinal muscular atrophy in over 40 countries (224), illustrating their relevance in neurodegenerative disease therapeutics. .

The development of novel, disease modifying therapeutics for PD hinges upon the thorough understanding of perturbed pathways and the identification of druggable targets that arise, often elucidated through gene functional studies. Substantial progress has been made in utilising *C. elegans* as a simple *in vivo* model for PD genes and as a platform for high-throughput screening of chemical and genetic modifiers (28), however there is extensive room for further development and understanding.

1.5.3 The Evolutionary Conservation of LRRK2 in *C. elegans*

The ROCO proteins are conserved even in simple Eukaryotes , such as the slime mould amoeba *Dictyostelium discoideum* (225), in which they were first described. Humans have two LRRK paralogs, LRRK1 and 2, while invertebrate models, such as *Drosophila melanogaster* and *C. elegans* have only one, dLRRK2 and LRK-1 respectively. It has been hypothesised that *LRRK2* arose as a gene duplication event, following the protostome-deuterostome split (226,227). Studies of evolutionary gene duplications have suggested that splits can lead to sub-functionalisation in which the ancestral gene functions are duplicated into 2 separate genes (228). In the instance of LRRK2, if sub-functionalisation has occurred, it may have retained similar functions to LRK-1. However, the functional conservation extent between *C. elegans* LRK-1 and LRRK2 is not yet established. Here, we will discuss current models of LRK-1 function, in contrast with established models of LRRK2 function in order to evaluate its suitability as a model for LRRK2 in PD.

Remarkably, protein sequence alignments between LRK-1 and LRRK2 demonstrate that many key residues mutated in *LRRK2* PD, or synthetically mutated to ablate catalytic activity in *in vitro* models, are conserved in *C. elegans* LRK-1 (229,230), implicating potential functional

conservation between LRK-1 and LRRK2. PD associated mutation or enzymatic residue conservation is not illustrated between human LRRK2, when aligned with LRRK1 and differential PPI networks between LRRK1 and 2 suggest divergent cellular function (231,232). In terms of sequence identity, the extent of conservation between LRK-1, LRRK1 and LRRK2 are broadly similar. Between LRK-1 and LRRK1, there is a 20.9% amino acid identity (35.9% similarity), while between LRK-1 and LRRK2, there is a 20.3% identity (36.3% similarity) (233,234). LRRK1 and LRRK2 phosphorylate distinct subsets of RAB proteins, downstream effectors of LRRK activity (235) and mutations of LRRK1 lead to a rare bone condition, osteosclerotic metaphyseal dysplasia (236–238), also indicative of divergent functionality. Future modelling of key PD pathogenic LRRK2 mutations and variants in *C. elegans* LRK-1, may shed light on the extent of functional conservation between *C. elegans* LRK-1 and mammalian LRRK1 and LRRK2. We have generated key PD relevant point mutants in C. elegans LRK-1, in order to further evaluate this and assess the suitability of *C. elegans* for dissecting the VPS35/LRRK2 interplay.

When contrasted with LRRK2 in mammalian *in vitro* and *in vivo* model systems, functional studies of *C. elegans* LRK-1 suggest it is a promising candidate as a LRRK2 model, which will be extensively detailed in this subchapter.

1.5.4 The relevance of LRK-1 deletion models for PD

Studies of *LRRK2* function in *C. elegans*, have often been limited to *lrk-1* gene deletion, or transgenic overexpression of human LRRK2 on a wildtype nematode background (76,79,229,230,239). Deletion models are useful in understanding physiological LRK-1 function, however in the context of understanding the biology of *LRRK2* mutation driven PD, the modelling needs to be extended to the individual gene variants with proven, or possible pathogenicity. PD-linked mutations in *LRRK2* have consistently been shown to act through a toxic gain of function mechanism, in which phosphorylation activity of LRRK2 is increased (134). Human genetic studies have illustrated that there are individuals with heterozygous loss of function variants in *LRRK2* (240), leading to an approximately 50% reduction in LRRK2 protein levels (240,241), these individuals do not present with PD and have no significant health complications (241). This suggests that in humans, there could be compensatory mechanisms for LRRK2 function reduction, and that drug delivered kinase inhibition, or application of ASO's in therapeutics may not be deleterious. However, in pre-clinical rodent and non-human primate animal models, LRRK2 inhibitor treatment presented reversible on-target side effects in the lung, showing abnormal accumulation of lysosomal related organelles known as lamellar bodies (242). Encouragingly, this phenotype was reversible (242), and early stage clinical trials of LRRK2 inhibitors have so far showed safety and tolerability (178,179). Pre-clinical *in vitro* models illustrate that LRRK2

inhibition does not significantly affect LRRK1 phosphorylation activity, supporting their distinct structure and function (243). In the context of *C. elegans*, deletion mutant and RNAi loss of function *lrk-1* models would not provide an orthologous tool to modelling the PD gain of function *LRRK2* mutations. Furthermore, *C. elegans lrk-1* deletion models do not show impaired dopaminergic phenotypes and behave similarly to wildtype (76), supporting the human genetics findings (241).

1.5.5 Insights from transgenic expression of LRRK2 in C. elegans

Using humanised *C. elegans* models, through overexpressing human LRRK2 in wildtype and PD mutant form, it is possible to model gain of function mutation effects (177). However, caution is needed when interpreting data, as little is known about the background phosphorylation activity and potential interplay, dimerization and functional redundancy, of wild-type *C. elegans* LRK-1, when human LRRK2 is co-expressed. Adult *C. elegans* with a wildtype *lrk-1* background, expressing LRRK2[G2019S] and LRRK2[R1441C] in the dopaminergic neurons, alongside a dopaminergic neuron specific GFP reporter, exhibit significantly reduced GFP fluorescence by day 3 of adulthood, indicative of dopaminergic neurodegeneration (244). This has been replicated in further studies, illustrating that these models have a robust, PD associated phenotype, relevant to *LRRK2* modelling (177,245). Often, rodent models do not recapitulate key PD hallmarks in terms of neuropathology (246), however viral-mediated PD mutant LRRK2 overexpression do induce dopaminergic neuron loss (247,248). The development of PD relevant phenotypes and neuropathology in rodents occurs over several months, while *C. elegans* have an advantage in speed, sample size and exhibition of robust phenotypes within days.

Furthermore, *C. elegans* are highly amenable to environmental toxin assays and drug screens to evaluate the interplay with transgenic expression of human proteins of interest (249,250). *C. elegans* strains overexpressing the PD associated LRRK2[G2019S] and LRRK2[R1441C] mutant proteins in neurons show reduced survival in response to oxidative stress induced by the environmental toxins rotenone and paraquat, widely used in toxin-based models of PD (80), when compared to animals expressing wildtype LRRK2 (79,244). However these studies did not examine whether protection was kinase dependent, through LRRK2 inhibition, or expression of kinase inactive LRRK2. Notably, *C. elegans* overexpressing wildtype LRRK2 show enhanced survival to oxidative stress and increased lifespan compared to non-transgenic wildtype animals. This suggests a LRRK2-driven protective effect, while deletion, or RNAi silencing of *lrk-1* in non-transgenic lines have shown a significantly reduced survival under these conditions (244,251). Overexpression of LRK-1 is yet to be utilised in oxidative stress assay, so it is currently unknown whether this would have a similar effect to heterologous expression of LRRK2. These results

suggests that PD mutant LRRK2 has a reduced efficacy in oxidative stress protection in *C. elegans*, However, the expression of these pathogenic LRRK2 variants in wildtype *C. elegans* background provides enhanced stress resistance than is observed in wildtype, non-transgenic *C. elegans*. This suggests that examination of the role of endogenous LRK-1 mutant proteins, with physiological expression levels, might provide better understanding of how these mutations impact survival of the organism, or the dopaminergic neurons. Nevertheless, this illustrates LRK-1's global role in oxidative stress survival, which may not be neuronal specific or restricted to neurons.

Additionally, the transgenic lines discussed above have been utilised as *in vivo* models to test early LRRK2 inhibitors LRRK2in1 and TTT-3002 (252,253). Vehicle treated nematodes expressing LRRK2[G2019S] or LRRK2[R1441C] show impaired dopaminergic behavioural phenotypes and significant dopaminergic neurodegeneration (177), which is rescued following treatment with any of the two LRRK2 inhibitors (177). However, the effect of LRRK2 inhibitors upon endogenous LRK-1 is unknown, as molecular readouts for LRK-1 phosphorylation activity remain to be identified. Similar effects in nematode behaviour, dopaminergic neurodegeneration and LRRK2 phosphorylation activity were demonstrated in a recent study utilising allosteric inhibition of LRRK2 kinase activity by Vitamin B12 in LRRK2[G2019S] expressing lines (245), in support of the robust, relevant phenotypes and promise of *C. elegans* in pharmacological assays.

The use of transgenic human LRRK2 expressing *C. elegans* models have contributed to our understanding of *LRRK2* function, while studies of LRK-1 suggest it may share functional conservation with LRRK2. Further characterisation and understanding of *C. elegans* LRK-1 function may shed further insight into LRRK2 mediated pathology from a novel model angle.

1.5.6 LRRK2 and *C. elegans* LRK-1 functionality in vesicle trafficking, endocytosis and WNT Signalling

Data obtained upon transgenic expression of *C. elegans* LRK-1 generally support the hypothesis that it may share some functional conservation with LRRK2. In 2007 *C. elegans* LRK-1 was suggested to have a role in regulating synaptic vesicle localisation to the dendrites of neurons, through modulating protein sorting in the Golgi in a kinase activity dependent manner (230), while deletion of LRK-1 leads to increased sensitivity to tunicamycin induced Endoplasmic Reticulum stress (229). Accordingly, enrichment at Golgi and the regulation of intraneuronal protein sorting through this network has also been reported in studies of LRRK2 in rat cortical neuron cultures *in vitro,* and in *D. melanogaster* and rodent models, *in vivo* (254). Expression of *C. elegans* LRK-1[K1726A] and LRK-1[I1877T] mutant proteins in the *C. elegans lrk-1* deletion mutant, carrying equivalent missense point mutations of the synthetic kinase ablation LRRK2[K2014A] and PD associated kinase hyperactive LRRK2[I2020T], respectively, has demonstrated that kinase activity

of LRK-1 is crucial to its function in determining polarised vesicle localisation in axons of *C. elegans* sensory neurons,, suggesting shared conservation in enzymatic activity and functionality between LRK-1 and LRRK2 (230,255). LRRK2 kinase activity has recently been shown to be essential in modulating axonal transport, with abnormal activation of kinesin *in vitro* and *in vivo* in PD LRRK2[G2019S] mutant models (256). Interestingly, in the 2007 study of LRK-1 localisation of synaptic vesicle proteins, localisation of synaptic vesicle proteins was shown to depend on the *C. elegans* protein UNC-101, an orthologue of the clathrin adaptor protein AP-1 (255) involved in vesicle trafficking from the Golgi to endosome. Clathrin adaptor proteins are integral to vesicle transport processes, including clathrin-mediated endocytosis (CME), a process also regulated by LRRK2 (257). Alterations to the CME process have been recognised in PD (258–260) and other neurodegenerative conditions (261,262), implicating potential functional overlap in the *C. elegans* model.

WNT/β-catenin signalling is an essential pathway in dopaminergic neurogenesis during development and also contributes to synapse formation and neuroprotection during ageing (263). As PD is caused by the loss of dopaminergic neurons, the WNT/β-catenin pathway is of great interest in the development of disease modifying therapeutics targeting neurogenesis (263). Importantly, LRRK2 plays key roles in the WNT signalling pathways (134,264–266). LRRK2 modulates axonal development through inducing phosphorylation of the WNT receptor Frizzled3, a component of the planar cell polarity (PCP) pathway in mice (264), with both loss of function and kinase overactive LRRK2 mutants presenting axon guidance defects. Likewise, in *C. elegans* the WNT signalling pathways modulate neuronal development (127,130,267). Interestingly, expression of the *C. elegans* LRK-1[G1876S] (the equivalent of human pathogenic LRRK2[G2019S]) in wildtype, or *lrk-1* deletion mutant background, revealed significant defects in canal-associated neuron development (229). Furthermore, in an RNAi screen targeting endogenous genes in wildtype *C. elegans* lines overexpressing human LRRK2[G2019S], endogenous nematode WNT signalling pathway components and axon guidance genes had the largest effect sizes in determining dopaminergic neuron survival (268). Thus, this shared phenotype of impaired neuronal development and survival through WNT pathways between transgenic *C. elegans* LRK-1 and vertebrate LRRK2 models further strengthens the conserved roles of LRK-1 and LRRK2.

1.5.7 The Shared Interactome of LRRK2 and *C. elegans* LRK-1

Comparative study of LRK-1 and LRRK2 interactomes further supports functional conservation and it might provide another strategy to identify candidate pathways as novel therapeutic targets (174) . LRRK2 has been shown to bind the BAG2-HSC70 chaperone complex, acting as a

chaperone for LRRK2 (269). In *C. elegans* UNC-23 and HSP-1, the orthologues of BAG2 and HSC70 respectively, interacts with LRK-1 , highlighting existing conservation of protein interactions (269). Further functional studies have illustrated that UNC-23 mediates Golgi localisation of LRK-1 in co-operation with HSP-1 and *unc-23* deletion mutants phenocopy the defects in synaptic vesicle localisation (269), as seen in *lrk-1* deletion mutants (229,230,269). This suggests that UNC-23 and LRK-1 function together in synaptic vesicle localisation.

LRRK2 has an extensively characterised interactome; a stringent search through PINOT, a resource for obtaining quality controlled PPIs in humans and *C. elegans* (270), indicated 1,440 interactor hits for LRRK2, replicated with multiple studies and methods (July 2021). In contrast, the LRK-1 interactome is poorly characterised, with only few interactors noted. Due to the existing conservation of interactions and of the molecular and cellular function between LRK-1 and LRRK2, *C. elegans* could provide an excellent tool to drive interactome-based functional studies.

1.5.8 The role of Parkinson's GWAS candidate risk gene RAB29 in LRRK2 and idiopathic PD

RAB proteins are a superfamily of small GTPases, with diverse regulatory roles in vesicle formation, trafficking and endosomal transport. A subset of these RABs are key effector substrates of LRRK2 phosphorylation (271). *RAB29*, also known as *RAB7L1*, has been a consistent PD GWAS hit (32) and the RAB29 protein has been shown to act upstream of LRRK2 (272), while RAB3, RAB5, RAB8, RAB10, RAB12, RAB35 and RAB43 have been demonstrated to be downstream effector substrates regulated by LRRK2 phosphorylation (273). *RAB29* has been stratified through unbiased LRRK2 PPI arrays as a candidate risk gene, which may bridge the gap between familial *LRRK2* and idiopathic PD (254,272,274). Thus, our understanding of the mechanisms of both *LRRK2* and idiopathic PD, may be furthered by functional studies of *RAB29*.

RAB29 has been demonstrated to be a selective master regulator of LRRK2, acting upstream and leading to LRRK2 kinase recruitment, localisation and activation on the Golgi membranes, via binding of RAB29 to LRRK2's ankyrin repeat domain (272,275,276)., with resultant increased LRRK2 kinase activity leading to changes in the trans-Golgi network morphology (277). However, in another study *RAB29* knockout had no impact on basal LRRK2 phosphorylation activity (278), suggesting a potentially more complex mechanism in LRRK2 modulation and PD pathogenesis. Furthermore, RAB29 is also a substrate of LRRK2 in human HEK293 cells. LRRK2 with kinase overactive PD mutations LRRK2[R1441C], LRRK2[Y1699C] and LRRK2[G2019S] present a 4-fold increase of LRRK2 mediated phosphorylation of RAB29 *in vitro* (271), suggesting interdependent regulation between these two proteins. Other key substrates of LRRK2 are RAB8A and RAB10, with RAB8A shown to accumulate at the trans-Golgi network following RAB29 mediated LRRK2 recruitment (275). Furthermore, upon stress induced lysosomal enlargement,

LRRK2 is targeted to the lysosomal membranes that is mediated by RAB29 (276). This leads to an accumulation of RAB8A and RAB10, which attenuates the enlargement of lysosomes, essential for maintaining their integrity and function (276). Thus, RAB29 is integral in LRRK2 biology and function, further highlighting the need to develop our understanding of the pathways in a range of models.

1.5.8.1 The conservation between RAB29 and *C. elegans* orthologue, GLO-1

C. elegans have an orthologue for *RAB29*, *glo-1*, which shows conservation in its function in the endolysosomal transport pathway (279). A coding variant RAB29[K157R] has been detected in an idiopathic PD patient (280), however its pathogenicity, as well as its mechanism of action is unconfirmed. This variant position is conserved in *C. elegans* GLO-1 and is located within the G5 loop, involved in tight binding of small G-proteins to nucleotides (174,281). Importantly, *C. elegans* GLO-1 has been shown to act upstream of *C. elegans* LRK-1 (282), congruent with studies of human LRRK2, further suggesting it may be relevant for further functional modelling of RAB29.However, GLO-1 is also the *C. elegans* orthologue for the closely related human RAB32 and RAB38, and it is most similar to these proteins in terms of protein sequence identity (41). GLO-1 shares 45.9% and 46.1% sequence identity with RAB32 and RAB38 respectively, while with RAB29 it shares a 40.7% identity (233,234). Functional studies of GLO-1 have demonstrated that it shares conservation with all three RAB proteins to varying extents. *In vivo* model organisms do not always show exact orthologue conservation with the human gene of interest. For example, mouse models display significant differences in biology and biochemistry of LRRK2 when compared to human (246). Despite this, much useful information has been gleaned through functional modelling of LRRK2 in mice (222,247,248), which can be contrasted or supported by consistent findings in alternate *in vivo*, *in vitro* and *in silico* models, along with findings reported in studies of PD patients. Thus, *C. elegans* GLO-1, when taken in conjunction with findings in other models, will be a useful model for further understanding RAB29 function, along with shedding insight into its close counterparts RAB32 and RAB38.

GLO-1 may not just be a potential functional model with relevance to PD, as *RAB29*, *RAB32* and *RAB38* have been highlighted as genes of interest in various neurodegenerative conditions. Functional studies of *RAB29* in the presence of *C9orf72* hexanucleotide repeat (283), causative of amyotrophic lateral sclerosis with FTD (ALS-FTD), have illustrated its role in vesicle trafficking (284). Additionally, *RAB38* has been identified as a significant GWAS hit in a behavioural variant subtype of FTD (285), while *RAB32* has been associated with ER stress and mitochondrial dysfunction in multiple sclerosis (286). This illustrates that this small sub-group of RABs may

play an important role in the maintenance of neuronal health and an *in vivo* reductionist model of their functions focusing on GLO-1 may be applicable to further research areas.

1.5.8.2 The LRK-1/GLO-1 interplay in *C. elegans*

Congruent with the human RAB29/LRRK2 axis, in *C. elegans* both endogenous LRK-1 and neuronally expressed human LRRK2 on a *lrk-1* deletion background have been shown to act downstream from GLO-1in axon termination (282). Notably, key residues of RAB29, routinely utilised to synthetically ablate or constitutively activate its GTPase function *in vitro* (283), are conserved in *C. elegans* GLO-1. On the other hand, key LRRK2 phosphorylation target sites T71 and S72 of RAB29 (287) are not conserved. GLO-1 and LRK-1/LRRK2 converge to regulate axonal morphology, highlighting their importance in the nematode central nervous system, and like RAB29 and LRRK2, they have lysosomal roles (282). In motor neuron axons, GLO-1 and LRK-1 act to modulate endo-lysosomal trafficking or endo-lysosomal maturation, suggesting similar functions to their human counterparts (282). Transgenic expression of PD mutant LRRK2[G2019S] or LRRK2[R1441C] in *lrk-1* deletion mutants, efficiently supresses the axonal abnormality phenotype exhibited in *lrk-1* or *glo-1* deletion mutants (282), suggesting high functional conservation. However, the effect of human RAB29/32/38 expression in *glo-1* deletion mutant background was not investigated, nor was the Golgi localisation of both proteins (282). Furthermore, the effect or presence of LRK-1/LRRK2 mediated phosphorylation of GLO-1 was not investigated (282), as robust phosphorylation readouts have not been developed for PD relevant orthologues in the worm. This highlights the need for additional studies to further assess the LRK-1/GLO-1 mechanistic conservation with the comparatively better understood LRRK2/RAB29 interplay.

1.5.8.3 The relevance of RAB32 and RAB38 in understanding RAB29 and LRRK2 function

Functional studies of human *RAB32* and *RAB38* implicate some shared pathways with *RAB29*, augmenting the relevance of *glo-1* for further study. RAB32 and RAB38 have been demonstrated to act co-operatively to regulate lysosomal biogenesis and modulation of lysosome-related organelles (LRO) (288). In *C. elegans*, GLO-1 modulates the biogenesis of LRO, which are intracellular compartments for storage, sharing some characteristics, but coexistent with conventional lysosomes (279,289). Furthermore, human RAB32 and RAB38 co-ordinate lysosomal biogenesis through the clathrin adaptor protein AP-3 (288), which is a known effector substrate of LRRK2, acting downstream from RAB29 (282). Likewise, studies of GLO-1 have identified modulation of LRO biogenesis through APB-3, the *C. elegans* orthologue of AP-3, via *C. elegans* LRK-1 (290), mirroring the human pathway (282). Additionally, nematodes with

deletion of *glo-1* or *apb-3*, or double deletion mutants of these genes, show decreased LRO biogenesis (282), suggesting convergent biology and importance in this function, as shared in the RAB32 and RAB38 interplay with AP-3 . These mutual processes, pathways and interactors suggest that GLO-1 shares high functional conservation with RAB32 and RAB38, retaining similar functions.

Similarly to RAB29, RAB32 and RAB38 also share convergent biology with LRRK2, although their mechanisms of interaction may differ. RAB32 and RAB38 have been shown to mediate phagosome restriction of intracellular pathogens, notably *Mycobacterium leprae*, the causative agent of leprosy, through phagosome restriction (291). Interestingly, single nucleotide polymorphisms (SNPs) in *LRRK2* have been identified through GWAS as predisposing towards leprosy (214) and a polymorphism in *RAB32* (292) has also been associated with disease susceptibility, implicating potential shared pathways in the immune response between LRRK2 and RAB32 and 38. It is currently unclear whether these immune pathways also contribute to PD pathogenesis (293). However, it has been hypothesised that PD associated mutations in *LRRK2*, prevalent in multiple human populations (294), may confer greater immunity to selected infectious diseases. This may have led to a balanced selection of *LRRK2* PD mutations, resulting in antagonistic pleiotropy, with potential advantageous roles of mutation in immunity, but increased risk of PD development in later adulthood (210,295).

LRRK2 physically interacts with RAB32 and 38 through its armadillo domain, (296), convergent with the LRK-1 and GLO-1 interaction (282). Furthermore, RAB32 and RAB38 bind to sortin-nexin 6 (SNX-6), a transient subunit of the retromer complex, affecting retromer dependent Golgi trafficking (297). Recent studies have demonstrated that LRRK2, bound to trans-Golgi localised RAB29, interacts with the GARP complex, stabilising syntaxin-6 and promoting retrograde transport to the trans-Golgi network in a kinase dependent manner (78). Importantly, syntaxin-6 and all GARP subunits are conserved in *C. elegans* and RNAi knockdown of GARP subunits in *C. elegans* expressing human $LRRK2^{G2019S}$ in the dopaminergic neurons (76) induces dopaminergic neurodegeneration (78). This proposed functional convergence of RAB29, 32 and 38 at the trans-Golgi network, with influences on trafficking and LRRK2 interaction suggest that GLO-1 may have retained similar functions of its three evolved human orthologues and may therefore be useful in gaining further mechanistic insight into the events linking these proteins to neurodegeneration.

1.5.9 The interplay of LRRK2/LRK-1 in α-synuclein transgenic models

Many pathways linking α-synuclein and LRRK2 have been suggested, including cytoskeletal dynamics, ER/Golgi transport, mitochondrial homeostasis and functionality of the degradative

systems, leading to the hypothesis that the use of LRRK2 inhibitors might be beneficial in the treatment of synuclein pathology (298,299). Lack or inhibition of LRRK2 kinase activity or LRRK2 deletion can mitigate neurodegeneration observed in rats after transduction of human α-synuclein via adeno-associated viral vectors (AAVs) (219,220), as can LRRK2 deletion (300). Indeed, AAVs, together with lentiviral vectors, have been extensively exploited to deliver wild-type and mutant human α-synuclein to the *substantia nigra* of rodents and primates, where they lead to Lewy body formation and neurodegeneration. Conversely, overexpression of the wild-type or mutant human α-synuclein in rodents does not correlate with pathological aggregate formation and degeneration of dopaminergic neurons in the *substantia nigra* (301). However, upon expression of human α-synuclein the invertebrate models *D. melanogaster* and *C. elegans*, recapitulate the major PD hallmarks such as impaired dopaminergic behaviour and neurodegeneration despite the lack of an orthologue (74,302).

Similar studies of α-synuclein propagation with regard to LRRK2 have been undertaken *in vivo* in rodent models and *in vitro* human derived SH-SY5Y cultures, and contrasted with *C. elegans* LRK-1 (300). Interestingly, *lrk-1* deletion mutant *C. elegans* show reduced aggregation of α-synuclein, expressed in the muscle (300). In the same study, this phenotype was recapitulated in the brain of *LRRK2* knockout rats, injected with AAV vectors of recombinant human α-synuclein. These animals showed significantly reduced number of axons immunoreactive for α-synuclein at 12 weeks (300), consistent with LRRK2 inhibitor studies (219,220). In a concurrent *in vitro* human SH-SY5Y culture study, this phenotype was determined as kinase activity dependent, with $LRRK2^{G2019S}$ enhancing α-synuclein propagation, through RAB35 phosphorylation, a mechanism later demonstrated to be conserved in *C. elegans* (300). Expression of a constitutively active RAB35 in the *lrk-1* deletion mutant, reversed the phenotype of reduced α-synuclein aggregation (300), further illustrating that key mechanisms and pathways in PD pathogenesis are readily modelled in *C. elegans*, despite the simplicity and evolutionary differences of the system.

However, deletion models of PD orthologues, when used in conjunction with α-synuclein expression still need to be approached with caution. A study developing a *C. elegans* model for neuron-neuron propagation of α-synuclein *in vivo* demonstrated that RNAi silencing of PD orthologue genes, including *lrk-1, pdr-1, pink-1, vps-35*, resulted in increased α-synuclein propagation between neurons (152). . Furthermore, more complex mechanisms may be at play, as *lrk-1* expression at the mRNA level has been shown to significantly increase in nematodes expressing α-synuclein in the muscle, in the presence of an apoptosis inducer wedelolactone (303) and flavonoid tambulin (304). Both of these have been demonstrated to reduce α-synuclein aggregation in *C. elegans* muscles. Dysregulation of *LRRK2* mRNA expression has been described in post-mortem studies of individuals with idiopathic and LRRK2[G2019S] PD (305). However,

these convergences and inconsistencies in *C. elegans*, with regards to the α-synuclein/LRRK2 interplay, further highlights the need to develop more precise genetic models of *LRRK2* pathology in *C. elegans*, rather than depending solely on deletion and RNAi silencing studies.

1.5.10 Modelling Tauopathies in *C. elegans*

C. elegans have a *MAPT*/tau-like orthologue, *ptl-1* (306,307) and multiple evidence suggests that this protein may cover essential roles in maintaining neuronal integrity through the lifespan when expressed at basal levels (308). Loss of *ptl-1* is not rescued by expression of human tau isoforms (308), suggesting potentially limited functional conservation between *ptl-1* and human tau. Multiple studies have used transgenic expression of human tau isoforms, investigating the impact of overexpression of wildtype or pathogenic mutant tau in *C. elegans* . Overexpression of wildtype tau *MAPT* in *C. elegans*, or neuronal expression of *MAPT[A152T]* mutant tau (309), a risk factor for FTD, PSP and atypical tauopathies (209,310) has been demonstrated to induce neuronal dysfunction, (311). .Expression of *MAPT[A152T]* in *C. elegans* leads to impaired associative memory, compared to worms expressing wildtype tau (312) and this may be explained by differential impacts on retrograde axonal transport (312), of which the retromer is a central component. The emergence of tau as a contributor to *LRRK2* and *VPS35* linked PD, the emerging aetiological overlap with the tauopathies and the existence of ready to use tauopathy models in *C. elegans,* provides further opportunities for functional studies and modifier screens of tau pathology, with impacts on multiple neurodegenerative conditions.

1.5.11 Potential of CRISPR/Cas9 modified *C. elegans* for understanding LRRK2 function

The use of transgenic human LRRK2 expressing *C. elegans* models have contributed to our understanding of *LRRK2* function, while studies of LRK-1 suggest it may share functional conservation with LRRK2. Further characterisation and understanding of *C. elegans* LRK-1 function may shed further insight into LRRK2 mediated pathology from a novel model angle. Consequently, this study has developed novel CRISPR/Cas9 point mutants in *C. elegans* LRK-1, generating novel mutants with Parkinson's associated mutations and catalytic ablations. Characterisation of these has enabled a catalytic dissection of the functionality of LRK-1 in *C. elegans* and the potential conservation extent between *C. elegans* LRK-1 and human LRRK2. These models could provide valuable future insights, as a reductionist model of LRRK biology. Assessment of conservation extent through functional modelling of LRK-1 mutants will also enable the evaluation of the suitability of *C. elegans* for dissecting the interaction of VPS35 with LRRK2. Characterisation of selected novel LRK-1 mutants will be discussed in Chapter 4.

1.6. Modelling the VPS35/LRRK2 interplay

There has been substantial evidence that VPS35 and LRRK2 converge upon similar cellular processes and pathways, the most notable being RAB proteins, the endosomal network and lysosomal biology. The conservation of these pathways in *C. elegans* appears promising, however this needs further characterisation. Review of the literature implicates several potential mechanisms of interplay between VPS35 and LRRK2, and how LRRK2 could contribute, or be causative of VPS35[D620N] PD. In this study, following evaluation of the conservation extent between *C. elegans* LRK-1 and LRRK2, one of these hypotheses will be tested, as detailed extensively in Chapter V.

1.6.1 LRRK2 and the downregulation of VPS35 expression

In recent post-mortem studies, LRRK2 was localised with the retromer in individuals carrying the G2019S mutation and in idiopathic PD (140). In LRRK2 mutation carriers, the expression of VPS35 was reduced by 50% in the frontal cortex, with a 77% reduction in the cargo CIMPR, suggesting retromer dysfunction (140). This was also reflected in idiopathic PD individuals, in which VPS35 expression was reduced by 32%, with a 38% reduction in CIMPR (140). This implicates retromer dysfunction as a marker of LRRK2 mediated pathology and suggests LRRK2 could have a role in regulating VPS35 expression. In addition, the consistency in phenotype between individuals carrying *LRRK2* PD mutations and individuals with idiopathic PD, further highlights the potential relevance of VPS35/LRRK2 studies for broader understanding of PD, rather than the Mendelian disease alone.

Coherently, VPS35 has been shown to be downregulated in neuroblastoma cells expressing LRRK2[G2019S] (254), suggesting a ‘double hit’ of toxicity, through VPS35 loss of function and LRRK2 gain of function. This idea is augmented by post-mortem transcriptomic studies of the substantia nigra of idiopathic PD patients, in which *VPS35* mRNA expression is downregulated (313). VPS35, as the key component of the retromer, could have a role in rescuing toxicity, initiated through α-synuclein aggregation or enhanced LRRK2 kinase activity, thus a potential mechanism for LRRK2 toxicity could be through the downregulation of retromer expression. Importantly, these studies further suggest that dysregulation of the retrograde transport in the endocytic system is a shared pathway to pathogenesis in idiopathic PD, illustrating that functional studies of LRRK2 and VPS35 PD could be representative in shedding further mechanistic insight.

1.6.2 VPS35 and LRRK2 share a Common Pathway

Conversely, alternative studies have illustrated that VPS35 acts in concert with LRRK2 indirectly (271), or directly (254), converging upon a common pathway, in which VPS35 does not appear to regulate the enzymatic activity of LRRK2 and their effect upon these cellular processes is additive. The pathogenic point mutations of LRRK2, R1441C, Y1699C and G2019S have been shown to enhance the phosphorylation of RAB29 fourfold (271). RAB29, a possible PD gene identified through GWAS and subsequent transcriptomic studies (314) and as discussed previously has an important role in recruiting LRRK2 to the TGN. Proportional increases in RAB29 phosphorylation enhance this, suggesting greater TGN recruitment of LRRK2 in the instance of mutation (271). The retromer is integral in the TGN and in recent studies, discussed in 1.5.8, LRRK2 localises to the retromer via interaction with TGN localised RAB29 and the GARP complex, promoting retrograde transport in a kinase dependent manner (78). Pertinently for this project, GARP complex subunits are well conserved in *C. elegans* (78).

Studies of RAB29 have shown that it interacts with LRRK2 to mediate intraneuronal protein sorting, PD associated mutations of *LRRK2* lead to Golgi sorting defects and retromer depletion, rescued by wildtype VPS35 overexpression, but not VPS35[D620N] (254). This could suggest that VPS35 is downstream in a common pathway with LRRK2. Furthermore, expression of VPS35[D620N] in primary neuron cultures exhibited CIMPR mis-sorting, reflected in LRRK2[G2019S] mutation or *VPS35* knockdown (254), illustrating a shared mechanism. With regards to VPS35[D620N], this suggests a dominant negative loss of function in neurodegeneration, also implicated in LRRK2[G2019S] mutation. Immuno-precipitation studies showed that VPS35 and LRRK2 were coprecipitated (254), contrasting the Mir theory of an intermediate interactor (111).

Studies undertaken in the *D. melanogaster* have reflected similar outcomes. Flies overexpressing human LRRK2 with the I2020T and Y1699C PD mutations lead to impaired locomotor activity, which was rescued by overexpression of VPS35 and exacerbated by *Vps35* knockdown (163). Conversely, research undertaken by Inoshita and colleagues, demonstrated that overexpression of the drosophila LRRK2 orthologue dLRRK, rescued locomotor deficits incurred VPS35[D620N] (141). Although there is debate regarding the functional conservation between dLRRK and human LRRK2, as like *C. elegans* dLRRK is orthologous for LRRK1 and 2, this further augments the idea that VPS35 and LRRK2 work in tandem, converging on the intracellular transport system.

1.6.3 VPS35[D620N] pathogenicity is induced through LRRK2 kinase hyperactivation

Mir and colleagues proposed in 2018, at the start of this research project, that VPS35[D620N] promotes the kinase activity of LRRK2, due to an altered interaction with an unknown effector (111), following illuminating functional studies. This supports the VPS35[D620N] gain of function theory proposed by Tsika et al in 2014 (109), but suggests LRRK2 is the effector, rather than VPS35, the D620N mutation of which may cause increased kinase activity through a loss of interaction with an unknown intermediate regulator.

In this study, mouse embryonic fibroblasts expressing the PD mutant VPS35[D620N] exhibited a six-fold increase of phosphorylation of RAB10, a downstream effector of LRRK2 and was rescued by pharmacological inhibition of LRRK2 (111). A three-fold increase in LRRK2 kinase activity through the readout of RAB10 phoshorylation was also reflected in neutrophil samples, taken from PD affected individuals carrying the VPS35[D620N] mutation, compared to idiopathic PD and control samples (111), rescued by pharmacological inhibition of LRRK2. This suggests that VPS35 mutation works through hyperactivation of LRRK2, with potentially enhanced pathogenicity compared to LRRK2 or idiopathic PD. The LRRK2[G2019S] mutation increases kinase activity between two and four-fold (73), hence this is an attractive concept in relation to understanding the varying age of onset and penetrance of VPS35 and LRRK2 Mendelian PD, a median of 49 (106) and 60 respectively (29) . Currently, it is clear that the endocytic pathway is heavily implicated in PD, but that there are many genes yet to be discovered in pathogenesis, potentially accounting for the unknown effector proposed (24).

Coherently, a recent 2021 study undertaken by Kadgien and colleagues illustrated that VPS35[D620N] increases the phosphorylation of RAB10 in mouse brain tissue *in vivo* and cortical neurons *in vitro* (139), further augmenting Mir and colleagues 2018 findings (111). Conversely, this study also illustrated that LRRK2 forms direct PPI complexes with VPS35, contradicting the hypothesis of an intermediate interactor previously proposed, and consistent with the co-immunoprecipitation noted by MacLeod and colleagues in 2013 (254). VPS35[D620N] did not impact the binding of LRRK2, however it did alter interaction with the WASH complex subunit FAM21 (139), a modulator of endocytic traffic. Reduced WASH complex interaction in VPS35[D620N] through FAM21 has previously been observed in the human derived in vitro model HeLa cells, leading to reduced autophagy, Glutamate receptor localisation and C1MPR transport (315) coherent with previous studies focused on understanding the WASH-VPS35 interaction (316). Pharmacological inhibition of LRRK2 in Kadgien's murine study did not rescue the impaired VPS35[D620N] interaction with the WASH complex and pathologies such as increased glutaminergic receptor expression, however glutamate receptor traffic was modulated by this (139). This new study heavily implicates LRRK2 kinase hyperactivation in VPS35[D620N]

pathogenesis, coherent with Mir and colleagues, but suggests it is not the only perturbed mechanism present and that a loss of alternative VPS35 functions also occurs.

1.6.4 Considerations for testing the VPS35/LRRK2 interplay in *C. elegans*

In this research project, the hypothesis that VPS35[D620N] induces toxicity through LRRK2 kinase hyperactivation, as detailed in 1.6.3 will be tested. Prior to this, considerations with regards to *C. elegans* suitability for this need to be made.

Pertinently in terms of VPS-35 function, the WASH complex is poorly characterised in *C. elegans*, with no known orthologue for FAM21 (41), thus this interaction would be very challenging to test in the novel model. Early research undertaken by MSc researcher J. Smolyn at Rutgers University, accessible in 2020, has promisingly suggested that the uncharacterised C05G5.2 *C. elegans* protein could be the orthologue, showing high protein sequence identity with human, catfish, mouse and *D. melanogaster* FAM21, specifically in the VPS35 binding region (317). This is hopeful that this pathway could be conserved, however it would be challenging to test the VPS35/FAM21 interplay in the novel model without any known or established orthologue.

Furthermore, the conservation extent between *C. elegans* LRK-1 and human LRRK1 and LRRK2 needs to be provisionally established and is achieved in chapter 4. Recent studies have demonstrated that LRRK1 and LRRK2 have divergent actions through phosphorylation of distinct RAB proteins and that VPS35[D620N] has no impact upon LRRK1 phosphorylation (235). As such, if *C. elegans* LRK-1 is orthologous to just human LRRK1, without shared functional conservation to LRRK2, it would not be a relevant model for dissecting this interplay in PD pathogenesis.

C. elegans are amenable to pharmacological assay and LRRK2 inhibitor treatment has alleviated impaired dopaminergic phenotypes in transgenic LRRK2[G2019S] expressing *C. elegans* (253), however it is unknown whether available LRRK2 inhibitors have any effect upon *C. elegans* LRK-1. In order to develop a pharmacological model for VPS35/LRRK2, the effect of human LRRK2 inhibitors upon *C. elegans* LRK-1 needs to be established. In addition, this model could be incomplete in terms of a biochemical readout, *C. elegans* possess well conserved RAB8a and RAB10 orthologues (RAB-8 and RAB-10), however phospho-sensitive antibodies specific for LRRK2 phosphorylation sites on these RABs have not been utilised in *C. elegans* before. Frequently, human antibodies do not show specificity for *C. elegans* orthologues, due to subtle evolutionary differences in sequence identity. Fortunately, *C. elegans* are also amenable to genetic crossing and the generation of lines with multiple mutations, as extensively detailed so far there are established *lrk-1* deletion models to potentially cross with VPS35[D620N] orthologous lines, to generate a genetic model to contrast with the pharmacological.

1.7 Research Aims and Hypotheses

As suggested throughout review of the literature, the PD modelling field could benefit from the development of novel, rapid and economical *in vivo* model systems, with endogenous knock in of mutations of interest. *In silico* analysis, comparing human PD genes of interest and their *C. elegans* orthologues, undertaken during this project, has highlighted the potential conservation of gene function in *C. elegans*. Most pertinently, many point mutations linked to PD are directly conserved in the *C. elegans* orthologous proteins. CRISPR/Cas9 modification of *C. elegans* embryos has made the knock in of endogenous point mutations into the *C. elegans* orthologues of PD linked genes a possibility, with great potential and novelty. For the first time, this approach will be employed to establish novel models for VPS35[D620N] and LRRK2, and to characterise them, gleaning insights into protein function, conservation and potential PD pathogenesis. The three key research aims and hypotheses tested throughout this project will be detailed here, organised through the three results chapters investigating each.

1.7.1. Chapter 3: Characterising the *vps-35[D638N]* mutation in *C. elegans*

Primarily, this project aims to develop a novel model with the orthologous [D638N] point mutation encompassed in *C. elegans* VPS-35. The process of CRISPR/Cas9 modification will be outsourced, but this model will be sufficiently outcrossed in the laboratory for characterisation and future use. The novel *C. elegans* will be assessed in terms of global organism health, dopaminergic outputs and molecular perturbations. Findings from this will be contrasted with existing models, in order to assess potential conservation. The potential mechanism of action of VPS35[D620N] will also be probed and contrasted with an established total loss of function *vps-35* deletion model, shedding insights into global VPS-35 function and integrating with our novel model angle.

Following review of the literature, this investigation hypothesises that *C. elegans* VPS-35 is likely to be well conserved with human VPS35. Through characterisation, the hypothesis that VPS35[D620N] acts through a gain of function will be tested.

1.7.2. Chapter 4: *C. elegans* LRK-1 as a model for human LRRK2 function

Previously, the Kevei laboratory in collaboration with Dr Patrick Lewis have developed a series of CRISPR/Cas9 modified *C. elegans* lines, with PD relevant or catalytic manipulations present in LRRK2, at orthologous residues in *C. elegans* LRK-1. However, these are yet to be characterised and could be very useful in understanding, if functional conservation is maintained between *C. elegans* LRK-1 and human LRRK2. Key point mutants with established phenotypes in alternative model systems will be tested in terms of dopaminergic behaviour and molecular outputs, in order to assess this. If promising conservation is shown, *C. elegans* could be a powerful

tool for dissecting the VPS35/LRRK2 interplay. LRRK2 has a diverse interactome, so understanding the interactome of *C. elegans* LRK-1 may shed further insight into potential conservation. However, there are currently no detection methods available for *C. elegans* LRK-1, so this project aims to establish a method for this.

Extensive review of the literature suggests that *C. elegans* LRK-1 shows some promising functional conservation with human LRRK2. Dissecting this with novel point mutants will help further establish this and this chapter will test the hypothesis that LRK-1 shares some functional conservation with LRRK2 and could be a relevant, reductionist model for LRRK2 function. If this is the case, LRK-1 could be investigated in conjunction with VPS-35.

1.7.3. Chapter 5: Modelling the VPS35/LRRK2 interplay in novel *C. elegans* models

Following the establishment of the novel *vps-35[D638N] C. elegans* model, the interplay between this mutation and alternative pathways to PD will be studied, if PD relevant phenotypes are shown. If study of *C. elegans* LRK-1 illustrates some functional conservation with human LRRK2, its interplay with VPS35 will be studied through the development of pharmacological and genetic models, testing phenotypes illustrated in the *vps-35[D638N]* model as behavioural and molecular outputs.

An overarching hypothesis of this project is that the mechanism of VPS35[D620N] mutation toxicity is through LRRK2 kinase hyperactivation, which will be tested from several angles in this chapter.

Chapter II: Materials and Methods

Common materials and methods are utilised throughout the results, chapter 3, 4 and 5 of this thesis, thus chapter 2 will contain extensive details of these.

2.1 *In silico* analysis methodology

In silico analysis of *C. elegans* orthologues with their human genes of interest was undertaken prior to CRISPR/Cas9 sourcing, to evaluate conservation extent and in the collaborative generation of a new bioinformatic database for PD and *C. elegans* researchers.

2.1.1 Literature Search

Prior to literature searching, confirmed PD genes were verified through Ortholist2 (http://ortholist.shaye-lab.org/) (41) and the resultant orthologs cross-referenced through WormBase (https://wormbase.org/) (61). PubMed was utilised for literature search (https://pubmed.ncbi.nlm.nih.gov/), including multiple search terms, for example 'LRK-1', 'LRK-1 and C. elegans', 'LRK-1 and "C. elegans"', 'LRRK2'. All articles were downloaded to CSV format and saved in Excel. Review articles and primary research articles were separated into different sheets and duplicates removed. The *C. elegans* orthologue was searched on WormBase and all references downloaded to csv, separating conference abstracts to a separate worksheet. The number of research article, review and abstract was quantified for each PD gene and *C. elegans* orthologue. These articles, along with orthologue searching methods were utilised in the development and writing of published literature review "Modelling the Functional Genomics of Parkinson's disease in *C. elegans: LRRK2* and beyond" (1).

2.1.2 Sequence Alignments

Protein sequences in FASTA format were obtained from UniProt (https://www.uniprot.org/) for human PD proteins, and WormBase for *C. elegans* orthologues. Alternative splice variants of both human and *C. elegans* proteins were also downloaded for analysis.

Pairwise sequence alignments were undertaken utilising EBI EMBOSS STRETCHER (https://www.ebi.ac.uk/Tools/psa/emboss_stretcher/) (234), parameters detailed in the table 2, along with the circumstance they were utilised. Protein similarity, identity and gap scores were recorded in Excel.

Use	EMBOSS	Matrix	Gap Penalty	Extend Penalty
Primary Sequence Alignment	Stretcher	EBLOSUM62	12	2
Secondary Sequence Alignment	Needle	EBLOSUM62	10	0.5
Low sequence identity. Evaluation of domain conservation.	Matcher	EBLOSUM62	14	4

Table 2-EBI EMBOSS Sequence Alignment Parameters

When there was more than one orthologue of the human PD gene of interest, multiple sequence alignments were undertaken, utilising EBI CLUSTAL OMEGA (https://www.ebi.ac.uk/Tools/msa/clustalo/). Output parameters are detailed in the table 3.

Parameters	Selection
Output format	ClustalW with character counts
Dealign Input Sequences	No
MBED-like clustering guide-tree	Yes
MBED-like clustering iteration	Yes
Number of Combined Iterations	Default(0)
Max Guide Tree Iterations	Default
Max HMM Iterations	Default
Order	Aligned

Table 3- EBI CLUSTAL OMEGA parameters for multiple sequence alignment

Protein domains were identified through UniProt, family and domains section, of the protein of interest. The search was continued through viewing the protein in ProSite (https://prosite.expasy.org/) with domain details listed. Domain ID, domain function, enzyme activity, regulatory role, protein description and amino acid domain borders were collated in Excel. Details were cross referenced in Interpro (https://www.ebi.ac.uk/interpro/) and functions inferred utilising G:profiler (https://biit.cs.ut.ee/gprofiler/gost) (318).

Comparative study of the proposed crystal structure of human VPS35 and *C. elegans* VPS-35 utilising the Artificial Intelligence (AI) protein structure database AlphaFold (https://alphafold.ebi.ac.uk/) (319,320). Proteins of interest were inputted and region of mutation residue identified through amino acid sequence toolbar.

Following collation of protein sequence identity and domains, known pathogenic residues in the human PD protein were mapped onto the alignments, to assess the conservation extent. Pathogenic

mutations were obtained from a gene search on ClinVar, filtered for pathogenic and single gene. These results were contrasted with searches on OMIM, UniProt Pathology and Biotech, Orphanet and PD specific GWAS browser. Publications detailing the known pathogenic variants were verified for PD relevance, mendelian segregation, or risk factor gene. Confirmed PD pathogenic mutations were mapped onto the protein sequence alignment, as well as key catalytic residues identified in functional studies.

2.1.3 Domain Visualisation

Human PD proteins and their *C. elegans* orthologues were visualised as linear diagrams, utilising the software DOG_2.0.1 (321). Domains were included, along with start and end amino acid residues and notable mutations. Diagrams were saved as .tif and .xml(DOG) files.

2.1.4 Interactome Analysis

Proteins of interest were searched in PINOT, the quality-controlled PPI database, using the stringent and lenient filter (http://www.reading.ac.uk/bioinf/PINOT/PINOT_form.html (270)). Data was saved in Excel and then the dataset manually filtered, to remove any non-PPI's, such as chemical, DNA and RNA interactions and saved separately. First layer *C. elegans* orthologue interactors were searched in PINOT, utilising stringent and lenient filters. *C. elegans* orthologue PPI's were cross referenced in WormBase, selecting for physical interactors and Excel sheet saved, filtering out non-physical PPIs. Proteins were also checked in IMEx and Biogrid. Functions of 1st layer interactors were noted.

2.2. Nematode Culturing and Maintenance

Standard culturing and maintenance methods for *C. elegans* populations were utilised throughout this study for all experiments, unless stated otherwise (64). The *C. elegans* lifecycle is summarised below. All *C. elegans* experiments are planned around the selected developmental stages and must also be considered throughout culturing and maintenance. *C. elegans* have a rapid lifecycle, growing from L1 larvae to reproductive adults in ~72 hours. Adults can live for 2-4 weeks, with a mean lifespan around 18 days and a maximum lifespan of approximately 30 days in wildtype *C. elegans* (64). Aged phenotypes are apparent much sooner, thus facilitating straightforward and high throughput laboratory study. *C. elegans* are reproductive adults from day 1-5 of adulthood, with peak egg laying occurring in day 1 of adulthood.

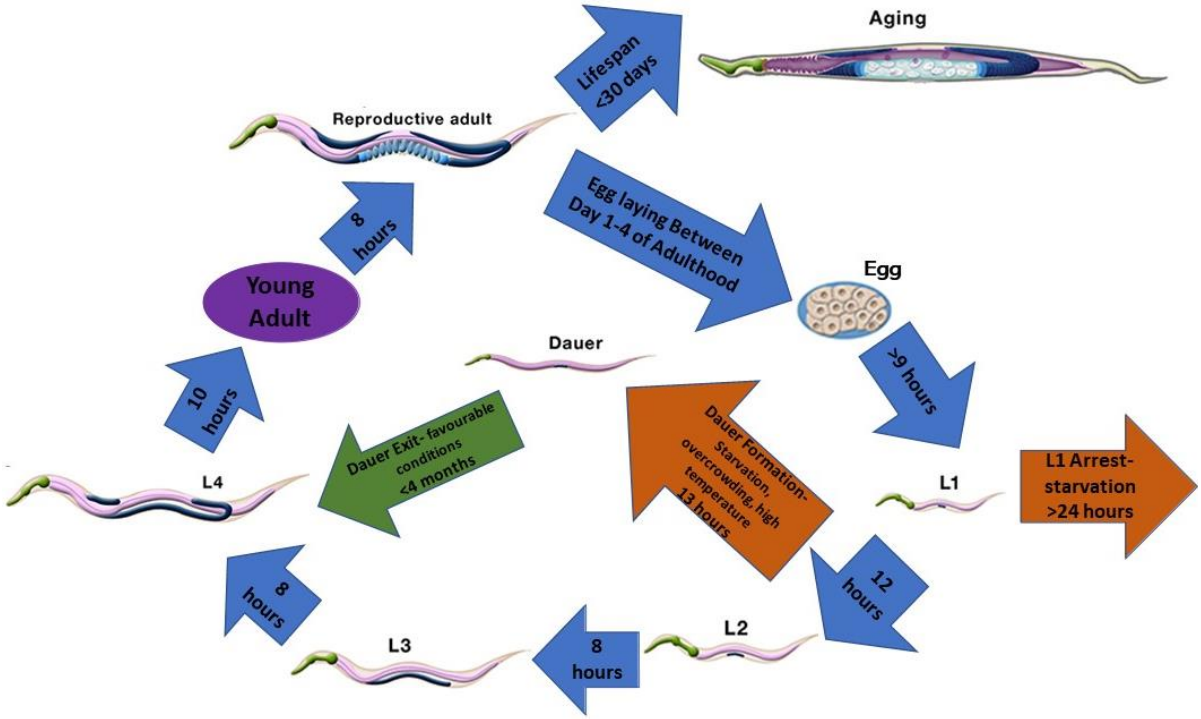

Figure 7- The developmental life stages of *C. elegans* hermaphrodites

Timing in hours between set developmental stages are indicated in the blue arrows. Stress conditions leading to a deviation from the normal development are indicated in orange. Green arrow indicates the loss of stress conditions and return to favourable environment, allowing the development of Dauer *C. elegans* to L4 and reproductive adults. *C. elegans* graphics indicating nematode morphology are taken from WormAtlas (61). The key differences between L2 and L3 larvae are size and development of the germline. L4 larvae are larger in size and have a developed reproductive tract, but no egg development, thus an empty crescent shaped uterine cavity is visible for nematode selection. Young adults have developed eggs, but these are yet to be laid. Reproductive adults are classified as egg laying and eggs present in utero, the first day of this is day 1 of adulthood. Fertility is highest between day 1 and day 2 of adulthood, with a cessation of egg laying by day 5 on average. *C. elegans* can live as adults for up to 30 days on average, but phenotypes of ageing are often present many days and weeks prior to this.

2.2.1 *C. elegans* mutant lines utilised throughout study

Table 4 displays all the *C. elegans* strains utilised throughout the course of this study. Wildtype N2 Bristol strain was consistently utilised as a control throughout every experiment in all results chapters. The table details the results chapter these lines will be described in, the original database number (DN), the strain, genotype and predicted or known function of the mutation. Several of these lines have been outcrossed (OC) through the course of this study in the Kevei lab, the number of generations detailed in the table where relevant and the OC database number (OC DN), of the new outcrossed strain for further characterisation. Mutant strains have been obtained from a range of sources, also detailed in table 4. Established strains shared by international research groups were obtained through the Caenorhabditis Genetics Centre (CGC, University of Minnesota, USA). Novel mutant lines devised by our research have been generated through outsourced CRISPR/Cas9 modification, by Knudra Transgenics (NemaMatrix, Murray, Utah, USA), or SunyBiotech (Fu Jian Province, China), as indicated in the table. Mutant lines encompassing multiple mutations were crossed in the Kevei lab as part of this project.

Result Chapt	DN	Strain	Genotype	Abbreviated Genotype/ Alternative Names in Thesis	Function	OC	OC DN	Source
1	194	FX30144	*tmC6[dpy-2(tm9710)]II*	*Dumpy* balancer	Balancer strain, prevents chromosomal rearrangement	-	-	CGC
1	270	VC1390	*vps-35(ok1880)II*	*vps35(ok1880)* *vps-35* deletion	*vps-35* knockout	-	-	CGC
1, 2, 3	222	MT15620	*cat-2(n4547)II*	*cat-2(n4547)* Tyrosine Hydroxylase deletion	Tyrosine hydroxylase knockout, no dopamine biosynthesis	-	-	CGC
1, 3	78	COP1676	*vps-35(knu618[D638N])*	Unbalanced *vps-35[D638N]*	PD mutant	4	202	Knundra
1, 3	274	COP1676 FX30144	*Vps-35(knu618[D638N]); tmC6[dpy9710)]II*	Balanced *vps-35[D638N]*	Heterozygous 4x OC VPS-35[D638N] PD mutant crossed with dpy balancer.	4	-	Crossed in Kevei lab
1, 3	60	TG2435	*vtIs1 [dat-1p::GFP + rol-6(su1006)] V.*	Wildtype:*dat:GFP*	Transgenic expression of GFP under control of dopaminergic reporter	-	-	CGC
1, 3	342	COP1676 FX30144 TG2435	*Vps-35(knu618[D638N]); tmC6[dpy9710)]II ; vtIs1 [dat-1p::GFP + rol-6(su1006)] V.*	*vps-35[D638N]: dat:GFP*	Balanced VPS-35[D638N] mutant with transgenic expression of GFP	4	-	Crossed in Kevei lab
2	133	WLZI	*wlzls1[snb-1p::Hsa-LRRK2 + lin15(+)]*	Transgenic Human *LRRK2* wildtype	Wildtype human LRRK2 neuronal transgenic overexpression	-	-	CGC
2	134	WLZ3	*Wlzls3[snb-1p::Hsa-LRRK2(G2019S) +lin15(+)]*	Transgenic Human *LRRK2[G2019S]*	PD mutant human LRRK2 neuronal transgenic overexpression	-	-	CGC
2	18	COP1576	*lrk-1(knu530[G1876S])*	*lrk-1[G1876S]*	PD mutant- LRK-1 kinase overactive?	3	348	Knundra
2	25	COP1585	*lrk-1(knu539[R1087C])*	*lrk-1[R1087C]*	PD mutant- LRK-1 kinase overactive?	-	-	Knundra
2	69	COP1671	*lrk-1(knu613[K988A])*	*lrk-1[K998A]*	Gatekeeper mutation- GTP binding defective	2	345	Knundra
2, 3	77	COP1680	*lrk-1(knu622[D1847A])*	*lrk-1[D1847A]]*	Gatekeeper mutation- kinase activity ablated	4	301	Knundra
2, 3	180	LG1	*lrk-1(tm1898)*	*lrk-1(tm1898)* *lrk-1* deletion	*lrk-1* knockout	4	302	CGC
3	357	COP1676 FX30144 TG2435	*Vps-35(knu618[D638N]); tmC6[dpy9710)]II ; vtIs1 [dat-1p::GFP + rol-*	Dopaminergic GFP expressing *vps-35[D638N];lrk-1[D1847A]* Double mutant	Balanced VPS-35[D638N] mutant, with homozygous kinase activity ablated LRK-1[D1847A], with	4	-	Crossed in Kevei lab

		COP1680	*6(su1006)] V: lrk-1(knu622[D1847A])*		transgenic expression of GFP			
3	359	COP1680 TG2435	*lrk-1(knu622[D1847A]): vtIs1 [dat-1p::GFP + rol-6(su1006)] V.*	*lrk-1[D1847A] dat-1:GFP*	Homozygous kinase activity ablated LRK-1[D1847A], with transgenic expression of GFP.	4	-	Crossed in Kevei lab
3	275	PHX1720	*lrk-1(syb1270)*	FLAG-LRK-1	LRK-1 FLAG tagged	3	326	Suny Biotech
3	339	PHX3732	*lrk-1 (syb3732[3XFLAG-LRK-1(G1876S)]knu530)*	FLAG-LRK-1[G1876S]	LRK-1 PD mutant FLAG tagged	-	-	Suny Biotech
3	340	PHX3781	*lrk-1(syb3732[3XFLAG-LRK-1(D1847A)]knu622)*	FLAG-LRK-1[D1847A]	LRK-1 kinase ablated FLAG tagged	-	-	Suny Biotech

Table 4- C. elegans mutant strains utilised throughout study

2.2.2 Culturing Media

C. elegans populations can be grown on solid Nematode Growth Media (NGM), or liquid media *S. complete*. In this study, *C. elegans* were grown on solid NGM media seeded with a bacterial lawn of *Escherichia Coli* OP50, unless stated otherwise.

2.2.2.1 Preparation of NGM plates

Plates are poured in sterile conditions. Standard medium maintenance plates are 6cm in diameter, with a volume of 10ml. Large plates, used for growing larger populations are 9cm across, with a volume of 25ml added. Small plates for genotyping and population establishment 3cm in diameter, with a volume of 5ml added. Plates are kept at room temperature overnight, prior to *E. coli* OP50 seeding. Where indicated, NGM plates were supplemented with 50μm of 5-fluorodeoxyuridine (FUDR) for *C. elegans* germline sterilisation when studying the effect of ageing. *C. elegans* are transferred to FUDR NGM plates at late L4 stage. FUDR NGM plates are seeded with concentrated *E. coli OP50*.

Reagent	**Mass/Volume**
Peptone	2.5g
Sodium Chloride (NaCl)	3g
Agar	17g
dH20	Up to 1 litre
Following autoclaving, media cooled to 56^{o}C and the following are added:	
1M Calcium Chloride ($CaCl_2$)	1ml
1M Magnesium Sulphate ($MgSO_4$)	1ml
5mg/ml Cholesterol (solubilised in ethanol)	1ml
1M Potassium Phosphate (KPO_4)	25ml

1000mg/ml Nystatin	2.5ml

Table 5- Reagents for preparation of 1 litre Nematode Growth Media

2.2.2.2 Preparation of liquid media *S. complete*

C. elegans can be grown in liquid media *S. complete* and cultivated for pharmacological assay in well plates under sterile conditions.

Reagent	Mass/Volume
Sodium Chloride (NaCl)	5.85g
Potassium Hydrogen Phosphate (K_2HPO_4)	1g
Potassium Dihydrogen Phosphate (KH_2PO_4)	6g
Cholesterol	1ml
dH_2O	Up to 1 litre
Following autoclaving, media cooled to room temperature and the following added under sterile conditions. Then, store at 4°C until use.	
1M Potassium Citrate (pH 6.0)	1ml
1M Calcium Chloride ($CaCl_2$)	1ml
1M Magnesium Sulphate ($MgSO_4$)	1ml
Trace Metals Solution*	1ml

Table 6- Preparation of 1 litre of liquid media S. complete

Reagent	Mass/Volume
EDTA	1.86g
Iron Sulphate ($FeSO_4$)	0.69g
Manganese Chloride ($MnCl_2$)	0.2g
Zinc Sulphate ($ZnSO_4$)	0.29g
Copper Sulphate ($CuSO_4$)	0.025g
dH_2O	Up to 1 litre
Autoclave and store in the dark until use.	

Table 7-Preperation of 1 litre of trace metals solution*

Concentrated *E. coli OP50* is washed in sterile deionised water three times and resuspended in *S. complete* to a concentration of 100mg/ml. 120µl of *S. complete E. coli OP50* solution was dispensed into selected wells of a 96 well plate under sterile conditions. *C. elegans* can be added to this for development as L1 larvae.

2.2.2.3 Preparation of *E. coli OP50* for Ad Libitum feeding

40ml of Luria Broth (Table 8) was inoculated with a colony of *E. coli OP50* with a sterile inoculation loop in sterile 50ml Falcon tube. This was placed in shaker at 80rpm overnight at 37°C. Store at 4°C. In sterile conditions, NGM plates seeded with 300µl *E. coli OP50* culture for 6cm plates, 150µl for 3cm and 600µl for 12cm. Once seeded on plate, *E. coli OP50* is grown overnight at 37°C.

Reagent	Mass/Volume
Tryptone	4g
NaCl	4g
Yeast Extract	2g
dH_2O	Up to 400ml
Sterilise through Autoclaving	

Table 8- Preparation of Luria Broth

2.2.2.4 Producing concentrated *E. coli OP50* food source

Inoculated 400ml of Luria Broth in a 500ml Duran, with a colony of OP50 in sterile conditions and placed in a shaker at 160rpm overnight at 37^{o}C. 45 ml decanted into 6 50ml falcon tubes and balanced for centrifugation at 2490rcf for 15 minutes. Under sterile conditions, supernatant disposed of and batcterial pellet is dispensed in the remaining 5ml LB and collated into 1 tube.

2.2.3 Freezing and Thawing

C. elegans populations can be stored at -80^{o}C long term and thawed when required. To freeze, C. elegans were washed from selected NGM plates with M9 into a 15ml falcon tube, when the population has an abundance of L1 larvae and minimal *E. coli OP50*, L1's are most resilient to freeze/thawing. Pellet was settled, supernatant removed and washed twice with M9. An equal volume of freezing buffer (Table 9) was added to the tube and 1ml of solution dispensed to labelled 1.5ml cryotube. Cryotubes were placed into a polystyrene cuvette box and freeze at -80^{o}C. 2 days later, 1 tube per genotype was removed and thawed. 300µl of solution dispensed per NGM plate, which was then stored at 20^{o}C. 48-72 hours later ensure there are live *C. elegans* present, confirming the freezing has been successful. Thawing for any lines of interest occurs through the above protocol.

Reagent	Mass/Volume
Sodium Chloride (NaCl)	5.8g
Potassium Dihydrogen Phosphate (KH_2PO_4)	6.8g
5M Sodium Hydroxide	1.12ml
Glycerol	300ml
dH2O	~700ml
Aliquot to 200ml and autoclave. Allow to cool to room temperature and add per bottle:	
1M Magnesium Sulphate (MgSO4)	60µl

Table 9-Preperation of 1 litre of *C. elegans* freezing buffer

2.2.4 *C. elegans* maintenance and growth

Nematodes were maintained on 6cm agar plates, seeded with bacterial lawn of *Escherichia coli* OP50 at 20^{o}C, unless otherwise indicated. *C. elegans* were transferred to a new plate every 3 days via NGM cube cutting a cube of NGM agar abundant with larvae using a sterile scalpel, or manual

individual *C. elegans* transfer utilising a platinum wire pick. 3 days following transfer of young larvae to a new plate, a mixed stage population will be optimal for age synchronisation. Developmental stages were synchronised following the isolation of eggs from gravid hermaphrodites and experiments undertaken at the indicated stage.

2.2.5 Age Synchronisation

Mixed stage plates, with a high abundance of day 1 adults were washed with M9 buffer (Table 10) into 1ml Eppendorf's in individual tubes, according to genotype.

Reagent	Mass/Volume
Potassium Dihydrogen Phosphate (KH_2PO_4)	3g
Monosodium Phosphate (NaH_2PO_4)	6g
Sodium Chloride (NaCl)	5g
dH2O	Up to 1 litre
Autoclave and allow to cool to room temperature	
1M Magnesium Sulphate ($MgSO_4$)	1ml

Table 10- Preparation of 1 litre of M9 buffer

C. elegans were settled by gravitation at room temperature and the M9 supernatant was removed. 1ml of Sodium Hypochlorite bleaching solution (Table 11) was added to the Eppendorf, agitated and regularly checked under stereomicroscope until adult bodies have broken down and eggs are free in the solution, taking between 5-7 minutes.

Reagent	Mass/Volume
Sodium Hypochlorite (Bleach)	10ml
dH20	27.5ml
1M NaOH	12.5ml
Do not add Bleach directly to 1M NaOH, add dH2O first	

Table 11-Sodium Hypochlorite Bleaching solution

Centrifuged at 1956rcf for 2 minutes, the supernatant was removed and pellet resuspend in 1ml M9, centrifuge at 1956rcf for 2 minutes. M9 washing repeated a further four times and then resuspend the pellet in 1ml M9. Allow the eggs to hatch in situ at 20^{o}C overnight. The following morning, this was centrifuged at 5000rpm for 2 minutes and 900µl of supernatant, removed then resuspend the pellet in the remaining 100µl. Dropped 3µl of solution onto a plate and count the number of L1 larvae in the droplet. Drop 200-300 L1 larvae onto a *E. coli* OP50 seeded NGM plate and allow to develop at 20^{o}C. *C. elegans* reach L4/Young Adult stage >48 hours after. If required and investigating *C. elegans* at an aged stage, *C. elegans* can be transferred through M9 washing to NGM plates containing 50mM FUDR to sterilise and prevent progeny development. Day 1 of adulthood is reached 72 hours after L1 larvae are added to NGM plate. This protocol can also be utilised to remove persistent bacterial infection from *C. elegans* mutant lines.

2.3 Genotyping *C. elegans* mutant lines

Genotyping was consistently utilised throughout this research project for multiple applications. Key Parkinson's mutant lines were outcrossed, to remove any background mutations incurred through outsourced CRISPR/Cas9 modification and is a requirement for publication of *C. elegans* data. Furthermore, gene segregation studies were undertaken utilising the heterozygous VPS-35[D638N] mutant line, gleaning insight into the genetics and mechanisms of this mutation.

2.3.1 Crossing

Crossing in *C. elegans* can be utilised for outcrossing or generating progeny with multiple mutations or transgene markers of interest. The same protocol, detailed below was utilised for all.

2.3.1.1 Male Generation

Although predominantly hermaphrodites, producing their own sperm for ovum fertilisation in utero at reproductive maturity, *C. elegans* can also reproduce sexually. Male *C. elegans* account for 0.2% of a wildtype population and their sperm is dominant in fertilisation, over hermaphrodites self-produced sperm. The proportion of males in the population can be increased and stably maintained, in order to generate crosses between hermaphrodites and males. 6 plates of 30 Late L4/Young Adult hermaphrodites were incubated at 30^{o}C for 6 hours, to heat shock developing eggs for increased X chromosome nondisjunction, which leads to the male genotype X0. Progeny were checked 4-5 days later and males were isolated. For maintenance of a stable male population, 10 males from the heat shocked plate were incubated at 20^{o}C with 2 L4 hermaphrodites. Progeny of this cross were 50% male and this maintenance cross was repeated every 4 days, when males were required for further crosses. Males a similar size to the hermaphrodite progeny should be selected for cross maintenance, as these will be in L4/young adulthood, the optimum age for crossing in the subsequent days, as fertility reduces in males after day 5 of adulthood.

2.3.1.2 Cross establishment

5 medium 6cm plates with 2 L4 hermaphrodites and 10 young males on each are incubated at 20^{o}C for 72-96 hours. For outcrossing, N2 wildtype males are utilised to cross with the selected L4 staged (mutant strain) hermaphrodite. Outcrossing removes background mutations from the mutant *C. elegans* genome, as mutagenesis in unspecific regions can occur, through off target effects of genome modification techniques. Double mutants can be generated also, utilising 2 mutant lines to understand the interplay of these mutations. Predominantly, mutations are studied in *C. elegans* in homozygous form, however this is mutation dependant. Heterozygous mutations can be maintained in a population through crossing with a balancer strain, which have

recombination resistant chromosomal regions, opposite the gene of interest, thus ensuring the heterozygous gene of interest in maintained in all offspring. Details of outcrossed lines, double mutants and balanced lines can be found in table 4.

2.3.1.3 Progeny Selection

72-96 hours after the cross establishment, individual *C. elegans* are selected for subsequent genotyping. The presence of approximately 50% male progeny confirms the success of the cross. 15-30 single hermaphrodites are transferred with a platinum pick to individual 3cm NGM small plate seeded with *E. coli* OP50 each and left to develop and lay eggs for 72 hours. It was ensured progeny of cross selected are of different sizes and ages, as some mutations are more prevalent in progeny laid later in the egg laying reproductive cycle.

2.3.1.4 Genotyping of Progeny

The hermaphrodites isolated on single small NGM plates are taken for genotyping after they had laid eggs, as their progeny will share this genotype. If the hermaphrodite mother is heterozygous, there will likely be homozygous progeny in the population. Once heterozygosity is confirmed, progeny from this individual can be separated as detailed in 2.3.1.3 and the genotyping steps illustrated in 2.3.1.4 repeated.

2.3.1.4.1.DNA Extraction

25µl of 20mg/ml Proteinase K (ThermoFisher) was added to 1 ml of lysis buffer, adult worms were added to 10µl of this with a platinum pick and incubated at 65ºC for 1 hour for removal of protein content, followed by 95ºC for 10 minutes for proteinase inactivation. Lysis buffer preparation is detailed in table 10. Following DNA extraction, lysates were stored at -20oC, or PCR undertaken subsequently.

Reagent	Mass/Volume
1M NaCl	10ml
1M Tris-HCL, pH 8.5	5ml
0.5M EDTA, pH 8	50µl
10% SDS	2.5ml
dH_2O	32.5ml

Table 12-Preperation of 50ml C. elegans lysis buffer

2.3.1.4.2 Polymerase Chain Reaction

Oligonucleotides indicated in Table 11, were designed using PerlPrimer software and ordered from SIGMA(Merk) LifeScience. 2µl of worm DNA lysate was used as a template, utilising 7.5µl PCR master mix (2xPCRbio HS Taq Mix Red. PCR Biosystems), diluted with 4.9µl of sterile dH_2O and

0.6µl of 10µM oligonucleotide mix, in a 40cycle PCR (95ºC-30seconds, 55ºC-30seconds, 72*o*C-30 seconds).

***C. elegans* strain**	**5' Sequence**	**Wildtype/ Mutant**	**Forward/ Reverse**
lrk-1[G1876S]	AGCAGCAGACAAATGGAAGAG	W/M	F
	GCAGGAAATCTCCATCCAAGTA	W	R
	ACCTCCAACCCAATACGTTTT	M	R
lrk-1[K988A]	CACGGCTCACACTTCTTTCAA	W/M	F
	TTGCACAGTGCATCCCAAATAA	W	R
	TCCTTACATAAAGCGTCCCAGA	M	R
lrk-1[D1847A]	TCTCGCAGCTTATAAGGCAGCA	W/M	F
	GCTCGAGCAACTTGAACTGCAG	W	R
	TGAAGGTACTCAAGGGCACGAG	M	R
lrk-1(tm1898)	TCTCTCTCCTCTTGATGCTCTTG	W/M	F
	ACCTTCTTCTACGCTGTACTCTG	W	R
	ATCTGAGCGATGGCATTTGG	M	R
FLAG-lrk-1	ACATCCAAAATGGACCTCTCAA	W	F
	TAAAGACGATGACGATAAGC	M	F
	TGAGTGGAATGATATTCTCGTTG	W/M	R
dat:GFP	CTACCTGTTCCATGGGTAAG	M	F
	CTTCCATCTTCAATGTTGTGTC	M	R
vps-35[D638N]	ACCATCGAGCACTTGTATCGA	W/M	F
	TGCCAGTGGTTGCCAATTTTCT	W	R
	GGTAAGGTGAAGGCAACGAACG	M	R
	CGTGCGATAAGCTCTTCAATC	W/M	R

Table 13-Oligonucleotides utilised for genotyping and outcrossing

2.3.1.4.3 Agarose Gel Electrophoresis

Agarose gel electrophoresis was performed using a 2% agarose gel in 1xTAE. For a medium gel, 3g of agarose was solubilised in 150ml 1xTAE and 1.5µl of 10,000x SYBRsafe (Invitrogen, S33102). A 1kb ladder (Ladder I. PCR Biosystems) was used as a molecular weight standard, half the PCR product sample volume was loaded for analysis. Gels were run in 1xTAE buffer, at a constant current of 100 volts for 30 minutes. DNA was visualised using gel documentation system (Syngene G-Box).

Reagent	Mass/Volume
Prepare a 10x concentrate solution	
TRIS	48.5g
Glacial Acetic Acid	11.4ml
0.5M EDTA (pH 8.0)	20ml
dH_2O	Up to 1 litre
Dilute 1:10 in dH2O to make 1xTAE solution	

Table 14- Preparation of 1xTAE buffer

2.3.2 VPS35 Gene Segregation

5 unbalanced, 4x outcrossed *vps-35[D638N]* heterozygote L4 larvae were singled and added to a medium NGM plate, seeded with *E. coli OP50* and raised under standard conditions. After 72 hours, the hermaphrodite mother was taken for genotyping, as detailed in 2.3.1, to confirm *vps-35[D638N]* heterozygosity. The progeny were left to develop for a further 24 hours, before they were taken for individual genotyping. The number of *vps-35[D638N]* homozygotes, heterozygotes and *vps-35* wildtype progeny were scored, following genotyping detailed in 2.3.1.

2.3.2.1 Optimisation of Progeny Selection

Subsequent fertility assays suggested that few *vps-35[D638N]* homozygote progeny were laid later in the egg laying period than *vps-35[D638N]* heterozygote and wildtype progeny, thus for subsequent gene segregation experiments, the egg laying period was extended to 96 hours. This ensured the whole progeny was captured and that younger progeny were at a feasible size to isolate for genotyping.

2.3.2.2 Optimisation of *vps-35* genotyping PCR

Outcrossing of the VPS-35[D638N] line was undertaken utilising the oligonucleotides detailed in table 11, however subsequent experiments indicated that the similarity between the wildtype and mutant size was too similar to accurately resolve at 300 and 244bp. A restriction enzyme, specific for wildtype cleavage, HincII (ThermoFisher) was subsequently utilised, along with a non-mutation specific reverse primer, 300bp downstream. 0.1units of HincII was incubated with 15ul of PCR product for 16 hours at 37^{o}C, prior to agarose gel electrophoresis. The PCR product has a size of 600base pairs, thus if the wildtype *vps-35* allele is present, a band of 400 and 200 base pairs are present. If the *C. elegans* is heterozygous for vps-35[D638N], an undigested PCR product band is present at 600 base pairs also.

2.3.2.3 Temperature Sensitive Allele Cultivation

Gene segregation as detailed in 2.3.2 was replicated, with the *C. elegans* populations raised at 15^{o}C. The deleterious effects of temperature sensitive alleles are due to protein instability and can

be rescued if *C. elegans* are cultivated at a lower temperature. Developmental timepoints slow when *C. elegans* are raised at 15^{o}C, hence the egg laying period was extended to 96 hours and the progeny selected for genotyping 72 hours after.

2.4 Organismal Health

In *C. elegans*, there are multiple whole organism outputs to measure, enabling characterisation of mutation effects on overall health (27,63,322,323), as detailed below.

2.4.1 Lifespan Analysis

C. elegans populations were age synchronised as detailed in 2.1. At L4 stage of development, 10 individual larvae were transferred via platinum picking to a concentrated *E. coli* OP50 seeded FUDR NGM plates, 5 replicates per mutant line studied. Every 24 hours, nematodes were scored for survival, via observance and responsiveness to platinum pick touch response, dead *C. elegans* were counted and removed from the plates. Assay continued until all *C. elegans* had died. Lifespan analysed through GraphPad Prism Software, utilising the Kaplan-Meyer survival analysis. Survival curve comparison undertaken through Mantel-Cox statistical test.

2.4.2 Progeny Count

Individual *C. elegans* were transferred via platinum picking to a medium NGM *E. coli* OP50 seeded plates at L4 larval stage of development and maintained overnight under standard conditions, 5 replicates per strain utilised. After 18 hours, the number of eggs laid was counted and the mother transferred to a new NGM *E. coli* OP50 seeded plate. The egg-lay plate was maintained under standard conditions and the number of day 1 adults counted 96 hours later. 24 hours after the maternal *C. elegans* transfer, the number of eggs laid was quantified, the plate maintained, and number of developed adults quantified 96 hours later. This is repeated for a further 3 consecutive days until egg-laying cessation at day 5 of adulthood, after which the mother *C. elegans* is taken for genotyping, as detailed in 2.3. Concurrently, *C. elegans* age matched to the egg-laying mothers were taken for DiC microscopy, as detailed in 2.4.3.1, to observe the eggs *in utero*. The number of progeny and developed adults plotted through GraphPad Prism software, utilising grouped data mode.

2.4.3 Germline Characterisation

Following progeny counting, the embryo, uterine and egg development was observed in *C. elegans*, to investigate if there were developmental differences in this between genotypes. Images were obtained though DiC microscopy.

2.4.3.1 DiC microscopy

Confocal-like microscopy was undertaken utilising Zeiss Apotome.2 (ZEISS Microscopy). *C. elegans* were immobilised utilising 5ul of 1mM levamisole, on a 2% agarose pad and transferred

via manual picking with platinum wire. DiC microscopy was undertaken utilising channel 1 DiC and channel 2 Brightfield. Intensity was set to 50% and auto exposure setting utilised. *C. elegans* were visualised with the 10x objective, capturing an image of the whole *C. elegans* body and developing uterus. Subsequently, images were taken at a 20x objective to image the progenitor cells, located at the distal tips of the uterus, and developing germline at a higher resolution. Images were analysed through manual scoring and observation, utilising ZenBlue 2.0 software (ZEISS Microscopy).

2.4.3.2 Embryo and uterine Morphology L4

Following progeny count, L4 *C. elegans* larvae were observed, as at this stage all somatic cells are developed and are uterine morphology is well established, gametes and embryos are under early development. The uterus was outlined utilising ZenBlue 2.0 software (ZEISS Microscopy), in order to compare the overall morphology between mutant strains and the presence of gamete nuclei in the distal tips of the uterus scored.

2.4.3.3 Egg Development and quantification *in utero* Day 1 Adult

DiC microscopy images taken in 2.4.2 were utilised to quantify the number of eggs *in utero*. The morphology of egg stacking *in utero* was also observed, to contrast between genotypes.

2.5 Behavioural Assays

C. elegans possess a plethora of behavioural outputs to test relevant to PD (28), often attributable to specific neuronal populations or neuromuscular function. This can give further insights into organismal health (27,63,322,323).

2.5.1 Determining Crawling Speed

Ad libitum fed *C. elegans* at the selected developmental stage were removed from NGM plates and washed twice with M9 buffer. 10µl of *C. elegans* pellet, containing approximately 30 *C. elegans* were dropped on the centre of an unseeded NGM plate and timer set for 10 minutes, allowing for evaporation, acclimatisation and locomotion. 20 second videos were captured were captured using Stereoblue trinocular stereomicroscope, with stereomicroscope USB camera (Euromex, CMEX.3 DC.3000C), attached to PC with ImageFocus4 software. Videos were captured at 6.2 frames per second and 1.5x (10x objective) magnification, with a scale photograph taken. For each condition, tracks from at least 20 *C. elegans* were obtained and analysed utilising Fiji ImageJ and the wrmTracker plugin, quantifying the average speed of each individual. Crawling speeds were mapped in GrahPad Prism column data setting, statistical analysis was undertaken through one-way ANOVA, with Welch-Forsyth correction, assuming unequal standard deviations between datasets.

2.5.2 Free Swimming/Thrashing Assay

Nematodes were removed from NGM plates and washed twice with M9 buffer. 10µl of worm pellet, containing approx. 30 worms were dropped onto the centre of an unseeded NGM plate. After 30 seconds, 5 videos of 20 seconds were taken, at a rate of 6.2 frames per second and 1.5 (10x objective) magnification. Analysis to quantify ‘thrashing’, as body bends per second (BBPS) was undertaken using Fiji ImageJ wrmTracker. Data was visualised utilising GraphPad Prism 8.0 software, column analyses with one-way ANOVA between datasets, with Brown-Forsyth Correction to adjust for differing Standard Deviations per dataset.

2.5.3 Basal Slowing Assay

Basal slowing was completed as described by Sawin et al (86). 60mm assay plates were prepared with a 1cm bacterial lawn around the edge of the plate and control plates were unseeded. Ad libitum fed worms at the selected developmental stage were removed from NGM plates and washed twice with M9 buffer. 10µl of worm pellet, containing approx. 30 worms were dropped onto the centre of the assay plate and timer set for 10 minutes, allowing for evaporation of the liquid, acclimatisation and crwling of the C. elegans towards the foodsource. Upon reaching the

bacterial lawn 20 second videos were captured using Stereoblue trinocular stereo microscope and Euromex camera with ImageFocus4 software, at 6.2 frames per second and 1.5x (10x objective) magnification. This was repeated for control plates. For each condition, tracks from at least 10 worms were obtained and analysed utilising Fiji ImageJ and the wrmTracker plugin, quantifying the average speed of each *C. elegans*. A % slowing was generated as detailed in equation 1. Data was visualised utilising GraphPad Prism 8.0 software, column analyses with one-way ANOVA between datasets, with Brown-Forsyth Correction to adjust for differing Standard Deviations per dataset.

$$Basal\ Slowing\ Response\ =\ 100 - ((\frac{Speed\ Upon\ Reaching\ Bacterial\ Lawn}{(Mean\ Crawling\ Speed\ on\ Unseeded\ NGM)}) \times 100)$$

Equation 1- Calculation of the Basal Slowing Response

2.6 *In vivo* Microscopy

C. elegans are highly amenable to *in vivo* microscopy, through the utilisation of fluorescent dyes and fluorescent transgene expression.

2.6.1 Mitochondrial staining with TMRE

Tetramethylrhodamine ethyl ester (TMRE) is an electron gradient sensitive dye, utilised in a range of systems to study mitochondrial membrane potential, indicative of mitochondrial function. TMRE (ThermoFisher) was added to *E. coli OP50* at a concentration of 10µM prior to seeding. 150µl of this solution was seeded onto small (50mm) plates. Plates were covered and incubated at 37^{o}C overnight. 100 L4 larvae were then dropped onto the plates, covered in foil and left to develop at 20^{o}C overnight. Ad libitum fed D1 adults were removed from the plates and washed twice with M9 buffer. Microscopy slides were prepared with a 2% agarose pad, worms were added to and immobilised with 5µl of 1mM levamisole (ACROS). Worms were imaged at a magnification of 4x objective, using Evos Fl Cell Imaging System (Invitrogen) at a light intensity of 70%. Experiments undertaken after July 2020, utilised the Zeiss Apotome2.0 for confocal-like microscopy. Channel1 and the TMRE filter utilised (Wavelength 561nM) at an intensity of 40%, and exposure of 2000miliseconds, optimised to wildtype quantification and without saturation. *C. elegans* were imaged at a 10x objective, to visualise the whole *C. elegans* body. Fluorescence was quantified using FijiImageJ, through the selection of a 500pixel diameter circle behind the pharynx. Background fluorescence was quantified for each image and subtracted from the fluorescence intensity. A mean fluorescence was quantified for the wildtype control, and utilised to normalise all values from each genotype. Fluorescence intensities were mapped in GraphPad Prism column data setting, statistical analysis was undertaken through one way ANOVA, with Welch-Forsyth correction for unequal standard deviations between datasets. Descriptive statistics, Mean, Standard Deviation and number were generated in GraphPad Prism.

2.6.2 DiI Amphid/Phasmid Neuron Staining

DiI is a fluorescent dye staining the lipid bilayer of highly ciliated cells, taken up through endocytosis. In *C. elegans*, the amphid, phasmid and IL sensory neurons are highly ciliated, a process that has been dysregulated in some alternative Parkinson's models (287,324–326). Ad libitum fed *C. elegans* of the selected developmental stage were removed from the plates and washed once with M9 buffer. *C. elegans* of the selected developmental stage were resuspended in 1ml M9 with 12ug/ml DiI dye, wrapped in foil and incubated on a slow shaker for 3 hours at room temperature. *C. elegans* were washed twice with M9, before addition of a 1ul *C. elegans* pellet to 5ul of 1mM levamisole, for immobilisation on a 2% agarose pad mounted on a glass slide. Glass

coverslip was added and visualisation was undertaken utilising the Zeiss Apotome2.0 for confocal-like microscopy. Channel1 and the DiI filter utilised (Wavelength 560nM) at an intensity of 40%, and exposure of 2000miliseconds, optimised to wildtype quantification and without saturation. *C. elegans* were imaged at a 20x objective, to visualise the *C. elegans* head, where the amphid and phasmid neurons are located. Fluorescence was quantified using ZenBlue2.0, through the selection of the neuronal area, background fluorescence was quantified and subtracted from the neuronal area intensity. A mean fluorescence was quantified for the wildtype control, and utilised to normalise all values from each genotype. Fluorescence intensities were mapped in GraphPad Prism column data setting, statistical analysis was undertaken through one way ANOVA, with Welch-Forsyth correction for unequal standard deviations between datasets. Descriptive statistics, Mean, Standard Deviation and number were generated in GraphPad Prism.

2.6.3 Nile Red Lipid Staining

Nile red is a fixative stain to quantify lipid accumulation across tissues and can be utilised to stain the *C. elegans* body following fixing (327). Nile Red stock solution prepared to a concentration of 5mg/ml, solubilised in acetone and stored in foil at room temperature. *C. elegans* grown to the selected developmental stage and washed from the plate with M9, then washed 2x with 0.01% PBS-T in 1.5ml Eppendorf. Supernatant removed and 500ul of 40% isopropanol added, for incubation at room temperature for 3 minutes. Eppendorf centrifuged at 2500rpm for 1 minute, supernatant removed and worm pellet washed 2x with 0.01% PBS-T, centrifugation repeated and supernatant removed. Nile Red working solution made, at a concentration of 30ug/ml in 40% isopropanol. 600uL of Nile Red working solution added to each sample, inverted three times and rotated on an orbital shaker for 2 hours at room temperature. Samples centrifuged at 2500rpm for 1 minute and washed 3x with 0.015% PBS-T. Following final supernatant removal, 2ul of worm pellet added to a slide mounted 2% agarose pad and glass coverslip added. Visualisation was undertaken utilising the Zeiss Apotome2.0 for confocal-like microscopy. Channel1 and the Nile Red filter utilised (Wavelength 560nM) at an intensity of 30%, and exposure of 2000miliseconds, optimised to wildtype quantification and without saturation. *C. elegans* were imaged at a 10x objective, to visualise the whole C. elegans body. Fluorescence was quantified using ZenBlue2.0 software, through the selection of the whole body, background fluorescence was quantified and subtracted from the neuronal area intensity. A mean fluorescence was quantified for the wildtype control, and utilised to normalise all values from each genotype. Fluorescence intensities were mapped in GraphPad Prism column data setting, statistical analysis was undertaken through one way ANOVA, with Welch-Forsyth correction for unequal standard deviations between datasets. Descriptive statistics, Mean, Standard Deviation and number were generated in GraphPad Prism.

2.6.4 GFP Dopaminergic Neurons

The dopaminergic neurons of *C. elegans* expressing GFP under the control of dopaminergic promoter can be visualised through in vivo confocal like microscopy. *C. elegans* are age synchronised and grown to the selected developmental stage, with or without pharmacological or toxicological treatment. Slides with 2% agarose pads were prepared, with 5ul of 1mM levamisole for immobilisation. For each genotype/treatment, 20-30 C. elegans were transferred to the levamisole droplet via platinum picking, minimising bacteria transferred. Glass coverslip was added and visualisation was undertaken utilising the Zeiss Apotome2.0 for confocal-like microscopy. Two channels with the eGFP filter were utilised (wavelength 510nm), channel 1 was optimised for wildtype quantification without saturation at an intensity of 25% at an exposure of 2000miliseconds, while channel 2 had an exposure of 5000 milliseconds, to generate stacked image in which CEP and ADE neurons were readily visible for morphology scoring. C. elegans were imaged at a 20x objective, to visualise the *C. elegans* head. Automated Z-stacking was not possible, as orientation and *C. elegans* morphology differed between individuals, so stack was adjusted according to each *C. elegans* imaged. 3-4 images were taken per *C. elegans*, with focus on each CEP and ADE neuron.

Images were analysed using ZenBlue2.0 software, fluorescence was quantified through circular selection of the CEP cell body at the nerve ring, background fluorescence was quantified and subtracted from the neuronal area intensity. Fluorescence intensities were mapped in GraphPad Prism column data setting, statistical analysis was undertaken through one way ANOVA, with Welch-Forsyth correction for unequal standard deviations between datasets. Descriptive statistics, Mean, Standard Deviation and number were generated in GraphPad Prism.

Dopaminergic neuronal morphology was scored for outgrowths, branching, blebbing and degeneration, utilising scoring method established by Guha, Caldwell and Kapahi (328). 20-30 *C. elegans* per mutant line were scored and percentage of neurons in a population with selected pathology were quantified. Additionally, the number of minor and major impairments per *C. elegans* were quantified and percentage of individuals in a population with this pathology quantified. This was broken down further, to calculate the number of *C. elegans* with minor and major impairments in the CEP and ADE neurons, to compare between genotypes and treatments.

2.7 Pharmacological and Toxicological Treatment

2.7.1 LRRK2 inhibitor treatment

C. elegans throughout this study were treated with the LRRK2 inhibitor Genetech0877. Initial studies utilised a liquid media treatment method, but following optimisation a solid media feeding method was established. Drug uptake in *C. elegans* is most efficient through liquid media cultivation (329), however this induces an exercise state, later shown to be neuroprotective (330).

2.7.1.1 Liquid Media cultivation

C. elegans can be developed in the liquid culture *S. complete*. 1 day prior to setting the inhibitor treatments, eggs were isolated through bleaching and left to hatch overnight, in M9 buffer at 20^{o}C. Concentrated *E. coli* OP50 was washed in sterile deionised water and resuspended in *S. complete* to a concentration of 100mg/ml. A dilution of the human LRRK2 inhibitor Genentech 0877, dissolved at 10µM in dimethylsulfoxide (DMSO), was made with S. complete to create a 10mM inhibitor stock solution. This was repeated for a 10mM DMSO control. 1ml aliquots of S. complete were produced, with final inhibitor/DMSO concentrations- of 0.2mM and/or 1.0mM, per *C. elegans* strain assayed, concentrations were chosen were utilised in prior studies by Saha et al, inhibiting transgenically expressed human LRRK2 in *C. elegans* (253). *E. coli* OP50 was added to the aliquots at a concentration of 6mg/ml. The number of L1 larvae in 10µl drops of M9 were quantified for each *C. elegans* strain,. The volume of L1 larvae solution required for 80-100 worms were added to each S. complete aliquot, containing 0.2/1.0mM inhibitor/DMSO and 6mg/ml *E. coli* OP50 . These aliquots were well mixed and dispensed into a 96 well plate, 120µl per well. Plates were incubated at 20^{o}C for 72 hours. *C. elegans* were removed from the plate the evening prior to phenotypic assay and habituated to crawling overnight on *E. coli* OP50 seeded NGM plates at 20^{o}C.

2.7.1.2 Solid Media cultivation

C. elegans were age synchronised through bleaching and left to develop under standard conditions, until selected developmental stage. Dilutions of the human LRRK2 inhibitor Genentech0877/Vehicle DMSO were created in deionised, sterile water at a concentration of 10mM, with 300µl added to FUDR plates, seeded with concentrated *E. coli* OP50. Plates were dried in a microbiological safety hood for 1 hour prior to transfer. *C. elegans* assayed on day 1 of adulthood were transferred to the inhibitor/vehicle plates through M9 washing from late L4 of development, while *C. elegans* assayed in day 5 were transferred late in day 4, utilising a 16 hour overnight incubation for both stages.

2.7.2 Dopamine Treatment

C. elegans developmental stages were synchronised through bleaching 400µL of 50mM dopamine hydrochloride, freshly dissolved in in deionised sterile water, was added to the surface of an *E. coli* OP50 seeded NGM plate. 300µL of deionised sterile water was added to control plates. Plates were dried in microbiological safety hood for 1 hour. *C. elegans* populations were transferred through washing at the selected developmental stage and incubated for 4 hours, then removed for phenotypic assay through M9 washing. Prior to assay, *C. elegans* populations were washed 2x with sterile M9.

2.7.3 Rotenone Oxidative Stress

Rotenone is a mitochondrial complex I inhibitor and pesticide epidemiologically linked to PD development, it has been frequently utilised in toxin-based models of PD and can be utilised as an oxidative stress inducer, to test the effect of our mutation upon environmental stress susceptibility/resistance.

2.7.3.1 Survival Assay

3cm NGM plates including 15µM of rotenone (ACROS) were prepared and seeded with concentrated *E. coli* OP50, then incubated at 37^{o}C overnight. 50 L4 larvae were then transferred to each plate, with 5 replicas for each mutant line. In the following 5 days, the number of surviving and dead worms were quantified, generating a survival ratio.

2.7.3.2 Toxicological treatment for GFP dopaminergic neuron visualisation

Concentrations of rotenone and a DMSO vehicle created in sterile, deionised water at concentrations of 500mM, 5, 7.5 and 10µM. 300µl of mixed rotenone or vehicle solution was added to the surface of 6cm E. coli OP50 seeded FUDR NGM plates and dried in a microbiological safety hood for 1 hour. *C. elegans* populations were transferred through washing with M9 at late L4/early young adult and incubated for 16 hours overnight. 20-30 animals were removed through picking, for in vivo microscopy of GFP expressing dopaminergic neurons.

2.8 Western Blotting

2.8.1 Lysate Preparation

Prior to protein extraction, worm populations were synchronised and developed in well fed conditions until the selected age. Aged worms were maintained on NGM plates containing 50µM 5-fluorodeoxyuridine (FUDR), following transfer as young adults, to prevent the hatching of progeny. At the selected stage, worms were washed from the plate with M9 and washed twice.

2.8.1.1 Extraction for Protein of Interest Detection

Undertaken when precise protein quantification was not required. Samples were concentrated to approx. 100µl. 100µl of 2xSDS (Table 15) was added to each sample and sonicated (Sonico Vibra-Cell) at 55% amplitude for 5x 30 seconds, with a 10 second interval. Samples were then heated for 2 minutes at 95ºC. Sonication and heating was repeated once and samples stored at –20ºC.

Reagent	**Mass/Volume**
125mM Tris pH 6.8	0.9g
4% SDS	2.4g
20% Glycerol	12g
0.03% Bromophenolblue	0.018g
Filter Sterilise under fume hood	
ß-Mercaptoethanol	3ml
Aliquot under fume hood, store at -20ºC	

Table 15-Preperation of 60ml 2xSDS Buffer

2.8.1.2 Extraction for Protein Quantification

Undertaken when precise protein quantification was required prior to sample loading. Samples were prepared in 100µl total volume. 50µl of both lysate (Table 16) and lysis buffer (Table 12) were added to each sample and frozen at -80ºC for 30 minutes. Samples were thawed on ice and sonicated as detailed in 2.10.1, then stored at -20ºC.

Reagent	**Mass/Volume**
Prepare lysis buffer fresh, on the day of protein extraction	
Triton x-100	20µl
PMSF (0.1M stock in propanol)	10µl
2x HALT protease inhibitor cocktail (ThermoFisher)	5µl
dH_2O	965µl
Add an equal volume of lysis buffer, as required for sample quantity	

Table 16- Preperation of 1ml C. elegans Protein Lysate Buffer

2.8.2 Protein Quantification

Protein quantification was undertaken dependent upon the protein extraction method. When method 2.8.1.1 was utilised, a Coomassie staining was undertaken as detailed in 2.8.2.1, while when method 2.8.1.2 was undertaken, a BCA assay was undertaken, as detailed in 2.8.2.2.

2.8.2.1 Quantification of protein via Coomassie staining

Standards with a total volume of 100µl were prepared utilising 2000µg/ml BSA, incorporating 50µl of 2xSDS, dilutions ranged from 1000, 750, 500, 250 and 125µg/ml. Prior to first use, standard proteins were linearised through heating at 95^{o}C for 5 minutes.

5µl of standards and unknown protein samples were loaded onto a 12% NuPage Bis-Tris Gel (ThermoFisher Scientific) and separated as detailed in 2.8.3. The gel was incubated in 25ml of InstantBlue™ Coomassie stain on an orbital shaker mixer (20rpm), for 1 hour at room temperature. Imaging was undertaken utilising visible protein gel application in GeneSys (Syn-Gene, G-Box) and exported as a TIFF file. The image was inverted in ImageJ and protein lanes quantified. A calibrations curve utilisng the standards were generated and the equation of the line of best fit obtained. This equation was utilised to calculate the concentration of the unknown samples.

2.8.2.2 Quantification via BCA assay

Prior to sample loading, protein was quantified via BCA assay, utilising Pierce^{TM} BCA protein assay kit, as detailed in the manufacturer instructions (ThermoFisher. 23225). Samples containing 15µg of protein were prepared and an equal volume of 2xSDS added. Protein samples were then heated at 100^{o}C for denaturation of protein prior to loading.

2.8.3 SDS-PAGE separation

15 µg of sample was loaded onto a 12% NuPage Bis-Tris Gel (ThermoFisherScientific) and run at 150 volts for 90 minutes (InvitrogenNovex XCell Lock) in 1x MOPS or 1x MES running buffer (ThermoFisher Scientific), dependent upon protein of interest molecular weight. Precision Plus PageRule Protein standard 10-250kDa (BIORAD) was loaded as a molecular weight standard.

2.8.3 Protein Transfer Conditions

Protein transfer conditions were optimised throughout the project, utilising wet and semi-dry protein transfer methods. Transfer conditions were adapted depending upon protein of interest molecular weight. High molecular weight proteins include LRRK2 (288kDa), LRK-1 (266kDa) and the *C. elegans* orthologue of SQSTM-1/P62, SQST-1 (68kDa). Low molecular weight proteins studied include RAB-8 (24kDa) and RAB-10 (23kDa).

2.8.3.1 Wet Protein Transfer

When studying SQST-1, proteins were transferred to a PDVF membrane by wet electrophoresis blot at room temperature, at 70 volts for 90 minutes, in 1x InstantBlot^{TM} Transfer buffer (Expedion). However, when studying very high molecular weight proteins, such as LRK-1 and LRRK2, wet transfer was undertaken to a PDVF membrane at 50 volts for 4 hours at room temperature. Both transfer methods undertaken at room temperature.

2.8.3.2 Semi-dry Protein Transfer

Semi-dry transfer undertaken using trans-blot turbo transfer system (BIO-RAD). Ready to Assemble (RTA) transfer kit with 0.2μm PDVF membrane utilised for transfer (BIO-RAD). Transfer undertaken for 20 minutes, 25 volts, 2.5A at room temperature.

2.8.4 Membrane Blocking

Prior to antibody incubation, blocking was undertaken for 1 hour in 5% milk PBS-T on a roller mixer at room temperature.

2.8.4.1 Primary Antibody Incubation

Membrane was cut according to molecular weight and primary antibodies were incubated with membrane overnight at 4ºC on a roller mixer in 5% Milk/PBS-T, the housekeeping gene of interest throughout experiments was β-actin. Prior to secondary antibody incubation, membrane was washed 5 times for 5 minutes in PBS-T on a roller mixer.

Antibody	Host	Provider	Product Code	Dilution
Anti-β-Actin	Mouse	Sigma	1978	1:5000
Anti-SQST-1	Rabbit	Supplied from collaborator (Prof Hoppe) at Institute for Genetics and CECAD Research Centre, University of Cologne, Germany		1:3000
Anti-LRK-1 Sera	Rabbit	Outscourced for generation by the Kevei laboratory		1:1000
Anti-FLAG	Mouse	Sigma	F3165	1:2500
RAB8A	Rabbit	Cell Signalling Technologies	#6975S	1:3000
RAB8A pT72	Rabbit	Abcam	230260	1:3000
RAB10	Rabbit	Cell Signalling Technologies	#8127S	1:3000
RAB10 pT73	Rabbit	Abcam	230261	1:3000
LRRK1 (475-523)	Rabbit	Aviva Systems Biology	ArP62030_P050	1:2500
LRRK1 (1339-1369)	Rabbit	Abcam	ab175839	1:2500

LRRK1 (1608-1744)	Rabbit	Sigma	HPA010537	1:2500
LRRK1 (1981-2014)	Rabbit	Aviva Systems Biology	OAAB16862	1:2500
LRRK2 (~950)	Rabbit	Abcam	ab133474	1:2500
LRRK2 pSer910	Rabbit	Abcam	ab133449	1:2500
LRRK2 pSer935	Rabbit	Abcam	ab133450	1:2500
LRRK2 pSer1292 (1250-1350)	Rabbit	Abcam	ab203181	1:2500
LRRK2 pT1491 (1450-1550)	Rabbit	Abcam	ab140106	1:2500

Table 17-Primary antibodies utilised or tested during research project

2.8.4.2 Secondary Antibody Incubation

Secondary antibodies were incubated in 5% milk PBS-T at room temperature on a roller mixer for 1 hour. Prior to imaging,, membranes were washed 4x for 5 minutes with PBS-T and 1xPBS for 5 minutes.

Antibody	**Host**	**Provider**	**Product Code**	**Dilution**
Anti-Rabbit IgG Peroxidase	Goat	Sigma/Merck	A0545	1:10,000
Anti-Mouse IgG Peroxidase	Rabbit	Sigma/Merck	A9044	1:10,000

Table 18-Secondary Peroxidase Conjugated Antibody utilised throughout study

2.8.5 Imaging

Blots were visualised following incubation with a lab prepared ECL solution and chemiluminescence imaged utilising the membrane documentation system (Syn-Gene, G-Box). ECL was prepared fresh prior to western blot imaging.

Reagent	**Volume/Mass**
Solution A (10ml)	
1M Tris pH8.5	1ml
250mM luminol	50µl
90mM coumaric acid	22µl
dH_2O	9ml
Solution B (10ml)	
H_2O_2	1ml
dH_2O	9ml
Combine equal volume as required for sample quantity.	

Table 19-Preperation of ECL for Western Blot Membrane Imaging

2.8.6 Membrane Drying and Reactivation

Following imaging, membranes were washed in PBS and air dried, prior to storage. If required, membranes were reactivated in methanol for 3 seconds, then washed 3 times prior to primary antibody re-incubation as detailed in 2.8.4

2.8.7 Protein Quantification

Analysis of proteins of interest was undertaken utilising ImageJ. Band intensity of the housekeeping protein was quantified for each sample and the protein of interest. The protein of interest intensity was corrected by dividing by the housekeeping protein intensity.

Chapter III: Characterising the *vps-35[D638N]* mutation in *C. elegans*

The first results chapter of this thesis will focus on studies of the novel, CRISPR/Cas9 modified *vps-35 C. elegans* line and establishment of it as a novel model for VPS35[D620N] mutation consequent Parkinson's. First the *in silico* conservation between human VPS35 and the *C. elegans* orthologue VPS-35 will be discussed, highlighting its suitability as a candidate for functional modelling. Following this, the characterisation of the novel VPS-35[D638N] mutant will be extensively detailed, in order for these observations to be later contrasted with findings in alternative models, further assessing its suitability and insights as a novel model. In addition, this model will be used to dissect the proposed mechanism of action of VPS35[D620N] mutation consequent Parkinson's, to assess whether it could be a loss of function, dominant negative, haploinsufficiency, or toxic gain of function mechanism implicated in mutation.

3.1 *C. elegans* VPS-35 shows conservation with human VPS35 *in silico*

Prior to the generation of a novel VPS-35 model, bioinformatic analysis was undertaken between the human VPS35 and *C. elegans* VPS-35, in order to assess its suitability as a novel disease model.

3.1.1 Advanced literature searching for VPS-35 and VPS35 relevant literature

Advanced literature searching for human and mammalian VPS35 and *C. elegans* VPS-35 illustrated that there was a substantial number of studies investigating human and mammalian VPS35, but very few covering *C. elegans* VPS-35. An advanced literature search of PubMed shows that there are 286 primary research papers and 68 review papers covering VPS35. However, *C. elegans* VPS-35 is only covered in 8 primary research papers and no reviews available on pubmed. Following an advanced literature search of WormBase, a database of *C. elegans* resources and literature, a further 18 primary research articles are shown to mention *C. elegans* VPS-35 (Accessed in April 2020). These research articles were also utilised in the development of the literature review "Modelling the Functional Genomics of Parkinson's Disease in *C. elegans: LRRK2* and Beyond" (1).

This demonstrates that VPS35 is well characterised in multiple model systems, but there is a gap in the literature investigating *C. elegans* VPS-35. This demonstrates that undertaking our novel, CRISPR/Cas9 approach would add valuable, new insights into this field. Furthermore, the well-established *in vivo, in vitro* and *in silico* alternative models of VPS35 function, could prove to be valuable resources, for us to evaluate the potential conservation extent of our novel *C. elegans* model and its relevance in VPS35 modelling, essential in establishing this.

3.1.2 Human and *C. elegans* VPS35 protein domains

VPS35 is the core subunit of the retromer complex and is highly conserved in functionality between humans and simple eukaryotic models. Human VPS35 is 781 amino acids long, while C. elegans VPS-35 is 799 amino acids in length, as shown in figure 8. Domain structural information was gathered from the databases ProSite and InterPro. Structurally, VPS35 and VPS-35 are composed of an armadillo fold, in which the Parkinson's consequent mutation D620N is located. Sequence alignment surrounding the D620N mutation in particular shows high conservation. The identified gaps between the two proteins located approximately 50 amino acids from the start of the armadillo fold, in which the 18 additional amino acids the *C. elegans* possess are located.

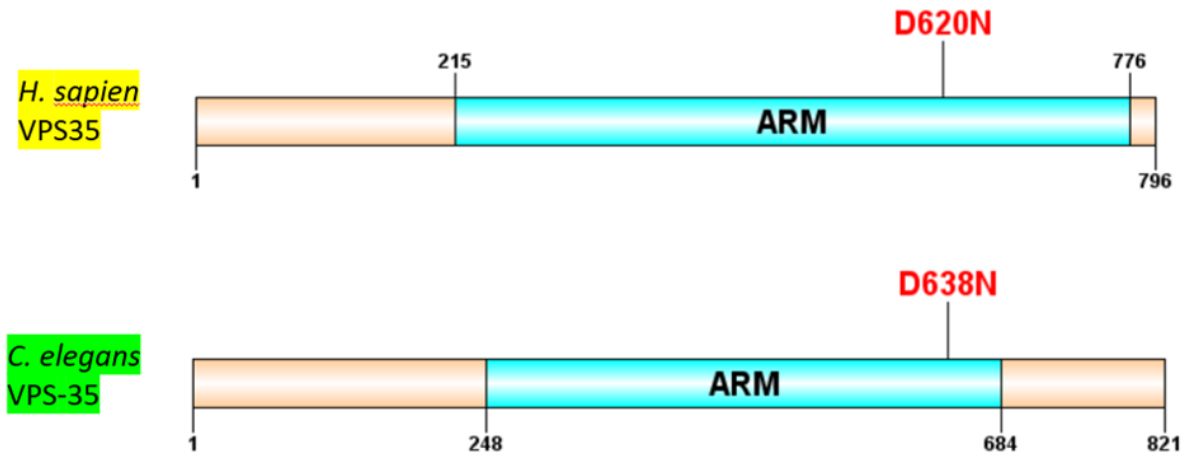

Figure 8- Protein domain structure of Human VPS35 and C. elegans VPS-35

Linear visualisations were generated through DOG2.0 software, as detailed in chapter 2 2.1. Domain information, including starting and end amino acid, was obtained from ProSite and InterPro prior to mapping. VPS35/VPS-35 has an Armadillo fold (ARM) domain, in which the D620/D638 residue is located, which is similar between species.

Comparative study of the proposed structure of human VPS35 and *C. elegans* VPS-35 utilising the Artificial Intelligence (AI) protein crystal structure database AlphaFold (https://alphafold.ebi.ac.uk/) (319,320) illustrates that broadly, the structure between human VPS35 and its *C. elegans* orthologue VPS-35 are similar, as shown in figure 9. In this model, the apical region of the J-domain in which the VPS35[D620N] mutation is located ([D638N] in *C. elegans*), is at a similar orientation in both proteins. The Aspartic acid (D) residue, forms similar hydrogen boding patterns with the surrounding amino acids, the sequence of which has a high conservation between humans and *C. elegans*. The mis-sense point mutation of this residue to Asparagine (N), leads to the loss of a hydroxyl (CH_2CO-OH) in the R-group of Aspartic acid, which is substituted for an amine (CH_2CO-NH_2) in the mutation to Asparagine. Both hydroxyl and amine groups are capable of hydrogen bonding, so it may be unlikely that VPS35 protein structure is affected by this mutation.

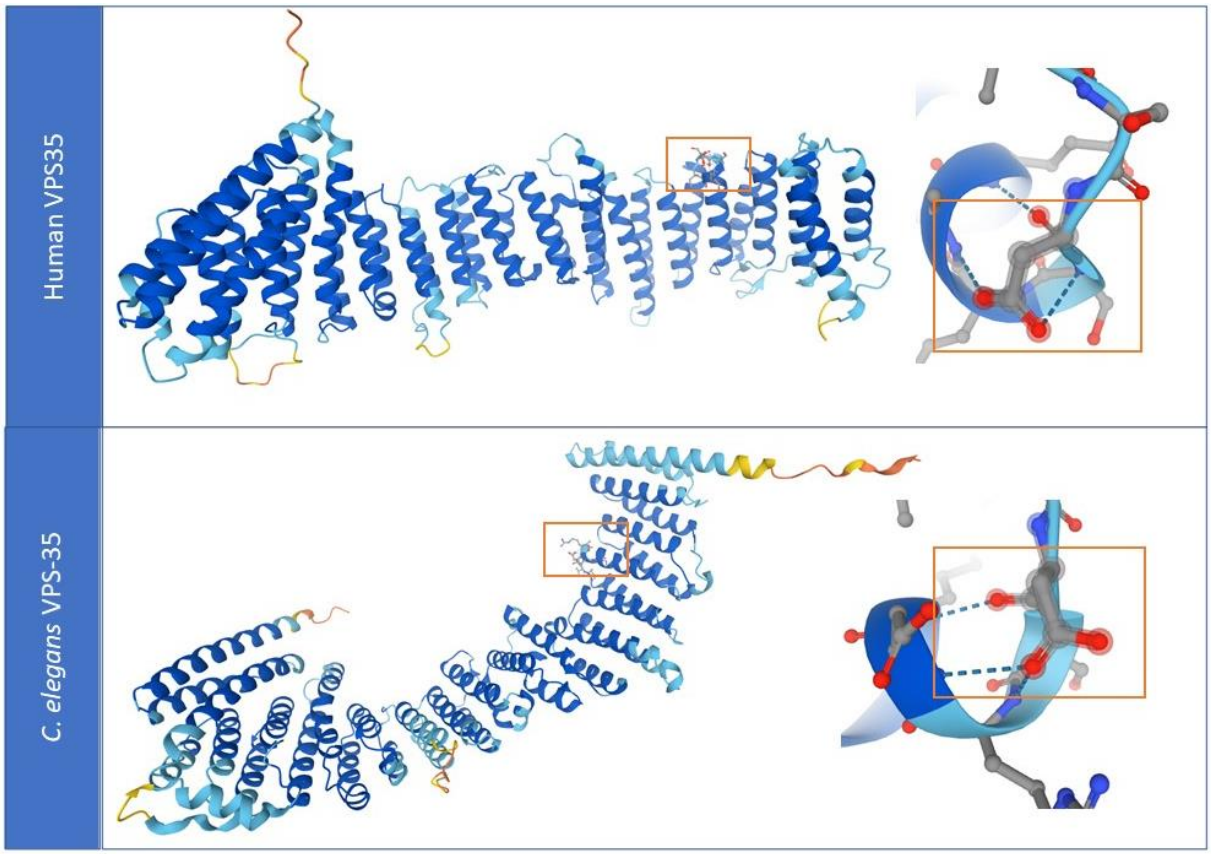

Figure 9- AlphaFold Crystal Structure of human VPS35 and C. elegans VPS-35

Location of PD pathogenic D620N mutation ([D638N] in *C. elegans*) highlighted in the orange box. Closer examination of D620/638 residue illustrates similarities in hydrogen bonding. AlphaFold utilised AI to predict protein crystal structure, including a per residue confidence score (pLDDT) (https://alphafold.ebi.ac.uk/) (319,320). Dark blue: Very high (>90pLDDT), light blue: confident (90>pLDDT>70), yellow: low (70>pLDDT>50), orange: very low (pLDDT<50).

3.1.3 Protein sequence Alignments between human VPS35 and *C. elegans* VPS-35

Protein sequence alignments of the full length protein were generated utilising EBI pairwise sequence alignment tool (234), using the parameters described in chapter 2, 2.1.2. As shown in table 20, utilising the Stretcher tool, there is a 47.2% amino acid identity and 67.4% similarity between human VPS35 and C. elegans VPS-35. There is very little change in these values, when the needle and matcher tools are utilised, demonstrating sustained similarity and conservation of the proteins.

Parameters			**Identity**	**Similarity**	**Gaps**
EBI Tool	**Gap Open**	**Gap Extend**			
Emboss_Stretcher	12	2	388/822 (47.2%)	554/882 (67.4%)	27/822 (3.3%)
Emboss_Needle	10	0.5	392/833 (47.1%)	557/833 (66.9%)	49/833 (5.9%)
Emboss_Matcher	14	4	385/790 (48.7%)	550/790 (69.6%)	19/790 (2.4%)

Table 20-EBI pairwise sequence alignments of full length human VPS35 and C. elegans VPS-35

The Parkinson's consequent D620N mutation is found at the apex of the retromer complex, of which VPS35 is the core subunit. This falls within the armadillo fold, any gaps in the sequence alignment between human VPS35 and *C. elegans* VPS-35 are found more than 50 amino acids upstream of this domain, suggesting high conservation. As demonstrated in Figure 8 and 9, the D620 amino acid residue is directly conserved in *C. elegans* VPS-35, D638. The surrounding amino acids illustrate high similarity, suggesting that there may be some structural conservation between human VPS35 and *C. elegans* VPS-35. This poses as a promising prospect for CRISPR/Cas9 modification, inducing a D638N mutation in *C. elegans* VPS-35, orthologous to the Parkinson's consequent D620N mutation.

3.1.4 Tissue expression of VPS35 in *C. elegans*

TextMining was undertaken in wormbase, in order to extract RNA sequencing data of VPS-35 in *C. elegans* to understand in which tissues VPS-35 is highly expressed. This will enable an evaluation of the relevance of VPS-35 in *C. elegans* for Parkinson's associated functional modelling, as summarised in table 21.

Expression Tissue	**Function and Location of Tissue in *C. elegans***	**Relevance to functional modelling of Parkinson's protein VPS35**
Amphid Neuron	Highly ciliated group of 12 chemosensory neurons, found in the head.	Cilia uptake can be a readout for endocytic function, in which retromer has an integral role. This can be monitored through DiI dye staining. Illustrates potential neuronal function for VPS-35.
Inner Labial Neuron	Ciliated sensory neurons, which are found in the head and terminate at the mouth of *C. elegans*	The alternative neurons which terminate at the mouth are 4 CEP Dopaminergic neurons, important in *C. elegans* models of Parkinson's related proteins. Cilia uptake is also important for inferring endocytic function. Illustrates potential neuronal function for VPS-35.
OLL Neuron	Mechanosensory neuron found in the head	Mechanosensory neurons are integral in *C. elegans* behaviour, phenotypes of which can be readouts for individual neuron function. Illustrates potential neuronal function for VPS-35.
Phasmid Neuron	2 highly ciliated chemosensory neurons, found to the posterior of the anus.	Cilia uptake can be a marker of endocytic function. Illustrates potential neuronal function for VPS-35.
DD Neuron	GABAergic inhibitory motor neuron, found in the ventral nerve cord	VPS-35 has a role in GLR-1 receptor trafficking, important in GABA-ergic neurons, study of this neuron could be an insightful model to understand Parkinson's mutation in this. Illustrates potential neuronal function for VPS-35.

PVD Neuron	Nociceptive, mechanosensation and thermosensation sensory neuron, found un the tail and lumbar ganglion	Illustrates potential neuronal function for VPS-35.
Head Ganglion	Largest cluster of neurons found in *C. elegans*, composed of the nerve ring, retrovesicular ganglion and ventral ganglion in the head	6 of the 8 dopaminergic neurons *C. elegans* possess are found in the head ganglion. Strongly suggests VPS-35 has role in neuronal function.
Coelomocyte	Scavenger organs that endocytose fluids in the body cavity. 6 found in pairs in adult *C. elegans* adjacent to somatic musculature	Coelomocytes are well established models for endocytosis in *C. elegans*. Further understanding of VPS-35 in relation to the processes of endocytosis would shed insights into core cell biology.
Gonad	Generation of gametes for reproduction, uterus incorporating distal tip for oocyte generation and spermatheca found in midsection of C. elegans body	In *C. elegans*, study of reproduction enables deeper understanding of developmental biology, cell signalling and cell death, relevant to understanding VPS-35 function.
Hypodermis	Epithelial system of C. elegans, made of main body syncytium and smaller hypodermal calls of head and tail	
Body Wall Musculature	Core muscle system found in C. elegans across body	

Table 21- Summarised tissue expression of VPS-35 in C. elegans and relevance for functional modelling

3.1.5 Interactome conservation

Studying the protein-protein interactions (PPI's) of a protein of interest may shed insight into their functionality, through guilt-by-association. Therefore, seeking to identify the interactors of VPS-35, could enable further assessment of its potential function in *C. elegans* and evaluate how conserved this is with human VPS35. Interactors were extracted through PINOT, an open resource for quality controlled PPI's in human and *C. elegans*, inferred through the number of detection methods and publications (270). From this, 4 interactors detailed in table 22 were identified for *C. elegans* VPS-35, 2 of which, SNX-1 and SNX-6 are conserved interactors for human VPS35. These two proteins are sortin-nexin dimers for adhesion of the retromer complex to membrane surfaces, thus illustrating the conservation of the retromer complex in *C. elegans*. To develop a greater understanding of VPS-35 functionality, the GO Biological Process functions of these proteins were investigated, highlighting diverse roles in the endolysosomal pathway, protein sorting, cell signalling and pathogen defence.

Interactor Protein	Notable GOBiological Functions	Human Paralog	Presence of Paralog in Human VPS35 interactome
SMA-6	•Protein phosphorylation •Regulation of cell adhesion •Regulation of cell morphogenesis •Bone Morphogenesis Protein signalling pathway •Reproduction •Cellular response to growth factor stimulus •Positive regulation of multicellular organism growth •Positive regulation of protein catabolic process •Positive regulation of transcription by RNA polymerase II •Dorsal/ventral pattern formation •Maintenance of protein interaction in the nucleus •Nematode male tail tip morphogenesis •Dauer larval development •Innate immune response •Defence response to fungus •Defence response to gram-positive bacterium •Positive regulation of TGF-β receptor signalling pathway	BMPR1A, BMPR1B	No
SNX-1	•Early endosome to Golgi transport •Protein localisation to postsynaptic membrane •Retrograde transport, endosome to Golgi •Mechanosensory behaviour •Execution phase of apoptosis •Phagolysosome assembly, fusion and phagosome maturation, involved in apoptotic cell clearance	SNX-1	Yes
SNX-6	•Execution phase of apoptosis •Phagolysosome assembly, fusion and phagosome maturation, involved in apoptotic cell clearance	SNX-6	Yes
RDE-8	•Positive regulation of RNA directed 5'→ 3' RNA polymerase activity. •Production of siRNA involved in RNA interference. •RNA phosphodiester bond hydrolysis.	Unknown	N/A

Table 22-VPS-35 interactors, notable functions and conservation in human VPS35 interactome

3.2 Generation of a heterozygous, balanced VPS-35[D638N] Mutant

Following bioinformatic analysis, a novel VPS35[D620N] orthologous model was generated in *C. elegans*, VPS-35[D638N], through outsourced CRISPR/Cas9 modification by Knundra Transgenics Ltd. Following obtaining this line in the laboratory, it was sufficiently outcrossed for extensive characterisation. The modification was undertaken as detailed below, recoding 232 base pairs of the 3333 base pairs in the *vps-35* gene. One point substitution was made at amino acid 24 indicated below, recoding an aspartic acid to asparagine. The DNA sequence 20-30 amino acids upstream and downstream from the D638N was recoded, as illustrated in pink in figure 10, generating synonymous point mutations in which the amino acid was not changed. This new sequence ensures that the DNA is not cleaved by the Cas enzyme after editing and introduction of D638N. Mutation presence was confirmed by Knundra Transgenics Ltd through PCR, prior to transportation.

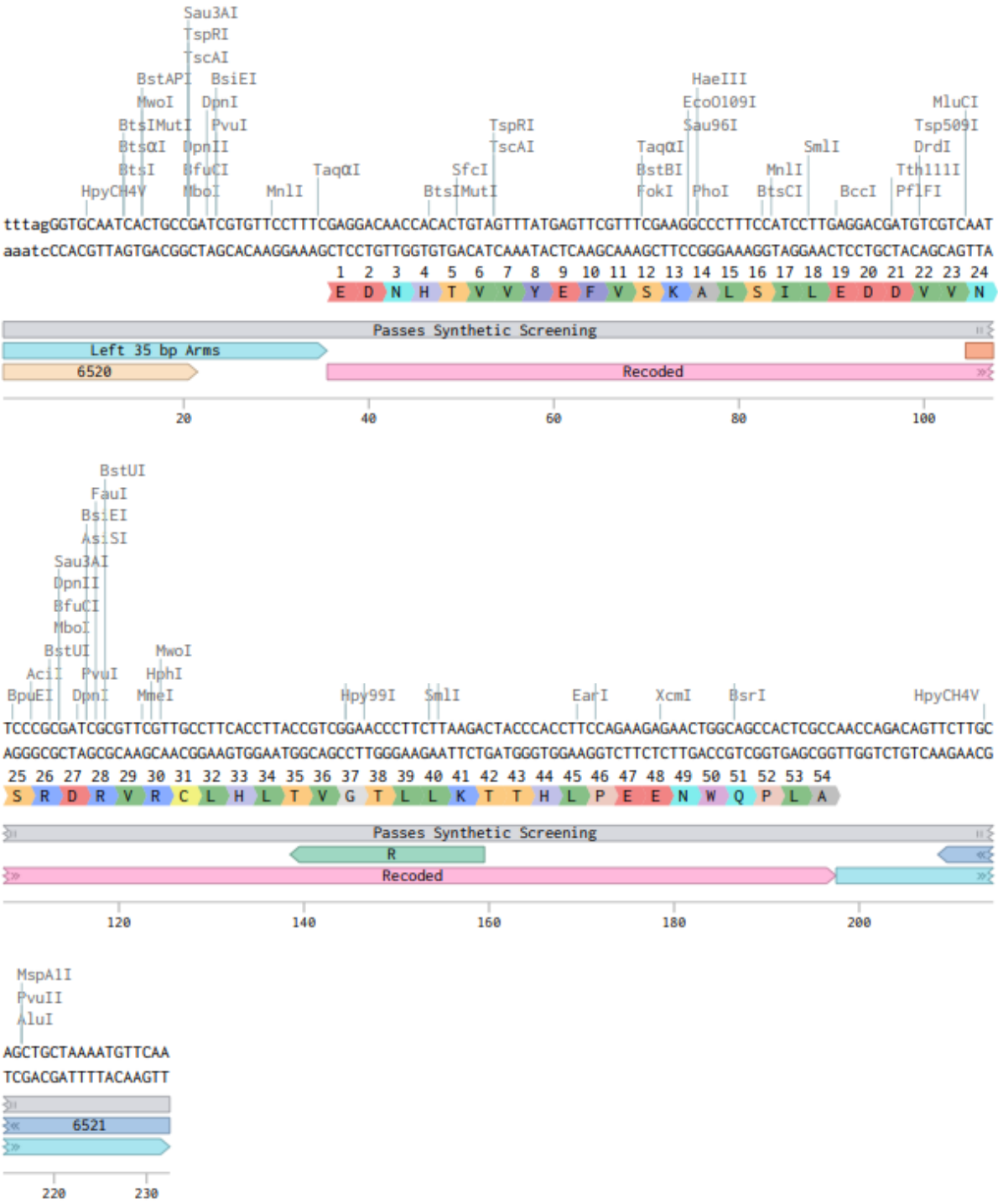

Figure 10- CRISPR/Cas9 recoded sequence for development of novel vps-35[D638N] point mutant C. elegans

Details of full modification illustrated provided by Knundra Transgenics Ltd, on Benchling Software. Recoded DNA sequence of 162 base pairs, generating synonymous point mutations to prevent recutting by the Cas9 enzyme and eliminate homology, is illustrated in pink. D638N residue is illustrated at amino acid 24, in orange. Region of reverse mutation specific primer for genotyping found in green. Unedited DNA sequence shown in blue.

3.2.1 Homozygous VPS-35[D638N] mutation induced through CRISPR/Cas9 modification is unviable

Production of a homozygous *vps-35[D638N]* mutant line was unviable, causing embryonic lethality, thus a heterozygous mutant line was generated by Knundra Transgenics Ltd. Deletion and therefore total loss of function of VPS-35, *vps-35(ok1880)* in *C. elegans* is viable. This suggests that the *vps-35[D638N]* mutation has a more complex cellular effect than retromer loss of function alone.

Mutations, when studied in *C. elegans*, are most easily maintained when they are in a homozygous state. *C. elegans* are self-fertilising hermaphrodites, producing their own oocytes and spermatozoa, thus in heterozygous gene mutation approx. ~¼ of the progeny will be wildtype, without the mutant gene, due to natural segregation. If the heterozygous mutation studied has deleterious, harmful consequences, as the *vps-35[D638N]* may, the gene is more likely to segregate out from the population after several generations. Experimentally, this can be overcome by the incorporation of a balancer strain, through mating with the outcrossed heterozygous mutant line, preventing recombination and segregation at the desired locus, *vps*-35. This has been undertaken in the laboratory following outcrossing and prior to extensive *vps-35[D638N]* characterisation.

3.2.2 Confirmation of VPS-35[D638N] presence and genotyping optimisation

Prior to outcrossing, the presence of the *vps-35[D638N]* mutation was confirmed through genotyping, utilising the primers suggested by Knundra Trangenics Ltd. This was a vital step, to confirm that the heterozygous *vps-35[D638N]* gene mutation had not filtered out of the population in the generations occurring from generation, through international transport and subsequent cryogenic freezing until use. This was a possibility, as if the *vp-35[D638N]* cannot be homozygous, suggesting lethality either at the embryonic stage, developmental arrest, or diminished fertility of homozygous *C. elegans*, strongly suggests that this mutation is deleterious in development. Prior to genotyping, 60 individuals were separated onto small plates, to found their own populations with confirmed genotype mothers. These individuals were taken for genotyping and 9 illustrated that the *vps-35[D638N]* mutation was present, shown in figure 11. These populations were rapidly frozen for the laboratory database, with population 21 chosen for subsequent outcrossing with wildtype males.

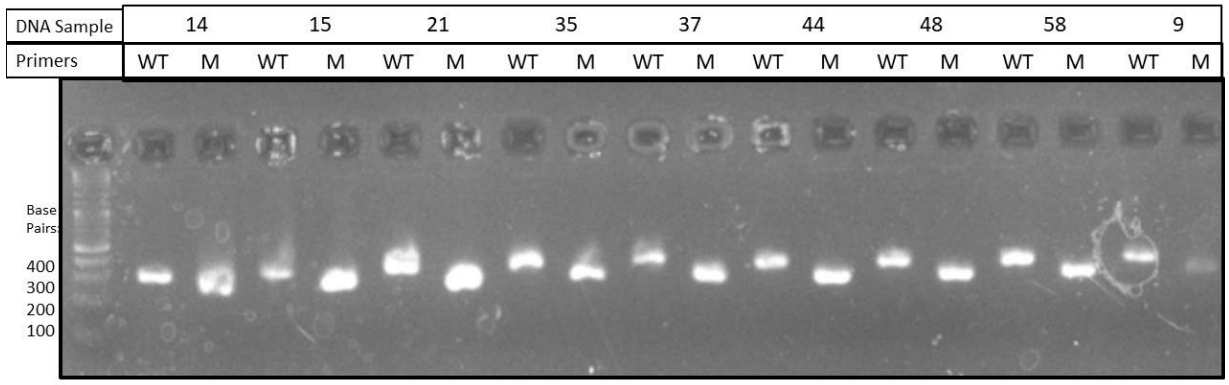

Figure 11- Genotyping for confirmation of vps-35[D638N] presence in population obtained from Knundra Transgenics Ltd

Oligonucleotides suggested by Knundra Transgenics Ltd, wildtype (WT) populations present with a PCR product band of 300bp and *vps-35[D638N]* mutant (M) a PCR product of 244bp. Illustrated are the 9 (out of 60) populations heterozygous for vps-35[D638N], utilised for subsequent outcrossing.

Following this provisional genotyping, the genotyping methods were optimised. The oligonucleotides suggested by Knundra Transgenics Ltd shared a forward primer, with mutational specific reverse primers for the *vps-35* wildtype or *vps-35[D638N]* mutant, however this generated PCR products of similar sizes, 300 and 243 base pairs respectively. A new reverse primer was obtained, approximately 300 base pairs downstream of the original reverse primers, generating a PCR product of approximately 600 base pairs, irrespective of mutational presence. A restriction enzyme HincII, specific for the wildtype sequence around the mutational site was utilised, generating a band of approximately 200 and 400 base pairs if a wildtype allele was present, while the *vps-35[D638N]* allele if present would not be cleaved (Shown in Figure 12). Therefore, *vps-35[D638N]* heterozygotes genotypes exhibited upon agarose gel electrophoresis an uncleaved band of 600base pairs and two additional bands of 400 and 200 base pairs, while homozygous *vps-35* wildtype would show only the 400 and 200 base pair bands. Restriction enzyme digestion of PCR products has greater specificity for mutational detection than the mutation specific reverse primers.

3.2.2 Generation of four times outcrossed, balanced heterozygous *vps-35[D638N]* mutant

Following the confirmation of the *vps-35[D638N]* mutation presence, this line was outcrossed for four generations with N2 wildtype males. Crosses were established with two L4 larvae progeny from a *vps-35[D638N]* heterozygote population, with 10 wildtype males. Multiple crosses were established, as although the L4 larvae were from confirmed *vps-35[D638N]* founded populations, if Mendelian gene segregation patterns are shown ¼ to 1/3rd of these could be wildtype. It is

impossible to verify whether the L4 larvae is heterozygous for vps-35[D638N] prior to mating, as this requires animal sacrifice. Following progeny production, two hermaphrodite mothers from the cross were taken for genotyping, to confirm *vps-35[D638N]* presence. Following confirmation of this, progeny from selected crosses were isolated onto small plates to found their own populations. Progeny from individuals with *vps-35[D638N]* were taken for crossing with wildtype males, as previously detailed. This was undertaken a following three times, in order to obtain a four times outcrossed *vps-35[D638N]* heterozygous population. The four times outcrossed population was stored, for future characterisation of gene segregation and fertility, as detailed in 3.3 and 3.4.

In *C. elegans* carrying heterozygous mutations, the gene of interest can filter out of the population throughout the generations, especially if the mutation is deleterious, as anticipated in the instance of *vps-35[D638N]*. In order to overcome this, the four times outcrossed populations were crossed with the balancer strain *dumpy (tmC6[dpy9710)]II*). The balancer lies on the adjacent chromosome II locus (-0.85 +/- 0.000 cM) to the *vps-35* gene and prevents chromosomal reorganisation during meiosis. *Dumpy C. elegans* lines have a substantially shorter, rounder phenotype for identification, when the recessive balancer is in homozygous form. Therefore balanced *vps-35[D638N]* heterozygotes do not exhibit this phenotype and any *dumpy* progeny, containing only wildtype *vps-35* alleles,. are discarded from investigation. Prior to crossing, L4 larvae from the unbalanced four times outcrossed *vps-35[D638N]* heterozygotes and the dumpy line were heat shocked in order to generate males. The *dumpy C. elegans* did not produce any male progeny, despite replication of L4 heat shocking, however males were readily generated from the *vps-35[D638N]* four times outcrossed population. These males were crossed with an L4 *dumpy* hermaphrodite, multiple crosses were established, as prior to crossing it was not possible to genotype the selected males for mating (as this requires animal sacrifice for DNA extraction) and it was unclear what proportion of the progeny of a heterozygous *vps-35[D638N]* hermaphrodite would be wildtype. Due to their morphology, the *dumpy* balancer carrying strain can be difficult for mating, as the male identifies the hermaphrodite for sexual reproduction through first contact and turning around the body to locate the vulva for spicule insertion. However, as the body shape is much shorter than wildtype *C. elegans*, these first steps of contact recognition and turning do not happen as rapidly. As such, these two obstacles presented challenges. Following cross establishment, the resulting progeny were observed for the presence of males- if a cross has been successful, approximately 50% of the population are male. In crosses with a high proportion of male progeny, individual hermaphrodites were singled onto small plates to establish their own populations. These were observed several days later and the hermaphrodite mothers taken for genotyping of the *vps-35[D638N]*. If the progeny also contained *dumpy C. elegans*, this illustrated that the remaining

progeny would be heterozygous for the dumpy balancer and the cross had been successful. Following genotyping, it was confirmed that multiple populations encompassing the heterozygous *vps-35[D638N]* mutation and the dumpy balancer had been obtained for future characterisation studies, as described in figure 12. These were maintained for extensive characterisation studies and cryogenically frozen for the laboratory database.

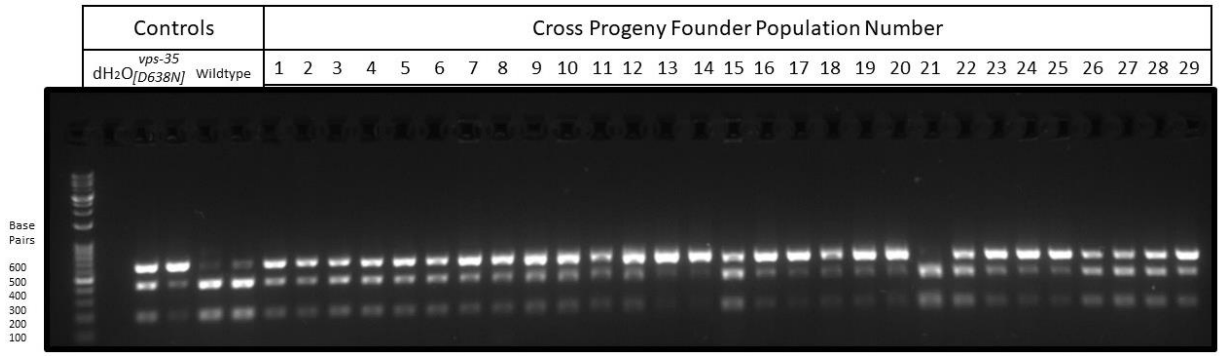

Figure 12- Genotyping of four times outcrossed vps-35[D638N] heterozygote, dumpy balancer cross progeny

29 populations were obtained from the vps-35[D638N] heterozygote and dumpy cross, the majority of which illustrated heterozygosity for vps-35[D638N]. The PCR product has a size of 600base pairs, this is cleaved by a wildtype specific restriction enzyme HincII, thus if the wildtype *vps-35* allele is present, a band of 400 and 200 base pairs are present. If the *C. elegans* is heterozygous for vps-35[D638N], an undigested PCR product band is present at 600 base pairs.

3.3 Unbalanced *vps-35[D638N]* heterozygotes show non-Mendelian progeny gene segregation patterns

Following the generation of four times outcrossed unbalanced *vps-35[D638N]* mutant, the gene segregation patterns of progeny were studied further in order to further investigate homozygous lethality, its penetrance and the potential effect of *vps-35[D638N]* upon developmental biology. Genotyping was undertaken for progeny as detailed in 3.2.

3.3.1 Gene segregation patterns of unbalanced heterozygous *vps-35[D638N]* mother

Homozygous embryonic lethality of *vps-35[D638N]* was studied further, through the investigation of gene segregation patterns, shown by unbalanced heterozygous *vps-35[D638N]* mutants. The progeny of single heterozygous nematodes were isolated and genotyped. Wildtype *C. elegans* can lay around 300 eggs each, while approximately 80 developed progeny from a *vps-35[D638N]* hermaphrodite were isolated. This suggests potential defects in fertility, egg laying and larval development. As homozygous *vps-35[D638N]* is embryonic lethal, according to mendelian gene segregation patterns 2/3rd's of the progeny should be *vps-35[D638N]* heterozygotes, with the remaining 1/3rd wildtype. As shown in figure 13, mendelian gene segregation patterns were approximately exhibited in a sample of 250 progeny. There was one homozygous *vps-35[D638N] C. elegans*, suggesting embryonic lethality is not 100% penetrant. However, this individual was sterile, with no progeny or visible eggs developed in the abdominal cavity. Despite the lack of complete penetrance, this demonstrates the severity of cellular dysfunction driven by *vps-35[D638N]*.

Genotype of *vps-35*(knu618[D638N])	**Population (%)**
VPS-35[D638N] Homozygous	0.4
VPS-35[D638N] Heterozygotes	73.2
VPS-35 Homozygous Wildtype	26.4

Figure 13- Gene Segregation Pattern of Progeny of unbalanced vps-35[D638N] Heterozygote

3.3.2 *vps-35[D638N]* is not a temperature sensitive allele

The lack of complete penetrance of embryonic lethality was investigated further. Selected *C. elegans* mutations which impair protein folding, or stability, can be temperature sensitive alleles. When *C. elegans* are cultivated at lower temperatures, 15^{o}C, rather than the standard 20^{o}C, the temperature sensitive allele phenotype and impairments in development are less severe, or even present with no phenotype. Due to the incomplete penetrance of homozygous embryonic lethality, the hypothesis that *vps-35[D638N]* is a temperature sensitive allele was tested. If so, maintenance at a lower temperature could be a viable option for the cultivation of homozygous populations and

simpler maintenance for future characterisation studies. The gene segregation experiment detailed in 3.3.1 was repeated at 15ºC. No increase in homozygous individuals was shown, as illustrated in Figure 14. This supports the idea that VPS35[D620N] does not lead to toxicity through protein mis-folding or impaired stability, consistent with alternative *in vivo* and *in vitro* models of VPS35 function (109), the comparative AlphaFold protein structure in 3.1 and suggesting a more complex mechanism may be in action.

Genotype of *vps-35*(knu618[D638N])	**Population (%)**
vps-35[D638N] Homozygous	0
vps-35[D638N] Heterozygotes	46.0
vps-35 Homozygous Wildtype	44.0

Figure 14-Gene Segregation Patterns of Progeny of unbalanced vps-35[D638N] Heterozygote, Maintained at 15ºC

3.3.3 Gene segregation patterns of *vps-35[D638N]* with optimised egglay period

Following on from the insights gleaned in the first progeny count that *vps-35[D638N]* homozygotes, if present are laid later in the egg laying cycle as discussed throughout 3.4, the progeny collection window in the gene segregation experiment was extended from 72 hours to 96, to ensure all larvae were collected for genotyping. A shorter window may mean that smaller larvae laid later in the cycle may be missed for genotyping. The entire progeny of 4 heterozygous hermaphrodites was isolated, utilising 419 progeny in total, collected within the 96 hour egg laying window. These clearly indicate an increased presence of *vps-35[D638N]* homozygosity in the population, with a mean of 3.7% of the progeny population carrying homozygous mutations, 65.61% heterozygous and 30.69% wildtype, shown in figure 15. Notably, the fertility appears to be lower for this genotype, as wildtype *C. elegans* produce over 300 eggs (64). This data augments earlier findings in the fertility assay and further confirms the results in gene segregation experiments.

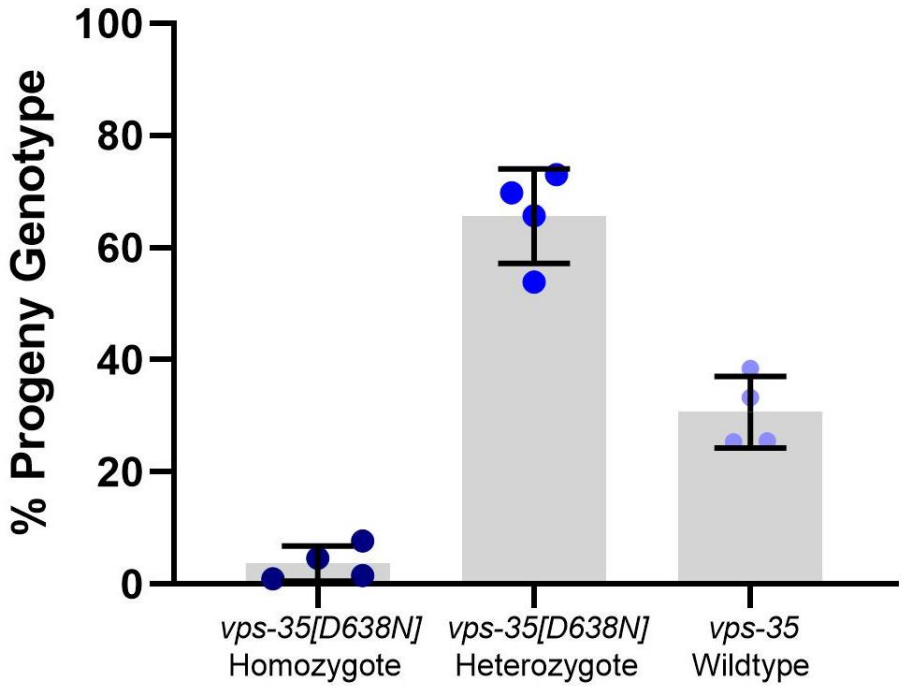

Replicate	Genotype			Number of Progeny Genotyped
	***vps-35[D638N]* Homozygote**	***vps-35[D638N]* Heterozygote**	***vps-35* Wildtype**	
1	7.69	53.85	38.46	52
2	0.93	65.74	33.33	108
3	4.65	69.77	25.58	129
4	1.54	73.08	25.39	130
Mean	**3.63**	**65.61**	**30.66**	**419**

Figure 15-Gene Segregation Patterns of Progeny of vps-35[D638N] Heterozygote

Whole progeny of four *vps-35[D638N]* heterozygotes taken for genotyping, incorporating ~500 individuals. Optimisation of egg lay period illustrates a greater number of *vps-35[D638N]* homozygotes, however its rarity further suggests lethality with incomplete penetrance. Genotyping undertaken as detailed in 3.2.

3.4 Progeny Count of *vps-35[D638N]* illustrates that *vps-35[D638N]* homozygosity induces larval arrest

Investigating the fertility of *C. elegans* through progeny counts of eggs and developed adults, sheds insight into perturbations in cell biology and development induced by selected mutations. This was particularly important for the characterisation of the *vps-35[D638N]* model, which has been demonstrated to be unviable for development in homozygous form, highlighting the potential functional implications of this mutation.

3.4.1. *vps-35* mutant progeny count

A progeny assay for the *vps-35[D638N]* unbalanced line was undertaken, to further investigate if homozygous mutation is embryonic lethal, or if these mutations prevent larval development. This line has been contrasted with the wildtype and the *vps-35* deletion mutant, the results from which can be found in figure 16.

In this experiment in day 1 of adulthood, *C. elegans* with the heterozygous *vps-35[D638N]* mutation lay approximately 30 eggs, while the wildtype lays 50, suggesting subtle fertility impairments at this timepoint, or a delay in egglaying (Figure 16A and B). All eggs laid by the *vps-35[D638N]* heterozygote on this day develop into adults, while in eggs laid on day 2, approximately half develop into adults and decomposing eggs were present on the plate 3-days post egg lay. This suggests that some of the eggs laid in day 2 may be homozygous for *vps-35[D638N]*, later in the reproductive cycle than other genotypes and exhibit larval development arrest with incomplete penetrance. The comparative rates of egg laying are further detailed in the supplementary.

Interestingly, one individual *C. elegans* was homozygous for *vps-35[D638N]* in the progeny count sample (Figure 16 C). In day 1 of adulthood, when wildtype worms are most fertile, there were no eggs laid by the homozygous mutant. In day 2, the homozygous worm laid 14 eggs, contrasting previous findings that the homozygous mutant was sterile, with egg production ceasing by day 3. However, when counting the adult *C. elegans* from the 14 eggs, there were no adults present, with decomposing eggs visible in the location they were counted. This suggests that this mutation has severe implications in larval development and leads to arrest in development to L1 larvae, however the penetrance of this is incomplete. Furthermore, the VPS35[D620N] mutation is so rare in human populations, there are no known individuals homozygous for this mutation, thus heterozygote *C. elegans* lines are a relevant model.

A *vps-35* deletion line has been utilised as a total loss of function model, to contrast against the novel *vps-35[D638N]* line. The *vps-35* deletion line shows distinct fertility phenotypes from the

vps-35[D638N] (Figure 16D). It has a very low fertility and latent egg laying compared to the wildtype. This is due to a severe egg laying defect known as 'bagging' in which ejection does not occur efficiently or at all and the developing eggs hatch into larvae *in utero*. This leads to the larvae killing the hermaphrodite mother and escaping from the body. As a result of this phenotype, there are more developed adults than eggs laid per individual. The *vps-35* deletion line exhibit premature vulval protrusions, suggesting muscular or neuromuscular impairments, preventing egg ejection. This phenotype is not shown in *vps-35[D638N]* further highlighting distinct mechanisms. Throughout the reproductive lifespan, the *vps-35[D638N]* heterozygotes show a reduced mean fertility compared to the wildtype, measured as mean egg number and developed adults from a mother. However this is not statistically significant (Figure 16 E). The *vps-35* deletion mutant exhibits a significantly reduced egg count, but not in the number of developed adults compared to the wildtype.

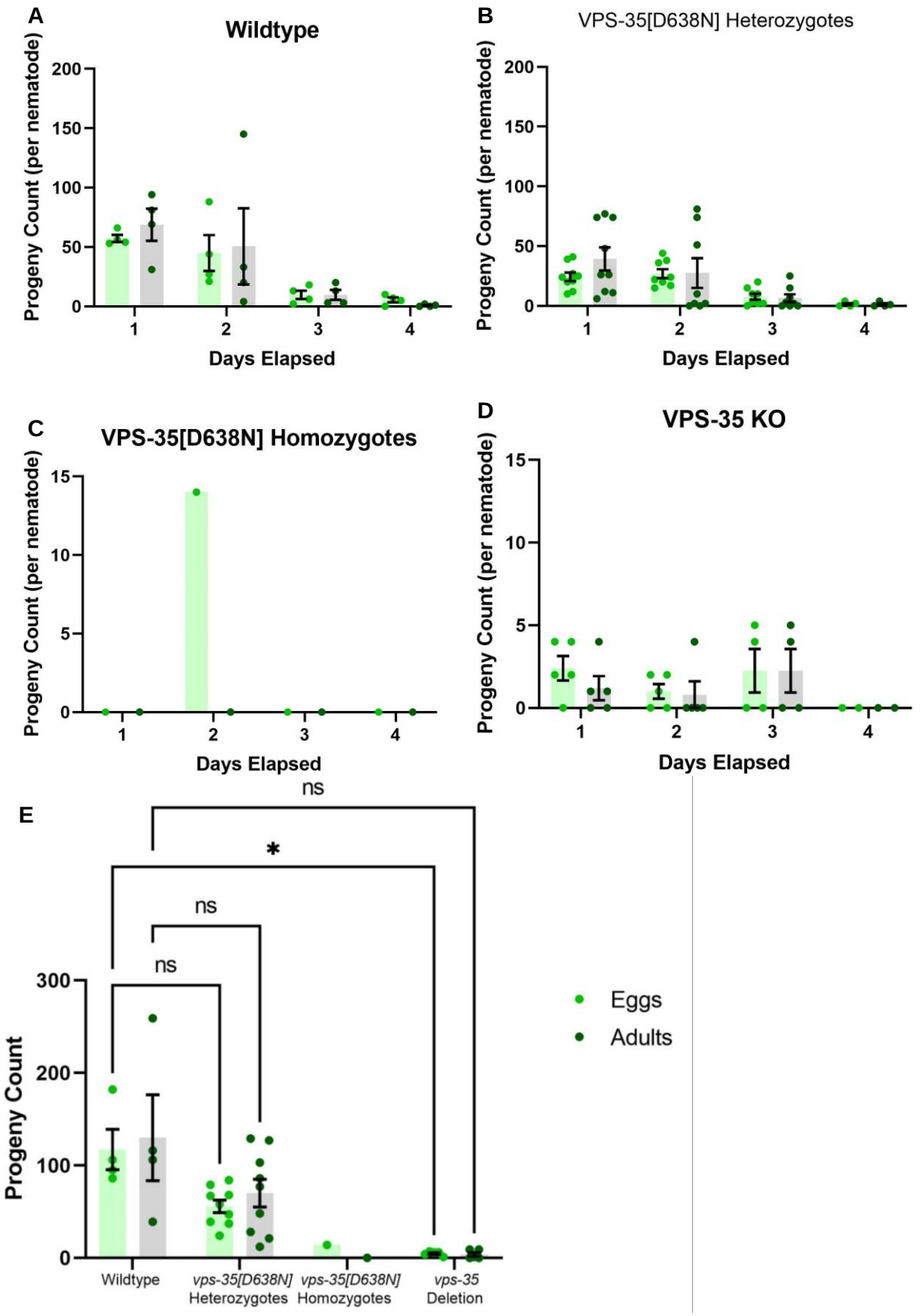

Figure 16- Fertility Assay for selected vps-35 mutants

Full descriptive statistics can be found in the supplementary 3.4.1, including mean and standard deviation for each gentoype, egg/adult progeny and day elapsed. Statistical analysis of total progeny count undertaken through two-way ANOVA, with stacked matching and assumed sphericity. Witin each column, rows were compared, with simple effects between columns compared, utilising Tukey's multiple comparisons test. Full descriptive statistics and P-values found in supplementary.

3.4.2 Optimised *vps-35* mutant progeny count

Following the first progeny count, this data was replicated, in order to further understand the effect of *vps-35* mutation upon fertility (Figure 17). In 3.4.1, the progeny count for the wildtype was substantially lower than anticipated, as a wildtype *C. elegans* hermaphrodite lay approximately 300 eggs. Furthermore, the balanced *vps-35[D638N]* line was not characterised in the preliminary count, as primarily, the egg laying patterns of the unbalanced line were characterised to understand the effect of potential homozygosity and further dissect the gene segregation studies data. Through contrasting the unbalanced and balanced line, we can further investigate and contrast the effect of consistent *vps-35[D638N]* heterozygosity in the progeny, to an unbalanced line in which there can be homozygous *vps-35[D638N]* and wildtype progeny. Alongside the progeny count, *in vivo* DiC confocal-like microscopy was undertaken on the uterus and reproductive system of age matched populations, to characterise any egg-laying impairments or egg morphology and number *in utero*. These are described in 3.5.

The wildtype *C. elegans* control utilised in this progeny count study illustrated a higher progeny count than in the preliminary test highlighted in 3.4.1 and is closer to the expected progeny count of *C. elegans* (Figure 17A). Furthermore, the egg laying and adult development was highest in day 2 of adulthood. Egg laying rate is included in the supplementary.

Balanced *vps-35[D638N]* heterozygotes show an increased mean adult progeny count compared to the unbalanced *vps-35[D638N]*, showing a similar fertility phenotype to the wildtype in day 2 and 3 of adulthood (Figure 17 B and C). This could suggest that homozygous *vps-35[D638N]* progeny in the unbalanced line could be laid at this developmental stage, as there are fewer developed adult progeny. Consistent with 3.4.1, *vps-35* deletion mutants show a distinct fertility phenotype from the *vps-35[D638N]* heterozygotes, with a low egg count and adult progeny (Figure 17D).

Analysis of the total progeny count have shed further insight into the fertility of selected *vps-35* mutants (Figure 17E). A notable observation, is that unbalanced *vps-35[D638N]* heterozygotes illustrate a significantly reduced number of developed adult progeny, compared to the wildtype, while the balanced *vps-35[D638N]* heterozygotes do not exhibit this significance. There is a greater variance of adult progeny in both *vps-35[D638N]* heterozygote populations compared to the wildtype, highlighting that the presence of this mutation may have an impact upon development, along with having significant impacts upon fertility in terms of egg laying. Consistent with 3.4.1, the *vps-35* deletion mutant shows a significantly reduced egg count and number of developed adult progeny.

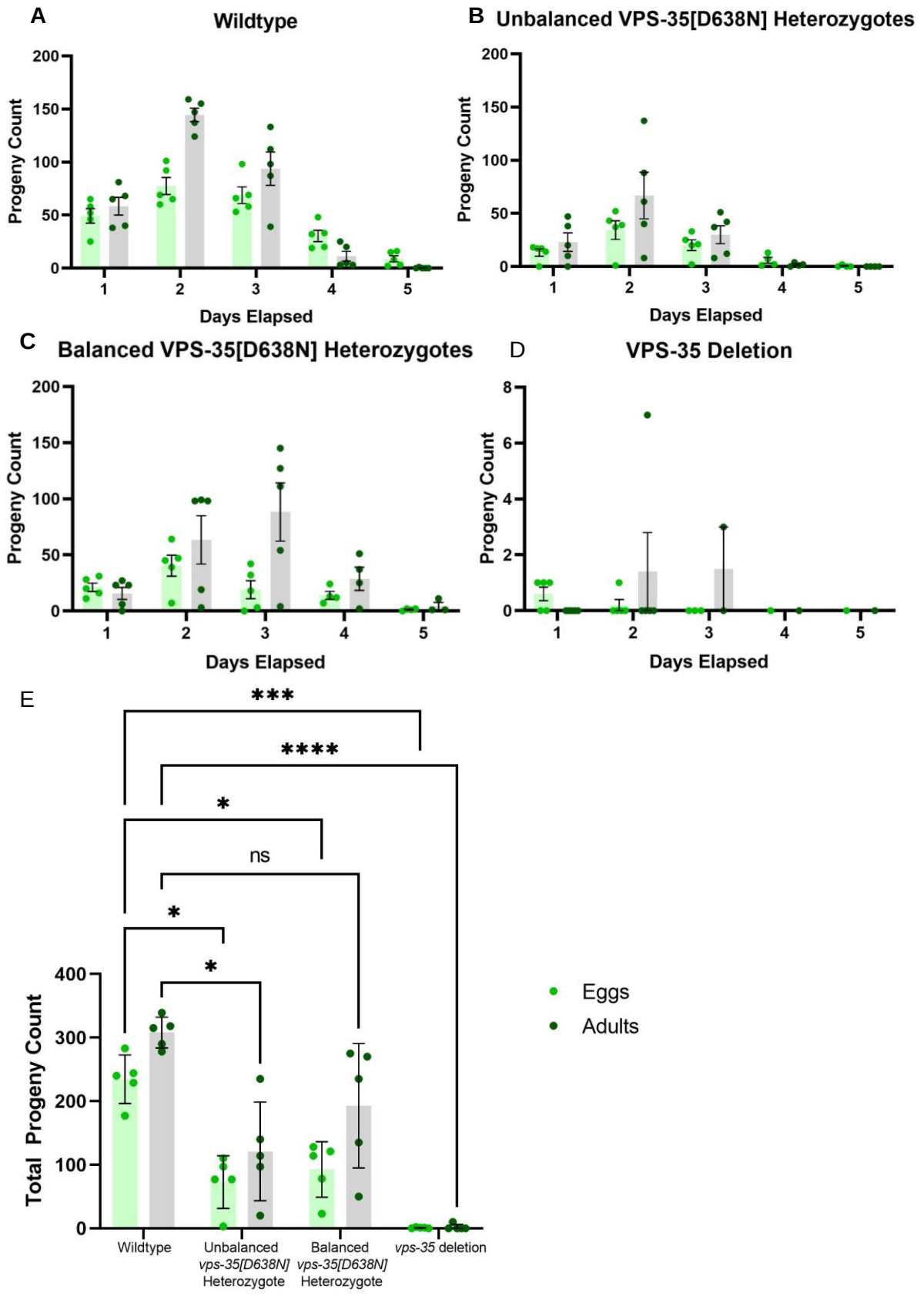

Figure 17- Optimised Fertility Assay of selected vps-35 mutants

Full descriptive statistics can be found in the supplementary 3.4.2, including mean and standard deviation for each gentoype, egg/adult progent and day elapsed. Statistical analysis of total progeny count undertaken through two-way ANOVA, with stacked matching and assumed sphericity. Within each column, rows were compared, with simple effects between columns compared, utilising Tukey's multiple comparisons test. Full descriptive statistics and P-values can be found in supplementary

3.5 Characterisation of the *vps-35* mutant germline *in utero*

Following the preliminary progeny count, detailed in 3.4.1, the *C. elegans* germline of selected *vps-35* mutants were studied through DiC *in vivo* confocal-like microscopy. The reproductive system is well developed, with identifiable structures and developing germline at L4 of larval development, so this stage was studied, along with day 1 of adulthood. At L4, the progenitor region is folded into the uterus epithelium, and the germ cells begin to differentiate along a folded path towards the developing spermatheca (331). By day 1 of adulthood, these germ cells form developed eggs, with fertilised eggs present between each spermatheca with the most developed ready for laying closest to the vulva (332).

3.5.1 No significant difference in germline development at L4 of larval stage

At L4 of larval stage, the stage prior to young adulthood, there is no notable difference in uterine morphology, mapped in green in figure 18. Early germline cells are present along the distal tips, with a similar density, highlighting that the *vps-35[D638N]* heterozygous and *vps-35* deletion mutants do not impair germline or reproductive development at this stage. A balanced *vps-35[D638N]* line was contrasted with the unbalanced utilised in the preliminary progeny count, as genotyping for mutation presence is challenging following microscopy. This data suggests that disruptions in cell biology because of these mutations may be later in egg developments or that there are impairments in egg laying, rather than impairments in early germline development.

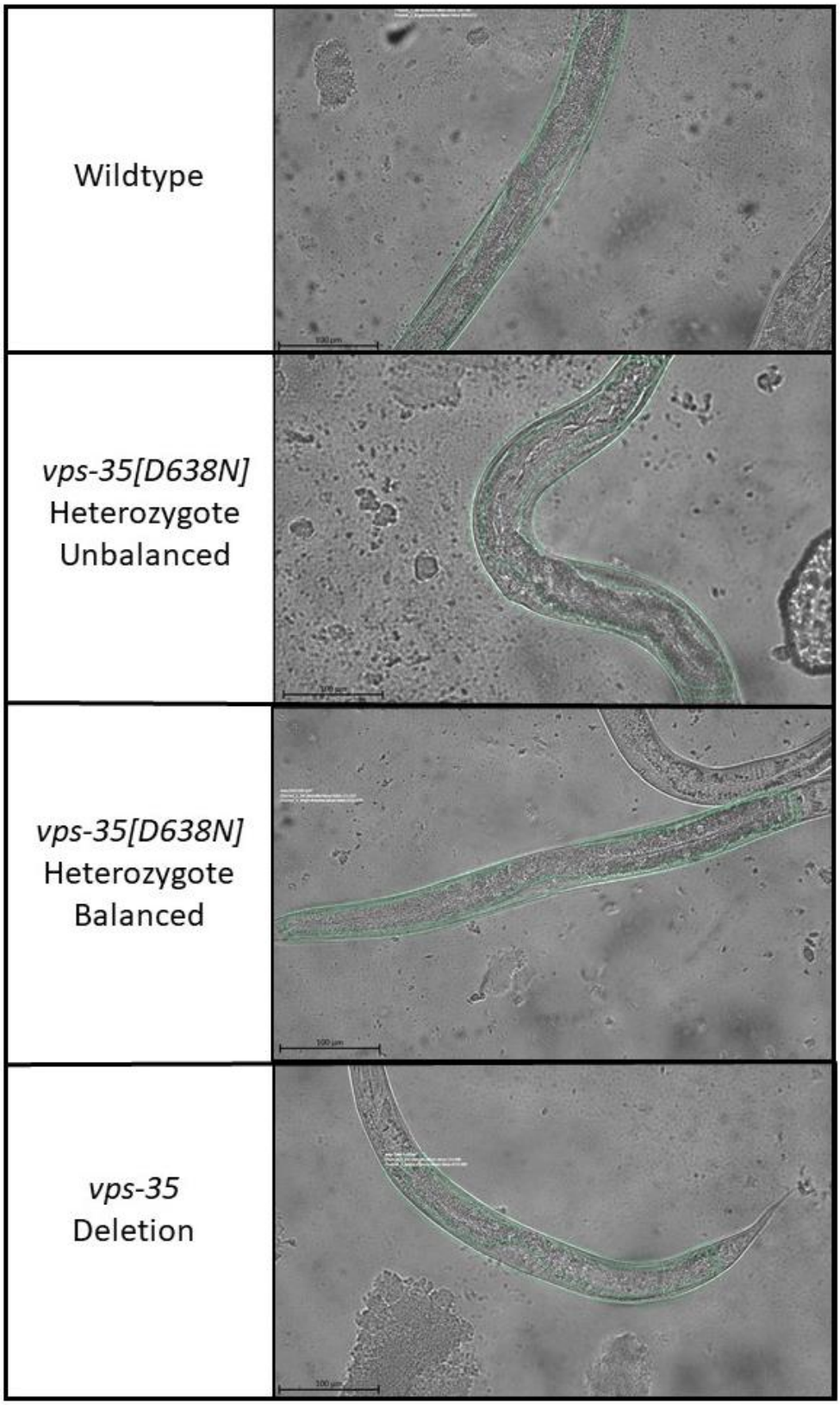

Figure 18-Reproductive tract and developing germline of vps-35 mutants at L4 stage of larval development

Images obtained utilising confocal-like DIC microscopy and studied utilising ZENBlue4.2 microscopy software. Diagram from WormBook (http://www.wormbook.org/chapters/www_introgermline/introgermline.html), detailing physiology of uterus and distal tips in late L4, utilised throughout study of microscopy images. Scale bar shows 100µm Uterine morphology encircled in green, distal tips encapsulating germline into uterus epithelia shown opposite uterus and vulva. Morphology is very similar between genotypes.

3.5.2 *vps-35* deletion show a 'cobblestone' phenotype of egg development *in utero,* while vps-35[D638N] show an atypical arrangement

Following DiC microscopy at day 1 of adulthood, the *vps-35* deletion shows abundant developed eggs *in utero,* illustrated in figure 23. However, these do not show a neatly stacked phenotype in the uterus, with newly fertilised eggs found adjacent to each spermatheca and mature eggs centred at the vulva, as shown consistently in the wildtype. The eggs in *vps-35* deletion mutants in utero are disordered, exhibiting a 'cobblestone' appearance. This demonstrates that *vps-35* deletion may not cause impairments in embryo development, but the issue may be due to egg ejection and laying, leading to retention of eggs *in utero,* which can lead to this disorganised appearance.

Similar to the *vps-35(ok1880)* deletion mutant, in *vps-35[D638N]* heterozygotes there is a disorganised appearance of eggs *in utero,* however this is not as severe as in deletion and there is still some stacking morphology present, similar to the wildtype, shown in figure 23. This suggests that reduced progeny count may be in part, due to issues in egg laying, convergent with the *vps-35* deletion model. However, the phenotype exhibited in *vps-35[D638N],* suggesting that loss of function in this mechanism may be partial, while gene segregation data and fertility of *vps-35[D638N]* homozygotes, show that homozygosity of *vps-35[D638N]* leads to larval arrest with incomplete penetrance.

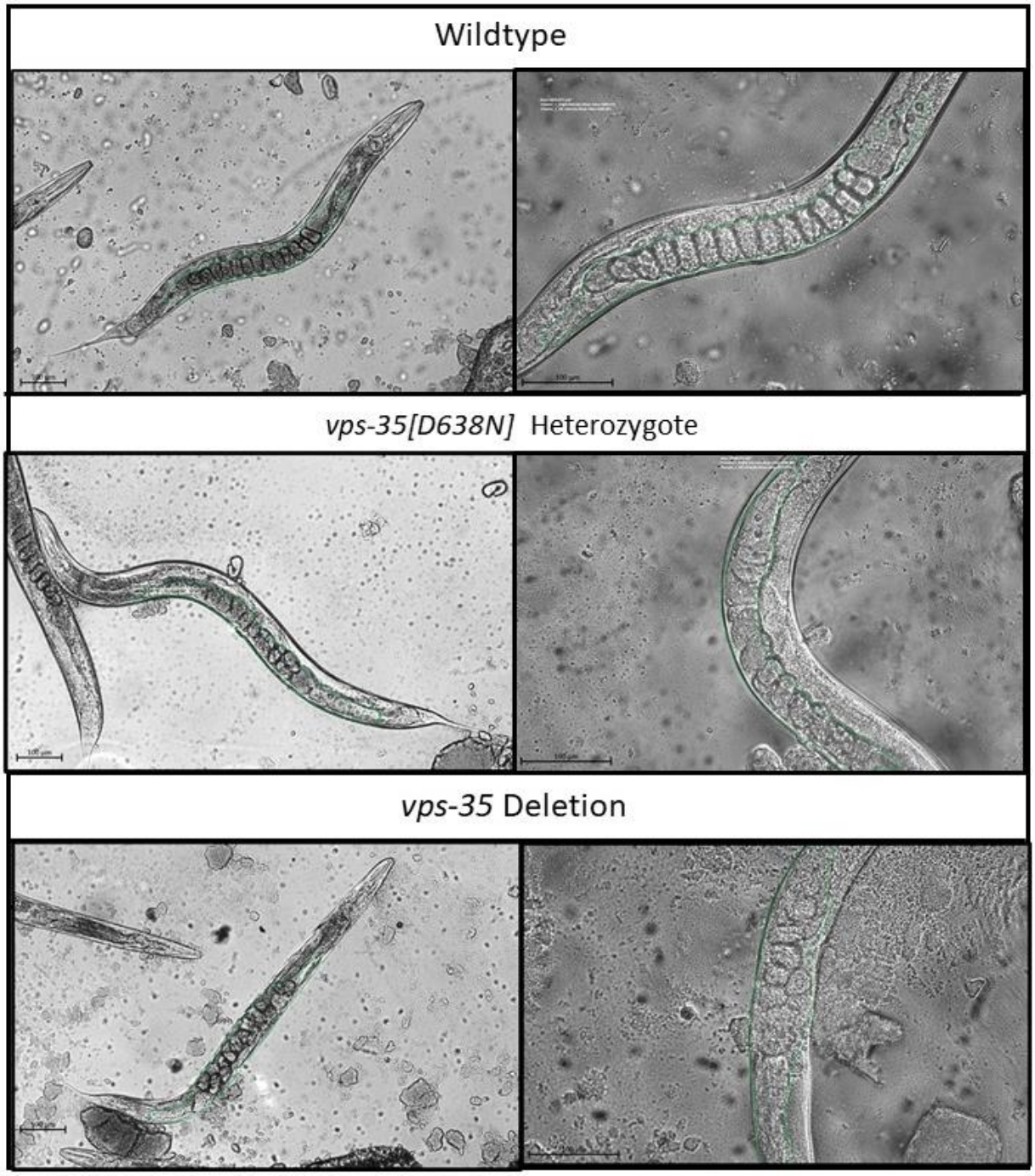

Figure 19- In utero morphology of developed eggs in day 1 adult vps-35 mutant C. elegans

Images obtained utilising confocal-like DIC microscopy and studied utilising ZENBlue4.2 microscopy software. Diagram obtained from WormBook (http://www.wormbook.org/chapters/www_introgermline/introgermline.html) , detailing physiology of uterus and distal tips, utilised throughout study of microscopy images. Eggs in the wildtype appear neatly stacked, with most developed eggs closest to the vulva. Unfertilised eggs (with nuclei, can be seen in the top left and bottom right of the 20x wildtype, with circular spermatheca adjacent. *vps-35[D638N]* show reduced organisation following fertilisation, *vps-35(ok1880)* deletion show no organisation, with mis-localised eggs in utero of different developmental stages.

3.5.3 Egg number *in utero* is not significantly different between wildtype and *vps-35* mutants

Quantification of visible eggs in utero illustrates that there is no significant difference in egg number between wildtype, *vps-35[D638N]* heterozygotes and *vps-35* deletion models. However, the *vps-35(ok1880)* deletion has a higher mean egg number in utero and greater variance in this This suggests that deletion of *vps-35* does not impair cellular development in embryogenesis and that the impairment is in egg laying. Furthermore, this suggests that in *vps-35[D638N]* heterozygosity, 1 wildtype allele is sufficient to rescue fertility phenotypes shown in homozygous *vps-35[D638N]*, but there may be a partial loss of function in egg laying.

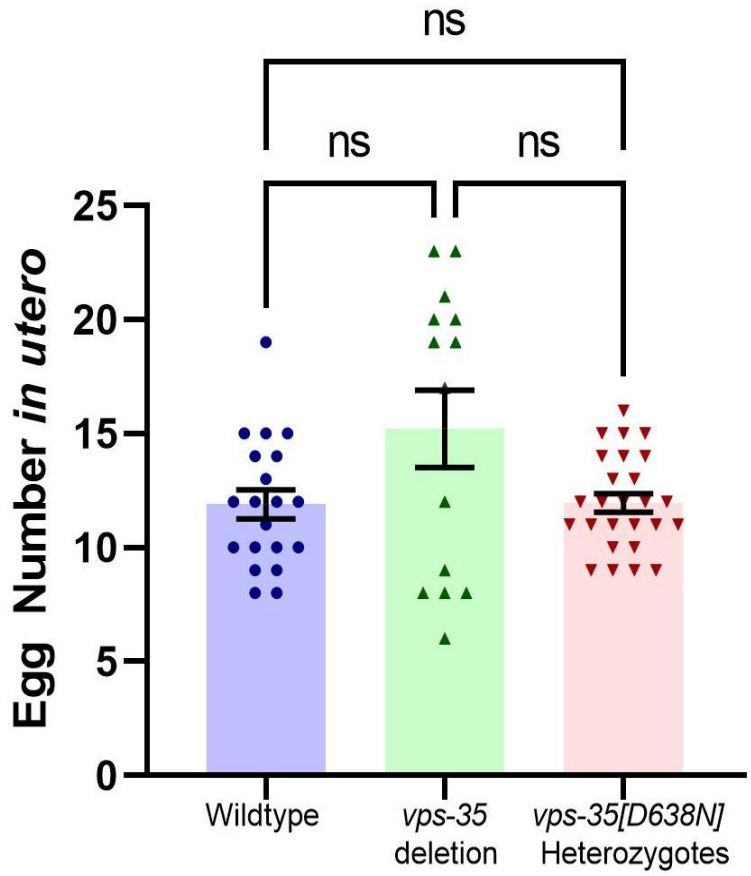

Figure 20-Egg number in utero for vps-35 mutants

Full descriptive statistics and P-Values found in supplementary 3.5.4. Brown-Forsyth and Welch ANOVA undertaken, for multiple comparisons. Egg number in utero manually counted, using image analysis in ZENBlue4.2 microscopy Data obtained from day 1 adult *C. elegans* microscopy images.

3.5.4 *In vivo* microscopy concurrent with 3.4.2 optimised progeny count

Following optimisation of the *vps-35* progeny count, brightfield microscopy was undertaken with age matched animals in day 1 of adulthood. Consistent with 3.5.2-3, the wildtype shows a neat stacking of eggs in utero. The unbalanced *vps-35[D638N]* heterozygote line, utilised in 3.5.2-3, coherently somewhat shows this stacking, but with more disorganised phenotype than the wildtype. Furthermore, the balanced *vps-35[D638N]* line illustrates a stacked phenotype similar to the wildtype, suggesting that the disorganised phenotype shown in the unbalanced line could be due to the mixed *vps-35* genotype in the progeny of the unbalanced line, or specific defects in egg laying. The *vps-35* deletion mutant shows a disorganised 'cobblestone' phenotype of eggs in utero, and in this microscopy, it is visible that the eggs closest to the vulva are at the 3-fold stage of embryonic development. This stage occurs approximately 600 minutes after fertilisation and occur 200 minutes prior to egg hatching. In wildtype *C. elegans*, eggs are laid at the gastrulation stage of development, which occurs between 100 and 300 minutes after fertilisation. This further demonstrates that *vps-35* deletion mutants have a delayed egg laying defect, leading to bagging.

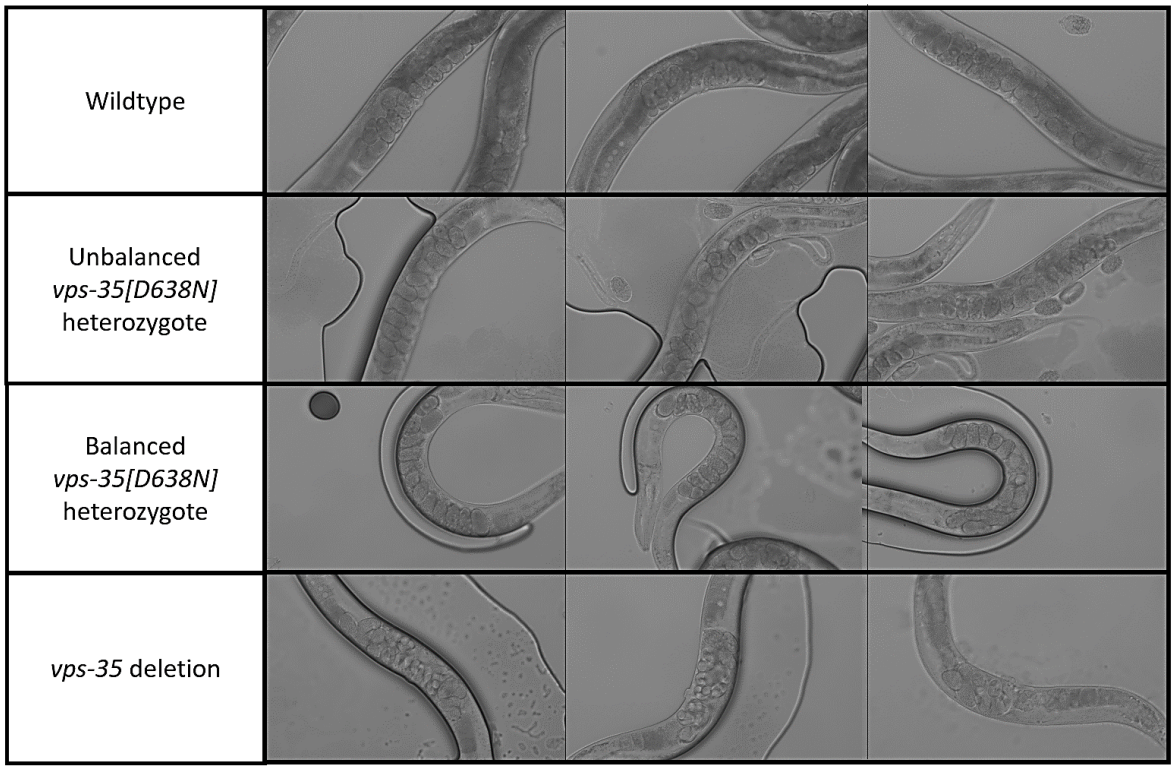

Figure 21- Optimised egg morphology in utero of vps-35 mutants

Images collected through brightfield DIC microscopy and analysed utilising ZenBlue4.2. 20x images captured for analysis. Day 1 adult *C. elegans* in images. *C. elegans* with *vps-35(ok1880)* deletion show eggs with larval development, close to hatching, further supporting the bagging phenotype, this is not illustrated in the balanced or unbalanced *vps-35[D638N]* lines. Wildtype shows a greater quantity of organised eggs *in utero*, further supporting the reduced egg laying phenotype in day 1 in *vps-35[D638N]* heterozygotes.

3.6 *vps-35* deletion mutants show a significantly reduced life and health span

3.6.1 vps-35 deletion show a significantly reduced lifespan

Lifespan can be a marker of overall health in *C. elegans* models and can be used to assess the effect of selected mutations upon ageing. Disease linked mutations frequently lead to deleterious impacts upon C. elegans longevity, especially when the gene of interest has no compensatory mechanism (27). 45-60 *C. elegans* per mutant line were assayed for survival on E. coli OP50 seeded FUDR NGM plates, over the course of up to 30 days. Two replicates were undertaken, with consistent findings between them. Full descriptive, tabulated lifespan and statistics are detailed in the supplementary 3.6.

Heterozygous mutant *vps-35*[D638N] in both the unbalanced and balanced form displayed no significant difference in lifespan compared to the wildtype. Furthermore, individuals with the VPS35[D620N] mutation develop Parkinson's in late adulthood at a mean age of 52 (3), with PD duration ranging from 6-31 years in affected individuals within a family (333), suggesting that VPS35[D620N] does not significantly reduce the age of death. This further illustrates the relevance of the *vps-35[D638N]* model for further understanding VPS35 PD.

In contrast, the *vps-35* deletion mutant model, showed a significantly reduced lifespan compared to wildtype and the *vps-35[D638N]* model. FUDR treatment prevented progeny development in this assay, eliminating the bagging phenotype, a frequent cause of *vps-35* deletion *C. elegans* death in day 2-4 of adulthood, however the lifespan of *vps-35* deletion *C. elegans* are still significantly shorter than the wildtype. This suggests that complete loss of *vps-35* function leads to reduced lifespan, however the *vps-35[D638N]* does not exhibit this phenotype, further implicating that complete loss of VPS-35 function is not the mechanism of *vps-35[D638N]* action.

Figure 22-Lifespan of VPS-35[D638N] heterozygote and VPS-35 deletion C. elegans populations

Analysis undertaken through Kaplan-Myer plot of survival, followed by curve comparison for statistical significance, through Mantel-Cox and Gehan-Breslow-Wilcoxon tests. Full descriptive statistics exhibited in supplementary 3.6

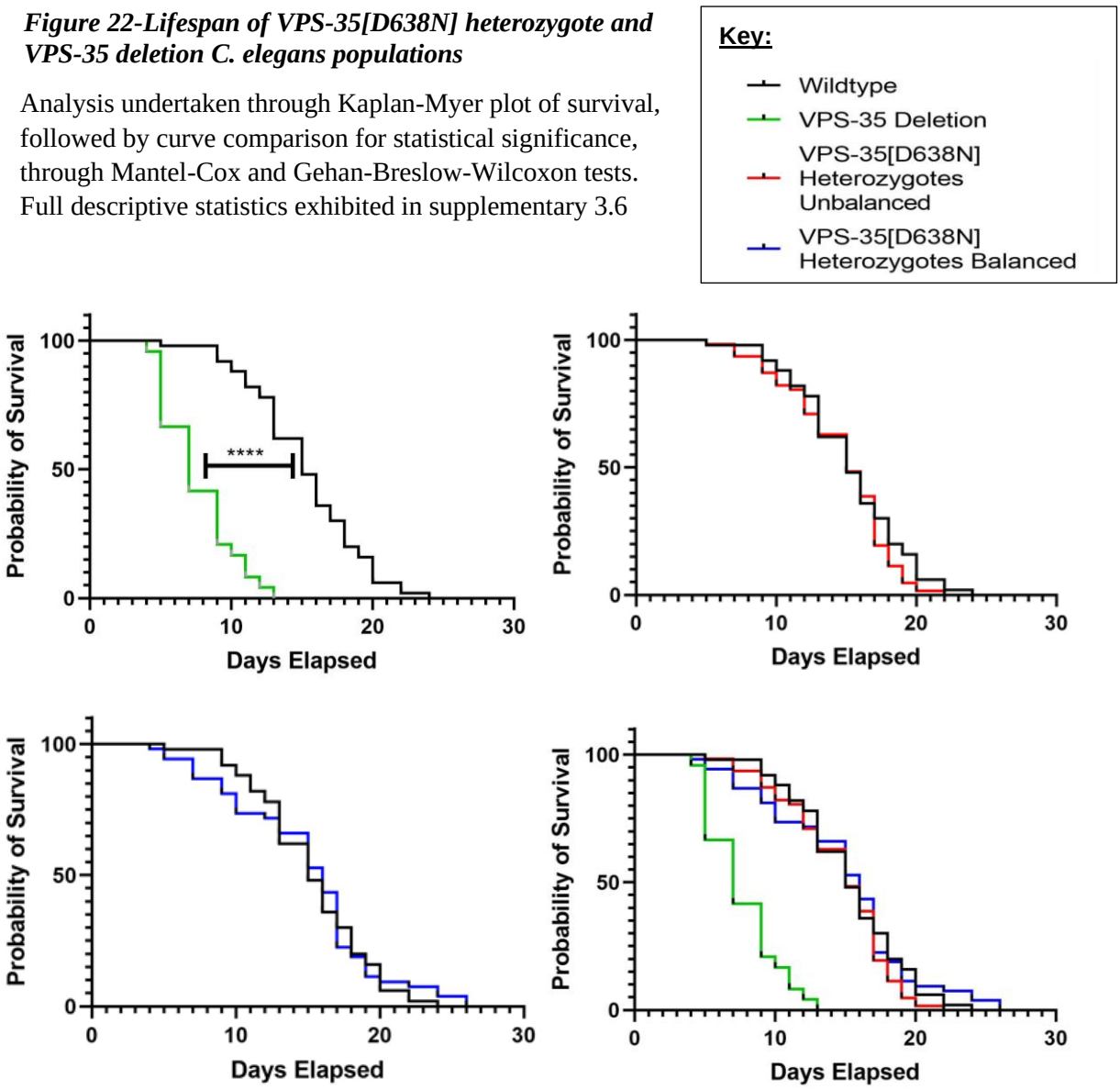

3.6.2 vps-35 deletion show a significantly reduced crawling speed

In recent years, lifespan analyses of *C.elegans* have become more sophisticated to incorporate health span measurements, such as motility (250,334,335). This gives a higher resolution to the phenotypes shown bey specific mutations, upon organism health and ageing, as health span is not always proportional to lifespan (336). through measuring the motility of *C. elegans*, a greater understanding of the mutation upon health rather than just its impact upon survival can be developed.

Previous study of these lines have likewise indicated that *vps-35* deletion models show reduced crawling speed, compared to wildtype, while *vps-35[D638N]* do not show any significant difference in day 1 of adulthood (Figure 23). This suggests that global health is not as affected by *vps-35[D638N]*, while *vps-35* deletion severely effects health. As seen in 3.5, *vps-35* deletion exhibits substantial impairments in egglaying leading to 'bagging',. By day 2 of adulthood, approx. 40% of *C. elegans* within a population show vulval protrusions, a phenotype associated with ageing and muscle weakness in *C. elegans* . The severity of this phenotype suggests that deletion of *vps-35* leads to severe muscular impairments, leading to reduced motility, exhibited in the significantly slower crawling speed of day 1 adult *vps-35* deletion *C. elegans*, despite sterilisation with FUDR. This is a distinct phenotype from the *vps-35[D638N]* heterozygotes.

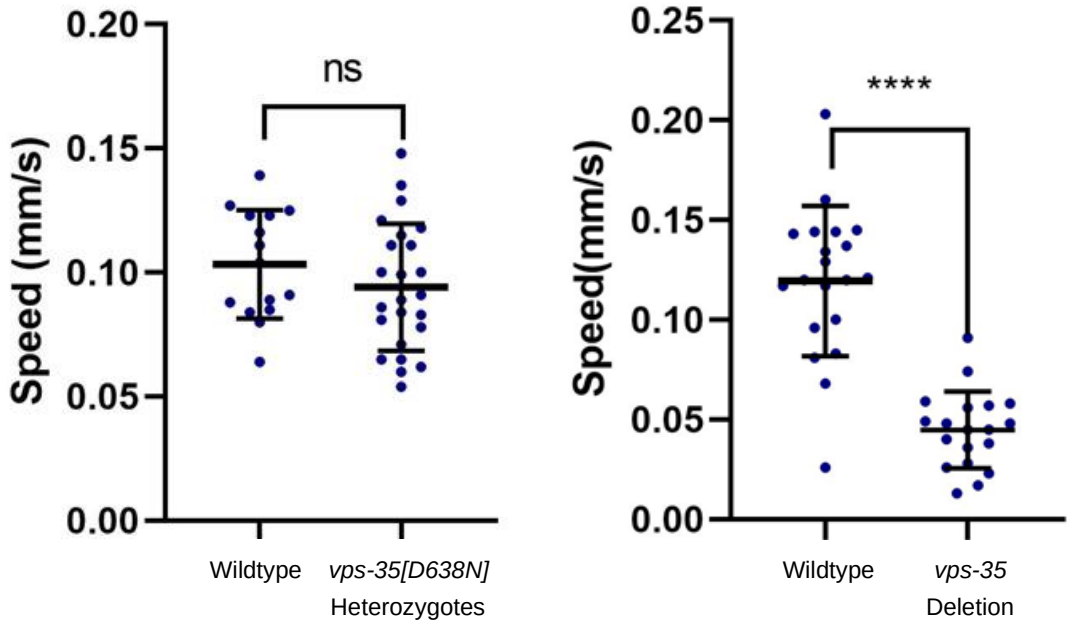

Figure 23-Crawling Speed of Day 1 Adult vps-35[D638N] heterozygotes

20-30 day 1 adult C. elegans were assayed. This experiment was undertaken prior to strain balancing and individuals from heterozygous populations were immediately taken for DNA extraction and genotyping following data collection in the instance of vps-35[D638N]. Descritive staistics and P-values of unpaired two-tailed T-test found in supplementary

3.7 Novel *vps-35*[D638N] heterozygotes show impaired dopaminergic behaviours

3.7.1 Establishment of the basal slowing response as a dopaminergic output

The basal slowing response, as described by Sawin et al (86), is a mechanosensory behavioural output modulated by the 4 CEP and 2 ADE dopaminergic neurons found in the *C. elegans* head. To establish basal slowing as a relevant dopaminergic output for study in the Kevei lab, a pharmacological assay with dopaminergic mutant was devised and optimised. The *C. elegans* strain *cat-2(n4547)* carries a deletion mutation in the gene encoding for the tyrosine hydroxylase deletion. This is a key enzyme implicated in the biosynthesis of dopamine, converting L-tyrosine to L-DOPA. Consequently, this mutant has ablated dopamine signalling activity, acting as a negative control. The dopaminergic basal slowing phenotype was validated following treatment with dopamine hydrochloride, the treatment conditions of which were optimised.

3.7.1.1 Treatment of *cat-2(n4547)* with dopamine for 24 hours improves the basal slowing response

A preliminary study was undertaken, in which day 1 adult *cat-2(n4547)* mutants were treated with 50mM dopamine hydrochloride for 16 hours overnight prior to assay (Figure 24). There is a great diversity in the basal slowing of the *cat-2(n4547)* population- previous groups have demonstrated that due to defective dopamine signalling, this line has abnormally high, or low average speeds and had impairments in speed adjustment, in the presence and absence of nutrients (337). Dopamine treatment demonstrated that the basal slowing response is significantly improved, from 40.48% to 68.72% following dopamine hydrochloride treatment. Following this assay, the dopamine administration period was tested and optimised in conjunction with a wildtype control.

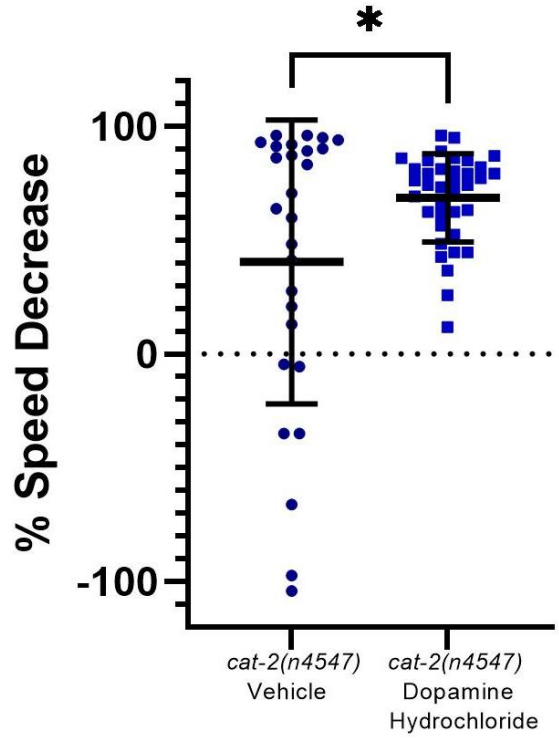

Figure 24-Basal Slowing Response of cat-2(n4547) treated with 50mM Dopamine Hydrochloride for 24 hours

20-40 day 1 adult *C. elegans* per condition utilised. % slowing was calculated by speed upon reaching bacteria/ unseeded control. Percentage slowing calculated by multiplying this value by 100, then 100- this number. Descriptive statistics, along with P values for Two-tailed unpaired T-test with Welch's correction found in supplementary.

3.7.1.2 Treatment of *cat-2(n4547)* with dopamine hydrochloride for 4 hours significantly rescues impairments in basal slowing

Wildtype *C. elegans* and *cat-2*(n4547) were assayed, following 4 hour treatment with 50mM dopamine hydrochloride and a vehicle, in this instance sterile deionised water. This time period is a closer model to dopamine therapeutics such as L-DOPA for PD, which are administered 3-5 times daily. There was no significant difference in slowing in vehicle and dopamine treated wildtype mutants, with a mean vehicle basal slowing response of 79.16%. The vehicle treated *cat-2(n4547)* mutant had an ablated basal slowing response of -17.34%. This phenotype was rescued to 79.82% following dopamine treatment. The dopamine hydrochloride treated *cat-2(n4547)* demonstrates almost identical basal slowing response to the wildtype and has a much smaller standard deviation than the 24 hour treatment detailed in 3.7.1.1, illustrating that 4 hours is optimal, after 24 hours dopamine may have been metabolised and excreted by the time of assay. This experiment verifies that basal slowing is a valid output for investigating dopaminergic behavioural phenotypes.

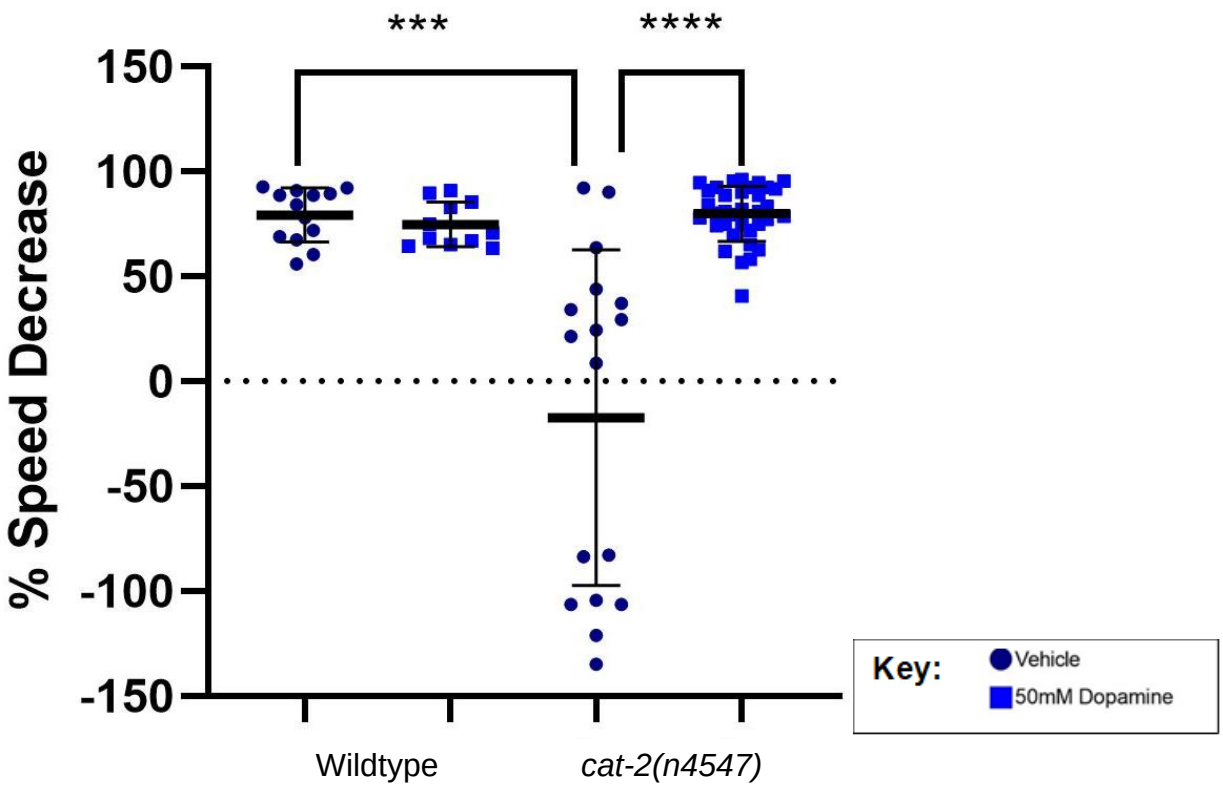

Figure 25-Basal Slowing Response of cat-2(n4547) mutant treated with 50mM Dopamine for 4 hours

15-30 day 1 adult worms were assayed per line and treatment. % slowing was calculated by speed upon reaching bacteria/ unseeded control. Percentage slowing calculated by multiplying this value by 100, then 100- this number. Descriptive statistics, along with P value for One way ANOVA with Brown-Forsyth Correction, performed between selected datasets.

3.7.2 *vps-35[D638N]* heterozygotes show impairments in the dopaminergic basal slowing response

The basal slowing response has been extensively tested in the novel *vps-35[D638N]* heterozygous mutants, as a behavioural readout for dopaminergic function. Consistently, the *vps-35[D638N]* heterozygote has shown impairments in the basal slowing response, suggesting the mutation has implications in dopaminergic function in our novel *C. elegans* model.

3.7.2.1 Unbalanced *vps-35[D638N]* show impaired basal slowing on day 1 of adulthood

Preliminary experiments illustrated that unbalanced *vps-35[D638N]* heterozygotes show an impaired basal slowing response in day 1 of adulthood, 66.87% compared to the wildtype 88.86%, with a greater standard deviation of individual variance, suggesting dysfunction of dopaminergic neuron signalling. As described in 3.7, *vps-35[D638N]* heterozygotes do not show any difference in crawling speed, suggesting these impairments are specific to the dopaminergic neuronal system.

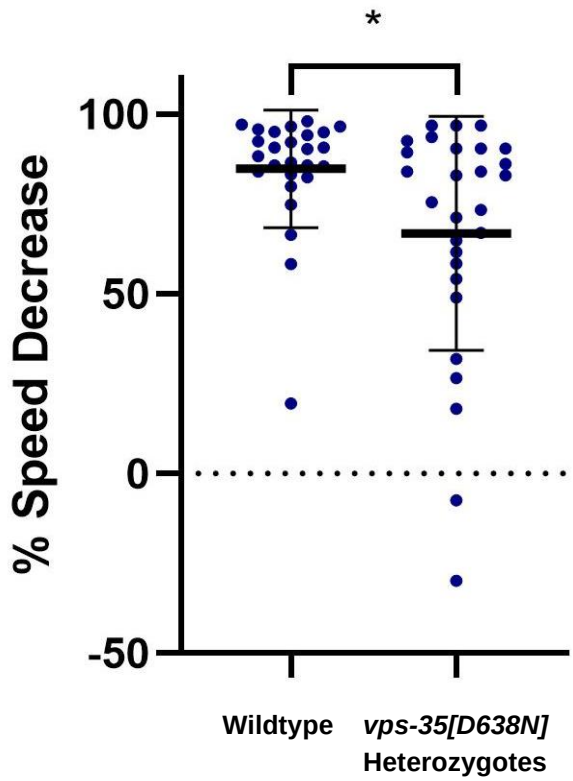

Figure 26-Basal Slowing Response of Day 1 Adult VPS-35[D638N] Heterozygote

20-30 day 1 adult worms were assayed. This experiment was undertaken prior to strain balancing, worms for heterozygous population were immediately taken for DNA extraction and genotyping following data collection. % slowing was calculated by speed upon reaching bacteria/ unseeded control. Percentage slowing calculated by multiplying this value by 100, then 100- this number. Descriptive statistics and P values of two-tailed t-test found in the supplementary.

3.7.2.2 Balanced *vps-35[D638N]* heterozygotes exhibit age exacerbated impairments in the basal slowing response in day 1 and 5 of adulthood, rescued by dopamine treatment

Following the development of the balanced heterozygous *vps-35[D638N]* line, the basal slowing response was extensively tested in day 1 and day 5 of adulthood, alongside the *cat-2(n4547)* as a negative control (Figure 27). Day 5 is the optimum stage to look at the effect of ageing upon the basal slowing response, as between day 5 and day 10, aged *C. elegans* slow in their motility for the remainder of their lifespan (94), remaining on bacterial food sources and therefore challenging to assay a basal slowing response. Furthermore, the basal slowing responses were assayed in conjunction with dopamine hydrochloride treatment, in order to further clarify if any exhibited phenotypes in our novel PD mutants were modulated by dopamine. Crawling speeds are included in the supplementary.

As illustrated in figure 27A, the balanced *vps-35[D638N]* heterozygote exhibits a significantly impaired basal slowing response of 63% compared to the wildtype 91% in day 1 of adulthood, coherent with preliminary studies undertaken utilising the unbalanced line in 3.7.2.1. When treated with 50mM dopamine hydrochloride for 4 hours, the day 1 adult *vps-35[D638N]* heterozygotes exhibit a significantly rescued basal slowing response of 86%. Consistent with 3.8.1, the *cat-2(n4547)* tyrosine hydroxylase deletion mutant exhibits a significantly impaired basal slowing response, also rescued by dopamine hydrochloride treatment. This suggests that the impairments shown in the basal slowing response in the *vps-35[D638N]* heterozygous mutant are modulated by dopaminergic impairments. That they can be rescued by administration of exogenous dopamine administration suggests our novel model may be relevant for PD modelling of VPS35 function and notably, people with VPS35[D620N] mutation consequent PD are responsive to L-DOPA therapeutics (103,104).

This experiment was repeated in day 5 of adulthood (Figure 27B), utilising individuals from the same populations as assayed in day 1. A significantly impaired basal slowing phenotype was shown in the *vps-35[D638N]* mutant line, of 17% compared to the wildtype basal slowing response of 71%. Administration of dopamine hydrochloride significantly rescued the basal slowing response of *vps-35[D638N]* heterozygotes to 65%. However, the spread of data and the standard deviation of the treated *vps-35[D638N]* in day 5, is much larger than in day 1 of adulthood. This suggests that there is not as strong an effect and individual *C. elegans* may have further impairments in their dopaminergic neurons, which cannot be as readily rescued with dopamine treatment. This further adds to the potential relevance of our model, as L-DOPA therapeutics in people with VPS35[D620N] PD are less effective at managing symptoms with condition progression (103,104), in which remaining dopaminergic neurons have been lost or impaired.

In day 1 of adulthood, the vps-35[D638N] shows a 63% basal slowing response, exacerbated when aged to day 5 to 17% (Figure 27C). Wildtype worms showed a significant reduction in the strength of their basal slowing response, from approx. 91% to 71% with age in these experiments. This progressive ageing phenotype is significantly exacerbated in the *vps-35[D638N]* mutant. Alongside these, we also tested the tyrosine hydroxylase knockout as a negative control. This showed a severely impaired basal slowing response in day 1 of adulthood, not significantly exacerbated with age. This is due to the genetically induced absence of dopamine biosynthesis, which ablates the response through the lifespan. This data further demonstrates that our novel *vps-35[D638N]* heterozygotes shows an impaired dopaminergic phenotype, exacerbated with age and may be a relevant phenotype to test in future characterisation studies, along with augmenting the potential relevance of the novel *vps-35[D638N]* heterozygote in PD modelling.

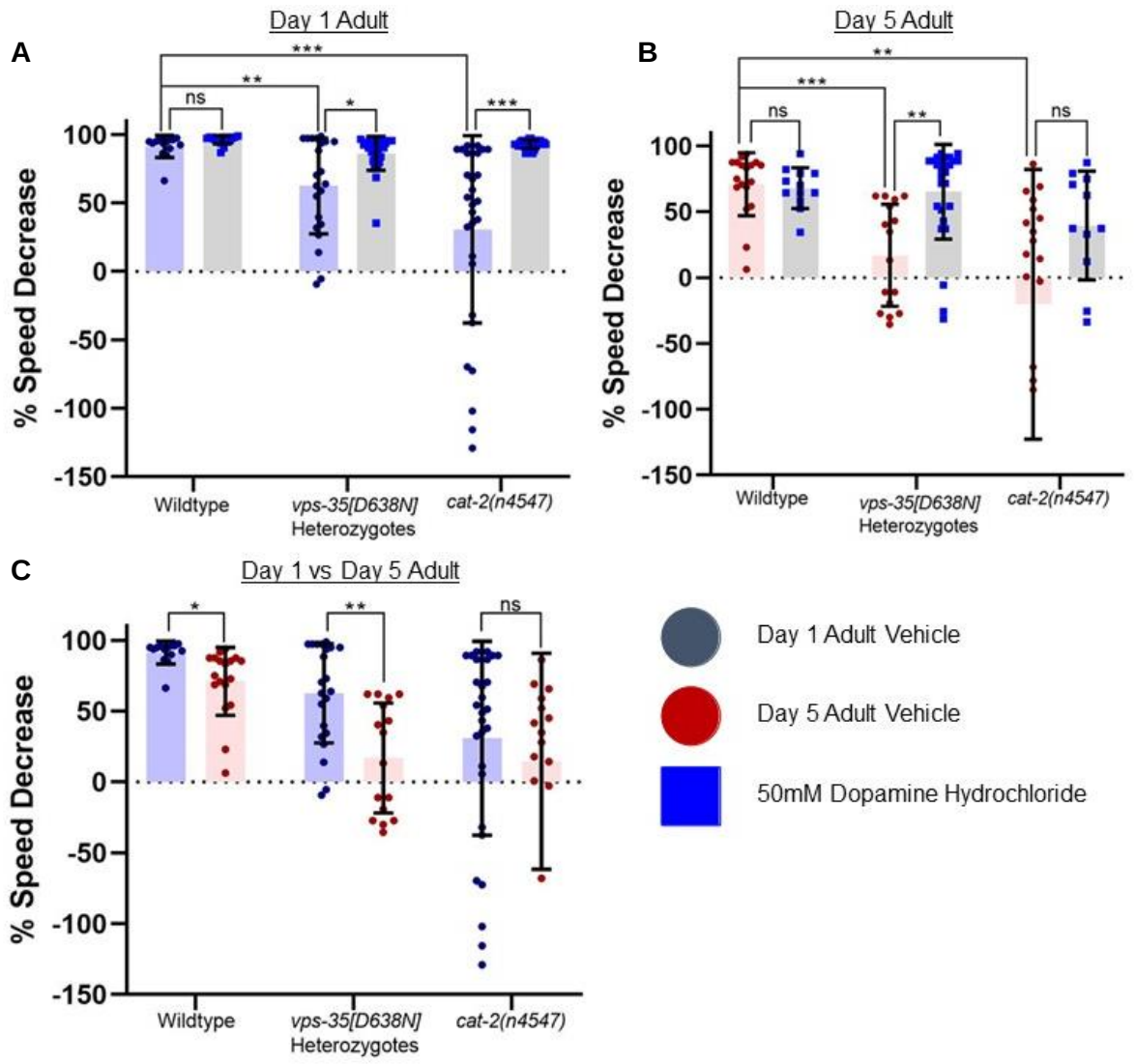

Figure 27- Balanced vps-35[D638N] heterozygotes exhibit an impaired basal slowing response in day 1 of adulthood, rescued by dopamine treatment

10-30 day 1 or day 5 adult worms were assayed per line and treatment. % slowing was calculated by speed upon reaching bacteria/ unseeded control. Percentage slowing calculated by multiplying this value by 100, then 100- this number. Descriptive statistics and P-values from One way ANOVA with Brown-Forsyth Correction detailed in the supplementary.

3.7.3 *C. elegans* with deletion of *vps-35* do not show impairments in the basal slowing response

The *vps-35* deletion model *vps-35(tm1880)* has been characterised in terms of the basal slowing response, in order to contrast a total loss of function model with our novel vps-35[D638N] heterozygote line, to shed further mechanistic insight into its mode of action.

3.7.3.1 *vps-35* deletion *C. elegans* do not show any significant difference in basal slowing in day 1 of adulthood

Preliminary experiments illustrated that *vps-35(ok1880)* does not show an impaired basal slowing response (Figure 28). However, its crawling speed is significantly lower than the wildtype, suggesting potential global, muscular effects of the deletion. Compared to the wildtype, *vps-35[D638N]* has no significant difference in crawling speed to wildtype, suggesting that mutation induced impairments may be localised to dopaminergic neurons, contrary to the VPS-35 deletion, suggesting distinct mechanisms.

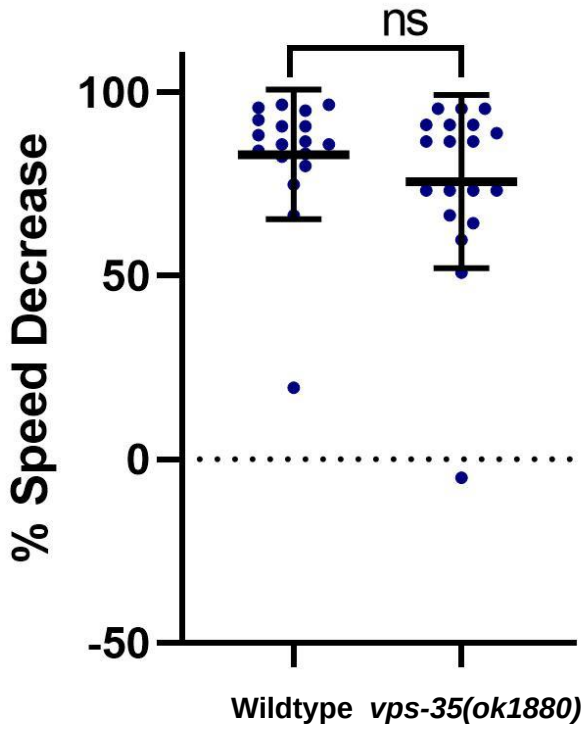

Figure 28-Basal Slowing Response of VPS-35(tm1880) deletion mutant

10-20 day 1 adult worms assayed, descriptive statistics found in the supplementary, along with P-values of unpaired, two tailed T-test.

3.7.3.2 *vps-35* deletion mutants do not show an impaired basal slowing response in day 1, but exhibit an impaired response following dopamine treatment

In day 1 of adulthood, *vps-35* deletion mutants do not show an impaired basal slowing response, as illustrated in figure 29, coherent with 3.7.3.1. Following dopamine treatment, the *vps-35* deletion mutant shows a significantly worsened basal slowing response, divergent to the phenotypes exhibited by *vps-35[D638N]* heterozygotes in 3.7.2.

In day 5 of adulthood, *vps-35* deletion mutants do not show an impaired basal slowing response and dopamine treatment has no impact upon this. However, there are important limitations to this data. As mentioned, *vps-35* deletion lines show a significantly reduced lifespan and healthspan compared to the wildtype. As a result of this, few replicate animals were available at day 5 of adulthood. Furthermore, effectively assaying the basal slowing response for a comparable reading to the wildtype is very challenging when the selected mutant line has a very low baseline motility, upon which the crawling speed upon reaching nutrients is compared.

The *vps-35* deletion mutant does not show a significantly impaired basal slowing response compared to the wildtype. Furthermore, the *vps-35* deletion does not show any significant reduction in the basal slowing response between day 1 and day 5 of adulthood. However, this is limited by the motility of the line, further details on the crawling speeds for this experiment are detailed in the supplementary.

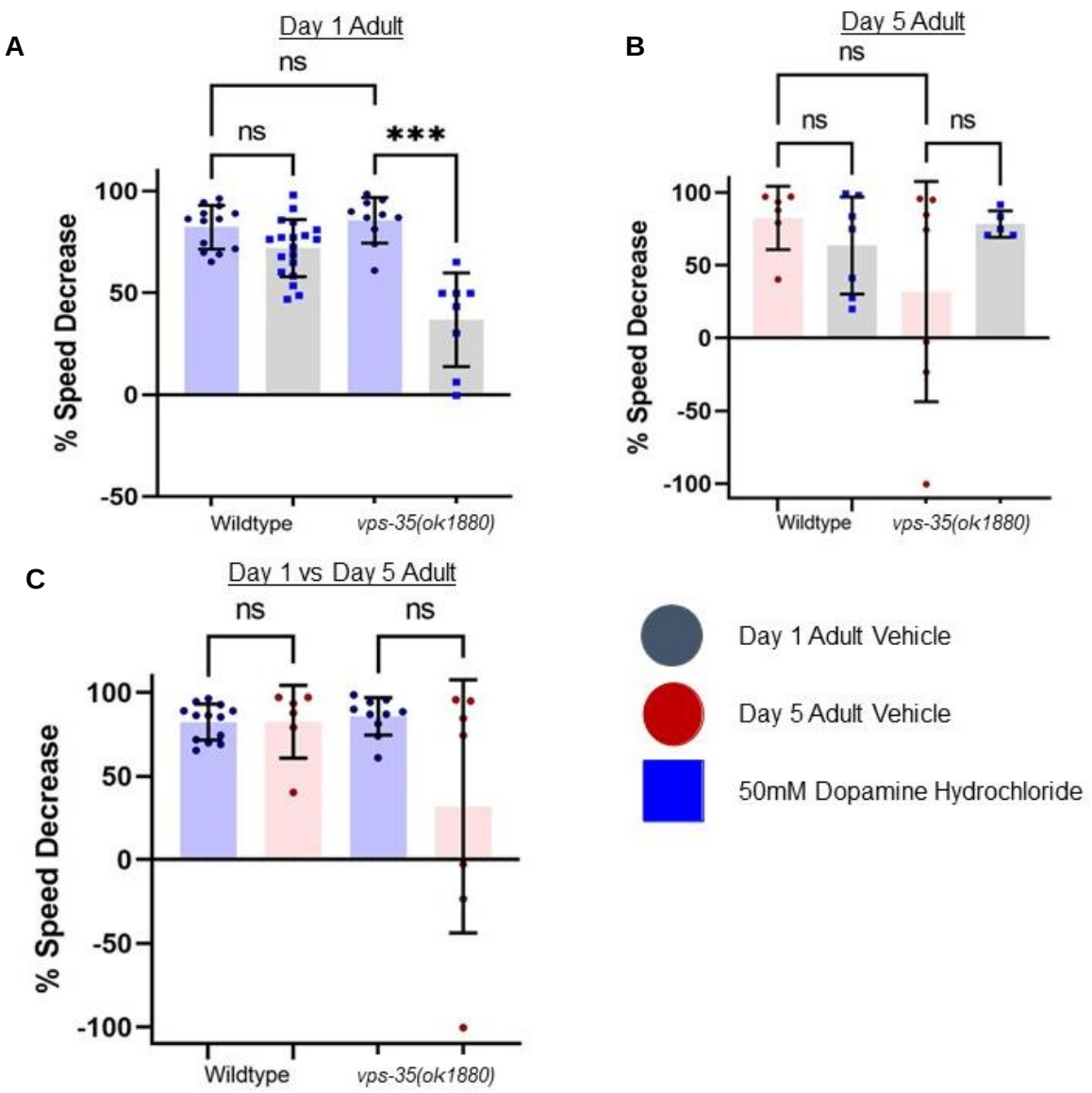

Figure 29-vps-35 deletion mutants do not show an impaired basal slowing response in day 1, but exhibit impairments following dopamine treatment

8-20 day 1 or day 5 adult worms were assayed per line and treatment. 10-30 day 1 adult worms were assayed per line and treatment. % slowing was calculated by speed upon reaching bacteria/ unseeded control. Percentage slowing calculated by multiplying this value by 100, then 100- this number. Descriptive statistics and P-values from One way ANOVA with Brown-Forsyth Correction detailed in the supplementary.

3.8 Cellular Phenotypes of *vps-35* mutants

C. elegans are highly amenable to the utilisation of fluorescent dyes, inferring functionality of multiple organelles and cellular pathways, utilising *in vivo* microscopy. Furthermore, *C. elegans* lysates can be utilised for immunoblotting for the presence and quantification of proteins of interest. These have been explored in the *vps-35* mutants, in terms of mitochondrial staining to infer function, lipid staining to infer lysosomal function and DiI amphid neuronal staining to infer cilia/endocytic function.

3.8.1.1 Inference of mitochondrial function through TMRE staining and optimisation of utilised protocol

Mitochondrial membrane potential can be a marker to infer potential mitochondrial function (338) and can be studied through quantifying the fluorescence of the electron gradient sensitive dye TMRE in selected *C. elegans* strains. Prior methods for TMRE uptake in *C. elegans* involved transferring L4 *C. elegans* to *E. coli* OP50 seeded NGM plates containing 1μM TMRE in the media, incubating for 24 hours and de-staining on a seeded NGM plate without TMRE for 1 hour prior to imaging (90). However, in multiple preliminary experiments this was unsuccessful in mitochondrial staining, with dye uptake consistently not illustrated upon microscopy.

To overcome this, method optimisation was undertaken utilising wildtype *C. elegans* under six different culturing conditions. Two populations were treated with 10μM TMRE in the NGM plates, utilising the same method as described above, with one population treated from L1 of development, to enable a 72-hour incubation. Four populations were trialled utilising an alternative method, in which TMRE was introduced into the *E. coli* OP50 prior to plate seeding, at a concentration of 1μM and 10μM. Plates were incubated for 16 hours overnight at 37ºC, for bacterial lawn growth, two *C. elegans* populations at L1 and two at L4 were transferred the following day.

Prior to imaging, all populations were de-stained for one hour. Treatment of *C. elegans* with 10μM TMRE in the NGM plates from L1 and L4 illustrated dye uptake, but excessive staining of the gut (Figure 30). This is unsuitable for microscopy and quantification, as this area shows fluorescence saturation and is not representative of the peripheral tissues. In contrast, *C. elegans* treated with TMRE in the *E. coli* OP50 from L1 and L4 showed dye uptake, with homogenous staining throughout the body and no excessive gut staining and saturation. TMRE was detectable at a concentration of 1μM, but optimal staining suitable for quantification was illustrated in *C. elegans* treated with 10μM TMRE in the *E. coli* OP50 bacterial lawn. L4 treatment showed a marginally reduced fluorescence compared to the L1 treatment, however this was still optimal for quantitative fluorescence microscopy. This illustrates that the administration method has a greater impact upon

dye uptake than the incubation period. Treatment of L4 *C. elegans* with 10µM TMRE *E. coli* OP50 for 24 hours was consistently utilised in all subsequent TMRE staining's, in order to avoid any potential developmental impact of TMRE treatment from L1.

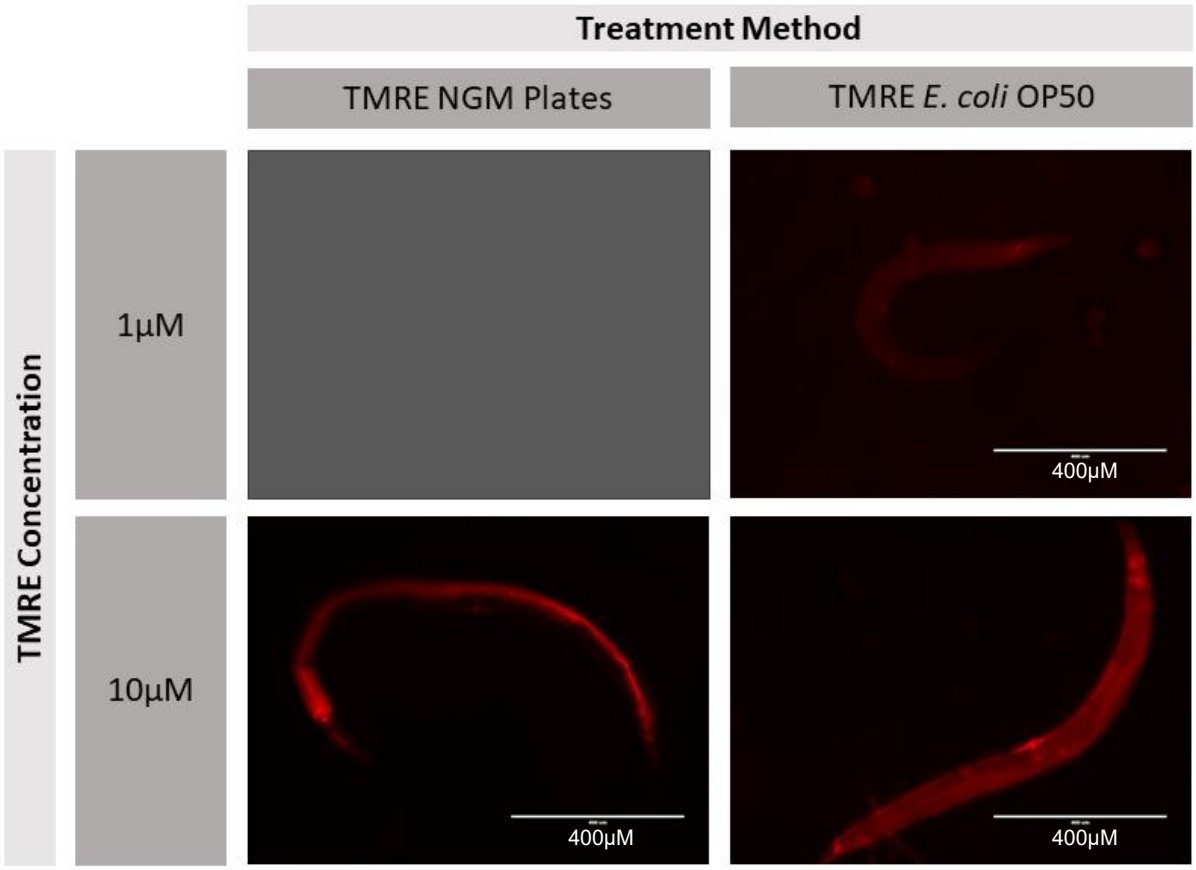

Figure 30-Optimisation of TMRE treatment protocol

5-10 well fed day 1 wildtype C. elegans imaged per condition to assess dye uptake, quantification not undertaken for qualitative method optimisation. *C. elegans* in images treated from L4 stage of development, undertaking different treatment methods. No detection of TMRE uptake in prior method, incorporating 1µM TMRE into the NGM media.

3.8.1.2 The *vps-35[D638N]* heterozygote exhibits an impaired mitochondrial phenotype, not exacerbated with age

VPS35[D620N] has been implicated in the dysregulation of mitochondrial fission, leading to mitochondrial fragmentation (159,160). The *vps-35[D638N]* heterozygote exhibits a significantly reduced mitochondrial membrane potential in day 1 of adulthood (Figure 31A), suggesting that this role may be conserved in *C. elegans* and is a potential mechanism implicated in neurodegeneration. This mutant line was re-examined with ageing, in day 5 of adulthood. There was no significant worsening of phenotype (Figure 31B). With age, the mitochondrial membrane potential of the wildtype *C. elegans* significantly reduces (Figure 31C). The mitochondrial membrane potential of a wildtype *C. elegans* in day 5 of adulthood is not significantly different from the membrane potential of a day 1 adult *vps-35[D638N]*. This suggests that the *vps-35[D638N]* may shows a prematurely aged phenotype, in relation to mitochondrial health.

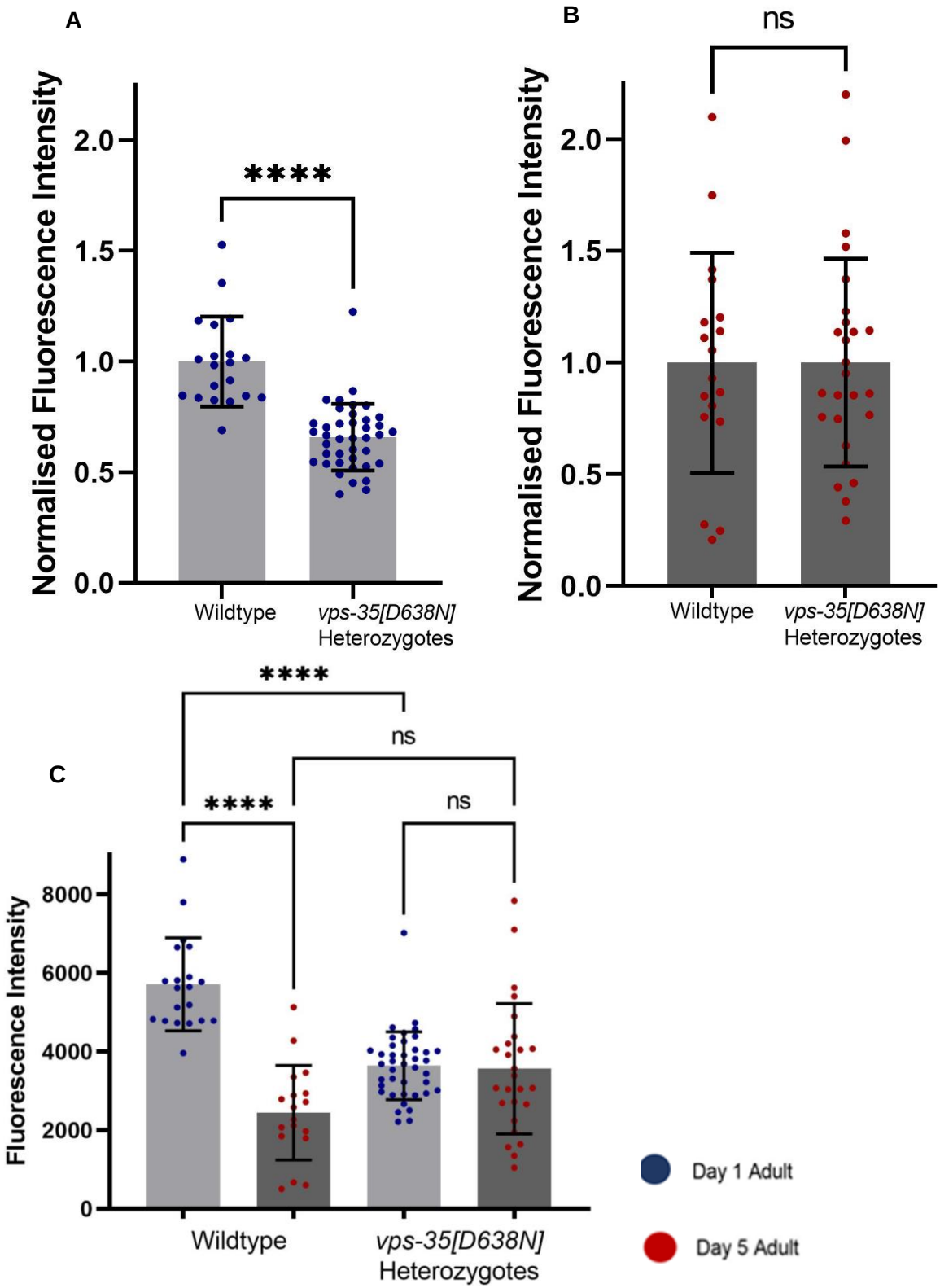

Figure 31-Mitochondrial Membrane Potential, inferred through TMRE fluorescence, of Day 1 and Day 5 Adult vps-35[D638N]

15-30 day 1 or day 5 adult *C. elegans* visualised per line. One-way ANOVA analysis utilising pre-selected columns and Welch's correction for unequal standard deviations, where multiple comparisons have been undertaken. Unpaired, two-tailed T-tests undertaken when for comparison between two datasets. Full descriptive statistics including the mean, standard deviation and number can be found in the supplementary.TMRE fluorescence normalised to the wildtype mean in the day 1 and day 5 graphs. Raw fluorescence intensity in comparative figure utilised, to contrast changes in fluorescence intensity between day 1 and 5 within genotypes.

3.8.2 *vps-35[D638N]* heterozygotes exhibit an impaired ciliation phenotype

Ciliation in *C. elegans* is partially modulated by endocytic genes, which regulate the transport of ciliary membrane proteins (339). One of these genes is the clathrin adaptor AP-2, which has previously been shown to modulate WNT signaling in *C. elegans* in tandem with VPS35 and the retromer complex (129). Furthermore, RAB-5 and RAB-8 are key endocytic genes in *C. elegans* relevant to ciliary membrane transport (339) and the human paralog of RAB-8, RAB8a is a key downstream effector substrate of LRRK2 (287). Whether this mechanism is conserved between *C. elegans* LRK-1 and RAB-8 is currently undefined. Furthermore, Parkinson's mutations in LRRK2 have been illustrated to disrupt ciliation in *in vitro* murine models (287,325), thus study of ciliation as a marker of endocytic function has been investigated in our novel model. *C. elegans* have highly ciliated neuronal groups in the head, the amphid and phasmid neurons, which have sensory functions. These neuronal populations readily uptake a fluorescent dye DiI, through cilia uptake relevant to endocytosis, thus the fluorescence of these stained neuronal populations can be a marker for cilia and endocytic function.

The *vps-35[D638N]* heterozygotes show in day 5 of adulthood a significantly reduced DiI fluorescence, indicating that they have reduced cilia function (Figure 32A). In day 5 of adulthood, *vps-35* deletion *C. elegans* do not exhibit this phenotype, illustrating that total loss of function of *vps-35* does not impact ciliation phenotype and once again, that the *vps-35[D638N]* is likely to be a more complex mechanism than complete loss of function alone. Following ageing to day 12 of adulthood, the *vps-35[D638N]* heterozygote maintains a significantly reduced DiI fluorescence compared to the wildtype (Figure 32B), whereas following ageing to day 19, there is no significant difference in DiI fluorescence between the wildtype and *vps-35[D638N]* heterozygote (Figure 34C).

When the DiI intensities are contrasted by age for each genotype, the wildtype shows no significant difference in DiI intensity between day 5 and 12, however between day 12 and 19, there is a significant reduction in DiI fluorescence, suggesting that in the wildtype model, cilia uptake and endocytic pathways are reduced in advanced age (Figure 33). In contrast, when the fluorescence intensities of the *vps-35[D638N]* heterozygote are compared, there is no significant difference between day 5, 12 or 19, suggesting that this mutation induces an impaired ciliation phenotype, irrespective of age and illustrates a phenotype most similar to a wildtype *C. elegans* in advanced age. Unfortunately, aged data was not available for *vps-35* deletion, as due to their shortened lifespan (3.6), there was no surviving animal to be used in the assay, however it is notable that complete loss of VPS-35 function illustrates a divergent phenotype from the *vps-35[D638N]* mutant in day 5 of adulthood.

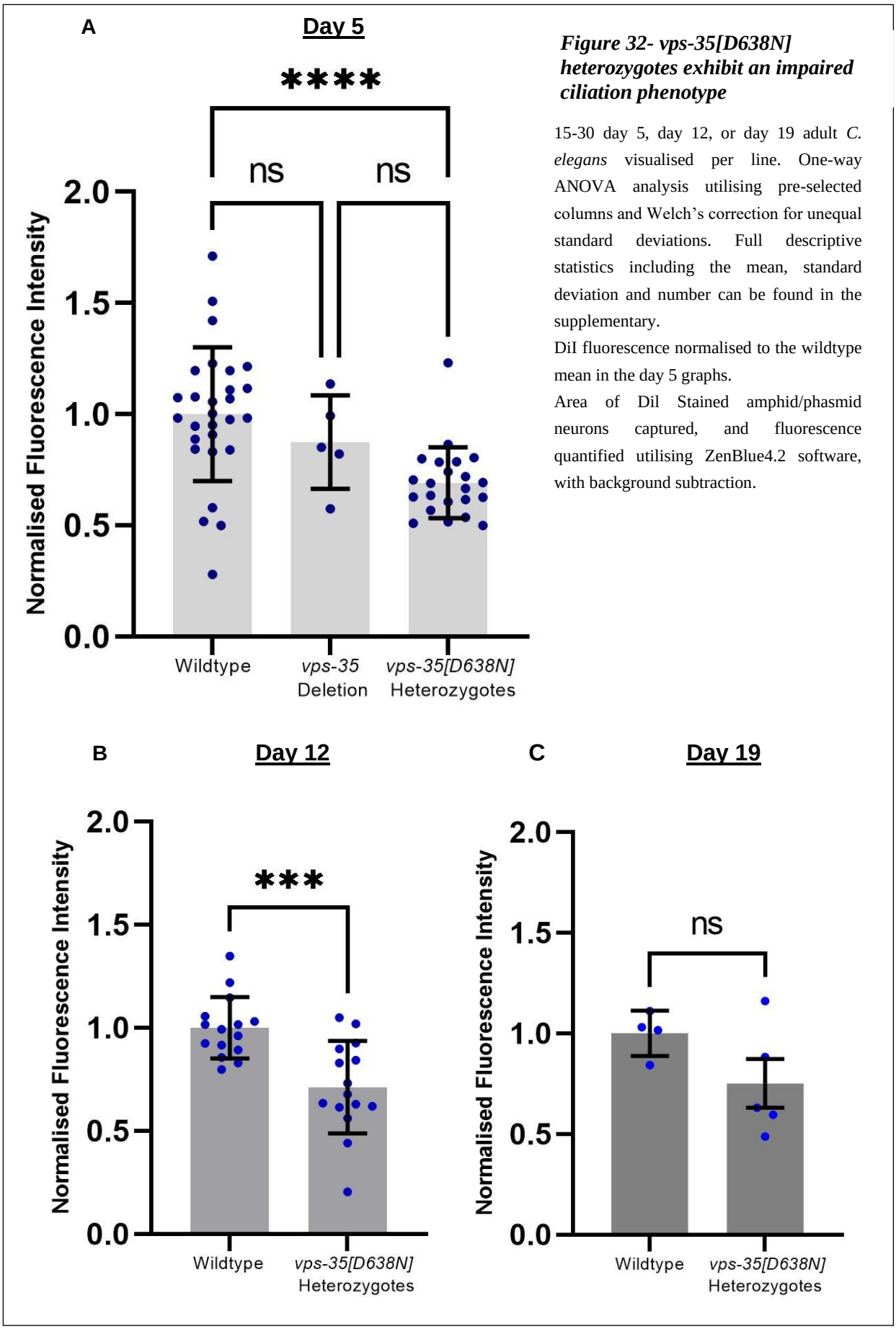

Figure 32- vps-35[D638N] heterozygotes exhibit an impaired ciliation phenotype

15-30 day 5, day 12, or day 19 adult *C. elegans* visualised per line. One-way ANOVA analysis utilising pre-selected columns and Welch's correction for unequal standard deviations. Full descriptive statistics including the mean, standard deviation and number can be found in the supplementary.

DiI fluorescence normalised to the wildtype mean in the day 5 graphs.

Area of Dil Stained amphid/phasmid neurons captured, and fluorescence quantified utilising ZenBlue4.2 software, with background subtraction.

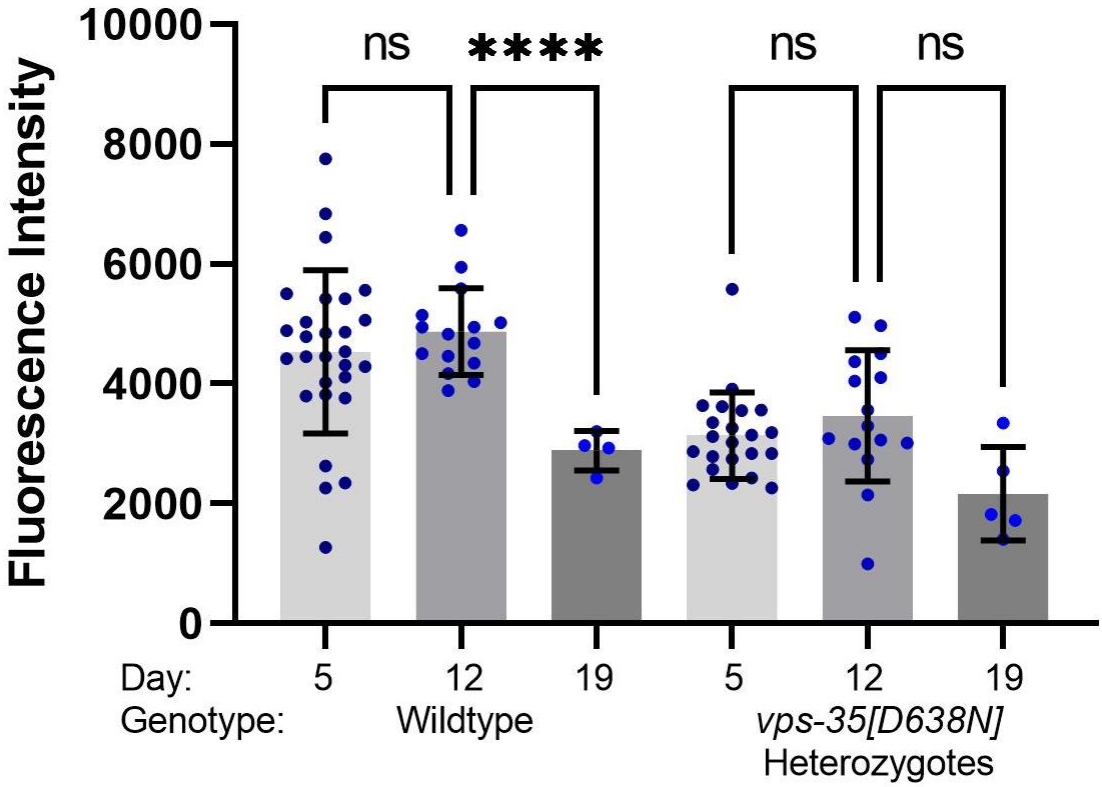

Figure 33- Impairments in ciliation phenotype exhibited by vps-35[D638N] heterozygotes is not age dependant

15-30 C. elegans visualised per line. One-way ANOVA analysis utilising pre-selected columns and Welch's correction for unequal standard deviations. Full descriptive statistics including the mean, standard deviation and number can be found in the supplementary.Raw fluorescence intensity in comparative figure utilised, to contrast changes in fluorescence intensity between day 1 and 5 within genotypes. Area of Dil Stained amphid/phasmid neurons captured and fluorescence quantified utilising ZenBlue4.2 software, with background subtraction.

3.8.3 *vps-35[D638N]* heterozygotes show reduced lipid accumulation as a marker for autophagy

In *C. elegans*, there are multiple readouts to infer autophagic function, including lipid accumulation. Lipid storage in *C. elegans* is partially modulated by autophagy, mutants with deletions of key autophagic genes show a reduction in the accumulation of lipids (340). Through Nile red staining for lipids of day 1 and day 5 *C. elegans*, followed by confocal-like fluorescent microscopy, utilizing a ZEISS Apotome 2.0 microscope, lipid content can be inferred by fluorescence in the whole body of the *C. elegans*.

Compared to the wildtype, our *vps-35[D638N]* heterozygote mutant lines, with and without the balancer strain, showed a significantly reduced lipid accumulation (Figure 34 A and B). This is again in contrast to the *vps-35* deletion model, which shows no significant difference in lipid storage compared to the *vps-35[D638N]* mutant, suggesting alternative mechanisms. The reduced lipid accumulation in the *vps-35[D638N]* mutant suggests impairments in key autophagy pathways; however this is not reflected in the total loss of function *vps-35* deletion model, suggesting that there could be a gain of function in *vps-35[D638N]* mutation. In order to further test the hypothesis that *vps-35[D638N]* acts through LRK-1 kinase hyperactivation, the lipid accumulation has been studied in selected LRK-1 mutants, detailed in chapter 4. Interestingly, the *cat-2(n4547)* tyrosine hydroxylase deletion model also shows significant reductions in lipid accumulation compared to the wildtype in day 1 and day 5 of adulthood, suggesting that impairments in dopamine signalling may have broader implications in lipid homeostasis. Between day 1 and day 5 of adulthood, the lipid content increases significantly in all three mutants studied at these timepoints (Figure 34 C), a commonly observed phenotype in ageing (304).

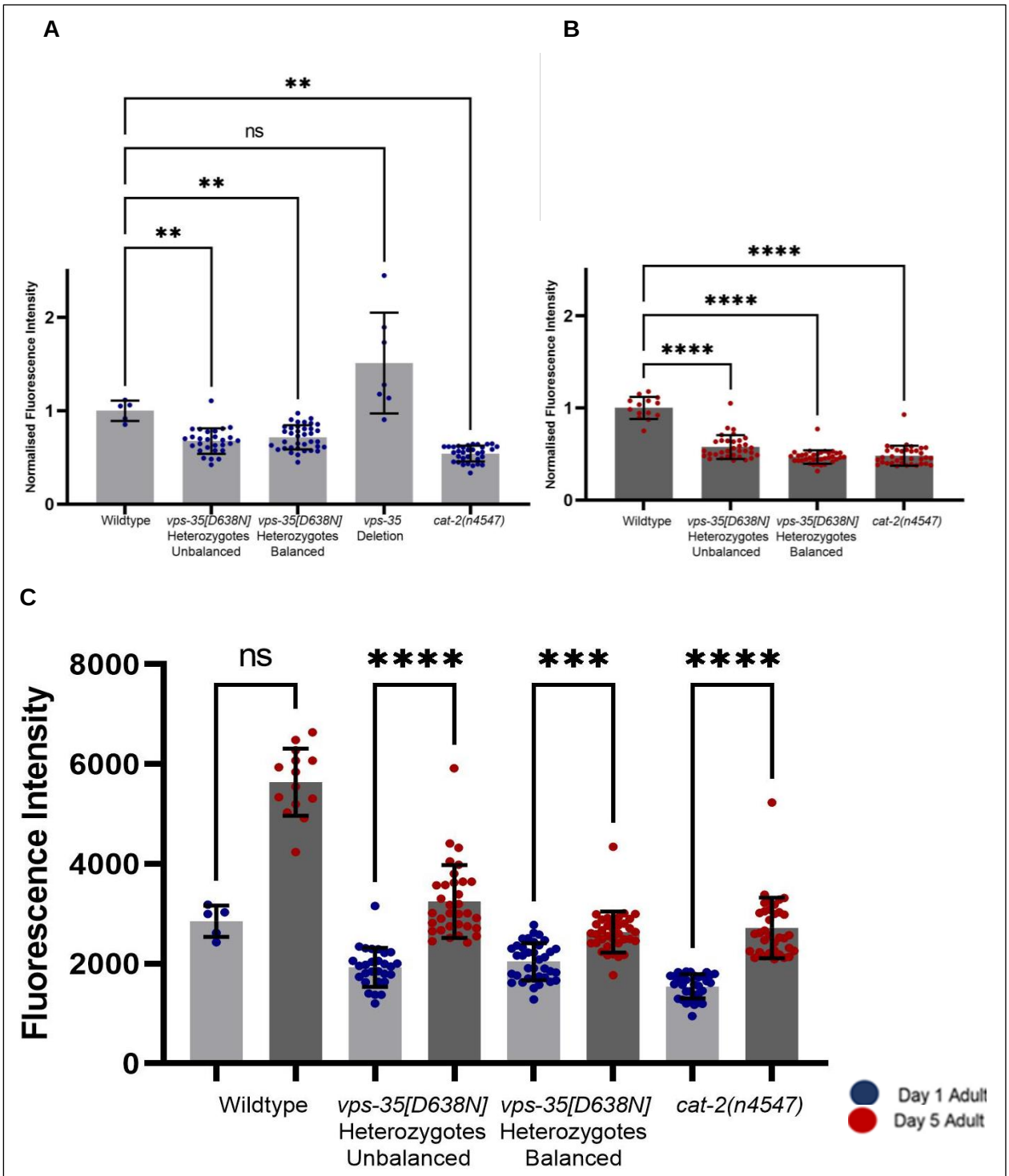

Figure 34- vps-35[D638N] heterozygotes show reduced lipid accumulation as a marker for autophagy

5-30 day 1 or day 5 adult *C. elegans* visualised per line. One-way ANOVA analysis utilising pre-selected columns and Welch's correction for unequal standard deviations. Full descriptive statistics including the mean, standard deviation and number can be found in the supplementary. Fluorescence normalised to the wildtype mean in the day 1 and day 5 graphs. Raw fluorescence intensity in comparative figure utilised, to contrast changes in fluorescence intensity between day 1 and 5 within genotypes.

3.9 Visualisation of VPS-35[D638N] Dopaminergic Neurons *in vivo*

A major benefit of *C. elegans* is that there are already a plethora of tools available to help investigate novel questions, *C. elegans* are translucent, thus tagging of proteins with fluorescent markers or cell type specific fluorescent transgenes are a viable option for multiple *in vivo* microscopy experiments. We obtained from the Caenorhabditis Genetics Centre (CGC), a platform for international *C. elegans* sharing, a *C. elegans* line which expressed a dopaminergic specific GFP transgene (88), enabling the study of dopaminergic neurons *in vivo*.

3.9.1 Generation of a vps-35[D638N] heterozygotes with dopaminergic neuron specific GFP expression

A cross was established, to generate balanced *vps-35[D638N]* heterozygotes expressing GFP in their dopamine neurons. Dopaminergic GFP expressing males (*vtIs1 [dat-1p::GFP + rol-6(su1006)]*.) were generated and crossed with a balanced L4 *vps-35[D638N]* heterozygote hermaphrodite (*Vps-35(knu618[D638N]);tmC6[dpy9710)]*), producing progeny with dopaminergic GFP transgene and the PD relevant *vps-35[D638N]* mutation. 20 progeny were separated onto small plates, to propagate their own populations. Founder *C. elegans* were genotyped (Figure 35), for GFP and *vps-35[D638N]*, which will be present in the progeny.

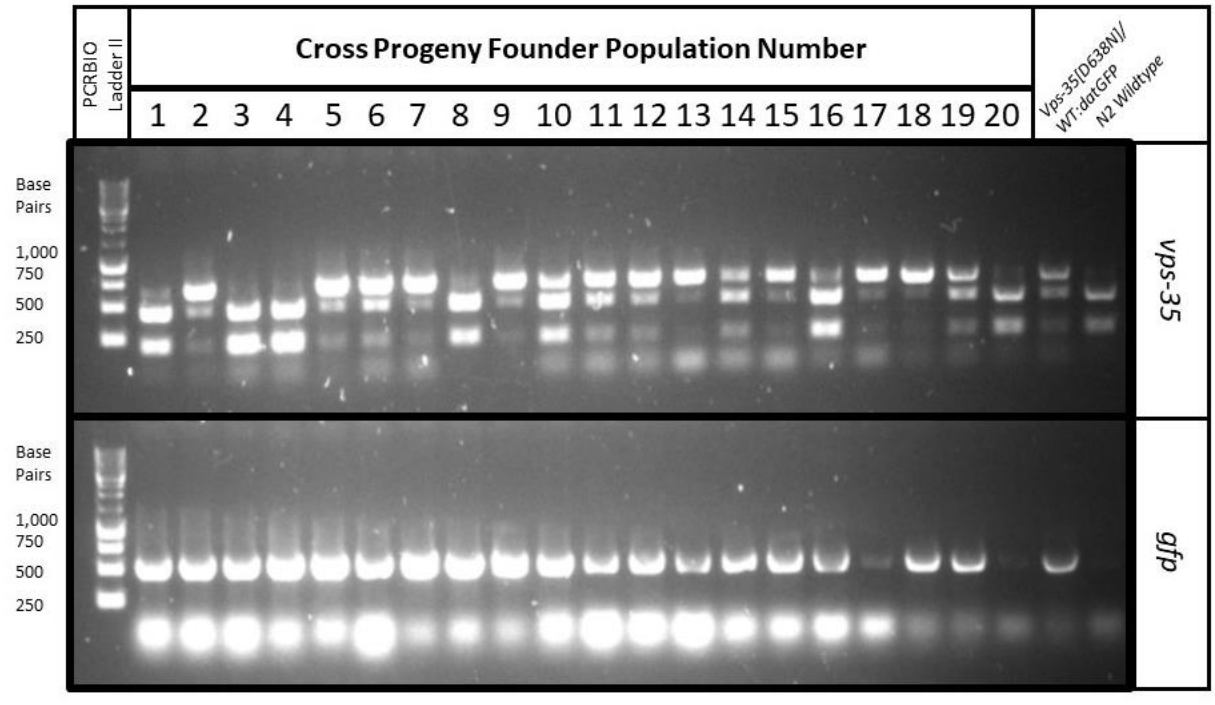

Figure 35- Genotyping for presence of vps-35[D638N] heterozygotes, expressing dopaminergic GFP

20 populations were obtained from the vps-35[D638N] heterozygote and dat:GFP cross, the majority of which illustrated heterozygosity for vps-35[D638N]. The PCR product has a size of 600base pairs, this is cleaved by a wildtype specific restriction enzyme HincII, thus if the wildtype *vps-35* allele is present, a band of 400 and 200 base pairs are present. If the *C. elegans* is heterozygous for vps-35[D638N], an undigested PCR product band is present at 600 base pairs.

14 of these individuals are heterozygous for the vps-35[D638N] mutation, demonstrated through the presence of one DNA fragment at approximately 650bp, one at approximately 200bp and another one at 400bp. The 400 and 200 base pairs are created through DNA cleavage at a wildtype specific restriction site, cleaved by the restriction enzyme HINCII, hence heterozygous *vps-35[D638N]* individuals possess these, along with a 650 base pair band encompassing the *vps-35[D638N]*, which is not subject to cleavage due to the mutations presence. The remaining 6 individuals do not possess the *vps-35[D638N]* mutation, showing a wildtype genotype, illustrating that the cross with the *vps-35* wildtype dopaminergic GFP expressing males has been successful. This is further confirmed that the cross has a high efficiency and success, as 19 individual founders possess the GFP transgene. As this is a transgene, this should be passed on to all the progeny of the male.

Populations founded from hermaphrodite mothers with both this mutation and transgene were maintained for further investigation and stored in our *C. elegans* database (*Vps-35(knu618[D638N]);tmC6[dpy9710)]II; vtIs1 [dat-1p::GFP + rol-6(su1006)] V*). The population maintained and studied throughout the remainder of this chapter and chapter 5, was population 10.

3.9.2 *vps-35[D638N]* induces impairments in dopaminergic neuronal morphology, not exacerbated with rotenone treatment

C. elegans have 6 dopaminergic neurons in the head, involved in mechanosensation of nutrient sources and are modulators of the basal slowing response (86). There are 4 CEP neurons, the long dendrites of which protrude from the cell body towards the mouth and have a sensory function in finding nutrients. Connected to the main cell body are 2 ADE neurons, directed towards the back of the head, which relay the sensory information. Neurons have been visualized through the capture of 3-4 images over a downward Z stack, as shown in figure 36, the parameters of which have been determined per *C. elegans*, utilizing a Zeiss Apotome 2.0 confocal-like fluorescent microscopy, with the images taken for analysis.

The fluorescence of the CEP cell bodies has been quantified, as reduced fluorescence indicates reduced activity of the *dat-1* promotor, which drives the expression of DAT-1 dopamine transporter (88). Reduced *dat-1* expression has been previously correlated with decreased dopaminergic function, as well as being used as a marker for dopaminergic neuron degeneration (251,341,342). Furthermore, the neuronal morphology of the CEP and ADE neurons have been scored, based upon phenotypes categorised by Guha and colleagues (328). There are 4 main types of neuronal impairments visible in *C. elegans*, 2 of which are minor and 2 major. Minor impairments include outgrowths, small protrusions in the cell body and branching, in which a short

branch has formed off from the main neuron. Major impairments include blebbing, in which the neuron is undergoing apoptosis and degeneration, in which the neuron has degenerated and has been lost altogether.

The neuronal morphology of *vps-35[D638N]* in day 1 of adulthood has been studied, in conjunction with acute treatment of rotenone, an agricultural pesticide epidemiologically linked to PD (343). Rotenone is routinely used in toxin induced models of PD (302), rather than the genetic approach undertaken here, but it is an inducer of oxidative stress, a process which may be key in PD pathogenesis (80). The effect of acute rotenone treatment upon the dopaminergic neurons in both the wildtype and *vps-35[D638N]* GFP expressing line was studied, as prior studies of VPS35[D620N] in alternative models had shown neurotoxin damage (133,163) and to establish this assay for future research. Rotenone was administered for 16 hours overnight at 3 concentrations, 5μM, 7.5μM and 10μM, as there was conflicting information in the literature, as to potential concentrations to test (251,341,342). 5μM was the most optimal, as there was no lethality and paralysis, as shown in 7.5 and 10μM, but neurodegeneration was illustrated. These higher concentrations did not show any greater impairments in neuronal fluorescence or morphology, suggesting that there is not a dose-dependent response in acute treatment in rotenone concentrations after an approximately 5μM threshold. The data for 7.5 and 10 μM rotenone treatment can be found in the supplementary.

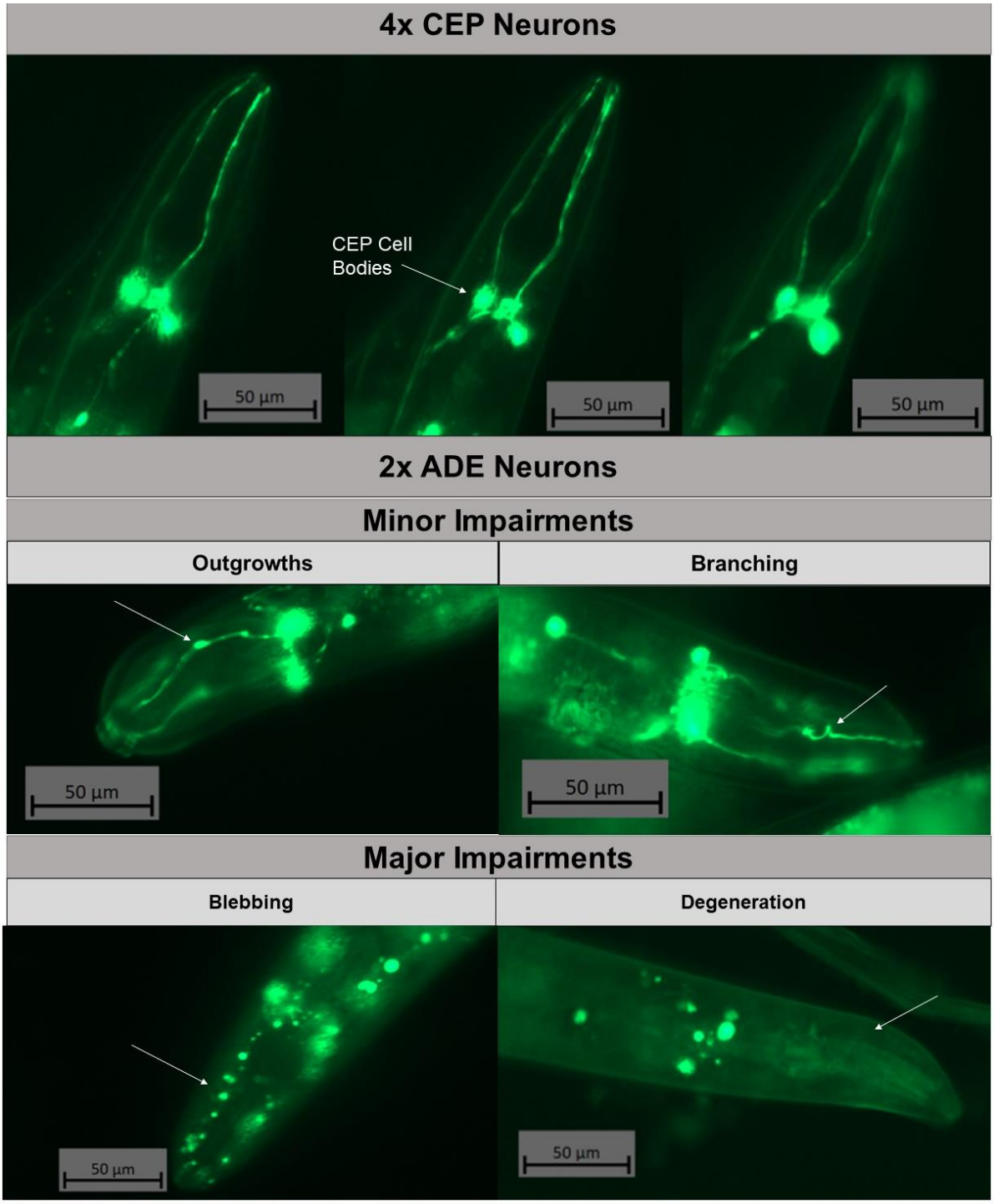

Figure 36- C. elegans dopaminergic CEP and ADE neurons, with scored pathologies

C. elegans CEP and ADE neurons visualised through a manual downward Z-stack and scored utilising existing method developed by Guha and colleagues (317) utilising ZenBlue4.2 software. Multiple analysis methods undertaken for datasets, to understand most prevalent pathologies in a population, the quantity of impairments per *C. elegans* and which impairments in which neuronal subset are common in each population. Images obtained during experiments in 3.9.2, to demonstrate pathologies scored utilising Guha and colleagues' methods.

3.9.2.1 *vps-35[D638N]* heterozygotes show reduced CEP cell body fluorescence, not exacerbated by 5µM rotenone treatment

In terms of CEP cell body fluorescence, in the wildtype GFP expressing line there is a significant reduction in fluorescence following acute rotenone treatment, compared to the vehicle (DMSO) treated wildtype (Figure 37). Furthermore, the GFP expressing *vps-35[D638N]* heterozygote exhibited a reduced fluorescence compared to the vehicle treated wildtype. Interestingly, there was no significant reduction in fluorescence in the rotenone treated *vps-35[D638N]* mutant compared to the vehicle *vps-35[D638N]*. This suggests that the mutation is as deleterious as a toxin induced model, in terms of cell signalling impairments and that induced oxidative stress is no more deleterious to *vps-35[D638N]*, which already shows a severely impaired phenotype.

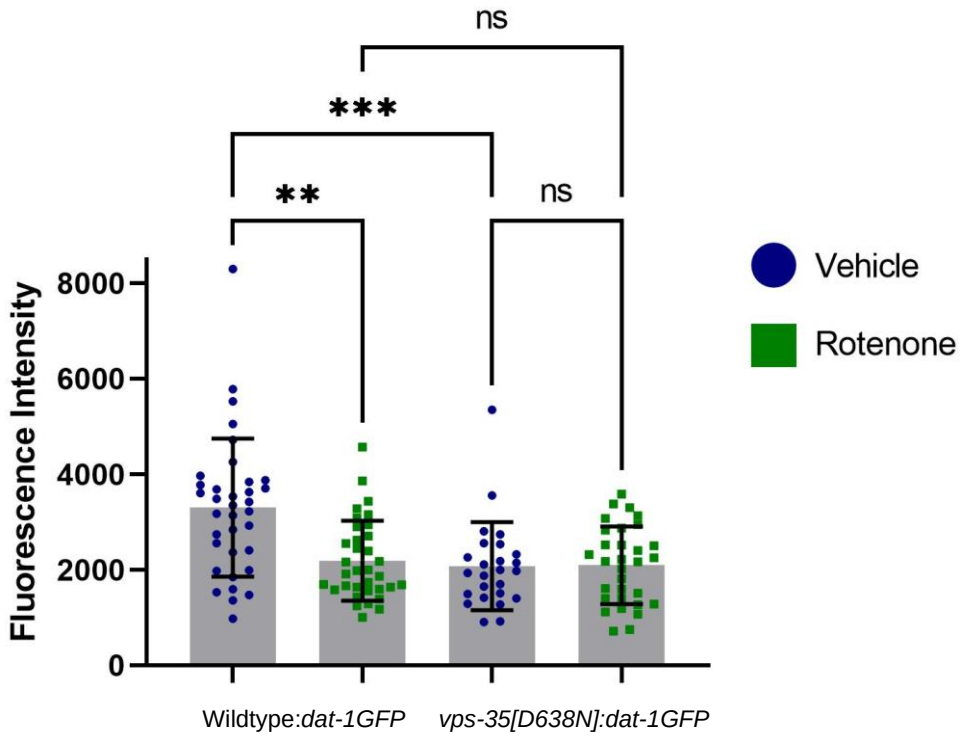

Figure 37-vps-35[D638N] show reduced CEP cell body fluorescence, independent of rotenone treatment

Day 1 adult *C. elegans*. CEP cell bodies fluorescence quantified per *C. elegans*, through selection of a 1000 pixel area. Analysis undertaken utilising ZenBlue4.2 software. Full descriptive statistics and One Way ANOVA with Brown-Forsyth Correction P values found in the supplementary.

3.9.2.2 *vps-35[D638N]* heterozygotes show impairments in CEP and ADE neuronal morphology, independent of 5µM rotenone treatment

As shown in Figure 38, the neuronal morphology of our rotenone treated *vps-35[D638N]* and wildtype lines was investigated. These graphs illustrate the proportion of neurons in a population of 20 *C. elegans* that show each of these impairments.

Approximately 90% of vehicle treated wildtype CEP neurons show a wildtype, healthy appearance, while the vehicle treated *vps-35[D638N]* shows over 40% have minor impairments,

such as branching and outgrowths. Following treatment with rotenone, there are modest increases in these minor impairments in both the wildtype and *vps-35[D638N]* mutant (Figure 38A). The ADE neurons appear to be more vulnerable than the CEP neurons to rotenone treatment and the *vps-35[D638N]* mutation. In the wildtype, vehicle treated *C. elegans*, over 95% show a healthy, wildtype morphology, while in the *vps-35[D638N]* 20% have degenerated, with a further 15% blebbing (Figure 38B). In the *vps-35[D638N]*, these major impairments are not substantially increased following rotenone treatment. However, in the wildtype rotenone treatment induced dopaminergic degeneration to a similar extent to the vehicle treated *vps-35[D638N]*. This contrasts the novel genetic modelling approach with a traditional toxin induced model and illustrates that the novel genetic approach exhibits cellular stress, seen in toxin-based models. This degeneration is not shown to the same extent in the wildtype rotenone treated CEP neurons, suggesting that the ADE neurons, are more sensitive to cellular perturbation, whether they are induced by cellular alterations caused by genetics, or environmental factors. Along with the impaired basal slowing response consistently seen in the *vps-35[D638N]*heterozygote, this enhanced dopaminergic neurodegeneration further augments the potential relevance of the model in understanding the VPS35 mutation in PD.

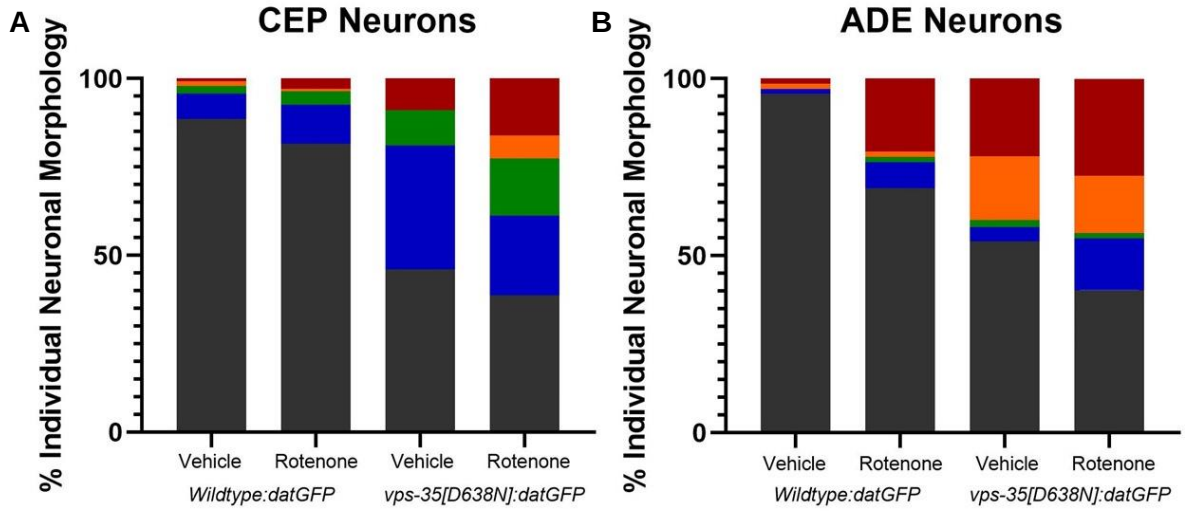

Figure 38- CEP and ADE neuronal morphology of rotenone treated Wildtype:datGFP and vps-35[D638N]:datGFP

Approximately 20 day 1 adult *C. elegans* scored per mutant line and treatment. Full tabulated values and number can be found in the supplementary. Proportions calculated from individual neurons in whole population, rather than individual *C. elegans*, in order to identify the most prevalent neuropathology within the

3.9.2.3 *vps-35[D638N]* heterozygotes show an increased number of impairments per *C. elegans*, irrespective of 5µM rotenone treatment

The neuronal morphologies have been dissected further, to quantify the number of minor or major impairments per *C. elegans* in the population, as the overall CEP and ADE neuron morphology was a readout of the individual neurons within the population of 20 as a whole, rather than individual (Figure 39).

The wildtype vehicle treated line, approximately 75% of individuals have no minor impairments, with the remaining 25% possessing 2 or fewer minor impairments. This increases slightly following rotenone treatment, with approximately 50% of *C. elegans* showing no minor impairments. In contrast, in the *vps-35[D638N]* heterozygotes, only 10% of the vehicle treated population show no minor impairments, while 65% show 1-2 impairments and the remainder, approximately 25% show 3 or 4 minor impairments per *C. elegans*. Following rotenone treatment, fewer *C. elegans* have 1-2 impairments and there is a greater proportion, approximately 35% of *C. elegans* with 3-5 impairments per worm. Again, this highlights how deleterious the *vps-35[D638N]* mutation is to dopaminergic neurons and that in terms of minor impairments caused by subtle alterations in cell signalling, this mutation is more harmful than rotenone treatment. Furthermore, in terms of major impairments, over 95% of vehicle treated wildtype worms do not show any major impairments, whereas in the *vps-35[D638N]* heterozygote treated with a vehicle, only 35% of the population do not have a major impairment- 45% have 1, with the remainder possessing 2-4 major impairments. With rotenone treatment, there is a drastic increase in major impairments shown, with 55% of the population exhibiting no major impairments, whereas in the rotenone treated *vps-35[D638N]* mutant, there is no change in the number of *C. elegans* without major impairments, however the number of impairments per *C. elegans* does modestly increase. This further illustrates that the *vps-35[D638N]* mutation is highly harmful to dopaminergic neurons, augmenting the use of *C. elegans* as a novel model for this.

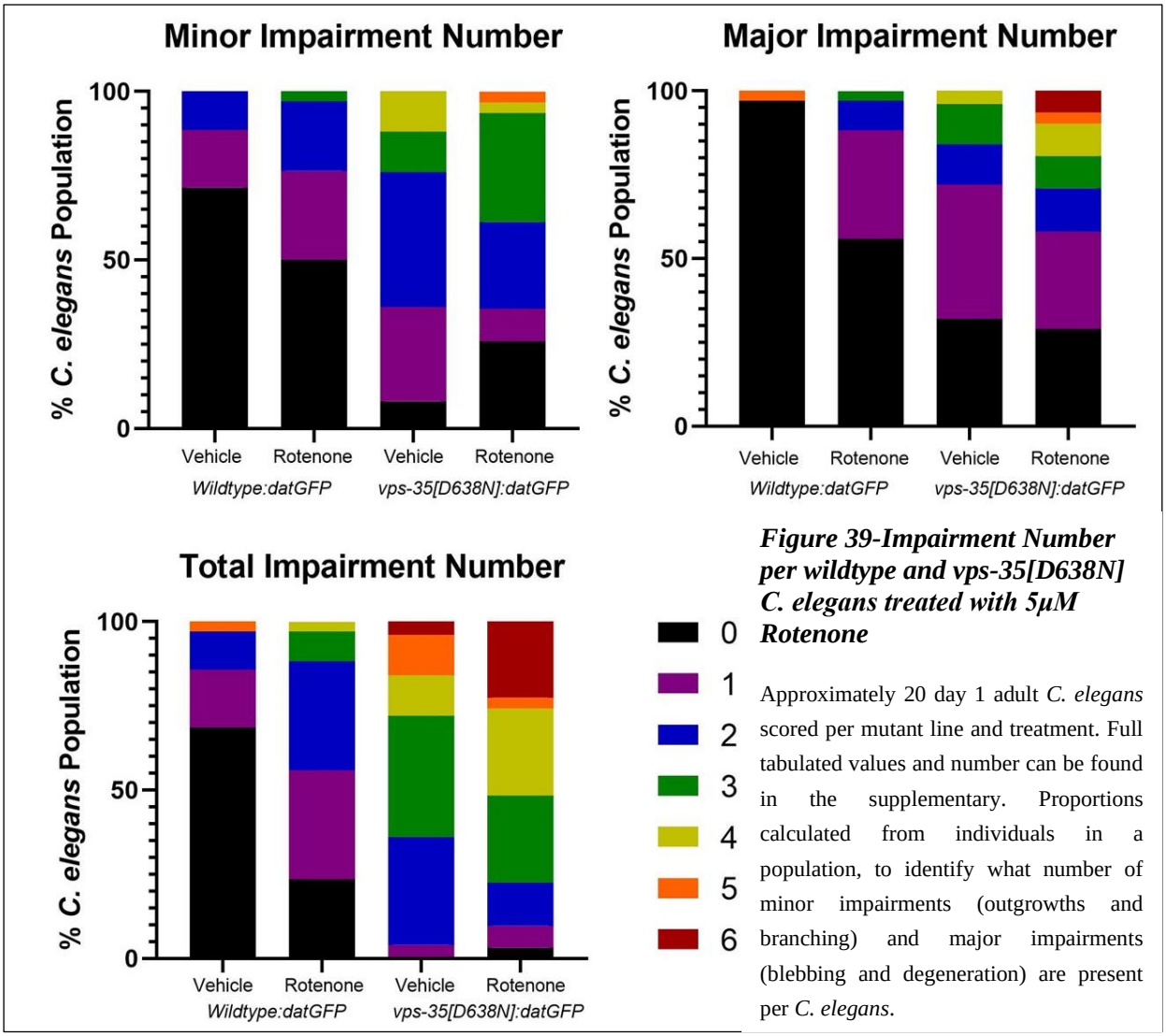

Figure 39-Impairment Number per wildtype and vps-35[D638N] C. elegans treated with 5µM Rotenone

Approximately 20 day 1 adult *C. elegans* scored per mutant line and treatment. Full tabulated values and number can be found in the supplementary. Proportions calculated from individuals in a population, to identify what number of minor impairments (outgrowths and branching) and major impairments (blebbing and degeneration) are present per *C. elegans*.

3.9.2.4 The most prevalent neuropathological changes in *vps-35[D638N]* are minor impairments in the CEP neurons and major impairments in the ADE neurons

In figure 40, it has been dissected further whether the minor or major impairments per *C. elegans* are found in the CEP and the ADE neurons, to determine which is the most common pathology per mutant line and with rotenone treatment, to assess if there are commonalities or divergences. The vehicle treated wildtype's most common pathology is minor impairments in the CEP neurons, affecting 25% of the population, with 15% of this population showing 1 and 10% 2. Often, these impairments are small outgrowths, the most minor of phenotypes. Following rotenone treatment, there is a drastic increase in CEP neuron minor impairments, affecting 45% of the population and an increase in major impairments in the ADE neurons, affecting 40% of the population. There is not such an increase in major impairments in the CEP neurons, further suggesting that the ADE neurons are more sensitive to induced oxidative stress. In the *vps-35[D638N]* heterozygote treated with a vehicle, the most common neuropathology are minor impairments in the CEP neurons, affecting 90% of the population, with 65% of the population with 1-2 impairments and the remaining 25% with 3-4- upon observation the majority of these are outgrowths. Furthermore, in

the vehicle treated *vps-35[D638N]* mutant 65% of the population show major impairments in the ADE neurons, with 55% of this showing impairments in just 1 of the 2 ADE neurons. When contrasted with the rotenone treated wildtype, this again suggests that the ADE neurons are more susceptible to insult form a genetic alteration and that our model causes substantially more damage to these ADE neurons than the traditional toxin-based approaches. Following rotenone treatment of the *vps-35[D638N]*, there is an increase in major impairments in the CEP neurons, suggesting that these may be vulnerable to toxin-based insult in conjunction with an environmental stressor, as this is not seen to the same extent in the rotenone treated wildtype. This data further suggests that the novel CRISPR/Cas9 modified *C. elegans* models could be useful in modelling the oligogenic and environmental interplay of PD pathogenesis, which could be further reaching than Mendelian forms of PD, such as caused by VPS35[D620N].

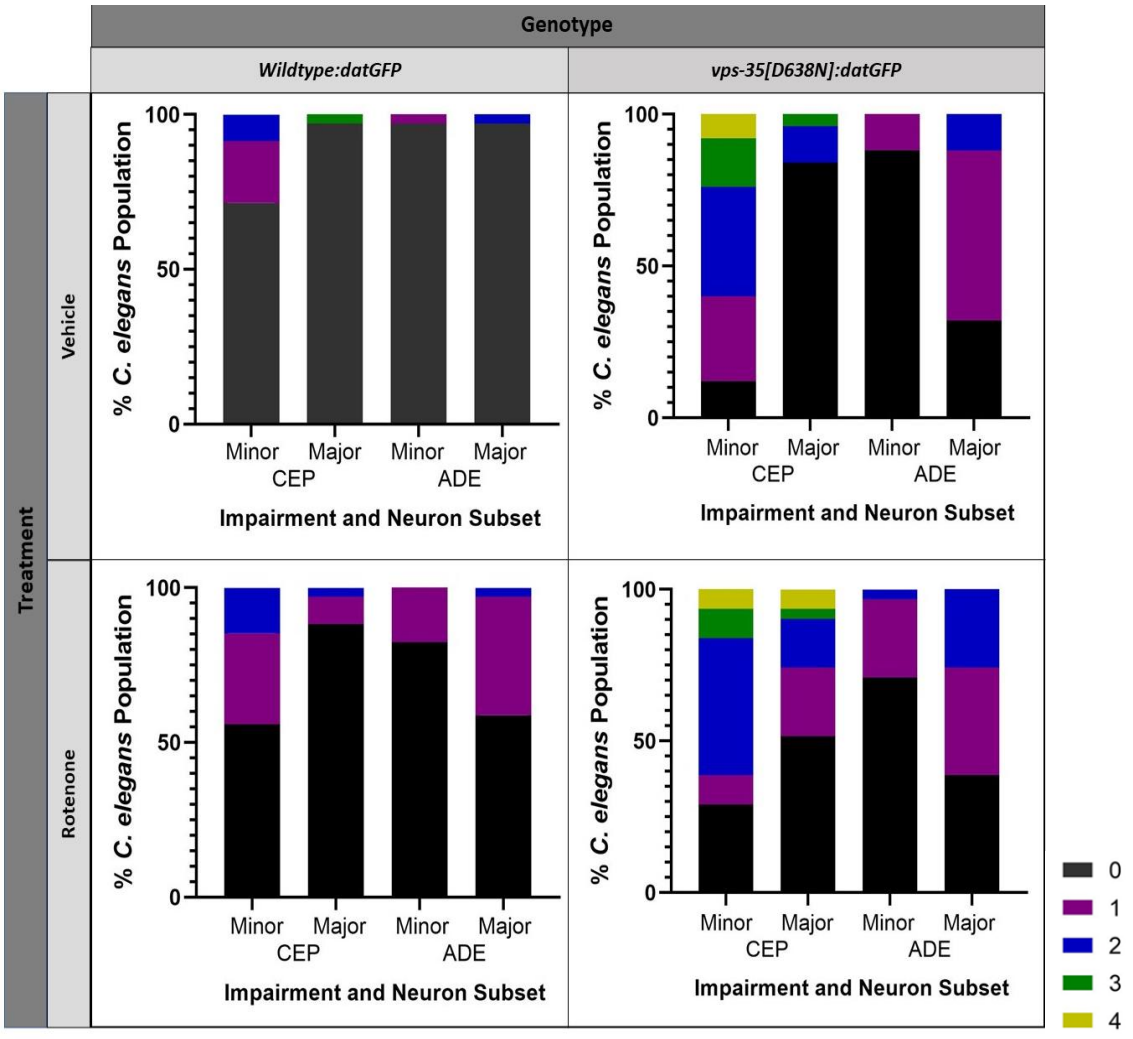

Figure 40- Impairment breakdown of wildtype and vps-35[D638N] C. elegans, treated with 5µM Rotenone

Approximately 20 day 1 adult *C. elegans* scored per mutant line and treatment. Full tabulated values and number can be found in the supplementary. Proportions calculated from individuals in a population, to identify what number of minor impairments (outgrowths and branching) and major impairments (blebbing and degeneration) are present per *C. elegans* in which specific neuronal subtypes

3.9.3. In advanced age, *vps-35[D638N]* heterozygotes show enhanced neurodegeneration

The two GFP expressing lines were studied in advanced age at day 15 and day 18 of adulthood, as at this time point neurodegeneration becomes more prevalent in wildtype populations and therefore optimal to contrast with the *vps-35[D638N]* heterozygotes. The effect of the mutation in advanced age is also vital to characterise, to further assess our model's relevance as a novel Parkinson's model. As detailed in 3.3, the *vps-35[D638N]* lifespan is not significantly reduced compared to the wildtype, so testing at this late age of development is possible. Animals from the same synchronised population were studied, several days apart. The dopaminergic neuronal fluorescence was quantified, and the dopaminergic neuronal pathologies were scored as detailed throughout 3.10.

3.9.3.1 vps-35[D638N] heterozygotes show reduced fluorescence in the CEP cell bodies in day 15 and day 18 of adulthood

In both day 15 and day 18 of adulthood, *vps-35[D638N]* heterozygotes show a reduced fluorescence of CEP cell bodies compared to the wildtype (Figure 41), consistent with observations in day 1 of adulthood. Furthermore, the mean fluorescence intensity reduces for both the wildtype and *vps-35[D638N]* heterozygotes between day 15 to day 18 of adulthood, suggesting that this period of advanced ageing is a vital timepoint for dopaminergic neuronal dysfunction.

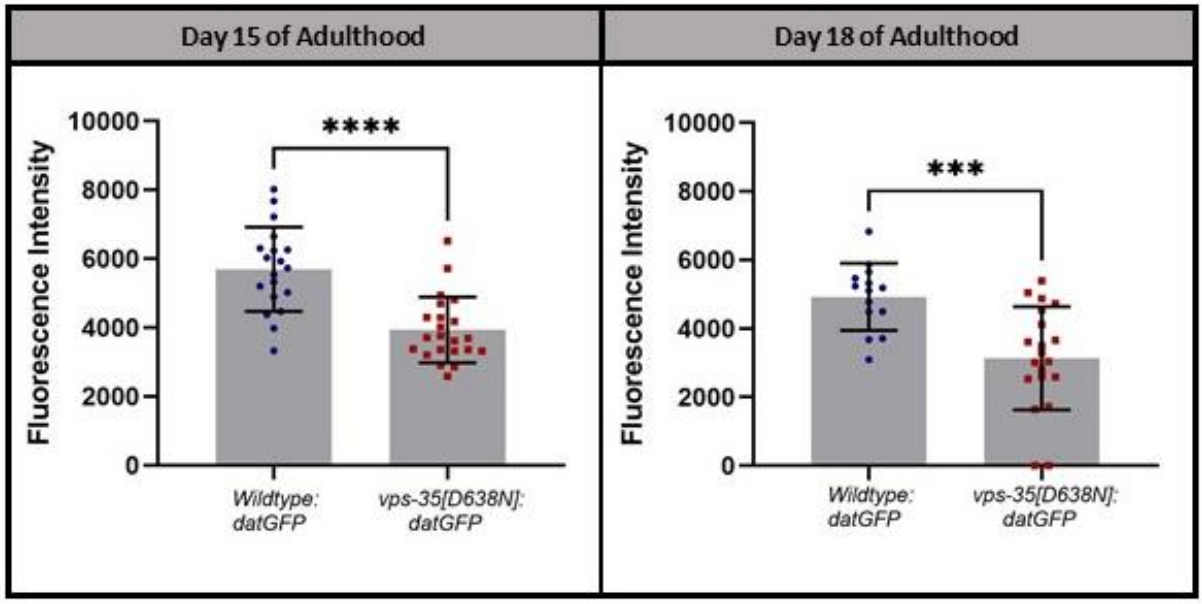

Figure 41-CEP cell body fluorescence of vps-35[D638N] heterozygotes in day 15 and day 18 of adulthood

Day 15 and day 18 adult *C. elegans* studied. CEP cell bodies fluorescence quantified per *C. elegans*, through selection of a 1000 pixel area. Analysis undertaken utilising ZenBlue4.2 software. Full descriptive statistics and. unpaired two-tailed T-test P values found in the supplementary.

3.9.3.2 *vps-35[D638N]* heterozygotes show enhanced degeneration and blebbing in the CEP and ADE neurons in day 15 and day 18 of adulthood

In day 15 of adulthood, the *vps-35[D638N]* heterozygotes show an increased proportion of ADE neuronal blebbing and degeneration compared to the wildtype and a greater proportion of CEP neuronal outgrowths than the wildtype (Figure 42). In day 18, approximately 35% of CEP neurons in the wildtype are blebbing or degenerating, while in *vps-35[D638N]* heterozygotes this proportion is approximately 65%. Furthermore, in day 18 of adulthood over 80% of *vps-35[D638N]* heterozygote ADE neurons are blebbing or degenerating, while 45% of wildtype *C. elegans* show this phenotype. This is a substantial change for both genotypes between day 15 and day 18 of adulthood and further highlights the deleterious impact of *vps-35[D638N]* heterozygotes upon dopaminergic neuronal health.

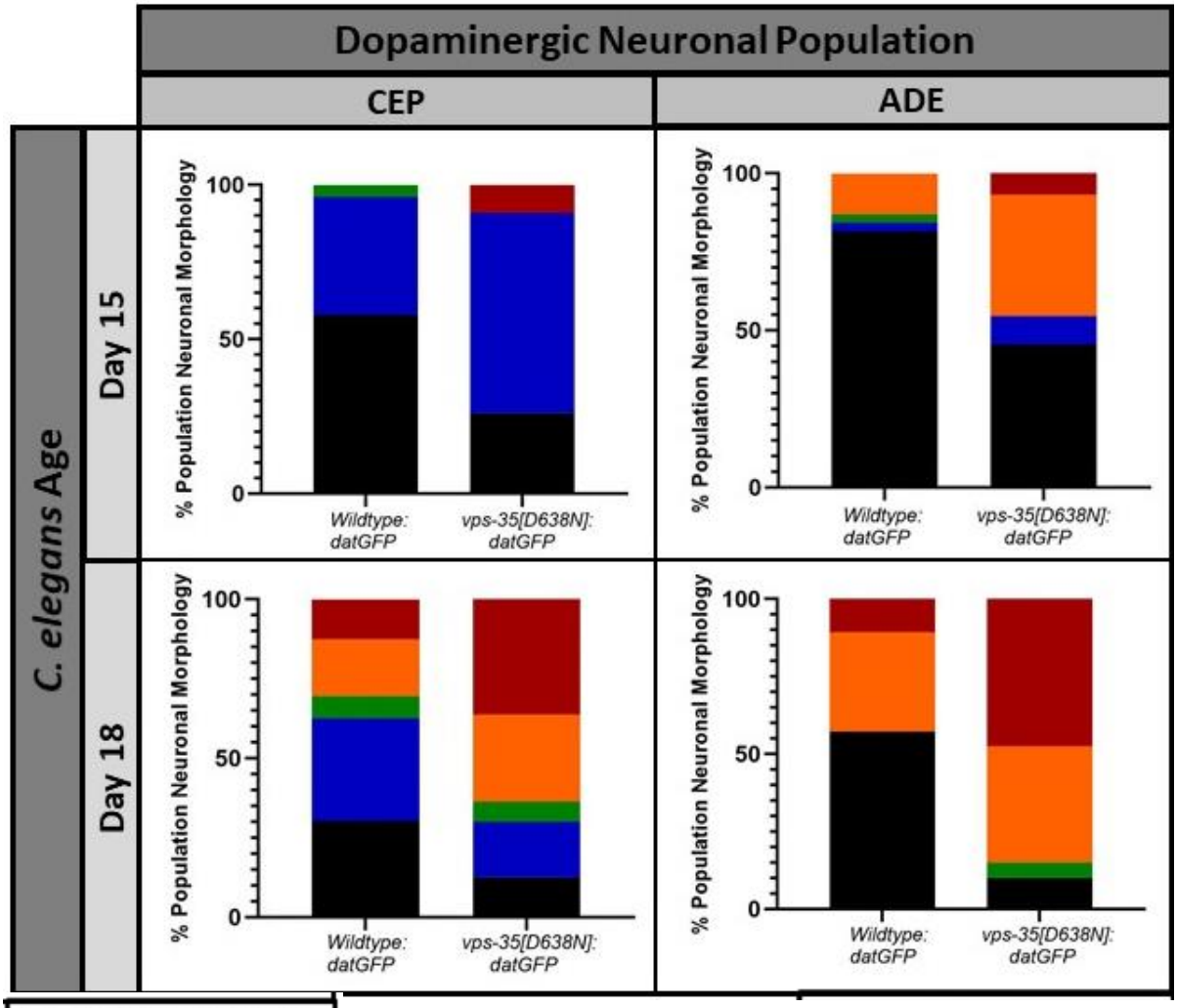

Figure 42-CEP and ADE dopaminergic Neuronal Morphology of vps-35[D638N] in day 15 and 18 of adulthood

Approximately 20 day 15 or day 18 adult *C. elegans* scored per mutant line and treatment. Full tabulated values and number can be found in the supplementary. Proportions calculated from individual neurons in whole population, rather than individual *C. elegans*, in order to identify the most prevalent neuropathology within the population.

3.9.3.3 *vps-35[D638N]* heterozygotes show substantially increased impairments per C. elegans in day 15 and day 18 of adulthood

In day 15 of adulthood *vps-35[D638N]* heterozygotes show an increased number of minor and major impairments per *C. elegans* (Figure 43). 45% of *vps-35[D638N]* heterozygotes have three or more minor impairments and 70% show one or more major impairments, while in the wildtype only 25% show three minor impairments and/or one major impairment. Furthermore, 45% of *vps-35[D638N]* heterozygotes show 5 or more impairments in total, while the whole wildtype population exhibit 4 or fewer impairments. In day 18 of adulthood, the *vps-35[D638N]* exhibits a reduced number of minor impairments compared to the wildtype, however over 50% of *vps-35[D638N] C. elegans* show major impairments in all 6 dopaminergic neurons, thus explaining the lack of minor impairments shown. In the wildtype, fewer than 15% of the population have major impairments in all 6 dopaminergic neurons. In terms of total impairments, over 75% of *vps-35[D638N]* heterozygotes exhibit impairments in all 6 of their dopaminergic neurons, while this remains at less than 15% in the wildtype line.

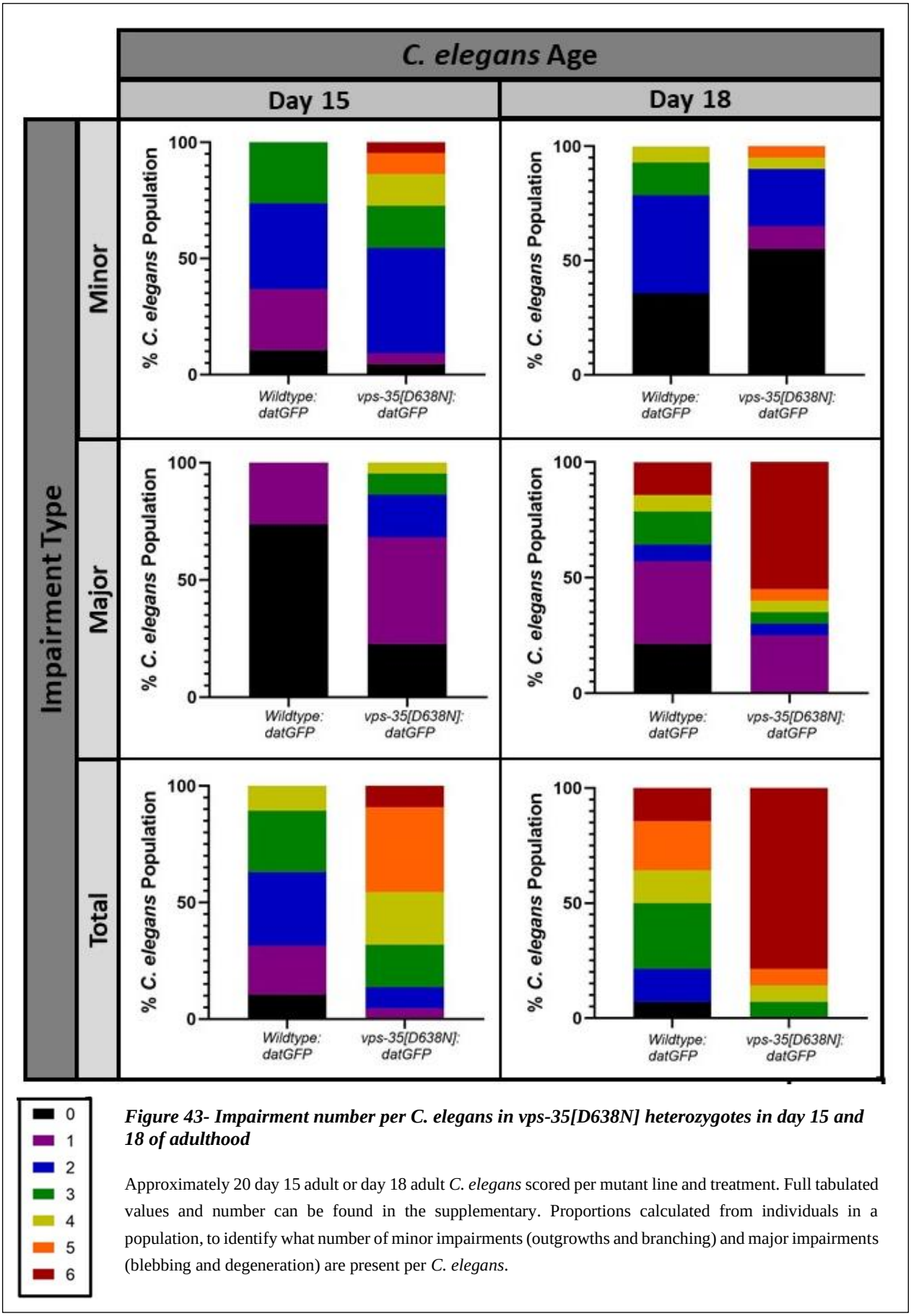

Figure 43- Impairment number per C. elegans in vps-35[D638N] heterozygotes in day 15 and 18 of adulthood

Approximately 20 day 15 adult or day 18 adult *C. elegans* scored per mutant line and treatment. Full tabulated values and number can be found in the supplementary. Proportions calculated from individuals in a population, to identify what number of minor impairments (outgrowths and branching) and major impairments (blebbing and degeneration) are present per *C. elegans*.

3.9.4.4 *vps-35[D638N]* heterozygotes show a similar, but exacerbated neuropathology profile to wildtype in day 15 and day 18 of adulthood

In day 15 of adulthood the most common impairments illustrated in both the wildtype and *vps-35[D638N]* heterozygotes are minor impairments in the CEP neurons and major impairments in the ADE neurons, this just differs in extent between genotypes (Figure 44). In the wildtype 90% of the population have one or more minor impairments in the CEP neurons, with 60% showing two or more, while over 90% of the *vps-35[D638N]* population show two or more minor impairments, with 25% showing this in all four CEP neurons. Furthermore, the second most common pathology for both genotypes are major impairments in the ADE neurons. In the wildtype approximately 25% of the population show major ADE impairments in one neuron, while in the *vps-35[D638N]* heterozygote, this is exhibited in 60% of the population, with a further 15% exhibiting impairments in both ADE neurons. By day 18 of adulthood, the wildtype is exhibiting minor and major impairments in the CEP neurons, with 50% of the population showing one or more major impairments in the CEP neurons. In the *vps-35[D638N]* heterozygote population, over 50% show major impairments in all four CEP neurons and all *C. elegans* in the population show major impairments in the ADE neurons, with over 65% of the population exhibiting blebbing or degeneration of both ADE neurons. For the wildtype, only 15% show major impairments of both ADE neurons, while 60% show impairments in one. This illustrates a similar pattern in neuropathology, but these pathologies are exhibited to a greater extent in the *vps-35[D638N]* heterozygote.

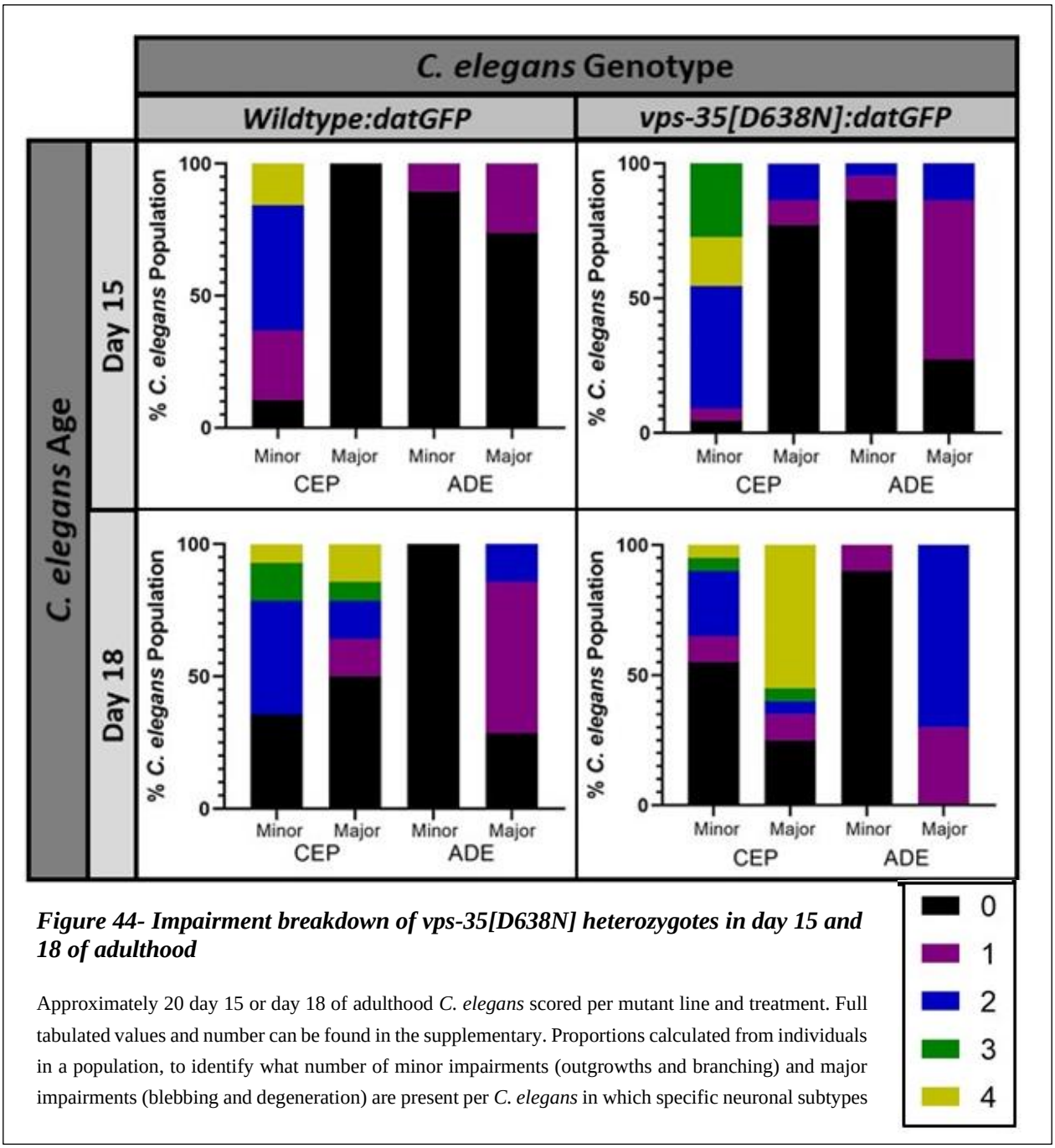

Figure 44- Impairment breakdown of vps-35[D638N] heterozygotes in day 15 and 18 of adulthood

Approximately 20 day 15 or day 18 of adulthood *C. elegans* scored per mutant line and treatment. Full tabulated values and number can be found in the supplementary. Proportions calculated from individuals in a population, to identify what number of minor impairments (outgrowths and branching) and major impairments (blebbing and degeneration) are present per *C. elegans* in which specific neuronal subtypes

Summary of Results Chapter I:

Characterising the *vps-35[D638N]* mutation in *C. elegans*

Characterisation of the novel *vps-35[D638N]* model for VPS35[D620N] PD has illustrated that this mutation in this orthologue leads to age-dependant impairments in dopaminergic behaviour, increased dopaminergic neurodegeneration compared to the wildtype and cellular perturbations which could underpin the dopaminergic impairments. This suggests that VPS-35[D638N] leads to PD relevant phenotypes for functional modelling and that this novel model developed and characterised here could be a beneficial new approach. Studies of the gene segregation patterns and fertility suggest that a more complex mechanism of action than loss of function alone could be implicated in VPS-35[D638N] mutation, supported by the contrasting phenotypes of the *vps-35* deletion model and the *vps-35[D638N]*. Following the establishment of relevant phenotypes in the *vps-35[D638N]*, its proposed interplay with LRRK2, (LRK-1 in *C. elegans*) will later be investigated. Prior to this, the conservation extent between *C. elegans* LRK-1 and human LRRK2 will be established, to verify if *C. elegans* are an appropriate model for dissecting the VPS35/LRRK2 interplay, as a mechanism of VPS-35[D638N] pathogenesis.

Chapter IV: *C. elegans* LRK-1 as a model for human LRRK2 function

C. elegans LRK-1 is an ancestral gene and potential ortholog of human LRRK1 and LRRK2. Early studies of LRK-1, utilising transgenic overexpression of LRK-1 in *C. elegans* have suggested it has shared roles with LRRK2 in synaptic vesicles trafficking (230), a function not associated with LRRK1. This suggests that *C. elegans* LRK-1 may share some functionality with LRRK2, posing as a potential reductionist model of LRRK2 function. However, the conservation extent needs to be established. In this chapter, novel CRISPR/Cas9 point mutant *C. elegans* with PD relevant and catalytic point mutations integrated into *C. elegans* LRK-1 have been characterised and contrasted against existing *lrk-1* deletion and human LRRK2 expressing models. The overall functional conservation has been assessed throughout this chapter, through contrasting the behavioural and cellular phenotypes of point mutants with proposed divergent catalytic consequences of mutation. This chapter will also cover the efforts made throughout this project to establish a method for LRK-1 detection, through the testing of existing antibodies, the development of novel sera and the establishment of FLAG tagged LRK-1 models. This chapter aims to assess LRK-1's suitability as a novel model for LRRK2 function.

4.1 *C. elegans* LRK-1 shows conservation with human LRRK2 *in silico*

Prior to and following the generation of a novel LRK-1 model of LRRK2 function, bioinformatic analysis was undertaken between the human orthologues LRRK1 and LRRK2 and C. elegans LRK-1, in order to assess its suitability as a novel disease model.

4.1.1. Sequence and domain conservation between human LRRK1 and LRRK2, with *C. elegans* LRK-1

In terms of amino acid sequence, LRK-1 has a similar sequence identity with LRRK1 and LRRK2, with an identity of 20.9% and 20.3%, a similarity of 35.9% and 36.3% and gaps of 25.6% and 25.7% respectively, shown in Table 23. LRK-1 differs from LRRK1 and LRRK2. However, these differences are very marginal, suggesting that there is may not be neofunctionalism in LRRK2, as it is not significantly different in conservation with LRK-1 from LRRK1.

Human Protein	PD Relevant	C. elegans Protein	Ebi tool	Matrix	Gap Open	Gap Extend	Identity	Similarity	Gaps
LRRK2	Yes	LRK-1	Emboss stretcher	BLOSUM 62	12	2	572/2823 (20.3%)	1025/2823 (36.3%)	726/2823 (25.7%)
LRRK2	Yes	LRK-1	Emboss needle	BLOSUM 62	10	0.5	571/3087 (18.5%)	990/3087 (32.1%)	1254/3087 (40.6%)
LRRK2	Yes	LRK-1	Emboss matcher	BLOSUM 62	14	4	164/649 (25.3%)	295/649 (45.5%)	42/649 (6.5%)
LRRK1	No	LRK-1	Emboss stretcher	BLOSUM 62	12	2	529/2528 (20.9%)	908/2528 (35.9%)	648/2528 (25.6%)
LRRK1	No	LRK-1	Emboss needle	BLOSUM 62	10	0.5	566/2635 (21.5%)	932/2635 (35.4%)	862/2635 (32.7%)
LRRK1	No	LRK-1	Emboss matcher	BLOSUM 62	14	4	122/463 (26.3%)	218/463 (47.1%)	16/463 (3.5%)

Table 23-Sequence Conservation between C. elegans LRK-1 with human LRRK1 and LRRK2

The differences between LRK-1 and its human paralogs are predominantly found in the scaffold domains of the proteins, shown in figure 45. *C. elegans* LRK-1 has a large ankyrin repeat of 400 amino acids, followed by leucine rich repeats. LRRK1 has a small ankyrin repeat, of 200 amino acids, followed by leucine rich repeats. LRRK2 diverges from this, as it has a 600 amino acid armadillo domain, follows by a 150 amino acid ankyrin domain and the characteristic leucine rich repeat. LRRK1 and LRRK2 diverge in their functionality due to differing PPI networks, in which physical interactions are modulated by these scaffold domains. In proportion to the protein length, this scaffold region is intermediate in size between LRRK1 and LRRK2, suggesting that these

differentiate it. The gaps in sequence identity between LRK-1 and both LRRK1 and 2 are predominantly found in these scaffold regions.

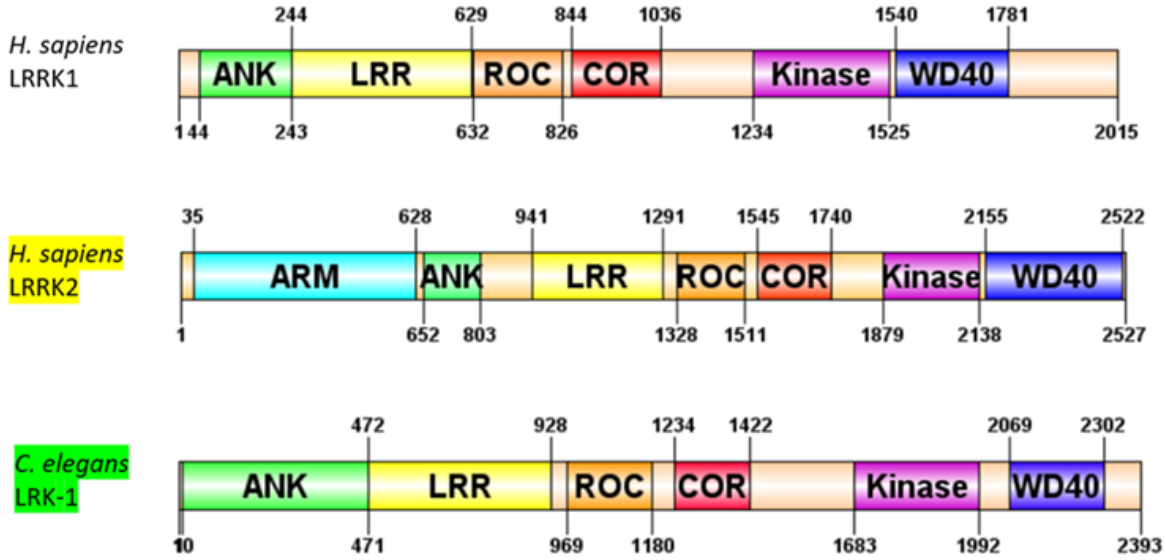

Figure 45-Protein Domain Organisation between C. elegans LRK-1 and human LRRK1 and LRRK2

Linear visualisations were generated through DOG2.0 software, as detailed in chapter 2 2.1. Domain information, including starting and end amino acid, was obtained from ProSite and InterPro prior to mapping. LRRK2 diffrs from human LRRK1 and C. elegans LRK-1 in that it has an armadillo domain (ARM turquoise). All three proteins have an ankyrin (ANK, green), Leucine Rich Repeat (LRR, yellow), Ras-like GTP-ase (ROC, orange), C-terminal of Roc (COR, red), Kinase (Purple) and WD40 (Blue) domains. The location of each of these domains differs slightly between proteins, but the sequential organisation is conserved.

Predominantly, these mutations are found in the catalytic ROC-COR and kinase domains and all are directly conserved in *C. elegans* LRK-1. Pathogenic point mutations in LRRK2 clearly have functional consequences, thus these residues are integral in LRRK2 function. The fact that all are conserved in *C. elegans* LRK-1 further suggests the evolutionary conservation of LRRK2 function with LRK-1 and that LRK-1 could be a promising, reductionist novel model for LRRK2 functionality.

Position	**Wildtype**	**Pathogenic**	**Wildtype Residue Conserved in *C. elegans* LRK-1?**
1437	N	H	Yes
1441	R	C	Yes
1441	R	G	Yes
1441	R	H	Yes
1699	Y	C	Yes
2019	G	S	Yes
2020	I	T	Yes

Table 24- Confirmed Parkinson's pathogenic point mutations in LRRK2 and conservation in C. elegans LRK-1

4.1.2 Tissue Expression of LRK-1 in C. elegans

TextMining was undertaken on Wormbase to establish the known tissues in which LRK-1 was highly expressed. Convergent with VPS-35, LRK-1 is highly expressed in head and tail neurons, as shown in table 25, suggesting potential neuronal function. It is highly expressed in the body wall musculature, hypodermis and intestine and pharynx.

Expression Tissue	**Function and Location of Tissue in *C. elegans***	**Relevance to functional modelling of Parkinson's protein LRK-1**
Head Neurons	Diverse functionality, most dense clusters if neurons found in the head of *C. elegans*	6 of the 8 dopaminergic neurons *C. elegans* possess are found in the head ganglion. Strongly suggests LRK-1 has role in neuronal function.
CAN Neurons	Mid-Body, lateral sides, neuron with unknown function.	Suggests LRK-1 has a role in neuronal function
Tail Neuron	Cluster of neurons found in the tail	Suggests LRK-1 has a role in neuronal function
Anterior/Posterior Distal Tip Cell	Progenitor cells of the hermaphrodite gonad, migrate in development, lay at the tip of each gonadal arm	Cell migration is important in immunity and development, LRRK2 has roles in immunity so could use LRK-1/distal cell tip as a potential model.
Vulva	External connection between environment, function in egg-laying and mating. Mid-section of body	
Pharynx	Muscular pump, import nutrients through mouth and to intestine	
Hypodermis	Epithelial system of *C. elegans*, made of main body syncytium and smaller hypodermal calls of head and tail	
Body Wall Musculature	Core muscle system found in *C. elegans* across body	

Table 25- Tissue expression of LRK-1 in C. elegans

4.1.3 Interactome conservation between human LRRK2 and C. elegans LRK-1

The first layer interactome of LRK-1 was studied (Table 26), in order to assess the conservation extent between LRK-1 and LRRK2. The ROCO proteins, particularly LRRK2, have a very extensive interactome, consisting of hundreds of proteins (232). LRRK2 is considered a 'hub' protein, which relocates to many interactome networks at different times, with different and wide reaching functions (174). Through PINOT analysis, LRK-1 has no validated physical interactors confirmed by multiple detection methods. PINOT servers obtain data from WormBase and IntAct,

in WormBase PPI's were filtered for physical interactors and IntAct interactors include genetic regulation and protein DNA interaction, along with physical PPI's. 14 proteins were obtained in the LRK-1 interactome, 3 of these have no human paralog and are *C. elegans* specific genes. Only 1 interactor of LRK-1, MIG-5, has paralogs DVL1, 2 and 3, found in the known interactome of LRRK2. MIG-5 is a particularly interesting LRK-1 interactor, as it has roles in canonical WNT signalling, a process implicated with VPS35 in *C. elegans* and in humans and regulates neuronal polarity in *C. elegans*. It is known that LRRK2 interplays with WNT signalling pathway (344). The functions of all LRK-1 interactors have been broadly categorised into neuronal development, cell fate differentiation and vesicle transport.

Protein	**Database**	**Notable functions. GO-Biological process**	**Human Paralog**	**Paralog present in human LRRK2 interactome**
MIG-5	IntAct	• Canonical Wnt signalling pathway • Cell fate determination and migration • Embryonic morphogenesis • Neuron migration Cell polarity	DVL1, DVL2 and DVL3.	Yes All Present in LRRK2 interactome
UNC-130	IntAct	• Anatomical structure morphogenesis • Axon extension involved in axon guidance • Cell differentiation • Embryo development • Nervous system development	FOXD1	No
MLS-2	IntAct	• Mitotic spindle orientation, • Nematode larval development • Neuron differentiation involved in amphid sensory neuron development • Regulation of mesodermal cell fate specification	HMX1	No
UNC-16	Wormbase	• Synaptic vesicle transport • Vesicle-mediated transport • Locomotion • Oviposition • Defecation	MAPK8IP3 and SPAG9	No
TBX-9	IntAct	• cell fate specification • Early morphogenesis of intestine, hypodermis and body wall muscle.	EOMES and TBR-1	No

LIN-54	IntAct	• cell cycle • Regulation of transcription • Repress induction of vulval development	LIN-54 and TESMIN	No
PHP-3	IntAct	• Positive regulation of male tail tip morphogenesis. • Regulation of transcription, DNA-templated	HOXA10	No
ATHP-1	IntAct	• Negative regulation of transcription by RNA polymerase II • Regulation of transcription DNA template	PHF12	No
DAC-1	IntAct	• Transcription regulation	DACH2	No
DIE-1	IntAct	• Neuron development amphid sensory organ. • Positive regulation of gene expression	No paralog	-
ZTF-8	IntAct	• double-strand break repair	No paralog	-
DMD-5	IntAct	Unknown	DMRTA2	No
CELE_R06C1.6	IntAct	Unknown	No paralog	-
CELE_ZC204.12	IntAct	Unknown	No paralog	-

Table 26-First Layer Protein Interactome of LRK-1

4.2 Selection of LRK-1 point mutants for characterisation studies

Prior to the start of this research project, a plethora of *C. elegans* strains with point mutations in LRK-1 had been generated for characterisation studies, through CRISPR/Cas9 modification outsourced to Knundra transgenics Ltd. Unlike the *vps-35[D638N]* mutant, detailed in 3.2, all of these selected lrk-1 mutants were viable in homozygous form. In some human populations, the most common LRRK2 PD mutation LRRK2[G2019S], which is also the most well characterised in terms of functional studies. is relatively prevalent in the population, thus there are individuals homozygous for this mutation (345). These individuals have an indistinguishable PD symptomatic presentation compared to heterozygous LRRK2[G2019S] carriers, suggesting there may not be gene dosage effects and study of the mutation in homozygous form in *C. elegans* may be insightful. Furthermore, maintenance and study of homozygous mutations in *C. elegans* is a more viable experimental approach, than maintaining a heterozygous gene in the population.

These point mutations are novel and have not been extensively studied before in *C. elegans*. A focus of this research project will be dissecting the interplay of VPS35 with other PD associated proteins, most notably LRRK2. However, as *C. elegans* LRK-1 has not been extensively characterised, it is unclear how well conserved it is with human LRRK2, how relevant *C. elegans* may be as a model for dissecting the VPS35/LRRK2 interplay and whether this avenue of VPS35 research should be pursued. Through characterising a subset of these LRK-1 point mutations, in contrast with existing models of LRK-1/LRRK2 function in *C. elegans*, the functional conservation of *C. elegans* LRK-1 has begun to be established.

4.2.1 Prioritisation of LRK-1 point mutants for characterisation

Key LRK-1 point mutants studied include the orthologous point mutant for the PD associated kinase hyperactive LRRK2[G2019S], the most common PD mutation, which is located in the kinase domain and well characterised in *in vitro* and *in vivo* model systems. To compliment this, the synthetic LRRK2 kinase ablation mutation LRRK2[D1994A] has also been characterised, along with the synthetic GTPase ablation LRRK2[K1347A] in order to gain a biochemical dissection of LRK-1 function, to assess its functional relevance. Following characterisation of these, another LRK-1 orthologous PD mutant LRRK2[R1441C] was studied to contrast. This point mutation is located in the GTPase domain, around a cluster of pathogenic PD point mutants, suggesting high functional relevance of this region. Preliminary characterisation of this point mutant will enable the contrasting of kinase located and GTPase located PD pathogenic mutants in *C. elegans* LRK-1, to further understand the functional conservation and relevance for further study.

To contrast with the novel point mutants, an already established *lrk-1(tm1898)* deletion mutant was tested alongside, in order to characterise the effect of total loss of *lrk-1* function. Also, the enables the assessment of the effect of point mutations in *lrk-1*, to assess whether they are more reflective models for gain of function point mutations than deletion models, as discussed in 1.5.4. Furthermore, transgenic dopaminergic neuron specific LRRK2 wildtype and PD LRRK2[G2019S] have been tested, as established LRRK2 models to contrast *lrk-1* point mutants with.

The nomenclature detailed on the ensuing graphs for our novel *lrk-1* point mutations and their human orthologous mutations in *LRRK2* can be found in table 27, along with the genotypes of the human LRRK2 expressing transgenic lines. Full details of the *C. elegans* genotypes can be found in the methodology, chapter 2.2.1.

Nomenclature on Graph	**Human orthologue and/or functionality**
lrk-1[G1876S]	LRRK2[G2019S], most common PD point mutation, found in kinase domain, 2-4-fold kinase hyperactivity illustrated *in vitro* and *in vivo*. Well characterised in multiple models.
lrk-1[D1847A]	LRRK2[D1994A], synthetic kinase ablation utilised in *in vitro* studies, ablates kinase activity of LRRK2.
lrk-1[K988A]	LRRK2[K1347A], synthetic GTPase ablation utilised in *in vitro* studies, prevents GTP binding to LRRK2.
lrk-1[R1087C]	LRRK2[R1441C], common PD point mutation, found in the GTPase domain, proposed 4-fold kinase hyperactive *in vitro*.
lrk-1(tm1898)	*lrk-1* gene deletion, established loss of function model
Hsa-LRRK2	Dopaminergic transgenic expression of wildtype human LRRK2
Hsa-LRRK2[G2019S]	Dopaminergic transgenic expression of PD mutant human LRRK2[G2019S]

Table 27- Nomenclature of Selected LRK-1 point mutants and transgenic human LRRK2 expressing C. elegans, characterised in chapter 4.

Following preliminary characterisation studied, the *lrk-1[G1876S]*, *lrk-1[D1847A]* and *lrk-1(tm1898)* were four times outcrossed, enabling characterisation to publication standard and crossing with the *vps-35[D638N]* heterozygote, as detailed in chapter 5.

4.3 Motility as a marker for neuromuscular health

Preliminary studies of *lrk-1* CRISPR/Cas9 point mutants prior to outcrossing have illustrated alterations in neuromuscular health in day 1 and day 5 of adulthood in crawling motility, shown in figure 46. Study of motility can shed insights into neuromuscular function, a global readout for *C. elegans* health.

4.3.1 Crawling speed in selected novel *lrk-1* CRISPR/Cas9 point mutants and transgenic human LRRK2 expressing *C. elegans*

The crawling speed of *lrk-1[G1876S]* mutant is not significantly different from the wildtype in day 1 of adulthood, suggesting there are not global impairments in development caused by this mutation, or in early adulthood. However, by day 5 of adulthood, the crawling speed of this mutant is significantly reduced compared to the wildtype and *lrk-1[G1876S]* population in day 1 of adulthood, suggesting global impairments and potentially decreased fitness.

In contrast, the GTP binding defective mutant *lrk-1[K988A]*, based on the synthetic gatekeeper mutation K1347A, prevents GTP binding in human LRRK2. This population has no significant difference in crawling motility compared to the wildtype in day 1 or day 5 of adulthood, however there is greater variance in speed of day 5 *lrk-1[K988A]* mutants. Despite this, there is no age dependant reduction in speed between day 1 and day 5 *lrk-1[K988A]* mutant populations.

Furthermore, the LRRK2 kinase ablation gatekeeper mutation D1994A, *lrk-1[D1847A]* in *C. elegans* in day 1 of adulthood, exhibit significantly increased motility, compared to the wildtype. This is inverted by day 5 of adulthood, with the *lrk-1[D1847A]* showing reduced motility, a convergent phenotype from both the *lrk-1[G1876S]* and *lrk-1[K988A]*.

Deletion *lrk-1* models have been extensively utilised in prior studies of LRK-1 function, however as discussed in 1.5.4, deletion models may not be as amenable as a model for LRRK2 Parkinson's mutations, which lead to increased kinase activity. We contrasted the *lrk-1(tm1898)* deletion model alongside our novel point mutants. Deletion of *lrk-1* does not affect the crawling speed of day 1 adult *C. elegans*, however by day 5 of adulthood, *lrk-1* deletion *C. elegans* are significantly slower than the wildtype, suggesting LRK-1 may have a role in global health.

Transgenic dopaminergic neuron specific LRRK2 wildtype and PD LRRK2[G2019S] expressing mutant lines were obtained and tested. From this we could evaluate transgene expression compared with endogenous CRISPR/Cas9 *lrk-1* knock in mutants. There was a small but significant decrease in motility in the day 1 adult LRRK2 G2019S expressing lines, however, this was not reflected in day 5 of adulthood, with a significantly enhanced crawling speed. Notably, these transgenic lines

generated by Saha and colleagues (244), show vastly differing expression levels of LRRK2, with the LRRK2[G2019S] expression almost 3-fold higher than the wildtype LRRK2 expressing strain. This suggests that endogenous *lrk-1* knock-in lines may be a more valid, insightful model to study, than transgenic lines with just dopaminergic specific expression at incomparable level.

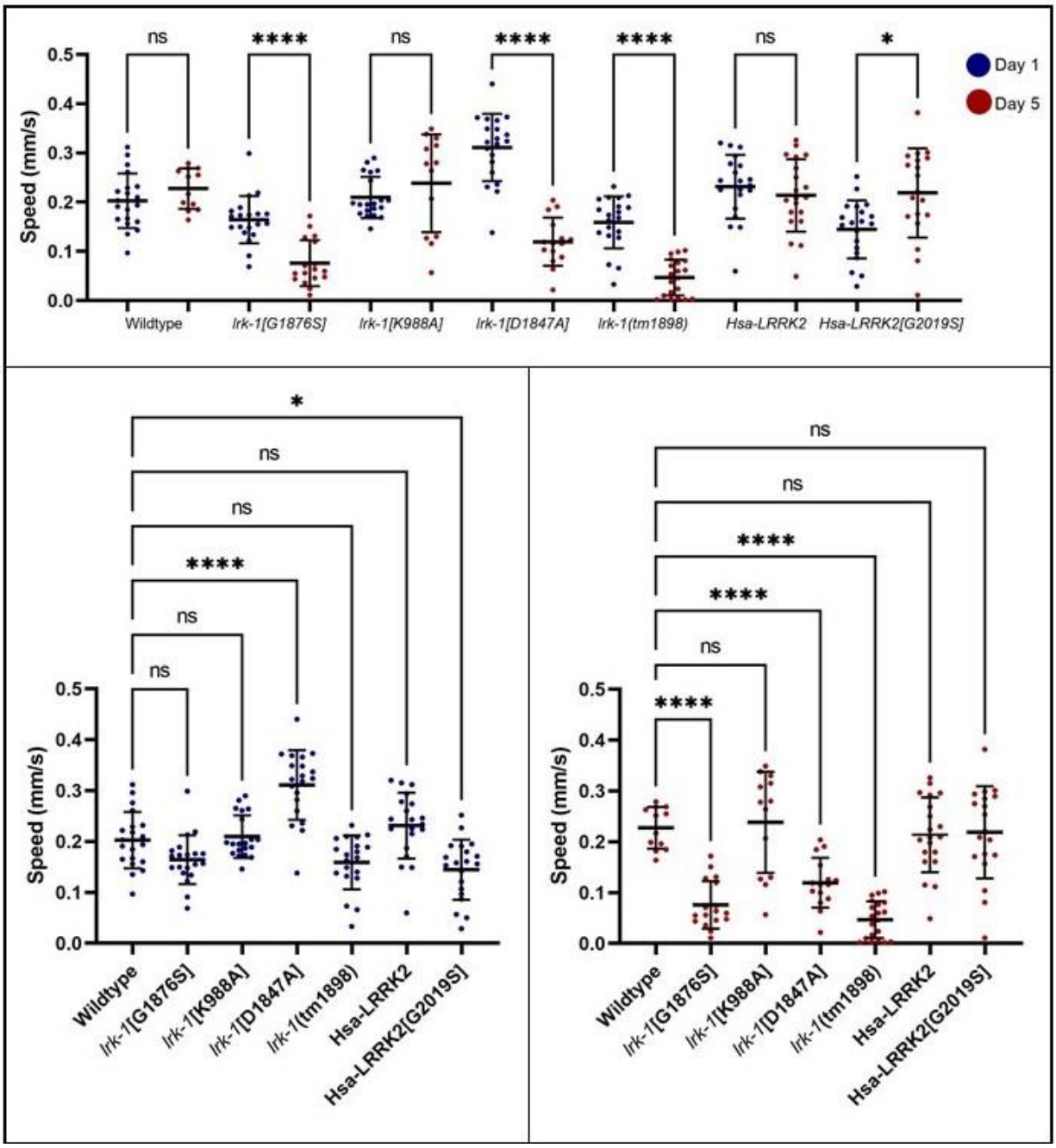

Figure 46-Crawling Speed of Day 1 and Day 5 Adult LRK-1 point mutants and human LRRK2 transgenic C. elegans

>12 *C. elegans* were assayed per line at each developmental stage. Day 1 and Day 5 adults were from the same age-synchronised population. One way ANOVA with Brown-Forsythe and Welch Correction for unequal standard deviations undertaken. Full P values and descriptive statistics including mean, standard deviation and number can be found in the supplementary, 4.3. Human orthologues and proposed functionality of mutants detailed on graphs can be found in table 27.

4.3.2 Crawling Speed of LRK-1 'R1441C PD mutant' is not significantly different in day 1 of adulthood, but impaired by day 5

Following characterisation of the *lrk-1[G1876S]* PD mutant, preliminary investigation of the *lrk-1[R1087C]* PD mutant was undertaken, to contrast the two pathogenic mutations located in different catalytic domains of LRRK2 and LRK-1 (Figure 47). This study illustrated that the crawling speed of *lrk-1[R1087C]* is not significantly different from the wildtype in day 1 of adulthood, but significantly slower by day 5 of adulthood. This suggests global impairments and potentially reduced fitness, convergent with phenotypes shown by *lrk-1[G1876S]*.

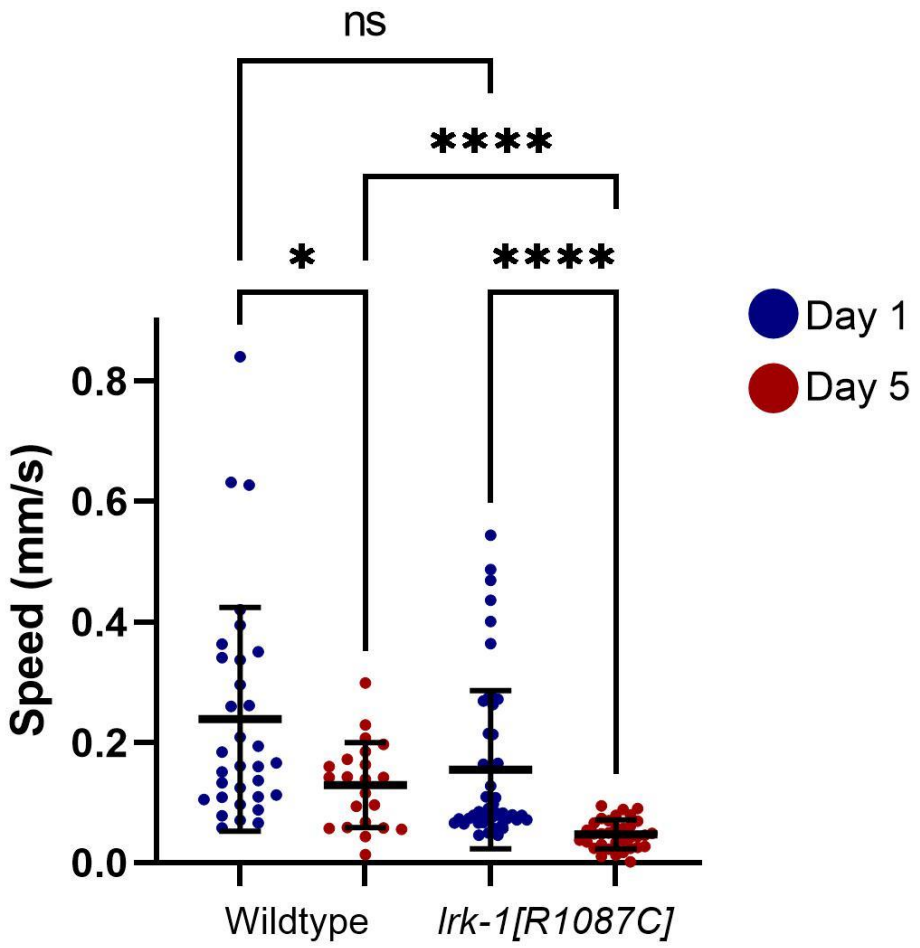

Figure 47-Crawling Speed of lrk-1[R1087C] PD mutant in Day 1 and Day 5 of Adulthood

>12 *C. elegans* were assayed per line at each developmental stage. Day 1 and Day 5 adults were from the same age-synchronised population. One way ANOVA with Brown-Forsythe and Welch Correction for unequal standard deviations undertaken. Full P values and descriptive statistics including mean, standard deviation and number can be found in the supplementary. Human orthologues and proposed functionality of mutants detailed on graphs can be found in table 27.

4.3.3 Swimming as a marker for neuromuscular health

Swimming in *C. elegans* is a thrashing motion, quantified as body bends per minute. Swimming has a high bioenergetic demand and speed is partially modulated by dopaminergic neurons (334). Motility depends upon neuronal and muscular function, along with the cellular energy status. The PD associated *lrk-1[G1876S]* shows a significantly reduced swimming motion in figure 48, congruent with its reduced crawling speed shown in figure 48. LRRK2[G2019S] induces toxicity through increasing kinase activity 2-4-fold in a toxic gain of function mechanism. Interestingly, the kinase activity ablated mutant *lrk-1[D1847A]* has been generated and does not exhibit this phenotype, along with the LRK-1 deletion *lrk-1(tm1898),* suggesting kinase dependant impairments in swimming. A GTP binding defective LRK-1 mutant has been generated, *lrk-1[K988A],* shows significantly reduced swimming motility. By contrasting these key mutants, we can begin to evaluate the functional conservation of LRK-1 with LRRK2 and then dissect the enzymatic roles of LRK-1, enabling further specific characterisation studies.

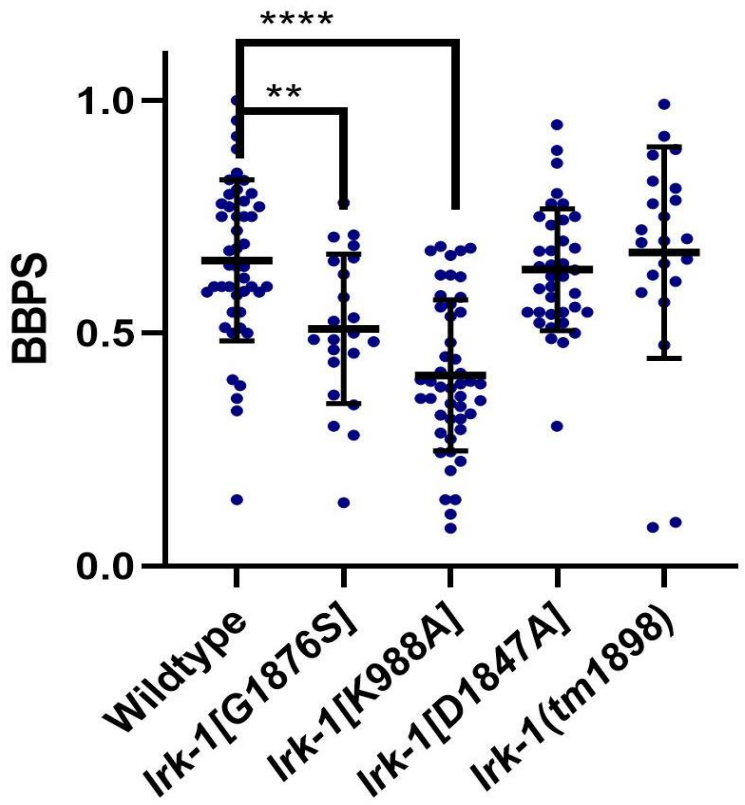

Figure 48- Free Swimming motility (BBPS) in selected C. elegans LRK-1 mutants

>12 day 1 adult *C. elegans* were assayed per line . One way ANOVA with Brown-Forsythe and Welch Correction for unequal standard deviations undertaken. Full P values and descriptive statistics including mean, standard deviation and number can be found in the supplementary. Human orthologues and proposed functionality of mutants detailed on graphs can be found in table 27.

4.4 LRK-1 and LRRK2 *C. elegans* mutant survival in response to oxidative stress

Novel LRK-1 point mutants were tested alongside established *lrk-1* deletion and dopaminergic human LRRK2 transgenic models for vulnerability to oxidative stress through rotenone treatment. Survival was assayed following transfer at L4 stage for the subsequent days. Rotenone is an established toxin model of PD and a mitochondrial complex I inhibitor, as an environmental pesticide linked to Parkinson's development its impact was studied against different genetic backgrounds. Key catalytic and the LRRK2[G2019S] equivalent LRK-1 point mutants were studied, alongside a *lrk-1* deletion model and the LRRK2 transgenic humanised models. 15mM within the NGM was utilised for this assay, with five populations per genotype studied. Prior experiments utilised 10mM rotenone, but this resulted in no lethality of the *C. elegans* after 5 days of exposure and 20mM rotenone, which resulted in excessive lethality with the loss of >60% *of C. elegans* overnight, thus 15mM was the optimal concentration for chronic assay.

4.4.1 Novel LRK-1 point mutants and human LRRK2 expressing *C. elegans* show altered survival in response to oxidative stress

In response to 15mM rotenone treatment, the Parkinson's associated and proposed kinase overactive *lrk-1[G1876S]* point mutant shows no significant difference in survival compared to the wildtype, shown in figure 49. In contrast, the synthetic kinase ablated mutant *lrk-1[D1847A]* shows enhances survival in response to oxidative stress, while the *lrk-1[K988A]* shows no significant difference in survival in response to oxidate stress, suggesting ablation of the GTPase domain has less impact upon oxidative stress response than the kinase domain. This could suggest that having an intact GTPase domain, with ablated kinase activity could contribute to oxidative stress resistance.

Established humanised LRRK2 transgenic and deletion of *lrk-1* models show divergent phenotypes in survival to oxidative stress exposure. Notably, the *lrk-1* deletion model shows a significantly reduced survival compared to the wildtype, suggesting LRK-1 may have a global role in oxidative stress protection. This may be independent of specific catalytic domains, as ablation of the GTPase and kinase domain do not result in this phenotype in the *lrk-1* point mutants. Furthermore, overexpression of wildtype LRRK2 in the dopaminergic neurons leads to increased survival, divergent to the *lrk-1* deletion, adding to the suggestion that LRK-1/LRRK2 may have a role in oxidative stress response, as additive protein expression results in this phenotype. However, human LRRK2 expression is not global and only localised to the dopaminergic neurons. The human LRRK2[G2019S] shows no significant difference in survival, suggesting that Parkinson's

mutation of this protein eliminates this additive protective effect, however this phenotype is not shown in the *lrk-1[G1876S]* equivalent point mutant.

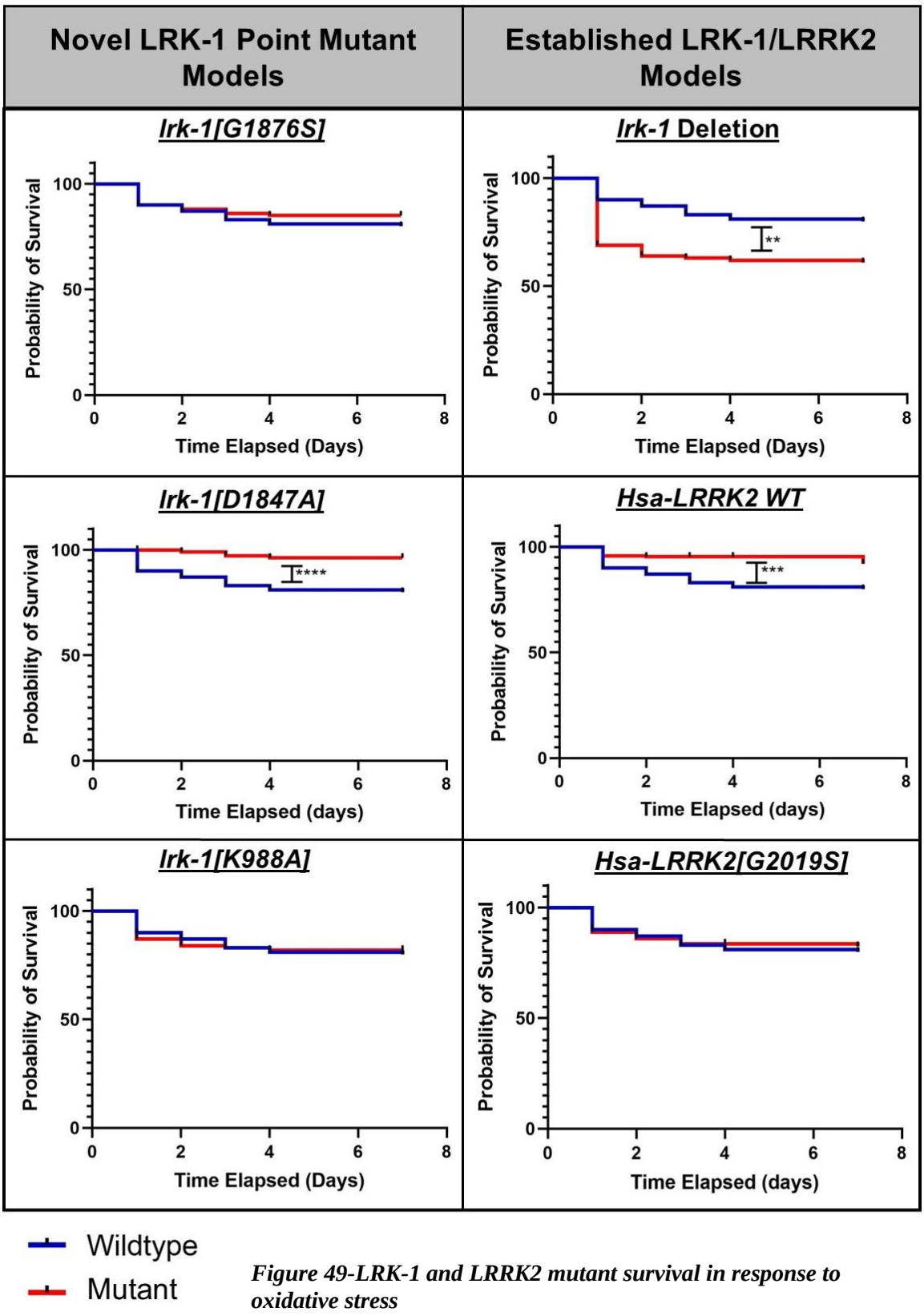

Figure 49-LRK-1 and LRRK2 mutant survival in response to oxidative stress

Analysis undertaken through Kaplan-Myer plot of survival, followed by curve comparison for statistical significance, through Mantel-Cox and Gehan-Breslow-Wilcoxon tests. Full descriptive statistics exhibited in supplementary. Approximately 50 C. elegans assayed per mutant line.

4.5 LRK-1 Parkinson's mutants show impaired dopaminergic phenotypes

4.5.1 Investigation of basal slowing phenotypes in established LRRK2 transgenic, *lrk-1* deletion and novel *lrk-1* CRISPR/Cas9 point mutants

The basal slowing response is an established dopaminergic function dependant behavioural phenotype, discussed and validated in 3.7.1. *C. elegans* with functional dopamine signalling slow to feed upon reaching a bacterial lawn (86), while *C. elegans* with defects in this system show impairments in this behaviour and is a PD relevant behavioural phenotype in *C. elegans* models. During the investigation of our novel point mutants, the basal slowing response of established LRRK2 *C. elegans* models were tested to be contrasted against. These include dopaminergic neuron expressing LRRK2 transgenic lines, established by Saha and colleagues (244) and the widely characterised *lrk-1* deletion mutant (230,244,269), as detailed in 4.3. The basal slowing response of these lines, along with the novel *lrk-1* point mutants were assayed in day 1 and day 5 of adulthood, in order to assess their dopaminergic function and potential suitability as novel, reductionist PD models of LRRK2 function. Through investigating key point mutants in LRK-1, orthologous to mutations in LRRK2 which are well characterised in alternative model systems, it has also been possible to begin to establish the conservation extent between LRK-1 and LRRK2. Orthologues of the LRRK2 PD mutant *lrk-1[G1876S]* was investigated, along with orthologous mutants to the GTP binding defective and kinase ablation mutation *lrk-1[K988A]* and *lrk-1[D1847A]* respectively (Figure 50).

The PD associated *lrk-1[G1876S]* was assayed for dopaminergic function. This proposed 'kinase overactive' PD mutation, exhibits an impaired basal slowing response in day 1 of adulthood. This is exacerbated with age, leading to an ablated basal slowing response by day 5 of adulthood, suggesting significant dopaminergic dysfunction.

The GTP binding defective mutant *lrk-1[K988A]* is orthologous to the synthetic gatekeeper mutation K1347A, resulting in a loss of GTP dependant GTPase activity in human LRRK2, shows a small but significant reduction in basal slowing compared to the wildtype in day 1 of adulthood. However, by day 5 of adulthood, the *lrk-1[K988A]* mutant shows no significant difference in basal slowing compared to the wildtype, suggesting the GTPase of LRK-1 may be important in its functionality in neuronal development. This enables the dissection of LRK-1's role with more specificity than the *lrk-1* deletion mutant, as a specific catalytic activity can be targeted. The lrk-1 deletion shows a similar basal slowing profile to the *lrk-1[K988A]*, suggesting that LRK-1 GTPase function may be implicated in day 1 neuronal health.

The kinase ablation *lrk-1[D1847A]*, shows no difference in basal slowing response compared to the wildtype in day 1 of adulthood. By day 5 of adulthood, this mutant shows no significant reduction in basal slowing, while the wildtype does, suggesting kinase ablation may be neuroprotective. In day 5 this is a divergent phenotype to the 'kinase overactive' PD orthologous *lrk-1[G1876S]* and *lrk-1[R1087C]* (discussed in 4.5.2) mutants, suggesting that there may be kinase dependant phenotypes in this model. This would suggest shared conservation between LRK-1 and LRRK2, augmenting its relevance as a potential novel model.

Deletion of *lrk-1* leads to a reduced basal slowing response in day 1 of adulthood, but no significant difference by day 5 of adulthood, illustrating that there is no age-dependant dopaminergic phenotype, and that LRK-1 may play a role in dopaminergic neuronal development. Prior RNAi silencing and deletion studies of LRK-1 have illustrated that there is no significant alterations in dopaminergic phenotypes from day 3 onwards, consistent with this data. Deletion studies are not orthologous to modelling gain of function mutations but demonstrate the global function of LRK-1 in *C. elegans*.

The basal slowing response of human LRRK2 expressing *C. elegans* models illustrate no significant difference in the basal slowing response in day 1 and day 5 of adulthood. Transgenic expression of wildtype LRRK2 shows no significant alterations, illustrating that increased LRRK2 protein levels do not impact dopaminergic function in *C. elegans*. Pertinently, transgenic expression of the Parkinson's mutant LRRK2 G2019S does not impact the basal slowing response in *C. elegans*. This expression is upon a wildtype background, rather than *lrk-1* deletion and it is unknown whether LRK-1 could have any compensatory effect in maintaining neuronal health, however our data suggests that there may not be an additive effect of kinase activity between LRK-1 and transgenic human LRRK2. Importantly, these transgenic lines show significantly different expression levels of LRRK2 (244), so are not directly comparable to each-other, illustrating a need for more reflective models.

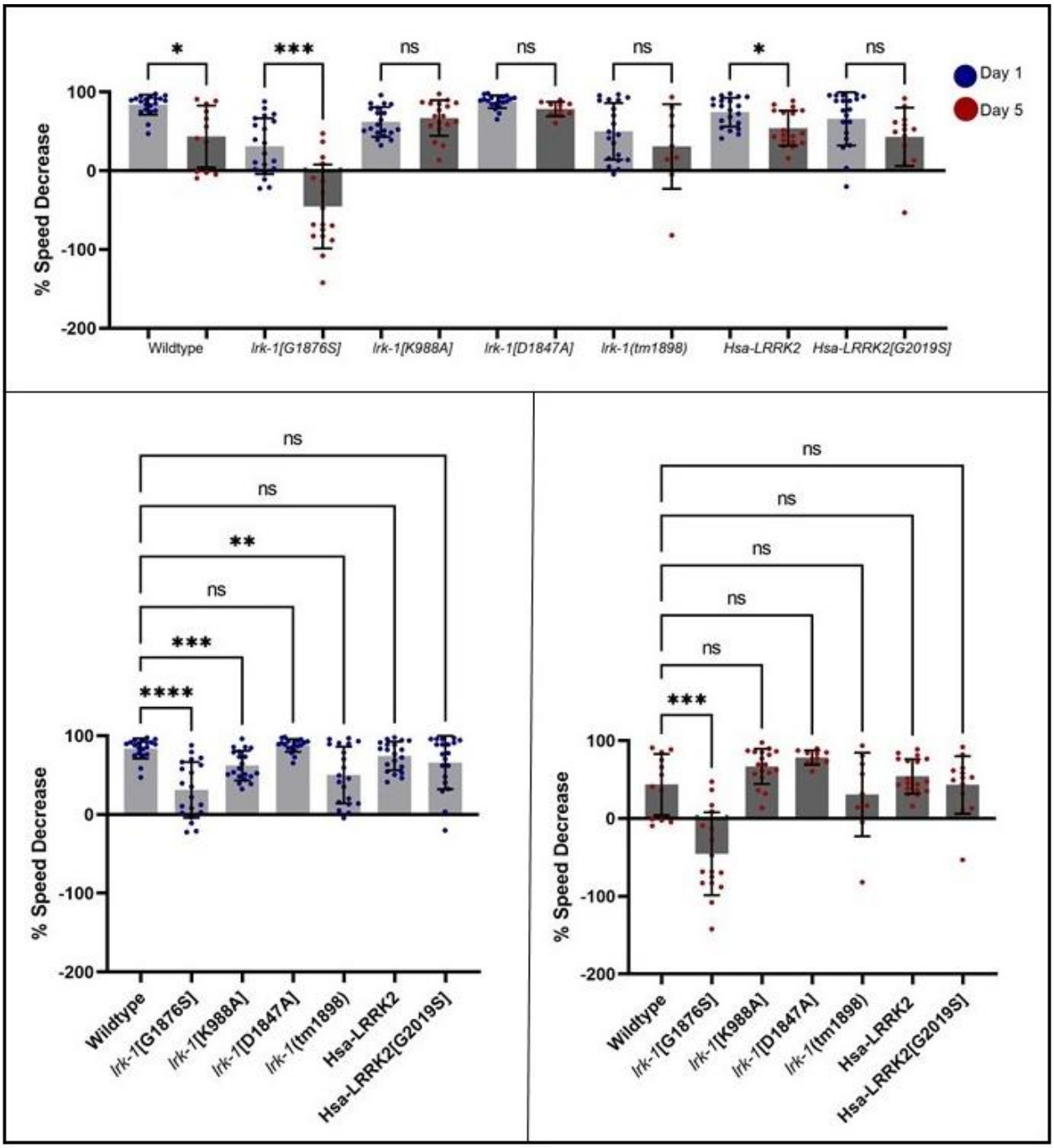

Figure 50-Basal Slowing response in established LRRK2 transgenic, lrk-1 deletion and novel lrk-1 CRISPR/Cas9 point mutants

>12 *C. elegans* were assayed per line at each developmental stage. Day 1 and Day 5 adults were from the same age-synchronised population. One way ANOVA with Brown-Forsythe and Welch Correction for unequal standard deviations undertaken. Full P values and descriptive statistics including mean, standard deviation and number can be found in the supplementary, 4.5. Human orthologues and proposed functionality of mutants detailed on graphs can be found in table 27.

4.5.2 LRK-1 Parkinson's mutant R1441C equivalent shows an impaired basal slowing response in day 5 of adulthood

Following the characterisation of the *lrk-1[G1876S]*, the LRRK2[R1441C] equivalent *lrk-1[R1087C]* was characterised, to assess the impact of a ROC-COR PD mutation against the kinase domain mutation *lrk-1[G1876S]* (Figure 51). In day 1 of adulthood, *lrk-1[R1087C]* does not show a significantly different basal slowing phenotype, however by day 5 of adulthood, the basal slowing response is significantly impaired. In people carrying LRRK2[R1441C] mutations, the age of PD onset and penetrance in comparison to LRRK2[G2019S] carriers is conflicting, with studies suggesting a similar age of onset (346) and other suggesting a later penetrance in LRRK2[R1441C] carriers (3), which may be reflected in this model. Notably, the wildtype in this assay does not show an age dependant decrease in basal slowing, as exhibited in other assays throughout this project.

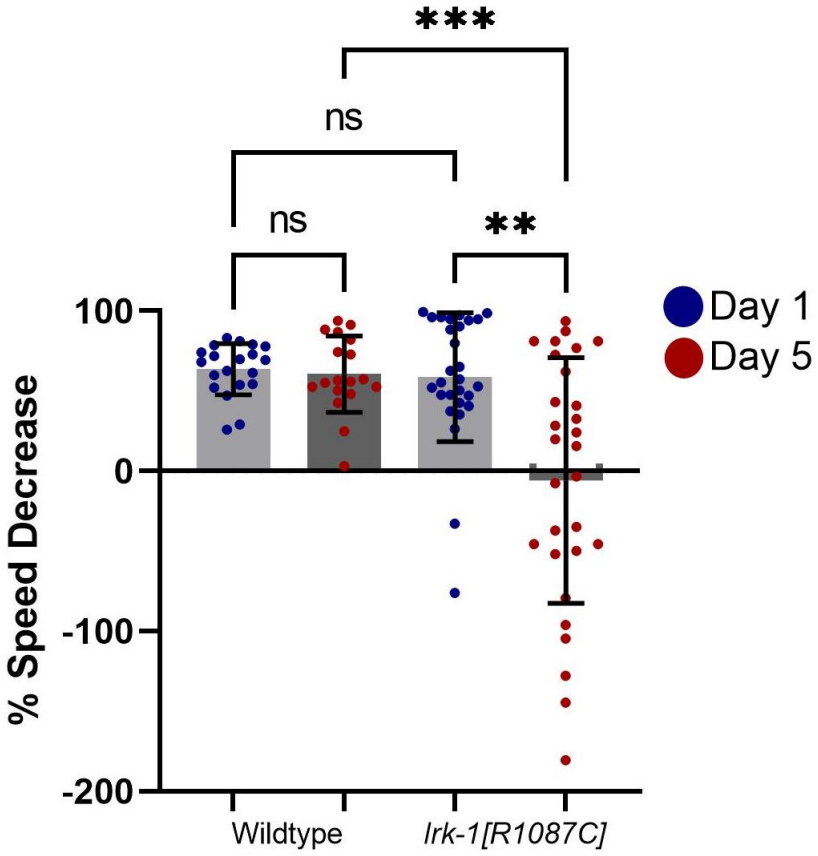

Figure 51- Basal Slowing Response of lrk-1[R1087C] Mutants in Day 1 and Day 5 of Adulthood

15-30 *C. elegans* were assayed per line at each developmental stage. Day 1 and Day 5 adults were from the same age-synchronised population. One way ANOVA with Brown-Forsythe and Welch Correction for unequal standard deviations undertaken. Full P values and descriptive statistics including mean, standard deviation and number can be found in the supplementary, 4.5. Human orthologues and proposed functionality of mutants detailed on graphs can be found in table 27.

4.6 Cellular Phenotypes of LRRK2/LRK-1 mutants

4.6.1 Inference of mitochondrial function of selected LRK-1 mutants through TMRE staining

Mitochondrial membrane potential can be inferred through the quantification of TMRE fluorescence, a mitochondria specific electron gradient sensitive dyes. The PD associated *lrk-1[G1876S]* shows a reduced mitochondrial membrane potential, 0.63 that of the wildtype, as measured by TMRE fluorescence in an area behind the pharynx (Figure 52). Notably, this is similar to the *vps-35[D638N]* heterozygotes. The GTP binding defective *lrk-1[K988A]* similarly shows a reduced mitochondrial membrane potential, of 0.74 of the wildtype. This is also reflected in the reduced swimming motility of this line, a high intensity exercise state with increased bioenergetic demand, highlighting a potential role of the ROC-COR domain in mitochondrial function. Interestingly, the kinase ablated mutant *lrk-1[D1847A]* exhibits the reverse phenotype, with a fluorescence twofold higher than the wildtype. This is particularly notable when the motility of these worms is considered, as they have a significantly faster crawling speed than the wildtype. No significant difference is shown in the knockout *lrk-1(tm1898)*, suggesting effects are catalytic activity dependant. Similarly, overexpression of human LRRK2 and LRRK2 G2019S have no effect, suggesting wildtype endogenous LRK-1 could be compensatory.

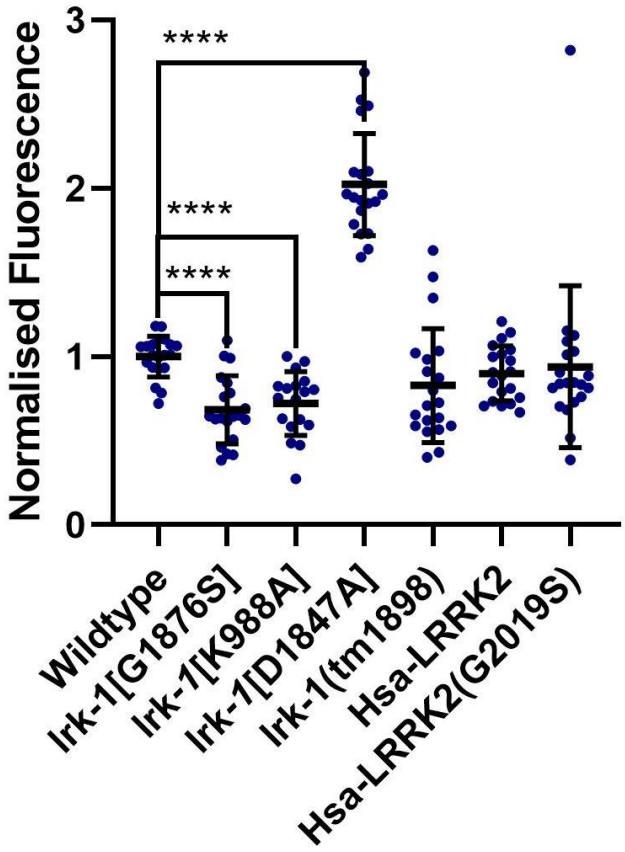

Figure 52-LRK-1 point mutants exhibit alterations in Mitochondrial Membrane Potential

15-20 worms analysed per line. Quantified 6000-pixel area behind the pharynx. Mean, Standard Deviation, number and P-values found in the supplementary. Undertook one-way ANOVA with multiple comparisons, all strains compared with Wildtype. Welch's correction, accounting for differing SDs. Full descriptive statistics can be found in the supplementary.

4.7 Treatment of selected LRK-1 point mutants with LRRK2 inhibitor Genentech 0877

LRRK2 inhibitors, targeting the kinase domain, are in early phase clinical trial for people with LRRK2 mutation consequent PD, with potential applications in idiopathic PD (167). *C. elegans* are a useful model in understanding the effects of pharmacological manipulation further. LRRK2 inhibitors developed by Genentech, GSK and Pfizer are available for fundamental research. These inhibitors could be a beneficial tool in the *C. elegans* lab, as an LRK-1 mutant phenotype has been established, in terms of the dopaminergic basal slowing response. The inhibitor Genentech0877 has been shown to rescue the basal slowing phenotype of *lrk-1[G1876S]* in a dose dependant manner, with no significant rescue exhibited in the deletion *lrk-1(tm1898),* kinase overactive *lrk-1[D1847A]*, or GTP binding defective *lrk-1[K988A]*. In murine preclinical models, Genentech0877 is selective and demonstrated to inhibit phosphor-serine1292 autophosphorylation in mice transgenically expressing LRRK2[G2019S], supporting their use in preclinical studies of LRRK2 function (347). Along with posing as a useful tool for further investigations, the suggested efficacy of Genetech0877 in improving dopaminergic phenotypes in *lrk-1[G1876S]* supports the hypothesis that LRK-1 is well conserved with LRRK2, in structure as well as function.

4.7.1 1.0mM Genentech0877 treatment in liquid culture leads to an improved basal slowing phenotype in *lrk-1[G1876S]*

Selected LRK-1 lines were treated with 1.0mM of LRRK2 inhibitor through larval development and assayed in day 1 of adulthood. Treatment of *lrk-1 [G1876S]*, lead to a significantly improved basal slowing response, suggesting LRK-1 inhibition and dopaminergic neuroprotection (Figure 53). This was not exhibited in the wildtype. Furthermore, the *lrk-1[G1876S]* does not exhibit a significantly impaired basal slowing response in this experiment, inconsistent with previous data, described in 4.5.1. For LRRK2 inhibitor administration, *C. elegans* were raised in liquid culture, placing them into a high bioenergetic exercise state of swimming, while in previous characterisation of the basal slowing response, *C. elegans* were raised on solid media. Recent publications have highlighted that swimming in *C. elegans* can enhance neuronal and neuromuscular health (330), thus alternative drug administration methods have been contrasted (4.7.2). Furthermore, GTP binding (*lrk-1[K988A]*) and Kinase ablated (*lrk-1[D1847A]*) mutants were treated with 1.0uM of Genentech 0877. This exhibited no significant difference in basal slowing, in both mutant lines.

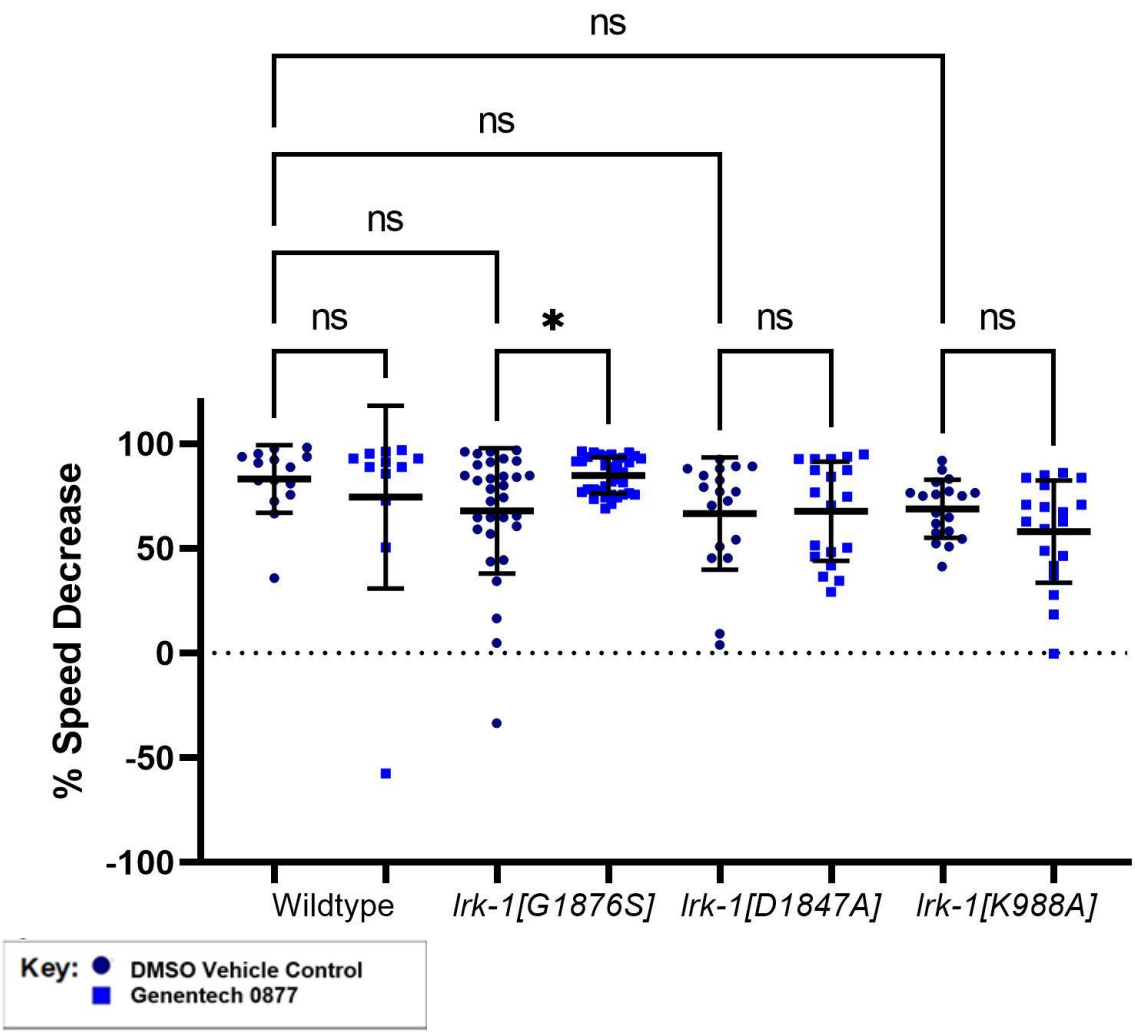

Figure 53-1.0mM Genentech 0877 leads to improved basal slowing in LRK-1[G1876S]

>12 *C. elegans* were assayed per line at each developmental stage. Day 1 and Day 5 adults were from the same age-synchronised population. One way ANOVA with Brown-Forsythe and Welch Correction for unequal standard deviations undertaken. Full P values and descriptive statistics including mean, standard deviation and number can be found in the supplementary, 4.5. Human orthologues and proposed functionality of mutants detailed on graphs can be found in table 27.

4.7.2 Administration through solid media treatment of a LRRK2 inhibitor to outcrossed LRK-1 lines demonstrate a rescued basal slowing response in *lrk-1[G1876S]*

Following preliminary data testing LRRK2 inhibitor Genentech 0877 in selected LRK-1 point mutants, the administration method was adapted to be utilised for solid media cultivation. In pharmacodynamic studies of *C. elegans*, liquid media feeding is most efficient (329), but swimming is a neuroprotective exercise state (330). As detailed in 4.7.1, this leads to an improved basal slowing response of *lrk-1[G1876S]* mutants compared to animals raised on solid media (4.5.1), thus eliminating our strong phenotype to test LRRK2 inhibitors against.

Prior to further investigation, selected LRK-1 mutants were outcrossed 3-4 times for further characterisation to publication standard. *C. elegans* were treated on solid media plates with 10mM Genentech0877 for 16 hours overnight, from late L4, for assay in day 1 of adulthood. *C. elegans* carrying the *lrk-1[G1876S]* mutation showed an impaired basal slowing response, consistent with 4.5.1, which was significantly rescued following Genentech0877 treatment, illustrated in figure 54A. Consistent with 4.7.1, *C. elegans* carrying the kinase ablated *lrk-1[D1847A]* mutation, GTP binding defective *lrk-1[K988A]* do not exhibit any significant alterations in basal slowing following Genentech 0877 treatment, nor do *lrk-1* deletion *C. elegans*, incorporated as an additional negative control.

Following on, the administration of Genentech 0877 was undertaken with day 5 adult *C. elegans*, to test if there was any impact upon the basal slowing response, shown in figure 54B. Treatment was undertaken overnight, from day 4 of adulthood. The *lrk-1[G1876S]* mutant line exhibited a significantly impaired basal slowing response, which was not rescued following Genentech0877 treatment, suggesting this timepoint may be too late to have a significant impact. The *lrk-1* deletion and *lrk-1[D1847A]* kinase ablated mutant did not show a significantly different basal slowing response from the wildtype, consistent with 4.5.1, with no impact following Genentech0877 treatment.

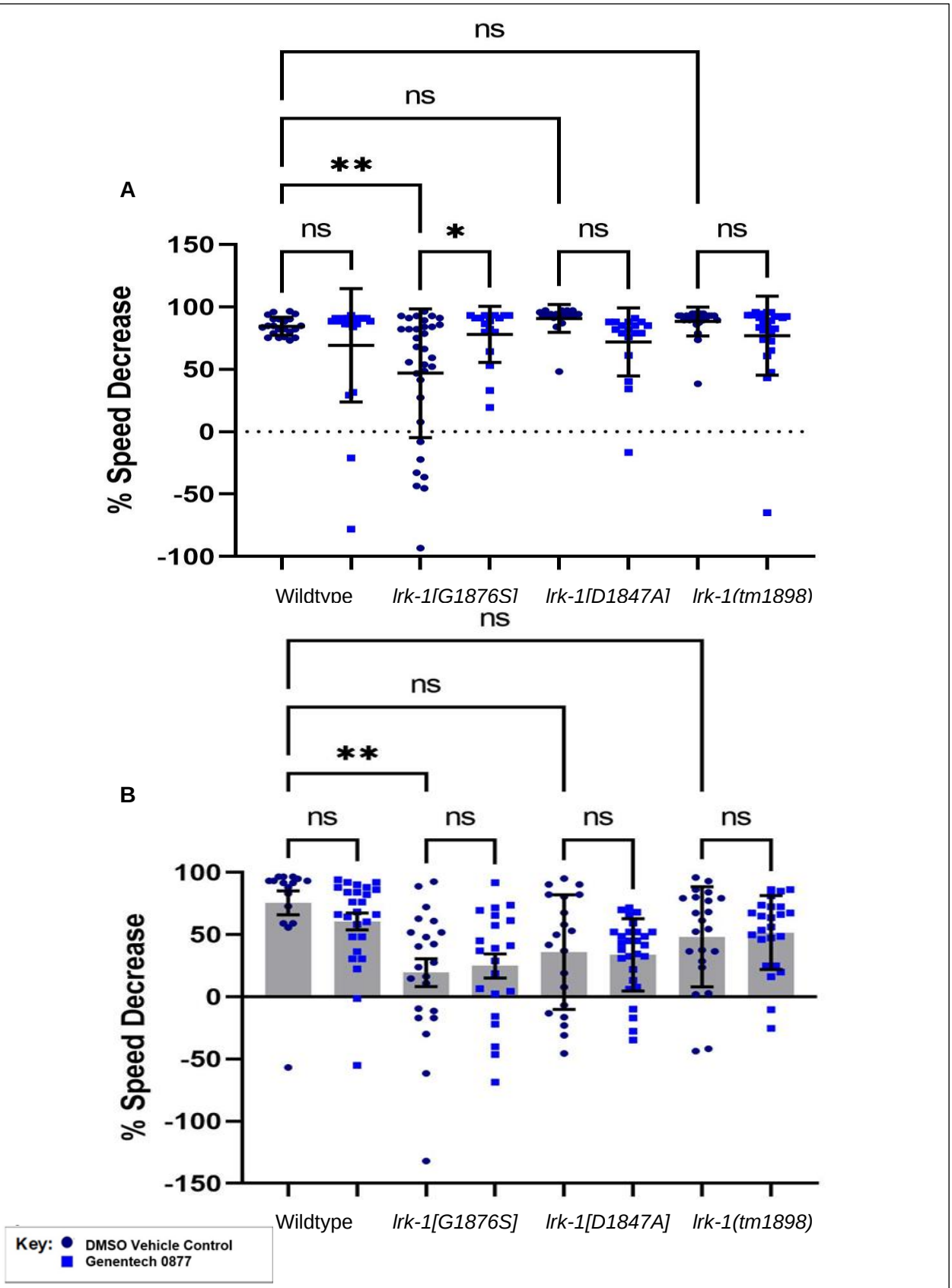

Figure 54- Basal Slowing Response of selected day 1 adult LRK-1 mutants treated with Genentech0877 on solid media

>12 day 1 adult *C. elegans* were assayed per line at each developmental stage. Day 1 and Day 5 adults were from the same age-synchronised population. One way ANOVA with Brown-Forsythe and Welch Correction for unequal standard deviations undertaken. Full P values and descriptive statistics including mean, standard deviation and number can be found in the supplementary, 4.5. Human orthologues and proposed functionality of mutants detailed on graphs can be found in table 27.

4.7.6 *lrk-1[G1876S]* mutants show reduced lipid accumulation, rescued by LRRK2 inhibitor administration

Lipid accumulation is regulated by autophagy in C. elegans (340,348) and as LRRK2 function is linked to the regulation of autophagy, lipid accumulation has been assessed through Nile Red staining. This has been undertaken in conjunction with Gnenetech0877 treatment, after improvements in the basal slowing response were shown in the *lrk-1[G1876S]*. This will enable the dissection of a cellular phenotype in conjunction with Genentech 0877 for these novel *lrk-1* lines, which may underpin dopaminergic behavioural phenotypes discussed throughout 4.8. As shown in Figure 55, in day 1 of adulthood, *lrk-1[G1876S]* mutants treated with a DMSO vehicle show a significantly reduced lipid accumulation compared to the wildtype, thus suggesting impaired autophagic function. Notably, this is a phenotype shared with *vps-35[D638N]* heterozygotes, as detailed in 3.3.9. The *lrk-1[D1847A]* kinase ablated model does not show a significantly different lipid accumulation to the wildtype, suggesting that this may be a kinase dependent phenotype. Additionally, deletion of *lrk-1* does not show a significantly different fluorescence intensity, suggesting that there may be compensatory pathways in the absence of *lrk-1*. Alternatively, it could be a lack of kinase activity, as this is also seen in the kinase ablated mutant. Following LRRK2 inhibitor administration, there is a significant rescue in the lipid accumulation phenotype of the *lrk-1[G1876S]*, further supporting our earlier findings that suggest LRRK2 inhibitors are specific enough for LRK-1 targeting and that the reduced lipid accumulation phenotype is kinase activity dependent. There is no alteration in phenotype for the *lrk-1[D1847A]* kinase ablated mutant, or the LRK-1 deletion following treatment, further suggesting this has some specificity for altering kinase hyperactive phenotypes.

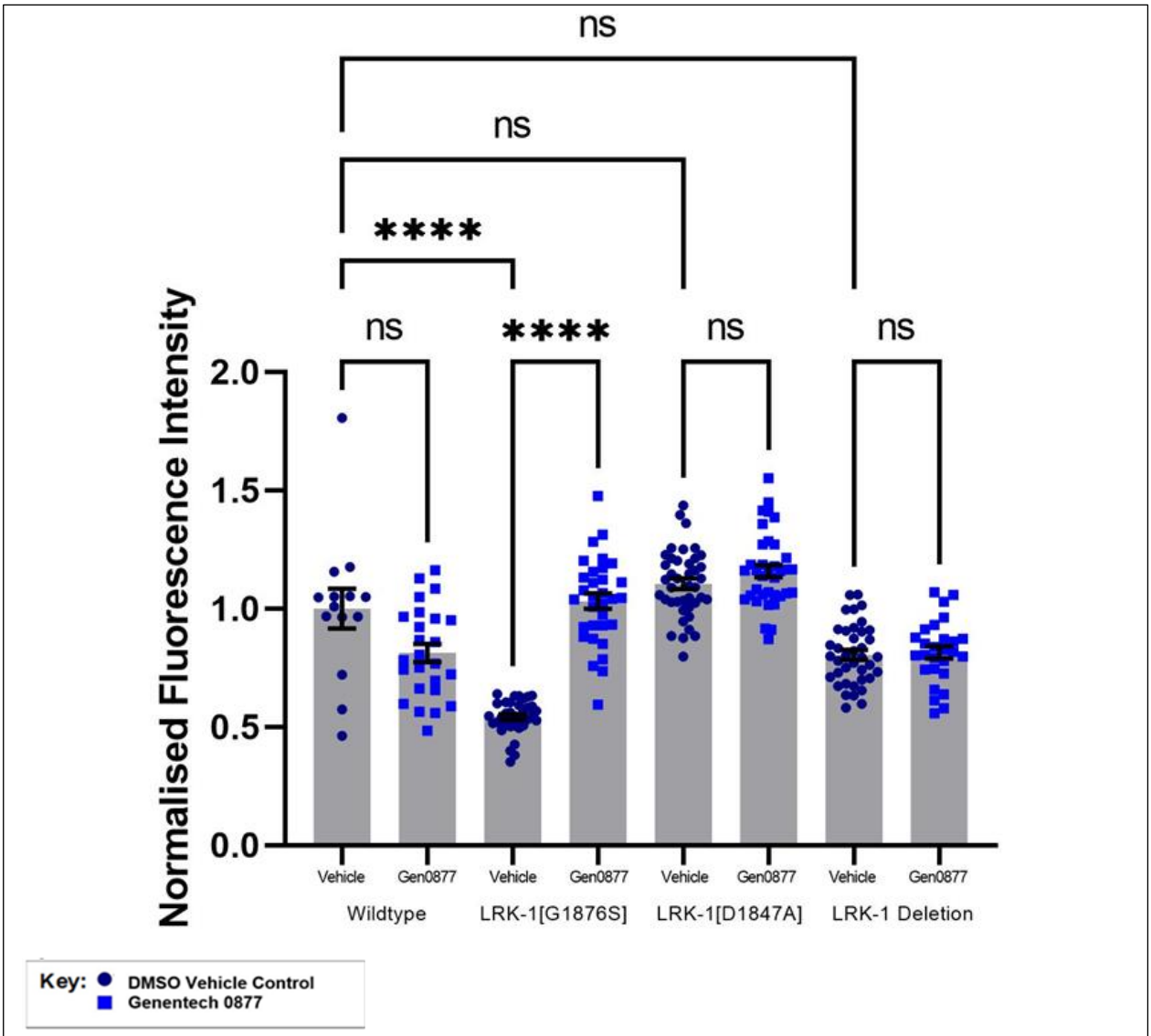

Figure 55-Lipid Accumulation as a marker of autophagic function in selected LRK-1 mutants, treated with 10mM Genentech 0877 on solid media

Lipid accumulation in day 1 of adulthood was quantified via Nile red staining, followed by confocal-like fluorescence microscopy. Fluorescence intensity was scored for each individual *C. elegans* in the population.
14-41 worms assayed per line and treatment. Mean (M) and Standard Deviation (SD) indicated. One-way ANOVA with Kruskal-Wallis test to account for differing standard deviations undertaken. Descriptive statistics and P-values detailed in the supplementary.

4.8 Novel Detection Methods for *C. elegans* LRK-1

The expression of LRK-1 through development has been vastly understudied, due to the absence of commercially available antibodies for this orthologue. Commercially available human LRRK1 and LRRK2 antibodies were tested, to examine if there was specificity for LRK-1, avoiding costly antibody or novel line generation. Unfortunately, these showed no specificity, however this issue has been overcome through the generation of a novel LRK-1-FLAG tagged line, for life stage expression analysis, localisation, and pull-down studies. Furthermore, a novel anti-LRK-1 rabbit sera has been generated, for further development of IgG LRK-1 antibody.

4.8.1 Commercially Available LRRK1 and LRRK2 antibodies are not specific for *C. elegans* LRK-1

Currently, there are no commercially available antibodies for C. elegans LRK-1, but there are a plethora for human LRRK1 and LRRK2. Several of the human LRRK1 and LRRK2 antibodies were available in the lab, so these were tested for LRK-1 specificity, as this would be a useful tool for future immunoblot investigations, without the costly need to generate and raise a novel antibody for *C. elegans* LRK-1. Wildtype and *lrk-1* knockout *C. elegans* lysates were tested, as detailed in Table 28, utilising the wet membrane transfer. Mixed stage N2 wildtype lines were tested, with *lrk-1(tm1898)* deletion utilised as a negative control and human LRRK2 transgenic *wlzls1[snb-1p::Hsa-LRRK2 + lin15(+)]* was employed as a positive control. No antibodies detailed in Table 5 showed specificity for C. elegans LRK-1, following 210 seconds exposure. This is unsurprising, as the amino acid sequence identity between LRK-1 and LRRK1 is 21%, while identity between LRK-1 and LRRK2 is 20%, thus highly specific antibody epitope residues are unlikely to be conserved. Due to this, a novel antibody specific for LRK-1 was concurrently generated, alongside the development of a FLAG tagged LRK-1 line, for future detection studies.

Antibody Epitope	Manufacturer	Product Code	LRK-1 Specificity in Western Blot	Epitope Sequence Identity (%)		
				Match	Similar	Gaps
LRRK2 (950)	Abcam	ab133474	-	15	26	44
LRRK1 (1339-1369)	Abcam	ab175839	-	23	56	6
LRRK1 (1981-2014)	AvivaSystems Biology	OAAB16862	-	15	24	66
LRRK1 (C1_C2)	GeneTex	GTX107407	-	-	-	-
LRRK2 pSer1292	Abcam	Ab203181	-	27	54	4
LRRK2 pSer935	Abcam	Ab133450	-	15	26	44
LRRK2pT1491	Abcam	Ab140106	-	23	37	27
LRRK2pSer910	Abcam	Ab133449	-	15	26	44

Table 28- Human LRRK1 and LRRK2 Antibodies tested for LRK-1 Specificity

4.8.2. Newly developed 3xFLAG-LRK-1 is detectable in *C. elegans* lysates

Following the unsuccessful detection of LRK-1 utilising commercially available antibodies, a N-Terminal 3xFLAG tagged LRK-1 line was designed (Supplementary). CRISPR/Cas9 modification was outsourced to SunyBiotech. Subsequently, the detection of this FLAG tag was tested to validate its viability for future experimentation utilising mixed stage lysates. As shown in Figure 56, FLAG-LRK-1, with an estimated size of 266kDa, is detectable in a mixed stage *C. elegans* population. Expression of LRK-1 protein is currently poorly understood and characterised in *C. elegans* adulthood. Thus, for future experiments, protein extraction will need to be optimised through investigating expression at different stages of development, facilitating optimal detection and insight into protein presence and potential function through the lifespan.

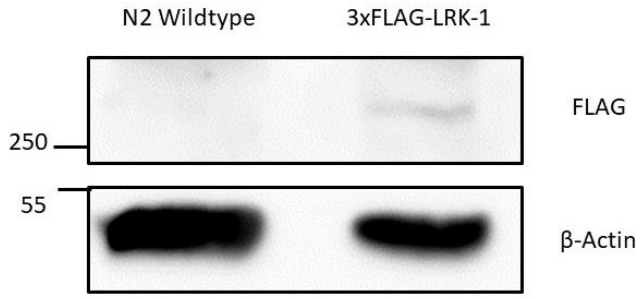

Figure 56-3xFLAG-LRK-1 is detectable in mixed stage C. elegans lysates

Detection for 3xFLAG-LRK-1 undertaken through western blot, gel was run in 1xMOPS as detailed in chapter 2, with the wet electrophoresis transfer method utilised, for 4 hours at 50 volts at room temperature. Following 5% milk PBS-T blocking, membrane was cut and FLAG antibody at a dilution of 1:3000 was incubated in 5% milk overnight at 4ºC, alongside β-actin housekeeping protein. Full details of antibodies can be found in table 17. HRP conjugated anti-mouse secondary antibody utilised for detection, using homemade ECL. Exposure for 210 seconds.

4.8.3 Development of anti-LRK-1 sera

Concurrent with the development of a novel LRK-1 FLAG tagged line, LRK-1 IgG sera from two rabbits were generated through outsourcing to Pepceuticals Ltd, to start developing a novel antibody for *C. elegans* LRK-1, as none are commercially available. Antibodies were raised against a short peptide sequence of *C. elegans* LRK-1, from 1613-28 amino acids, found approximately 50 amino acids upstream from the kinase domain; this region was selected by Pepceuticals Ltd (Supplementary 4.8.3). Preliminary testing through western blotting was undertaken as part of this project with these sera, to understand whether they showed any specificity and detection for *C. elegans* LRK-1. These did not show specificity for LRK-1 in early studies. Furthermore, this sera testing highlighted that LRK-1-FLAG in *C. elegans* was readily detectable and this method was carried forward for future expression, localisation and interactome studies. Details of anti-LRK-1 sera testing can be found in the supplementary, 4.8.3.

4.8.4 Expression of LRK-1-FLAG through the *C. elegans* adult lifespan

Available on WormBase is RNAseq data of LRK-1 mRNA expression through development, from eggs to adult, as indicated in figure 57. However, mRNA transcript levels are not always indicative of protein expression and there is no data specific for the specific timepoints and days of adulthood. Therefore this requires further study, in order to optimise the timepoints of future investigations and validate if LRK-1 is present at the key timepoints investigated throughout this study.

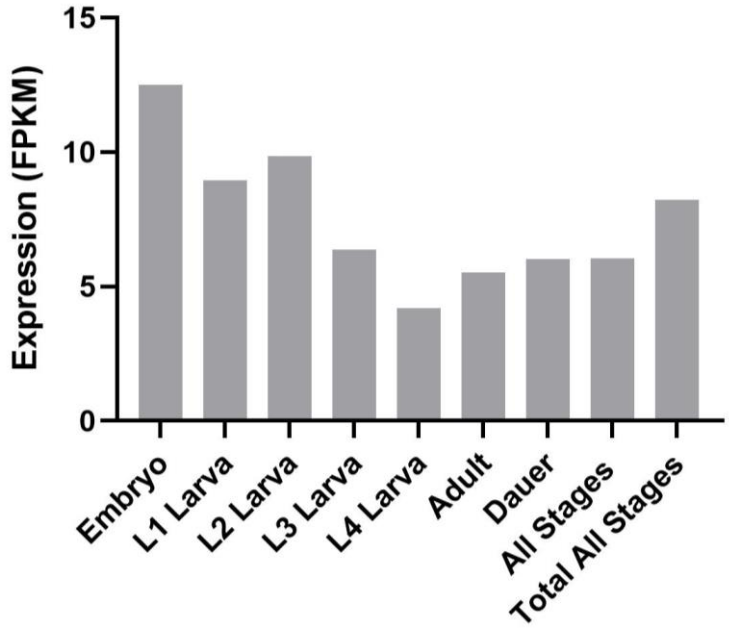

Figure 57- WormBase Mean Aggregate mRNA expression estimates of lrk-1 through development

Aggregate RNA expression estimates, obtained from WormBase, are mapped. These have been calculated in the database through the calculation of FPKM (Fragments Per Kilobase of exon per Million), for all untreated samples at each life stage. Lifestages so far have only focused on development, day 1 of adulthood or mixed stage populations. More accuracy is needed at specific adulthood timepoints, along with data on protein expression.

Testing of lysates from egg, L1-4 larvae and day 1 adulthood showed no detection of FLAG-LRK-1 during novel sera testing (4.8.3, supplementary). Subsequently, expression through the adult lifespan was tested (figure 58), as these developmental timepoints have been utilised extensively in our phenotypic assays. Following promising data in the anti-LRK-1 sera testing, FLAG-LRK-1 protein expression was studied in triplicate at day 1, 3, 5, 7 and 10 of adulthood, to investigate how expression changes through the lifespan and to further pinpoint the optimal life stages for future localisation and protein pull-down studies. Contrary to 4.9.4.1, high expression was illustrated in day 1 of adulthood, while expression remained high in day 5 of adulthood. Prior to lysate preparation, these lines were treated with FUDR from late L4 of adulthood, hence the effect of FUDR upon LRK-1 protein expression in day 1 of adulthood must be understood. LRK-1 expression remains in day 7-10 of adulthood in this experiment, highlighting the protein's potential role in ageing.

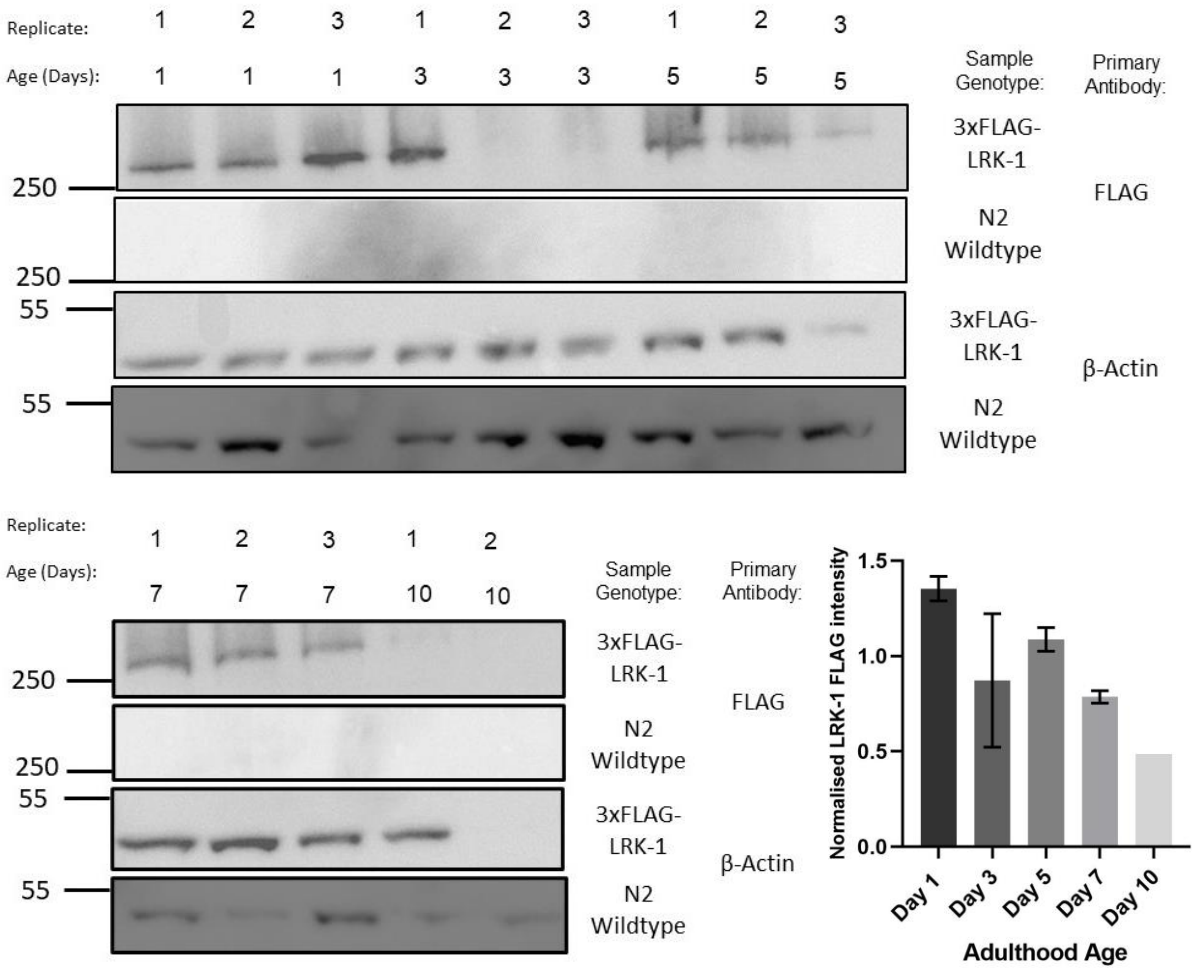

Figure 58-FLAG-LRK-1 protein expression from day 1 to day 10 of adulthood

Semi-quantitative western blot for 3xFLAG LRK-1 protein expression. Samples collected in triplicate, following FUDR treatment at late L4, in order to collect aged samples. Low number of *C. elegans* in day 10 samples, posing challenge to adequate sample collection. Quantification was undertaken through normalisation of 3xFLAG-LRK-1 against β-actin controls.
Detection for 3xFLAG-LRK-1 undertaken through western blot, gel was run as detailed in chapter 2, with the wet electrophoresis transfer method utilised, for 4 hours at 50 volts at room temperature. Following 5% milk PBS-T blocking, membrane was cut and FLAG antibody at a dilution of 1:3000 was incubated in 5% milk overnight at 4^{o}C, alongside β-actin housekeeping protein. Full details of antibodies can be found in table 17. HRP conjugated anti-mouse secondary antibody utilised for detection, using homemade ECL. Exposure for 210 seconds.

4.8.5 Development of LRK-1[G1876S] and LRK-1[D1847A] FLAG tagged mutant lines

Following the success of the readily detectable FLAG-LRK-1 2 novel lines have been generated, FLAG-LRK-1[G1876S] and FLAG-LRK-1[D1847A], through outsourcing to SunyBiotech. The design method for the 3xFLAG tag detailed in 4.9.2 and already generated *lrk-1[G1876S]* and *lrk-1[D1847A]* lines were sent for further CRISPR/Cas9 modification. The induction of key catalytic point mutants, already characterized in terms of behavioral and molecular phenotypes, will enable future mutation specific co-immunoprecipitation interactome studies and localization studies.

4.8.5.1 FLAG-LRK-1[G1876S] and FLAG-LRK-1[G1876S] are readily detectable at day 1 of adulthood and FUDR treatment does not impact FLAG-LRK-1 expression

Following obtaining these lines, it was validated whether there was detection utilizing the FLAG antibody. Both the FLAG-LRK-1[G1876S] and FLAG-LRK-1[D1847A] lines are readily detectable in day 1 and are not substantially impacted by FUDR treatment, an important observation for all functional study phenotypes (Figure 59), in which FUDR was utilised. This further elucidates the conflicting data between 4.8.4 and 4.9.4, regarding FLAG-LRK-1 expression in day 1 of adulthood and suggests that FUDR does not have an impact upon expression.

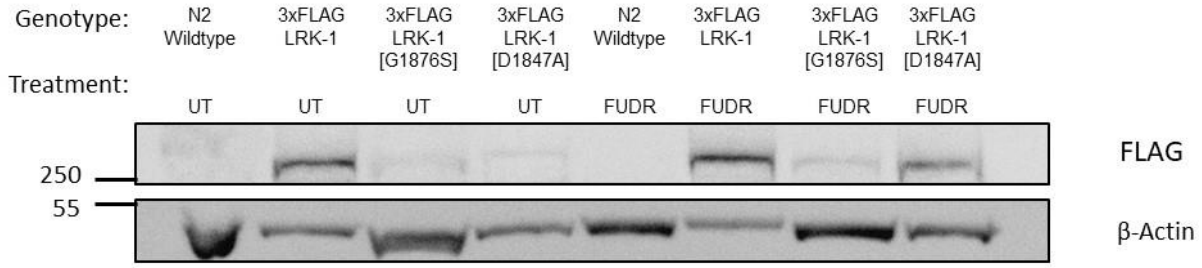

Figure 59-FLAG-LRK-1 protein expression at day 1 of adulthood, with and without FUDR treatment

Western blot, to determine protein expression of FLAG-LRK-1 following FUDR treatment, which was utilised throughout the majority of characterisation studies. .Detection for 3xFLAG-LRK-1 undertaken through western blot, gel was run as detailed in chapter 2, with the semi-dry transfer method used. . Following 5% milk PBS-T blocking, membrane was cut and FLAG antibody at a dilution of 1:3000 was incubated in 5% milk overnight at 4ºC, alongside β-actin housekeeping protein. Full details of antibodies can be found in table 17. HRP conjugated anti-mouse secondary antibody utilised for detection, using homemade ECL. Exposure for 210 seconds. UT=Untreated.

4.8.5.2 FLAG-LRK-1[G1876S] and FLAG-LRK-1[D1847A] may show increased expression in day 5 of adulthood

Furthermore, the expression of these novel FLAG-LRK-1 mutants in day 5 was tested, to contrast with day 1 expression and confirm the presence of these proteins at this developmental stage. Compared to wildtype LRK-1, there is a lower expression of FLAG-LRK-1[G1876S] in day 1 of adulthood, but this drastically increases by day 5, while the increase in wildtype with ageing is modest, as shown in Figure 60. LRK-1[D1847A] shows a similar expression in day 1 of adulthood to wildtype LRK-1, which substantially increases by day 5 of adulthood. This data confirms the presence of mutant LRK-1 proteins at the developmental stages investigated, further validating the functional consequences observed. However, in order to interpret the potential mutation specific effects upon expression, replicates are required to undertake a study similar to the wildtype LRK-1FLAG expression throughout adulthood, as shown in figure 58.

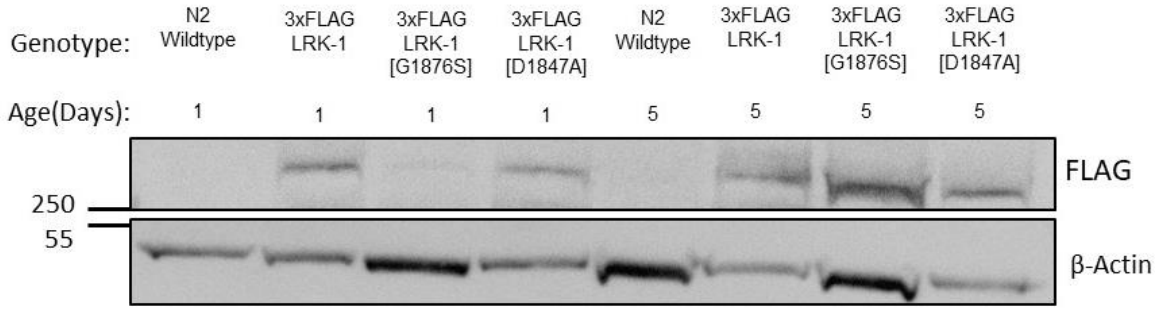

Figure 60-FLAG-LRK-1[G1876S] and FLAG-LRK-1[D1847A] expression at day 1 and day 5 of adulthood

Novel FLAG-LRK-1 mutants are readily detectable in day and day 5 of adulthood the most extensively utilised development stages in all characterisation studies. Detection for 3xFLAG-LRK-1 undertaken through western blot, gel was run in 1xMOPS as detailed in chapter 2, with the semi-dry transfer method used. . Following 5% milk PBS-T blocking, membrane was cut and FLAG antibody at a dilution of 1:3000 was incubated in 5% milk overnight at 4ºC, alongside β-actin housekeeping protein. Full details of antibodies can be found in table 17. HRP conjugated anti-mouse secondary antibody utilised for detection, using homemade ECL. Exposure for 210 seconds.

4.9 Detection of LRK-1 Phosphorylation Activity as a Biochemical Readout for novel mutant function

Upon kinase activation, LRRK2 autophoshorylates at selected sites (71,192). Using phospho-site sensitive antibodies is a good molecular readout for LRRK2 phosphorylation activity and would be a valuable tool in novel studies of LRK-1. This depends upon whether these phosphor-sites are conserved and if the available antibodies show specificity.

Furthermore, LRRK2 phosphorylates downstream effector proteins, predominantly RAB proteins and specifically RAB8A and RAB10 (277,287). These RABs are conserved in *C. elegans* and commercially available antibodies are available, sensitive for phosphor-sites. The conservation extent between human RAB8A and RAB10, with their *C. elegans* orthologues, RAB-8 and RAB-10 respectively, has been evaluated and existing antibodies tested.

4.9.1 Antibodies for human LRRK2 pSer1292 are unspecific for LRK-1

The LRRK2 autophosphorylation site, pSer1292, is conserved in *C. elegans*, with similar amino acid residues surrounding the phosphorylation site. Furthermore, *in vivo* mammalian studies of the LRRK2 inhibitor utilised throughout this study Genentech0877 demonstrate inhibition of pSer1292 autophosphorylation as a biochemical readout (347).

Following testing, the commercially available antibody LRRK2pSer1292 (Abcam, Ab203181) is not specific for LRK-1 and shows no detection, shown in figure 61. This is further supported by the low epitope similarity, highlighted in table 28. To overcome this, a novel *C. elegans* line encompassing an orthologous point mutation in LRK-1 of a S1292 ablation, for future characterisation has been developed.

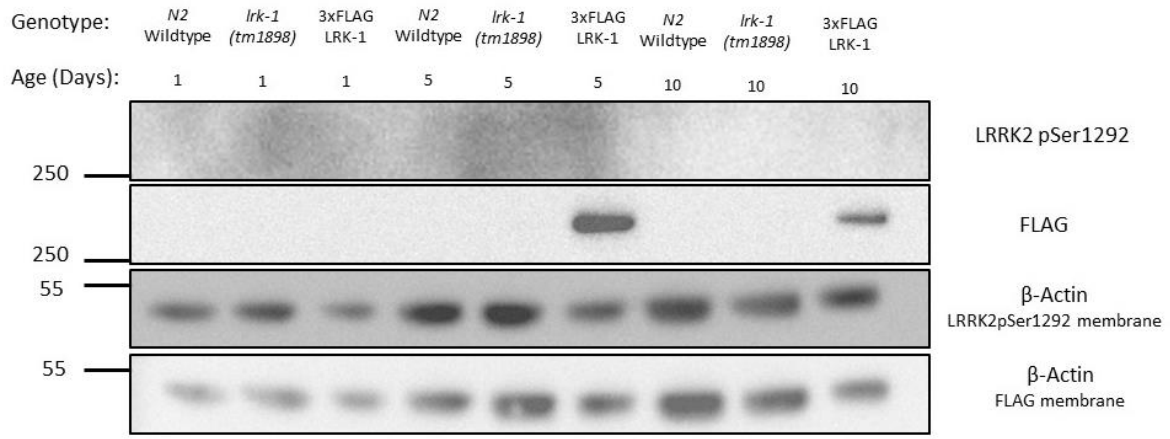

Figure 61- Antibodies for human LRRK2 pSer1292 are unspecific for LRK-1

Detection for LRK-1 undertaken through western blot, 2 gels were run in 1xMOPS as detailed in chapter 2, with the wet electrophoresis transfer method utilised, for 4 hours at 50 volts at room temperature. Following 5% milk PBS-T blocking, membrane was cut, one was incubated with antiLRRK2pSer1292 (1:2500) and the other anti-FLAG antibody (1:3000) in 5% milk overnight at 4^{o}C, alongside β-actin housekeeping protein. Full details of antibodies can be found in table 17. HRP conjugated anti-mouse secondary antibody utilised for detection, using homemade ECL. Exposure for 210 seconds.

4.9.2 Testing of human RAB8A and RAB10 antibodies in *C. elegans*

A challenge of *C. elegans* research is a lack of commercially available phosphor-antibodies, specific to *C. elegans* proteins. As increased phosphorylation activity of LRRK2 substrates such as RAB8A and RAB10 is a key hallmark of LRRK2 Parkinson's and VPS-35[D620N] (111), thus commercially available antibodies have been tested. Proteomic analysis highlights there is promising protein sequence conservation between human RAB8A and *C. elegans* RAB-8 and human RAB10 and *C. elegans* RAB-10, with key epitope sites of available antibodies conserved, as shown in figure 62. However, it is currently unknown how well conserved the LRRK2/RAB8a and RAB10 interplay is with *C. elegans* LRK-1/RAB-8 and RAB-10, due to the novelty of this work and the lack of prior LRK-1 pathway characterisation. Preliminary experiments were undertaken, to test if these antibodies detected *C. elegans* RAB proteins. Antibodies detecting RAB8a and RAB10, along with phospho-antibodies for RAB8a phospho-T72 and RAB10 phospho-T73, were tested utilising day 5 adult *C. elegans* lysates, in which LRK-1 is established to be present. Notably, these phosphor-sites are conserved in *C. elegans* RAB-8 and RAB-10.

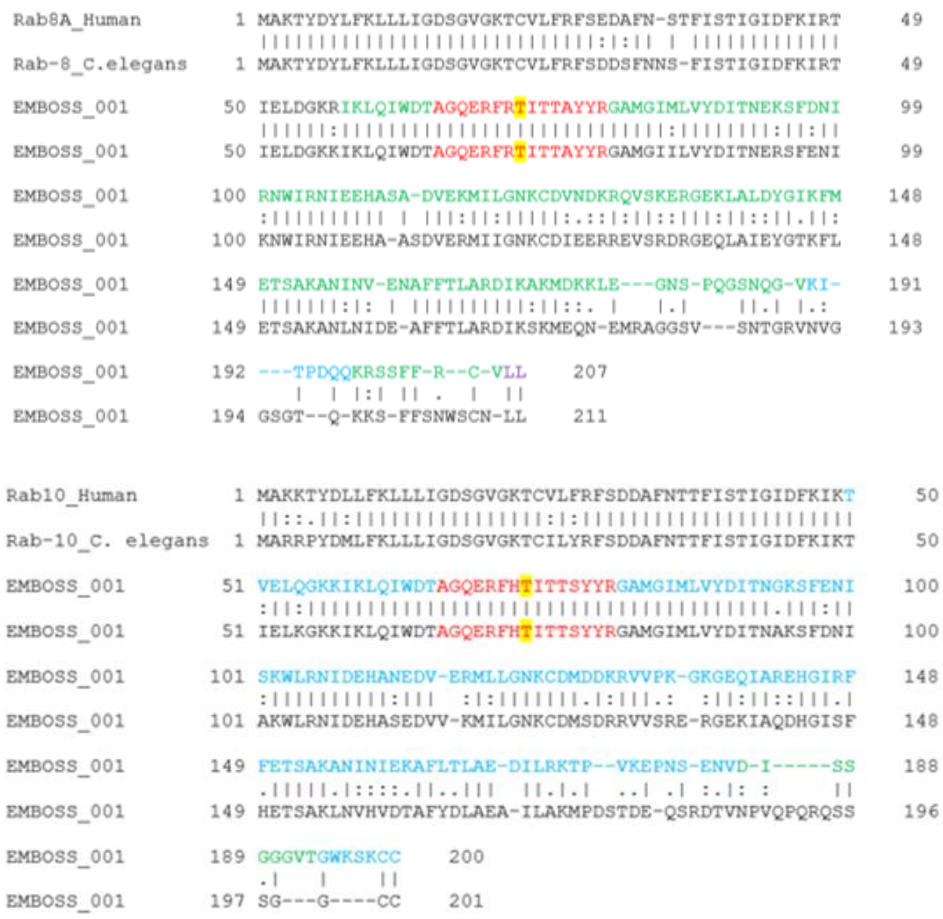

Figure 62-EMBOSS sequence alignments between human RAB8A and RAB10 with C. elegans orthologues

Protein sequence alignment undertaken utilising EBI EMBOSS sequence alignment, parameters as detailed in 2.1. FASTA amino acid sequence obtained from UniProt, for human proteins and WormBase for C. elegans orthologues. Green highlights the catalytic GTPase domain of the Rab protein. Phospho-antibody epitopes visualised in red, with phosphosite indicated in yellow. The sequence for non-phospho antibodies is highlighted in blue, this sequence was proprietary for RAB10, but is within the amino acid region highlighted. Full antibody details can be found in Table 17, chapter 2.

4.9.2.2 Phospho-antibodies for RAB8A show promise in the detection of C. elegans RAB-8

The antibodies to detect RAB8a and RAB10 are not specific for *C. elegans* RAB-8 and RAB-10 respectively. The sequence identity for the RAB8A antibody is proprietary, the available range in which the epitope is located covers the majority of the protein length, as shown in green in figure 63. The epitope for RAB10 is found close to the C-terminus of the protein, highlighted in green, in which the conservation with *C. elegans* RAB-10. This supports our findings that these human antibodies are not specific for *C. elegans* orthologues.

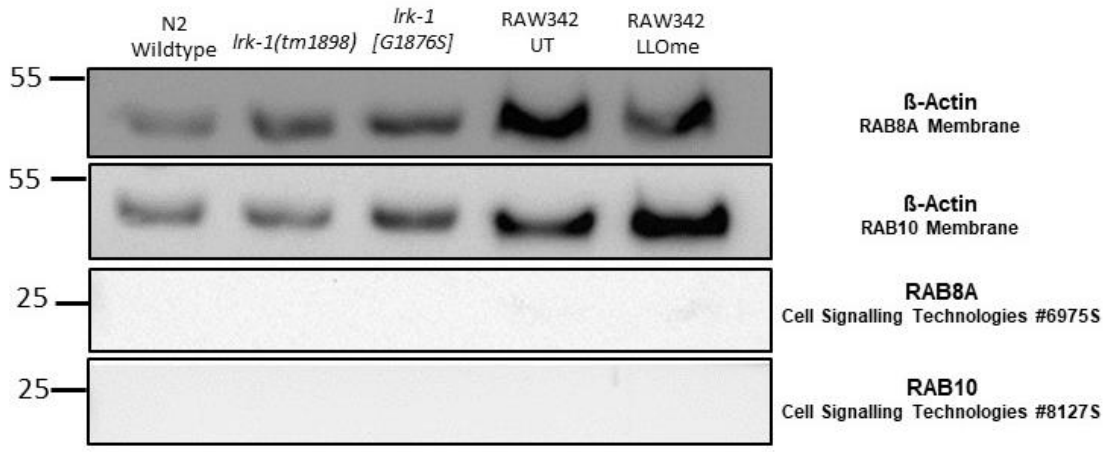

Figure 63- Testing of RAB8A and RAB10 antibodies for detection of C. elegans orthologues

Detection for 3xFLAG-LRK-1 undertaken through western blot, gel was run in 1xMES as detailed in chapter 2, with the semi-dry transfer method used. . Following 5% milk PBS-T blocking, membrane was cut and FLAG antibody at a dilution of 1:3000 was incubated in 5% milk overnight at 4ºC, alongside β-actin housekeeping protein. Full details of antibodies can be found in table 17. HRP conjugated anti-mouse secondary antibody utilised for detection, using homemade ECL. Exposure for 210 seconds.

The phospho-antibody for RAB8A pT72 showed very promising detection in *C. elegans* lysates, shown in figure 64. Interestingly, there was reduced RAB8A pT72 present in the *lrk-1* deletion sample. This could be a great tool for understanding the kinase activity of LRK-1, however in future research this needs further validation. The RAB proteins in *C. elegans* are very closely related (349), so there is a chance of epitope cross-specificity. Hence, a RAB-8 deletion mutant needs to be obtained, along with several of the most closely related RABs, to fully confirm that the RAB8A pT72 antibody is detecting RAB-8. However, the RAB10pT73 antibody shows no specificity for *C. elegans* RAB-10, suggesting this may not be as directly conserved as RAB-8.

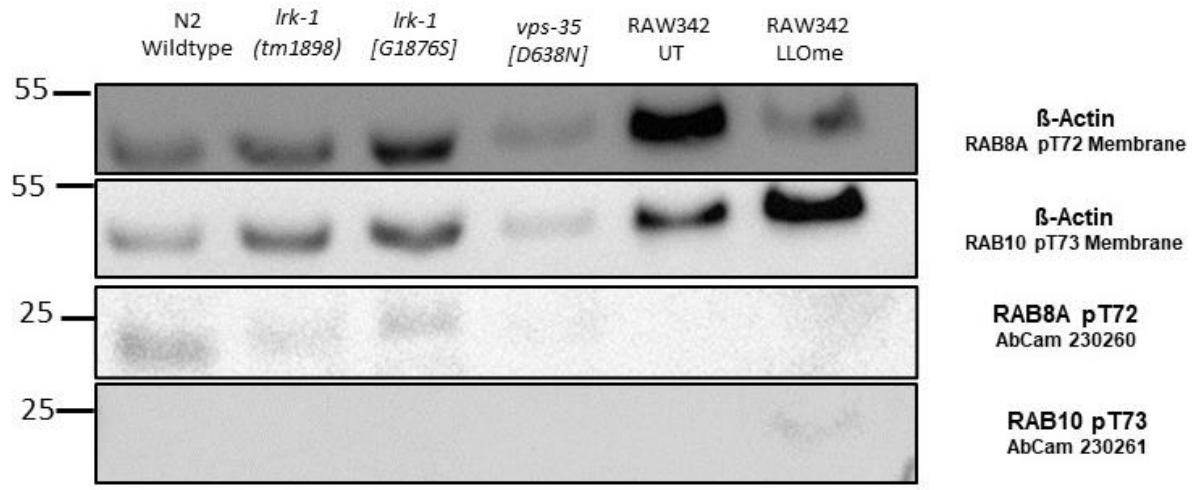

Figure 64- Testing of phosphor-RAB8A and phosphor-RAB10 antibodies for C. elegans orthologue detection

Detection for 3xFLAG-LRK-1 undertaken through western blot, gel was run in 1xMES as detailed in chapter 2, with the semi-dry transfer method used. . Following 5% milk PBS-T blocking, membrane was cut and FLAG antibody at a dilution of 1:3000 was incubated in 5% milk overnight at 4ºC, alongside β-actin housekeeping protein. Full details of antibodies can be found in table 17. HRP conjugated anti-mouse secondary antibody utilised for detection, using homemade ECL. Exposure for 210 seconds.

A molecular readout for LRK-1 phosphorylation activity, potentially through detection of phosphorylation of RAB-8 would be an important addition to our research, for validation of our observations at a phosphorylation level and further validating LRK-1 as an effective novel model for *C. elegans* LRK-1 and further dissecting the *vps-35[D638N]* interplay

Summary of Chapter IV: *C. elegans* LRK-1 as a model for human LRRK2 function

Overall, this chapter has suggested that *C. elegans* LRK-1 shows some promising conservation with human LRRK2, in the exhibition of phenotypes correlating with proposed kinase activity. The proposed kinase overactive LRRK2[G2019S] PD mutant equivalent, *lrk-1[G1876S]* shows an impaired dopaminergic behaviour, exacerbated with age and in day 1 of adulthood this can be rescued following treatment with a human LRRK2 inhibitor Genenetech0877. Meanwhile, the proposed kinase inactive catalytic mutant *lrk-1[D1847A]* has shown consistently divergent phenotypes from this mutant. The phenotypes shown by the novel LRK-1 point mutants are more distinctive than the existing human LRRK2 transgenic expressing models, suggesting this novel approach may be advantageous. Furthermore, this is a more relevant method for modelling PD gain of function mutations than *lrk-1* deletion models, further augmenting the relevance of CRISPR/Cas9 modification in modelling LRRK2 function in *C. elegans*. The development of a detection method for LRK-1 has been successful, in the generation of FLAG tagged lines. Protein expression analysis through the first 10 days of adulthood has highlighted that LRK-1 protein expression is highest in day 5, with the protein present at day 1, the two developmental timepoints most characterised throughout this project. Following the promising functional relevance of LRK-1 to LRRK2 function, the interplay between VPS-35[D638N] and LRK-1 will be investigated.

Chapter V: Modelling the VPS35/LRRK2 interplay in novel *C. elegans* models

In this chapter, the hypothesis that LRRK2 kinase hyperactivation is implicated in VPS35[D620N] mutation consequent PD will be tested in the novel *vps-35[D638N]* model and examined from multiple angles. After the success of LRRK2 inhibitor treatment in rescuing *lrk-1[G1876S]* dopaminergic phenotypes and proposed effect upon LRK-1, a pharmacological model has been developed, in which the *vps-35[D638N]* has been treated with inhibitor prior to dopaminergic behavioural assay, scoring of dopaminergic neuronal morphology and cellular phenotypes. To contrast with this, a genetic model has been established with *vps-35[D638N]* mutation and homozygous *lrk-1[D1847A]* kinase ablation mutation incorporated. The dopaminergic behavioural phenotype and dopaminergic morphology have been scored for this double mutant, further elucidating the VPS35/LRRK2 interplay in *C. elegans*.

5.1 *In Silico* convergence between Parkinson's associated pathways in *C. elegans*

C. elegans have orthologues of multiple PD associated genes, many of which have yet to be studied in the context of PD modelling, as shown in figure 2. As discussed previously, functional studies of LRRK2 have highlighted its interplay with multiple PD associated genes, of which VPS35 could be one (101,130,131), this will be investigated in *C. elegans* throughout this chapter. Prior to the dissection of the VPS35/LRRK2 interplay in *C. elegans* through pharmacological and genetic models, *in silico* analysis of three PD associated genes and their conservation with the *C. elegans* orthologues has been undertaken, to further assess the conservation of PD associated pathways in *C. elegans* and their suitability as a chosen novel model. Three key genes with relevance to LRRK2 or effector RAB proteins were chosen, which had been previously stratified for future PPI network analysis (33). The analysis detailed here includes, as in 3.1 and 4.1, protein sequence alignments, assessment of domain conservation, mutational analysis, tissue expression and PPI networks. This will enable the assessment of proposed functional conservation for these orthologues, enabling the targeting of new PD relevant genes for future functional study and further elucidation of the broader networks that may be implicated in the modelling pf PD relevant genes in *C. elegans*.

The genes stratified for *in silico* analysis include lysosomal glucocerebrosidase (GBA1), heterozygous mutations of which are a common risk factor in PD development and its function in the endolysosomal pathway is known to interplay with LRRK2 (351,352). Also selected is RAB29, a consistent GWAS candidate (32), upstream regulator and downstream effector of LRRK2 function (276) will also be investigated, as this protein may be integral in LRK-1 function. Review of the literature suggests that the LRRK2/RAB29 axis may be conserved in *C. elegans* (282) and as such, gaining new information about the *C. elegans* orthologue could further understanding of LRK-1 function and pinpoint future development of oligogenic disease models. Furthermore, this could shed insight into wider RAB protein biology in *C. elegans*, downstream effectors of LRRK2 function and the VPS35[D620N] mutation consequent kinase activity in mouse embryonic fibroblast models (111). To broaden understanding of RAB biology in *C. elegans* further, rather than just those directly affected by LRRK2, RAB39B has been selected, mutations of which are responsible for X-linked Parkinsonism. RAB39B parkinsonism has an atypical presentation, affecting only males, with juvenile onset and concurrent with intellectual disability (162). This is opposed to typical PD which affects both sexes, has a later-adulthood age of onset and cognitive impairments are heterogeneous in their presence between individuals late in PD progression (6). Study of RAB39B suggests that investigation may give broader insights into the application of *C. elegans* as a neurodegenerative disease model for rare, genetic conditions, with molecular phenotypes potentially shared with PD.

5.1.1 Conservation human GBA1 with *C. elegans* GBA-1, GBA-2, GBA-3 and GBA-4

Heterozygous mutations in lysosomal glucocerebrosidase (GBA) are a major and common risk factor in the development of late onset PD. Homozygous GBA mutations are also responsible for the lysosomal storage disorder Gaucher's disease (353). GBA has vital roles in the degradation of glucosylceramides and complex lipids such as sphingolipids and lipid membranes (352). GBA is involved in the endolysosomal system and autophagic pathways, integral in alpha-synuclein catabolism(15,354,355). *C. elegans* have four lysosomal GBA orthologues (encoded by four independent genes), while there are five splice isoforms of human lysosomal GBA. The conservation between each *C. elegans* GBA ortholog with each human lysosomal GBA isoform has been addressed, in order to evaluate which *C. elegans* GBA genes could be used to model GBA1 associated lysosomal defects in PD.

When aligned with the longest human GBA splice isoform (RefSeq ID: P04062-1), *C. elegans* GBA-3 and GBA-4 show the highest conservation, with 40% identity, 57-59% similarity and 5.5-7.8% gaps (Table 29). This is in contrast with *C. elegans* GBA-1 and GBA-2, which shows a 35% identity, 53% similarity and 5% gaps. Analysis of each of these *C. elegans* GBA genes in sequence alignment with each of the human isoforms, does not show any distinct groupings or specific conservation between the *C. elegans* orthologs and certain human GBA isoforms. GBA-3 is consistently the most conserved of the *C. elegans* genes in all the human GBA isoforms as highlighted in yellow in table 26, suggesting that this *C. elegans* lysosomal GBA may be most closely linked to model human lysosomal GBA.

Human Protein	PD Relevant	C. elegans Protein	Paramaters				Identity	Similarity	Gaps	score	Mean score
			Ebi tool	Matrix	Gap Open	Gap Extend					
GBA Long Isoform	Yes	GBA-1	Emboss stretcher	BLOSUM62	12	2	194/545 (35.6%)	290/545 (53.2%)	31/545 (5.7%)	787	837.5
	Yes		Emboss needle	BLOSUM62	10	0.5	199/551 (36.1%)	296/551 (53.7%)	43/551 (7.8%)	874.5	
	Yes		Emboss matcher	BLOSUM62	14	4	183/467 (39.2%)	268/467 (57.4%)	7/467 (1.5%)	851	
GBA Long Isoform	Yes	GBA-2	Emboss stretcher	BLOSUM62	12	2	191/542 (35.2%)	287/542 (53.0%)	32/542 (5.9%)	783	821.8333
	Yes		Emboss needle	BLOSUM62	10	0.5	190/562 (33.8%)	289/562 (51.4%)	72/562 (12.8%)	859.5	
	Yes		Emboss matcher	BLOSUM62	14	4	183/477 (38.4%)	269/477 (56.4%)	10/477 (2.1%)	823	
GBA Long Isoform	Yes	GBA-3	Emboss stretcher	BLOSUM62	12	2	218/544 (40.1%)	310/544 (57.0%)	30/544 (5.5%)	1001	1037

	Yes		Emboss needle	BLOSUM62	10	0.5	215/546 (39.4%)	311/546 (57.0%)	34/546 (6.2%)	1074	
	Yes		Emboss matcher	BLOSUM62	14	4	210/501 (41.9%)	299/501 (59.7%)	11/501 (2.2%)	1036	
GBA Long Isoform	Yes	GBA-4	Emboss stretcher	BLOSUM62	12	2	222/549 (40.4%)	327/549 (59.6%)	43/549 (7.8%)	962	1005.167
	Yes		Emboss needle	BLOSUM62	10	0.5	223/554 (40.3%)	329/554 (59.4%)	53/554 (9.6%)	1059.5	
	Yes		Emboss matcher	BLOSUM62	14	4	199/453 (43.9%)	287/453 (63.4%)	5/453 (1.1%)	994	
GBA Short Isoform	Yes	GBA-1	Emboss stretcher	BLOSUM62	12	2	194/528 (36.7%)	287/528 (54.4%)	17/528 (3.2%)	819	847.8333
	Yes		Emboss needle	BLOSUM62	10	0.5	199/532 (37.4%)	295/532 (55.5%)	25/532 (4.7%)	873.5	
	Yes		Emboss matcher	BLOSUM62	14	4	183/467 (39.2%)	268/467 (57.4%)	7/467 (1.5%)	851	
GBA Short Isoform	Yes	GBA-2	Emboss stretcher	BLOSUM62	12	2	191/526 (36.3%)	287/526 (54.6%)	20/526 (3.8%)	809	831.1667
	Yes		Emboss needle	BLOSUM62	10	0.5	195/532 (36.7%)	293/532 (55.1%)	32/532 (6.0%)	861.5	
	Yes		Emboss matcher	BLOSUM62	14	4	183/477 (38.4%)	269/477 (56.4%)	10/477 (2.1%)	823	
GBA Short Isoform	Yes	GBA-3	Emboss stretcher	BLOSUM62	12	2	215/526 (40.9%)	308/526 (58.6%)	14/526 (2.7%)	1038	1048.167
	Yes		Emboss needle	BLOSUM62	10	0.5	214/526 (40.7%)	308/526 (58.6%)	14/526 (2.7%)	1070.5	
	Yes		Emboss matcher	BLOSUM62	14	4	210/501 (41.9%)	299/501 (59.7%)	11/501 (2.2%)	1036	
GBA Short Isoform	Yes	GBA-4	Emboss stretcher	BLOSUM62	12	2	221/531 (41.6%)	325/531 (61.2%)	27/531 (5.1%)	989	1013.167
	Yes		Emboss needle	BLOSUM62	10	0.5	222/536 (41.4%)	328/536 (61.2%)	37/536 (6.9%)	1056.5	
	Yes		Emboss matcher	BLOSUM62	14	4	199/453 (43.9%)	287/453 (63.4%)	5/453 (1.1%)	994	
GBA Isoform3	Yes	GBA-1	Emboss stretcher	BLOSUM62	12	2	115/526 (21.9%)	155/526 (29.5%)	266/526 (50.6%)	-12	346.8333
	Yes		Emboss needle	BLOSUM62	10	0.5	113/526 (21.5%)	154/526 (29.3%)	266/526 (50.6%)	533.5	
	Yes		Emboss matcher	BLOSUM62	14	4	112/261 (42.9%)	153/261 (58.6%)	4/261 (1.5%)	519	
GBA Isoform3	Yes	GBA-2	Emboss stretcher	BLOSUM62	12	2	138/548 (25.2%)	191/548 (34.9%)	317/548 (57.8%)	522	502.8333
	Yes		Emboss needle	BLOSUM62	10	0.5	110/524 (21.0%)	153/524 (29.2%)	269/524 (51.3%)	505.5	
	Yes		Emboss matcher	BLOSUM62	14	4	108/261 (41.4%)	149/261 (57.1%)	6/261 (2.3%)	481	
GBA Isoform3	Yes	GBA-3	Emboss stretcher	BLOSUM62	12	2	115/526 (21.9%)	160/526 (30.4%)	267/526 (50.8%)	57	416.8333

	Yes		Emboss needle	BLOSUM62	10	0.5	114/526 (21.7%)	160/526 (30.4%)	267/526 (50.8%)	606.5	
	Yes		Emboss matcher	BLOSUM62	14	4	113/261 (43.3%)	159/261 (60.9%)	5/261 (1.9%)	587	
GBA Isoform3	Yes	GBA-4	Emboss stretcher	BLOSUM62	12	2	125/521 (24.0%)	171/521 (32.8%)	260/521 (49.9%)	104	458.3333
	Yes		Emboss needle	BLOSUM62	10	0.5	124/521 (23.8%)	169/521 (32.4%)	260/521 (49.9%)	641	
	Yes		Emboss matcher	BLOSUM62	14	4	123/261 (47.1%)	168/261 (64.4%)	3/261 (1.1%)	630	
GBA Isoform4	Yes	GBA-1	Emboss stretcher	BLOSUM62	12	2	180/526 (34.2%)	265/526 (50.4%)	80/526 (15.2%)	657	763.6667
	Yes		Emboss needle	BLOSUM62	10	0.5	183/529 (34.6%)	271/529 (51.2%)	86/529 (16.3%)	825	
	Yes		Emboss matcher	BLOSUM62	14	4	167/403 (41.4%)	242/403 (60.0%)	5/403 (1.2%)	809	
GBA Isoform4	Yes	GBA-2	Emboss stretcher	BLOSUM62	12	2	174/523 (33.3%)	258/523 (49.3%)	81/523 (15.5%)	620	724
	Yes		Emboss needle	BLOSUM62	10	0.5	171/526 (32.5%)	255/526 (48.5%)	87/526 (16.5%)	788	
	Yes		Emboss matcher	BLOSUM62	14	4	165/415 (39.8%)	240/415 (57.8%)	8/415 (1.9%)	764	
GBA Isoform4	Yes	GBA-3	Emboss stretcher	BLOSUM62	12	2	194/526 (36.9%)	273/526 (51.9%)	81/526 (15.4%)	822	928.5
	Yes		Emboss needle	BLOSUM62	10	0.5	191/526 (36.3%)	271/526 (51.5%)	81/526 (15.4%)	993.5	
	Yes		Emboss matcher	BLOSUM62	14	4	191/451 (42.4%)	271/451 (60.1%)	6/451 (1.3%)	970	
GBA Isoform4	Yes	GBA-4	Emboss stretcher	BLOSUM62	12	2	196/524 (37.4%)	289/524 (55.2%)	80/524 (15.3%)	790	891.8333
	Yes		Emboss needle	BLOSUM62	10	0.5	196/528 (37.1%)	285/528 (54.0%)	88/528 (16.7%)	955.5	
	Yes		Emboss matcher	BLOSUM62	14	4	181/394 (45.9%)	259/394 (65.7%)	4/394 (1.0%)	930	
GBA Isoform5	Yes	GBA-1	Emboss stretcher	BLOSUM62	12	2	178/526 (33.8%)	259/526 (49.2%)	42/526 (8.0%)	612	697.1667
	Yes		Emboss needle	BLOSUM62	10	0.5	181/548 (33.0%)	265/548 (48.4%)	86/548 (15.7%)	759.5	
	Yes		Emboss matcher	BLOSUM62	14	4	152/356 (42.7%)	213/356 (59.8%)	5/356 (1.4%)	720	
GBA Isoform5	Yes	GBA-2	Emboss stretcher	BLOSUM62	12	2	179/542 (33.0%)	264/542 (48.7%)	81/542 (14.9%)	612	685.3333
	Yes		Emboss needle	BLOSUM62	10	0.5	177/560 (31.6%)	263/560 (47.0%)	117/560 (20.9%)	762	
	Yes		Emboss matcher	BLOSUM62	14	4	151/366 (41.3%)	213/366 (58.2%)	8/366 (2.2%)	682	
GBA Isoform5	Yes	GBA-3	Emboss stretcher	BLOSUM62	12	2	201/544 (36.9%)	281/544 (51.7%)	79/544 (14.5%)	798	870.1667

	Yes		Emboss needle	BLOSUM62	10	0.5	199/546 (36.4%)	283/546 (51.8%)	83/546 (15.2%)	945.5	
	Yes		Emboss matcher	BLOSUM62	14	4	171/387 (44.2%)	237/387 (61.2%)	6/387 (1.6%)	867	
GBA Isoform5	Yes	GBA-4	Emboss stretcher	BLOSUM62	12	2	206/545 (37.8%)	301/545 (55.2%)	84/545 (15.4%)	784	855.5
	Yes		Emboss needle	BLOSUM62	10	0.5	207/550 (37.6%)	303/550 (55.1%)	94/550 (17.1%)	943.5	
	Yes		Emboss matcher	BLOSUM62	14	4	165/362 (45.6%)	236/362 (65.2%)	4/362 (1.1%)	839	

Table 29- Sequence conservation between human GBA1 isoforms and C. elegans GBA orthologues

In terms of domain structure, human lysosomal GBA is a glycosyl hydrolase, composed of a TIMM-Barrel domain and a Beta-sandwich domain and this domain structure is conserved in the C. elegans GBA proteins (Figure 65). This consistency between the *C. elegans* GBA's shows that there are no highly distinct genes that directly match human GBA, however GBA-3 interestingly has the longest protein chain prior to TIMM barrel formation, at 105 amino acids.

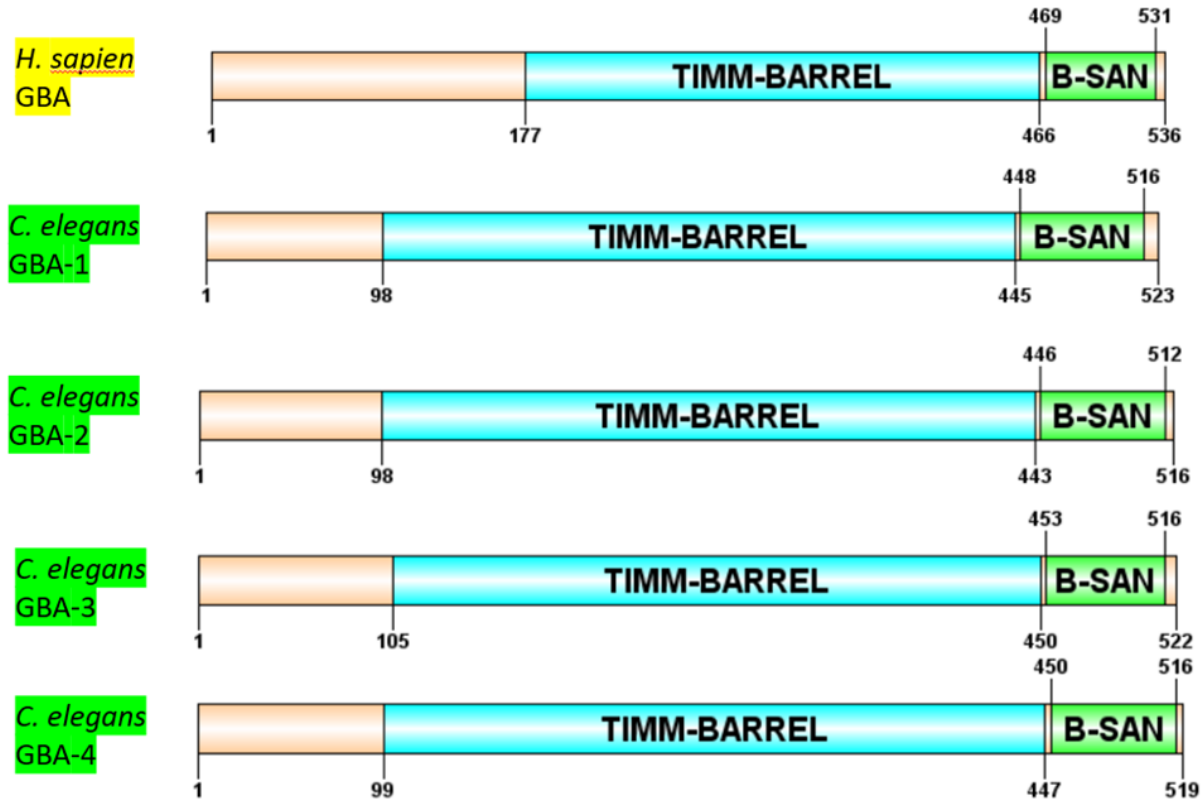

Figure 65-Linear Protein domain structure of long-isoform human GBA1 and C. elegans GBA orthologues GBA-1, GBA-2, GBA-3 and GBA-4

Linear visualisations were generated through DOG2.0 software, as detailed in chapter 2 2.1. Domain information, including starting and end amino acid, was obtained from ProSite and InterPro prior to mapping. High similarity is suggested between the C. elegans GBA proteins, with an extended TIMM-Barrel domain (Turquoise), compared to human GBA. All proteins include a β-Sandwich domain (B-SAN, green).

PD mutations in human GBA were identified through ClinVar databases, through pathogenic, single gene filtering. Many mutations identified for Gaucher's disease are confirmed pathogenic, however fewer are categorised in this way in PD, as many mutations are classed as a risk factor. The conservation of all confirmed pathogenic PD associated mutations was evaluated in all the *C. elegans* GBA proteins, aligned with each of the five human GBA isoforms. Table 27 shows the PD relevant mutations in the long isoform of GBA1, which were mapped on sequence alignments between human GBA splice isoforms and *C. elegans* GBA. Additional mutations identified to be pathogenic in causing Gaucher disease were incorporated , to gain higher resolution in evaluating the potential conservation extent between human lysosomal GBA and *C. elegans* GBA-1, GBA-2, GBA-3 and GBA-4.

Position	**Pathogenicity**	**Wildtype**	**Mutation**
115+1	Parkinson's Disease	G	A
32	Gaucher's Disease	Q	Frameshift
29	Gaucher's Disease	L	Lx18
25	Gaucher's Disease	L	Frameshift
496	Parkinson's Disease	R	H
463	Parkinson's Disease	R	G
483	Parkinson's Disease	L	P
448	Parkinson's Disease	D	H
433	Parkinson's Disease	V	L
432	Parkinson's Disease	W	R
409	Parkinson's Disease	N	S
296	Parkinson's Disease	R	Q

Table 30- Pathogenic GBA1 mutations mapped in C. elegans GBA orthologues

Each of these 12 mutations was mapped on each sequence alignment, to assess the conservation between these human isoforms and each *C. elegans* orthologue, full details of which are tabulated in the supplementary. *C. elegans* GBA-1 and GBA-3 showed the highest conservation in terms of point mutations, each with four directly conserved mutations in the long isoform, with two and three alternate, very similar amino acids found in the place of other mutations sites respectively. This suggests that GBA-3 may be the most conserved. Evaluation of each of the human GBA isoforms with each of the *C. elegans* GBA orthologues did not show distinct groupings, or consistent identities between *C. elegans* proteins and particular human splice isoforms.

TextMining was undertaken to evaluate the expression pattern tissue for each of the *C. elegans* genes. This data was not available for any of GBA-1,2,3 or 4, as these are relatively understudied. However, there was genomic study tissue data available, in which the protein of interest has been detected in specific tissues when genomic analysis was undertaken, for GBA-1, GBA-3, (the most promising candidates for conservation) and GBA-4. In GBA-1, the genomic study tissues include dopaminergic neurons, the I5 neuron, retrovesicular ganglion, VA neuron and the intestine. This focus on neuronal tissues suggests there may be some relevance in studying GBA-1 as a GBA PD model. Additionally, in GBA-3, the tissues studied include the GABAergic neuron, OLL and PVD neuron, as well as in the body wall muscle. GBA-4 has only been studied in the intestine.

***C. elegans* orthoogue**	**Expression Tissue**	**Function and Location of Tissue in *C. elegans***	**Relevance to functional modelling of Parkinson's protein GBA1**
GBA-1	DA Neuron	Motor Neuron located in the ventral nerve cord	Illustrates potential neuronal function for GBA-1
	I5 Neuron	Pharangeal interneuron, can also be a posterior sensing neuron.	Illustrates potential neuronal function for GBA-1
	VA Neuron	Motor Neuron located in the ventral nerve cord	Illustrates potential neuronal function for GBA-1
	PVD Neuron	Nociceptive, mechanosensation and thermosensation sensory neuron, found un the tail and lumbar ganglion	Illustrates potential neuronal function for GBA-1
	SAB Neuron	Interneuron found in the head resoventricular ganglion	Illustrates potential neuronal function for GBA-1
	Head Mesodermal Cell	Found in the head, function unknown	
	Intestine	Found along the *C. elegans* body, digestion and storage of macromolecules	Model for vesicular trafficking, ageing and stress responses, which may be relevant for PD modelling.
	Pharyngeal Muscle Cell	Found in the pharynx, in the head of *C. elegans*, pumping for bacterial uptake via the mouth.	
GBA-3	PVD Neuron	Nociceptive, mechanosensation and thermosensation sensory neuron, found un the tail and lumbar ganglion	Illustrates potential neuronal function for GBA-3
	GABAergic Neuron	Found throughout *C. elegans* CNS, primarily neuromuscular synapses	Illustrates potential neuronal function for GBA-3

	OLL Neuron	Glutaminergic sensory neuron found in the head, implicated in mechanosensation and pathogen avoidance	Illustrates potential neuronal function for GBA-3
	Body Wall Muscle Cell	Found throughout body wall, locomotion	
GBA-4	Intestine	Found along the *C. elegans* body, digestion and storage of macromolecules	Model for vesicular trafficking, ageing and stress responses, which may be relevant for PD modelling.

Table 31 C. elegans GBA1 orthologue tissue expression, functionality, and Parkinson's modelling relevance

The first and second layer interactome was studied, in order to assess the conservation extent between the *C. elegans* GBA's and human lysosomal GBA. Through PINOT analysis, there was only interactome data available for GBA-1 and GBA-3, with only one interactor found for each. GBA-1 interacts with SMO-1, the human paralog SUMO-1 is not found in GBA's interactome. SUMO-1 has roles in development, gene expression, protein degradation and multicellular locomotion. SCC-1 interacts with GBA-3, its human paralog RAD21L1 is again, not found in the interactome of GBA. SCC-1 is a cohesion complex component implicated in cell division and synaptonemal complex assembly.

C. elegans orthologue	**Protein**	**Database**	**Notable functions. GO-Biological process**	**Human Paralog**	**Paralog present in human GBA1 interactome**
GBA-1	SMO-1	WormBase	• Embryo development ending in birth or egg hatching • Mitotic metaphase plate congression • Mitotic sister chromatid separation • Multicellular organismal locomotion • Muscle cell cellular homeostasis • Negative regulation of transcription. DNA templated • Negative regulation of transcription by RNA polymerase II • Nematode larval development • Positive regulation of male tail tip morphogenesis • Protein localisation to chromosome • Protein sumoylation • Regulation of gene expression	SUMO-1	No

			• Regulation of protein stability • Synaptonemal complex disassembly		
GBA-3			• Cell division • Double-strand break repair • Meiotic cell cycle • Sister chromatid cohesion • Synaptonemal complex assembly	RAD21L1	No

Table 32- First Layer Interactors of C. elegans GBA orthologues

The *C. elegans* GBA genes have been vastly understudied, thus there are no known deletion, RNAi or transgenic models available. If utilised in future research, our data suggests that GBA-3, closely followed by GBA-1 would be most orthologous to human GBA and may be the most relevant for further study.

5.1.2 Conservation between human RAB29 and *C. elegans* GLO-1

GLO-1 is the *C. elegans* orthologue for human Rab29, Rab32 and Rab38. Rab29 is a consistent GWAS hit in Parkinson's cohort studies (24,356) and is a known interactor of LRRK2, converging upon similar pathways in vesicle trafficking. RAB29 also plays a role in retrograde transport between the endosomes and trans-Golgi network, mediated by the retromer, of which VPS35 is the core subunit. Specifically, Rab29 has a role in the transport of the Mannose-6-Phosphate receptor, responsible for the uptake and transport of acid hydrolases, such as cathepsin D from the endosome to the lysosome(276,357). Rab29 recruits LRRK2 to the Golgi complex, stimulating its kinase activity(272). Rab32, a non-Parkinson's associated paralog of GLO-1 is also an activator of LRRK2 and interacts with the retromer complex via the Sortin-Nexin dimers(297). *C. elegans* GLO-1 is predicted to have GTPase activity and is involved in lipid storage and lysosome organisation. In *C. elegans*, it is localised to the gut granule membrane and is highly expressed in the intestine.

In terms of protein sequence identity, GLO-1 shows a high sequence identity with RAB29, but also with RAB32 and RAB38, for which GLO-1 is also the C. elegans orthologue. The key domain site of these three proteins is a GTPase domain, which starts at amino acid 9 in human RAB29 and amino acid 12 in *C. elegans* GLO-1.

Human Protein	PD Relevant	C. elegans Protein	Ebi tool	Matrix	Gap Open	Gap Extend	Identity	Similarity	Gaps
Rab29	Yes	GLO-1	Emboss_stretcher	BLOSUM62	12	2	87/214 (40.7%)	131/214 (61.2%)	13/214 (6.1%)
Rab29	Yes	GLO-1	Emboss_needle	BLOSUM62	10	0.5	91/216 (42.1%)	134/216 (62.0%)	17/216 (7.9%)
Rab29	Yes	GLO-1	Emboss_matcher	BLOSUM62	14	4	79/162 (48.8%)	110/162 (67.9%)	1/162 (0.6%)
Rab32	No	GLO-1	Emboss_stretcher	BLOSUM62	12	2	106/231 (45.9%)	142/231 (61.5%)	25/231 (10.8%)
Rab32	No	GLO-1	Emboss_needle	BLOSUM62	10	0.5	104/231 (45.0%)	140/231 (60.6%)	25/231 (10.8%)
Rab32	No	GLO-1	Emboss_matcher	BLOSUM62	14	4	100/203 (49.3%)	135/203 (66.5%)	5/203 (2.5%)
Rab38	No	GLO-1	Emboss_stretcher	BLOSUM62	12	2	100/217 (46.1%)	131/217 (60.4%)	11/217 (5.1%)
Rab38	No	GLO-1	Emboss_needle	BLOSUM62	10	0.5	102/228 (44.7%)	138/228 (60.5%)	33/228 (14.5%)
Rab38	No	GLO-1	Emboss_matcher	BLOSUM62	14	4	93/172 (54.1%)	120/172 (69.8%)	3/172 (1.7%)

Table 33- Sequence Identity between human RAB29, RAB32 and RAB38 with C. elegans GLO-1

There are no confirmed pathogenic mutations identified in RAB29 to be causative of PD, it is a loci consistently observed in GWAS, but several of the risk variants are coding variants (32). However, *in vitro* studies have identified point mutations in which the GTPase activity of RAB29 is constitutively active or ablated (283), as shown in figure 66.

Small GTP binding protein
P-loop nucleoside triphosphate hydrolase
PD Mutations
Catalytic Ablations
Catalytic constitutive activation
+ charge- ablation does not alter LRRK2 interaction in Rab29
Emboss stretcher, Matrix: EBLOSUM62, Gap Penalty: 12, Extend Penalty: 2.

```
Rab29              1 MGS---RDHL-FKVLVVGDAAVGKTSLVQRYSQDSFSKHYKSTVGVDFAL     46
                     |.:   .|.: :||||:||..|||||:::|:..:.||.:||:|:|||||
Glo-1                MAALTNNDKISYKVLVIGDPGVGKTSIIRRFVHNVFSSNYKTTIGVDFAL     50

EMBOSS_001        47 KVLQWSDYEIVRLQLWDIAGQERFTSMTRLYYRDASACVIMFDVTNATTF     96
                     |:|...:..:|.||:|||:||:|:..|||:||:||.|.:|:.|.|...|.
EMBOSS_001        51 KILPVDENTVVHLQIWDISGQDRYGVMTRVYYKDAHAAIIVLDSTRERTI    100

EMBOSS_001        97 SNSQRWKQDLDSKLTLPNGEPVPCLLLANKCDLSPWAVSRDQIDRFSKEN    146
                     ..:.|||.|||.|:||.:|.|||.:|||||||:.. .:..|::.....|
EMBOSS_001       101 EGALRWKTDLDQKVTLADGSPVPAILLANKCDIDN-KLGDDKLYDLETNN    149

EMBOSS_001       147 GFTGWTETSVKENKNINEAMRVLIEKMM---RNSTEDIMSLSTQGDYINL    193
                     ||.|...||.||:..|.||.:.|...::   :....|:..:.:|: :||
EMBOSS_001       150 GFVGSFRTSAKESVGIEEAFKFLANTVISTEQGGQYDVPFMNREGN-VNL    198

EMBOSS_001       194 QTKSS----SWSCC    203
                     ...::    ...||
EMBOSS_001       199 DDNTTHSRYDSKCC    212
```

Figure 66- Protein Sequence Alignment Between human Rab29 and C. elegans GLO-1

Protein sequence alignment undertaken utilising EBI EMBOSS sequence alignment, parameters as detailed in 2.1. FASTA amino acid sequence obtained from UniProt, for human proteins and WormBase for *C. elegans* orthologues. Structures and key enzymatic residues illustrated in selected colours, small GTP binding loop (Blue), P-loop (Orange), catalytic ablations (purple), catalytic activation (Green).

The tissue expression of GLO-1 is yet to be extensively characterised, but it is noted to be highly expressed in the intestines. The interactome of GLO-1 has suggested three interactors in the first layer, with broad roles in development, protein transport and organisation, lipid transport and storage and lysosomal function. One of these interactors, APB-3 is the *C. elegans* orthologue of the clathrin adaptor protein AP3B, a LRK-1 and LRRK2 interacting protein (282). Together with LRK-1/LRRK2, APB-3/AP3B modulates the recycling of lysosomal membrane proteins LAMP1 and LAMP2 (358). This key convergence illustrates the potential conservation of LRRK2 Parkinson's relevant pathways in *C. elegans*, the relevance of this model for dissecting the VPS35/LRRK2 interplay and the potential for future development of oligogenic models.

Protein	Database	Notable functions. GO-Biological process	Human Paralog	Paralog present in human RAB29 interactome
APB-3	WormBase	• Lysosome organisation • Intracellular protein transport • Vesicle-mediated transport • Embryo development ending in birth or egg hatching	AP3B1 and AP3B2	Yes, acts with LRRK2
MRP-4	WormBase	• Lysosome organisation • Transmembrane transport • Lipid transport, involved in lipid storage	ABCC2	No
PGP-2	WormBase	• Lipid Storage • Organelle organisation	ABCB1 and ABCB11	No

Table 34- First Layer Interactome of C. elegans RAB29 orthologue GLO-1

Multiple transgenic knock-in point mutation models of GLO-1 have been generated and are available for study, with a wide range of phenotypes reported. Phenotypes reported include defects in axon termination(359), endocytic transport defects and misplacement of gut granules. They have also shown variants in lysosome organisation(289), embryonic lethality and hypersensitivity to zinc deficiency(360). The conserved roles in neuronal development and endocytic transport make GLO-1 a potentially insightful model of RAB29, hence it will be studied in future research in oligogenic PD models. Furthermore, GLO-1's convergence with LRK-1, mirroring the LRRK2/RAB29 interplay, further augments our model for dissecting *LRRK2* PD and associated pathways in *C. elegans*.

5.1.3 Conservation between human RAB39B and C. elegans RAB-39

Following the conservation of LRRK2 relevant RAB29 with *C. elegans* GLO-1 and potential conservation of LRRK2 effector RAB8a and RAB10 with *C. elegans* RAB-8 and RAB-10, as detailed in results chapter II, further Parkinson's relevant RAB proteins were studied. RAB39B was selected to diversify the RAB subsets studied, as it has no direct links with LRRK2 function, but loss of function mutations in RAB39B have been demonstrated to cause early onset, X-linked recessive Parkinsonism, often accompanied by intellectual disabilities, highlighting its importance in neuronal health and atypical, inherited Parkinsonism pathogenesis. Rab39B is highly expressed in the neurons and is localised to the plasma membrane, recycling endosome and Golgi network. Functional studies have suggested that RAB39B is implicated in the regulation of alpha-synuclein homeostasis (57,161,361). *C. elegans* RAB-39 is an ortholog for RAB39B and is predicted to have GTPase activity, convergent with the human protein.

In terms of sequence identity, *C. elegans* RAB-39 is highly conserved with RAB39B, specifically within the small GTP binding protein. There are two mutations that cause Parkinsonism with intellectual disability- these are loss of function mutations, leading to mis localisation of the protein. One is directly conserved in *C. elegans*, while the second has a similar amino acid substitution.

Small GTP binding protein
P-loop nucleoside triphosphate hydrolase
X-linked early onset Parkinsonism mutations
X-linked intellectual disability mutations
Emboss stretcher, Matrix: EBLOSUM62, Gap Penalty: 12, Extend Penalty: 2.

```
HumanRab39B         1 MEAIWL---------YQFRLIVIGDSTVGKSCLIRRFTEGRFAQVSDPTV     41
                      ||..::          ||:|||||||||||||.|:|.||||:.|::||||| 
C.elRab-39          1 METNFIGDDYGPLFHYQYRLIVIGDSTVGKSSLLRYFTEGKMAEISDPTV     50

EMBOSS_001         42 GVDFFSRLVEIEPGKRIKLQIWDTAGQERFRSITRAYYRNSVGGLLLFDI     91
                      ||||::|::|:.||.|:|||:|||||||:||||::|||||||.|.::|.
EMBOSS_001         51 GVDFYARMIELRPGYRVKLQLWDTAGQEKFRSITKSYYRNSVGVLAIYDT    100

EMBOSS_001         92 TNRRSFQNVHEWLEETKVHV---QPYQIVFVLVGHKCDLDTQRQVTRHEA    138
                      |||.||::|..|::|..:::    .|.:.||.|||.|.|:|:||||...|.
EMBOSS_001        101 TNRESFEHVENWVKEAALNLGGPSPSKCVFQLVGTKSDMDSQRQVNYEEG    150

EMBOSS_001        139 EKLAAAYGMKYIETSARDAINVEKAFTDLTRDIYELVKRGEITIQEGWEG    188
                      |..|..:.||:||||:|...||.:||..:.::|...|..||:...:||||
EMBOSS_001        151 EYFAKYHKMKFIETSSRTGDNVNEAFHMIAQEIQNRVDDGELRPVDGWEG    200

EMBOSS_001        189 VKSGFVPNV-VHSSEEVV---KSERRCLC    213
                      :|:|.:.:. |..||...    .|...|.|
EMBOSS_001        201 LKTGIMRSQSVCLSERSFPQNSSAGACGC    229
```

Figure 67- Sequence conservation between human RAB39B and C. elegans RAB-39

Protein sequence alignment undertaken utilising EBI EMBOSS sequence alignment, parameters as detailed in 2.1. FASTA amino acid sequence obtained from UniProt, for human proteins and WormBase for *C. elegans* orthologues. Structures and key enzymatic residues illustrated in selected colours, small GTP binding loop (Blue), P-loop (Orange), intellectual disability mutation (purple), X-linked parkinsonism mutation (red).

In order to further evaluate the conservation, we mapped mutations known to cause intellectual disability exclusive of Parkinsonism, in order to give a greater predictive resolution. Three of these four mutations are directly conserved- two result in premature termination of the protein synthesis, while the third leads to mis-localisation. This high conservation in mutation sites with consequent mechanisms of neurodegeneration illustrate the promise of utilising *C. elegans* to further understand RAB39B linked Parkinsonism.

Position	Wildtype	Pathogenic Mutation	Condition	Conserved in C. elegans
192	G	R	Parkinsonism with Intellectual Disability	Yes
168	T	K	Parkinsonism with Intellectual Disability	No, Similar amino acid alanine.
187	E	* Mislocalisation	Intellectual Disability without Parkinsonism	Yes
215+1		Alters 5' splice site	Intellectual Disability without Parkinsonism	No
7	Y	Termination	Intellectual Disability without Parkinsonism	Yes
1	M	Termination	Intellectual Disability without Parkinsonism	Yes

Table 35- Pathogenic Mutations identified in RAB39B

In *C. elegans*, RAB-39 is expressed in the head, in the mesodermal cells, muscles and neurons. It is also found in the tail neurons, intestine, rectal gland and the hypodermis. The expression in neuronal tissues may be relevant for further Parkinson's relevant modelling.

Expression Tissue	Function and Location of Tissue in *C. elegans*	Relevance to functional modelling of Parkinson's protein RAB39B
AFD Neuron	Thermosensory neuron found in the head	Illustrates potential neuronal function for RAB39B
ASER Neuron	Chemosensory amphid neuron, highly ciliated and found in the head	Illustrates potential neuronal function for RAB39B.
NSM Neuron	Mechanosensory neuron found in the pharyngeal sub ventral nerve cord	Illustrates potential neuronal function for RAB39B.
OLL Neuron	Glutaminergic sensory neuron found in the head, implicated in mechanosensation and pathogen avoidance	Illustrates potential neuronal function for RAB39B
PVD Neuron	Nociceptive, mechanosensation and thermosensation sensory neuron, found un the tail and lumbar ganglion	Illustrates potential neuronal function for RAB39B

Intestine	Found along the C. elegans body, digestion and storage of macromolecules	Model for vesicular trafficking, ageing and stress responses, which may be relevant for Parkinson's modelling.
Germline	Reproduction, found in the gonad and uterus	

Table 36- Tissue expression of RAB-39 in C. elegans

PINOT analysis of the interactome of RAB-39 indicated 2 interactors, IGDB-2 and RSF-1. IGDB-1 has no known functions, but is expressed in the amphid sheath and socket cells. Amphid neurons are implicated in sensory behaviour in *C. elegans*, so this could be relevant for further Parkinson's associated studies. There are no known human paralogs for this gene. RSF-1 is involved in intracellular signal transduction, it has paralogs RASSF1 and 5, but these are not conserved in the known RAB39B interactome.

Protein	**Database**	**Notable functions. GO-Biological process**	**Human Paralog**	**Paralog present in human RAB39B interactome**
IGDB-2	WormBase	• No known functions • Expressed in amphid sheath and socket cells	None	-
RSF-1	WormBase	• Intracellular signal transduction	RASSF1 and RASSF5	No

Table 37- Protein interactome of C. elegans RAB-39

RAB-39 has been studied in *C. elegans* through RNAi knockdown studies. These showed neuroblast lineage migration variation (362) and hypersensitivity to oxidative stress response (363), phenotypes which may be relevant for future PD research. However, as with *C. elegans* GLO-1, the RAB29 orthologue and the orthologues for human GBA1, the characterisation of RAB-39 is very limited, opening a window for further novel functional studies.

5.2 The administration of a human LRRK2 inhibitor rescues *vps-35[D638N]* impaired dopaminergic function

In *in vitro* mouse embryonic fibroblasts encompassing VPS35[D620N] and neutrophils isolated from people with VPS35[D620N] consequent PD, increased LRRK2 kinase activity is shown, which can be rescued through treatment with a LRRK2 inhibitor (111). Following promising data regarding the efficacy of LRRK2 inhibitor treatment in LRK-1 point mutants (Figure 54), the *vps-35[D638N]* heterozygote model has been treated, in order to utilise a pharmacological model for dissecting the VPS-35/LRRK2 interplay in *C. elegans*. This has shed insight into the potential conservation extent of this pathway in *C. elegans* and alluded to the pathological mechanisms of *vps-35[D638N]* mutation in *C. elegans*. Following treatment, the basal slowing response as a dopaminergic behavioural phenotype had been assessed and in later subchapters, the impact upon dopaminergic morphology and cellular perturbations. This is also an approach to test the working hypothesis, that VPS35[D620N] mutation leads to LRRK2 kinase hyperactivation and toxicity. If correct, this could indicate the potential utility of LRRK2 inhibitors for the treatment of VPS35[D620N] linked PD.

5.2.1 Administration of a LRRK2 inhibitor rescues the impaired basal slowing response of *vps-35[D638N]* Heterozygotes

In order to test the hypothesis that VPS35[D620N] induces toxicity through LRRK2 hyperactivation, the *vps-35[D638N]* strain was incubated with human LRRK2 inhibitor Genentech 0877 in liquid media (Figure 68). Following this, basal slowing was assayed as a robust dopaminergic readout. Previous studies have suggested that LRK-1 is inhibited by the LRRK2 inhibitor Genentech0877, improving a kinase overactive phenotype (Figure 54). Selected LRK-1 mutants can be incubated with 2 concentrations of Genentech0877, 1mM and 0.2mM. When *vps-35[D638N]* were incubated with 1mM of inhibitor, the same concentration effective for rescuing *lrk-1[G1876S]* phenotype, exhibited severe developmental delay, whereas the wildtype and DMSO vehicle controls developed at the usual rate. This suggests that kinase inhibition may have a greater global effect on this mutant, than LRK-1 mutants alone. One possible explanation is off target effects on kinases which are vital for development and may be already working at a suboptimal level in the *vps-35[D638N]* heterozygote, but not the wildtype. Incubation of *vps-35[D638N]* with 0.2mM Genentech0877 through development leads to a modest rescue in the impaired basal slowing response, augmenting the theory that VPS35[D620N] acts through LRRK2 hyperactivation.

The most efficient method of drug delivery and uptake in *C. elegans* is through raising the worms in liquid culture from larval development with the drug incorporated, as utilised here (329), and also the method we utilised in preliminary LRRK2 inhibitor experiments. *C. elegans* raised in liquid culture are swimming, rather than crawling. This requires high bioenergetic demand, is an exercise state and in a 2019 study has been shown to be protective in neuromuscular function and neurodegeneration in the model (330). Despite the lack of statistical significance in the vehicle phenotype of the *lrk-1[G1876S]* raised in liquid culture as detailed in 4.8, our data appears promising as the basal slowing response was significantly improved in this line, despite the impairments of the *lrk-1[G1876S]* not being statistically significantly different from the wildtype. *C. elegans* heterozygous for the *vps-35[D638N]* mutation, raised in liquid culture, maintain impairments in the basal slowing response, as shown in figure. This is to a similar extent as when they are raised crawling, on solid media, as detailed in chapter 3. This is interesting alone, as even when raised under exercise neuroprotective conditions, the *vps-35[D638N]* (a mutation with reported higher penetrance than the LRRK2[G2019S] (3)) still shows dopaminergic impairments.

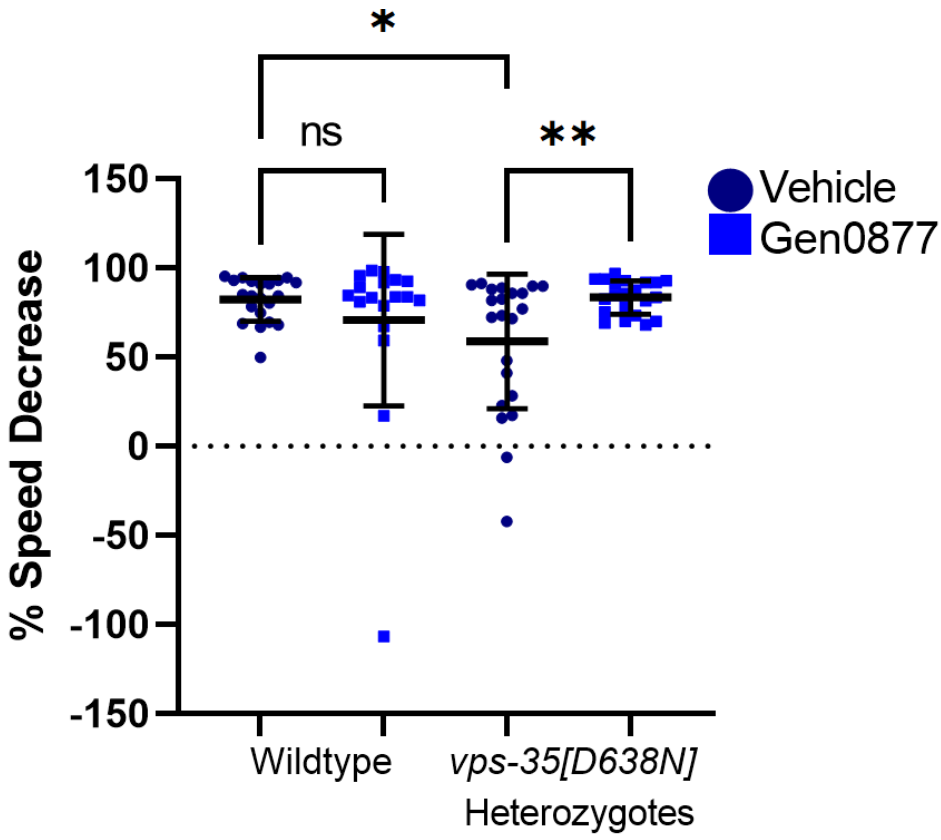

Figure 68-Basal slowing response of VPS-35[D638N] heterozygotes treated with 0.2mM of human LRRK2 inhibitor Genentech0877

20-30 day 1 adult *C. elegans* were assayed perline, following developmental incubation with 0.2mM Genentech 0877 (Gen0877). No significant difference in crawling speed between wildtype and vps-35[D638N] heterozygotes. Full descriptive statistics and P values found in supplementary.
Performed One-way ANOVA with Brown-Forsyth correction between selected datasets.

5.2.2 Administration of a LRRK2 inhibitor through solid media feeding rescues impairments in the basal slowing response in day 1 adult *vps-35[D638N]* heterozygotes

Solid media feeding of Genentech0877 to the *vps-35[D638N]* heterozygote for 16 hours overnight significantly rescues impairments in the basal slowing response in day 1 of adulthood (Figure 69A), suggesting that impairments illustrated may be due to LRK-1 kinase hyperactivation, consistent with findings in 5.2.1. This also suggests that solid media feeding is effective in drug administration and may be beneficial for future experiments, as the *C. elegans* are not raised under exercise conditions. The *cat-2(n4547)* tyrosine hydroxylase deletion model was utilised as a dopaminergic dysfunction negative control, showing a significantly reduced basal slowing response unaffected by Genentech0877 treatment. In day 5 of adulthood, there is no significant difference in basal slowing response between the wildtype and the *vps-35[D638N]* heterozygote (Figure 69B). In this experiment, animals were treated with Genentech0877 overnight from day 4 of adulthood. Treatment caused no significant difference in the basal slowing response. The *cat-2(n4547)* illustrated a significantly reduced basal slowing response compared to the wildtype, to a lesser extent than in day 1.

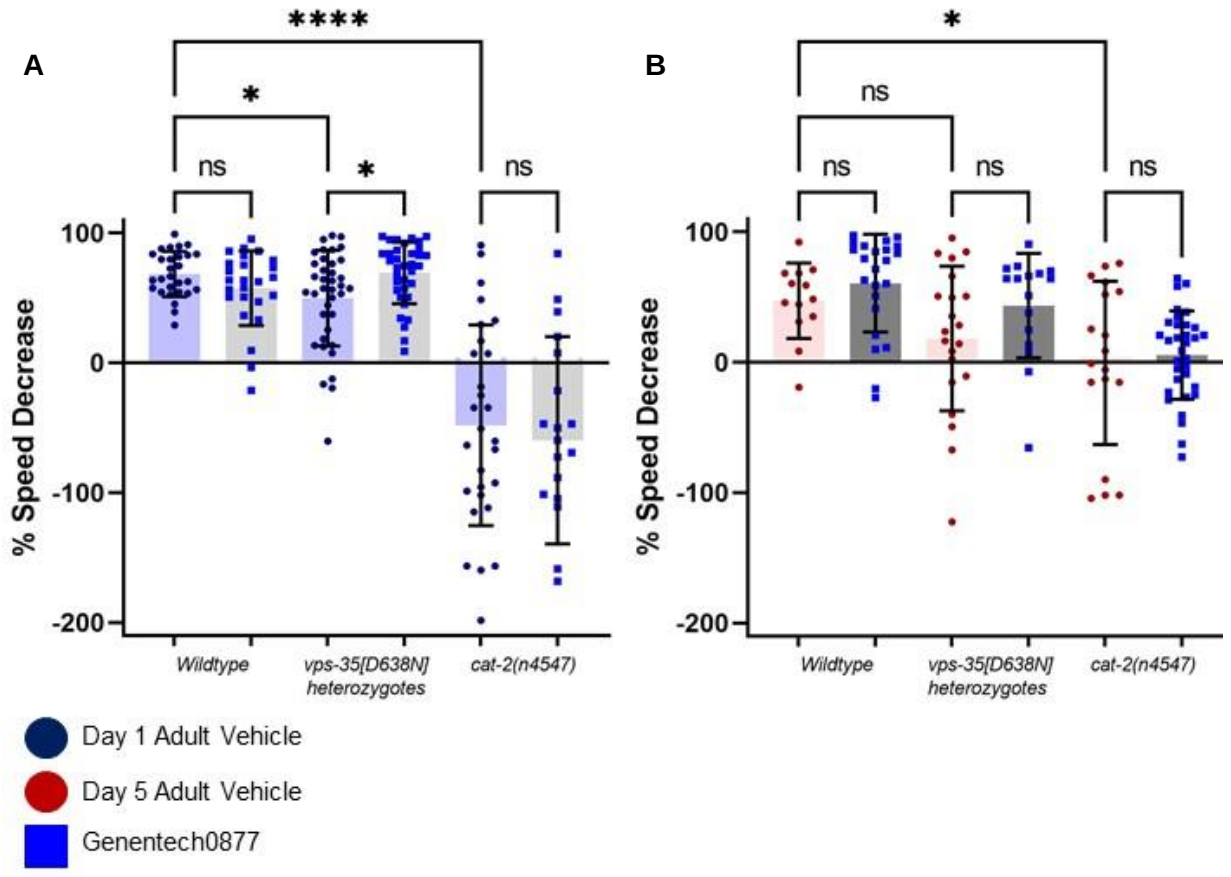

Figure 69- Administration of Genentech0877 on solid media rescues impairments in the basal slowing response of vps-35[D638N] heterozygotes in day 1 of adulthood, but not day 5

>12 *C. elegans* were assayed per line at each developmental stage. Day 1 and Day 5 adults were from the same age-synchronised population. One way ANOVA with Brown-Forsythe and Welch Correction for unequal standard deviations undertaken. Full P values and descriptive statistics including mean, standard deviation and number can be found in the supplementary.

5.2.3 The basal slowing response is not significantly impaired with ageing in vehicle and LRRK2 inhibitor treatment

The basal slowing responses discussed in 5.2.2 have been alternatively contrasted, to determine if there is a significant difference between day 1 and day 5 of adulthood, in animals treated with the vehicle (Figure 70A) and Genentech0877 (Figure 70B). There is no significant difference in the basal slowing response in vehicle treated animals of all three genotypes between day 1 and day 5 of adulthood. Furthermore, there is no significant difference in basal slowing response in day 1 or day 5 of adulthood in Genentech0877 treated wildtype and *vps-35[D638N]* heterozygous animals, however in the *cat-2(n4547)* mutant the day 5 Genentech0877 treatment leads to an enhanced basal slowing response compared to day 1, however this is not significantly different from the age-matched vehicle, as discussed in 5.2.2.

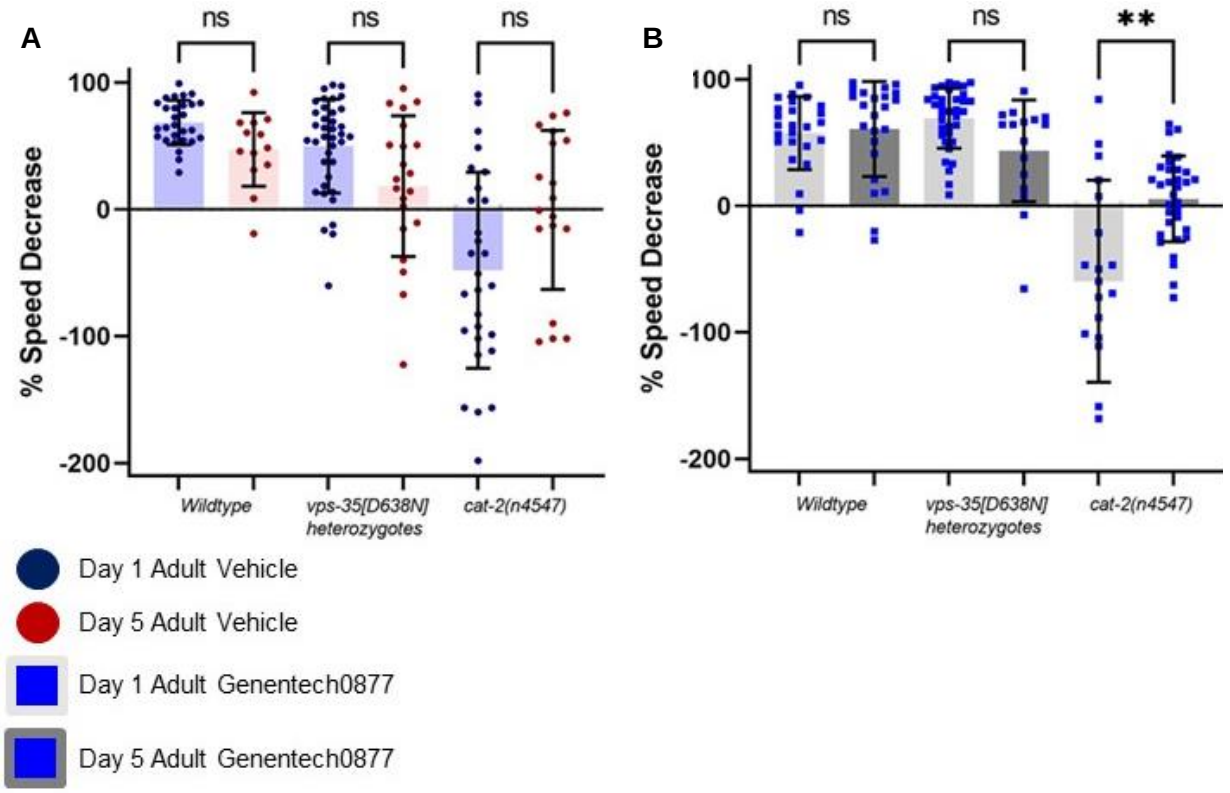

Figure 70- The basal slowing response is not significantly impaired in ageing in vehicle and Genentech0877 treatment

>12 *C. elegans* were assayed per line at each developmental stage. Day 1 and Day 5 adults were from the same age-synchronised population. One way ANOVA with Brown-Forsythe and Welch Correction for unequal standard deviations undertaken. Full P values and descriptive statistics including mean, standard deviation and number can be found in the supplementary.

5.2.4 The crawling speeds of wildtype and *vps-35[D638N]* heterozygote *C. elegans* are significantly altered by Genentech0877 treatment

The crawling speeds of *C. elegans* on unseeded NGM and upon reaching the *E. coli* OP50 bacterial lawn were quantified in day 1 and day 5 of adulthood (figure 71), to contrast with the basal slowing data detailed in 5.2.2.

In day 1 of adulthood, vehicle treated *vps-35[D638N]* heterozygotes do not show significantly different crawling speeds to the wildtype on unseeded NGM, consistent with prior studies, while the *cat-2(n4547)* mutant shows a significantly reduced crawling speed. Following Genentech0877 treatment, the wildtype shows a significantly reduced crawling speed, as does the *vps-35[D638N]* heterozygote to a greater extent than the wildtype, suggesting possible non-dopaminergic impairments. The crawling speeds upon reaching the bacterial lawn are significantly different between the wildtype and the *vps-35[D638N]* heterozygote and *cat-2(n4547),* illustrating impairments in basal slowing. Importantly, the crawling speed upon reaching the bacterial lawn is significantly (***) reduced following Genentech0877 treatment in the *vps-35[D638N]* heterozygote, consistent with improvements in basal slowing as seen in 5.2.2.

In day 5 of adulthood, the wildtype and *vps-35[D638N]* heterozygote do not show any significant differences in crawling speed on unseeded NGM, while the *cat-2(n4547)* consistently shows a reduced crawling speed compared to the wildtype. following Genentech0877 treatment, there is a significant reduction in crawling speed on unseeded NGM, which is not demonstrated in the wildtype at this age. Upon reaching *E. coli* OP50, the *vps-35[D638N]* heterozygotes and the *cat-2(n4547)* do not show significant differences in crawling speed to the wildtype. however, upon Genentech0877 treatment, the *vps-35[D638N]* heterozygote illustrates significant reductions in crawling speed under this condition. This may be suggestive if basal slowing, however when contrasted with the unseeded NGM crawling speed for this line following Genentech0877 treatment, this may be due to broader impacts upon crawling speed illustrated in the inhibitor treated *vps-35[D638N]* heterozygote at this stage.

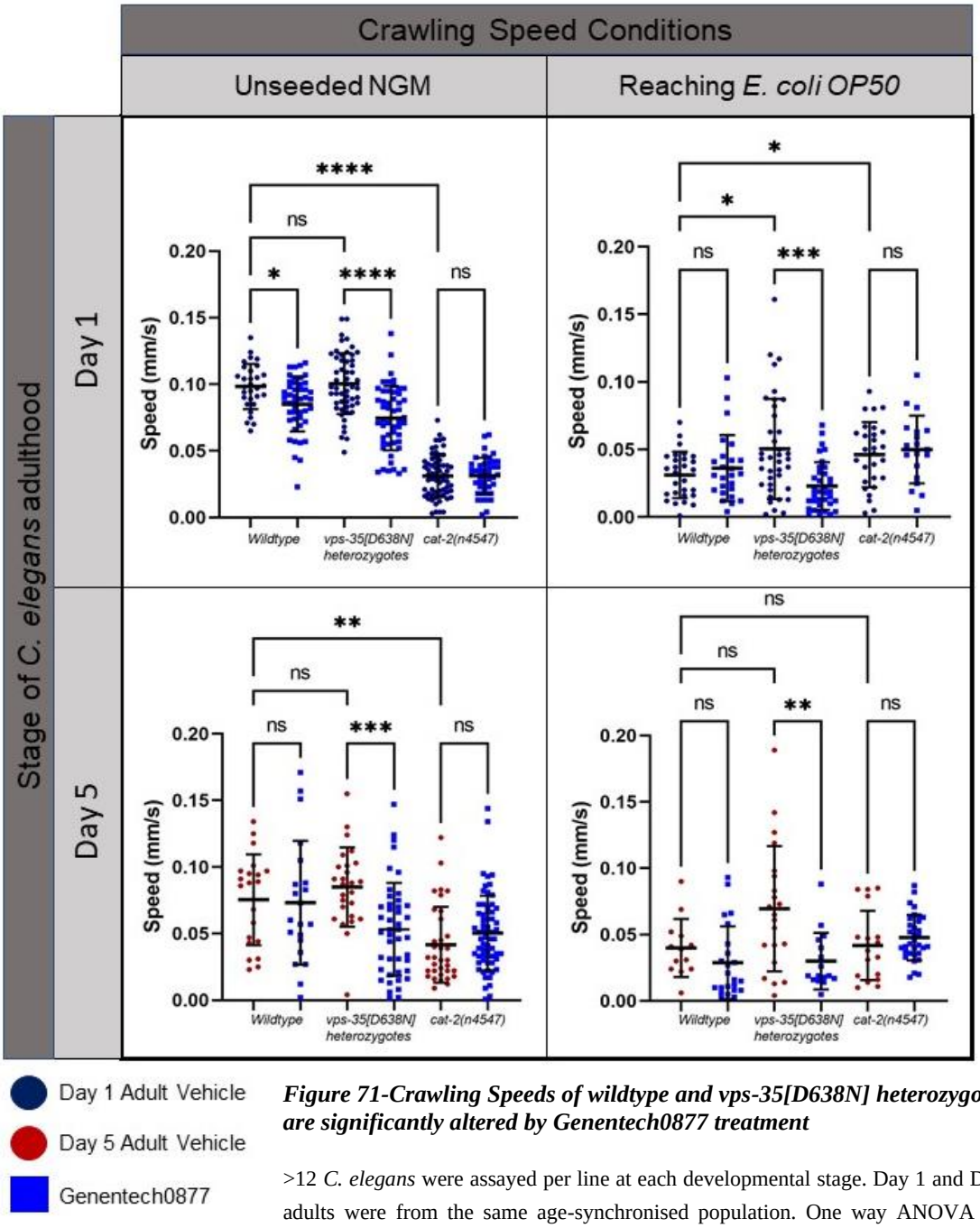

Figure 71-Crawling Speeds of wildtype and vps-35[D638N] heterozygotes are significantly altered by Genentech0877 treatment

>12 *C. elegans* were assayed per line at each developmental stage. Day 1 and Day 5 adults were from the same age-synchronised population. One way ANOVA with Brown-Forsythe and Welch Correction for unequal standard deviations undertaken. Full P values and descriptive statistics including mean, standard deviation and number can be found in the supplementary.

5.2.5 The crawling speed is not altered in *vps-35[D638N]* heterozygotes between day 1 and day 5 in vehicle and Genentech0877 treated conditions

As with the basal slowing responses contrasted in 5.2.3, the crawling speeds have been compared in day 1 and day 5 of adulthood under vehicle and LRRK2 inhibitor treated conditions (Figure 72). Under vehicle treated conditions, the wildtype shows a significantly reduced crawling speed in day 5 of adulthood on unseeded NGM, while there are no significant differences in the *vps-35[D638N]* heterozygote and *cat-2(n4547)*. Upon reaching the *E. coli OP50* lawn, there is no significant difference in crawling speed between day 1 and day 5 of adulthood for all genotypes.

Under Genentech0877 treated conditions, there is no significant difference in crawling speed between day 1 and day 5 of adulthood for the wildtype and *vps-35[D638N]* heterozygote, however there is a significant increase in crawling speed in the *cat-2(n4547)*, which accounts for the improved basal slowing response illustrated in 5.2.3. There is no significant difference in crawling speed of the *cat-2(n4547)* upon reaching the *E. coli OP50*, suggesting there is no improvement in slowing at this developmental stage. Furthermore, no significant differences in crawling speed between day 1 and day 5 of adulthood in Genentech0877 treated wildtype and *vps-35[D638N]* heterozygotes are illustrated.

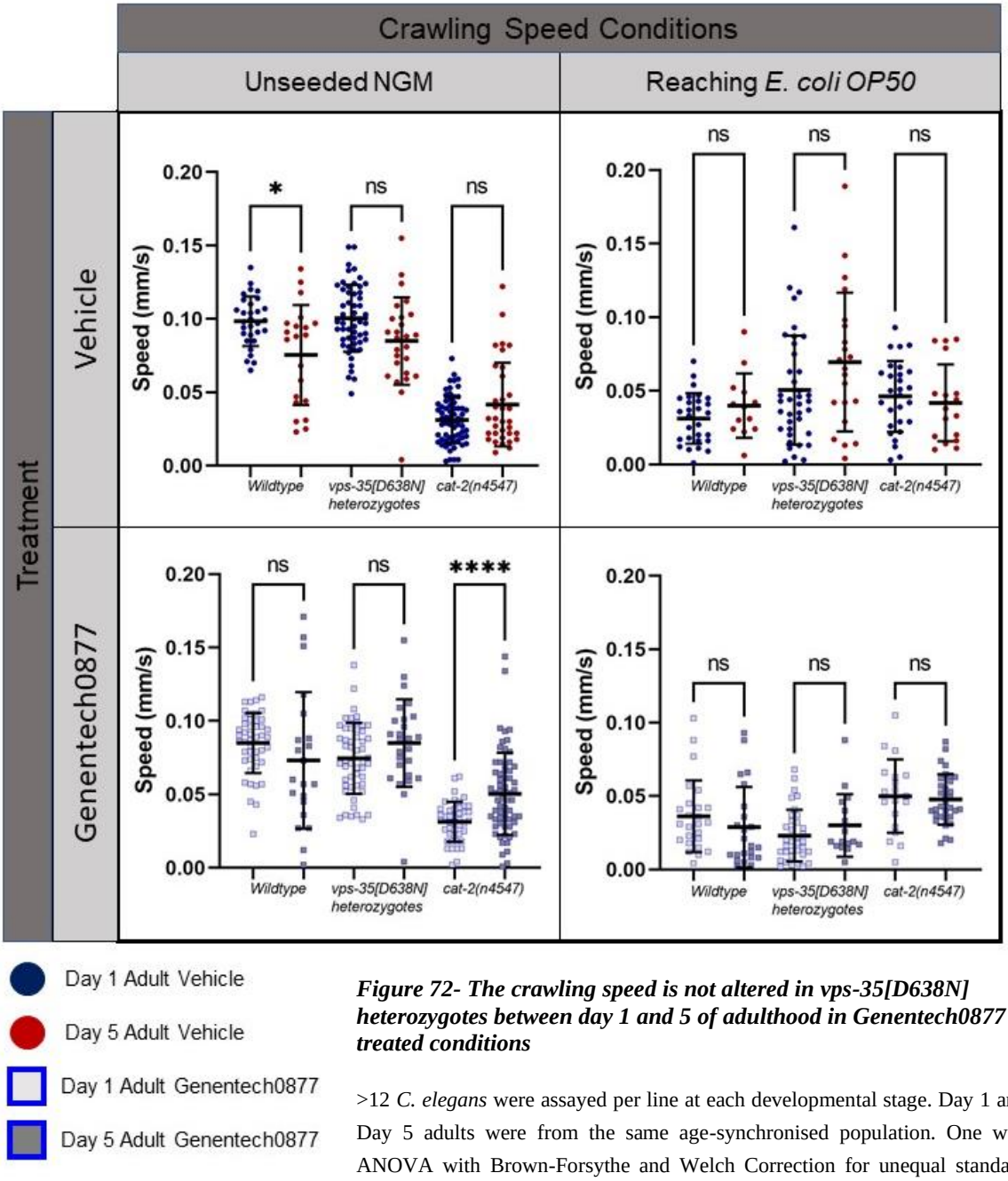

Figure 72- The crawling speed is not altered in vps-35[D638N] heterozygotes between day 1 and 5 of adulthood in Genentech0877 treated conditions

>12 *C. elegans* were assayed per line at each developmental stage. Day 1 and Day 5 adults were from the same age-synchronised population. One way ANOVA with Brown-Forsythe and Welch Correction for unequal standard deviations undertaken. Full P values and descriptive statistics including mean, standard deviation and number can be found in the supplementary.

5.3Administration of a LRRK2 inhibitor alleviates impairments in dopaminergic neuronal morphology in *vps-35[D638N]*

Following the successful generation of a dopaminergic neuronal GFP expressing *vps-35[D638N]* heterozygote, as detailed in chapter 3.10, the effect of Genentech0877 treatment through solid media feeding overnight was further examined. The dopaminergic neuronal morphology and fluorescence in day 1 and day 5 of adulthood was tested. A rescue in the impaired basal slowing response had been previously seen in the *vps-35[D638N]* following inhibitor treatment in day 1, but not day 5 of adulthood, thus it was examined whether these phenotype alleviations were due to improvements in dopaminergic function, or prevention of dopaminergic neurodegeneration and neuropathology's. Utilising the novel dat1:GFP expressing line, it has been possible to investigate the presence or extent of these at the key day 1 and 5 timepoints, utilised throughout this study.

5.3.1.1 LRRK2 inhibitor treatment improves the fluorescence intensity of *vps-35[D638N]* heterozygotes in day 1 of adulthood

Firstly, the fluorescence intensity of day 1 adult wildtype and *vps-35[D638N]* heterozygotes was quantified, following overnight vehicle or inhibitor treatment. Contrary to the data in 3.10, there was no significant difference in fluorescence intensity between the vehicle treated wildtype and *vps-35[D638N]* heterozygotes. However, following LRRK2 inhibitor treatment, there is a significant increase in *vps-35[D638N]* fluorescence and no change in the wildtype.

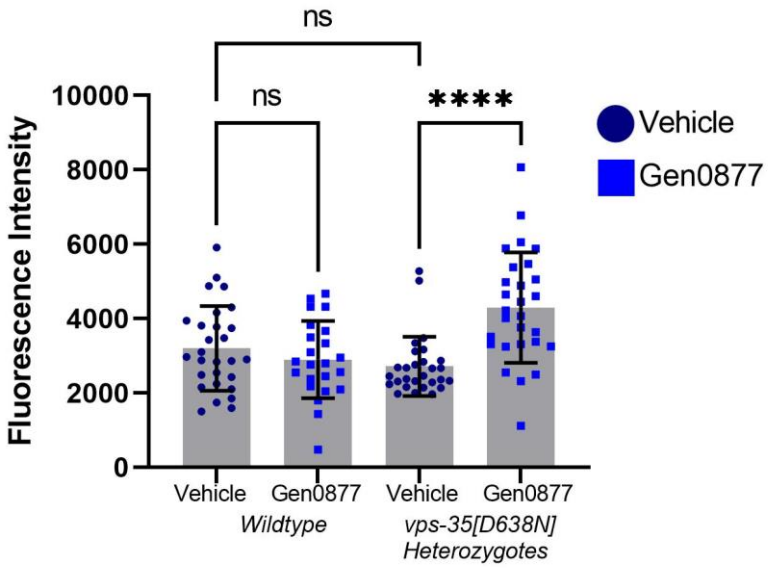

Figure 73-LRRK2 inhibitor treatment improves the fluorescence intensity of vps-35[D638N] heterozygotes in day 1 of adulthood

Day 1 adult CEP cell bodies fluorescence quantified per *C. elegans*, through selection of a 1000 pixel area. Analysis undertaken utilising ZenBlue4.2 software. Full descriptive statistics and One Way ANOVA with Brown-Forsyth Correction P values found in the supplementary.

5.3.1.2 Treatment with a LRRK2 inhibitor improves outgrowths in CEP neurons and blebbing in ADE neurons in the *vps-35[D638N]* heterozygotes in day 1 of adulthood

Upon observing the dopaminergic neuronal morphology of these lines following LRRK2 inhibitor treatment, there are noticeable differences in the type and extent of pathology seen in the CEP and ADE dopaminergic neurons (Figure 74). In a population of ~20 *C. elegans*, the wildtype vehicle treated line shows approximately 95% wildtype healthy appearance of the CEP neurons, opposed to just 70% in the vehicle treated *vps-35[D638N]* heterozygotes, consistent with findings in 3.10. Following treatment with the LRRK2 inhibitor Genentech0877, there are highly deleterious impacts upon the wildtype *C. elegans*, with ~20% of the neuronal population exhibiting CEP neuronal degeneration, a further ~5% exhibiting blebbing and a further ~15% showing minor impairments such as branching and outgrowths. This is in contrast to the inhibitor treated *vps-35[D638N]* heterozygote, which shows modest improvements in the minor impairments seen in the vehicle treated CEP neurons, from affecting approximately 30% to 20%.

In addition, when the ADE neurons are examined, which have previously been reported to be more sensitive to toxic insults in 3.10, through genetic alterations or toxin induction, this picture is further expanded. In the wildtype vehicle treated, ~95% show wildtype morphology, but following inhibitor treatment, this drastically reduces to ~60%, with 10% of the population exhibiting blebbing and the remaining 30% exhibiting ADE neuron degeneration. In contrast, the vehicle treated *vps-35[D638N]* heterozygote shows 10% of the population have neuronal degeneration and approximately 20% present with blebbing. Following inhibitor treatment, only 10% of the ADE neurons show major impairments such as degeneration in the *vps-35[D638N]* heterozygote population. This data is highly important in testing our main hypothesis that *vps-35[D638N]* acts through LRK-1 hyperactivation, as in both neuronal groups, neuropathology in *vps-35[D638N]* is improved, rescuing impairments not seen in the wildtype. Furthermore, the deleterious impacts seen in the wildtype inhibitor treated line is consistent with behavioural data, on the dopaminergic basal slowing response, in which improvements were seen in the *vps-35[D638N]* heterozygotes, but modest worsening of the basal slowing response demonstrated in the wildtype.

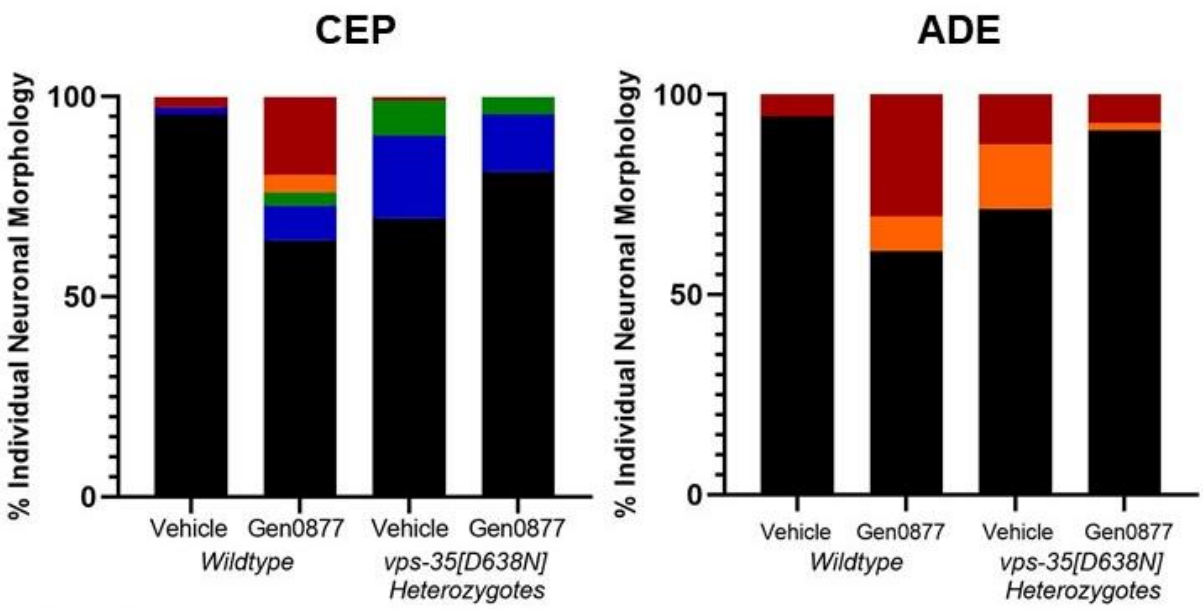

Figure 74- Treatment with Genentech0877 improves the dopaminergic impairments exhibited in vps-35[D638N] heterozygotes in day 1 of adulthood

Approximately 20 day 1 adult *C. elegans* scored per mutant line and treatment. Full tabulated values and number can be found in the supplementary. Proportions calculated from individual neurons in whole population, rather than individual *C. elegans*, in order to identify the most prevalent neuropathology within the population.

5.3.1.3 LRRK2 inhibitor treatment improves the number of impairments per *vps-35[D638N]* heterozygote in day 1 of adulthood

As well as studying the impairment type in the whole *C. elegans* population, the number of minor and major impairments shown per *C. elegans* within the population have been scored (figure 75), to understand the typical extent of neuropathology per *C. elegans*, as opposed to how common a pathology is within a population. Minor impairments include outgrowths and branching, indicative of perturbed cellular signalling, while major impairments include blebbing and degeneration. In the wildtype line treated with a vehicle, only 5% of the population show 1 minor impairment, while following treatment with Genentech0877, almost 20% show 1 impairment, with a further 10% exhibiting 2 impairments and 5% exhibiting 3, further illustrating the deleterious impact of the inhibitor in wildtype populations. As reported in 3.10, the *vps-35[D638N]* heterozygote treated with a vehicle, a very high proportion of the population present with 1 or more minor impairment, notably outgrowths. Almost 50% of the population show 1 impairment, with a further 35% showing 2. Following Genentech0877 treatment, this is reduced to 25% and 15% respectively, highlighting the improvement seen in individual *C. elegans*, rather than the population as a whole. In terms of major impairments, the wildtype again sees a dramatic increase in the number of major impairments per worm following Genentech0877 administration, with 1 or more major impairment seen in 55% of the population, with over 15% of the population showing major

impairments in all 6 dopaminergic neurons, highlighting further the severe impacts of drug treatment. This impact is completely differential in the *vps-35[D638N]*, in the vehicle 45% of the population show 1 or more major impairment and this reduces to 20% following inhibitor treatment.

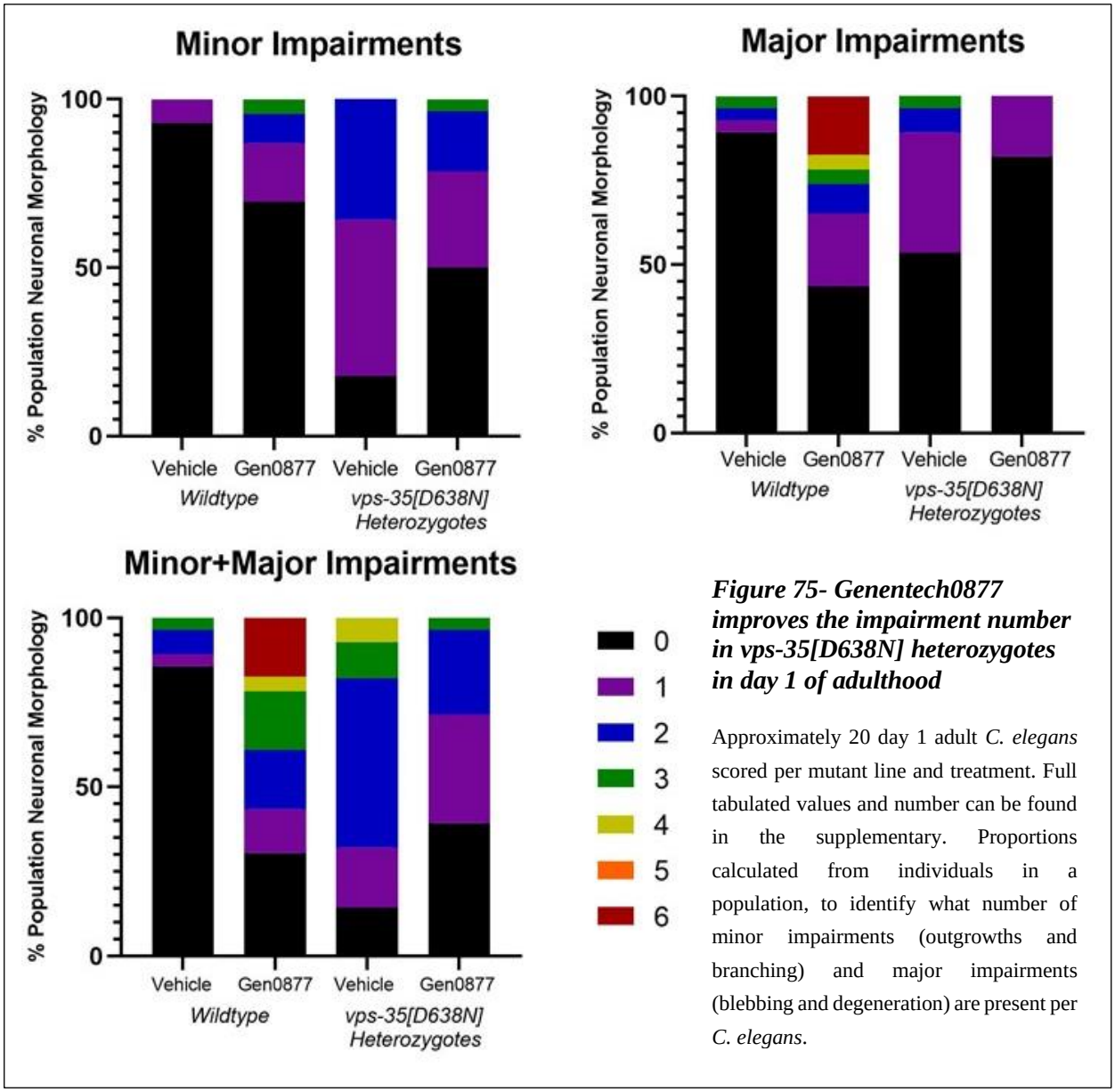

Figure 75- Genentech0877 improves the impairment number in vps-35[D638N] heterozygotes in day 1 of adulthood

Approximately 20 day 1 adult *C. elegans* scored per mutant line and treatment. Full tabulated values and number can be found in the supplementary. Proportions calculated from individuals in a population, to identify what number of minor impairments (outgrowths and branching) and major impairments (blebbing and degeneration) are present per *C. elegans*.

5.3.1.4 Prevalence of major impairments in ADE neurons of *vps-35[D638N]* heterozygotes are reduced following LRRK2 inhibitor treatment in day 1 of adulthood

In addition, insights were gleaned into which neuronal groups the minor and major impairments commonly occur per *C. elegans* (Figure 76). In the *vps-35[D638N]* heterozygotes treated with a vehicle, the most common impairments are minor impairments in the CEP neurons, affecting over 85% of the population and major impairments in the ADE neurons, affecting 45%. In Genentech0877 treatment, these are still the most prevalent impairment, but are reduced to affecting 50% and 20% of individuals respectively. This again, is in contrast to the wildtype, as

following inhibitor treatment the most prevalent impairment are major impairments in the ADE neurons, impacting almost 50% of *C. elegans* in the population. This further supports our data in 3.10, that ADE neurons are more sensitive to cellular aberrations. Furthermore, this population uniquely shows a high proportion of major impairments in the CEP neurons, with 35% of the population showing 1 or more of these, highlighting the harmful impact as these neurons are more resistant to cellular stress. This data further augments our working hypothesis that VPS-35[D638N] mutation acts through LRK-1 hyperactivation, consistent with alternative models of VPS35[D620N] function.

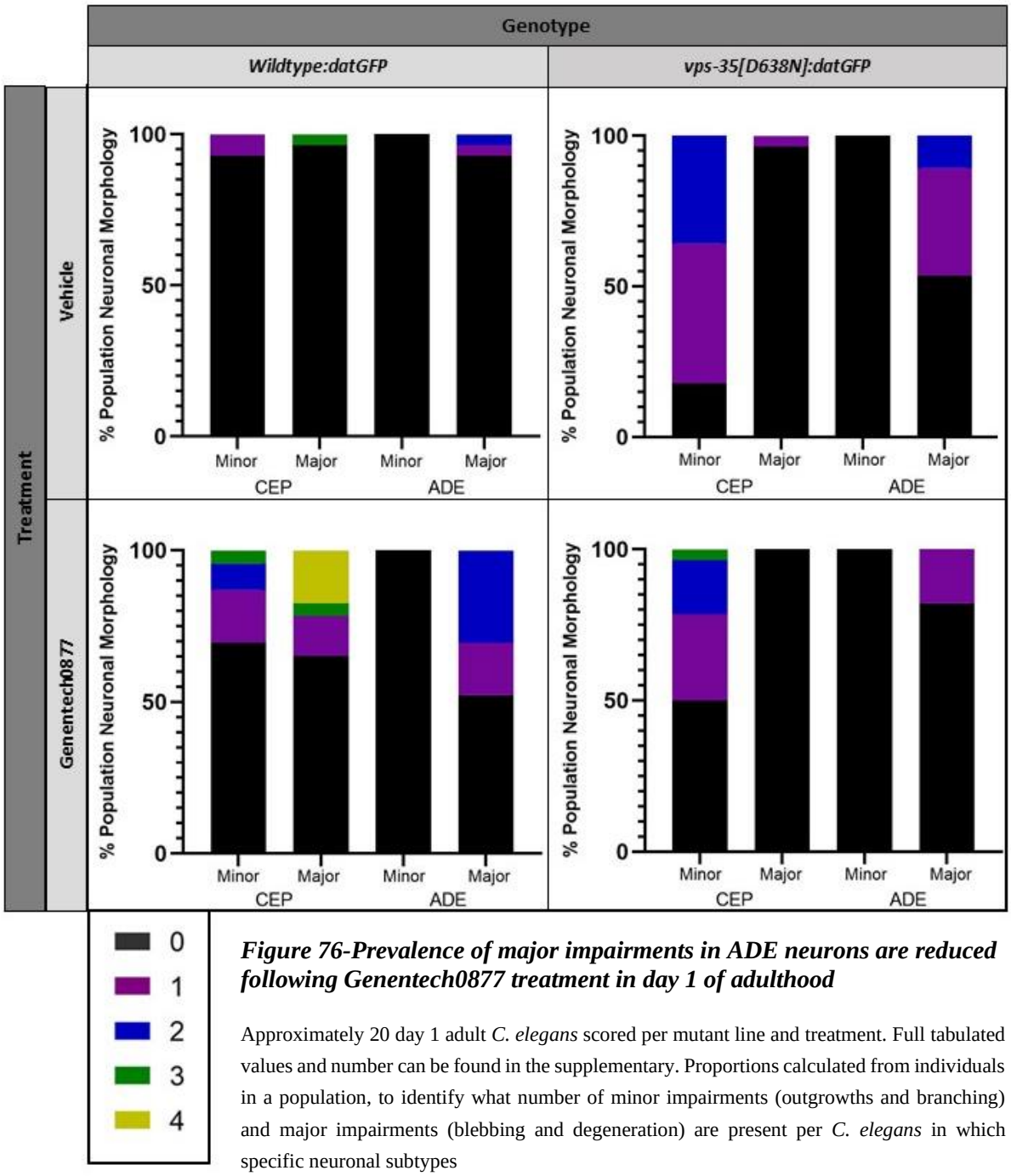

Figure 76-Prevalence of major impairments in ADE neurons are reduced following Genentech0877 treatment in day 1 of adulthood

Approximately 20 day 1 adult *C. elegans* scored per mutant line and treatment. Full tabulated values and number can be found in the supplementary. Proportions calculated from individuals in a population, to identify what number of minor impairments (outgrowths and branching) and major impairments (blebbing and degeneration) are present per *C. elegans* in which specific neuronal subtypes

5.3.2.1 LRRK2 inhibitor treatment reduces the fluorescence intensity of *vps-35[D638N]* heterozygotes in day 5 of adulthood

The impact of ageing to day 5 was investigated in *vps-35[D638N]* heterozygotes, in conjunction with Genentech0877. At day 5 of adulthood, the *vps-35[D638N]* heterozygotes shows a further impaired basal slowing response compared to day 1 and this is not significantly rescued following Genentech0877 treatment, thus the dopaminergic neuronal morphology and fluorescence was investigated. The fluorescence intensity was quantified, as in day 1. At day 5, the *vps-35[D638N]* heterozygotes show no significant difference from the wildtype following vehicle treatment, in terms of fluorescence intensity. However, interestingly the *vps-35[D638N]* heterozygotes show a significantly reduced fluorescence intensity following LRRK2 inhibitor treatment, while the wildtype does not. This is juxtaposed to the day 1 data, in which LRRK2 inhibitor treatment significantly increases GFP fluorescence in the *vps-35[D638N]* heterozygotes, suggesting age determined effects of LRRK2 inhibitor treatment, as this dosage regimen began at day 4 adult, opposed to L4 larval.

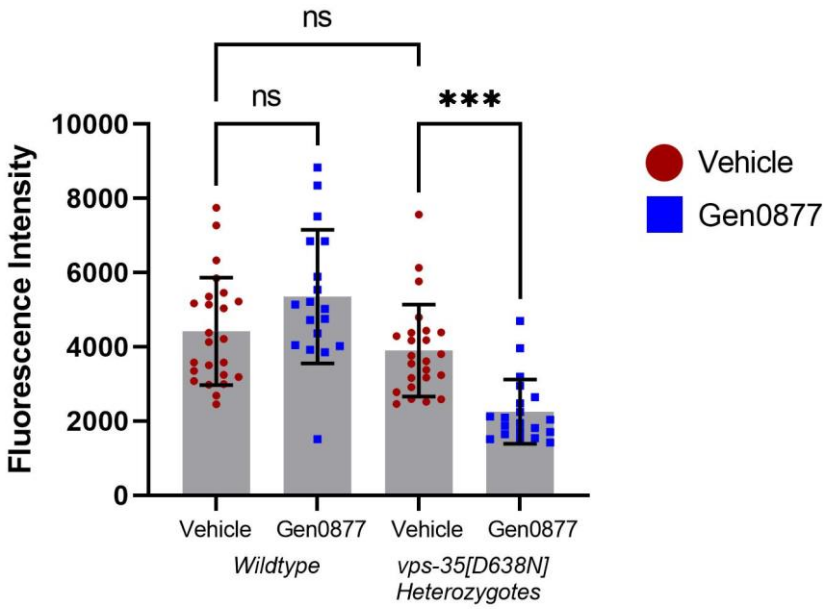

Figure 77- Fluorescence intensity of day 5 adult vps-35[D638N] treated with Genentech0877

Day 5 adult CEP cell bodies fluorescence quantified per *C. elegans*, through selection of a 1000 pixel area. Analysis undertaken utilising ZenBlue4.2 software. Descriptive statistics and One Way ANOVA with Brown-Forsyth Correction P values in

5.3.2.2 Treatment with a LRRK2 inhibitor improves the dopaminergic impairments exhibited in *vps-35[D638N]* heterozygotes in day 5 of adulthood

In terms of neuronal pathologies, these are more prevalent or more severe with age in both vehicle treated populations in the CEP (figure 78). In the wildtype, almost 15% of the population show outgrowths in the CEP neurons, while in the *vps-35[D6638N]* there remains 25% of individuals showing outgrowths and more than 5% showing severe phenotypes such as degeneration. Following LRRK2 inhibitor treatment, there is no change in neuronal pathology in the wildtype,

a substantial difference from the day 1 data. In the *vps-35[D638N]* there is a reduction in degeneration, but a consistent level of outgrowths, suggesting that there may be some inhibitor benefit at this developmental stage, but this is relatively small.

In terms of the sensitive ADE neurons, in the wildtype nearly 25% are blebbing or degenerated, a much greater proportion than in day 1. Meanwhile in the *vps-35[D638N]*, 65% of ADE neurons are blebbing or have degenerated. This highlights the age dependent, dopaminergic neurodegeneration shown in our model, which is a very relevant phenotype to PD modelling and further understanding VPS35. Moreover, this correlates with the age dependent decline in basal slowing data previously seen in chapter 3, augmenting *C. elegans* as a model that could be approached from multiple angles for *in vivo* modelling. In the inhibitor treated wildtype populations, there is an increase in ADE neuron degeneration, as opposed to blebbing in the wildtype vehicle, suggesting that in already impaired neurons, inhibition increases the speed of the process of degeneration. Whereas in the *vps-35[D638N]*, again the opposite phenotype is shown, with just 35% of the population showing impairments in the ADE neurons, suggesting that LRK-1 inhibition is beneficial for this neuronal subgroup in day 5.

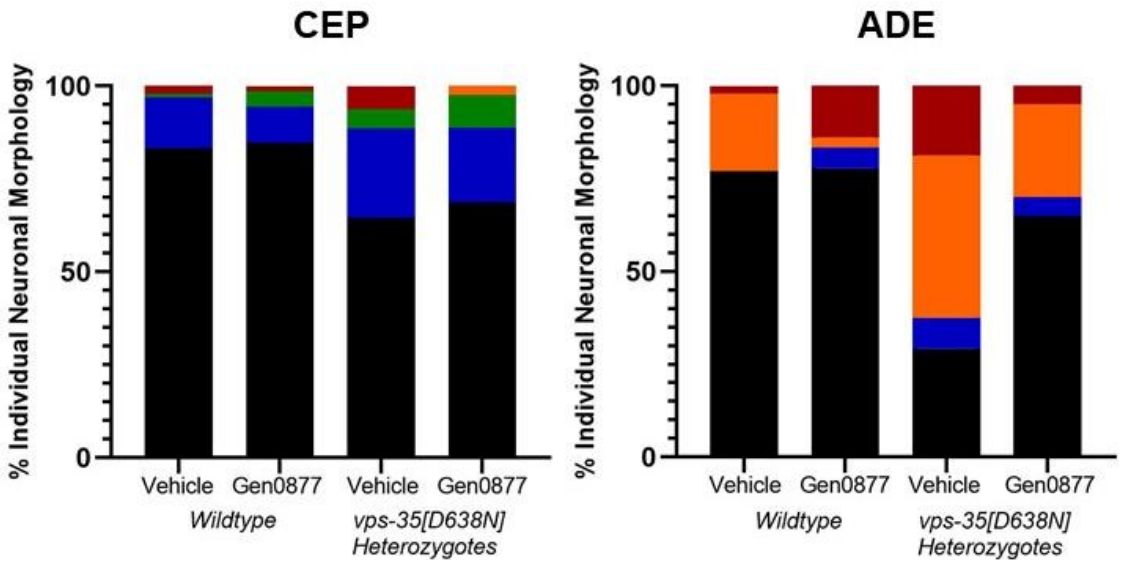

Figure 78- CEP and ADE neuronal morphology of day 5 adult vps-35[D638N] treated with Genentech0877

Approximately 20 day 5 adult *C. elegans* scored per mutant line and treatment. Full tabulated values and number can be found in the supplementary. Proportions calculated from individual neurons in whole population, rather than individual *C. elegans*, in order to identify the most prevalent neuropathology within the population.

5.3.2.3 LRRK2 inhibitor treatment improves the number of impairments in vps-35[D638N] heterozygotes in day 5 of adulthood

The number of impairments per *C. elegans* in the population was quantified, to evaluate the impact age and inhibition had upon individuals, rather than a proportion of neurons. In the wildtype

vehicle, approximately 40% of individuals had one or more minor impairment, which was modestly increased to 50% following inhibitor treatment (Figure 79). In contrast, the *vps-35[D638N]* showed almost 60% of the population had 1 or more minor impairments and following inhibitor treatment, this increased to over 65%, however the proportion of animals showing three or more minor impairments reduced by almost half, suggesting a beneficial effect. In terms of major impairments, in the wildtype 40% of animals show one or more while this increased to 80% in the *vps-35[D638N]*. LRRK2 inhibitor treatment leads to no substantial change in this proportion in the wildtype, but in the *vps-35[D638N]*, this number reduces to approximately 50%, further suggesting inhibition may still be beneficial at this stage of the lifespan for neuroprotection. However, this is still a large proportion of the inhibitor treated *vps-35[D638N]* population with impairments, which may be reflected in the basal slowing data, in which improvements in behaviour are not shown at day 5 (Figure 69).

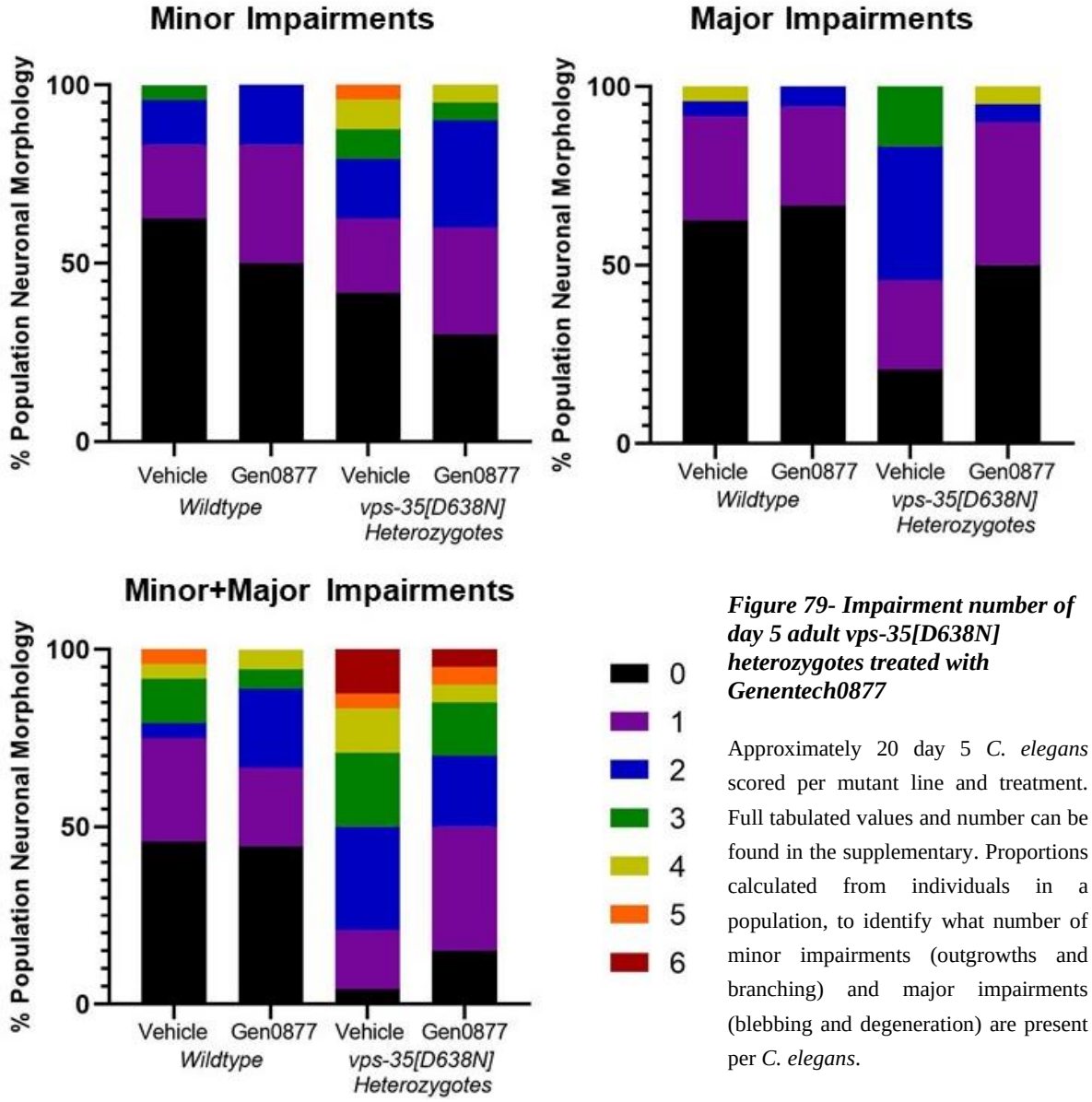

Figure 79- Impairment number of day 5 adult vps-35[D638N] heterozygotes treated with Genentech0877

Approximately 20 day 5 *C. elegans* scored per mutant line and treatment. Full tabulated values and number can be found in the supplementary. Proportions calculated from individuals in a population, to identify what number of minor impairments (outgrowths and branching) and major impairments (blebbing and degeneration) are present per *C. elegans*.

5.3.2.4 Prevalence of major impairments in ADE neurons of *vps-35[D638N]* heterozygotes are reduced following LRRK2 inhibitor treatment in day 5 of adulthood

The most prevalent impairment in each neuronal group has been scored, to evaluate how this differs with ageing and Genentech0877 treatment between wildtype and *vps-35[D638N]* (Figure 80). In the vehicle treated *vps-35[D638N],* the most common impairments are minor impairments in the CEP neurons, closely followed by major impairments in the ADE neurons, reflecting prior data suggesting that these are the most common neuropathology's in response to cellular stresses. Following inhibitor treatment, these neuropathology's remain the most prevalent, the proportion of *C. elegans* with 1 or more minor impairments in the CEP neurons does not change, however there is a modest reduction in the proportion of *C. elegans* with 1 or more major impairment in the ADE neurons. Compared to the *vps-35[D638N]* heterozygote, the wildtype vehicle treated population shows a reduced proportion of *C. elegans* exhibiting one or more minor impairment in the CEP neurons and one or more major impairments in the ADE neurons. This remains similar in the Genentech0877 treated population, with no substantial difference in neuropathology type or extent shown.

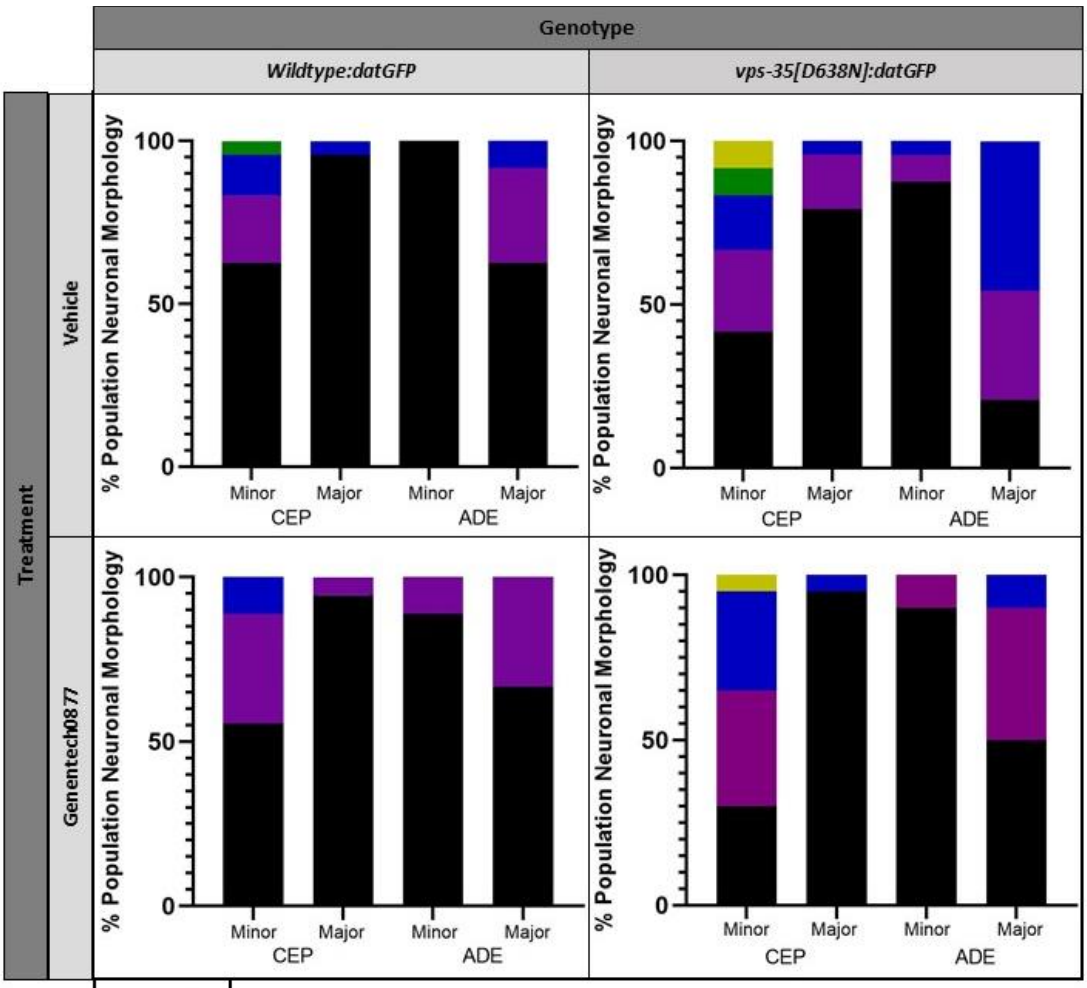

Figure 80- Impairment breakdown of Day 5 Adult vps-35[D638N] treated with Genentech0877

Approximately 20 day 5 adult *C. elegans* scored per mutant line and treatment. Full tabulated values and number can be found in the supplementary. Proportions calculated from individuals in a population, to identify what number of minor impairments (outgrowths and branching) and major impairments (blebbing and degeneration) are present per *C. elegans* in which specific neuronal subtypes

5.4 Effect of LRRK2 inhibitor treatment upon selected *vps-35[D638N]* heterozygote cellular phenotypes

As reported in chapter 3, the *vps-35[D638N]* heterozygote shows multiple alterations in different cellular phenotypes, in mitochondrial, autophagic and endocytic/cilia function. Several of these have been linked to LRRK2 function in alternative model systems, notably ciliation (287,325,326). These outputs can be studied in *C. elegans* through DiI uptake in the amphid neurons. Thus, this phenotype has been investigated in conjunction with treatment with the LRRK2 inhibitor Genentech0877, following promising data described in section 5.2, demonstrating that this alleviates impaired dopaminergic basal slowing phenotypes in day 1 of adulthood.

5.4.1 Treatment with LRRK2 inhibitor does not rescue impairments in *vps-35[D638N]* ciliation phenotypes

vps-35[D638N] heterozygotes show a reduced DiI fluorescence, indicative of an impaired ciliation phenotype and endocytic traffic, while LRRK2 has been associated with impaired cilia formation. As such, this phenotype was investigated following LRRK2 inhibitor treatment in order to investigate if LRK-1 function was implicated in this process in *C. elegans* and further test the VPS-35/LRK-1 interplay through a cellular readout.

Consistent with prior data, the *vps-35[D638N]* heterozygote shows reduced DiI fluorescence in day 1 of adulthood, indicative of reduced dye uptake through ciliation and endocytic traffic. In contrast to data in chapter 3, in which this ciliation was studied from day 5 onwards and showed no age dependant reduction. The fact that reduced ciliation is shown in day 1 of adulthood in *vps-35[D638N]* further highlights that this phenotype is not age dependant and likely due to cellular aberrations induced by the *vps-35[D638N]* mutation. Following treatment with a LRRK2 inhibitor overnight, there is no significant difference in DiI fluorescence intensity, suggesting that impairments may be independent of LRK-1 kinase activity in this mutant.

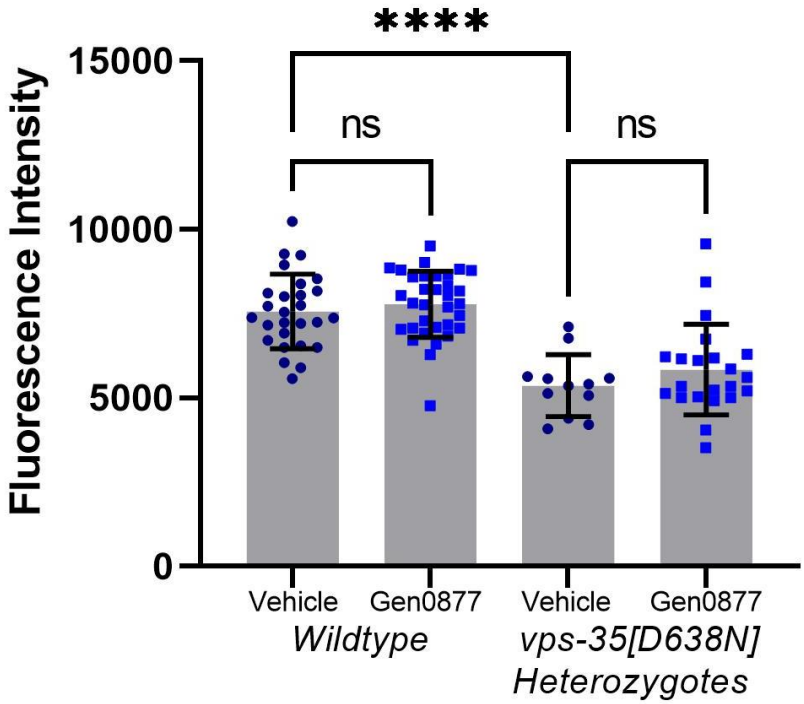

Figure 81- Treatment with Genentech0877 does not rescue impairments in vps-35[D638N] ciliation phenotypes

15-30 day 1 adult C. elegans visualised per line. One-way ANOVA analysis utilising pre-selected columns and Welch's correction for unequal standard deviations. Full descriptive statistics including the mean, standard deviation and number can be found in the supplementary.Raw fluorescence intensity in comparative figure utilised, to contrast changes in fluorescence intensity between day 1 and 5 within genotypes. Area of Dil Stained amphid/phasmid neurons captured and fluorescence quantified utilising ZenBlue4.2 software, with background subtraction.

5.5 Generation of a VPS-35[D638N] mutant with homozygous LRK-1[D1847A] kinase ablation mutation

Following the establishment of a pharmacological model to dissect the VPS-35/LRK-1 interplay in *C. elegans*, a novel genetic model was established for characterisation, to further test the working hypothesis that mutation in VPS35 increases LRRK2 phosphorylation activity. The *vps-35[D638N]*:datGFP mutant was crossed with the four times outcrossed homozygous *lrk-1[D1847A]* kinase ablated mutant, with the aim to generate progeny with dopaminergic GFP expression for neuronal morphology characterisation, heterozygous for *vps-35[D638N]* and homozygous for the *lrk-1[D1847A]* kinase ablated mutant.

Males were generated through heat-shocking the L4 larvae of the *lrk-1[D1847A]* mutant line, these male populations were propagated and young adult male *lrk-1[D1847A]* were crossed with L4 *vps-35[D638N]:datGFP* hermaphrodites. 15 resultant progeny from this cross were separated onto small plates, to found their own populations. Founding hermaphrodite mothers were taken for genotyping, to test for GFP presence. 10 of the progeny showed this, highlighting that the transgene for dopaminergic visualisation had been passed on.

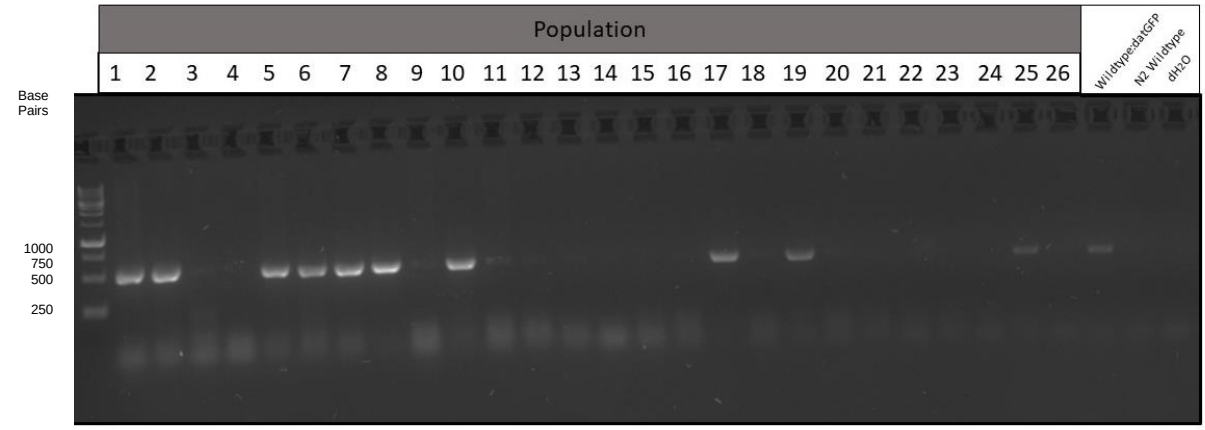

Figure 82- Genotyping for GFP presence in VPS-35[D638N]:LRK-1[D1847A] double mutant cross

26 populations were obtained from the *vps-35[D638N]:dat:GFP* and *lrk-1[D1847A]* cross, 10 of which illustrated *dat:GFP* presence, illustrated through the ~500bp GFP PCR product.

All progeny from the cross will be heterozygous for *lrk-1[D1847A]*, however for the genetic model of complete LRK-1 kinase ablation, homozygous mutation is required. As *C. elegans* self-fertilise, there should be homozygous *lrk-1[D1847A]* in the progeny of the heterozygous *lrk-1[D1847A]*, if Mendelian gene segregation patterns are shown. 18 progeny of population 1 were separated and then genotyped for both vps-35[D638N] heterozygosity and lrk-1[D1847A] homozygosity. One population, population 9 shown in green on figure 86, illustrated this genotype. The population was expanded for characterisation and cryogenically frozen for the laboratory database.

vps-35[D638N]

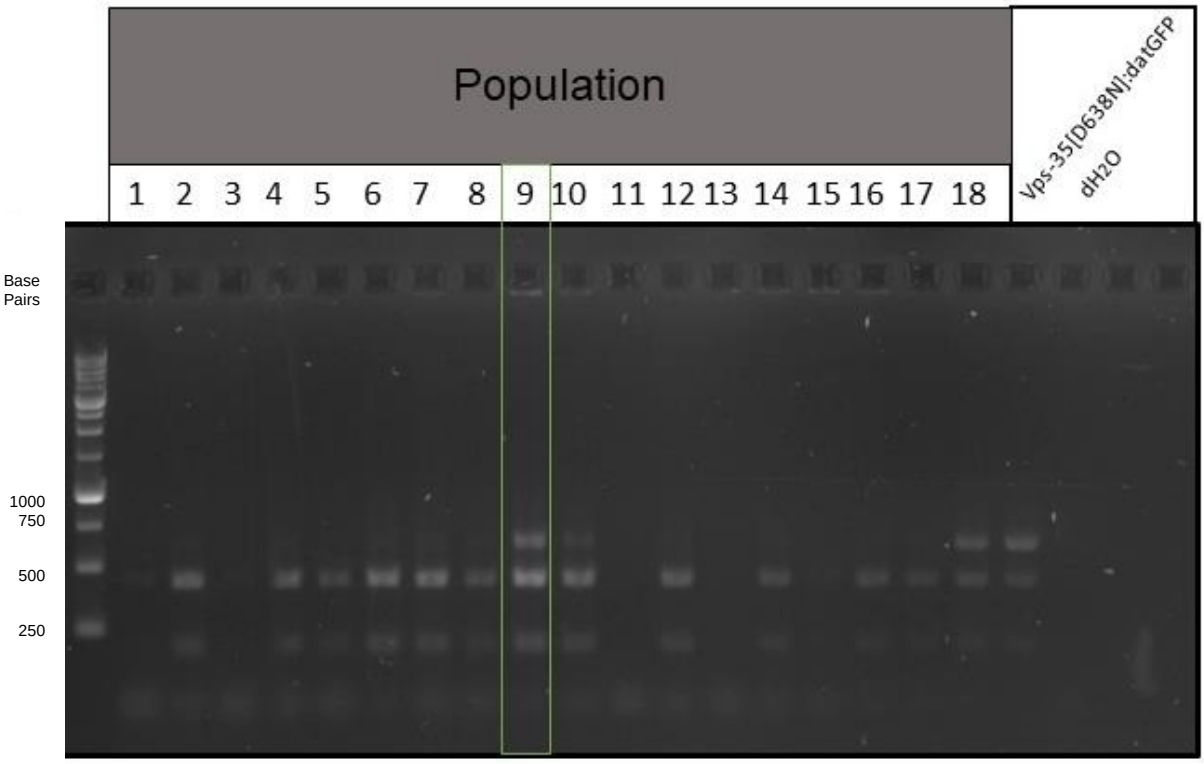

lrk-1[D1847A]

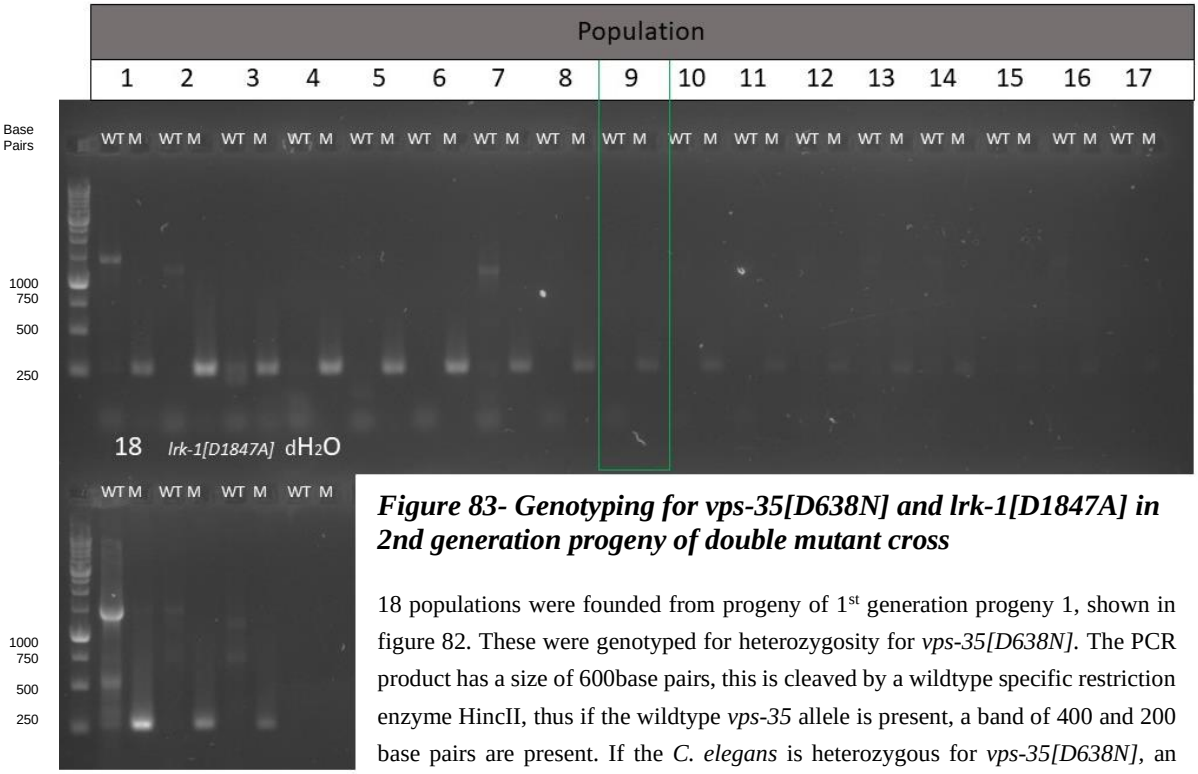

Figure 83- Genotyping for vps-35[D638N] and lrk-1[D1847A] in 2nd generation progeny of double mutant cross

18 populations were founded from progeny of 1st generation progeny 1, shown in figure 82. These were genotyped for heterozygosity for *vps-35[D638N]*. The PCR product has a size of 600base pairs, this is cleaved by a wildtype specific restriction enzyme HincII, thus if the wildtype *vps-35* allele is present, a band of 400 and 200 base pairs are present. If the *C. elegans* is heterozygous for *vps-35[D638N]*, an undigested PCR product band is present at 600 base pairs, shown in population 9. Concurrently, genotyping was undertaken for lrk-1[D1847A], utilising mutation specific primers, wildtype creates a PCR product of 1250bp and mutant, ~200bp. Of the three populations heterozygous for *vps-35[D638N]* (9, 10 and 18), population 9 and 10 appear to be homozygous for *lrk-1[D1847A]*.

Notably, the generation of a *vps-35[D638N]* heterozygote with homozygous *lrk-1[D1847A]* proved very challenging and multiple unsuccessful attempts were undertaken, prior to this success in August 2021. Frequently, second generation populations heterozygous for *vps-35[D638N]* would be heterozygous for *lrk-1[D1847A]* (as illustrated in population 18), or *lrk-1* wildtype, or vice versa- homozygous for *lrk-1[D1847A]*, but wildtype for *vps-35*. This suggests that the combination of these two mutations may have broader impacts on development and organism health. Detailed study of genetic interaction and progeny genotype of crosses between *vps-35[D638N]* and selected *lrk-1* mutations would provide great insight into the broader interplay of these two mutations about the cellular and organismal consequences.

As the novel double mutant will be utilised for GFP dopaminergic neuron visualisation, a single mutant homozygous *lrk-1[D1847A] C. elegans* expressing *dat:GFP* was generated in tandem, through crossing the *lrk-1[D1847A]* males generated with the *wildtype;datGFP* expressing line. These progeny were separated, genotyped and populations expressing *dat:GFP* were selected for progeny separation, in order to obtain second generation *lrk-1[D1847A]* homozygous mutants, obtained through self-fertilisation. This line will be utilised as a control in future studies of dopaminergic neuronal morphology.

5.6 *vps-35[D638N]* heterozygotes with homozygous *lrk-1[D1847A]* genetic kinase ablation show improved basal slowing responses

Following double mutant generation, the basal slowing response was assayed, which has been illustrated to be a robust output of *vps-35[D638N]* heterozygote impaired dopaminergic function. As detailed in 5.2, this impaired phenotype is alleviated following LRRK2 inhibitor treatment in day 1 of adulthood but not day 5 of adulthood. Thus, assay utilising our genetic model will be a helpful output for contrasting with the pharmacological model and may provide additional validation of the phenotypes illustrated. During this basal slowing assay, three replicates of each novel mutant line were assayed in tandem and analysed utilising nested parameters.

5.6.1 *vps-35[D638N]* heterozygotes with homozygous *lrk-1[D1847A]* kinase ablation show a significantly improved basal slowing response on day 1 of adulthood

Consistent with data discussed in chapter 3 and in 5.3, the *vps-35[D638N]* heterozygote shows a significantly impaired basal slowing response compared to the wildtype, while conversely the *lrk-1[D1847A]* mutant, utilised as a control for LRK-1 kinase ablated dopaminergic function, showed a significantly enhanced basal slowing response (Figure 84). Pertinently, the newly developed *vps-35[D638N]* heterozygote with homozygous *lrk-1[D1847A]* kinase ablation illustrated no significant difference in basal slowing response compared to the wildtype, suggesting a rescue in basal slowing. This is a similar phenotype to that shown in the pharmacological model utilised to test the working hypothesis that *vps-35[D638N]* may act through LRK-1 kinase hyperactivation. However, this may not be a complete rescue, as the *lrk-1[D1847A]* shows a significantly enhanced basal slowing compared to the wildtype and is very highly (****) significantly different from the *vps-35[D638N]* heterozygote, while the *vps-35[D638N]:lrk-1[D1847A]* model shows no significant difference from the wildtype and is significantly different to a lower extent (**) to the *vps-35[D638N]* heterozygote. This suggests that although LRK-1 kinase ablation rescues defects in basal slowing function and could be a key pathological pathway in VPS-35[D638N] neuropathology, additional mechanisms may be in action linked to this mutation.

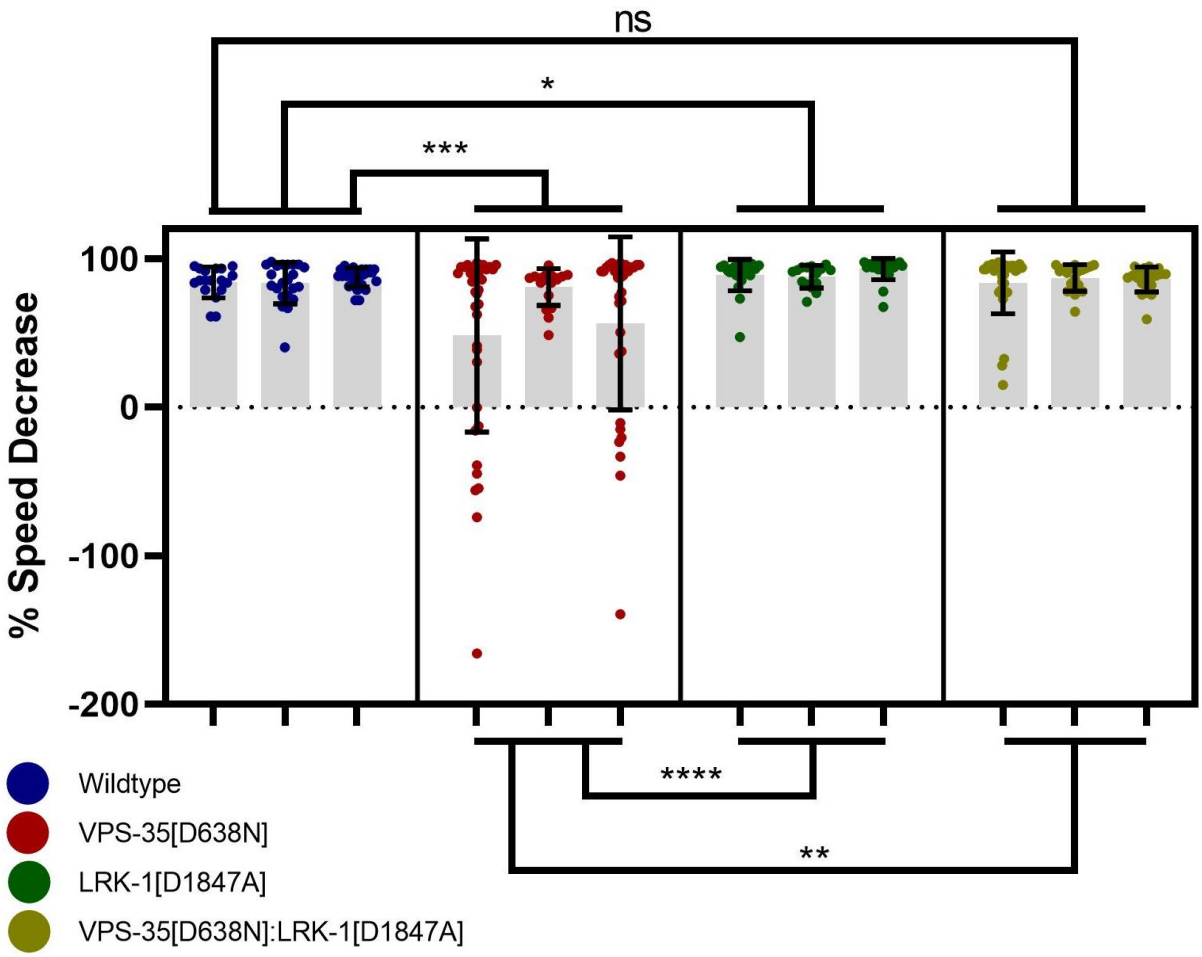

Figure 84- vps-35[D638N] heterozygotes with homozygous lrk-1[D1847A] kinase ablation show improved basal slowing in day 1 of adulthood

Three replicates undertaken in tandem in same experimental setup for each genotype. Statistical analysis undertaken through nested one-way ANOVA, utilising averages from each of the three replicates for comparison. Descriptive statistics for each genotype and replicate, along with P-values can be found in the supplementary.

5.6.2 *vps-35[D638N]* heterozygotes with homozygous *lrk-1[D1847A]* kinase ablation do not show significantly different crawling speeds in day 1 of adulthood

As part of this basal slowing assay, the crawling speeds of the different *C. elegans* genotypes and replicates were quantified on an unseeded NGM plated and upon reaching a bacterial lawn on an *E. coli OP50* seeded NGM plate (Figure 85). The novel *vps-35[D638N]:lrk-1[D1847A]* double mutant does not show any significant differences in crawling speed compared to the wildtype, on unseeded NGM or upon reaching a bacterial lawn. However, upon reaching the bacterial lawn the *vps-35[D638N]:lrk-1[D1847A]* double mutant shows a significantly (*) slower crawling speed than the *vps-35[D638N]*, indicative of improved dopaminergic function. However, the *lrk-1[D1847A]* homozygote is significantly slower than the *vps-35[D638N]* heterozygote to a greater extent (***), further suggesting that LRK-1 kinase activity is implicated in *vps-35[D638N]* mutation, but may not be the sole mechanism.

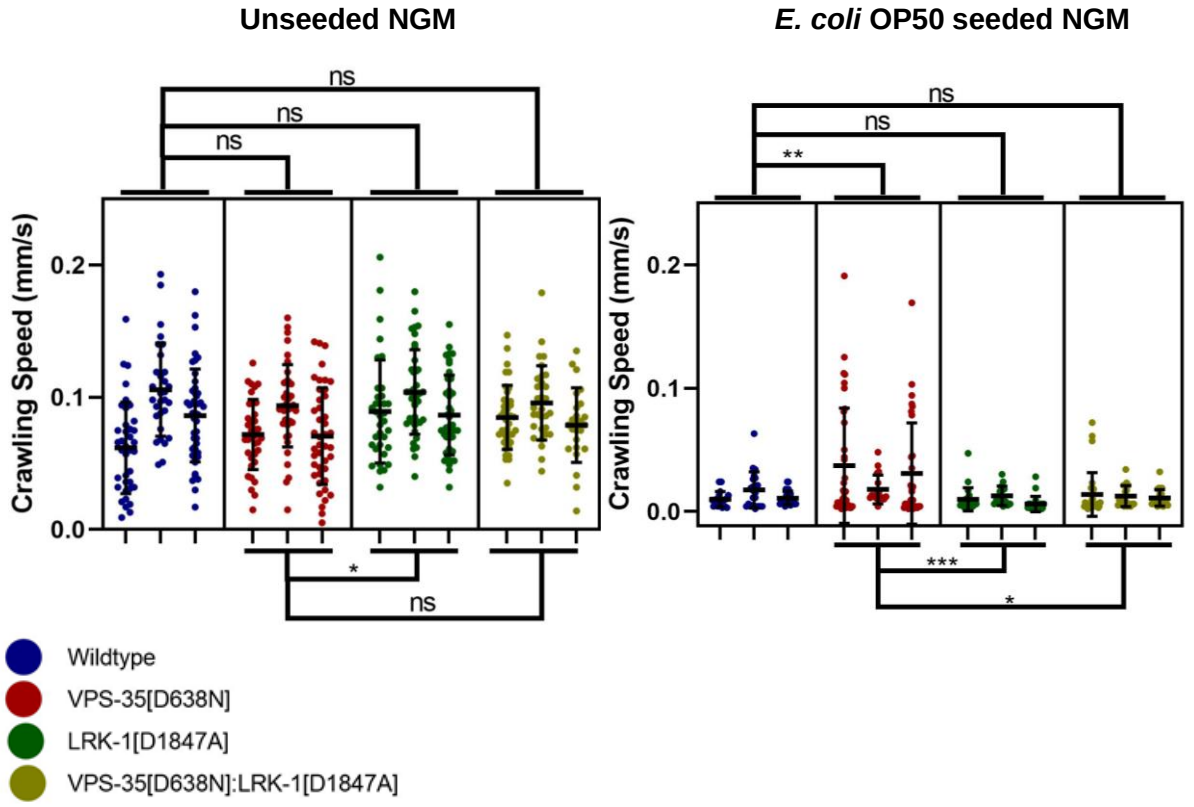

Figure 85-vps-35[D638N] heterozygotes with homozygous lrk-1[D1847A] kinase ablation do not show significantly different crawling speeds in day 1 of adulthood

Three replicates undertaken in tandem in same experimental setup for each genotype. Statistical analysis undertaken through nested one-way ANOVA, utilising averages from each of the three replicates for comparison. Descriptive statistics for each genotype and replicate, along with P-values can be found in the supplementary.

5.6.3 *vps-35[D638N]* heterozygotes with homozygous *lrk-1[D1847A]* kinase ablation show a significantly improved basal slowing response in day 5 of adulthood

In day 5 of adulthood, *vps-35[D638N]* heterozygotes show a significantly impaired basal slowing response, consistent with prior findings, while the *lrk-1[D1847A]* kinase ablated mutant do not show any significant difference (figure 86). Furthermore, the novel *vps-35[D638N]:lrk-1[D1847A]* double mutant shares this phenotype, showing no significant difference in basal slowing compared to the wildtype, further suggesting that LRK-1 kinase ablation improves *vps-35[D638N]* neuropathology's. This genetic model is in contrast to 5.4, which demonstrates that LRRK2 inhibitor treatment does not alleviate this phenotype at day 5 of adulthood. Furthermore, the *vps-35[D638N]:lrk-1[D1847A]* double mutant shows a significantly (*) improved basal slowing response compared to the *vps-35[D638N]* heterozygote. Congruent with the data obtained from day 1 of adulthood, this is to a lesser extent of significance than between the *vps-35[D638N]* heterozygote and the *lrk-1[D1847A]* homozygote (***), further suggesting that there may be wider implications of *vps-35* mutation than just LRK-1 kinase hyperactivation alone.

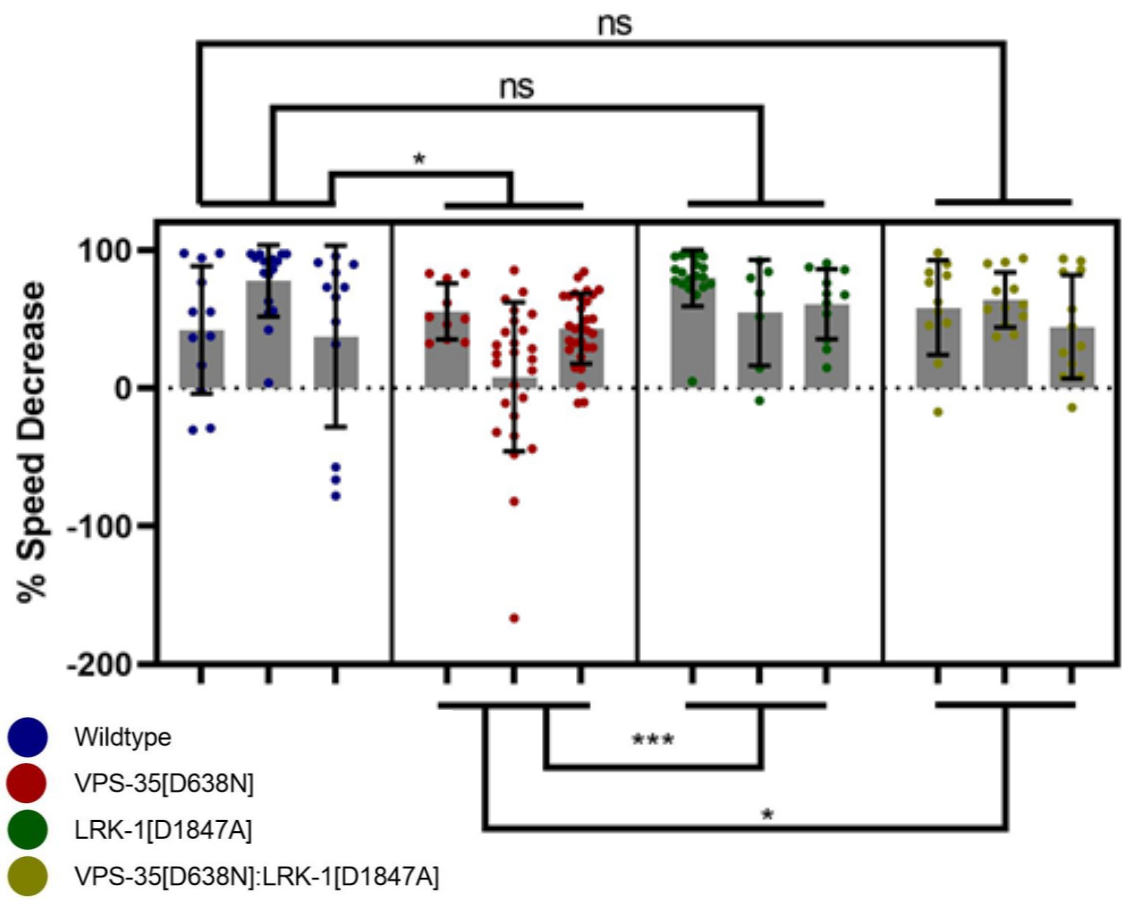

Figure 86-vps-35[D638N] heterozygotes with homozygous lrk-1[D1847A] kinase ablation show a significantly improved basal slowing response in day 5 of adulthood

Three replicates undertaken in tandem in same experimental setup for each genotype. Statistical analysis undertaken through nested one-way ANOVA, utilising averages from each of the three replicates for comparison. Descriptive statistics for each genotype and replicate, along with P-values in supplementary.

5.6.4 *vps-35[D638N]* heterozygotes with homozygous *lrk-1[D1847A]* kinase ablation do not show significantly different crawling speeds from wildtype in day 5 of adulthood

In day 5 of adulthood, the *vps-35[D638N]* heterozygote shows enhanced crawling speeds on unseeded NGM compared to the wildtype, *lrk-1[D1847A]* and *vps-35[D638N]:lrk-1[D1847A]* (Figure 87). The *lrk-1[D1847A]* and *vps-35[D638N]:lrk-1[D1847A]* do not show significantly altered crawling speeds from wildtype. Importantly, this is reflected in the crawling speed upon reaching the bacterial lawn, the hallmark of basal slowing. The *vps-35[D638N]* shows a highly significantly different crawling speed in this state (****), however the basal slowing has a lower significance in 5.6.5 (*), as the slowing is a ration between the genotypes crawling speed on unseeded NGM against the bacterial lawn speed. However, this further illustrates those alterations in crawling speed in the *vps-35[D638N]* heterozygote are restored to wildtype matched phenotypes following the addition of *lrk-1[D1847A]* in the *vps-35[D638N]:lrk-1[D1847A]* double mutant.

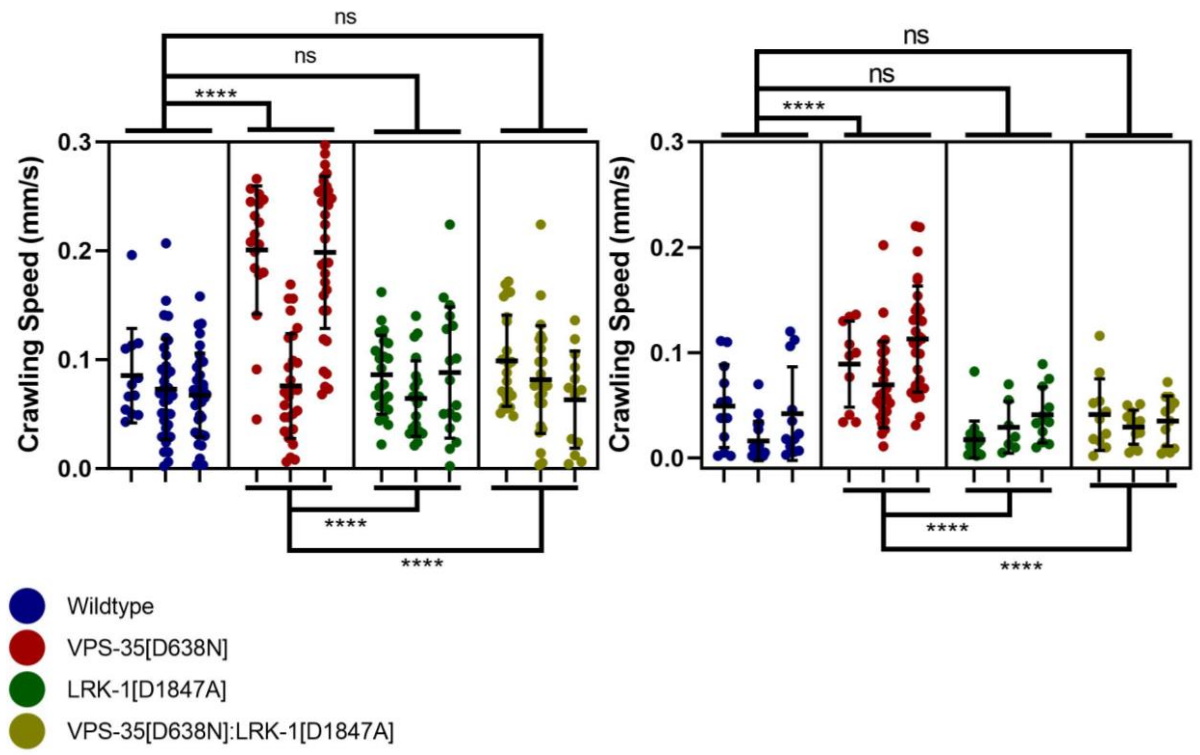

Figure 87- vps-35[D638N] heterozygotes with homozygous lrk-1[D1847A] kinase ablation do not show significantly different crawling speeds in day 5 of adulthood

Three replicates undertaken in tandem in same experimental setup for each genotype. Statistical analysis undertaken through nested one-way ANOVA, utilising averages from each of the three replicates for comparison. Descriptive statistics for each genotype and replicate, along with P-values in supplementary.

5.7 Dopaminergic Neuronal Morphology of *vps-35[D638N]* Heterozygotes with homozygous *lrk-1[D1847A]* mutation

Alongside assay of the basal slowing response, the dopaminergic neuronal morphology of the four selected mutants, in three genotype population replicates, were scored as undertaken in 5.3. this enables the contrasting of the genetic model against the pharmacological model and further probe the hypothesis that VPS-35[D638N] mutation acts through LRK-1 kinase hyperactivation. The *vps-35[D638N]* heterozygote has consistently shown impairments in dopaminergic neuronal morphology, and is therefore readily applicable to testing the LRK-1 interplay. This will be enabled through characterisation of the dopaminergic GFP expressing *vps-35[D638N];lrk-1[D1847A]* double mutant and *lrk-1[D1847A]* control alongside. Summary data utilising mean morphology scores of each genotype will be discussed throughout 5.7, with replicates incorporated into the supplementary.

5.7.1 The *vps-35[D638N]:lrk-1[D1847A]* double mutants show improved CEP and ADE neuropathology's in day 1 of adulthood

In day 1 of adulthood, the *vps-35[D638N]* heterozygote shows outgrowths and branching in the CEP neurons, affecting a mean of approximately 25% between the three replicates (Figure 88), consistent with prior studies. Furthermore, major impairments such as blebbing and neurodegeneration are illustrated in 20% of ADE neurons of the *vps-35[D638N]* heterozygotes. The *lrk-1[D1847A]* mutant shows improved CEP minor impairments and ADE major impairments compared to the wildtype, suggesting potential neuroprotection. The novel *vps-35[D638N]:lrk-1[D1847A]* double mutant shows a similar neuropathology profile to the *lrk-1[D1847A]* mutant, with substantial improvements compared to the *vps-35[D638N]*, suggesting LRK-1 kinase hyperactivation is implicated in *vps-35[D638N]* neuropathology.

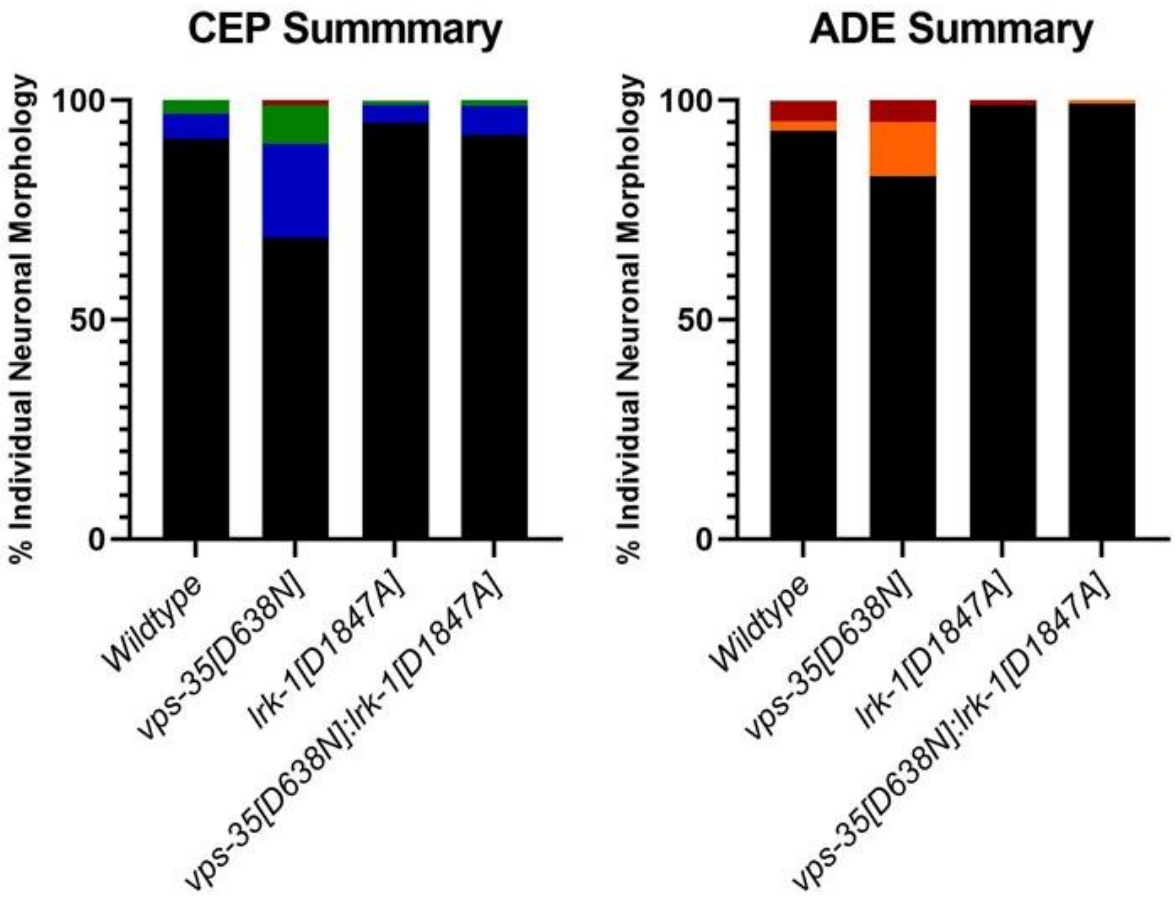

Figure 88- vps-35[D638N]:lrk-1[D1847A] double mutants show improved CEP and ADE neuropathology's in day 1 of adulthood

Characterization of three replicate populations undertaken in the same experiment for each genotype, Between 15-22 *C. elegans* scored per population. Data displayed is the mean proportion shown per genotype, across the three replicates. Score of individual neurons within a population, rather than proportion of worms exhibiting this phenotype. Later data describes individual pathologies. Data of replicate populations included into the supplementary

5.7.2 The *vps-35[D638N]:lrk-1[D1847A]* double mutant shows a reduced minor, major and total impairment number per *C. elegans* than *vps-35[D638N]* heterozygotes in day 1 of adulthood

The number of minor, major and total impairments per *C. elegans* were scored for the four genotypes, with a mean generated for each impairment type and genotype, shown in figure 89. in the *vps-35[D638N]* heterozygote, over 75% of individual *C. elegans* show one or more minor impairments, with 35-40% showing one or more major impairments, consistent with prior studies. The *lrk-1[D1847A]* kinase ablated mutant shows a reduced number of *C. elegans* showing 2 or more minor impairments compared to the wildtype and <5% showing 1 or more major impairment compared to 10% in the wildtype, suggesting that this mutation may have a moderately neuroprotective effect. Furthermore, the *vps-35[D638N]:lrk-1[D1847A]* shows a similar profile to the *lrk-1[D1847A]* and the wildtype, further suggesting VPS-35[D638N] may require LRK-1 kinase activity.

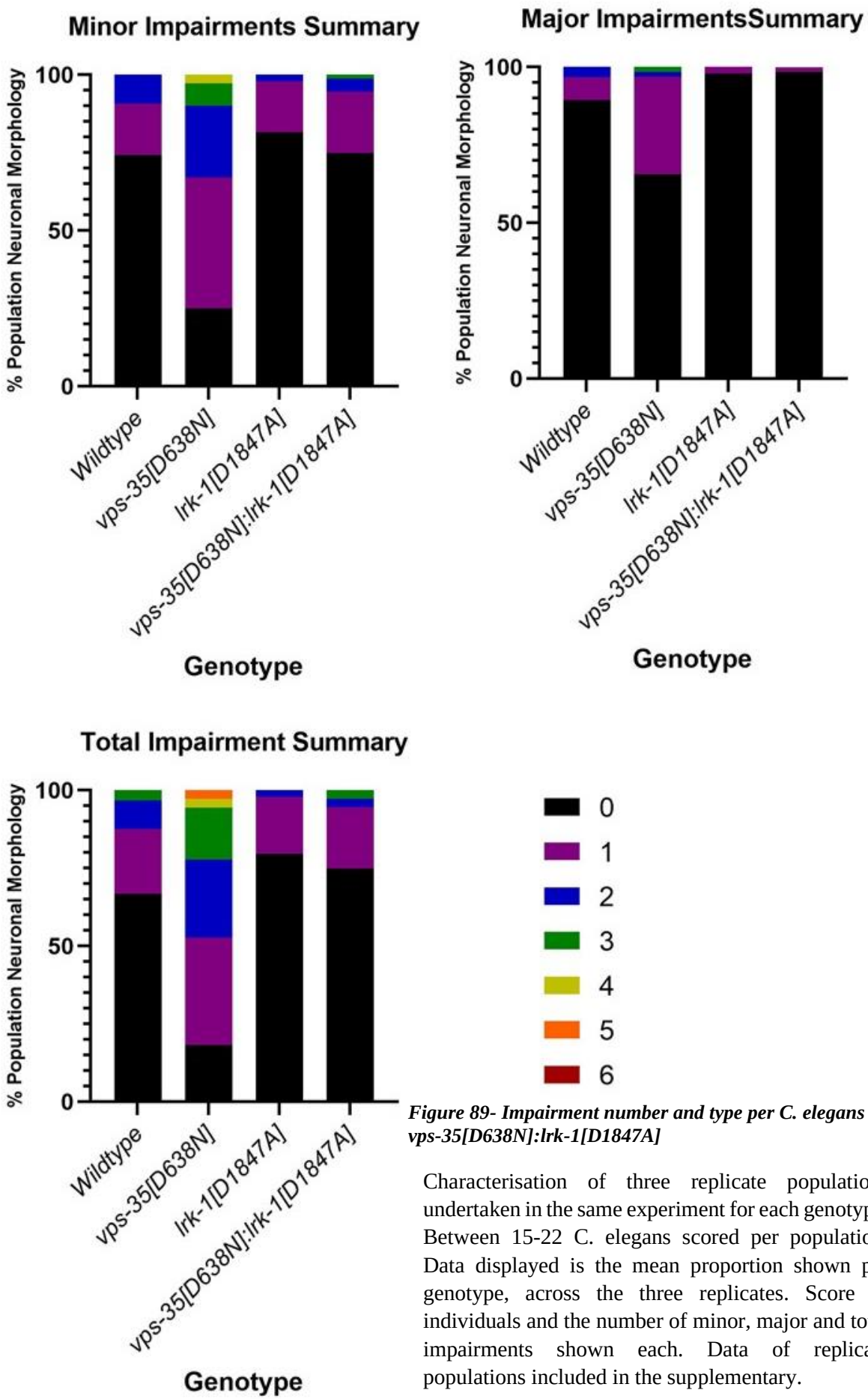

Figure 89- Impairment number and type per C. elegans of vps-35[D638N];lrk-1[D1847A]

Characterisation of three replicate populations undertaken in the same experiment for each genotype. Between 15-22 C. elegans scored per population. Data displayed is the mean proportion shown per genotype, across the three replicates. Score of individuals and the number of minor, major and total impairments shown each. Data of replicate populations included in the supplementary.

5.7.3 The *vps-35[D638N]:lrk-1[D1847A]* double mutant shows a similar individual neuropathology profile to the wildtype and *lrk-1[D1847A]* in day 1 of adulthood

The mean neuropathology profile of the three replicates for each genotype has been generated, in order to break down which impairments are most prevalent in each genotype. In the wildtype, 25% of the population show one or more minor impairment in the CEP neurons, with 10% showing one or more major impairment in the CEP neurons (figure 90). As with prior studies, this profile is exacerbated in the *vps-35[D638N]* heterozygote, with 75% showing one or more minor impairments in the CEP neurons and 35% showing major impairments in the ADE neurons. This profile is reduced in the *lrk-1[D1847A]* kinase ablated mutant, which illustrates one or more minor impairments in 20% of the CEP neurons and major impairments in the ADE neurons in <5% of individuals. This is similar to the *vps-35[D638N]:lrk-1[D1847A]* double mutant, which shows minor impairments in the CEP neurons in 25% of the population and major impairments in the ADE neurons in <5% of the population. This further highlights the rescue in the *vps-35[D638N]* phenotype through genetic kinase ablation, however the lack of full rescue of the minor CEP impairments to *lrk-1[D1847A]* levels suggests that alternative mechanisms may be at play and that this ablation is most protective to the ADE neurons.

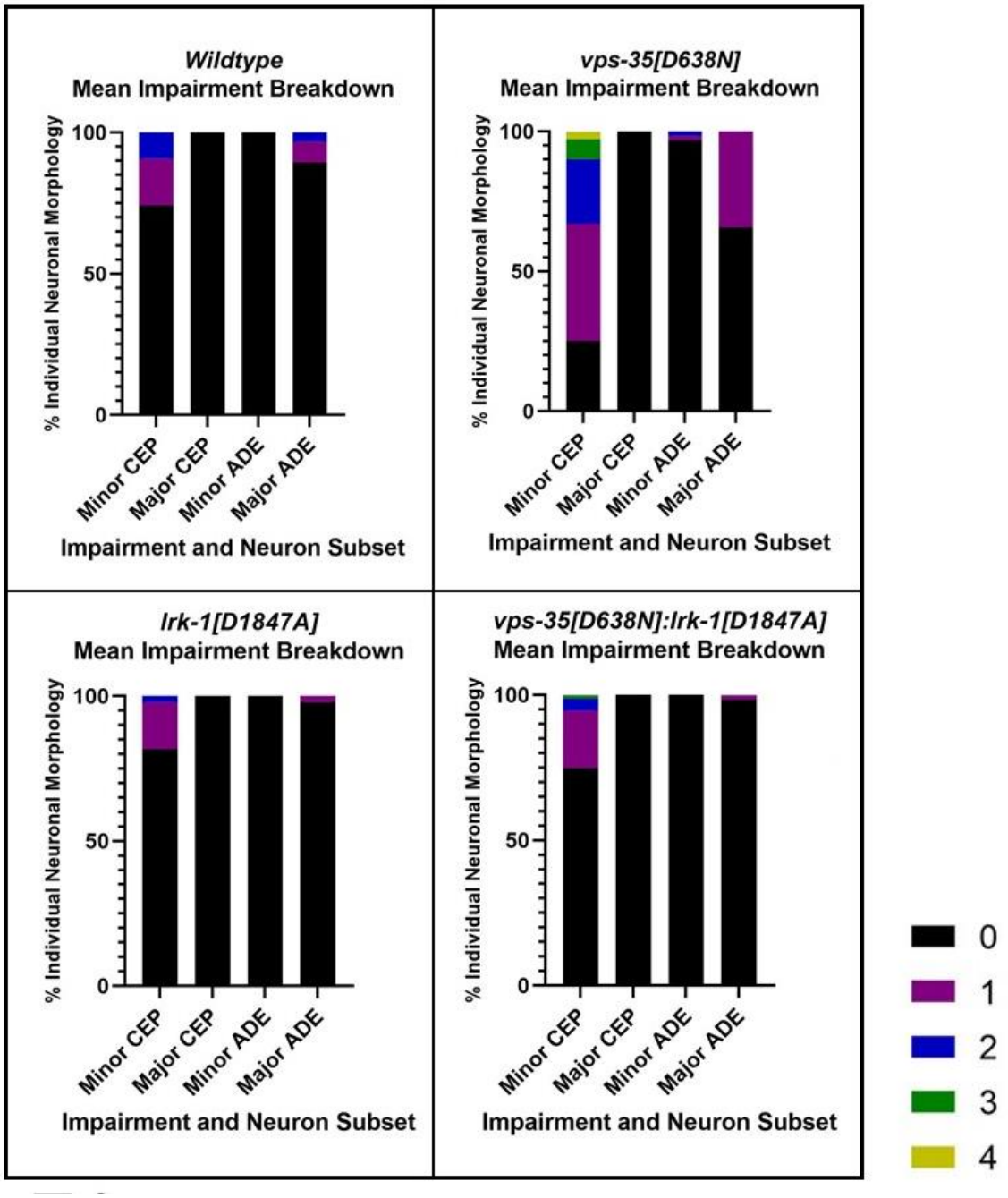

Figure 90- Impairment Breakdown of vps-35[D638N]:lrk-1[D1847A] double mutants

Characterisation of three replicate populations undertaken in the same experiment for each genotype. Between 15-22 C. elegans scored per population. Data displayed is the mean proportion shown per genotype, across the three replicates. Score of individuals and the type of neuronal impairments shown and in which subset. Data of replicate populations included in the supplementary.

Summary of Chapter V: Modelling the VPS35/LRRK2 interplay in novel *C. elegans* models

The development of pharmacological and genetic models to test the hypothesis that VPS35[D620N] acts through LRRK2 hyperactivation have both suggested that this hypothesis could be correct and that in *C. elegans*, LRK-1 kinase activity may be implicated in *vps-35[D638N]* mutation. Treatment with a LRRK2 inhibitor led to the rescue of dopaminergic behavioural impairments in *vps-35[D638N]* heterozygotes and improved dopaminergic neuronal morphology. This effect was also demonstrated in the genetic model, the *vps-35[D638N]:lrk-1[D1847A]* double mutant exhibited improvements in dopaminergic behaviour and dopaminergic neuronal morphology compared to the *vps-35[D638N]*. This convergence in phenotypes through the two different approaches augments that LRRK2 hyperactivation is likely to be a key pathogenesis implicated in VPS35[D620N] and that this pathway could be conserved in *C. elegans*.

However currently, there is no biochemical readout for LRK-1 phosphorylation activity, thus it cannot be fully ascertained if there is indeed increased LRK-1 kinase activity upon vps-35[D638N] mutation, or if this is impacted by pharmacological intervention, or genetic kinase ablation. Further development for this is needed and currently, mammalian cell or mouse models with robust biochemical redouts (111,139) may be the preferred model for further dissecting the VPS35/LRRK2 interplay. Despite this, the proposed presence of this pathway conservation further suggested from the behavioural and cellular data discussed here, supports the relevance, future application and promise for further development of *C. elegans* as a model, for the functional modelling of PD relevant genes.

Chapter VI: Discussion

6.1 *vps-35[D638N]* may be a relevant, novel model for VPS35[D620N] function

Over the last 25 years, great advances have been made in understanding the molecular pathogenesis of PD through the study of Mendelian genes through functional modelling. A decade ago, VPS35[D620N] was identified to be causative of an autosomal-dominant, late onset PD with complete penetrance in mutation carriers (103,104) and a high similarity in symptomatic presentation to idiopathic PD (22,106). Since then, multiple *in vivo* and *in vitro* functional models have been developed, linking VPS35[D620N] to impaired lysosomal function (142,148,350,364), mitochondrial dynamics (136,160,365), endosomal sorting (136,315,350,366–368) and pertinently, interaction with the most common Mendelian PD gene *LRRK2* (111,139–141). Each functional model is compromised by their own limitations, in terms of conservation with humans, ease, cost and rapidity of study, along with the exhibition of PD relevant phenotypes. As such, multiple models need to be compared for thorough understanding of disease pathways.

Prior to this research project, the *C. elegans* orthologue for human *VPS35*, *vps-35* had been relatively understudied and only through gene deletion and RNAi knockdown studies, providing vital information in overall gene function (121,124). However the human genetics of VPS35[D620N] do not suggest that its mechanism of action is a complete loss of function, carriers of VPS35[D620N] are heterozygous (103,104) and the mutation is dominant, suggesting dominant negative toxicity, or a toxic gain of function, with the potential for haploinsufficiency. Therefore, gene silencing and deletion studies in *C. elegans* may not be a reflective model for VPS35[D620N], but shed broader insights into VPS-35 function and pathology in its reduction. In fact, recent VPS35 neuronal deletion mouse models presented with rapid motor neuron degeneration, most closely related to MND (137), further developing understanding of the retromers pivotal role in neurodegeneration, but lacking a suitable pathogenic phenotype for PD modelling.

The precision of gene functional models in modelling disease pathology in *C. elegans* partially hinges upon the genetic methods undertaken to study the gene of interest (27,28). Humanised expression models, in which the gene of interest is transgenically overexpressed, can model the effect of specific mutations, rather than gene function as a whole (76,244). However, the human protein of interest is likely to differ from the orthologous gene in the model system and unless a deletion background is utilised (230), it is unclear how the orthologous protein could interplay with the humanised protein. The advent of CRISPR/Cas9 technologies have enabled the addition

of precise point mutations in the orthologous gene of interest and can be applied to *in vitro* cell models (102,371), or to *in vivo* mammalian models such as mice (372). However, the development of murine models is costly and relatively low throughput (153,372). *C. elegans* overcome this pitfall, CRISPR/Cas9 modification is simple, economical and due to their rapid and expansive reproduction, coupled with a short lifespan, experiments can be undertaken at a higher throughput and speed (51,82) for functional modelling of PD genes of interest. This has been applied in this study, to further understand VPS35[D620N] mutation consequent PD.

6.1.1 Bioinformatic assessment of conservation between human VPS35 and *C. elegans* VPS-35

The novel *vps-35[D638N]* model described in chapter 3 and 5, has been suggested to be a potentially relevant novel model for dissecting VPS35[D620N] function. Bioinformatic analysis demonstrated that the exact mutation residue is highly conserved in *C. elegans*, with a high sequence identity between human VPS35 and *C. elegans* VPS-35, similar protein structure and orientation of the D620/D638 residue, congruent with previous literature detailing the high conservation of the retromer throughout evolution (110). This is further supported by the consistent interaction of *C. elegans* VPS-35 with the orthologous retromer components SNX-1 and SNX-6. Furthermore, the expression in neuronal tissues further suggests VPS-35 may have a pertinent role in the *C. elegans* neurons and consistent with the high expression of VPS35 in the human brain (373). Likewise, there is high expression of VPS35/VPS-35 in the human and *C. elegans* gonad (373). In *C. elegans*, there is notably high expression in the amphid and phasmid neurons, these are highly ciliated and can be studied through DiI dye uptake as undertaken in this study, to infer endocytic function. Similarly, VPS-35 is expressed in the coelomocyte as anticipated, this organ endocytoses fluid in the body cavity and is utilised as a generic model for endocytic function, further supporting the hypothesis that VPS-35 function is well conserved in *C. elegans.*

6.1.2 *vps-35[D638N]* gene segregation studies suggest more complex mechanism than loss of function in *C. elegans*

The data thus far, utilising the novel *C. elegans vps-35[D638N]* model, supports the hypothesis that VPS35 mutation leads to neurodegeneration through a toxic gain of function or dominant negative mechanism. Lethality through larval arrest with incomplete penetrance is exhibited in homozygous *vps-35[D638N]* (Figure 13, 15 and 16), whereas homozygous deletion of *vps-35* is viable for development in *C. elegans* (Figure 16 and 17), suggesting a total loss of function is not implicated in *vps-35[D638N]* mutation. Mir and colleagues noted that VPS35[D620N] leads to a

six-fold increase in phosphorylation of Rab10 through LRRK2 (111), while LRRK2[G2019S] causes a modest 2 fold increase in kinase activity and phosphorylation of substrates *in vitro* (71) and *in vivo* (196) , while increasing the $LRRK2^{G2019S}$ autophosphorylation activity 4-fold (197). The LRRK2[G2019S] equivalent, *lrk-1[G1876S]* is viable in homozygous form in *C. elegans*, but previous studies in which *lrk-1[G1876S]* and *lrk-1* wildtype was vastly transgenically overexpressed in *C. elegans* with wildtype and *lrk-1* deletion backgrounds, resulted in larval arrest of over 50% of the population (229). This data together suggests a toxicity threshold of LRRK2/LRK-1 kinase activity, in which past a certain high level, development may not be viable. This could be implicated in homozygous *vps-35[D638N]* mutation, if does activates LRK-1. However, conversely and interestingly, progeny of two heterozygous cre/lox mice, encompassing a knock-in of the VPS35[D620N] mutation in the murine VPS35 orthologue show Mendelian gene segregation patterns, with VPS35[D620N] homozygous progeny present alongside heterozygous and wildtype littermates. The homozygous VPS35[D620N] animals show a similar lifespan and fertility to the VPS35[D620N] heterozygote and wildtype littermates (113). This could be due to evolutionary differences in models and a potentially broader role for the retromer in the simplistic *C. elegans* system, leading to larval arrest with incomplete penetrance in mutation.

A potential 50% increase in LRRK2 kinase activity in heterozygous VPS35[D620N] carriers, compared to LRRK2[G2019S] may be an explanation for the complete PD penetrance, compared to LRRK2[G2019S] cohorts in which penetrance of PD onset is incomplete (29), along with a slightly earlier average age of PD onset in VPS35[D620N] carriers (104) (164). Due to its rarity, homozygosity for the VPS35[D620N] mutation has not, to date, been identified in human populations. Whereas the LRRK2[G2019S] is a common mutation in several human populations, such as the north African Berber's and Ashkenazi Jewish populations, where homozygous individuals have been identified (3). Furthermore, the LRRK2[R1441G] mutation is prevalent in the Basque region of Spain, accounting for 50% of cases of familial PD and homozygous individuals have been identified (374), while individuals homozygous for LRRK2[R1441H] have been identified in a family in Japan (198). Individuals homozygous for these LRRK2 mutations show a very similar PD presentation compared to individuals heterozygous for these mutations (198,345,374), suggesting there is not an additive gene dosage effect in kinase overactive LRRK2 mutation. Further experiments investigating the gene dosage LRK-1 mutants could be devised in *C. elegans*, through the crossing of *lrk-1* knock in PD mutants with the wildtype, to obtain PD mutant heterozygotes. Furthermore, it could be insightful to cross the *vps-35[D638N]* heterozygote with *vps-35* deletion, in order to assess the functionality of *vps-35[D638N]* when no wildtype *vps-35* allele is present.

In line with studies in alternate models, gene segregation data collected here suggests that stability and/or protein folding of VPS35 is not affected by the [D620N] mutation (109), as *vps-35[D638N]* has been shown to not be a temperature sensitive allele. Non-mendelian gene segregation patterns in the progeny of a *vps-35[D638N]* heterozygote raised at 15^{o}C, instead of the standard 20^{o}C are exhibited, in which no homozygous individuals are viable (Figure 14). In *C. elegans*, protein misfolding/ impaired stability alleles can sometimes be rescued by cultivation at a lower temperature (375) and if this was true of *vps-35[D638N],* a higher proportion of homozygous individuals would have developed, however gene segregation patterns remained consistent, with no increase in *vps-35[D638N]* homozygotes (Figure 13 and 14). This supports the idea that the *C. elegans* model is a reflective, novel angle to take and that mutation is likely to induce toxicity through a more complex mechanism than impairing the stability and presence of the protein. To maintain heterozygosity of *vps-35[D638N]* in the *C. elegans* population, a balancer line was successfully incorporated for subsequent characterisation. All individuals with VPS35[D620N] PD are heterozygous (103,104) ; therefore characterisation of a heterozygote model may be more reflective of the mechanisms of action.

Fertility assays utilising the balanced and unbalanced *vps-35[D638N]* populations further validated the lethality with incomplete penetrance phenotype of *vps-35[D638N]* homozygosity (Figure 16 and 17). Along with ascertaining the fertility of selected lines, this assay sheds an insight into mutational effects on cell biology and development. In a preliminary screen utilising individuals from an unbalanced *vps-35[D638N]* population, a rare homozygous individual was selected for characterisation by chance. Previous data, shown in Figure 13, had suggested that rare homozygous individuals were infertile, as no eggs were laid or present in the body cavity of the individual selected for genotyping in day 1 of adulthood. Consistent with this, the homozygote studied in the fertility assay (Figure 16) showed no egg development or laying in day 1 of adulthood, but in day 2 of adulthood laid 14 eggs. As part of this assay, the number of adults developed from eggs laid was quantified. None of these eggs hatched, suggesting that lethality occurs through larval arrest, rather than embryonic lethality. Following this discovery, the egglaying period for gene segregation studies was extended (Figure 15), in order to isolate the whole progeny of a *vps-35[D638N]* heterozygote laid throughout the reproductive lifespan. This coherently illustrated a mean of 3.63% of progeny homozygous for *vps-35[D638N]*, when prior studies has suggested only 0.6% of progeny were *vps-35[D638N]* homozygotes (Figure 13). The incomplete penetrance of larval arrest could be due to subtle alterations in genetic background between individuals within a population genotype, however further investigation is needed.

Consistent with the larval arrest reported, unbalanced *vps-35[D638N]* heterozygote *C. elegans* produce significantly fewer progeny that develop to adulthood than the wildtype, producing a

mean of 308 and 121 progeny per individual in their reproductive lifespan respectively (Figure 16). Wildtype *C. elegans* produce >300 progeny (85) and these findings are consistent with this. Interestingly, the mean adult progeny count for the balanced *vps-35[D638N]* is 193 individuals per *C. elegans* and statistically, is not significantly different from the wildtype (Figure 16). This suggests that in the unbalanced line, there could be a substantial proportion of the progeny that undergo larval or embryonic arrest, consistent with *vps-35[D638N]* homozygosity. Balancing eliminates recombination and as such, no *vps-35[D638N]* homozygotes will be produced in the progeny of this line, potentially accounting for the higher progeny count. A challenge of this assay is that egg counting is manual and frequently, *C. elegans* lay eggs in a stacked cluster, particularly when the brood size is larger, so it can be challenging to differentiate individuals. As a result, the egg counts frequently are lower than the developed adults and an underestimate of eggs present. Adults are easier to count, as they are larger, more diffuse and immobilised via cold shock. With inconsistencies in this data, it is difficult to quantify the number of eggs that may undergo larval arrest and not reach adulthood.

Alongside the *vps-35[D638N]* heterozygote lines, the fertility phenotype of *vps-35* deletion *C. elegans* model was studied (Figure 16 and 17), in order to contrast a total loss of *vps-35* function. These individuals showed a significantly low progeny count, with a mean of 2 adults produced per *C. elegans,* further implicating the vital role of VPS-35 in development. This is a divergent phenotype to the *vps-35[D638N]* heterozygote, further suggesting total loss of retromer function is not implicated. *In utero*, the *vps-35* deletion does not show a significantly different egg number to the wildtype or the *vps-35[D638N]* heterozygote (Figure 20) and upon DiC microscopy the eggs are at a later stage of larval development (Figure 19 and 21), suggesting impairments in egg laying, further supported by a penetrant bagging phenotype. This is in contrast to alternative model systems, in which *VPS35* deletion is unviable, in D. melanogaster *Vps35* null flies exhibit larval arrest at the pupal stage (141). *C. elegans* are evolutionarily simpler than the *D. melanogaster* model, which may account for this divergent phenotype. In addition, in murine haploinsufficiency models of VPS35, embryos homozygous for *VPS35* deletion underwent embryonic lethality at day 10 (376), embryonic lethality due to *VPS35* insufficiency has been reported in multiple mouse models (113,377) and most recently, a viable mouse model has been developed with *VPS35* deletion only in the neurons (137). Like the homozygosity of VPS35[D620N] in mouse models, the viability of *C. elegans* with *vps-35* deletion is likely to be due to evolutionary divergences in the system, however as suggested by the fertility assay this mutant line is severely perturbed by this deletion.

6.1.3 *vps-35* deletion *C. elegans* show reduced lifespan and significant health impairments, while *vps-35[D638N]* heterozygotes do not

Following outcrossing and the generation of a balanced, heterozygous *vps-35[D638N]* model, multiple organism phenotypes were characterised. Markers of global organism health include lifespan and crawling motility, the novel *vps-35[D638N]* model showed no significant difference in lifespan compared to the wildtype (Figure 22), or crawling motility in day 1 of adulthood (Figure 23). This suggests that in terms of lifespan, *vps-35[D638N]* heterozygotes may be reflective of VPS35[D620N] consequent PD. Individuals with VPS35[D620N] PD show symptomatic onset in late adulthood and disease progression ranges from 6-31 years (103) a similar rate to idiopathic PD (6), thus individuals do not have a significantly earlier age of death. This is in contrast to the total loss of function *vps-35* deletion model, observed alongside (Figure 22), which shows a significantly reduced lifespan compared to the wildtype, with a median age of death at 5-6 days. Interestingly, this is congruent with recent *VPS35* pan-neuronal deletion mice which showed early lethality (137), suggesting some potential conservation across species. There are no known humans with variants in *VPS35* leading to homozygous deletion and as mentioned previously, it is embryonic lethal in multiple models. Reduced copy number variants of *VPS35* have been linked to rare developmental conditions and intellectual disabilities of unknown aetiology, but these are poorly ascertained (378).

Furthermore, the crawling motility illustrates that impairments induced by the *vps-35[D638N]* mutation may be partial in organism health, as they have a comparable speed to the wildtype in day 1 of adulthood (Figure 23 and supplementary 3.8). In contrast to the *vps-35[D638N]* heterozygote, the *vps-35* deletion model demonstrates a significantly slower crawling speed than the wildtype. This phenotype is consistent with the *vps-35* pan-neuronal deletion mice (137), suggesting potential severe motor neuron impairments. In addition, the *vps-35* deletion model illustrates a severe egg laying defect from day 1 of adulthood (Figure 16 and 17), eggs are not ejected at the correct stage and embryos hatch inside the mother's uterus, leading to a bagging phenotype and maternal lethality (Figure 21). Egg ejection in *C. elegans* is partially controlled by motor neurons (379), further suggesting that this neuronal group could be affected by *VPS35* deletion, consistent with the murine model. This egg laying defect is not reflected in the *vps-35[D638N]*, further suggesting that this mutation acts in a distinct mechanism from total loss of function.

6.1.4 *vps-35[D638N]* heterozygotes present with impaired dopaminergic phenotypes

Prior to and following the generation of a balanced *vps-35[D638N]* mutant, dopaminergic behavioural phenotypes were established and examined. The basal slowing response, in which a

C. elegans slows upon reaching a bacterial food source, is partially modulated by 4 dopaminergic CEP and 2 dopaminergic ADE neurons, found in the *C. elegans* head (86,380,381). Although this phenotype is recognised as a dopaminergic output following the establishment of the *C. elegans* neural connectome, but prior to use as an assay this output was validated through the utilisation of a tyrosine hydroxylase deletion *C. elegans cat-2(n4547)* (337), in which dopamine biosynthesis is ablated. Following exogenous dopamine treatment, the impaired basal slowing response was rescued to a greater extent following 4 hour treatment (Figure 25) than 16 hours overnight (Figure 24). A shorter treatment window is more reflective of dopamine replacement therapeutics in PD (18) and in *C. elegans*, exogenous dopamine may be metabolised in a longer treatment window, leading to a reduced efficacy in basal slowing response rescue. Subsequently, the basal slowing response of the *vps-35[D638N]* model was assayed in day 1 of adulthood. Prior to balancing, the four times outcrossed *vps-35[D638N]* population were assayed, with each individual recorded taken for genotyping following video capture, the results of which are detailed in figure 26. These individuals, whether genotyped as wildtype or *vps-35[D638N]* heterozygote, were from the same age matched population and somewhat orthologous to wildtype matched littermates in mammalian models, rather than contrasting the genotype of interest with an independent N2 wildtype population. Furthermore, as genotyping could only be undertaken following video capture, this was in effect a genotype blind assay. An impaired basal slowing response was exhibited in vps-35[D638N] heterozygote, suggesting dopaminergic impairments, these could be underpinned by defects in neuronal health, or dopamine signalling, to be ascertained. VPS35 and the retromer have been implicated in neurite outgrowth and synaptic transmission (132) (136), but it is as yet unclear which is implicated in this mutation in *C. elegans*.

Further examination of this in the established, balanced *vps-35[D638N]* heterozygote model, illustrated a coherent phenotype with the unbalanced *vps-35[D638N]* heterozygotes of an impaired basal slowing response in day 1 of adulthood (Figure 27). This was exacerbated by day 5 of adulthood, showing a highly significant worsening of dopaminergic function with age, an orthologous, simplistic behavioural phenotype for PD modelling. Although *C. elegans* have a lifespan of between 20-30 days, motility and crawling drastically slows by day 7-10 of adulthood (94) and as a consequence, it is challenging to track and contrast with other genotypes. Day 1 of adulthood is a standard developmental timepoint tested, utilised to understand the phenotypes when development is complete, but there has been minimal effect of ageing. *C. elegans* have all their somatic cells developed by late L4/Young adulthood and there is no subsequent replication for replenishment, so cells gradually senesce (94). As a result of this, the impacts of ageing can be seen by day 5 of adulthood.

In conjunction with 4 hour dopamine hydrochloride treatment, the basal slowing response of day 1 adult *vps-35[D638N]* is significantly rescued, with a significant rescue also established in day 5 of adulthood (Figure 27). However, the significance of the rescue in day 5 of adulthood is to a lesser extent than day 1 of adulthood, suggesting further neuronal impairments and reduced efficacy with age. People with VPS35[D620N] mutation consequent PD are responsive to L-DOPA therapeutics (22), somewhat orthologous to the exogenous dopamine treatment undertaken in the *C. elegans* model. The parallel of improved dopaminergic impairments in *vps-35[D638N]* heterozygote *C. elegans* (Figure 27), with responsiveness to L-DOPA therapeutics in VPS35[D620N] patients (103,104), illustrates the translational relevance of the novel model in future studies. Coherently, L-DOPA therapeutics reduce in efficacy throughout PD progression (106), as also seen in our day 5 adult *C. elegans*. Congruent with other models, VPS35[D620N] knock in mice illustrate a reduced speed and motor deficits, however this is only apparent at 14 months (382), while mouse models raised in an independent laboratory also show this phenotype and illustrate improvements in motor function following L-DOPA treatment (133). This novel *C. elegans* model recapitulates orthologous, but simplistic phenotypes and has the advantage that robust dopaminergic behavioural phenotypes are shown in days, rather than months to years, enabling rapid assay.

In order to contrast *vps-35[D638N]* with a total loss of function allele, the basal slowing response of the *vps-35* deletion has been studied (Figure 28 and 29). Interestingly, this does not show impairments in the basal slowing response in day 1 or 5 of adulthood, unaffected by dopamine treatment (Figure 29). This suggests that dopaminergic neuronal health could be maintained without retromer in *C. elegans* and that the effects of *vps-35* deletion upon health are global. Furthermore, it supports the hypothesis that dysfunction induced through mutation is not be due to a total loss of function. The motility of *vps-35[D638N]* in crawling speed does not significantly alter compared to wildtype, however *vps-35* deletion shows significantly reduced motility (Supplementary, 3.8). It is important to consider that the basal slowing response is a ratio of the crawling speed on plain NGM and on an *E. coli* OP50 bacterial lawn, therefore there is likely to have less sensitivity when assaying *vps-35* deletion models which have significantly slower crawling speeds, so this finding should not be overstated. However, the divergent phenotype further suggests that *vps-35[D638N]* has pertinent roles in dopaminergic neuron dysfunction.

One major limitation of *C. elegans* in the modelling of PD is the lack of an orthologue of the PD hallmark α-synuclein (27). Transgenic humanised models have been established (74), transgenically overexpressing human α-synuclein in wildtype and PD pathogenic form (181, 246), recapitulating major PD pathologies (384–387). These have not been utilised in this study and yet,

impaired dopaminergic phenotypes are shown in the *vps-35[D638N]* heterozygote. It is currently unknown whether α-synuclein pathology is implicated in VPS35[D620N] PD as due to its rarity, no individuals have had a full autopsy study. One individual from a Swiss family, later identified to be a VPS35[D620N] carrier, underwent autopsy however key PD relevant brain areas were missed and α-synuclein pathology was not reported (333). Although mice have strong limitations in modelling human diseases, a VPS35[D620N] knock-in mouse model does not show α-synuclein pathology (113) and crossing with established humanised α-synuclein mouse models does not lead to a significant difference in lifespan reduction between VPS35[D620N] homozygotes, heterozygotes or VPS35 wildtype animals (113). Furthermore, in this study injection of pre-formed α-synuclein fibrils into the striatum of 6 month old mice lead to similar pathology between VPS35 wildtype and VPS35[D620N] mice 30 days post injection (113). This suggests that α-synuclein pathology may not be such a pertinent feature of VPS35 PD and in this model, tau accumulation was shown to be the major pathogenic hallmark (113). However, this is controversial and there are discrepancies between knock-in mouse models between laboratories. A recent homozygous VPS35[D620N] mouse model has demonstrated age dependent motor impairments, dopaminergic neurodegeneration and a greater immunoreactivity for α-synuclein in the substantia nigra pars compacta in 16 month old VPS35[D620N] homozygotes, compared to wildtype controls (382). The neuropathology of VPS35 PD is currently unknown (104), therefore despite its clinical and symptomatic similarity to idiopathic PD, it could be classified as an atypical PD, if the hallmark α-synuclein pathology is not shown in future autopsy studies. To overcome this shortfall of a lack of α-synuclein in the *vps-35[D638N]* heterozygote model, crosses could be established utilising humanised transgenic α-synuclein expressing lines, to further understand if there is an interplay between *vps-35[D638N]* mutation and α-synuclein in *C. elegans*. Furthermore, *C. elegans* have a tau like orthologue *ptl-1,* however its functional conservation may be limited (306,307). Similarly, transgenic humanised tau expression models have been developed (309,312) and could be a valuable tool in further understanding the impact of *vps-35[D638N]* in protein aggregation.

The *vps-35[D638N]* has shown a robust, impaired dopaminergic phenotype, relevant to PD modelling. This phenotype will be very valuable in investigating the pathways to VPS35 PD and further understanding whether impairments are due to dopaminergic dysfunction or degeneration.

6.1.5 *vps-35[D638N]* heterozygotes exhibit dopaminergic neurodegeneration

Following the establishment of impaired dopaminergic behaviour in the *vps-35[D638N]* heterozygote, this mutant line was crossed with a *C. elegans* line expressing a GFP transgene (88) in the dopaminergic neurons (Figure 35 and 36), facilitating *in vivo* microscopy. This is

challenging in *in vivo* models such as mice, in which dopaminergic degeneration is frequently quantified following sacrifice , while utilising *C. elegans* a sample of a population can be taken for microscopy while live and immobilised. Initially, the *vps-35[D638N]* heterozygote was studied in day 1 of adulthood, in which impaired dopaminergic phenotypes are shown (Figure 27). This was studied in conjunction with acute rotenone treatment, an agricultural pesticide epidemiologically linked to PD (343). Rotenone is a mitochondrial complex I inhibitor, utilised in toxin induced models of PD (302), in contrast with the novel genetic approach undertaken here. Toxin-induced models of PD are less widely used in recent years, although substantial research has been undertaken utilising these in prior decades (302). Functional models of Mendelian disease genes are likely to be more precise in modelling PD pathology (102), than global oxidative stress inducers such as rotenone. Oxidative stress and mitochondrial dysfunction are likely to be key pathologies in PD (80), however functional studies in the last decade through studying Mendelian PD genes have illustrated broader cellular perturbations in the lysosomal, autophagic and endosomal transport systems (66,389,390). However, it is known that PD is likely to be oligogenic and a complex interplay between the environment and an individual's genetics (30,2,11,28,29). Although VPS35[D620N] has a high penetrance in PD, the age of onset and disease progression varies between individuals carrying the mutation (3,105), which may be due to subtle alterations in individual's genetic background or environment. Through testing the *vps-35[D638N]* heterozygotes *C. elegans* dopaminergic neuronal morphology in conjunction with known oxidative stress inducers, the interplay of this can be studied. Furthermore, following the establishment of novel CRISPR/Cas9 modified *C. elegans* as a model for Mendelian PD, future research directions in the laboratory will focus on generating oligogenic disease models, utilising orthologues of known risk factors or GWAS loci, in conjunction with environmental stressors.

The method for rotenone treatment in C. elegans varies between laboratories, with conflicting literature regarding treatment concentrations and incubation times (251,341,342). An acute method of treatment was chosen, as the dopaminergic phenotypes were shown in day 1 of adulthood, with treatment for 16 hours overnight prior to microscopy, at concentrations of 5μM, 7.5μM and 10μM. 5μM was selected as the most optimal, with degeneration exhibited in the wildtype dopaminergic GFP expressing line, but no lethality and paralysis, as shown in 7.5 and 10μM. These two high concentrations did not show any greater impairments in morphology (supplementary 3.10), suggesting that there is not a dose-dependent response in acute treatment in rotenone concentrations after an approximately 5μM threshold. Further experiments could investigate the effect of chronic treatment at these concentrations.

C. elegans have eight dopaminergic neurons, four CEP neurons, the long dendrites of which reach the end of the nose from the nerve ring, which is close to the pharynx, projecting backwards from

the nerve ring and CEP are two ADE neurons (Figure 36) (67,88). A further two dopaminergic PDE neurons are found along the dorsal body wall muscle. Functionally, the CEP and ADE neurons are implicated in the basal slowing response (86). CEP neurons are cephalic sensilla, the cilium of which are exposed to the environment through a hole in the cuticle surrounding the mouth, with sheath cells serving glial functions (391). CEP neurons have a mechanosensory role for bacteria sensing (391). Furthermore, the ADE neurons characterised in this study form a synapse with the nerve ring, including the CEP neurons, they are classed as anterior deirid sensilla, with ciliated sensory endings embedded in the cuticle (391). Divergent to CEP neurons, ADE neurons possess both sheath and socket cells at the sensillum (391).

Throughout the characterisation of the CEP and ADE neurons in *C. elegans*, the ADE neurons were most sensitive to cellular perturbations, whether induced by rotenone or *vps-35[D638N]* mutation. These neurons frequently exhibited blebbing or neurodegeneration, major impairments, while the CEP neurons most frequently exhibited minor impairments, such as branching and outgrowths (Figure 38 and 40). This suggests that there could be some selective vulnerability in the ADE neurons, compared to the CEP neurons- functioning of both of these is required for basal slowing behaviour (86). This is somewhat surprising, as CEP neurons have the greater dendrite length, a proposed reason for selective vulnerability of dopamine neurons in the human striatum (97) and a greater connection with the environment than ADE neurons (391) and thus more exposed to environmental stressors. However, the presence of socket cells differentiates the glia of ADE neurons from CEP neurons, socket cells are poorly characterised glia in *C. elegans* with unclear function (99), while sheath cells, present in surrounding both CEP and ADE neurons encasing the ciliated projections in contact with the environment. Furthermore, *C. elegans* glia has been implicated in neurite outgrowth and synapse formation (392), processes noted to be impaired in *lrk-1* null *C. elegans* transgenically expressing *lrk-1[I1877T]*, orthologous to the PD mutation LRRK2[I2020T] (230). These two types of glial cells in *C. elegans* are not directly orthologous to specific glia found in humans (393), so it is not possible to draw direct parallels between these and for example, astrocyte function. However, glial activation has been observed in LRRK2 PD models (371), idiopathic PD (394–396) and astrocytes differentiated from VPS35[D620N] iPSC's have shown aberrant mannose-6phosphate receptor localisation (397), a key retromer cargo and congruent with alternative studies of VPS35[D620N] function (109,142,397,398). This suggests that the neuron-glia crosstalk could be implicated in VPS35[D620N] PD pathogenesis, although this is relatively understudied. The presence of socket cells in the ADE neurons could potentially exacerbate impaired neuron-glia crosstalk under stress conditions, whether induced by ageing, *vps-35[D638N]* or environmental oxidative stress induction, however this is yet to be ascertained.

Interestingly, there was no substantial exacerbation in minor or major impairments in dopaminergic morphology in the *vps-35[D638N]* heterozygote treated with rotenone (Figure 37-40), suggesting that the perturbations induced by the *vps-35[D638N]* mutation and rotenone treatment were not additive. This interplay between environment and genetics suggests that the *vps-35[D638N]* mutation is the stronger determinant in the induction of dopaminergic neuronal damage, as impairments in the vehicle *vps-35[D638N]* heterozygote are modestly higher compared to the wildtype *C. elegans* treated with 5μM rotenone (Figure 38-40). It is possible that *vps-35[D638N]* causes defects in the same pathways damaged by rotenone, such as mitochondrial dysfunction, which cannot be further exacerbated by rotenone treatment. In future, more subtle, chronic treatments with compounds linked to PD development, or neuroprotection which are not utilised in toxin models could be tested. Specifically in relation to rotenone, inhibitors of other mitochondrial complexes could be tested, to elucidate if *vps-35[D638N]* could induce toxicity through one specifically, if additive effects are shown. In the literature, cortical neurons expressing VPS35 wildtype and VPS35[D620N] under the control of a lentiviral vector treated with rotenone do not show any significant difference in viability from each other (109), supporting findings from this study that there is no substantial difference in rotenone toxicity between *VPS35* genotypes. The presence of these alterations in dopaminergic neuronal morphology in the *vps-35[D638N]* heterozygote is congruent with the impaired basal slowing response exhibited by this mutant line, furthering its relevance for PD modelling, as both a behavioural and cellular phenotype are exhibited in day 1 od adulthood, a valuable tool for modelling the effect of different genetic interactors upon *vps-35[D638N]* function in future research studies.

Following the examination of rotenone toxicity upon *vps-35[D638N]* heterozygotes, the effect of advanced ageing upon dopaminergic neuronal morphology was examined. Wildtype *C. elegans* begin to substantially exhibit dopaminergic neurodegeneration at approximately day 15 of adulthood (28). Prior investigation within the laboratory team had shown this, thus this timepoint was chosen as optimal to contrast with the *vps-35[D638N]* heterozygote, despite the fact that behavioural assays such as basal slowing are challenging to perform at this timepoint. Lifespan analysis had illustrated that the *vps-35[D638N]* heterozygote does not show a significantly different lifespan compared to the wildtype (Figure 22), so this timepoint was possible. Upon examination, the *vps-35[D638N]* heterozygote illustrated a substantial increase in major impairments in both the CEP and ADE neurons, compared to the wildtype (Figure 41-44). *C. elegans* from this population were examined on day 18, to explore the progression of neurodegeneration and again, the *vps-35[D638N]* heterozygote illustrated increased neurodegeneration compared to the wildtype. When each genotype at day 18 was contrasted to their phenotype at day 15, neurodegeneration had increased in an age dependent manner. This

long-term, progressive neurodegeneration phenotype exacerbated in the *vps-35[D638N]* heterozygote will be a relevant model for testing the effect of chronic treatment with disease modifiers or environmental risks. Furthermore, this is a relevant phenotype for PD modelling, highlighting that VPS35 function is conserved in maintaining neuronal function in *C. elegans* and that endogenous knock-in point mutations through CRISPR/Cas9 in *C. elegans* may be a useful, functional model, as PD relevant consequences are shown.

6.1.6 *vps-35[D638N]* Cellular Phenotypes are conserved with alternative model systems

An advantage of *C. elegans* modelling, as stated previously, is that multiple cellular functions can be inferred through a range of *in vivo* microscopy methods. These cellular aberrations studied could play a role in the dopaminergic dysfunction and degeneration illustrated so far in the *vps-35[D638N]* heterozygote model and be tested to further validate the models relevance.

Interestingly the *vps-35[D638N]* heterozygote illustrates a reduced mitochondrial membrane potential in day 1 of adulthood, inferred through TMRE staining of the whole tissue of live animals (Figure 31). Upon study in day 5 of adulthood, using a sample of animals from the same population, the TMRE fluorescence of the *vps-35[D638N]* heterozygote is not significantly different from the wildtype, while the wildtype exhibits a significant reduction in fluorescence from day 1 to day 5 (Figure 31). This highlights that the *vps-35[D638N]* heterozygote could be showing a prematurely aged phenotype, or exhibit impairments in mitochondrial function. Prior functional modelling of VPS35 has highlighted that it has a role in modulating mitochondrial fission and fusion, a delicate balance of which is needed for the maintenance of mitochondrial health (136,143,368). Furthermore, VPS35[D620N] knock in mouse models illustrate dopaminergic dysfunction, a reduced mitochondria size and mitofusin2 activity (133), a key substrate for mitochondrial fusion (157). Pertinently, this model illustrated that the dopaminergic neurons in the Substantia Nigra pars compacta of mice carrying VPS-35[D620N] showed significantly reduced mitochondrial complex I and IV activity, with a reduced ATP output (133). Rotenone is a mitochondrial complex I inhibitor (80) and as detailed previously, does not exacerbate the impairments in dopaminergic neuronal morphology illustrated in our *vps-35[D638N]* heterozygotes (Figure 38-40). This could be potentially due to already reduced mitochondrial complex I activity seen in VPS35[D620N], if this phenotype is shared in the *C. elegans* model. The reduced activity of mitochondrial complexes suggested in VPS35[D620N] would lead to the reduced fluorescence illustrated in TMRE staining detailed here, as it is electron gradient sensitive (90). To further validate and probe the mitochondrial phenotype illustrated in the novel *vps-35[D638N]* heterozygote, immunoblotting could be undertaken utilising population lysates to probe for mitochondrial complexes. This could be undertaken semi-quantitatively to

infer mitochondrial number and validate whether the reduced fluorescence was due to reduced mitochondria size and function, or quantity. However, the shared phenotype of inferred mitochondrial dysfunction in the novel *vps-35[D638N]* heterozygote *C. elegans* further augments its potential relevance as a novel disease model.

In *C. elegans*, there are multiple readouts to infer autophagic function, including lipid accumulation (Figure 33). In VPS35[D620N] models, reduced autophagy has been illustrated through impaired WASH interaction (399). Lipid storage in *C. elegans* is partially modulated by autophagy, mutants with deletions of key autophagic genes show a reduction in the accumulation of lipids (340). Compared to the wildtype, the *vps-35[D638N]* heterozygote mutant lines, with and without the balancer strain, show a significantly reduced lipid accumulation, inferred through nile red staining. This suggests that this mutation leads to a loss of normal autophagic function and is again in contrast to the *vps-35* deletion model, which shows a significantly enhanced lipid storage compared to the *vps-35[D638N]* heterozygote. The loss of function implicated in *vps-35[D638N]* is most likely to be through a dominant negative, haploinsufficiency or gain of function, as this is not demonstrated in the total loss of function.

Ciliation in *C. elegans* is partially modulated by endocytic genes, which regulate the transport of ciliary membrane proteins (339) and could be used as an output to infer endocytic function, in which the retromer is a master regulator (258). One of these genes is the clathrin adaptor AP-2, which has previously been shown to modulate WNT signaling in *C. elegans* in tandem with VPS35 and the retromer complex (129). Furthermore, RAB-5 and RAB-8 are key endocytic genes in *C. elegans* relevant to ciliary membrane transport (339) and the human paralog of RAB-8, RAB8a is a key downstream effector substrate of LRRK2 (287). Whether this mechanism is conserved between *C. elegans* LRK-1 and RAB-8 is currently undefined. Furthermore, Parkinson's mutations in LRRK2 have been illustrated to disrupt ciliation in *in vitro* murine models (287,325), thus study of ciliation as a marker of endocytic function has been investigated in our novel model. *C. elegans* have highly ciliated neuronal groups in the head, the amphid and phasmid neurons, which have sensory functions, the endocytic function of which can be inferred through the uptake of a fluorescent dye DiI. In day 5 of adulthood, *vps-35[D638N]* heterozygotes show a significantly reduced DiI fluorescence, indicating that they have reduced cilia function, while *vps-35* deletion *C. elegans* do not exhibit this phenotype (Figure 32). This illustrates that total loss of function of VPS-35 does not impact ciliation phenotype and once again, that the *vps-35[D638N]* is likely to be a more complex mechanism than complete loss of function alone. Following ageing to day 12 of adulthood, the *vps-35[D638N]* heterozygote maintains a significantly reduced DiI fluorescence compared to the wildtype, whereas following ageing to day 19, there is no significant difference in DiI fluorescence between the wildtype and *vps-35[D638N]* heterozygote. When the DiI

intensities are contrasted by age for each genotype, the wildtype shows no significant difference in DiI intensity between day 5 and 12, however between day 12 and 19, there is a significant reduction in DiI fluorescence, suggesting that in the wildtype model, cilia uptake and endocytic pathways are reduced in advanced age (Figure 33). In contrast, when the fluorescence intensities of the *vps-35[D638N]* heterozygote are compared, there is no significant difference between day 5, 12 or 19, suggesting that this mutation induces an impaired ciliation phenotype, irrespective of age. Unfortunately, aged data was not available for *vps-35* deletion, as due to their shortened lifespan, there were no surviving animals to be included in the assay, however it is notable that complete loss of VPS-35 function illustrates a divergent phenotype from the *vps-35[D638N]* mutant in day 5 of adulthood (Figure 32). The maintenance of impaired endocytic function further implicates this novel model as functionally relevant for studying VPS35[D620N].

As PD relevant phenotypes have been established in the *vps-35[D638N]* heterozygote at a behavioural, cellular, and molecular level, it can be utilised to test the effect of alternative pathways to PD, most pertinently its proposed interplay with LRRK2. Prior to this, the functional conservation between human LRRK2 and *C. elegans* LRK-1 needs to be established.

6.2 LRK-1 may be a relevant novel model for human LRRK2

Mutations in *LRRK2* represent the most common cause of Mendelian PD (21), leading to increased kinase activity and substrate phosphorylation (59, 101,178,186), resulting in substantial downstream effects including autophagic dysfunction, impaired lysosomal function and defective vesicle trafficking (358,400,401). LRRK2 kinase hyperactivation has also been implicated in some instances of idiopathic PD (168–170), while inhibitors for LRRK2 kinase activity are in early phase clinical trial (Clinical Trial ID:NCT03710707 (178), NCT04056689 (179)), as a prospective, novel druggable target for LRRK2 PD , with potential relevance to idiopathic PD. Appurtenant to this study, VPS35[D620N] PD mutation has a proposed interplay with LRRK2 (66,151,153, 244,261,303, 304), with multiple models proposing that this mutation in VPS35 leads to LRRK2 kinase activation (101,152). This suggested mechanism for VPS35[D620N], has been examined in this study through novel *C. elegans* modelling. Prior to this, the functional conservation between *C. elegans* LRK-1 and human LRRK2 has been established, as LRK-1 is also the orthologue for human LRRK1 (226,227), mutations of which are not associated with PD (236–238).

Prior studies of LRRK2 in *C. elegans* have been achieved through the transgenic overexpression of LRRK2 or deletion models in which *lrk-1* has been removed from the genetic background (76,79,229,230,239). Deletion models have gleaned insight into the mechanism of LRK-1 activity and function, however these are not so relevant to study in the context of PD, as PD linked LRRK2 mutations act through a toxic gain of function mechanism (134). Transgenic overexpression models have illustrated that overexpression of PD mutant LRRK2 have led to dopaminergic dysfunction (76,244). The development of CRISPR/Cas9 technologies has enabled the addition of point mutations in *C elegans lrk-1*, the first study of which has been undertaken in this project. An array of PD mutants and catalytic ablations have been generated, for characterization in *C. elegans* LRK-1, in order to assess the functional conservation extent in comparison to alternative models. A subset of point mutations have been provisionally characterised. These have shown proposed kinase activity dependent phenotypes, suggesting that *C .elegans lrk-1* could be conserved with human LRRK2 in terms of functionality and catalytic biochemistry.

In terms of this research project, this suggests that study of *C. elegans lrk-1* in conjunction with *vps-35* could be a good model to study the VPS35/LRRK2 interplay. More broadly, the novel *lrk-1* models could be utilised in modifier screens for neuroprotective agents or environmental risk factors. *LRRK2* mutations present the most common cause of familial PD, with each showing different pathogenicity and PD risk (402). Between individuals with a specific *LRRK2* mutation, the age of PD onset/diagnosis and disease progression varies (3), this is likely to be due to environmental or oligogenic risk factors (403). New models to test this could be achieved in *C.*

elegans, with *lrk-1* mutants incorporating multiple risk genes to generate rapid oligogenic models, and different culturing conditions to test environmental factors. The groundwork for this idea has been started here, in validating potential conservation between human LRRK2 and *C. elegans* LRK-1. As suggested by this data, LRK-1 could pose as a relevant, powerful and reductionist model for LRRK2 function.

One challenge of *C. elegans* modelling is that frequently antibodies are not available for the orthologous proteins of interest and due to evolutionary differences, the epitopes developed in human or mammalian antibodies are not conserved in the *C. elegans* protein. To overcome this a new IgG sera against LRK-1 has been developed, but the most effective method for detection of LRK-1 has been through the addition of a FLAG tagging to *lrk-1* through CRISPR/Cas9 technologies. This has enabled the study of LRK-1 protein expression through the *C. elegans* adulthood up to day 10, along with confirming the presence of LRK-1 at the selected time points in which phenotypic characterization has taken place for *vps-35* and *lrk-1* mutants. Importantly in the instance of LRRK2 models, in *C. elegans* there are no established molecular readouts for LRK-1 kinase activity, which would be useful in validating the model further. Additionally, this would generate a biochemical readout, to contrast with the organismal, behavioural, molecular and cellular outputs observed and enable the probing of mutation upon biochemical activity.

6.2.1 Proposed kinase activity dependant phenotypes are exhibited in *lrk-1* CRISPR/Cas9 Point Mutants

In silico analysis further highlighted the conservation between *C. elegans* LRK-1 and human LRRK2, most pertinently the direct conservation of the seven PD pathogenic residues (Table 24). CRISPR/Cas9 point mutants of these have been generated for characterisation, with two, the *lrk-1[G1876S]* and *lrk-1[R1087C]* stratified for characterisation alongside catalytic mutants *lrk-1[K988A]* and *lrk-1[D1847A]*, as discussed in 4.2. This has enabled the dissecting of proposed 'kinase dependant' phenotypes.

The LRK-1 PD mutant G2019S equivalent, *lrk-1[G1876S]*, exhibits a drastically impaired dopaminergic basal slowing phenotype, significantly worsened with age (Figure 50). LRRK2[G2019S] causes a modest 2 fold increase in kinase activity and phosphorylation of substrates *in vitro* (71) and *in vivo* (196) , while increasing the LRRK2[G2019S] autophosphorylation activity 4-fold (197). Congruent with this, preliminary study of the *lrk-1[R1087C]*, orthologous to the LRRK2[R1441C], showed an impaired basal slowing response in day 5 of adulthood, but not day 1 (Figure 51). In people carrying LRRK2[R1441C] mutations, the age of PD onset and penetrance in comparison to LRRK2[G2019S] carriers is conflicting, with studies suggesting a similar age of onset (346) and other suggesting a later penetrance in

LRRK2[R1441C] carriers (3), which may be reflected in this model. Furthermore, the LRRK2[R1441C] mutation enhances both substrate phosphorylation and autophosphorylation activity by approximately 3-4 fold (111,188,196) Dopaminergic neuron impairments correlated with proposed kinase activity, as the kinase ablated orthologous LRK-1 mutation *lrk-1[D1847A]* and the GTP binding defective *lrk-1[K988A]* do not exhibit this phenotype (Figure 50). Furthermore, these two genotypes do not exhibit a significantly impaired basal slowing response in day 5 compared to their response in day 1, suggesting neuroprotection, as in wildtype *C. elegans* a significant reduction in basal slowing is shown between day 1 and 5 (Figure 50). Deletion of LRK-1 has a similar effect to deletion of *vps-35*, in which the basal slowing response is not impaired in day 5 adulthood, suggesting that *lrk-1* is not integral for neuronal health, but has significantly reduced crawling speed (Figure 46) indicative of impaired global health. This augments the idea that neuronal toxicity is dependent upon the increased kinase activity of LRK-1, as is the case in LRRK2 PD mutation, rather than the presence of the protein alone.

The basal slowing data of the novel endogenous point mutants suggests CRISPR/Cas9 induced mutation is a more efficacious approach than transgenic overexpression of LRRK2. Transgenic LRRK2 expression levels differ between the wildtype and G2019S mutants studied and expression is not on an *lrk-1* null background (244), so it is unknown whether there are background effects, dimerization or compensatory action between LRK-1 and LRRK2. In terms of basal slowing, there are no significant differences between the wildtype and day 5 aged human LRRK2, or human LRRK2(G2019S) transgenic lines (Figure 50), despite there being 2500 and 8000 relative expression respectively (244). Through biochemically dissecting LRK-1 via the characterisation of selected CRISPR/Cas9 catalytic mutants, the functional relevance to LRRK2 can be assessed, compared with available results from alternative *in vitro* and *in vivo* systems.

LRK-1 has a role in several cellular processes, including the oxidative stress response, maintenance of mitochondrial health and autophagy. Deletion of LRK-1 leads to significantly increased vulnerability to oxidative stress (Figure 49) (229), suggesting a pertinent global role, while genetic kinase ablation of *lrk-1[D1847A]* leads to increased survival. Oxidative stress was induced through rotenone treatment, a mitochondrial complex I inhibitor (302) and coherently, the *lrk-1[D1847A]* illustrate phenotypes correlating with improved mitochondrial health (Figure 52). The *lrk-1[D1847A]* illustrate a two-fold increase in mitochondrial membrane potential inferred through TMRE fluorescence, compared to the wildtype (Figure 52) and exhibit a significantly enhanced crawling speed (Figure 46), suggestive of high cellular metabolism and ATP biosynthesis. Conversely, mitochondrial membrane potential, indicative of mitochondrial function is reduced in *lrk-1[G1876S]* (Figure 52) to a similar extent to *vps-35[D638N]* (Figure 31). A similar reduction is shown in *lrk-1[K988A]*, suggesting that the GTPase domain could have a role

in mitochondrial health (Figure 52). Both *lrk-1[G1876S]* and *lrk-1[K988A]* mutants showed impairments in free swimming (Figure 48), a high bioenergetic demand motion for *C. elegans*, an explanation for which is supported by this mitochondrial observation. As divergent phenotypes are shown depending upon proposed kinase activity, this further suggests functional conservation between human LRRK2 and *C. elegans* LRK-1. Like the basal slowing response, deletion of *lrk-1* does not lead to any alterations in mitochondrial membrane potential and neither does transgenic human LRRK2 overexpression (Figure 52). This further supports the idea that study of endogenous, knock in point mutants gives clearer detail into the molecular mechanisms of LRK-1 and that it could be utilised to further understand human LRRK2.

Impaired autophagic function has been illustrated to be integral in LRRK2 PD in multiple models (246,264), so it was investigated in the novel *lrk-1* point mutants through lipid staining, as lipid accumulation is partially mediated by autophagy genes in *C. elegans* (340). Convergent with the *vps-35[D638N]* heterozygote, the *lrk-1[G1876S]* showed reduced lipid accumulation in day 1 of adulthood (Figure 34 and Figure 55). This suggests that impairments in autophagy illustrated in LRRK2[G2019S] models (102,401) are conserved in endogenous knock-in mutations in *C. elegans* LRK-1. In this assay, the kinase ablated *lrk-1[D1847A]* and the *lrk-1* deletion model showed a similar lipid accumulation profile to the wildtype (Figure 55). Importantly, the reduced lipid accumulation phenotype was rescued through administration of the LRRK2 inhibitor Genentech0877. This suggests that this inhibitor could illustrate some specificity for LRK-1, suggesting that there could be some structural similarity in the kinase domain to LRRK2. This is already suggested through protein sequence alignments and high functional conservation of PD relevant and catalytic residues of LRRK2 in LRK-1.

Harmonious with this, the *lrk-1[G1876S]* illustrates a rescued basal slowing response in day 1 of adulthood, when treated with Genentech0877 on solid media, suggesting that inhibition of LRK-1 kinase activity improves dopaminergic impairments (Figure 54). Following liquid media treatment, the *lrk-1[G1876S]* exhibits an improved basal slowing response compared to the vehicle treated of this genotype, however the vehicle is not significantly different to the wildtype, loosing the strong basal slowing phenotype exhibited in liquid media (Figure 53). Swimming in *C. elegans* is an exercise state and in late 2019, after the liquid media studies were undertaken, studies illustrated that exercise improves neuronal and neuromuscular health in *C. elegans* (330). Follow up experiments on solid media further validated this, that impairments in basal slowing are still shown when not raised under exercise conditions (Figure 54). The validation of a LRRK2 inhibitor showing functional behavioural consequences in proposed kinase overactive LRK-1 PD mutant *C. elegans*, enabled the development of a pharmacological model to test the working hypothesis that VPS-35[D638N] acts through LRK-1 kinase hyperactivation in *C. elegans*. In future studies,

the effect of Genentech0877 upon LRK-1 kinase activity could be further verified through investigation of LRK-1 mediated phosphorylation, after the establishment of a phosphorylation readout.

6.2.2 Development of novel detection methods for LRK-1

Currently, there are no commercially available antibodies for the detection of *C. elegans* LRK-1. A plethora are available for the detection of human LRRK1 and LRRK2, however upon testing of these against *C. elegans* lysates, these illustrated no specificity for C. elegans LRK-1 (Table 28). Despite the potential functional conservation in catalytic activity suggested in the phenotypic assays (Figure 46-55), this suggests that in terms of amino acid sequence LRK-1 is distinct, as reflected in sequence alignments (Table 23). Prior bioinformatic analysis of known antibody epitopes against the orthologous region of LRK-1 further suggests that there are subtle alterations in sequence, leading to a lack of antibody specificity (Table 28). The availability of a viable detection method for *C. elegans* LRK-1 is pivotal for this investigation, in terms of validating the presence and expression of LRK-1 at selected developmental timepoints studied in phenotypic assay. As existing antibodies are not a viable option, this project undertook two potential routes for the development of a novel detection method, the generation of novel IgG sera raised against LRK-1 and the development of novel *C. elegans* lines CRISPR/Cas9 modified to include a FLAG tag at the C-terminus of LRK-1, for detection utilising generic anti FLAG antibodies.

Through the early development of both of these, it quickly became apparent that detecting FLAG-tagged LRK-1 through the use of established FLAG antibodies was the most appropriate method, compared to the use of anti-LRK-1 sera to probe for the protein. The IgG sera showed unspecific detection (Supplementary), while testing lysates of the FLAG tagged LRK-1 populations with generic FLAG antibodies showed specific detection in mixed stage populations (Figure 56). Little is known about the protein expression of LRK-1 during development and adulthood, however this has been identified through this study. LRK-1 is present in day 1 of adulthood and expressed at a similar level in day 5 of adulthood (Figure 58). Pertinently to this research project, these timepoints are most characterised in phenotypic assays, in which divergent phenotypes from the wildtype are shown in not only the *vps-35[D638N]* heterozygotes, but also the selected *lrk-1* point mutants. The confirmation that LRK-1 is present at these developmental stages further supports that these *lrk-1* point mutations could have functional consequences mediated by LRK-1. Furthermore, high expression at day 5 of adulthood further implicates LRK-1 as having a potential role in ageing in *C. elegans*, augmenting its relevance in PD modelling.

Following the success of detection following LRK-1-FLAG tagging, two novel *lrk-1* mutants, the LRK-1[G1876S] kinase overactive PD mutant and LRK-1[D1847A] kinase ablated were FLAG

tagged, these two lines were prioritised as the most characterised, with clear divergent phenotypes shown between the two (Figure 46-55). The LRRK2[G2019S] mutation is the most characterised LRRK2 mutation (246), so further characterisation in LRK-1 could be further validated or contrasted with alternative models, while the LRRK2[D1994A] kinase ablation has the opposite biochemical consequence to the G2019S in terms of kinase activity (77). As with the wildtype LRK-1 FLAG tagged line, these two novel mutants are readily detectable at day 1 and 5, irrespective of FUDR treatment (Figure 58 and 59), further supporting the model and phenotypic observations.

Future development of the anti-LRK-1 IgG sera will involve extensive purification and further validation. However, further experiments are now possible as a detection method has been established for wildtype LRK-1, LRK-1[G1876S] and LRK-1[D1847A]. These lines could be employed for immunocytochemistry and immunohistochemistry, in order to understand the localisation of LRK-1 in the cells or tissues and contrast if differences are shown between these genotypes. Interactome studies, through protein pulldown and immunoprecipitation, followed by mass spectrometry could develop understanding of the LRK-1 interactome and whether this changes depending upon the catalytic activity of the kinase domain in PD mutation. The interactome of LRRK2 is extensive and well characterised (174,232), therefore comparison of the *C. elegans* interactome will enable further elucidation of the conservation extent of the orthologues and whether similar pathways could be conserved in *C. elegans*.

6.2.3 Development of a phosphor-readout for LRK-1 function

Kinase dependant dopaminergic phenotypes, which can be modulated by inhibitors, suggest that LRK-1 has phosphorylation activity, exacerbated by *vps-35[D638N]* and *lrk-1[G1876S]* mutations. However, a robust molecular readout for this is lacking, specifically a phosphor-antibody for LRK-1 autophosphorylation activity, or phosphorylation of potential downstream substrates. The lack of a biochemical readout for LRK-1 phosphorylation activity is a major shortfall of this research study. As with LRK-1 detection as a whole, there are no phosopho-specific antibodies available for LRK-1, or downstream LRK-1 substrates. In addition, LRK-1 is so under characterised in *C. elegans*, it is uncertain which key substrates and pathways are conserved, which could be overcome through future FLAG-LRK-1 pulldown studies. In the meantime, a LRRK2 autophosphorylation antibody has been tested, along with phosphor-specific antibodies for LRRK2's main substrates, RAB8a and RAB10 for specificity for *C. elegans* orthologues RAB-8 and RAB-10.

LRRK2 has multiple autophosphorylation sites (Figure 6) (175,197), the phosphorylation of which has been demonstrated to increase in in PD mutation. One of these, the pSer1292 is directly

conserved in *C. elegans* and there are human/mammalian antibodies specific for this. Bioinformatic analysis suggested the epitope of this antibody was the most conserved with *C. elegans* LRK-1, compared to the alternative LRRK1/LRRK2 antibodies tested for detection, however the similarity remained low. Testing of this antibody in day 1, 5 and 10 of adulthood, when LRK-1-FLAG lysates had proven LRK-1 presence showed no specificity, further suggesting that the epitopes need to be highly conserved with LRK-1 and the amino acid sequence identity differences are too great.

Two of the most important LRRK2 substrates, RAB8a and RAB10 are well conserved in *C. elegans*, RAB-8 and RAB-10 show a high sequence identity with their human counterparts, specifically phosphorylation sites, targeted by the phosphor-antibody epitopes (Figure 62). Notably, the Rab8apT72 antibody showed detection for day 5 adult *C. elegans* lysates (Figure 64), when LRK-1 is most highly expressed (Figure 58 and 61), with a reduced intensity band illustrated in the *lrk-1* deletion mutant, suggesting some potential specificity. This is promising, however this needs further validation before use as a molecular readout for LRK-1 kinase activity. The RAB superfamily in *C. elegans* are closely related, with overlapping sequence identity (349). Therefore, to prove whether this antibody is certainly detecting RAB-8 phosphorylation, rather than a closely related RAB, a *rab-8* deletion line needs to be obtained and day 5 adult lysates tested as a negative control, along with a selection of the most closely related RABs. Furthermore, RAB29 a key substrate and regular of LRRK2 kinase activity (272) and consistent GWAS loci (32), has an orthologue in *C. elegans* GLO-1, which according to the literature may share substantial conservation in this function (282). GLO-1 could be an alternative molecular readout for LRK-1 kinase activity to further explore, while key catalytic sites are well conserved in *C. elegans* (Figure 66). Elucidation of the molecular pathways of LRK-1 will further enable the validation of this model, in understanding how well conserved *C. elegans* LRK-1 is with LRRK2.

The data described in Chapter 4 suggests that there are *lrk-1* phenotypes present, which are distinct based upon whether the mutation has proposed alterations in phosphorylation activity. Behavioural and cellular assays support this conservation; however, a biochemical readout is further needed to validate changes in kinase activity. Following the data that LRK-1 could be conserved with human LRRK2 in functionality and phenotypes, this project sought to dissect the VPS35/LRRK2 interplay in *C. elegans*, through pharmacological and genetic models.

6.3 VPS35[D620N] acts through LRRK2 kinase hyperactivation

Succeeding the establishment of a robust, impaired dopaminergic phenotype in vps-35[D638N] heterozygotes and the phenotypes suggesting that *C. elegans lrk-1* shares some functional conservation with LRRK2, it has been possible to develop pharmacological and genetic models to test the hypothesis that VPS35[D620N] acts through a toxic gain of LRRK2 function. At the start of this research project, one paper suggested that mutation of VPS35[D620N] leads to LRRK2 kinase hyperactivation six-fold in mouse embryonic fibroblasts and neutrophils isolated from people with VPS35[D620N] PD, proposed through an unknown interactor (111). Since then, novel murine and cortical neurons studies have highlighted that VPS35 and LRRK2 directly interact and coherently, that VPS35[D620N] leads to increased LRRK2 kinase hyperactivation and endosomal sorting defects can be partially rescued through LRRK2 inhibition (350). However the impaired interaction of VPS35 with the WASH complex caused by mutation continues to cause impairments in autophagy, irrespective of LRRK2 inhibition (350). This suggests both a toxic gain of function through LRRK2 and a partial loss of VPS35 function concurrently.

To test this hypothesis in *C. elegans* would further add to the resolution in understanding VPS35[D620N] and LRRK2 PD. This could have translational relevance, as LRRK2 inhibitors are in early phase trial for LRRK2 PD (Clinical Trial ID:NCT03710707 (178), NCT04056689 (179)), if this hypothesis is true inhibitors could potentially be of therapeutic benefit for people with VPS35[D620N]. Furthermore, antisense oligonucleotides are in development for the silencing of LRRK2 as a targeted genetic therapy (Clinical trial ID:NCT03976349 (223)). To testing the hypothesis, both pharmacological and genetic models have been utilised, further elucidating this proposed mechanism. This data strongly suggests that in *vps-35[D638N]* mutation, LRK-1 kinase activity is increased leading to dopaminergic impairments and degeneration in *C. elegans*, coherent with mammalian models (111,350). This not only suggests that this pathway may be conserved in *C. elegans*, but that as a result they could be a beneficial, relevant model for further understanding Mendelian PD.

6.3.1 Findings from the pharmacological model of VPS35/LRRK2 interplay

Following the establishment of a dopaminergic phenotype in *vps-35[D638N]* heterozygote, it has been possible to design experiments to pharmacologically modulate this. Previously, it had been established that the human LRRK2 inhibitor Genentech 0877 rescues dopaminergic phenotypes exhibited in the *lrk-1[G1876S]* kinase overactive PD mutant. To test the theory that VPS35[D620N] incurs toxicity through LRRK2 activation (111,350), *vps-35[D638N]* mutants were treated with 2 doses of LRRK2 inhibitor in liquid culture from L1 of development. In the *lrk-1[G1876S]*, treatment with 1mM lead to a significant improvement in basal slowing compared

to the vehicle (figure 53), while 0.2mM resulted in modest, non-significant alterations (supplementary). Upon treatment with 1mM inhibitor, the *vps-35[D638N]* heterozygotes failed to develop, suggesting that the LRRK2 inhibitor has a more complex effect in the presence of this mutation. One possible explanation could be off target effects of Genentech0877 on kinases, which are vital for development and may be already working at a suboptimal level in the *vps-35[D638N]* heterozygote, but not the wildtype or *lrk-1[G1876S]*. Treatment with 0.2mM resulted in normal development and a significant rescue of the impaired basal slowing phenotype in day 1 of adulthood, suggesting that this mutant is responsive to a lower dosage (Figure 68). Notably the *vps-35[D638N]* heterozygote still showed an impaired basal slowing response after being raised in liquid culture, an exercise state shown to be neuroprotective in *C. elegans* (330). Culturing in liquid media lead to non-significant impairments in the basal slowing response in the *lrk-1[G1876S]* PD mutants, which exhibit significant impairments when raised on solid media, suggesting improvements (Figure 55 and 56). The penetrance of VPS35[D620N] PD is higher than LRRK2[G2019S] PD, with an earlier age of onset (3,105). In addition, this experiment was undertaken utilising the *vps-35[D638N]* unbalanced heterozygotes, with individuals taken for genotyping following assay, hence this was performed genotype blind. This data supports the theory of LRRK2 hyperactivation by VPS35[D620N] and the working hypothesis that *vps-35[D638N]* leads to a toxic gain of function via LRK-1.

Subsequently, this experiment was replicated utilising a solid media feeding method, after it had been noted that raising in liquid culture induces a neuroprotective exercise state. Balanced, *vps-35[D638N]* heterozygotes were utilised and tested in day 1 and day 5 of adulthood (Figure 69 and 70), the key timepoints studied in the characterisation experiments and when LRK-1 protein is highest expressed (Figure 58). Animals tested on day 1 were treated for 16 hours overnight, from late L4/young adulthood (Figure 69) and assayed subsequently, an age matched inhibitor naïve population from the same synchronisation were maintained and then treated with LRRK2 inhibitor for 16 hours overnight in day 4 of adulthood, with assay taking place on day 5 (Figure 69). This was to test the developmental timepoints in which LRRK2 inhibition could be most beneficial. In LRRK2 therapeutics, this is challenging as at the time of PD onset, 80% of dopaminergic neurons in the *substantia nigra pars compacta* are already lost (9), therefore for most clinical benefit, individuals carrying PD mutations in LRRK2 would need to be identified (167), or early biomarkers of PD onset detected (216,217), prior to the onset of cardinal motor symptoms. In *vps-35[D638N]*, significant impairments are illustrated in the day 1 adult, but these are significantly exacerbated further by day 5, mirroring the progressive nature of PD (Figure 27). In day 1 of adulthood, treatment with a LRRK2 inhibitor significantly rescues the impairments in the basal slowing response (Figure 69) , coherent with the earlier data. By day 5 of adulthood, there was no

significant rescue in the basal slowing response, suggesting that treatment at this timepoint is too late to have significant impacts upon dopaminergic function in *C elegans*. Future experiments could validate this through chronic treatment, investigating the basal slowing response in day 5 with *C. elegans* treated from day 1 of adulthood. Again, this data suggests that in the instance of *vps-35[D638N]*, LRK-1 kinase hyperactivation may be implicated.

The same treatment regimen was utilised to test the effect of LRK-1 inhibition upon the dopaminergic neuronal morphology, following the establishment of a *vps-35[D638N]* heterozygote expressing GFP in the dopaminergic neurons. In day 1 of adulthood, treatment with a LRRK2 inhibitor substantially improved the proportion of impairments shown in the *vps-35[D638N]* population (Figure 74-76), notably reducing the number of minor impairments such as outgrowths and branching in the CEP neurons and major impairments in the ADE neurons, which continued to show selective vulnerability. This is coherent with the basal slowing data, suggesting that the improvements in behavioural phenotype are due to improvements in the dopaminergic neuronal impairments. Treatment at day 5 also leads to modest improvements in the dopaminergic morphology (Figure 77-80), however this is to a lesser extent than shown in day 1 of adulthood, again congruent with the basal slowing data. Importantly, treatment of the wildtype with LRRK2 inhibitor induces dopaminergic impairments such as outgrowths in the CEP neurons and blebbing in the ADE neurons in day 1 of adulthood. In the first liquid media treated basal slowing assay, the wildtype showed significantly impaired basal slowing compared to the vehicle, suggesting that there are off target effects, or on target functional consequences of LRK-1 inhibition in wildtype *C. elegans* at this developmental timepoint. This phenotype is not so substantially reflected in day 5 adult *C. elegans* treated with LRRK2 inhibitor, suggesting that day 1 of adulthood is a particularly sensitive stage for LRK-1 kinase activity. In terms of translational potential, this suggests that LRRK2 inhibitors may not be beneficial as a preventative treatment for the general population, or individuals with idiopathic PD without LRRK2 hyperactivation, patient groups receiving treatment should be stratified to only LRRK2 mutation carriers, or individuals with idiopathic PD and LRRK2 kinase hyperactivation. This data further implicates LRK-1 kinase activity in the modulation of *vps-35[D638N]* heterozygote neuronal morphology.

Cellular phenotypes established in *vps-35[D638N]* heterozygotes have been investigated in *C. elegans*, in conjunction with LRRK2 inhibitor treatment.

Furthermore, the established impaired ciliation phenotype shown in the *vps-35[D638N]* heterozygote was tested through DiI staining, after LRRK2 inhibitor treatment. Previous literature has linked LRRK2 kinase activity to cilia function (325,326), so this experiment tested whether the impaired phenotype exhibited could be through LRK-1 kinase hyperactivation, or general endosomal impairments induced by the *vps-35[D638N]* mutation. The LRRK2 inhibitor had no

impact upon rescuing this phenotype (Figure 81), suggesting that this is due to endocytic impairments which occur independently. This is coherent with the most recent studies investigating the VPS35/LRRK2 interplay in mice, in which LRRK2 inhibition did not rescue all impairments illustrated in VPS35[D620N] models, suggesting that LRRK2 kinase activity is a key pathogenic process, but there are other cellular perturbations present in VPS35[D620N] mutation (350).

As discussed previously, this study has limitations in that there is no established biochemical readout for LRK-1 phosphorylation activity. The RAB8apT72 antibody shows some promising specificity for *C. elegans* RAB-8, with a lower intensity band in *lrk-1* deletion, however as stated previously this needs further validation. Once this is established and if specificity is confirmed, this should be tested against lysates obtained from populations treated with LRRK2 inhibitor, grown alongside these experiments and currently in -80^{o}C storage. Overall, the pharmacological model of VPS35/LRRK2 function in *C. elegans* suggests that *vps-35[D638N]* mutation leads to increased LRK-1 kinase activity, in line with alternative models.

6.3.2 Findings from the genetic model of VPS35/LRRK2 interplay

After the development of the pharmacological model, a genetic model was established, in which a line heterozygous for *vps-35[D638N]* and homozygous for *lrk-1[D1847A]*, with GFP expression in its dopaminergic neurons was developed. Alongside, a *lrk-1[D1847A]* line expressing dopaminergic GFP was developed, as a control for microscopy experiments. Of these mutants, the basal slowing response was assayed and the dopaminergic neuronal morphology scored, in tandem with the wildtype and *vps-35[D638N]* heterozygote. Strikingly, the development of a *vps-35[D638N]:lrk-1[D1847A]* mutant was very challenging, with multiple unsuccessful attempts. The first generation progeny were frequently heterozygous for both the *vps-35[D638N]* and *lrk-1[D1847A]* as expected, however there were often no progeny from these founder populations heterozygous for *vps-35[D638N]* and homozygous for *lrk-1[D1847A]*, as required for this model of kinase ablation. This suggests a potential genetic interaction between *vps-35* and *lrk-1* and that *lrk-1* kinase activity may be required in this mutation for development, as previously reported in the *vps-35[D638N]* heterozygotes treated with 1mM LRRK2 inhibitor in liquid media, which arrested in growth at L1. However, one population with *vps-35[D638N]* and homozygous *lrk-1[D1847A]* was obtained in late August 2021 for characterisation.

The basal slowing response has proven to be a robust dopaminergic phenotype throughout this study and as such, it was utilised as a key readout in the novel genetic model. In day 1 of adulthood, triplicate populations of *vps-35[D638N]* illustrated a significantly impaired basal slowing response compared to the wildtype, as seen throughout this study, while the *lrk-1[D1847A]*

showed a disparate phenotype of significantly improved basal slowing compared to the wildtype. The *vps-35[D638N]:lrk-1[D1847A]* mutant illustrated no significant impairments in basal slowing, illustrating a similar phenotype to the wildtype, further confirming the hypothesis that LRK-1 kinase hyperactivation is implicated in *vps-35[D638N]* (Figure 84). In day 5 of adulthood, a similar pattern is shown, the *vps-35[D638N]* maintains an impaired basal slowing response, while the *lrk-1[D1847A]* and the *vps-35[D638N];lrk-1[D1847A]* demonstrate a similar basal slowing to the wildtype (Figure 89). Compared to *the vps-35[D638N]*, the *lrk-1[D1847A]* shows a more highly significant improvement than the *vps-35[D638N]:lrk-1[D1847A]*, suggesting that there may be additional impairments induced by the *vps-35[D638N]* mutation, although when taken in conjunction with LRK-1 kinase ablation these are not substantial enough to cause behavioural impairments.

These lines were developed to include dopaminergic GFP in order to undertake *in vivo* microscopy, to contrast with the basal slowing data and the pharmacological model. This demonstrated that in day 1 of adulthood in triplicate independent populations, impairments are maintained in the *vps-35[D638N]* heterozygotes, showing the key pathologies of CEP outgrowths and ADE blebbing (Figure 88-90). The *lrk-1[D1847A]* and *vps-35[D638N]:lrk-1[D1847A]* lines show a similar phenotype to the wildtype in terms of neuronal morphology, further augmenting the working hypothesis and underpinning the basal slowing phenotypes shown. Lysates grown in triplicate in parallel to these lines have been obtained and are in storage for future immunoblot analysis, for autophagic markers such as SQST-1, or for RAB phosphorylation, once a biochemical readout for LRK-1 kinase activity is established.

In terms of translational potential, the genetic model could be most orthologous to LRRK2 silencing through ASO's, although further work would be needed to model this with greater acuity. This approach has genetically ablated the kinase domain of LRK-1, but other catalytic domains are proposed to be active. Crossing with the *vps-35[D638N]* with a *lrk-1* deletion model could develop the understanding of the whole LRK-1 function in conjunction with *vps-35[D638N]* mutation, rather than the kinase domain alone. More pertinently in the case of ASO's, *C. elegans* are readily amenable to RNAi (405), so employing an RNAi against *lrk-1* and feeding at selected timepoints, for example day 1, day 5 or chronically through development could glean information on LRK-1s function and model ASO effects. This could also be utilised to contrast the pharmacological and genetic model undertaken in this study, to further validate and dissect the *vps-35/lrk-1* interplay in *C. elegans*, as suggested in this study.

This genetic model has further contributed to confirming that LRK-1 kinase hyperactivation is implicated in *vps-35[D638N]* mutation, coherent with the pharmacological model developed in this study and mammalian models of the VPS35[D620N]/LRRK2 interplay (111,350). This not

only sheds insight into the pathologies of VPS35 and LRRK2 PD, but most importantly this proposed pathway conservation, establishes novel CRISPR/Cas9 modified *C. elegans* as potential PD gene functional models of the future, an approach which has been first attempted here.

Chapter VII: Future Directions and Final Conclusions

7.1 Future Research Directions

Following the results of this research study, multiple follow up experiments could be undertaken to further develop the novel models established throughout this project. Broadly, these involve developing understanding of the molecular and biochemical readouts of the new model and including PD relevant protein aggregates, to overcome the limitations of the *vps-35[D638N]* and *lrk-1* CRISPR/Cas9 *C. elegans* models.

A major challenge of these novel models is that there is no established output for LRK-1 kinase activity. Testing of RAB8aPT72 illustrated that there could be detection for *C. elegans* RAB-8 and encouragingly, in a day 5 adult *lrk-1* deletion lysate there was reduced band intensity compared to the wildtype sample. This tentatively suggests that RAB-8 could be a phosphorylated substrate of LRK-1, showing conservation with LRRK2, which phosphorylates RAB8a. This antibody could be a promising phosphorylation readout, however prior to use it needs to be thoroughly validated. The members of the *C. elegans* RAB superfamily are closely related, with some RABs as orthologues for multiple human genes, as a result there is often high sequence similarity between proteins. To validate this detection is specific for RAB-8 a *rab-8* deletion mutant needs to be obtained. *C. elegans* RABs with the highest sequence identity to RAB-8, particularly around the RAB8aPT72 antibody epitope need to be pinpointed through sequence alignment analysis and subsequently, deletion lines of the RABs most closely related to RAB-8 would need to be obtained for verification. As there is no biochemical readout for LRK-1 phosphorylation activity, it cannot be fully ascertained from this study whether *vps-35[D638N]*, *lrk-1[G1876S]*, or *lrk-1[D847A]* lead to alterations in kinase activity, despite the behavioural and cellular phenotypes suggesting this could be the case. Further development of this is urgently needed and currently, mammalian or mouse models with established biochemical readouts may be the preferred model for dissecting the VPS35/LRRK2 interplay.

Another challenge of this research, is that the interplay of key PD aggregate proteins α-synuclein and potentially tau, have not been assessed in conjunction with the novel point mutants (181, 246). It is currently unknown whether individuals with VPS35[D620N] present with α-synuclein aggregation (333). Furthermore, α-synuclein is not ubiquitously present in all individuals with LRRK2 mutation consequent PD (29,164), however tauopathy is a consistent feature (115,164,165,198,199). Despite the lack of α-synuclein orthologue or transgenic expression in the

novel *vps-35* and *lrk-1* models, dopaminergic impairments are still shown, however it would be insightful and important to understand the effect of *vps-35* and *lrk-1* mutations upon this. This could be achieved through crossing these novel mutants with previously established transgenic α-synuclein lines. Prior studies utilising deletion models of *vps-35* and *lrk-1* have been very conflicting, as to whether these genes promote α-synuclein propagation and aggregation or not (152,303,304), so testing this with novel point mutants would develop understanding from a new angle and potentially add to the translational relevance of the model.

Following the successful characterisation of the *vps-35[D638N], lrk-1[G1876S], lrk-1[D1847A]* and *lrk-1* deletion as part of this study, these lines are to be collected for RNA extraction in day 1 and 5 of adulthood, for outsourced RNA sequencing. This would enable understanding of the *C. elegans* transcriptome in the presence of these mutations, develop a stronger understanding of the molecular consequences and differential expression between genotypes, rather than observing phenotypic and cellular outputs alone. This would further enable an assessment of functional conservation of these novel models, as the transcriptome in LRRK2 mutation and PD is a large area of study in *in vitro* studies, mammalian models and patient studies.

Furthermore, the interactome of LRK-1 will be studied, utilising protein pull down followed by mass spectrometry, with the *lrk-1* wildtype, *lrk-1[G1876S]* and *lrk-1[D1847A]* FLAG tagged lines in day 1 and 5 of adulthood. This would enable an understanding of the PPI network in *C. elegans* LRK-1, again gleaning functional insight and a greater understanding of the molecular consequences of mutation. Furthermore, the LRK-1-FLAG line could be crossed with the *vps-35[D638N]* model, in order to understand if this mutation has any effect upon the LRK-1 interactome, as chapter 5 has illustrated LRK-1 kinase hyperactivation is likely to be implicated in *vps-35[D638N]* and in mammalian models, VPS35 has been shown to directly interact with LRRK2 (254,350). The interactome of human LRRK2 is extensive (232), so comparative study of the LRK-1 interactome will further enable assessment of conservation extent and pathway maintenance in *C. elegans*.

More broadly, the PD genetics field is moving towards understanding idiopathic PD through the emerging oligogenic nature of the condition and loci identified through GWAS (32), rather than just focusing on Mendelian gene functional models. These have been for the last 25 years and continue to be an insightful model, since the first identification of families with PD in 1997 (92). Functional models of Mendelian genes give greater acuity to PD pathogenesis than previous, toxin based models and importantly, they have enabled the development of targeted novel therapeutics for PD (167), pertinently inhibitors (Clinical Trial ID:NCT03710707 (178), NCT04056689 (179)) and ASO's for LRRK2 (Clinical trial ID:NCT03976349 (223)). LRRK2 has some relevance to idiopathic PD, however oligogenic modelling of newly identified, common risk loci would be of

closer translational relevance to understanding idiopathic PD. A major challenge of this is that currently, many of the GWAS loci identified, as shown in figure 3, are yet to be functionally validated and modelled in the context of PD. New, rapid, genetically tractable and economical models, with the viability to induce multiple mutations are needed (1). Through this study, CRISPR/Cas9 modified *C. elegans* have been established as a novel model that could be used to begin to understand this, opening up the field for further research. Following on from this project and utilising some preliminary data from it, a 3-year Parkinson's UK funded Post-Doctoral Researcher position has been awarded to the Kevei laboratory, in collaboration with Dr Patrick Lewis, to Dr Susanna Cogo, to continue the functional modelling of PD relevant genes in *C. elegans*, generate and characterise oligogenic novel models, in conjunction with potential disease modifiers.

7.2 Final Conclusions

In conclusion, this research project suggests that CRISPR/Cas9 modified *C. elegans* may pose as useful, reductionist functional model for PD genes. Human VPS35 is likely to share functional conservation with *C. elegans* VPS-35, PD orthologous mutation VPS35[D620N], *vps-35[D638N]* in *C. elegans*, leads to impaired dopaminergic behavioural phenotypes and increased dopaminergic neuronal pathologies in more rapid timescales than mammalian models. This robust phenotype and characterisation of this novel model has established it for future research studies. Furthermore, this research project has ascertained that *C. elegans* LRK-1 is likely to share functional conservation with human LRRK2 and be a relevant orthologue for future research, as proposed kinase activity dependent phenotypes are shown. The establishment of LRK-1 expression through the first 10 days of adulthood further augment its relevance for PD modelling and establish that LRK-1 is present at the timepoints most characterised throughout this study, opening a window for extensive future work.

An overarching aim of this research project was to dissect the mechanism of VPS35[D620N] and through this novel *C. elegans* model, new insights have been gained. The *C. elegans* modelling undertaken here suggests that VPS35[D620N] mutation acts through a more complex mechanism than loss of function alone, conferring dominant negative toxicity, leading to impairments in some retromer functions. Most pertinently, this novel model coherently suggests VPS35[D620N] leads to altered interaction with LRRK2, leading to LRRK2 kinase hyperactivation and toxicity through a concurrent toxic gain of function mechanism, although biochemical readouts are yet to be established. This pathway conservation suggested in the *C. elegans* model, that LRK-1 is kinase hyperactivated in *vps-35[D638N]* mutation, further augments the potential relevance and conservation of *C. elegans* models for future functional modelling of PD relevant genes. This could readily be undertaken through the novel CRISPR/Cas9 modified orthologue approach, first undertaken in this study.

Bibliography

1. Chandler RJ, Cogo S, Lewis PA, Kevei E. Modelling the functional genomics of Parkinson's disease in Caenorhabditis elegans: LRRK2 and beyond. Biosci Rep [Internet]. 2021 Sep 30 [cited 2021 Sep 14];41(9):20203672. Available from: /bioscirep/article/41/9/BSR20203672/229558/Modelling-the-functional-genomics-of-Parkinson-s
2. Parkinson J. An essay on the shaking palsy. 1817. J Neuropsychiatry Clin Neurosci [Internet]. 2002 Mar [cited 2022 Jan 11];14(2). Available from: https://pubmed.ncbi.nlm.nih.gov/11983801/
3. Trinh J, Guella I, Farrer MJ. Disease penetrance of late-onset parkinsonism: A meta-analysis. JAMA Neurol. 2014;71(12):1535–9.
4. Postuma RB, Berg D, Stern M, Poewe W, Olanow CW, Oertel W, et al. MDS clinical diagnostic criteria for Parkinson's disease. Mov Disord. 2015;30(12):1591–601.
5. Dickson DW, Braak H, Duda JE, Duyckaerts C, Gasser T, Halliday GM, et al. Neuropathological assessment of Parkinson's disease: refining the diagnostic criteria. Lancet Neurol [Internet]. 2009;8(12):1150–7. Available from: http://dx.doi.org/10.1016/S1474-4422(09)70238-8
6. Ali K, Morris HR. Parkinson's disease: Chameleons and mimics. Pract Neurol. 2015;15(1):14–25.
7. Schrag A, Horsfall L, Walters K, Noyce A, Petersen I. Prediagnostic presentations of Parkinson's disease in primary care: A case-control study. Lancet Neurol [Internet]. 2015;14(1):57–64. Available from: http://dx.doi.org/10.1016/S1474-4422(14)70287-X
8. Muller T, Kuhn W, Przuntek H. [Non-motor symptoms of Parkinson disease. Significant impact on quality of life--using possible treatments]. Fortschr Med. 1997;115(14):45–8.
9. Wu YH, Lee WJ, Chen YH, Chang MH, Lin CH. Premotor symptoms as predictors of outcome in parkinsons disease: A case-control study. PLoS One. 2016;
10. Wider C, Skipper L, Solida A, Brown L, Farrer M, Dickson D, et al. Autosomal dominant dopa-responsive parkinsonism in a multigenerational Swiss family. Park Relat Disord. 2008;14(6):465–70.
11. Braak H, Del K, Rüb U, Vos RAI De, Jansen ENH, Braak E. Staging of Brain Pathology related to sporadic Parkinson's Disease. 2003;24:197–211.
12. Braak H, Rüb U, Gai WP, Del Tredici K. Idiopathic Parkinson's disease: Possible routes by which vulnerable neuronal types may be subject to neuroinvasion by an unknown pathogen. J Neural Transm. 2003;110(5):517–36.
13. Stokholm MG, Danielsen EH, Hamilton-Dutoit SJ, Borghammer P. Pathological α-synuclein in gastrointestinal tissues from prodromal Parkinson disease patients. Ann Neurol. 2016;79(6):940–9.
14. Stoessl AJ. Salivary gland biopsy for diagnosis of Parkinson's disease? Lancet Neurol. 2016;15(7):654–6.
15. Zeng XS, Geng WS, Jia JJ, Chen L, Zhang PP. Cellular and molecular basis of neurodegeneration in Parkinson disease. Front Aging Neurosci. 2018;10(APR):1–16.

16. Johnson ME, Labrie V, Brundin L, Brundin P. Triggers, Facilitators, and Aggravators: Redefining Parkinson's Disease Pathogenesis. Trends Neurosci [Internet]. 2018;xx:1–10. Available from: https://www.sciencedirect.com/science/article/pii/S0166223618302534?dgcid=rss_sd_all
17. García-Lorenzo D, Longo-Dos Santos C, Ewenczyk C, Leu-Semenescu S, Gallea C, Quattrocchi G, et al. The coeruleus/subcoeruleus complex in rapid eye movement sleep behaviour disorders in Parkinson's disease. Brain. 2013;136(7):2120–9.
18. Fahn S. The 200-year journey of Parkinson disease: Reflecting on the past and looking towards the future. Park Relat Disord [Internet]. 2018;46:S1–5. Available from: https://doi.org/10.1016/j.parkreldis.2017.07.020
19. Oertel W, Schulz JB. Current and experimental treatments of Parkinson disease: A guide for neuroscientists. J Neurochem. 2016;139:325–37.
20. Borovac JA. Side effects of a dopamine agonist therapy for Parkinson's disease: A mini-review of clinical pharmacology. Yale J Biol Med. 2016;89(1):37–47.
21. Hernandez DG, Reed X, Singleton AB. Genetics in Parkinson disease: Mendelian versus non-Mendelian inheritance. J Neurochem. 2016;139:59–74.
22. Struhal W, Presslauer S, Spielberger S, Zimprich A, Auff E, Bruecke T, et al. VPS35 Parkinson's disease phenotype resembles the sporadic disease. J Neural Transm. 2014;121(7):755–9.
23. Li Y, Ikeda A, Yoshino H, Oyama G, Kitani M, Daida K, et al. Clinical characterization of patients with leucine-rich repeat kinase 2 genetic variants in Japan. J Hum Genet [Internet]. 2020; Available from: http://dx.doi.org/10.1038/s10038-020-0772-4
24. Bandres-Ciga S, Saez-Atienzar S, Bonet-Ponce L, Billingsley K, Vitale D, Blauwendraat C, et al. The endocytic membrane trafficking pathway plays a major role in the risk of Parkinson's disease. Mov Disord. 2019;1–9.
25. Lubbe SJ, Escott-Price V, Gibbs JR, Nalls MA, Bras J, Price TR, et al. Additional rare variant analysis in Parkinson's disease cases with and without known pathogenic mutations: evidence for oligogenic inheritance. Assoc Stud Artic [Internet]. 2016;25:5483–9. Available from: https://academic.oup.com/hmg/article-abstract/25/24/5483/2608636
26. Keogh MJ, Wei W, Aryaman J, Wilson I, Talbot K, Turner MR, et al. Oligogenic genetic variation of neurodegenerative disease genes in 980 postmortem human brains. J Neurol Neurosurg Psychiatry. 2018;89(8):813–6.
27. Caldwell KA, Willicott CW, Caldwell GA. Modeling neurodegeneration in Caenorhabditiselegans. Dis Model Mech. 2020;13(10).
28. Cooper JF, Van Raamsdonk JM. Modeling Parkinson's disease in C. elegans. J Parkinsons Dis. 2018;8(1):17–32.
29. Marder K, Wang Y, Alcalay RN, Mejia-Santana H, Tang MX, Lee A, et al. Age-specific penetrance of LRRK2 G2019S in the Michael J. Fox Ashkenazi Jewish LRRK2 Consortium. Neurology. 2015;85(1):89–95.
30. Ma C, Liu Y, Neumann S, Gao X. Nicotine from cigarette smoking and diet and Parkinson

disease: A review. Transl Neurodegener. 2017;6(1):1–7.

31. Blauwendraat C, Nalls MA, Singleton AB. The genetic architecture of Parkinson's disease. Lancet Neurol [Internet]. 2020;19(2):170–8. Available from: http://dx.doi.org/10.1016/S1474-4422(19)30287-X
32. Nalls MA, Blauwendraat C, Vallerga CL, Heilbron K, Bandres-Ciga S, Chang D, et al. Identification of novel risk loci, causal insights, and heritable risk for Parkinson's disease: a meta-analysis of genome-wide association studies. Lancet Neurol. 2019;18(12):1091–102.
33. Ferrari R, Kia DA, Tomkins JE, Hardy J, Wood NW, Lovering RC, et al. Stratification of candidate genes for Parkinson's disease using weighted protein-protein interaction network analysis. BMC Genomics. 2018;19(1):1–8.
34. Germer EL, Imhoff S, Vilariño-Güell C, Kasten M, Seibler P, Brüggemann N, et al. The Role of Rare Coding Variants in Parkinson's Disease GWAS Loci. Front Neurol. 2019;10(December):1–6.
35. Bandres-Ciga S, Saez-Atienzar S, Kim JJ, Makarious MB, Faghri F, Diez-Fairen M, et al. Large-scale pathway specific polygenic risk and transcriptomic community network analysis identifies novel functional pathways in Parkinson disease. Acta Neuropathol [Internet]. 2020;140(3):341–58. Available from: https://doi.org/10.1007/s00401-020-02181-3
36. Singleton A, Hardy J. Progress in the genetic analysis of Parkinson's disease. Hum Mol Genet. 2019;28(R2):R215–8.
37. Smolders S, Van Broeckhoven C. Genetic perspective on the synergistic connection between vesicular transport, lysosomal and mitochondrial pathways associated with Parkinson's disease pathogenesis. Acta Neuropathol Commun. 2020;8(1):1–28.
38. Sarasija S, Laboy JT, Ashkavand Z, Bonner J, Tang Y, Norman KR. Presenilin mutations deregulate mitochondrial Ca2+ homeostasis and metabolic activity causing neurodegeneration in Caenorhabditis elegans. Elife. 2018;7:1–30.
39. Bieschke J, Cohen E, Murray A, Dillin A, Kelly JW. A kinetic assessment of the C. elegans amyloid disaggregation activity enables uncoupling of disassembly and proteolysis. Protein Sci. 2009;18(11):2231–41.
40. Sandhof CA, Hoppe SO, Tittelmeier J, Nussbaum-Krammer C. C. Elegans models to study the propagation of prions and prion-like proteins. Biomolecules. 2020;10(8):1–23.
41. Kim W, Underwood RS, Greenwald I, Shaye DD. Ortholist 2: A new comparative genomic analysis of human and caenorhabditis elegans genes. Genetics. 2018;210(2):445–61.
42. Bargmann CI. Neurobiology of the Caenorhabditis elegans genome. Science (80-). 1998;282(5396):2028–33.
43. Equence CES, Iology TOB, The C, Consortium S. Genome sequence of the nematode C. elegans: A platform for investigating biology. Science (80-). 1998;282(5396):2012–8.
44. Walther DM, Kasturi P, Zheng M, Pinkert S, Vecchi G, Ciryam P, et al. Widespread proteome remodeling and aggregation in aging C. elegans. Cell [Internet]. 2015;161(4):919–32. Available

from: http://dx.doi.org/10.1016/j.cell.2015.03.032

45. Azulay A, Itskovits E, Zaslaver A. The C. elegans Connectome Consists of Homogenous Circuits with Defined Functional Roles. PLoS Comput Biol. 2016;12(9):1–16.
46. Cook SJ, Jarrell TA, Brittin CA, Wang Y, Bloniarz AE, Yakovlev MA, et al. Whole-animal connectomes of both Caenorhabditis elegans sexes. Nature [Internet]. 2019;571(7763):63–71. Available from: http://www.nature.com/articles/s41586-019-1352-7
47. Maulik M, Mitra S, Bult-Ito A, Taylor BE, Vayndorf EM. Behavioral phenotyping and pathological indicators of Parkinson's disease in C. elegans models. Front Genet. 2017;8(JUN):1–21.
48. Smith LL, Ryde IT, Hartman JH, Romersi RF, Markovich Z, Meyer JN. Strengths and limitations of morphological and behavioral analyses in detecting dopaminergic deficiency in Caenorhabditis elegans. Neurotoxicology [Internet]. 2019;74(June):209–20. Available from: https://linkinghub.elsevier.com/retrieve/pii/S0161813X19300695
49. Chase DL, Koelle MR. Biogenic amine neurotransmitters in C. elegans. WormBook. 2007;1–15.
50. Ségalat L, Elkes DA, Kaplan JM. Modulation of serotonin-controlled behaviors by Go in Caenorhabditis elegans. Science (80-). 1995;267(5204):1648–51.
51. Paix A, Folkmann A, Rasoloson D, Seydoux G. High efficiency, homology-directed genome editing in Caenorhabditis elegans using CRISPR-Cas9ribonucleoprotein complexes. Genetics. 2015;201(1):47–54.
52. Ibáñez P, Lesage S, Lohmann E, Thobois S, De Michele G, Borg M, et al. Mutational analysis of the PINK1 gene in early-onset parkinsonism in Europe and North Africa. Brain. 2006;129(3):686–94.
53. Lesage S, Lunati A, Houot M, Romdhan S Ben, Clot F, Tesson C, et al. Characterization of Recessive Parkinson Disease in a Large Multicenter Study. Ann Neurol [Internet]. 2020 Oct 28 [cited 2021 Jan 15];88(4):843–50. Available from: https://onlinelibrary.wiley.com/doi/10.1002/ana.25787
54. Pankratz N, Pauciulo MW, Elsaesser VE, Marek DK, Halter CA, Wojcieszek J, et al. Mutations in DJ-1 are rare in familial Parkinson disease. Neurosci Lett. 2006;408(3):209–13.
55. Olgiati S, Quadri M, Fang M, Rood JPMA, Saute JA, Chien HF, et al. DNAJC6 Mutations Associated with Early-Onset Parkinson's Disease. Ann Neurol [Internet]. 2016 Feb 1 [cited 2021 Jan 15];79(2):244–56. Available from: https://pubmed.ncbi.nlm.nih.gov/26528954/
56. Vilariño-Güell C, Rajput A, Milnerwood AJ, Shah B, Szu-Tu C, Trinh J, et al. DNAJC13 mutations in Parkinson disease. Hum Mol Genet [Internet]. 2014 Apr 1 [cited 2021 Jan 15];23(7):1794–801. Available from: https://pubmed.ncbi.nlm.nih.gov/24218364/
57. Wilson GR, Sim JCH, McLean C, Giannandrea M, Galea CA, Riseley JR, et al. Mutations in RAB39B cause X-linked intellectual disability and early-onset parkinson disease with α-synuclein pathology. Am J Hum Genet [Internet]. 2014;95(6):729–35. Available from: http://dx.doi.org/10.1016/j.ajhg.2014.10.015

58. Di Fonzo A, Chien HF, Socal M, Giraudo S, Tassorelli C, Iliceto G, et al. ATP13A2 missense mutations in juvenile parkinsonism and young onset Parkinson disease. Neurology [Internet]. 2007 May 7 [cited 2021 Jan 15];68(19):1557–62. Available from: https://pubmed.ncbi.nlm.nih.gov/17485642/
59. Puschmann A. New Genes Causing Hereditary Parkinson's Disease or Parkinsonism. Curr Neurol Neurosci Rep. 2017;17(9).
60. Landrum MJ, Kattman BL. ClinVar at five years: Delivering on the promise. Hum Mutat [Internet]. 2018 Nov 11 [cited 2021 Jan 27];39(11):1623–30. Available from: https://onlinelibrary.wiley.com/doi/abs/10.1002/humu.23641
61. Harris TW, Arnaboldi V, Cain S, Chan J, Chen WJ, Cho J, et al. WormBase: a modern Model Organism Information Resource. Nucleic Acids Res. 2020;48(D1):D762–7.
62. Stein L, Sternberg P, Durbin R, Thierry-Mieg J, Spieth J. WormBase: Network access to the genome and biology of Caenorhabditis elegans. Nucleic Acids Res. 2001;29(1):82–6.
63. Hodgkin J, Horvitz HR, Brenner S. Nondisjunction Mutants of the Nematode CAENORHABDITIS ELEGANS. Genetics [Internet]. 1979;91(1):67–94. Available from: http://www.pubmedcentral.nih.gov/articlerender.fcgi?artid=1213932&tool=pmcentrez&rendertype=abstract%5Cnhttp://www.genetics.org/content/91/1/67.short
64. Brenner S. The Genetics of Caenorhabditis Elegans. Genetics. 1974;77:71–94.
65. Jadiya P, Fatima S, Baghel T, Mir SS, Nazir A. A Systematic RNAi Screen of Neuroprotective Genes Identifies Novel Modulators of Alpha-Synuclein-Associated Effects in Transgenic Caenorhabditis elegans. Mol Neurobiol [Internet]. 2016;53(9):6288–300. Available from: http://dx.doi.org/10.1007/s12035-015-9517-3
66. Jansen IE, Ye H, Heetveld S, Lechler MC, Michels H, Seinstra RI, et al. Discovery and functional prioritization of Parkinson's disease candidate genes from large-scale whole exome sequencing. Genome Biol. 2017;18(1):1–26.
67. Hamamichi S, Rivas RN, Knight AL, Cao S, Caldwell KA, Caldwell GA. Hypothesis-based RNAi screening identifies neuroprotective genes in a Parkinson's disease model. Proc Natl Acad Sci U S A. 2008;105(2):728–33.
68. Thompson O, Edgley M, Strasbourger P, Flibotte S, Ewing B, Adair R, et al. The million mutation project: A new approach to genetics in Caenorhabditis elegans. Genome Res. 2013;23(10):1749–62.
69. Barstead R, Moulder G, Cobb B, Frazee S, Henthorn D, Holmes J, et al. Large-scale screening for targeted knockouts in the caenorhabditis elegans genome. G3 Genes, Genomes, Genet. 2012;2(11):1415–25.
70. Cuppen E, Gort E, Hazendonk E, Mudde J, Van De Belt J, Nijman IJ, et al. Efficient target-selected mutagenesis in Caenorhabditis elegans: Toward a knockout for every gene. Genome Res. 2007;17(5):649–58.
71. West AB, Moore DJ, Biskup S, Bugayenko A, Smith WW, Ross CA, et al. Parkinson's disease-

associated mutations in leucine-rich repeat kinase 2 augment kinase activity. Proc Natl Acad Sci U S A. 2005;102(46):16842–7.

72. Greggio E, Jain S, Kingsbury A, Bandopadhyay R, Lewis P, Kaganovich A, et al. Kinase activity is required for the toxic effects of mutant LRRK2/dardarin. Neurobiol Dis. 2006;23(2):329–41.
73. Smith WW, Pei Z, Jiang H, Dawson VL, Dawson TM, Ross CA. Kinase activity of mutant LRRK2 mediates neuronal toxicity. Nat Neurosci. 2006;9(10):1231–3.
74. Lakso M, Vartiainen S, Moilanen AM, Sirviö J, Thomas JH, Nass R, et al. Dopaminergic neuronal loss and motor deficits in Caenorhabditis elegans overexpressing human α-synuclein. J Neurochem. 2003;86(1):165–72.
75. Bodhicharla R, Nagarajan A, Winter J, Adenle A, Nazir A, Brady D, et al. Effects of α-Synuclein Overexpression in Transgenic Caenorhabditis elegans Strains. CNS Neurol Disord - Drug Targets [Internet]. 2013;11(8):965–75. Available from: http://www.eurekaselect.com/openurl/content.php?genre=article&issn=1871-5273&volume=11&issue=8&spage=965
76. Yao C, El Khoury R, Wang W, Byrd TA, Pehek EA, Thacker C, et al. LRRK2-mediated neurodegeneration and dysfunction of dopaminergic neurons in a Caenorhabditis elegans model of Parkinson's disease. Neurobiol Dis [Internet]. 2010;40(1):73–81. Available from: http://dx.doi.org/10.1016/j.nbd.2010.04.002
77. Long S, Guo W, Hu S, Su F, Zeng Y, Zeng J, et al. G2019S LRRK2 increases stress susceptibility through inhibition of DAF-16 nuclear translocation in a 14-3-3 associated-manner in caenorhabditis elegans. Front Neurosci. 2018;12(NOV):1–14.
78. Beilina A, Bonet-Ponce L, Kumaran R, Kordich JJ, Ishida M, Mamais A, et al. The Parkinson's Disease Protein LRRK2 Interacts with the GARP Complex to Promote Retrograde Transport to the trans-Golgi Network. Cell Rep. 2020;31(5).
79. Luth ES, Stavrovskaya IG, Bartels T, Kristal BS, Selkoe DJ. LRRK2 modulates vulnerability to mitochondrial dysfunction in C. elegans. J Biol Chem. 2014;289(31):21490–507.
80. Ray A, Martinez BA, Berkowitz LA, Caldwell GA, Caldwell KA. Mitochondrial dysfunction, oxidative stress, and neurodegeneration elicited by a bacterial metabolite in a C. elegans Parkinson's model. Cell Death Dis [Internet]. 2014;5(1):e984-12. Available from: http://dx.doi.org/10.1038/cddis.2013.513
81. Langston, R, G. Rudenko, I, N. Cookson, M R. The functions of orthologues of the human Parkinson's disease gene LRRK2 across species: implications for disease modeling in preclinical research. Biochem J. 2016;473(3):221–32.
82. Dickinson DJ, Goldstein B. CRISPR-based methods for caenorhabditis elegans genome engineering. Genetics. 2016;202(3):885–901.
83. Mojumder S, Sawamura R, Murayama Y, Ogura T, Yamanaka K. Functional characterization of UBXN-6, a C-terminal cofactor of CDC-48, in C. elegans. Biochem Biophys Res Commun [Internet]. 2019;509(2):462–8. Available from: https://doi.org/10.1016/j.bbrc.2018.12.155

84. Dokshin GA, Ghanta KS, Piscopo KM, Mello CC. Robust Genome Editing with Short Single-Stranded. Genetics. 2018;210(November):781–7.
85. Corsi AK, Wightman B, Chalfie M. A transparent window into biology: A primer on Caenorhabditis elegans. Genetics. 2015;200(2):387–407.
86. Sawin ER, Ranganathan R, Horvitz HR. C. elegans locomotory rate is modulated by the environment through a dopaminergic pathway and by experience through a serotonergic pathway. Neuron. 2000;26(3):619–31.
87. Hills T, Brockie PJ, Maricq A V. Dopamine and Glutamate Control Area-Restricted Search Behavior in Caenorhabditis elegans. J Neurosci [Internet]. 2004 Feb 4 [cited 2021 Sep 15];24(5):1217–25. Available from: https://www.jneurosci.org/content/24/5/1217
88. Nass R, Hall DH, Miller DM, Blakely RD. Neurotoxin-induced degeneration of dopamine neurons in Caenorhabditis elegans. Proc Natl Acad Sci [Internet]. 2002 Mar 5 [cited 2021 Sep 16];99(5):3264–9. Available from: https://www.pnas.org/content/99/5/3264
89. Lapierre LR, Silvestrini MJ, Nuñez L, Ames K, Wong S, Le TT, et al. Autophagy genes are required for normal lipid levels in C. elegans. Autophagy [Internet]. 2013 [cited 2021 Apr 15];9(3):278–86. Available from: /pmc/articles/PMC3590250/
90. Dingley S, Polyak E, Lightfoot R, Ostrovsky J, Rao M, Greco T, et al. Mitochondrial respiratory chain dysfunction variably increases oxidant stress in Caenorhabditis elegans. Mitochondrion. 2010;10(2):125–36.
91. Minniti AN, Labarca M, Hurtado C, Brandan E. Caenorhabditis elegans syndecan (SDN-1) is required for normal egg laying and associates with the nervous system and the vulva. J Cell Sci. 2004;117(21):5179–90.
92. Polymeropoulos MH, Lavedan C, Leroy E, Ide SE, Dehejia A, Dutra A, et al. Mutation in the α-synuclein gene identified in families with Parkinson's disease. Science (80-). 1997;276(5321):2045–7.
93. Kuwahara T, Koyama A, Gengyo-Ando K, Masuda M, Kowa H, Tsunoda M, et al. Familial Parkinson mutant α-synuclein causes dopamine neuron dysfunction in transgenic Caenorhabditis elegans. J Biol Chem. 2006;281(1):334–40.
94. Tissenbaum HA. Using C. elegans for aging research. Invertebr Reprod Dev [Internet]. 2015 Jan 30 [cited 2021 Dec 9];59(sup1):59. Available from: /pmc/articles/PMC4464094/
95. Goya ME, Xue F, Sampedro-Torres-Quevedo C, Arnaouteli S, Riquelme-Dominguez L, Romanowski A, et al. Probiotic Bacillus subtilis Protects against α-Synuclein Aggregation in C. elegans. Cell Rep. 2020;30(2):367-380.e7.
96. Zheng J, Wang M, Wei W, Keller JN, Adhikari B, King JF, et al. Dietary Plant Lectins Appear to Be Transported from the Gut to Gain Access to and Alter Dopaminergic Neurons of Caenorhabditis elegans, a Potential Etiology of Parkinson's Disease. Front Nutr [Internet]. 2016 Mar 7 [cited 2021 Dec 9];3. Available from: https://pubmed.ncbi.nlm.nih.gov/27014695/
97. Fu H, Hardy J, Duff KE. Selective vulnerability in neurodegenerative diseases. Nat Neurosci

[Internet]. 2018;21(10):1350–8. Available from: http://dx.doi.org/10.1038/s41593-018-0221-2

98. Giguère N, Nanni SB, Trudeau LE. On cell loss and selective vulnerability of neuronal populations in Parkinson's disease. Vol. 9, Frontiers in Neurology. Frontiers Media S.A.; 2018.
99. Shaham S. Glial Development and Function in the Nervous System of Caenorhabditis elegans. [cited 2021 Mar 26]; Available from: www.cshperspectives.org
100. Salari S, Bagheri M. In vivo, in vitro and pharmacologic models of Parkinson's disease. Physiol Res [Internet]. 2019 [cited 2021 Dec 9];68(1):17–24. Available from: https://pubmed.ncbi.nlm.nih.gov/30433804/
101. Moraes ÂM, Jorge SAC, Astray RM, Suazo CAT, Calderón Riquelme CE, Augusto EFP, et al. Drosophila melanogaster S2 cells for expression of heterologous genes: From gene cloning to bioprocess development. Biotechnol Adv. 2012 May 1;30(3):613–28.
102. Vermilyea SC, Babinski A, Tran N, To S, Guthrie S, Kluss JH, et al. In Vitro CRISPR/Cas9-Directed Gene Editing to Model LRRK2 G2019S Parkinson's Disease in Common Marmosets. Sci Rep [Internet]. 2020;10(1):3447. Available from: http://www.ncbi.nlm.nih.gov/pubmed/32103062
103. Zimprich A, Benet-Pagès A, Struhal W, Graf E, Eck SH, Offman MN, et al. A mutation in VPS35, encoding a subunit of the retromer complex, causes late-onset parkinson disease. Am J Hum Genet. 2011;89(1):168–75.
104. Vilariño-Güell C, Wider C, Ross OA, Dachsel JC, Kachergus JM, Lincoln SJ, et al. VPS35 mutations in parkinson disease. Am J Hum Genet. 2011;89(1):162–7.
105. Sharma M, Ioannidis JPA, Aasly JO, Annesi G, Brice A, Bertram L, et al. A multi-centre clinico-genetic analysis of the VPS35 gene in Parkinson disease indicates reduced penetrance for disease-associated variants. J Med Genet. 2012;49(11):721–6.
106. Trinh J, Zeldenrust FMJ, Huang J, Kasten M, Schaake S, Petkovic S, et al. Genotype-phenotype relations for the Parkinson's disease genes SNCA, LRRK2, VPS35: MDSGene systematic review. Mov Disord. 2018;33(12):1857–70.
107. Seaman MNJ, McCaffery JM, Emr SD. A membrane coat complex essential for endosome-to-Golgi retrograde transport in yeast. J Cell Biol. 1998;142(3):665–81.
108. Erro R. VPS35 and EIF4G1 interactions and novel candidate genes for PD: From genes to pathways and back. Mov Disord. 2015;30(4):499–499.
109. Tsika E, Glauser L, Moser R, Fiser A, Daniel G, Sheerin UM, et al. Parkinson's disease-linked mutations in VPS35 induce dopaminergic neurodegeneration. Hum Mol Genet. 2014;23(17):4621–38.
110. Seaman MNJ, Marcusson EG, Cereghino JL, Emr SD. Endosome to Golgi retrieval of the vacuolar protein sorting receptor, Vps10p, requires the function of the VPS29, VPS30, and VPS35 gene products. J Cell Biol. 1997;137(1):79–92.
111. Mir R, Tonelli F, Lis P, Macartney T, Polinski NK, Martinez TN, et al. The Parkinson's disease VPS35[D620N] mutation enhances LRRK2-mediated Rab protein phosphorylation in mouse and

human. Biochem J [Internet]. 2018;475(11):1861–83. Available from: http://biochemj.org/lookup/doi/10.1042/BCJ20180248

112. Williams ET, Chen X, Moore DJ. VPS35, the retromer complex and Parkinson's disease. J Parkinsons Dis. 2017;7(2):219–33.
113. Chen X, Kordich JK, Williams ET, Levine N, Cole-Strauss A, Marshall L, et al. Parkinson's disease-linked D620N VPS35 knockin mice manifest tau neuropathology and dopaminergic neurodegeneration. Proc Natl Acad Sci U S A [Internet]. 2019; Available from: http://feedproxy.google.com/~r/Pnas-RssFeedOfEarlyEditionArticles/~3/C7bqG4EsbJ8/1814909116.short
114. Carosi JM, Hein LK, van den Hurk M, Adams R, Milky B, Singh S, et al. Retromer regulates the lysosomal clearance of MAPT/tau. Autophagy [Internet]. 2020;00(00):1–21. Available from: https://doi.org/10.1080/15548627.2020.1821545
115. Henderson MX, Sengupta M, Trojanowski JQ, Lee VMY. Alzheimer's disease tau is a prominent pathology in LRRK2 Parkinson's disease. Acta Neuropathol Commun [Internet]. 2019 Dec 16;7(1):183. Available from: https://actaneurocomms.biomedcentral.com/articles/10.1186/s40478-019-0836-x
116. McGough IJ, Steinberg F, Jia D, Barbuti PA, McMillan KJ, Heesom KJ, et al. Retromer binding to FAM21 and the WASH complex is perturbed by the Parkinson disease-linked VPS35(D620N) mutation. Curr Biol [Internet]. 2014;24(14):1670–6. Available from: http://dx.doi.org/10.1016/j.cub.2014.06.024
117. Harrison MS, Hung C-S, Liu T -t., Christiano R, Walther TC, Burd CG. A mechanism for retromer endosomal coat complex assembly with cargo. Proc Natl Acad Sci [Internet]. 2014;111(1):267–72. Available from: http://www.pnas.org/cgi/doi/10.1073/pnas.1316482111
118. Cui Y, Carosi JM, Yang Z, Ariotti N, Kerr MC, Parton RG, et al. Retromer has a selective function in cargo sorting via endosome transport carriers. 2018;218(2):615–31.
119. Hierro A, Rojas AL, Rojas R, Murthy N, Effantin G, Kajava A V., et al. Functional architecture of the retromer cargo-recognition complex. Nature. 2007;449(7165):1063–7.
120. Kovtun O, Leneva N, Bykov YS, Ariotti N, Teasdale RD, Schaffer M, et al. Structure of the membrane-assembled retromer coat determined by cryo-electron tomography. Nature [Internet]. 2018;561(7724):561–4. Available from: http://dx.doi.org/10.1038/s41586-018-0526-z
121. Small SA, Kent K, Pierce A, Leung C, Kang MS, Okada H, et al. Model-guided microarray implicates the retromer complex in Alzheimer's disease. Ann Neurol. 2005;58(6):909–19.
122. Bhalla, Akhil. Vetanovetz, Christopher. Morel, Etienne. Chamoun, Zeina. Di Paolo, Gilbert. Small S. Characterizing the location and trafficking routes of the neuronal retromer and its role in amyloid precursor protein transport. Neurobiol Dis. 2012;47(1):126–34.
123. Hardy J, Allsop D. Amyloid deposition as the central event in the aetiology of Alzheimer's disease. Vol. 12, Trends in Pharmacological Sciences. Elsevier Current Trends; 1991. p. 383–8.
124. Hu F, Padukkavidana T, Vægter CB, Brady OA, Mackenzie IR, Feldman HH, et al. Sortilin-

Mediated Endocytosis Determines Levels of the Fronto- Temporal Dementia Protein, Progranulin. Neuron. 2011;68(4):654–67.

125. Kim E, Lee Y, Lee HJ, Kim JS, Song BS, Huh JW, et al. Implication of mouse Vps26b-Vps29-Vps35 retromer complex in sortilin trafficking. Biochem Biophys Res Commun [Internet]. 2010;403(2):167–71. Available from: http://dx.doi.org/10.1016/j.bbrc.2010.10.121
126. Verpoorten N, Timmerman V, Coen K, Schmedding E, Van Gerwen V, Hartung H-P, et al. Mutations in the Small GTP-ase Late Endosomal Protein RAB7 Cause Charcot-Marie-Tooth Type 2B Neuropathy. Am J Hum Genet. 2003;72(3):722–7.
127. Maro GS, Klassen MP, Shen K. A β-catenin-dependent Wnt pathway mediates anteroposterior axon guidance in C. elegans motor neurons. PLoS One. 2009;4(3).
128. Coudreuse, Damien Y M. Roel, Giulietta. Betist, Marco C. Destree, Olivier. Korswagen HC. Wnt Gradient Formation Requires Retromer Function in Wnt-Producing Cells. Science (80-). 2006;312(May):921–5.
129. Pan CL, Baum PD, Gu M, Jorgensen EM, Clark SG, Garriga G. C. elegans AP-2 and Retromer Control Wnt Signaling by Regulating MIG-14/Wntless. Dev Cell. 2008;14(1):132–9.
130. Prasad BC. Wnt signaling establishes anteroposterior neuronal polarity and requires retromer in C. elegans. Development [Internet]. 2006;133(9):1757–66. Available from: http://dev.biologists.org/cgi/doi/10.1242/dev.02357
131. Belenkaya TY, Wu Y, Tang X, Zhou B, Cheng L, Sharma Y V., et al. The Retromer Complex Influences Wnt Secretion by Recycling Wntless from Endosomes to the Trans-Golgi Network. Dev Cell. 2008;14(1):120–31.
132. de Groot REA, Farin HF, Macůrková M, van Es JH, Clevers HC, Korswagen HC. Retromer Dependent Recycling of the Wnt Secretion Factor Wls Is Dispensable for Stem Cell Maintenance in the Mammalian Intestinal Epithelium. PLoS One. 2013;8(10):1–9.
133. Chiu CC, Weng YH, Huang YZ, Chen RS, Liu YC, Yeh TH, et al. (D620N) VPS35 causes the impairment of Wnt/β-catenin signaling cascade and mitochondrial dysfunction in a PARK17 knockin mouse model. Cell Death Dis [Internet]. 2020;11(11). Available from: http://dx.doi.org/10.1038/s41419-020-03228-9
134. Berwick DC, Javaheri B, Wetzel A, Hopkinson M, Nixon-Abell J, Grannò S, et al. Pathogenic LRRK2 variants are gain-of-function mutations that enhance LRRK2-mediated repression of β-catenin signaling. Mol Neurodegener [Internet]. 2017;12(1):29–39. Available from: http://dx.doi.org/10.1186/s13024-017-0153-4
135. Zhang D, Isack NR, Glodowski DR, Liu J, Chen CCH, Shawn Xu XZ, et al. RAB-6.2 and the retromer regulate glutamate receptor recycling through a retrograde pathway. J Cell Biol. 2012;196(1):85–101.
136. Munsie LN, Milnerwood AJ, Seibler P, Beccano-Kelly DA, Tatarnikov I, Khinda J, et al. Retromer-dependent neurotransmitter receptor trafficking to synapses is altered by the Parkinson's disease VPS35 mutation p.D620N. Hum Mol Genet. 2015;24(6):1691–703.

137. Sargent D, Cunningham LA, Dues DJ, Ma Y, Kordich JJ, Mercado G, et al. Neuronal VPS35 deletion induces spinal cord motor neuron degeneration and early post-natal lethality. Brain Commun [Internet]. 2021 Jul 1 [cited 2021 Dec 8];3(3). Available from: https://pubmed.ncbi.nlm.nih.gov/34704029/
138. Rahman AA, Morrison BE. Contributions of VPS35 mutations to Parkinson's Disease. Neuroscience [Internet]. 2019;401:1–10. Available from: https://linkinghub.elsevier.com/retrieve/pii/S030645221930017X
139. Kadgien CA, Kamesh A, Milnerwood AJ. Endosomal traffic and glutamate synapse activity are increased in VPS35 D620N mutant knock-in mouse neurons, and resistant to LRRK2 kinase inhibition. Mol Brain 2021 141 [Internet]. 2021 Sep 16 [cited 2021 Sep 21];14(1):1–20. Available from: https://molecularbrain.biomedcentral.com/articles/10.1186/s13041-021-00848-w
140. Zhao Y, Perera G, Takahashi-Fujigasaki J, Mash DC, Vonsattel JPG, Uchino A, et al. Reduced LRRK2 in association with retromer dysfunction in post-mortem brain tissue from LRRK2 mutation carriers. Brain. 2018;141(2):486–95.
141. Inoshita T, Arano T, Hosaka Y, Meng H, Umezaki Y, Kosugi S, et al. Vps35 in cooperation with LRRK2 regulates synaptic vesicle endocytosis through the endosomal pathway in Drosophila. Hum Mol Genet. 2017;26(15):2933–48.
142. Miura E, Hasegawa T, Konno M, Suzuki M, Sugeno N, Fujikake N, et al. VPS35 dysfunction impairs lysosomal degradation of α-synuclein and exacerbates neurotoxicity in a Drosophila model of Parkinson's disease. Neurobiol Dis [Internet]. 2014;71:1–13. Available from: http://dx.doi.org/10.1016/j.nbd.2014.07.014
143. Tang F, Liu W, Hu J, Erion JR, Ye J, Mei L, et al. VPS35 deficiency or mutation causes dopaminergic neuronal loss by impairing mitochondrial fusion and function. Cell Rep. 2015;12(10):1631–43.
144. Tang FL, Erion JR, Tian Y, Liu W, Yin DM, Ye J, et al. VPS35 in dopamine neurons is required for endosome-to- golgi retrieval of Lamp2a, a receptor of chaperone- mediated autophagy that is critical for α-synuclein degradation and prevention of pathogenesis of Parkinson's disease. J Neurosci [Internet]. 2015 Jul 22 [cited 2021 Apr 15];35(29):10613–28. Available from: https://pubmed.ncbi.nlm.nih.gov/26203154/
145. Lee Y, Karuppagounder SS, Shin JH, Lee Y Il, Ko HS, Swing D, et al. Parthanatos mediates AIMP2-activated age-dependent dopaminergic neuronal loss. Nat Neurosci. 2013;16(10):1392–400.
146. Kitada T, Aakawa S, Hattori N, Matsumine H, Yokochi M, Mizuno Y, et al. Mutations in the parkin gene cause autosomal recessive juvenile parkinsonism. Nat Lett [Internet]. 1998;169(1993):166–9. Available from: https://www.nature.com/articles/33416.pdf
147. Kam TI, Mao X, Park H, Chou SC, Karuppagounder SS, Umanah GE, et al. Poly(ADP-ribose) drives pathologic a-synuclein neurodegeneration in Parkinson's disease. Science (80-). 2018;362(6414).

148. PilYun S, Kim H, Ham S, Kwon SH, Lee GH, Shin JH, et al. VPS35 regulates parkin substrate AIMP2 toxicity by facilitating lysosomal clearance of AIMP2. Cell Death Dis [Internet]. 2017;8(4):e2741-13. Available from: http://dx.doi.org/10.1038/cddis.2017.157
149. Goswami D, Arendt K, Malenka R, Chen L, Temkin P, Morishita W. The Retromer Supports AMPA Receptor Trafficking During LTP. Neuron [Internet]. 2017;94(1):74-82.e5. Available from: http://dx.doi.org/10.1016/j.neuron.2017.03.020
150. Olanow CW, Prusiner SB. Is Parkinson's disease a prion disorder? Proc Natl Acad Sci [Internet]. 2009;106(31):12571–2. Available from: http://www.pnas.org/cgi/doi/10.1073/pnas.0906759106
151. Mao X, Ou MT, Karuppagounder SS, Kam TI, Yin X, Xiong Y, et al. Pathological α-synuclein transmission initiated by binding lymphocyte-activation gene 3. Science (80-). 2016;353(6307).
152. Tyson T, Senchuk M, Cooper JF, George S, Van Raamsdonk JM, Brundin P. Novel animal model defines genetic contributions for neuron-to-neuron transfer of α-synuclein. Sci Rep. 2017;7(1):1–10.
153. Ishizu N, Yui D, Hebisawa A, Aizawa H, Cui W, Fujita Y, et al. Impaired striatal dopamine release in homozygous Vps35 D620N knock-in mice. Hum Mol Genet [Internet]. 2016;25(20):4507–17. Available from: http://www.ncbi.nlm.nih.gov/pubmed/27562021
154. Bu G, Wang C, Tian Y, Niu M, Zheng X, Zhang L, et al. VPS35 regulates cell surface recycling and signaling of dopamine receptor D1. Neurobiol Aging [Internet]. 2016;46:22–31. Available from: http://dx.doi.org/10.1016/j.neurobiolaging.2016.05.016
155. Gurevich E V., Gainetdinov RR, Gurevich V V. G protein-coupled receptor kinases as regulators of dopamine receptor functions. Pharmacol Res [Internet]. 2016;111:1–16. Available from: http://dx.doi.org/10.1016/j.phrs.2016.05.010
156. Pickrell AM, Youle RJ. The roles of PINK1, Parkin, and mitochondrial fidelity in parkinson's disease. Neuron [Internet]. 2015;85(2):257–73. Available from: http://dx.doi.org/10.1016/j.neuron.2014.12.007
157. Knott AB, Perkins G, Schwarzenbacher R, Bossy-Wetzel E. Mitochondrial fragmentation in neurodegeneration. Nat Rev Neurosci. 2008;9(7):505–18.
158. Yang H, Puri R, Yun J, Sheng Z-H, Guo M, Lizzio MA, et al. MUL1 acts in parallel to the PINK1/parkin pathway in regulating mitofusin and compensates for loss of PINK1/parkin. Elife. 2014;3:1–26.
159. Fujioka H, Cullen PJ, Zhu X, Hoppel C, Liu J, Whone AL, et al. Parkinson's disease–associated mutant VPS35 causes mitochondrial dysfunction by recycling DLP1 complexes. Nat Med. 2015;22(1):54–63.
160. Wang W, Ma X, Zhou L, Liu J, Zhu X. A conserved retromer sorting motif is essential for mitochondrial DLP1 recycling by vps35 in parkinson's disease model. Hum Mol Genet. 2017;26(4):781–9.
161. Lesage S, Bras J, Cormier-Dequaire F, Condroyer C, Nicolas A, Darwent L, et al. Loss-of-Function Mutations in RAB39B are associated with Typical Early-Onset Parkinson's Disease.

Neurol Genet. 2015;1(1).

162. Wilson GR, Sim JCH, McLean C, Giannandrea M, Galea CA, Riseley JR, et al. Mutations in RAB39B cause X-linked intellectual disability and early-onset parkinson disease with α-synuclein pathology. Am J Hum Genet [Internet]. 2014 Dec 4 [cited 2021 Jan 15];95(6):729–35. Available from: /pmc/articles/PMC4259921/?report=abstract

163. Linhart, Radek. Wong, Sarah Anne. Cao, Jieyun. Tran, Melody. Huynh, Anne. Adrey, Casey. Park, Jong Min. Hsu, Christine. Taha, Saher. Peterson, Retia. Shea, Shannon. Kurian, Jason. Venderova K. Vaculolar protein sorting 35 (Vps35) rescues locomotor defecits and shortened lifespan in Drosophila expressing a Parkinson's disease mutant of Leucine-rich repeat kinase 2 (LRRK2). Mol Neurodegener. 2014;9(23).

164. Zimprich A, Biskup S, Leitner P, Lichtner P, Farrer M, Lincoln S, et al. Mutations in LRRK2 Cause Autosomal-Dominant Parkinsonism with Pleomorphic Pathology families, we have found six disease-segregating muta- tions (five missense and one putative splice site muta- tion) in a gene encoding a large, multifunctional pro- kinase. Neuron [Internet]. 2004;44:601–7. Available from: https://ac.els-cdn.com/S0896627304007202/1-s2.0-S0896627304007202-main.pdf?_tid=ebd5617e-a372-11e7-afe0-00000aacb35d&acdnat=1506510143_82eab12b4d7b5a09922edc129e4b414c

165. Paisán-Ruíz C, Jain S, Evans EW, Gilks WP, Simón J, Van Der Brug M, et al. Cloning of the gene containing mutations that cause PARK8-linked Parkinson's disease. Neuron. 2004;44(4):595–600.

166. Ross OA, Soto-Ortolaza AI, Heckman MG, Aasly JO, Abahuni N, Annesi G, et al. Association of LRRK2 exonic variants with susceptibility to Parkinson's disease: A case-control study. Lancet Neurol [Internet]. 2011 Oct 1 [cited 2021 Jan 14];10(10):898–908. Available from: http://www.thelancet.com/article/S1474442211701752/fulltext

167. Tolosa E, Vila M, Klein C, Rascol O. LRRK2 in Parkinson disease: challenges of clinical trials [Internet]. Vol. 16, Nature Reviews Neurology. Nature Research; 2020 [cited 2021 Jan 12]. p. 97–107. Available from: https://www.nature.com/articles/s41582-019-0301-2

168. Di Maio R, Hoffman EK, Rocha EM, Keeney MT, Sanders LH, De Miranda BR, et al. LRRK2 activation in idiopathic Parkinson's disease. Sci Transl Med. 2018;10(451):1–13.

169. Kluss JH, Mamais A, Cookson MR. LRRK2 links genetic and sporadic Parkinson's disease. Biochem Soc Trans. 2019;47(2):651–61.

170. Tolosa E, Vila M, Klein C, Rascol O. LRRK2 in Parkinson disease: challenges of clinical trials. Nat Rev Neurol [Internet]. 2020; Available from: http://www.ncbi.nlm.nih.gov/pubmed/31980808

171. Wauters L, Versées W, Kortholt A. Roco Proteins: GTPases with a Baroque Structure and Mechanism. Int J Mol Sci [Internet]. 2019;20(1):147. Available from: http://www.mdpi.com/1422-0067/20/1/147

172. Sejwal K, Chami M, Rémigy H, Vancraenenbroeck R, Sibran W, Sütterlin R, et al. Cryo-EM analysis of homodimeric full-length LRRK2 and LRRK1 protein complexes. Sci Rep. 2017;7(1):1–12.

173. Guaitoli G, Raimondi F, Gilsbach BK, Gómez-Llorente Y, Deyaert E, Renzi F, et al. Structural model of the dimeric Parkinson's protein LRRK2 reveals a compact architecture involving distant interdomain contacts. Proc Natl Acad Sci [Internet]. 2016;113(30):E4357–66. Available from: http://www.pnas.org/lookup/doi/10.1073/pnas.1523708113
174. Gloeckner CJ, Porras P. Guilt-by-Association – Functional Insights Gained From Studying the LRRK2 Interactome. Front Neurosci. 2020;14(May):1–14.
175. Taymans JM, Vancraenenbroeck R, Ollikainen P, Beilina A, Lobbestael E, de Maeyer M, et al. LRRK2 kinase activity is dependent on LRRK2 gtp binding capacity but independent of LRRK2 GTP binding. PLoS One. 2011;6(8).
176. West AB, Moore DJ, Choi C, Andrabi SA, Li X, Dikeman D, et al. Parkinson's disease-associated mutations in LRRK2 link enhanced GTP-binding and kinase activities to neuronal toxicity. Hum Mol Genet. 2007;16(2):223–32.
177. Yao C, El Khoury R, Wang W, Byrd TA, Pehek EA, Thacker C, et al. LRRK2-mediated neurodegeneration and dysfunction of dopaminergic neurons in a Caenorhabditis elegans model of Parkinson's disease. Neurobiol Dis [Internet]. 2010;40(1):73–81. Available from: http://dx.doi.org/10.1016/j.nbd.2010.04.002
178. Study to Evaluate DNL201 in Subjects With Parkinson's Disease - Full Text View - ClinicalTrials.gov [Internet]. [cited 2021 Jan 14]. Available from: https://clinicaltrials.gov/ct2/show/NCT03710707
179. Study to Evaluate DNL151 in Subjects With Parkinson's Disease - Full Text View - ClinicalTrials.gov [Internet]. [cited 2021 Jan 14]. Available from: https://clinicaltrials.gov/ct2/show/NCT04056689
180. Lewis PA, Greggio E, Beilina A, Jain S, Baker A, Cookson MR. The R1441C mutation of LRRK2 disrupts GTP hydrolysis. Biochem Biophys Res Commun. 2007;357(3):668–71.
181. Li X, Tan YC, Poulose S, Olanow CW, Huang XY, Yue Z. Leucine-rich repeat kinase 2 (LRRK2)/PARK8 possesses GTPase activity that is altered in familial Parkinson's disease R1441C/G mutants. J Neurochem. 2007;103(1):238–47.
182. Li Y, Dunn L, Greggio E, Krumm B, Jackson GS, Cookson MR, et al. The R1441C mutation alters the folding properties of the ROC domain of LRRK2. Biochim Biophys Acta - Mol Basis Dis [Internet]. 2009;1792(12):1194–7. Available from: http://dx.doi.org/10.1016/j.bbadis.2009.09.010
183. Huang X, Wu C, Park Y, Long X, Hoang QQ, Liao J. The Parkinson's disease–associated mutation N1437H impairs conformational dynamics in the G domain of LRRK2. FASEB J [Internet]. 2018;fj.201802031R. Available from: https://www.fasebj.org/doi/10.1096/fj.201802031R
184. Hovemann B, Ziegler AB, Trifunovic A, Nolte H, Krüger M, Moore DJ, et al. Human R1441C LRRK2 regulates the synaptic vesicle proteome and phosphoproteome in a Drosophila model of Parkinson's disease . Hum Mol Genet. 2016;25(24):ddw352.

185. Nguyen APT, Tsika E, Kelly K, Levine N, Chen X, West AB, et al. Dopaminergic neurodegeneration induced by Parkinson's disease-linked G2019S LRRK2 is dependent on kinase and GTPase activity. Proc Natl Acad Sci U S A. 2020;117(29):17296–307.
186. Chen ML, Wu RM. LRRK 2 gene mutations in the pathophysiology of the ROCO domain and therapeutic targets for Parkinson's disease: A review Julie Y.H. Chan. J Biomed Sci. 2018;25(1):1–11.
187. Gloeckner CJ, Kinkl N, Schumacher A, Braun RJ, O'Neill E, Meitinger T, et al. The Parkinson disease causing LRRK2 mutation I2020T is associated with increased kinase activity. Hum Mol Genet. 2006;15(2):223–32.
188. Liu Z, Bryant N, Kumaran R, Beilina A, Abeliovich A, Cookson MR, et al. LRRK2 phosphorylates membrane-bound Rabs and is activated by GTP-bound Rab7L1 to promote recruitment to the trans-Golgi network. Hum Mol Genet. 2018;27(2):385–95.
189. Tsika E, Moore DJ. Contribution of GTPase activity to LRRK2-associated Parkinson disease. Small GTPases. 2013;4(3).
190. Biosa A, Trancikova A, Civiero L, Glauser L, Bubacco L, Greggio E, et al. GTPase activity regulates kinase activity and cellular phenotypes of parkinson's disease-associated LRRK2. Hum Mol Genet [Internet]. 2013 Mar 15 [cited 2021 Jun 23];22(6):1140–56. Available from: https://academic.oup.com/hmg/article/22/6/1140/583376
191. Ramírez MB, Ordóñez AJL, Fdez E, Madero-Pérez J, Gonnelli A, Drouyer M, et al. GTP binding regulates cellular localization of Parkinson's disease-associated LRRK2. Hum Mol Genet. 2017;26(14).
192. Civiero L, Vancraenenbroeck R, Belluzzi E, Beilina A, Lobbestael E, Reyniers L, et al. Biochemical Characterization of Highly Purified Leucine-Rich Repeat Kinases 1 and 2 Demonstrates Formation of Homodimers. PLoS One. 2012;7(8).
193. Greggio E, Zambrano I, Kaganovich A, Beilina A, Taymans JM, Daniëls V, et al. The Parkinson disease-associated leucine-rich repeat kinase 2 (LRRK2) is a dimer that undergoes intramolecular autophosphorylation. J Biol Chem. 2008;283(24):16906–14.
194. Deyaert E, Wauters L, Guaitoli G, Konijnenberg A, Leemans M, Terheyden S, et al. A homologue of the Parkinson's disease-associated protein LRRK2 undergoes a monomer-dimer transition during GTP turnover. Nat Commun [Internet]. 2017;8(1):1–12. Available from: http://dx.doi.org/10.1038/s41467-017-01103-4
195. Berwick DC, Heaton GR, Azeggagh S, Harvey K. LRRK2 Biology from structure to dysfunction: research progresses, but the themes remain the same. [cited 2021 Jul 19]; Available from: https://doi.org/10.1186/s13024-019-0344-2
196. Steger M, Tonelli F, Ito G, Davies P, Trost M, Vetter M, et al. Phosphoproteomics reveals that Parkinson's disease kinase LRRK2 regulates a subset of Rab GTPases. Elife. 2016 Jan 29;5(JANUARY2016).
197. Sheng Z, Zhang S, Bustos D, Kleinheinz T, Le Pichon CE, Dominguez SL, et al. Ser1292

autophosphorylation is an indicator of LRRK2 kinase activity and contributes to the cellular effects of PD mutations. Sci Transl Med [Internet]. 2012 Dec 12 [cited 2021 Jan 12];4(164):164ra161-164ra161. Available from: https://stm.sciencemag.org/content/4/164/164ra161

198. Takanashi M, Funayama M, Matsuura E, Yoshino H, Li Y, Tsuyama S, et al. Isolated nigral degeneration without pathological protein aggregation in autopsied brains with LRRK2 p.R1441H homozygous and heterozygous mutations. Acta Neuropathol Commun. 2018;6(1):105.
199. Guerreiro PS, Gerhardt E, Lopes da Fonseca T, Bähr M, Outeiro TF, Eckermann K. LRRK2 Promotes Tau Accumulation, Aggregation and Release. Mol Neurobiol [Internet]. 2016;53(5):3124–35. Available from: http://dx.doi.org/10.1007/s12035-015-9209-z
200. Rhodes SL, Sinsheimer JS, Bordelon Y, Bronstein JM, Ritz B. Replication of GWAS Associations for GAK and MAPT in Parkinson's Disease. Ann Hum Genet [Internet]. 2010 Nov 1 [cited 2021 Jan 5];75(2):no-no. Available from: http://doi.wiley.com/10.1111/j.1469-1809.2010.00616.x
201. Smith C, Malek N, Grosset K, Cullen B, Gentleman S, Grosset DG. Neuropathology of dementia in patients with Parkinson's disease: A systematic review of autopsy studies [Internet]. Vol. 90, Journal of Neurology, Neurosurgery and Psychiatry. BMJ Publishing Group; 2019 [cited 2021 Jan 14]. p. 1234–43. Available from: http://dx.doi.org/10.1136/jnnp-2019-321111
202. Kim WS, Kagedal K, Halliday GM. Alpha-synuclein biology in Lewy body diseases. Alzheimer's Res Ther. 2014;6(1):1–9.
203. Zhang X, Gao F, Wang D, Li C, Fu Y, He W, et al. Tau pathology in Parkinson's disease. Front Neurol. 2018;9(OCT):1–7.
204. Guerreiro R, Escott-Price V, Darwent L, Parkkinen L, Ansorge O, Hernandez DG, et al. Genome-wide analysis of genetic correlation in dementia with Lewy bodies, Parkinson's and Alzheimer's diseases. Neurobiol Aging. 2016;38:214.e7-214.e10.
205. Stanley B. Prusinera, b, c, 1, Amanda L. Woermana, Daniel A. Mordesd, Joel C. Wattsa, b, 2, Ryan Rampersauda, David B. Berrya, Smita Patela, Abby Oehlere, Jennifer K. Lowef, Stephanie N. Kravitzf, Daniel H. Geschwindf, g, David V. Gliddenh, Glenda M. Hall B. Evidence for α-synuclein prions causing multiple system atrophy in humans with parkinsonism. PNAS. 2015;79(6):5308–17.
206. Lippa CF, Fujiwara H, Mann DMA, Giasson B, Baba M, Schmidt ML, et al. Lewy bodies contain altered α-synuclein in brains of many familial Alzheimer's disease patients with mutations in presenilin and amyloid precursor protein genes. Am J Pathol [Internet]. 1998;153(5):1365–70. Available from: http://dx.doi.org/10.1016/S0002-9440(10)65722-7
207. Bateman RJ, Xiong C, Benzinger TLS, Fagan AM, Goate A, Fox NC, et al. Clinical and Biomarker Changes in Dominantly Inherited Alzheimer's Disease. N Engl J Med [Internet]. 2012;367(9):795–804. Available from: http://www.nejm.org/doi/abs/10.1056/NEJMoa1202753
208. Boxer AL, Yu JT, Golbe LI, Litvan I, Lang AE, Höglinger GU. Advances in progressive supranuclear palsy: new diagnostic criteria, biomarkers, and therapeutic approaches. Lancet

Neurol [Internet]. 2017;16(7):552–63. Available from: http://dx.doi.org/10.1016/S1474-4422(17)30157-6

209. Kara E, Ling H, Pittman AM, Shaw K, de Silva R, Simone R, et al. The MAPT p.A152T variant is a risk factor associated with tauopathies with atypical clinical and neuropathological features. Neurobiol Aging [Internet]. 2012;33(9):2231.e7-2231.e14. Available from: http://dx.doi.org/10.1016/j.neurobiolaging.2012.04.006
210. Lewis PA. Leucine rich repeat kinase 2: a paradigm for pleiotropy. J Physiol. 2019;597(14):3511–21.
211. Jabbari E, Koga S, Valentino RR, Reynolds RH, Ferrari R, Tan MMX, et al. Genetic determinants of survival in progressive supranuclear palsy: a genome-wide association study. Lancet Neurol [Internet]. 2020 Dec [cited 2021 Jan 5];0(0). Available from: https://linkinghub.elsevier.com/retrieve/pii/S147444222030394X
212. Hakimi M, Selvanantham T, Swinton E, Padmore RF, Tong Y, Kabbach G, et al. Parkinson's disease-linked LRRK2 is expressed in circulating and tissue immune cells and upregulated following recognition of microbial structures. J Neural Transm [Internet]. 2011 May 7 [cited 2021 Jan 14];118(5):795–808. Available from: https://link.springer.com/article/10.1007/s00702-011-0653-2
213. Cook DA, Kannarkat GT, Cintron AF, Butkovich LM, Fraser KB, Chang J, et al. LRRK2 levels in immune cells are increased in Parkinson's disease. npj Park Dis [Internet]. 2017;3(1):11. Available from: http://www.nature.com/articles/s41531-017-0010-8
214. Zhang F-R, Huang W, Chen S-M, Sun L-D, Liu H, Li Y, et al. Genomewide Association Study of Leprosy. N Engl J Med. 2009;361(27):2609–18.
215. Hui KY, Fernandez-Hernandez H, Hu J, Schaffner A, Pankratz N, Hsu NY, et al. Functional variants in the LRRK2 gene confer shared effects on risk for Crohn's disease and Parkinson's disease. Sci Transl Med [Internet]. 2018 Jan 10 [cited 2021 Jan 14];10(423):7795. Available from: http://stm.sciencemag.org/
216. Rideout HJ, Chartier-Harlin MC, Fell MJ, Hirst WD, Huntwork-Rodriguez S, Leyns CEG, et al. The Current State-of-the Art of LRRK2-Based Biomarker Assay Development in Parkinson's Disease [Internet]. Vol. 14, Frontiers in Neuroscience. Frontiers Media S.A.; 2020 [cited 2021 May 19]. p. 865. Available from: www.frontiersin.org
217. Kelly K, West AB. Pharmacodynamic Biomarkers for Emerging LRRK2 Therapeutics [Internet]. Vol. 14, Frontiers in Neuroscience. Frontiers Media S.A.; 2020 [cited 2021 May 19]. p. 807. Available from: www.frontiersin.org
218. Lee BD, Shin JH, Vankampen J, Petrucelli L, West AB, Ko HS, et al. Inhibitors of leucine-rich repeat kinase-2 protect against models of Parkinson's disease. Nat Med. 2010;16(9):998–1000.
219. Daher JPL, Volpicelli-Daley LA, Blackburn JP, Moehle MS, West AB. Abrogation of α-synuclein -mediated dopaminergic neurodegeneration in LRRK2-deficient rats. Proc Natl Acad Sci U S A. 2014;111(25):9289–94.

220. Daher JPL, Abdelmotilib HA, Hu X, Volpicelli-Daley LA, Moehle MS, Fraser KB, et al. Leucine-rich repeat kinase 2 (LRRK2) pharmacological inhibition abates α-synuclein gene-induced neurodegeneration. J Biol Chem. 2015;290(32):19433–44.
221. Korecka JA, Thomas R, Hinrich AJ, Moskites AM, Macbain ZK, Hallett PJ, et al. Splice-Switching Antisense Oligonucleotides Reduce LRRK2 Kinase Activity in Human LRRK2 Transgenic Mice. Mol Ther - Nucleic Acids [Internet]. 2020;21(September):623–35. Available from: https://doi.org/10.1016/j.omtn.2020.06.027
222. Zhao HT, John N, Delic V, Ikeda-Lee K, Kim A, Weihofen A, et al. LRRK2 Antisense Oligonucleotides Ameliorate α-Synuclein Inclusion Formation in a Parkinson's Disease Mouse Model. Mol Ther - Nucleic Acids [Internet]. 2017;8(September):508–19. Available from: http://dx.doi.org/10.1016/j.omtn.2017.08.002
223. A Study to Evaluate the Safety, Tolerability, and Pharmacokinetics of BIIB094 in Adults With Parkinson's Disease - Full Text View - ClinicalTrials.gov [Internet]. [cited 2021 Jan 14]. Available from: https://www.clinicaltrials.gov/ct2/show/NCT03976349
224. Chen I. An antisense oligonucleotide splicing modulator to treat spinal muscular atrophy. Nat Res 2020. 2019;
225. Lewis PA. The function of ROCO proteins in health and disease. Biol Cell. 2009;101(3):183–91.
226. Marín I. The Parkinson disease gene LRRK2: Evolutionary and structural insights. Mol Biol Evol. 2006;23(12):2423–33.
227. Marín I. Ancient origin of the parkinson disease gene LRRK2. J Mol Evol. 2008;67(1):41–50.
228. Force, A. Lynch, M. Pickett, F, B. Amores, A. Yan, Y. Postlethwait J. Preservation of Duplicte Genes by Complementary, Degenerative Mutations. Genetics. 1999;151:1531–45.
229. Sämann J, Hegermann J, von Gromoff E, Eimer S, Baumeister R, Schmidt E. Caenorhabditits elegans LRK-1 and PINK-1 act antagonistically in stress response and neurite outgrowth. J Biol Chem. 2009;284(24):16482–91.
230. Sakaguchi-Nakashima A, Meir JY, Jin Y, Matsumoto K, Hisamoto N. LRK-1, a C. elegans PARK8-Related Kinase, Regulates Axonal-Dendritic Polarity of SV Proteins. Curr Biol. 2007;17(7):592–8.
231. Reyniers L, Del Giudice MG, Civiero L, Belluzzi E, Lobbestael E, Beilina A, et al. Differential protein protein interactions of LRRK1 and LRRK2 indicate roles in distinct cellular signaling pathways. J Neurochem. 2014;131(2):239–50.
232. Tomkins JE, Dihanich S, Beilina A, Ferrari R, Ilacqua N, Cookson MR, et al. Comparative Protein Interaction Network Analysis Identifies Shared and Distinct Functions for the Human ROCO Proteins. Proteomics. 2018;18(10):1–12.
233. Rice P, Longden L, Bleasby A. EMBOSS: The European Molecular Biology Open Software Suite [Internet]. Vol. 16, Trends in Genetics. Elsevier Ltd; 2000 [cited 2021 Jan 27]. p. 276–7. Available from: http://www.cell.com/article/S0168952500020242/fulltext
234. EMBOSS Stretcher < Pairwise Sequence Alignment < EMBL-EBI [Internet]. [cited 2021 Jun 22].

Available from: https://www.ebi.ac.uk/Tools/psa/emboss_stretcher/

235. Malik AU, Karapetsas A, Nirujogi RS, Mathea S, Chatterjee D, Pal P, et al. Deciphering the LRRK code: LRRK1 and LRRK2 phosphorylate distinct Rab proteins and are regulated by diverse mechanisms. Biochem J [Internet]. 2021 Jan 18 [cited 2021 Feb 1]; Available from: http://portlandpress.com/biochemj/article-pdf/doi/10.1042/BCJ20200937/902248/bcj-2020-0937.pdf
236. Iida A, Xing W, Docx MKF, Nakashima T, Wang Z, Kimizuka M, et al. Identification of biallelic LRRK1 mutations in osteosclerotic metaphyseal dysplasia and evidence for locus heterogeneity. J Med Genet [Internet]. 2016 Aug 1 [cited 2021 Feb 1];53(8):568–74. Available from: https://pubmed.ncbi.nlm.nih.gov/27055475/
237. Miryounesi M, Nikfar A, Changi-Ashtiani M, Shahrooei M, Dinmohammadi H, Shahani T, et al. A novel homozygous LRRK1 stop gain mutation in a patient suspected with osteosclerotic metaphyseal dysplasia. Ann Hum Genet [Internet]. 2020 Jan 1 [cited 2021 May 21];84(1):102–6. Available from: https://onlinelibrary.wiley.com/doi/full/10.1111/ahg.12352
238. Howaldt A, Hennig AF, Rolvien T, Rössler U, Stelzer N, Knaus A, et al. Adult Osteosclerotic Metaphyseal Dysplasia With Progressive Osteonecrosis of the Jaws and Abnormal Bone Resorption Pattern Due to a LRRK1 Splice Site Mutation. J Bone Miner Res [Internet]. 2020 Jul 1 [cited 2021 Feb 1];35(7):1322–32. Available from: https://pubmed.ncbi.nlm.nih.gov/32119750/
239. Kamath RS, Fraser AG, Dong Y, Poulin G, Durbin R, Gotta M, et al. Systematic functional analysis of the Caenorhabditis elegans genome using RNAi. Nature. 2003;421(6920):231–7.
240. Blauwendraat C, Reed X, Kia DA, Gan-Or Z, Lesage S, Pihlstrøm L, et al. Frequency of loss of function variants in LRRK2 in Parkinson disease. JAMA Neurol [Internet]. 2018 Nov 1 [cited 2021 Jan 14];75(11):1416–22. Available from: /pmc/articles/PMC6248108/?report=abstract
241. Whiffin N, Armean IM, Kleinman A, Marshall JL, Minikel E V, Goodrich JK, et al. The effect of LRRK2 loss-of-function variants in humans. Nat Med [Internet]. 2020; Available from: http://www.ncbi.nlm.nih.gov/pubmed/32461697
242. Fuji RN, Flagella M, Baca M, Baptista MAS, Brodbeck J, Chan BK, et al. Effect of selective LRRK2 kinase inhibition on nonhuman primate lung. Sci Transl Med [Internet]. 2015 Feb 4 [cited 2021 Jan 14];7(273):273ra15. Available from: https://stm.sciencemag.org/content/7/273/273ra15
243. Reyniers L, Del Giudice MG, Civiero L, Belluzzi E, Lobbestael E, Beilina A, et al. Differential protein protein interactions of LRRK1 and LRRK2 indicate roles in distinct cellular signaling pathways. J Neurochem. 2014;131(2):239–50.
244. Saha S, Guillily MD, Ferree A, Lanceta J, Chan D, Ghosh J, et al. LRRK2 modulates vulnerability to mitochondrial dysfunction in Caenorhabditis elegans. J Neurosci. 2009;29(29):9210–8.
245. Schaffner A, Li X, Gomez-Llorente Y, Leandrou E, Memou A, Clemente N, et al. Vitamin B 12 modulates Parkinson's disease LRRK2 kinase activity through allosteric regulation and confers neuroprotection. Cell Res [Internet]. 2019;29(4):313–29. Available from: http://dx.doi.org/10.1038/s41422-019-0153-8

246. Langston RG, Rudenko IN, Kumaran R, Hauser DN, Kaganovich A, Ponce LB, et al. Differences in Stability, Activity and Mutation Effects Between Human and Mouse Leucine-Rich Repeat Kinase 2. Neurochem Res [Internet]. 2019;44(6):1446–59. Available from: http://dx.doi.org/10.1007/s11064-018-2650-4
247. Bieri G, Brahic M, Bousset L, Couthouis J, Kramer NJ, Ma R, et al. LRRK2 modifies α-syn pathology and spread in mouse models and human neurons. Acta Neuropathol [Internet]. 2019;137(6):961–80. Available from: https://doi.org/10.1007/s00401-019-01995-0
248. Nguyen APT, Daniel G, Valdés P, Islam MS, Schneider BL, Moore DJ. G2019S LRRK2 enhances the neuronal transmission of tau in the mouse brain. Hum Mol Genet. 2018;27(1):120–34.
249. Kim H, Perentis RJ, Caldwell GA, Caldwell KA. Gene-by-environment interactions that disrupt mitochondrial homeostasis cause neurodegeneration in C. elegans Parkinson's models. Cell Death Dis [Internet]. 2018;9(5). Available from: http://dx.doi.org/10.1038/s41419-018-0619-5
250. Smith LL, Ryde IT, Hartman JH, Romersi RF, Markovich Z, Meyer JN. Strengths and limitations of morphological and behavioral analyses in detecting dopaminergic deficiency in Caenorhabditis elegans. Neurotoxicology [Internet]. 2019;74(June):209–20. Available from: https://doi.org/10.1016/j.neuro.2019.07.002
251. Wolozin B, Saha S, Guillily M, Ferree A, Riley M. Investigating convergent actions of genes linked to familial Parkinson's disease. Neurodegener Dis. 2008;5(3–4):182–5.
252. Deng X, Dzamko N, Prescott A, Davies P, Liu Q, Yang Q, et al. Characterization of a selective inhibitor of the Parkinson's disease kinase LRRK2. Nat Chem Biol [Internet]. 2011 Mar 6 [cited 2021 Jan 27];7(4):203–5. Available from: https://www.nature.com/articles/nchembio.538
253. Yao C, Johnson WM, Gao Y, Wang W, Zhang J, Deak M, et al. Kinase inhibitors arrest neurodegeneration in cell and C. elegans models of LRRK2 toxicity. Hum Mol Genet. 2013;22(2):328–44.
254. MacLeod DA, Rhinn H, Kuwahara T, Zolin A, Di Paolo G, MacCabe BD, et al. RAB7L1 Interacts with LRRK2 to Modify Intraneuronal Protein Sorting and Parkinson's Disease Risk. Neuron [Internet]. 2013;77(3):425–39. Available from: http://dx.doi.org/10.1016/j.neuron.2012.11.033
255. Choudhary B, Kamak M, Ratnakaran N, Kumar J, Awasthi A, Li C, et al. UNC-16/JIP3 regulates early events in synaptic vesicle protein trafficking via LRK-1/LRRK2 and AP complexes. Murphy CT, editor. PLOS Genet [Internet]. 2017 Nov 16 [cited 2021 Jan 12];13(11):e1007100. Available from: https://dx.plos.org/10.1371/journal.pgen.1007100
256. CA B, J G, D D, GG C, ELF H. Increased LRRK2 kinase activity alters neuronal autophagy by disrupting the axonal transport of autophagosomes. Curr Biol [Internet]. 2021 May 24 [cited 2021 Jul 15];31(10):2140-2154.e6. Available from: https://pubmed.ncbi.nlm.nih.gov/33765413/
257. Heaton GR, Landeck N, Mamais A, Nalls MA, Nixon-Abell J, Kumaran R, et al. Sequential screening nominates the Parkinson's disease associated kinase LRRK2 as a regulator of Clathrin-mediated endocytosis. Neurobiol Dis [Internet]. 2020;141(April):104948. Available from:

https://doi.org/10.1016/j.nbd.2020.104948

258. Vidyadhara DJ, Lee JE, Chandra SS. Role of the endolysosomal system in Parkinson's disease. J Neurochem. 2019;150(5):487–506.

259. Connor-Robson N, Booth H, Martin JG, Gao B, Li K, Doig N, et al. An integrated transcriptomics and proteomics analysis reveals functional endocytic dysregulation caused by mutations in LRRK2. Neurobiol Dis [Internet]. 2019;127(March):512–26. Available from: https://doi.org/10.1016/j.nbd.2019.04.005

260. Medeiros AT, Soll LG, Tessari I, Bubacco L, Morgan JR. A-Synuclein Dimers Impair Vesicle Fission During Clathrin-Mediated Synaptic Vesicle Recycling. Front Cell Neurosci. 2017;11(December):1–15.

261. Kuboyama T, Lee YA, Nishiko H, Tohda C. Inhibition of clathrin-mediated endocytosis prevents amyloid β-induced axonal damage. Neurobiol Aging [Internet]. 2015;36(5):1808–19. Available from: http://dx.doi.org/10.1016/j.neurobiolaging.2015.02.005

262. Gorenberg EL, Chandra SS. The role of co-chaperones in synaptic proteostasis and neurodegenerative disease. Front Neurosci. 2017;11(MAY):1–16.

263. Marchetti B, Tirolo C, L'Episcopo F, Caniglia S, Testa N, Smith JA, et al. Parkinson's disease, aging and adult neurogenesis: Wnt/β-catenin signalling as the key to unlock the mystery of endogenous brain repair [Internet]. Vol. 19, Aging Cell. Blackwell Publishing Ltd; 2020 [cited 2021 Jan 12]. Available from: https://pubmed.ncbi.nlm.nih.gov/32050297/

264. Onishi K, Tian R, Feng B, Liu Y, Wang J, Li Y, et al. LRRK2 mediates axon development by regulating Frizzled3 phosphorylation and growth cone–growth cone communication. Proc Natl Acad Sci U S A. 2020;117(30):18037–48.

265. Salašová A, Yokota C, Potěšil D, Zdráhal Z, Bryja V, Arenas E. A proteomic analysis of LRRK2 binding partners reveals interactions with multiple signaling components of the WNT/PCP pathway. Mol Neurodegener. 2017;12(1):1–19.

266. Sancho RM, Law BMH, Harvey K. Mutations in the LRRK2 Roc-COR tandem domain link Parkinson's disease to Wnt signalling pathways. Hum Mol Genet. 2009;18(20):3955–68.

267. Harterink M, Kim D h., Middelkoop TC, Doan TD, van Oudenaarden A, Korswagen HC. Neuroblast migration along the anteroposterior axis of C. elegans is controlled by opposing gradients of Wnts and a secreted Frizzled-related protein. Development [Internet]. 2011;138(14):2915–24. Available from: http://dev.biologists.org/cgi/doi/10.1242/dev.064733

268. Dusonchet J, Li H, Guillily M, Liu M, Stafa K, Derada Troletti C, et al. A Parkinson's disease gene regulatory network identifies the signaling protein RGS2 as a modulator of LRRK2 activity and neuronal toxicity. Hum Mol Genet. 2014;23(18):4887–905.

269. Fukuzono T, Pastuhov SI, Fukushima O, Li C, Hattori A, Iemura S ichiro, et al. Chaperone complex BAG2-HSC70 regulates localization of Caenorhabditis elegans leucine-rich repeat kinase LRK-1 to the Golgi. Genes to Cells. 2016;21(4):311–24.

270. Tomkins JE, Ferrari R, Vavouraki N, Hardy J, Hardy J, Hardy J, et al. PINOT: An intuitive

resource for integrating protein-protein interactions. Cell Commun Signal. 2020;18(1):1–11.
271. Liu Z, Bryant N, Kumaran R, Beilina A, Abeliovich A, Cookson MR, et al. LRRK2 phosphorylates membrane-bound Rabs and is activated by GTP-bound Rab7L1 to promote recruitment to the trans-Golgi network. Hum Mol Genet. 2018;27(2):385–95.
272. Purlyte E, Dhekne HS, Sarhan AR, Gomez R, Lis P, Wightman M, et al. Rab29 activation of the Parkinson's disease-associated LRRK2 kinase. EMBO J. 2018;37(1):1–18.
273. Seol W, Nam D, Son I. Rab GTPases as physiological substrates of LRRK2 kinase. Vol. 28, Experimental Neurobiology. Korean Society for Neurodegenerative Disease; 2019. p. 134–45.
274. Beilina A, Rudenko IN, Kaganovich A, Civiero L, Chau H, Kalia SK, et al. Unbiased screen for interactors of leucine-rich repeat kinase 2 supports a common pathway for sporadic and familial Parkinson disease. Proc Natl Acad Sci U S A. 2014;111(7):2626–31.
275. Madero-Pérez J, Fernández B, Lara Ordóñez AJ, Fdez E, Lobbestael E, Baekelandt V, et al. RAB7L1-mediated relocalization of LRRK2 to the golgi complex causes centrosomal deficits via RAB8A. Front Mol Neurosci. 2018;11(November):1–19.
276. Eguchi T, Kuwahara T, Sakurai M, Komori T, Fujimoto T, Ito G, et al. LRRK2 and its substrate Rab GTPases are sequentially targeted onto stressed lysosomes and maintain their homeostasis. Proc Natl Acad Sci U S A. 2018;115(39):E9115–24.
277. Fujimoto T, Kuwahara T, Eguchi T, Sakurai M, Komori T, Iwatsubo T. Parkinson's disease-associated mutant LRRK2 phosphorylates Rab7L1 and modifies trans-Golgi morphology. Biochem Biophys Res Commun [Internet]. 2017;495(2):1708–15. Available from: https://doi.org/10.1016/j.bbrc.2017.12.024
278. Kalogeropulou AF, Freemantle JB, Lis P, Vides EG, Polinski NK, Alessi DR. Endogenous Rab29 does not impact basal or stimulated LRRK2 pathway activity. Biochem J. 2020;0:4397–423.
279. Morris C, Foster OK, Handa S, Peloza K, Voss L, Somhegyi H, et al. Function and regulation of the Caenorhabditis elegans Rab32 family member GLO-1 in lysosome-related organelle biogenesis. Vol. 14, PLoS Genetics. 2018. 1–36 p.
280. Tucci A, Nalls MA, Houlden H, Revesz T, Singleton AB, Wood NW, et al. Genetic variability at the PARK16 locus. Eur J Hum Genet. 2010;18(12):1356–9.
281. Vetter IR, Wittinghofer A. The guanine nucleotide-binding switch in three dimensions. Science (80-). 2001;294(5545):1299–304.
282. Kuwahara T, Inoue K, D'Agati VD, Fujimoto T, Eguchi T, Saha S, et al. LRRK2 and RAB7L1 coordinately regulate axonal morphology and lysosome integrity in diverse cellular contexts. Sci Rep. 2016;6(March):1–12.
283. Aoki Y, Manzano R, Lee Y, Dafinca R, Aoki M, Douglas AGL, et al. C9orf72 and RAB7L1 regulate vesicle trafficking in amyotrophic lateral sclerosis and frontotemporal dementia. Brain. 2017;140(4):887–97.
284. Balendra R, Isaacs AM. C9orf72-mediated ALS and FTD: multiple pathways to disease. Nat Rev Neurol [Internet]. 2018;14(9):544–58. Available from: http://dx.doi.org/10.1038/s41582-018-

0047-2

285. Ferrari R, Hernandez DG, Nalls MA, Rohrer JD, Ramasamy A, Kwok JBJ, et al. Frontotemporal dementia and its subtypes: A genome-wide association study. Lancet Neurol. 2014;13(7):686–99.
286. Haile Y, Deng X, Ortiz-Sandoval C, Tahbaz N, Janowicz A, Lu JQ, et al. Rab32 connects ER stress to mitochondrial defects in multiple sclerosis. J Neuroinflammation [Internet]. 2017;14(1):1–13. Available from: http://dx.doi.org/10.1186/s12974-016-0788-z
287. Steger M, Diez F, Dhekne HS, Lis P, Nirujogi RS, Karayel O, et al. Systematic proteomic analysis of LRRK2-mediated rab GTPase phosphorylation establishes a connection to ciliogenesis. Elife. 2017;6(i):1–22.
288. Bultema JJ, Di Pietro SM. Cell type-specific Rab32 and Rab38 cooperate with the ubiquitous lysosome biogenesis machinery to synthesize specialized lysosome-related organelles. Small GTPases. 2013;4(1):16–21.
289. Hermann, Greg J. Schroeder, Lena K. Hieb, Caroline A. Kershner, Aaron M. Rabbitts, Beverly M. Fonarev, Paul. Grant, Barth D. Priess JR. Genetic Analysis of Lysosomal Trafficking in Caenorhabditis elegans. Mol Biol Cell. 2005;16(November):3273–88.
290. Grill B, Bienvenut W V., Brown HM, Ackley BD, Quadroni M, Jin Y. C. elegans RPM-1 Regulates Axon Termination and Synaptogenesis through the Rab GEF GLO-4 and the Rab GTPase GLO-1. Neuron. 2007;55(4):587–601.
291. Solano-Collado V, Rofe A, Spanò S. Rab32 restriction of intracellular bacterial pathogens. Small GTPases. 2018;9(3):216–23.
292. Wang N, Wang Z, Wang C, Fu X, Yu G, Yue Z, et al. Prediction of leprosy in the Chinese population based on a weighted genetic risk score. PLoS Negl Trop Dis. 2018;12(9):1–12.
293. Herbst S, Gutierrez MG. LRRK2 in Infection: Friend or Foe? ACS Infect Dis. 2019;5(6):809–15.
294. Saunders-Pullman R, Mirelman A, Alcalay RN, Wang C, Ortega RA, Raymond D, et al. Progression in the LRRK2-Asssociated Parkinson disease population. JAMA Neurol. 2018;75(3):312–9.
295. Fijarczyk A, Babik W. Detecting balancing selection in genomes: Limits and prospects. Mol Ecol. 2015;24(14):3529–45.
296. McGrath E, Waschbüsch D, Baker BM, Khan AR. LRRK2 binds to the Rab32 subfamily in a GTP-dependent manner via its armadillo domain. Small GTPases [Internet]. 2019;00(00):1–14. Available from: https://doi.org/10.1080/21541248.2019.1666623
297. Waschbüsch D, Hübel N, Ossendorf E, Lobbestael E, Baekelandt V, Lindsay AJ, et al. Rab32 interacts with SNX6 and affects retromer-dependent Golgi trafficking. PLoS One. 2019;14(1):1–18.
298. Dues DJ, Moore DJ. LRRK2 and Protein Aggregation in Parkinson's Disease: Insights From Animal Models. Front Neurosci. 2020;14(July).
299. Liu G, Aliaga L, Cai H. α-synuclein, LRRK2 and their interplay in Parkinson's disease. Future Neurol. 2012;7(2):145–53.

300. Bae E-J, Kim D-K, Kim C, Mante M, Adame A, Rockenstein E, et al. LRRK2 kinase regulates α-synuclein propagation via RAB35 phosphorylation. Nat Commun [Internet]. 2018;9(1):3465. Available from: http://www.nature.com/articles/s41467-018-05958-z
301. Goedert M, Jakes R, Spillantini MG. The Synucleinopathies: Twenty Years on. J Parkinsons Dis. 2017;7(s1):S53–71.
302. Chia SJ, Tan EK, Chao YX. Historical perspective: Models of Parkinson's disease. Int J Mol Sci. 2020;21(7):1–14.
303. Sharma S, Trivedi S, Pandey T, Ranjan S, Trivedi M, Pandey R. Wedelolactone Mitigates Parkinsonism Via Alleviating Oxidative Stress and Mitochondrial Dysfunction Through NRF2/SKN-1. Mol Neurobiol. 2021;58(1):65–77.
304. Pandey T, Sammi SR, Nooreen Z, Mishra A, Ahmad A, Bhatta RS, et al. Anti-ageing and anti-Parkinsonian effects of natural flavonol, tambulin from Zanthoxyllum aramatum promotes longevity in Caenorhabditis elegans. Exp Gerontol [Internet]. 2019;120(February):50–61. Available from: https://doi.org/10.1016/j.exger.2019.02.016
305. Sharma S, Bandopadhyay R, Lashley T, Renton AEM, Kingsbury AE, Kumaran R, et al. LRRK2 expression in idiopathic and G2019S positive Parkinson's disease subjects: A morphological and quantitative study. Neuropathol Appl Neurobiol. 2011;37(7):777–90.
306. McDermott JB, Aamodt S, Aamodt E. ptl-1, a Caenorhabditis elegans gene whose products are homologous to the τ microtubule-associated proteins. Biochemistry. 1996;35(29):9415–23.
307. Goedert M, Baur CP, Ahringer J, Jakes R, Hasegawa M, Spillantini MG, et al. PTL-1, a microtubule-associated protein with tau-like repeats from the nematode Caenorhabditis elegans. J Cell Sci. 1996;109(11):2661–72.
308. Chew YL, Fan X, Götz J, Nicholas HR. PTL-1 regulates neuronal integrity and lifespan in C. elegans. J Cell Sci. 2013;126(9):2079–91.
309. Pir GJ, Choudhary B, Mandelkow E, Mandelkow EM. Tau mutant A152T, a risk factor for FTD/PSP, induces neuronal dysfunction and reduced lifespan independently of aggregation in a C. elegans Tauopathy model. Mol Neurodegener [Internet]. 2016;11(1):1–21. Available from: http://dx.doi.org/10.1186/s13024-016-0096-1
310. Coppola G, Chinnathambi S, Lee JJY, Dombroski BA, Baker MC, Soto-ortolaza AI, et al. Evidence for a role of the rare p.A152T variant in mapt in increasing the risk for FTD-spectrum and Alzheimer's diseases. Hum Mol Genet. 2012;21(15):3500–12.
311. Miyasaka T, Shinzaki Y, Yoshimura S, Yoshina S, Kage-Nakadai E, Mitani S, et al. Imbalanced expression of tau and tubulin induces neuronal dysfunction in C. elegans models of tauopathy. Front Neurosci. 2018;12(JUN):1–13.
312. Butler VJ, Salazar DA, Soriano-Castell D, Alves-Ferreira M, Dennissen FJA, Vohra M, et al. Tau/MAPT disease-associated variant A152T alters tau function and toxicity via impaired retrograde axonal transport. Hum Mol Genet. 2019;28(9):1498–514.
313. Macleod DA, Rhinn H, Kuwahara T, Zolin A, Paolo G Di, Mccabe BD, et al. NIH Public Access.

2014;77(3):425–39.

314. Li YI, Wong G, Humphrey J, Raj T. Prioritizing Parkinson's Disease genes using population-scale transcriptomic data. bioRxiv [Internet]. 2017;(2019):1–10. Available from: http://biorxiv.org/content/early/2017/12/08/231001.abstract

315. Zavodszky E, Seaman MNJ, Moreau K, Jimenez-Sanchez M, Breusegem SY, Harbour ME, et al. Mutation in VPS35 associated with Parkinson's disease impairs WASH complex association and inhibits autophagy. Nat Commun [Internet]. 2014 May 13 [cited 2021 Apr 15];5. Available from: https://pubmed.ncbi.nlm.nih.gov/24819384/

316. McGough IJ, Steinberg F, Jia D, Barbuti PA, McMillan KJ, Heesom KJ, et al. Retromer binding to FAM21 and the WASH complex is perturbed by the Parkinson disease-linked VPS35(D620N) mutation. Curr Biol. 2014;24(14):1670–6.

317. Smolyn J. The first characterization of the WASH complex in C. elegans endocytic recycling. 2020;

318. Raudvere U, Kolberg L, Kuzmin I, Arak T, Adler P, Peterson H, et al. g:Profiler: a web server for functional enrichment analysis and conversions of gene lists (2019 update). Nucleic Acids Res [Internet]. 2019 Jul 2 [cited 2022 May 11];47(W1):W191–8. Available from: https://academic.oup.com/nar/article/47/W1/W191/5486750

319. Varadi M, Anyango S, Deshpande M, Nair S, Natassia C, Yordanova G, et al. AlphaFold Protein Structure Database: massively expanding the structural coverage of protein-sequence space with high-accuracy models. Nucleic Acids Res [Internet]. 2021 Nov 17 [cited 2022 Jan 3]; Available from: https://academic.oup.com/nar/advance-article/doi/10.1093/nar/gkab1061/6430488

320. Jumper J, Evans R, Pritzel A, Green T, Figurnov M, Ronneberger O, et al. Highly accurate protein structure prediction with AlphaFold. Nat 2021 5967873 [Internet]. 2021 Jul 15 [cited 2022 Jan 3];596(7873):583–9. Available from: https://www.nature.com/articles/s41586-021-03819-2

321. Ren J, Wen L, Gao X, Jin C, Xue Y, Yao X. DOG 1.0: Illustrator of protein domain structures [Internet]. Vol. 19, Cell Research. Nature Publishing Group; 2009 [cited 2021 Jan 27]. p. 271–3. Available from: www.cell-research.com

322. Stroustrup N, Ulmschneider BE, Nash ZM, López-Moyado IF, Apfeld J, Fontana W. The caenorhabditis elegans lifespan machine. Nat Methods [Internet]. 2013 Jul 12 [cited 2021 Feb 8];10(7):665–70. Available from: http://www.lifespanmachine.org/

323. Javer A, Currie M, Lee CW, Hokanson J, Li K, Martineau CN, et al. An open-source platform for analyzing and sharing worm-behavior data. Nat Methods [Internet]. 2018;15(9):645–6. Available from: http://dx.doi.org/10.1038/s41592-018-0112-1

324. Wu KY, Tang FL, Lee D, Zhao Y, Song H, Zhu XJ, et al. Ependymal Vps35 promotes ependymal cell differentiation and survival, suppresses microglial activation, and prevents neonatal hydrocephalus. J Neurosci [Internet]. 2020 May 6 [cited 2021 Mar 16];40(19):3862–79. Available from: https://pubmed.ncbi.nlm.nih.gov/32291328/

325. Dhekne HS, Yanatori I, Gomez RC, Tonelli F, Diez F, Schüle B, et al. A pathway for parkinson's

disease LRRK2 kinase to block primary cilia and sonic hedgehog signaling in the brain. Elife. 2018;7:1–26.

326. Sobu Y, Wawro PS, Dhekne HS, Yeshaw WM, Pfeffer SR. Pathogenic LRRK2 regulates ciliation probability upstream of tau tubulin kinase 2 via Rab10 and RILPL1 proteins. Proc Natl Acad Sci [Internet]. 2021 Mar 9 [cited 2021 Mar 16];118(10):e2005894118. Available from: http://www.pnas.org/lookup/doi/10.1073/pnas.2005894118
327. O'Rourke EJ, Soukas AA, Carr CE, Ruvkun G. C. elegans Major Fats Are Stored in Vesicles Distinct from Lysosome-Related Organelles. Cell Metab [Internet]. 2009 Nov 4 [cited 2021 Dec 22];10(5):430. Available from: /pmc/articles/PMC2921818/
328. Guha S, Caldwell G, Kapahi P. Morphological Analysis of Dopaminergic Neurons with Age Using Caenorhabditis elegans GFP Reporter Strains. BIO-PROTOCOL. 2018;8(9).
329. Zheng SQ, Ding AJ, Li GP, Wu GS, Luo HR. Drug Absorption Efficiency in Caenorhbditis elegans Delivered by Different Methods. PLoS One. 2013;8(2):1–9.
330. Laranjeiro R, Harinath G, Hewitt JE, Hartman JH, Royal MA, Meyer JN, et al. Swim exercise in Caenorhabditis elegans extends neuromuscular and gut healthspan, enhances learning ability, and protects against neurodegeneration. Proc Natl Acad Sci U S A. 2019;116(47):23829–39.
331. Seidel HS, Smith TA, Evans JK, Stamper JQ, Mast TG, Kimble J. C. elegans germ cells divide and differentiate in a folded tissue. Dev Biol. 2018 Oct 1;442(1):173–87.
332. Pazdernik N, Schedl T. Introduction to Germ Cell Development in C. elegans. Adv Exp Med Biol [Internet]. 2013 [cited 2022 Jan 10];757:1. Available from: /pmc/articles/PMC3781019/
333. Wider C, Skipper L, Solida A, Brown L, Farrer M, Dickson D, et al. Autosomal dominant dopa-responsive parkinsonism in a multigenerational Swiss family. Park Relat Disord [Internet]. 2008 Aug 1 [cited 2021 Jan 5];14(6):465–70. Available from: http://www.prd-journal.com/article/S1353802007002507/fulltext
334. Salam S, Ansari A, Amon S, Rezai P, Selvaganapathy PR, Mishra RK, et al. A microfluidic phenotype analysis system reveals function of sensory and dopaminergic neuron signaling in C. elegans electrotactic swimming behavior . Worm. 2013;2(2):e24558.
335. Senchuk MM, Van Raamsdonk JM, Moore DJ. Multiple genetic pathways regulating lifespan extension are neuroprotective in a G2019S LRRK2 nematode model of Parkinson's disease. Neurobiol Dis. 2021 Jan 1;151:105267.
336. Rollins JA, Howard AC, Dobbins SK, Washburn EH, Rogers AN. Assessing Health Span in Caenorhabditis elegans: Lessons From Short-Lived Mutants. Journals Gerontol Ser A [Internet]. 2017 Apr 1 [cited 2022 Jan 10];72(4):473–80. Available from: https://academic.oup.com/biomedgerontology/article/72/4/473/2966371
337. Omura DT, Clark DA, Samuel ADT, Horvitz HR. Dopamine signaling is essential for precise rates of locomotion by C. elegans. PLoS One. 2012;7(6).
338. Connolly NMC, Theurey P, Adam-Vizi V, Bazan NG, Bernardi P, Bolaños JP, et al. Guidelines on experimental methods to assess mitochondrial dysfunction in cellular models of

neurodegenerative diseases [Internet]. Vol. 25, Cell Death and Differentiation. Springer US; 2018. 542–572 p. Available from: http://dx.doi.org/10.1038/s41418-017-0020-4

339. Kaplan OI, Doroquez DB, Cevik S, Bowie R V., Clarke L, Sanders AAWM, et al. ENDOCYTOSIS GENES FACILITATE PROTEIN AND MEMBRANE TRANSPORT IN C. ELEGANS SENSORY CILIA. Curr Biol [Internet]. 2012 Mar 20 [cited 2021 Sep 16];22(6):451. Available from: /pmc/articles/PMC3678972/
340. Lapierre LR, Silvestrini MJ, Nuñez L, Ames K, Wong S, Le TT, et al. Autophagy genes are required for normal lipid levels in C. elegans View supplementary material. Autophagy [Internet]. 2013;9:278–86. Available from: https://www.tandfonline.com/action/journalInformation?journalCode=kaup20http://dx.doi.org/10.4161/auto.22930
341. Wu S, Lei L, Song Y, Liu M, Lu S, Lou D, et al. Mutation of hop-1 and pink-1 attenuates vulnerability of neurotoxicity in C. elegans: the role of mitochondria-associated membrane proteins in Parkinsonism. Exp Neurol [Internet]. 2018;309(February):67–78. Available from: https://doi.org/10.1016/j.expneurol.2018.07.018
342. Ved R, Saha S, Westlund B, Perier C, Burnam L, Sluder A, et al. Similar patterns of mitochondrial vulnerability and rescue induced by genetic modification of α-synuclein, parkin, and DJ-1 in Caenorhabditis elegans. J Biol Chem. 2005;280(52):42655–68.
343. Salama M, Arias Carrion O. Natural toxins implicated in the development of Parkinson's disease. Ther Adv Neurol Disord. 2011;4(6):361–73.
344. Sancho RM, Law BMH, Harvey K. Mutations in the LRRK2 Roc-COR tandem domain link Parkinson's disease to Wnt signalling pathways. Hum Mol Genet. 2009;18(20):3955–68.
345. Ishihara L, Warren L, Gibson R, Amouri R, Lesage S, Dürr A, et al. Clinical features of Parkinson disease patients with homozygous leucine-rich repeat kinase 2 G2019S mutations. Arch Neurol. 2006;63(9):1250–4.
346. K. Haugarvoll, R. Rademakers, J.M. Kachergus, K. Nuytemans, MSc, O.A. Ross, J.M. Gibson, E.-K. Tan, C. Gaig, E. Tolosa, S. Goldwurm, M. Guidi, G. Riboldazzi, L. Brown, U. Walter, R. Benecke, D. Berg, T. Gasser, J. Theuns, P. Pals, P. Cras, P. Paul De Deyn and ZKW. LRRK2 R1441C Parkinsonism is Clinically Similar to Sporadic Parkinson disease. Neurology. 2008;70(1602):1456–60.
347. Estrada AA, Chan BK, Baker-Glenn C, Beresford A, Burdick DJ, Chambers M, et al. Discovery of highly potent, selective, and brain-penetrant aminopyrazole Leucine-rich repeat kinase 2 (LRRK2) small molecule inhibitors. J Med Chem. 2014;57(3):921–36.
348. Lapierre LR, Gelino S, Meléndez A, Hansen M. Autophagy and lipid metabolism coordinately modulate life span in germline-less C. elegans. Curr Biol. 2011 Sep 27;21(18):1507–14.
349. Gallegos ME, Balakrishnan S, Chandramouli P, Arora S, Azameera A, Babushekar A, et al. The C. elegans Rab Family: Identification, Classification and Toolkit Construction. PLoS One [Internet]. 2012 Nov 21 [cited 2022 Jan 5];7(11). Available from: /pmc/articles/PMC3504004/

350. Kadgien CA, Kamesh A, Milnerwood AJ. Endosomal traffic and glutamate synapse activity are increased in VPS35 D620N mutant knock-in mouse neurons, and resistant to LRRK2 kinase inhibition. Mol Brain [Internet]. 2021 Dec 1 [cited 2021 Dec 10];14(1). Available from: https://pubmed.ncbi.nlm.nih.gov/34530877/
351. Alcalay RN, Levy OA, Waters CC, Fahn S, Ford B, Kuo SH, et al. Glucocerebrosidase activity in Parkinson's disease with and without GBA mutations. Brain. 2015;138(9):2648–58.
352. Ferrazza R, Cogo S, Melrose H, Bubacco L, Greggio E, Guella G, et al. LRRK2 deficiency impacts ceramide metabolism in brain. Biochem Biophys Res Commun [Internet]. 2016;478(3):1141–6. Available from: http://dx.doi.org/10.1016/j.bbrc.2016.08.082
353. Riboldi, G M, Di Fonzo, A B. GBA, Gaucher Disease, and Parkinson's Disease: From Genetic to Clinic to New Therapeutic Approaches. Cells. 2019;8(364):16.
354. Cullen PJ, Steinberg F. To degrade or not to degrade: mechanisms and significance of endocytic recycling. Nat Rev Mol Cell Biol [Internet]. 2018;19(11):679–96. Available from: http://dx.doi.org/10.1038/s41580-018-0053-7
355. Hansen M, Rubinsztein DC, Walker DW. Autophagy as a promoter of longevity: insights from model organisms. Nat Rev Mol Cell Biol [Internet]. 2018;19(9):579–93. Available from: http://dx.doi.org/10.1038/s41580-018-0033-y
356. Nalls MA, Blauwendraat C, Vallerga CL, Heilbron K, Bandres-Ciga S, Chang D, et al. Identification of novel risk loci, causal insights, and heritable risk for Parkinson's disease: a meta-analysis of genome-wide association studies. Lancet Neurol. 2019;18(12):1091–102.
357. Taylor M, Alessi DR. Advances in elucidating the function of leucine-rich repeat protein kinase-2 in normal cells and Parkinson's disease. Curr Opin Cell Biol [Internet]. 2020;63:102–13. Available from: https://doi.org/10.1016/j.ceb.2020.01.001
358. Erb ML, Moore DJ. LRRK2 and the Endolysosomal System in Parkinson's Disease. J Parkinsons Dis. 2020;10(4):1271–91.
359. Tulgren ED, Baker ST, Rapp L, Gurney AM, Grill B. PPM-1, a PP2Cα/β phosphatase, regulates axon termination and synapse formation in caenorhabditis elegans. Genetics. 2011;189(4):1297–307.
360. Roh HC, Collier S, Guthrie J, Robertson JD, Kornfeld K. Lysosome-related organelles in intestinal cells are a zinc storage site in C. elegans. Cell Metab [Internet]. 2012;15(1):88–99. Available from: http://dx.doi.org/10.1016/j.cmet.2011.12.003
361. Mata IF, Jang Y, Kim CH, Hanna DS, Dorschner MO, Samii A, et al. The RAB39B p.G192R mutation causes X-linked dominant Parkinson's disease. Mol Neurodegener [Internet]. 2015;10(1):4–11. Available from: http://dx.doi.org/10.1186/s13024-015-0045-4
362. Lorenowicz MJ, Macurkova M, Harterink M, Middelkoop TC, de Groot R, Betist MC, et al. Inhibition of late endosomal maturation restores Wnt secretion in Caenorhabditis elegans vps-29 retromer mutants. Cell Signal [Internet]. 2014;26(1):19–31. Available from: http://dx.doi.org/10.1016/j.cellsig.2013.09.013

363. Takenaka M, Inoue H, Takeshima A, Kakura T, Hori T. C. elegans Rassf homolog, rasf-1, is functionally associated with rab-39 Rab GTPase in oxidative stress response. Genes Cells [Internet]. 2013 Mar [cited 2022 Jan 5];18(3):203–10. Available from: https://pubmed.ncbi.nlm.nih.gov/23294242/

364. Carosi JM, Hein LK, van den Hurk M, Adams R, Milky B, Singh S, et al. Retromer regulates the lysosomal clearance of MAPT/tau. Autophagy [Internet]. 2020 [cited 2021 Apr 15]; Available from: https://pubmed.ncbi.nlm.nih.gov/32960680/

365. Hanss Z, Larsen SB, Antony P, Mencke P, Massart F, Jarazo J, et al. Mitochondrial and Clearance Impairment in p.D620N VPS35 Patient-Derived Neurons. Mov Disord [Internet]. 2020 Mar 1 [cited 2021 Apr 15];36(3). Available from: https://pubmed.ncbi.nlm.nih.gov/33142012/

366. Vazquez-Sanchez S, Bobeldijk S, Dekker MP, Van Keimpema L, Van Weering JRT. VPS35 depletion does not impair presynaptic structure and function. Sci Rep [Internet]. 2018;8(1):1–12. Available from: http://dx.doi.org/10.1038/s41598-018-20448-4

367. Tang F-L, Yin D-M, Tang B, Erion JR, Mei L, Ye J, et al. VPS35 in Dopamine Neurons Is Required for Endosome-to-Golgi Retrieval of Lamp2a, a Receptor of Chaperone-Mediated Autophagy That Is Critical for -Synuclein Degradation and Prevention of Pathogenesis of Parkinson's Disease. J Neurosci. 2015;35(29):10613–28.

368. Malik BR, Godena VK, Whitworth AJ. VPS35 pathogenic mutations confer no dominant toxicity but partial loss of function in Drosophila and genetically interact with parkin. Hum Mol Genet. 2015;24(21):6106–17.

369. Prasad BC, Clark SG. Wnt signaling establishes anteroposterior neuronal polarity and requires retromer in C. elegans. Development. 2006;133(9):1757–66.

370. Zhang Q, Wu X, Chen P, Liu L, Xin N, Tian Y, et al. The Mitochondrial Unfolded Protein Response Is Mediated Cell-Non-autonomously by Retromer-Dependent Wnt Signaling. Cell [Internet]. 2018;174(4):870-883.e17. Available from: https://doi.org/10.1016/j.cell.2018.06.029

371. di Domenico A, Carola G, Calatayud C, Pons-Espinal M, Muñoz JP, Richaud-Patin Y, et al. Patient-Specific iPSC-Derived Astrocytes Contribute to Non-Cell-Autonomous Neurodegeneration in Parkinson's Disease. Stem Cell Reports [Internet]. 2019 Feb 12 [cited 2021 Dec 15];12(2):213–29. Available from: http://www.cell.com/article/S2213671118305307/fulltext

372. Jin LF, Li JS. Generation of genetically modified mice using CRISPR/Cas9 and haploid embryonic stem cell systems. Zool Res [Internet]. 2016 Jul 18 [cited 2021 Dec 13];37(4):205. Available from: /pmc/articles/PMC4975102/

373. Edgar AJ, Polak JM. Human Homologues of Yeast Vacuolar Protein Sorting 29 and 35. Biochem Biophys Res Commun. 2000 Nov 2;277(3):622–30.

374. Vinagre-Aragón A, Campo-Caballero D, Mondragón-Rezola E, Pardina-Vilella L, Hernandez Eguiazu H, Gorostidi A, et al. A More Homogeneous Phenotype in Parkinson's Disease Related to R1441G Mutation in the LRRK2 Gene. Front Neurol [Internet]. 2021 Mar 2 [cited 2022 Jan 11];12. Available from: https://pubmed.ncbi.nlm.nih.gov/33763016/

375. Edgely M. Genetic balancers. WormBook [Internet]. 2006;(1995):1–32. Available from: http://www.wormbook.org/chapters/www_geneticbalancers/geneticbalancers.html
376. Wen L, Tang FL, Hong Y, Luo SW, Wang CL, He W, et al. VPS35 haploinsufficiency increases Alzheimer's disease neuropathology. J Cell Biol [Internet]. 2011 Nov [cited 2021 Dec 14];195(5):765. Available from: /pmc/articles/PMC3257571/
377. Jiang M, Tu HT, Zhang K, Zhang W, Yu WP, Xu J, et al. Impaired neurogenesis in the hippocampus of an adult VPS35 mutant mouse model of Parkinson's disease through interaction with APP. Neurobiol Dis [Internet]. 2021 Jun 1 [cited 2021 Dec 8];153. Available from: https://pubmed.ncbi.nlm.nih.gov/33636388/
378. Kaminsky EB, Kaul V, Paschall J, Church DM, Bunke B, Kunig D, et al. An evidence-based approach to establish the functional and clinical significance of copy number variants in intellectual and developmental disabilities. Genet Med [Internet]. 2011 Sep 1 [cited 2021 Dec 13];13(9):777–84. Available from: http://www.gimjournal.org/article/S1098360021036418/fulltext
379. Collins KM, Bode A, Fernandez RW, Tanis JE, Brewer JC, Creamer MS, et al. Activity of the C. elegans egg-laying behavior circuit is controlled by competing activation and feedback inhibition. Elife. 2016 Nov 16;5(NOVEMBER2016).
380. Oranth A, Schultheis C, Tolstenkov O, Erbguth K, Nagpal J, Hain D, et al. Food Sensation Modulates Locomotion by Dopamine and Neuropeptide Signaling in a Distributed Neuronal Network. Neuron [Internet]. 2018;100(6):1414-1428.e10. Available from: https://doi.org/10.1016/j.neuron.2018.10.024
381. Maulik M, Mitra S, Bult-Ito A, Taylor BE, Vayndorf EM. Behavioral phenotyping and pathological indicators of Parkinson's disease in C. elegans models. Front Genet. 2017;8(JUN):1–21.
382. Niu M, Zhao F, Bondelid K, Siedlak SL, Torres S, Fujioka H, et al. VPS35 D620N knockin mice recapitulate cardinal features of Parkinson's disease. Aging Cell [Internet]. 2021 May 1 [cited 2021 Dec 8];20(5). Available from: https://pubmed.ncbi.nlm.nih.gov/33745227/
383. Xun Z, Sowell RA, Kaufman TC, Clemmer DE. Proteomics of a Drosophila Model of Parkinson ' s Disease. Nat Rev Neurol. 2000;404(March):47405.
384. Kim DK, Lim HS, Kawasaki I, Shim YH, Vaikath NN, El-Agnaf OMA, et al. Anti-aging treatments slow propagation of synucleinopathy by restoring lysosomal function. Autophagy [Internet]. 2016;12(10):1849–63. Available from: http://dx.doi.org/10.1080/15548627.2016.1207014
385. Qiao L, Hamamichi S, Caldwell KA, Caldwell GA, Yacoubian TA, Wilson S, et al. Lysosomal enzyme cathepsin D protects against alpha-synuclein aggregation and toxicity. Mol Brain. 2008;1(Cl):17.
386. Cooper JF, Dues DJ, Spielbauer KK, Machiela E, Senchuk MM, Van Raamsdonk JM. Delaying aging is neuroprotective in Parkinson's disease: A genetic analysis in C. Elegans models.

Parkinsons Dis [Internet]. 2015;1(May). Available from: http://dx.doi.org/10.1038/npjparkd.2015.22

387. Goya ME, Xue F, Sampedro-Torres-Quevedo C, Arnaouteli S, Riquelme-Dominguez L, Romanowski A, et al. Probiotic Bacillus subtilis Protects against α-Synuclein Aggregation in C. elegans. Cell Rep [Internet]. 2020 Jan 14 [cited 2021 Dec 9];30(2):367-380.e7. Available from: https://pubmed.ncbi.nlm.nih.gov/31940482/
388. Seegobin SP, Heaton GR, Liang D, Choi I, Blanca Ramirez M, Tang B, et al. Progress in LRRK2-Associated Parkinson's Disease Animal Models. Front Neurosci. 2020;14(July).
389. Abe T, Kuwahara T. Targeting of Lysosomal Pathway Genes for Parkinson's Disease Modification: Insights From Cellular and Animal Models. Front Neurol. 2021 Jun 14;12:978.
390. Xilouri M, Brekk OR, Stefanis L. Autophagy and Alpha-Synuclein: Relevance to Parkinson's Disease and Related Synucleopathies. Mov Disord. 2016;31(2):178–92.
391. Stout Jr RF, Verkhratsky A, Parpura V, Kuhn B, Liu P, Dominick TP. CELLULAR NEUROSCIENCE Caenorhabditis elegans glia modulate neuronal activity and behavior INTRODUCTION: A BRIEF ON EVOLUTION OF NEUROGLIA. 2014; Available from: www.frontiersin.org
392. Shao Z, Watanabe S, Christensen R, Jorgensen EM, Colón-Ramos DA. Synapse location during growth depends on glia location. Cell. 2013;154(2):337.
393. Shaham S. Glial Development and Function in the Nervous System of Caenorhabditis elegans. Cold Spring Harb Perspect Biol [Internet]. 2015 [cited 2021 Dec 9];7(4). Available from: /pmc/articles/PMC4382739/
394. Reynolds RH, Botía J, Nalls MA, Hardy J, Gagliano Taliun SA, Ryten M. Moving beyond neurons: the role of cell type-specific gene regulation in Parkinson's disease heritability. npj Park Dis. 2019;5(1).
395. Arenas E. Unleashing the neuronal side of astrocyte cells. Nature [Internet]. 2020;582(25 June):489–90. Available from: http://www.nature.com/articles/d41586-020-01817-4
396. Stefanis L, Emmanouilidou E, Pantazopoulou M, Kirik D, Vekrellis K, Tofaris GK. How is alpha-synuclein cleared from the cell? J Neurochem. 2019;150(5):577–90.
397. Bono K, Hara-Miyauchi C, Sumi S, Oka H, Iguchi Y, Okano HJ. Endosomal dysfunction in iPSC-derived neural cells from Parkinson's disease patients with VPS35 D620N. Mol Brain [Internet]. 2020 Oct 8 [cited 2021 Dec 15];13(1):1–15. Available from: https://molecularbrain.biomedcentral.com/articles/10.1186/s13041-020-00675-5
398. Zavodszky E, Seaman MNJ, Moreau K, Jimenez-Sanchez M, Breusegem SY, Harbour ME, et al. Mutation in VPS35 associated with Parkinson's disease impairs WASH complex association and inhibits autophagy. Nat Commun 2014 51 [Internet]. 2014 May 13 [cited 2021 Dec 10];5(1):1–16. Available from: https://www.nature.com/articles/ncomms4828
399. Zavodszky E, Seaman MNJ, Moreau K, Jimenez-Sanchez M, Breusegem SY, Harbour ME, et al. Mutation in VPS35 associated with Parkinson's disease impairs WASH complex association and

inhibits autophagy. Nat Commun. 2014;5(May):1–16.

400. Cogo S, Manzoni C, Lewis PA, Greggio E. Leucine-rich repeat kinase 2 and lysosomal dyshomeostasis in Parkinson disease. J Neurochem. 2020;152(3):273–83.
401. Albanese F, Novello S, Morari M. Autophagy and LRRK2 in the Aging Brain. Front Neurosci. 2019;13(December):1–23.
402. Shu L, Zhang Y, Pan H, Xu Q, Guo J, Tang B, et al. Clinical heterogeneity among lrrk2variants in Parkinson's disease: A Meta-analysis. Front Aging Neurosci. 2018;10(SEP):1–10.
403. Chittoor-Vinod VG, Nichols RJ, Schüle B. Genetic and Environmental Factors Influence the Pleomorphy of LRRK2 Parkinsonism. Int J Mol Sci [Internet]. 2021 Jan 21 [cited 2021 Feb 2];22(3):1045. Available from: https://www.mdpi.com/1422-0067/22/3/1045
404. Manzoni C. The LRRK2–macroautophagy axis and its relevance to Parkinson's disease. Biochem Soc Trans [Internet]. 2017;45(1):155–62. Available from: http://biochemsoctrans.org/lookup/doi/10.1042/BST20160265
405. Fire A, Xu S, Montgomery MK, Kostas SA, Driver SE, Mello CC. Potent and specific genetic interference by double-stranded RNA in Caenorhabditis elegans. Nat 1998 3916669 [Internet]. 1998 Feb 19 [cited 2021 Jul 27];391(6669):806–11. Available from: https://www.nature.com/articles/35888
406. Waterman MS, Eggert M. A new algorithm for best subsequence alignments with application to tRNA-rRNA comparisons. J Mol Biol. 1987 Oct 20;197(4):723–8.
407. Needleman SB, Wunsch CD. A general method applicable to the search for similarities in the amino acid sequence of two proteins. J Mol Biol. 1970 Mar 28;48(3):443–53.

Appendix

3.1 *C. elegans* VPS-35 shows conservation with human VPS35 *in silico*

3.1.3 Protein sequence Alignments between human VPS35 and C. elegans VPS-35
Full annotated sequence alignment between human VPS35 and C. elegans VPS-35. EBI pairwise sequence alignment. Parameters: Tool-Emboss_Stretcher. Gap Open-12. Gap Extend- 2.

```
Armadillo fold
J domain
PD mutation

HumanVPS35        11 EQEKLLDEAIQAVKVQSFQMKRCLDKNKLMDALKHASNMLGELRTSMLSP     60
                     :|||.||::|:.||.:||:|||||||.|.|||||||..||.|:||:.|||
C.elVPS-35        10 DQEKFLDQSIRVVKAESFEMKRCLDKGKTMDALKHALQMLNEMRTAELSP     59

EMBOSS_001        61 KSYYELYMAISDELHYLEVYLTDEFAKG-RKVADLYELVQYAGNIIPRLY    109
                     |.||.|||....||..|||.|..|:|:. .|:.:|||.||||..||||||
EMBOSS_001        60 KFYYRLYMDSMHELQCLEVNLVQEYAQEPAKLGNLYECVQYASAIIPRLY    109

EMBOSS_001       110 LLITVGVVYVKSFPQSRKDILKDLVEMCRGVQHPLRGLFLRNYLLQCTRN    159
                     ||:|:|.|::|....|||:|||||||||||||||||||||:||||:
EMBOSS_001       110 LLVTIGGVFIKCGLGSRKEILKDLVEMCRGVQHPLRGLFLRNYLMQCTRS    159

EMBOSS_001       160 ILPD----------------EGEPTDEETTGDISDSMDFVLLNFAEMNKL    193
                     :|||                 :|.|..:...|.:.|::||||:||||||||
EMBOSS_001       160 VLPDFPETEEMLVAHNDNLSKGTPKLKPRDGTVDDTIDFVLINFAEMNKL    209

EMBOSS_001       194 WVRMQHQGHSRDREKRERERQELRILVGTNLVRLSQLEGVNVERYKQIVL    243
                     ||||||||.|:::||||::|.|||||||||||||:|||.:..|.|.:.||
EMBOSS_001       210 WVRMQHQGPSKEKEKREKDRMELRILVGTNLVRLAQLEALTEEMYVKDVL    259

EMBOSS_001       244 TGILEQVVNCRDALAQEYLMECIIQVFPDEFHLQTLNPFLRACAELHQNV    293
                     ..||||:|:|||.::|||||||:||||.|:|||.||..||.||.:|.|:|
EMBOSS_001       260 PSILEQIVSCRDPISQEYLMECVIQVFADDFHLATLTEFLNACGQLQQDV    309

EMBOSS_001       294 NVKNIIIALIDRLALFAHR-EDGPGIPADIKLFDIFSQQVATVIQSRQDM    342
                     |:|.::|||:|||||:... .:|...|..::||:|||:|..|:|::|.||
EMBOSS_001       310 NIKILLIALVDRLALYTTSYNEGQPAPTKMQLFEIFSEQATTLIKNRPDM    359

EMBOSS_001       343 PSEDVVSLQVSLINLAMKCYPDRVDYVDKVLETTVEIFNKLNLEHIATSS    392
                     |.:|:|:|.|||::||:||||||.||.:...:...:..:..:..|....
EMBOSS_001       360 PLDDIVALHVSLVSLAVKCYPDRQDYANMTFQGLRQVIEEKGVTDIEAFG    409

EMBOSS_001       393 AVSKELTRLLKIPVDTYNNILTVLKLKHFHPLFEYFDYESRKSMSCYVLS    442
                     .|.:|||:||.||:|.|.|:|.:.:|..:..:..||||..:.:::::.|::.
EMBOSS_001       410 KVGRELTKLLNIPIDEYKNVLRLSQLPEYIKVMNYFDYRGQCNIASYMIQ    459

EMBOSS_001       443 NVLDYNTEIVSQDQVDSIMNLVSTLIQDQPDQPVEDPDPEDFADEQSLVG    492
                     |:|:..|...:||.|||..:|:|:|::||..|..:..:.|:|||||:||.
EMBOSS_001       460 NMLEEETVFRNQDDVDSAFSLISSLLKDQEKQSSDSHETEEFADEQNLVA    509

EMBOSS_001       493 RFIHLLRSEDPDQQYLILNTARKHFGAGGNQRIRFTLPPLVFAAYQLAFR    542
                     |.:||:|::|.|.|:|:||:|||..|.||..|:|:||||::|..|:|..:
EMBOSS_001       510 RLLHLIRADDVDSQFLLLNSARKTLGEGGRHRLRYTLPPIIFELYRLVLQ    559

EMBOSS_001       543 YKENSKVDDKWEKKCQKIFSFAHQTISALIK-AELAELPLRLFLQGALAA    591
                     :.:....||||:.|.:|:|..|..||.||:. |||||||::|:|.||:.|
EMBOSS_001       560 FSDMKDEDDKWDAKIRKMFVCAMGTIGALVSTAELAELPMKLYLNGAITA    609

EMBOSS_001       592 GEIGFENHETVAYEFMSQAFSLYEDEISDSKAQLAAITLIIGTFERMKCF    641
```

```
                    ..:.||::.||.|||:|:|.|:.||::.||:.::..:.|.:||..:....
EMBOSS_001      610 DRVPFEDNHTVVYEFVSKALSILEDDVVDSRDRVRCLHLTVGTLLKTTHL    659

EMBOSS_001      642 SEENHEPLRTQCALAASKLLKKPDQGRAVSTCAHLFWSGRNTDKNGEELH    691
                    .|||.:||..|..|||:|:.|||||.|::.|.|.|:|.|:..:.|||::.
EMBOSS_001      660 PEENWQPLANQTVLAAAKMFKKPDQVRSLVTVAALYWHGQTLETNGEKMK    709

EMBOSS_001      692 GGKRVMECLKKALKIANQCMDPSLQVQLFIEILNRYIYFYEKENDAVTIQ    741
                    .||:|::.|:||.|||.:|::|.:|.||||::|:.|.|:||.....|.:.
EMBOSS_001      710 NGKKVVDILRKAAKIARECLEPLVQQQLFIQLLSAYTYYYEDNCSEVNVD    759

EMBOSS_001      742 VLNQLIQKIREDLPNLESSEETEQINKHFHNTLEHLRLRR    781
                    .:.:||.:.:::...|:.|.|.:.:.|.....:..|:|.:
EMBOSS_001      760 HIEELIARTQDNAVQLDVSAEADSLEKQLGEAIRRLQLAK    799
```

3.4 Progeny Count of *vps-35[D638N]* illustrates that *vps-35[D638N]* homozygosity induces larval arrest.

3.4.1. *vps-35* mutant progeny count

Full descriptive statistics for fertility assay per genotype per day

Genotype	Progeny	Days Elapsed							
		1		2		3		4	
		M	SD	M	SD	M	SD	M	SD
Wildtype	Eggs	57.25	5.97	45	30.28	9.75	7.14	5.5	4.20
	Adults	68.75	27.16	50.5	64.12	9.75	8.30	0.75	0.96
vps-35[D638N] heterozygotes	Eggs	17.6	6.35	20	15.31	11.6	6.35	2	2
	Adults	23.6	16.21	39.25	44.27	10	12.25	1.25	1.89
vps-35[D638N] homozygotes	Eggs	0	-	14	-	0	-	0	-
	Adults	0	-	0	-	0	-	0	-
vps-35 deletion	Eggs	2.4	1.67	1	1	2.25	2.63	0	0
	Adults	1.2	1.64	0.8	1.79	2.23	2.63	0	0

Descriptive dataset of total progeny count.

Genotype	Progeny Lifestage	Total Progeny Count		Significance compared to wildtype	
		M	SD	P Value	Significance
Wildtype	Eggs	117.25	43.94		
	Adults	130	92.55		
vps-35[D638N] heterozygotes	Eggs	55.89	20.42	0.2233	ns
	Adults	70.111	44.91	0.7524	ns
vps-35[D638N] homozygotes	Eggs	14	0		
	Adults	0	0		
vps-35 deletion	Eggs	4.8	2.39	0.0352	*
	Adults	3.8	4.76	0.1719	ns

vps-35[D638N] heterozygotes show a different rate of egg laying compared to the wildtype

The data described in 3.3.1, has been mapped to visualise the rate of egg laying of the *vps-35* mutants, compared to the wildtype and how this translates into larval development of eggs laid

throughout the lifespan. The wildtype control shows the highest egg count in day 1 of adulthood (A), with a substantial reduction between day 2 and 3, whereas the *vps-35[D638N]* heterozygote shows a substantially reduced egg count on day 1 compared to the wildtype, with a slower rate of egg laying decrease and similar fertility to the wildtype in day 3 and 4. Studying the adult development of eggs laid on specific days (B) also sheds insight into the viability of eggs laid on specific days. In the *vps-35[D638N]* mutant, more adults develop from eggs laid on day 2.

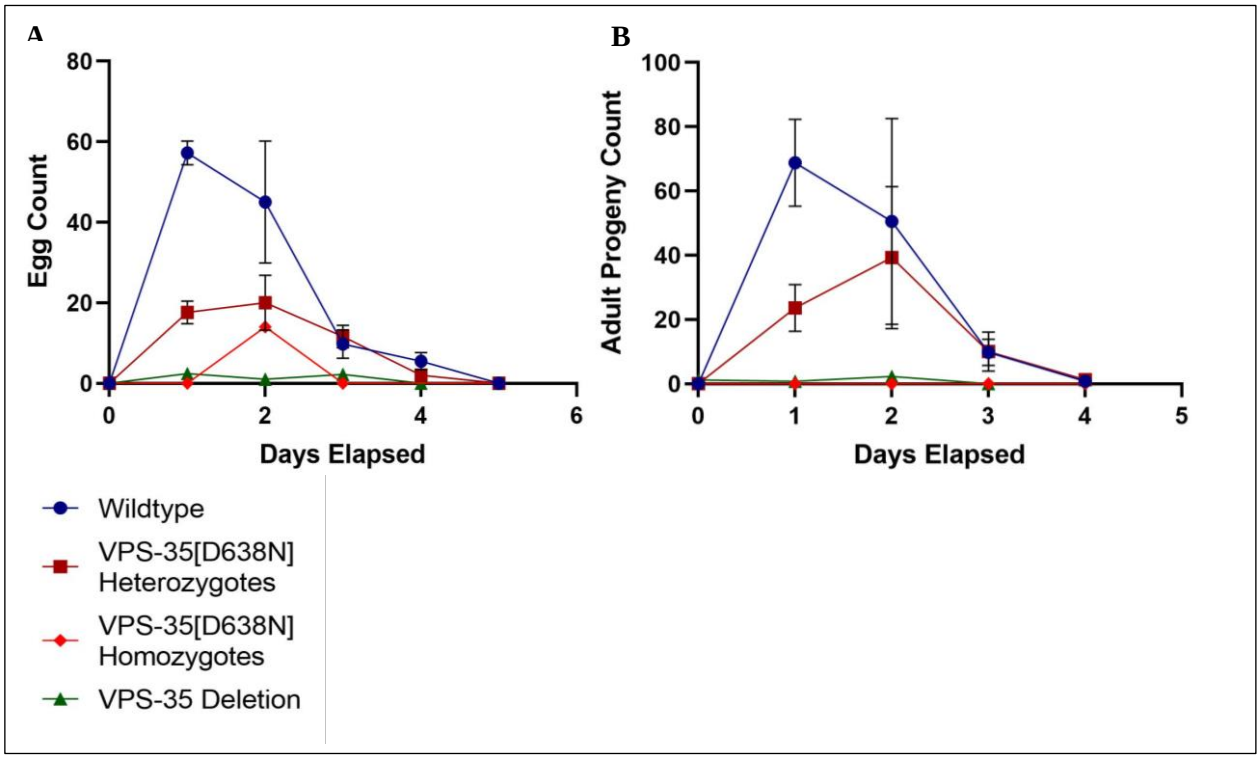

3.4.2 Optimised *vps-35* mutant progeny count

Descriptive statistics for progeny count in genotype, days elapsed and egg/adult progeny.

Genotype	Progeny	Days Elapsed									
		1		2		3		4		5	
		M	SD	M	SD	M	SD	M	SD	M	SD
Wildtype	Eggs	49.2	15.25	77.4	18.01	68.8	17.51	30.4	11.80	8.8	6.53
	Adults	58.4	18.72	144.4	14.17	93.8	35.12	11.2	10.5	0.2	0.45
Unbalanced *vps-35[D638N]* heterozygotes	Eggs	13.2	7.53	34.4	19.54	20.2	11.39	5.75	5.5	0.5	1
	Adults	23	19.42	66.8	48.96	30	18.99	1.75	1.71	0	0
Balanced *vps-35[D638N]* heterozygotes	Eggs	21.2	8.29	40.4	20.85	19	18.14	14	7.17	1.25	0.96
	Adults	15.8	11.99	63.4	48.17	88.2	58.12	28.75	20.76	4.33	5.77
vps-35 deletion	Eggs	0.6	0.55	0.2	0.45	0	0	0	0	0	0
	Adults	0	0	1.4	3.13	1.5	2.12	0	0	0	0

Full descriptive dataset from preliminary total progeny count, as shown in "Figure 17- Optimised Total progeny count of selected vps-35 mutants."

Genotype	Progeny Lifestage	Total Progeny Count	Significance compared to wildtype

		M	SD	P Value	Significance
Wildtype	Eggs	234.6	38.12		
	Adults	308.0	24.16		
Unbalanced *vps-35[D638N]* heterozygotes	Eggs	72.8	41.46	0.0101	*
	Adults	121.200	77.75	0.0477	*
Balanced *vps-35[D638N]* homozygotes	Eggs	92.8	43.52	0.0325	*
	Adults	193	97.76	0.2658	NS
vps-35 deletion	Eggs	0.8	0.83	0.0006	***
	Adults	2	4.47	<0.0001	****

Balanced *vps-35[D638N]* heterozygotes show altered egg laying patterns compared to wildtype

Contrary to 3.4.1, unbalanced *vps-35[D638N]* heterozygotes show a similar egg laying profile to the wildtype, with egg laying and developed adults from these eggs exhibiting a peak in day 2 of adulthood (A). However, the *vps-35[D638N]* balanced line exhibits a peak in progeny development to adults in day 3 of adulthood (B), with an enhanced number of adult progeny in day 4 of adulthood compared to the wildtype. This suggests that presence of *vps-35[D638N]* heterozygosity in progeny may induce some delay in larval development and progeny viability, with the most viable eggs laid later in the reproductive cycle.

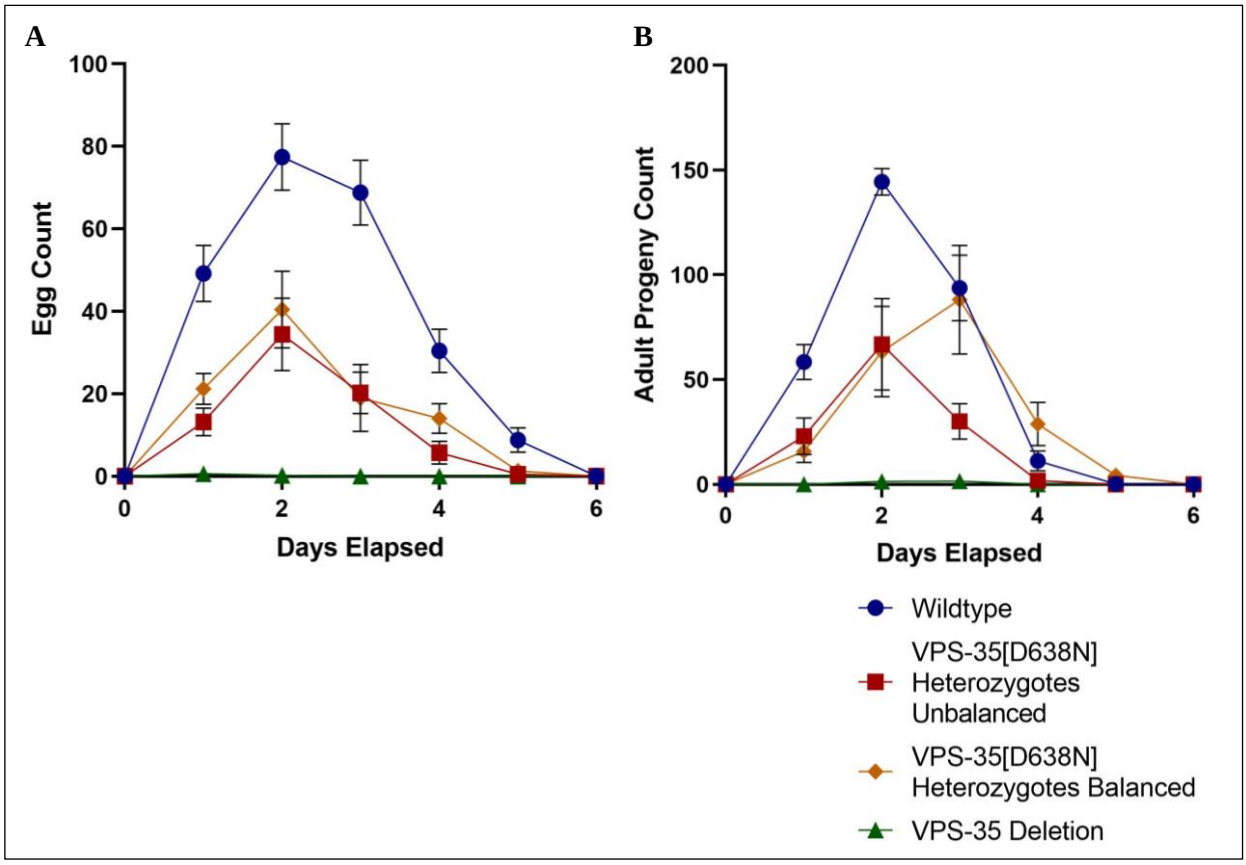

3.5 Characterisation of the *vps-35* mutant germline in utero

3.5.3 Egg number *in utero* is not significantly different between wildtype and *vps-35* mutants

Full descriptive statistics for egg number *in utero*

Genotype	*In utero* egg count		
	M	SD	N
Wildtype	11.9	2.83	20
vps-35 deletion	15.21	6.34	14
vps-35[D638N] heterozygotes	11.96	2.07	26

Brown-Forsyth and Welch ANOVA undertaken, for multiple comparisons.

Comparison	P value	Significant
Wildtype vs *vps-35* deletion	0.224	NS
Wildtype vs *vps-35[D638N]* heterozygotes	0.999	NS
vps-35 deletion vs *vps-35[D638N]* heterozygotes	0.216	NS

3.6 *vps-35* deletion mutants show a significantly reduced life and health span

3.6.1 *vps-35* deletion shows a significantly reduced lifespan

Full Descriptive Statistics for figure 22- Lifespan of *vps-35[D638N]* heterozygote and *vps-35* deletion populations

Genotype		Median Survival			
Wildtype		15			
vps-35 deletion		7			
vps-35[D638N] heterozygote unbalanced		15			
vps-35[D638N] heterozygote balanced		16			
Days Elapsed	Number of Surviving *C. elegans* per genotype				
	Wildtype	VPS-35 Deletion	VPS-35[D638N] Heterozygotes Unbalanced	VPS-35[D638N] Heterozygotes Balanced	
0	50	48	62	53	
1	50	48	62	53	
2	50	48	62	53	
3	50	48	62	53	
4	50	48	62	53	
5	50	46	62	52	
6	50	46	62	52	
7	50	32	61	50	
8	50	32	61	50	
9	49	20	58	46	
10	46	10	54	43	
11	44	8	51	43	
12	41	4	50	39	
13	39	2	44	38	
14	39	0	44	38	
15	31	0	39	35	
16	24	0	30	28	
17	18	0	24	23	
18	15	0	12	12	
19	10	0	7	10	
20	8	0	3	6	
21	8	0	3	6	
22	3	0	1	5	
23	3	0	0	5	
24	1	0	0	4	
25	0	0	0	4	
26	0	0	0	2	
27	0	0	0	0	

Statistical analysis undertaken through Mantel-Cox test of curve comparison, wildtype compared to *vps-35* mutant

Genotype	P Value	Significant	Median Survival	Ratio
vps-35 deletion	<0.0001	****	7	2.143
vps-35[D638N] heterozygote unbalanced	0.2218	NS	15	1.000
vps-35[D638N] heterozygote balanced	0.7667	NS	16	0.9375

Replicate of lifespan assay descriptive statistics

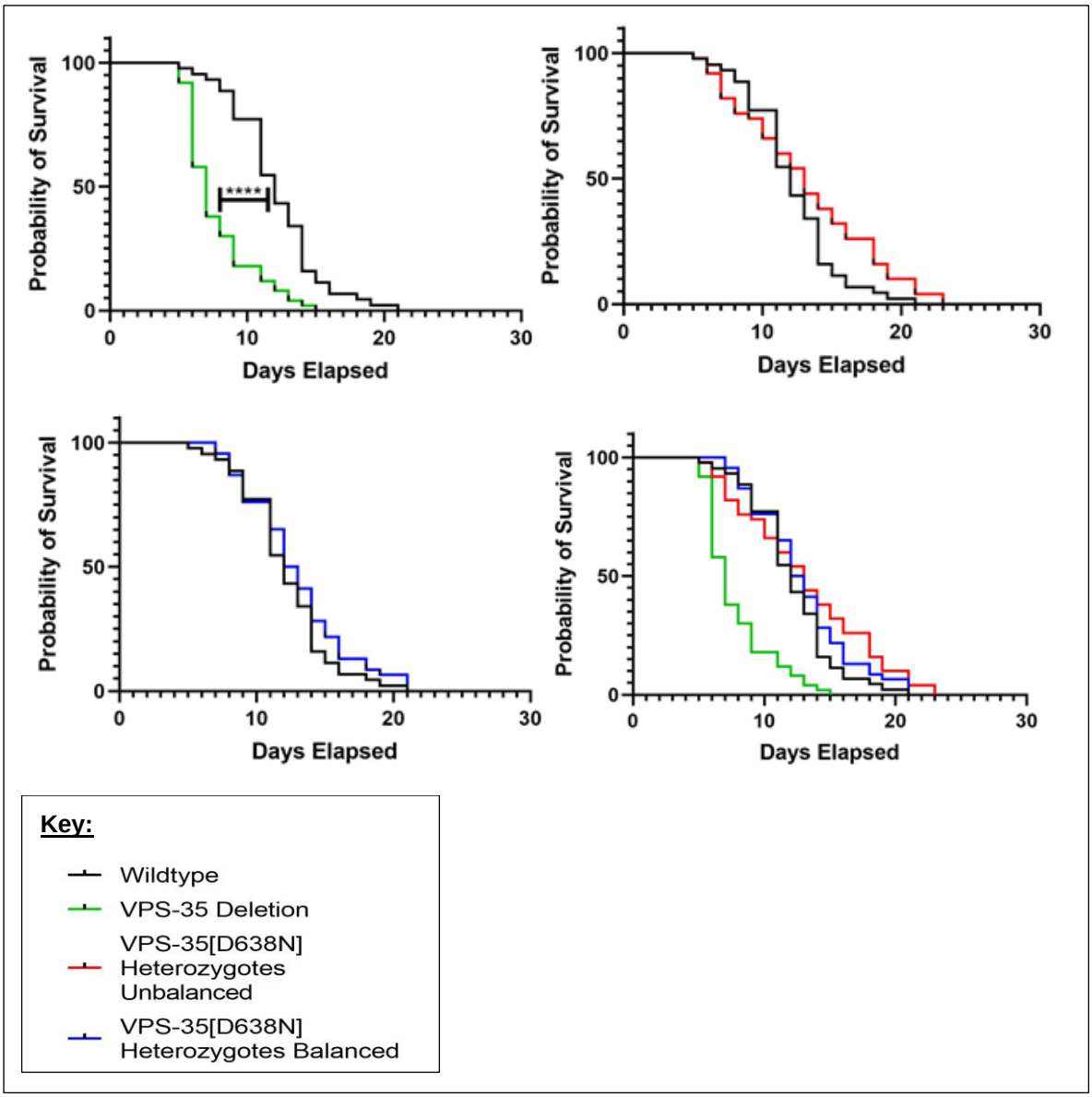

Genotype	Median Survival
Wildtype	12
vps-35 deletion	7
vps-35[D638N] heterozygote unbalanced	13
vps-35[D638N] heterozygote balanced	12.5

Days Elapsed	Number of Surviving *C. elegans* per genotype			
	Wildtype	VPS-35 Deletion	VPS-35[D638N] Heterozygotes Unbalanced	VPS-35[D638N] Heterozygotes Balanced
0	44	50	50	46
1	44	50	50	46
2	44	50	50	46
3	44	50	50	46
4	44	50	50	46
5	44	50	50	46
6	43	46	49	46
7	42	29	46	46
8	41	19	41	44
9	39	15	38	40
10	39	15	37	40

11	34	9	33	35
12	24	4	30	30
13	19	2	27	23
14	15	1	22	19
15	7	0	19	13
16	5	0	16	10
17	5	0	16	10
18	3	0	13	6
19	2	0	8	4
20	2	0	8	4
21	1	0	5	3
22	0	0	5	0
23	0	0	2	0
24	0	0	0	0
25	0	0	0	0
26	0	0	0	0
27	0	0	0	0

Statistical analysis undertaken through Mantel-Cox test of curve comparison, wildtype compared to vps-35 mutant

Genotype	P Value	Significant	Median Survival	Ratio
vps-35 deletion	<0.0001	****	7	1.714
vps-35[D638N] heterozygote unbalanced	0.3980	NS	13	0.9231
vps-35[D638N] heterozygote balanced	0.2349	NS	12.5	0.96

3.6.2 vps-35 deletion show a significantly reduced crawling speed

Line	M (mm/s)	SD	N
Wildtype	0.1033	0.02186	15
vps-35[D638N] heterozygote	0.0940	0.02552	23

Unpaired two-tailed T-test undertaken. Welch's correction. P=0.2361, not significant.

Line	M(mm/s)	SD	N
Wildtype	0.1194	0.03754	20
vps-35(tm1880)	0.04479	0.01932	19

Unpaired two-tailed T-test with Welch's correction. P<0.0001, significant****

3.7 Novel *vps-35*[D638N] heterozygotes show impaired dopaminergic behaviours

3.7.1.1 Treatment of cat-2(n4547) with dopamine hydrochloride for 24 hours improves the basal slowing response

	M	SD	N
Vehicle	40.48	68.72	27
Dopamine Hydrochloride	62.33	19.35	35

Two-tailed unpaired T-test with Welch's correction undertaken.
P=0.0303, significant*

3.7.1.2 Treatment of cat-2(n4547) with dopamine hydrochloride for 4 hours significantly rescues impairments in basal slowing

Line	Dopamine	M (%)	SD	N
Wildtype	-	79.16	12.87	14
Wildtype	+	74.4	10.52	12
cat-2(n4547)	-	-17.34	79.96	17
cat-2(n4547)	+	79.82	13.15	28

	Wildtype Vehicle	*cat-2*(n4547)II Dopamine
cat-2(n4547)II vehicle	P=0.0007 Sig***	P<0.0001 Sig****
Wildtype Dopamine	P>0.999 NS	P=0.8961 NS

3.7.2.1 Unbalanced vps-35[D638N] show impaired basal slowing on day 1 of adulthood

Line	M (%)	SD	N
Wildtype	84.85	16.34	26
vps-35[D638N]	66.87	32.5	29

Unpaired two tailed T-test undertaken. Welch's correction. P=0.0139, significant*

3.7.2.2 Balanced *vps-35[D638N]* heterozygotes exhibit age exacerbated impairments in basal slowing response in day 1 and 5 of adulthood, rescued by dopamine treatment

Descriptive statistics and P-Values from one-way ANOVA with Brown-Forsyth correction

Day 1

Genotype	Treatment	Mean % (M)	Standard Deviation (SD)	Number (N)
Wildtype	Vehicle	91.341	8.135	14
	Dopamine	96.277	3.051	19
vps-35[D638N] heterozygotes	Vehicle	62.578	35.057	22
	Dopamine	86.381	12.422	28
cat-2(n4547)	Vehicle	30.746	68.498	30
	Dopamine	92.972	3.012	26

Comparison	P Value	Significance
Wildtype Vehicle vs *vps-35[D638N]* heterozygote Vehicle	0.0067	**
Wildtype Vehicle vs *cat-2(n4547)* Vehicle	0.0002	***
Wildtype Vehicle vs Wildtype Dopamine	0.2285	NS
vps-35[D638N] heterozygote Vehicle vs *vps-35[D638N]* heterozygote Dopamine	0.0317	*
cat-2(n4547) Vehicle vs *cat-2(n4547)* Dopamine	0.0002	***

Day 5

Genotype	Treatment	Mean % (M)	Standard Deviation (SD)	Number (N)
Wildtype	Vehicle	71.065	23.902	18
	Dopamine	68.015	15.544	12
vps-35[D638N] heterozygotes	Vehicle	16.881	38.809	16
	Dopamine	65.205	35.946	27
cat-2(n4547)	Vehicle	-20.306	102.447	19
	Dopamine	39.546	41.249	11

Comparison	P Value	Significance
Wildtype Vehicle vs *vps-35[D638N]* heterozygote Vehicle	0.0003	***
Wildtype Vehicle vs *cat-2(n4547)* Vehicle	0.0058	**
Wildtype Vehicle vs Wildtype Dopamine	0.9958	NS
vps-35[D638N] heterozygote Vehicle vs *vps-35[D638N]* heterozygote Dopamine	0.0016	**
cat-2(n4547) Vehicle vs *cat-2(n4547)* Dopamine	0.1491	NS

Day 1 vs Day 5

Genotype	Age	Mean % (M)	Standard Deviation (SD)	Number (N)
Wildtype	1	91.341	8.135	14
	5	71.065	23.902	18
vps-35[D638N] heterozygotes	1	62.578	35.057	22
	5	16.881	38.809	16
cat-2(n4547)	1	30.746	68.498	30
	5	20.306	102.447	19

Comparison	P Value	Significance
Wildtype Day 1 vs Wildtype Day 5	0.0191	*
vps-35[D638N] heterozygotes Day 1 vs *vps-35[D638N]* heterozygotes Day 5	0.0055	**
cat-2(n4547) Day 1 vs *cat-2(n4547)* Day 5	0.3583	NS

Balanced *vps-35[D638N]* do not show a significantly different crawling speed to the wildtype in day 1 of adulthood following dopamine treatment

In day 1 of adulthood, the *vps-35[D638N]* balanced heterozygotes do not show any significant impairments in crawling speed compared to the wildtype, consistent with previous findings. Crawling speed is not significantly impacted by dopamine administration in either the wildtype, or the *vps-35[D638N]* heterozygote. However, the tyrosine hydroxylase *cat-2(n4547)* mutant shows a significantly reduced crawling speed compared to the wildtype under both conditions. The crawling speed is significantly enhanced in the *cat-2(n4547)* following dopamine treatment.

In day 5 of adulthood, *vps-35[D638N]* heterozygotes do not show a significantly different crawling speed to the wildtype. Following dopamine treatment, the wildtype shows a significantly reduced crawling speed compared to the vehicle. This phenotype is not exhibited in the vps-35[D638N] heterozygote line, or the cat-2(n4547), suggesting that dopamine may not have a deleterious effect upon these mutants. Consistent with day 1 of adulthood, the *cat-2(n4547)* show a significantly reduced crawling speed compared to the wildtype under both conditions.

Between day 1 and day 5 of adulthood, vehicle treated *vps-35[D638N]* heterozygotes show a significant reduction in crawling speed. This is not illustrated in the *cat-2(n4547)* mutant, suggesting that impairments in the novel *vps-35[D638N]* heterozygotes are age dependant, while the *cat-2(n4547)* has a genetic dopamine signalling ablation. The wildtype shows a significant reduction in crawling speed between day 1 and 5 of adulthood; however this is not as significant as the *vps-35[D638N]* heterozygotes. As previously discussed, the *cat-2(n4547)* mutant demonstrates a reduced crawling speed compared to the wildtype in day 1 and day 5 of adulthood.

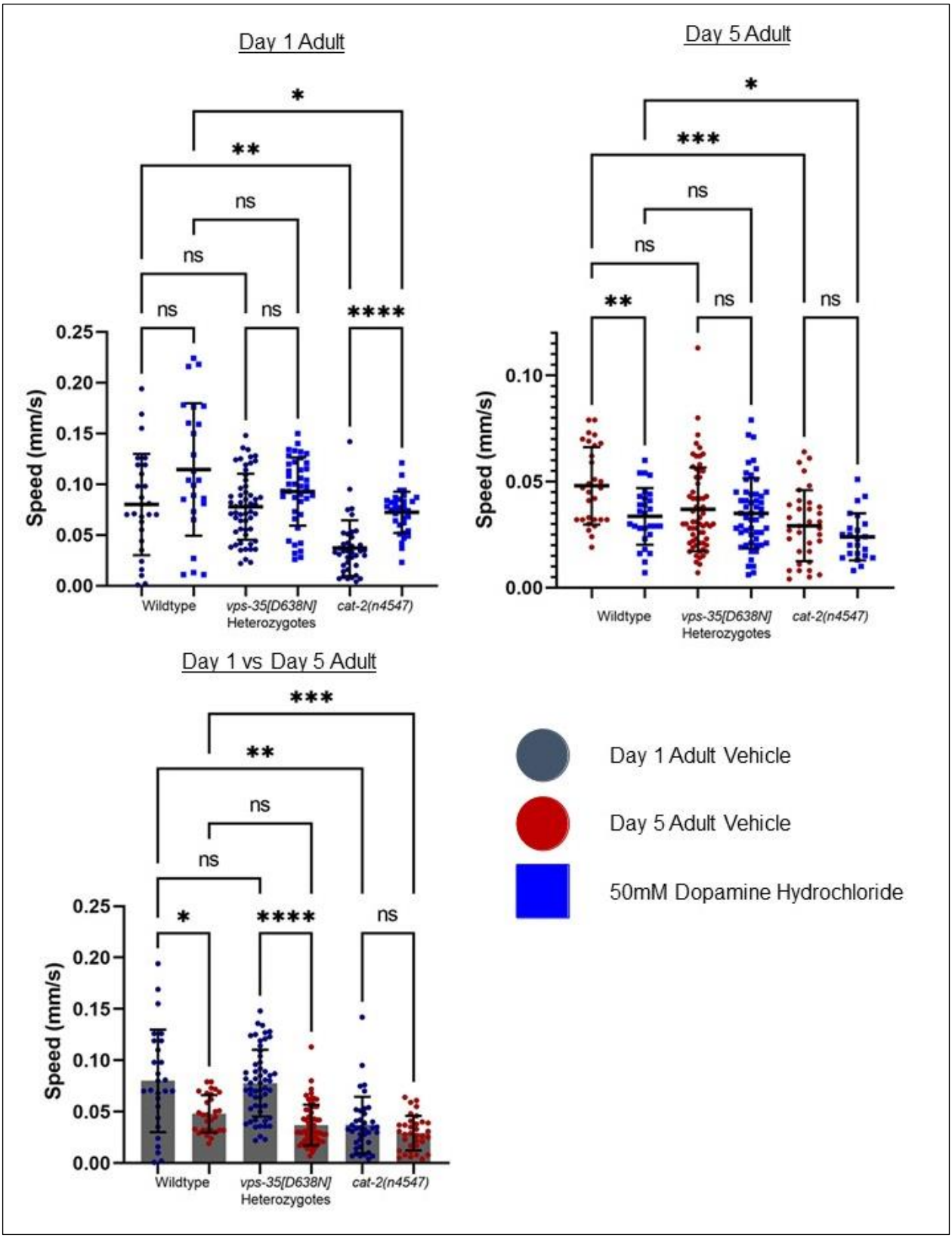
Day 1 Adult
Speed (mm/s)
0.25
0.20
0.15
0.10
0.05
0.00
*
**
ns
ns
ns
****
Wildtype
vps-35[D638N] Heterozygotes
cat-2(n4547)
Day 5 Adult
Speed (mm/s)
0.10
0.05
0.00
*
***
ns
ns
**
ns
ns
Wildtype
vps-35[D638N] Heterozygotes
cat-2(n4547)
Day 1 vs Day 5 Adult
Speed (mm/s)
0.25
0.20
0.15
0.10
0.05
0.00
***
**
ns
ns
*
****
ns
Wildtype
vps-35[D638N] Heterozygotes
cat-2(n4547)
Day 1 Adult Vehicle
Day 5 Adult Vehicle
50mM Dopamine Hydrochloride

Crawling Speed Descriptive Statistics and P-Values

Descriptive statistics and P-Values from one-way ANOVA with Brown-Forsyth correction

Day 1

Genotype	Treatment	Mean (mm/s)	Standard Deviation (SD)	Number (N)
Wildtype	Vehicle	0.08002	0.04988	27
	Dopamine	0.1145	0.06518	24
vps-35[D638N] heterozygotes	Vehicle	0.07784	0.03257	55
	Dopamine	0.09283	0.03362	41
cat-2(n4547)	Vehicle	0.03711	0.02743	38
	Dopamine	0.07232	0.02027	34

Comparison	P Value	Significance
Wildtype Vehicle vs *vps-35[D638N]* heterozygote Vehicle	>0.9999	NS
Wildtype Vehicle vs *cat-2(n4547)* Vehicle	0.0017	**
Wildtype Dopamine vs *vps-35[D638N]* heterozygote Dopamine	0.6279	NS
Wildtype Dopamine vs *cat-2(n4547)* Dopamine	0.0334	*
Wildtype Vehicle vs Wildtype Dopamine	0.2485	NS
vps-35[D638N] heterozygote Vehicle vs *vps-35[D638N]* heterozygote Dopamine	0.1961	NS
cat-2(n4547) Vehicle vs *cat-2(n4547)* Dopamine	<0.0001	****

Day 5

Genotype	Treatment	Mean (mm/s)	Standard Deviation (SD)	Number (N)
Wildtype	Vehicle	0.04800	0.01821	29
	Dopamine	0.03361	0.01336	28
vps-35[D638N] heterozygotes	Vehicle	0.03692	0.01975	64
	Dopamine	0.03502	0.01654	53
cat-2(n4547)	Vehicle	0.02918	0.01673	34
	Dopamine	0.02391	0.01111	23

Comparison	P Value	Significance
Wildtype Vehicle vs *vps-35[D638N]* heterozygote Vehicle	0.0699	NS
Wildtype Vehicle vs *cat-2(n4547)* Vehicle	0.0006	***
Wildtype Dopamine vs *vps-35[D638N]* heterozygote Dopamine	0.9996	NS
Wildtype Dopamine vs *cat-2(n4547)* Dopamine	0.0455	*
Wildtype Vehicle vs Wildtype Dopamine	0.0088	**
vps-35[D638N] heterozygote Vehicle vs *vps-35[D638N]* heterozygote Dopamine	0.9972	NS
cat-2(n4547) Vehicle vs *cat-2(n4547)* Dopamine	0.6892	NS

Day 1 vs Day 5

Genotype	Treatment	Mean (mm/s)	Standard Deviation (SD)	Number (N)
Wildtype	Vehicle	0.04800	0.01821	29
	Dopamine	0.03361	0.01336	28
vps-35[D638N] heterozygotes	Vehicle	0.03692	0.01975	64
	Dopamine	0.03502	0.01654	53
cat-2(n4547)	Vehicle	0.02918	0.01673	34
	Dopamine	0.02391	0.01111	23

Comparison	P Value	Significance
Wildtype Vehicle vs *vps-35[D638N]* heterozygote Vehicle	0.0699	NS
Wildtype Vehicle vs *cat-2(n4547)* Vehicle	0.0006	***
Wildtype Dopamine vs *vps-35[D638N]* heterozygote Dopamine	0.9996	NS

Wildtype Dopamine vs *cat-2(n4547)* Dopamine	0.0455	*
Wildtype Vehicle vs Wildtype Dopamine	0.0088	**
vps-35[D638N] heterozygote Vehicle vs *vps-35[D638N]* heterozygote Dopamine	0.9972	NS
cat-2(n4547) Vehicle vs *cat-2(n4547)* Dopamine	0.6892	NS

3.7.3 *C. elegans* with deletion of *vps-35* do not show impairments in the basal slowing response

Line	M (%)	SD	N
Wildtype	83.06	17.68	17
vps-35(tm1880)	75.68	23.60	19

Unpaired, two tailed T-test with Welch's correction. P=0.3230, not significant.

3.7.3.2 *vps-35* deletion mutants do not show an impaired basal slowing response in day 1, but exhibit an impaired response following dopamine treatment

Descriptive statistics and P-Values from one-way ANOVA with Brown-Forsyth correction

Day 1

Genotype	**Treatment**	**Mean % (M)**	**Standard Deviation (SD)**	**Number (N)**
Wildtype	Vehicle	82.3	10.74	13
	Dopamine	71.99	14.04	19
vps-35(tm1880)	Vehicle	85.70	11.22	10
	Dopamine	36.76	23.02	8

Comparison	**P Value**	**Significance**
Wildtype Vehicle vs *vps-35(tm1880)* Vehicle	0.8439	NS
Wildtype Vehicle vs Wildtype Dopamine	0.0735	NS
vps-35(tm1880) Vehicle vs *vps-35(tm1880)* Dopamine	0.0008	***

Day 5

Genotype	**Treatment**	**Mean % (M)**	**Standard Deviation (SD)**	**Number (N)**
Wildtype	Vehicle	82.46	21.76	6
	Dopamine	63.47	33.37	7
vps-35(tm1880)	Vehicle	31.85	75.63	7
	Dopamine	78.21	9.086	5

Comparison	**P Value**	**Significance**
Wildtype Vehicle vs *vps-35(tm1880)* Vehicle	0.3246	NS
Wildtype Vehicle vs Wildtype Dopamine	0.5474	NS
vps-35(tm1880) Vehicle vs *vps-35(tm1880)* Dopamine	0.3712	NS

Day 1 vs Day 5

Genotype	**Age**	**Mean % (M)**	**Standard Deviation (SD)**	**Number (N)**
Wildtype	1	82.3	10.74	13
	5	82.46	21.76	6
vps-35(tm1880)	1	85.70	11.22	10
	5	31.85	75.63	7

Comparison	**P Value**	**Significance**
Wildtype Day 1 vs Wildtype Day 5	>0.9999	NS
vps-35(tm1880) Day 1 vs *vps-35(tm1880)* Day 5	0.2688	NS

***vps-35* deletion mutants show a significantly impaired crawling speed in day 1 of adulthood, exacerbated with dopamine treatment**

Coherent with 3.7, the vps-35 deletion mutant exhibits a reduced crawling speed in day 1 of adulthood compared to the wildtype. This is significantly exacerbated following treatment with dopamine, which is not exhibited in the wildtype in this experiment. This phenotype is not illustrated in the *vps-35[D638N]* heterozygote, suggesting distinct mechanisms of action. In day 5 of adulthood, *vps-35* deletion mutants show a highly significantly reduced crawling speed compared to the wildtype. Administration of dopamine has no effect upon the crawling speed of either the *vps-35* deletion mutant or the wildtype, contradictory to 3.8.3.1.4. As discussed previously, this low crawling speed poses challenges to effective assaying of the basal slowing response in these mutants. As mentioned in 3.8.3.2.2, assaying the basal slowing response of *vps-35* deletion mutants in day 5 of adulthood is challenging, as their baseline crawling motility, upon which the speed on a bacterial lawn is compared, is very low. In day 1 of adulthood, as discussed in 3.7, the *vps-35* deletion mutant illustrates a significantly reduced crawling speed compared to the wildtype. Ageing to day 5 of adulthood significantly reduces the crawling speed of *vps-35* deletion mutants further, suggesting that impairments in this mutants are not dopaminergic neuronal specific and could be neuromuscular.

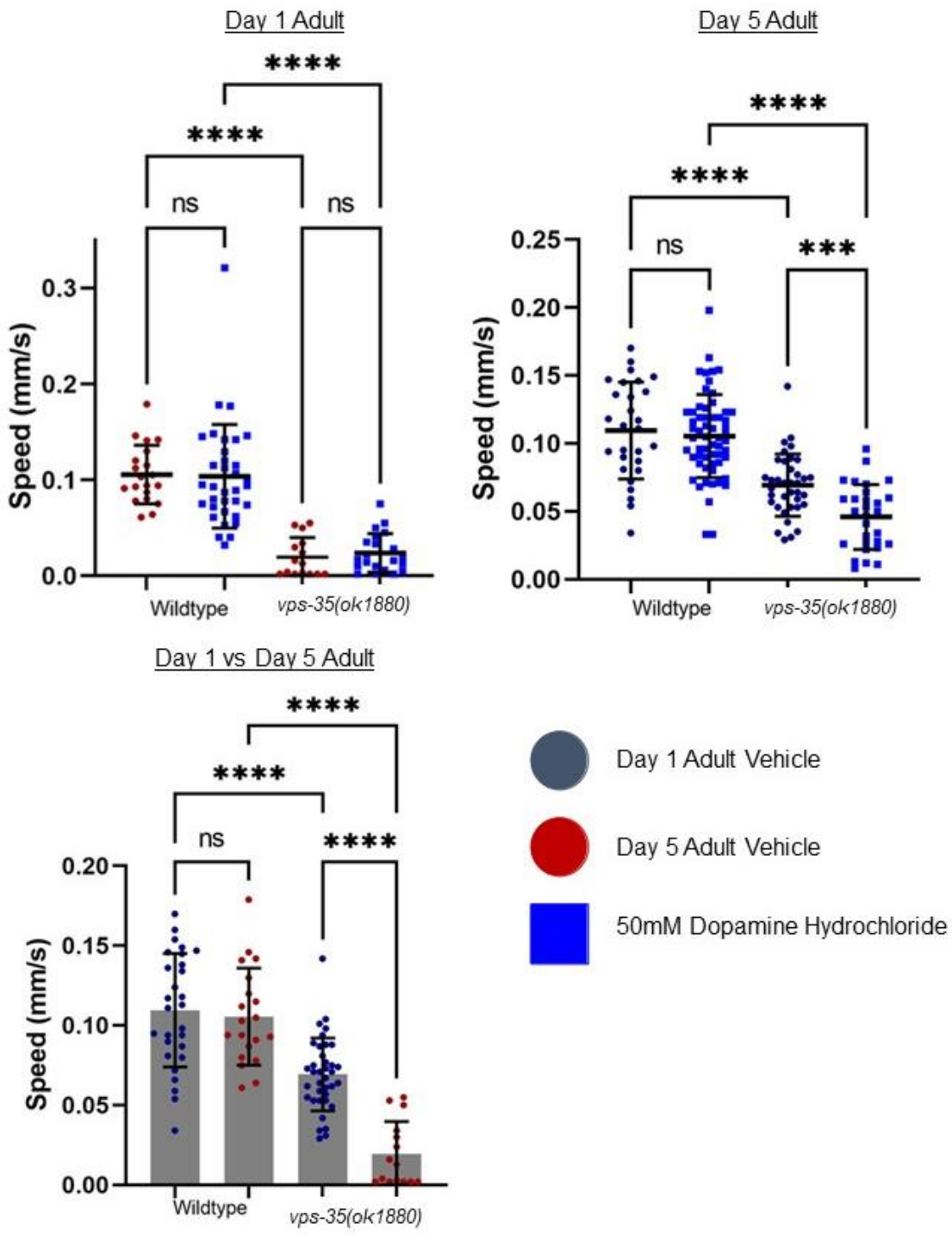

25-60 day 1 adult worms were assayed per line and treatment. Descriptive statistics and One way ANOVA with Brown-Forsyth Correction was performed between selected datasets, which can be found in the supplementary

Crawling speed statistics

Descriptive statistics and P-Values from one-way ANOVA with Brown-Forsyth correction

Day 1

Genotype	Treatment	Mean % (M)	Standard Deviation (SD)	Number (N)
Wildtype	Vehicle	0.1095	0.03561	28
	Dopamine	0.1054	0.03054	59
vps-35(tm1880)	Vehicle	0.06924	0.02286	37
	Dopamine	0.04586	0.02386	29

Comparison	P Value	Significance
Wildtype Vehicle vs *vps-35(tm1880)* Vehicle	<0.0001	****
Wildtype Dopamine vs *vps-35(tm1880)* Dopamine	<0.0001	****
Wildtype Vehicle vs Wildtype Dopamine	NS	0.9738
vps-35(tm1880) Vehicle vs *vps-35(tm1880)* Dopamine	0.0007	***

Day 5

Genotype	Treatment	Mean % (M)	Standard Deviation (SD)	Number (N)
Wildtype	Vehicle	0.1055	0.03043	20
	Dopamine	0.1036	0.05400	34
vps-35(tm1880)	Vehicle	0.01947	0.02027	15
	Dopamine	0.02386	0.02009	21

Comparison	P Value	Significance
Wildtype Vehicle vs *vps-35(tm1880)* Vehicle	<0.0001	****
Wildtype Dopamine vs *vps-35(tm1880)* Dopamine	<0.0001	****
Wildtype Vehicle vs Wildtype Dopamine	0.9997	NS
vps-35(tm1880) Vehicle vs *vps-35(tm1880)* Dopamine	0.9452	NS

Day 1 vs Day 5

Genotype	Age	Mean (mm/s)	Standard Deviation (SD)	Number (N)
Wildtype	1	0.1095	0.03561	28
	5	0.1055	0.03043	20
vps-35(tm1880)	1	0.06924	0.02286	37
	5	0.01947	0.02027	15

Comparison	P Value	Significance
Wildtype Day 1 vs *vps-35(tm1880)* Day 1	<0.0001	****
Wildtype Day 5 vs *vps-35(tm1880)* Day 5	<0.0001	****
Wildtype Day 1 vs Wildtype Day 5	0.9886	NS
vps-35(tm1880) Day 1 vs *vps-35(tm1880)* Day 5	<0.0001	****

3.8 Selected Cellular Phenotypes of *vps-35* mutants

3.9.1.2 The *vps-35[D638N]* heterozygote exhibits an impaired mitochondrial phenotype, not exacerbated with age

Descriptive statistics and unpaired, two-tailed t-test P-values for wildtype mean normalised fluorescence intensities in day 1 and day 5 of adulthood.

Age (Days)	**Genotype**	**Mean**	**Standard Deviation**	**Number**	**P Value**	**Significance**
1	Wildtype	1.000	0.2032	20		
	vps-35[D638N] Heterozygote	0.6583	0.1501	40	<0.0001	****
5	Wildtype	1.000	0.4922	18		
	vps-35[D638N] Heterozygote	1.000	0.4655	26	0.9291	NS

Descriptive statistics and One-way ANOVA for fluorescence intensity, with comparisons between day 1 and day 5 of adulthood

Genotype	Age (days)	Mean	Standard Deviation	Number
Wildtype	1	5715	1183	20
	5	2444	1203	18
vps-35[D638N] heterozygote	1	3638	864.8	40
	5	3561	1658	26

Comparison	**P Value**	**Significance**
Wildtype Day 1 Adult vs. Wildtype Day 5 Adult	<0.0001	****
vps-35[D638N] Day 1 Adult vs. vps-35[D638N] Day 5 Adult	0.9991	ns
Wildtype Day 1 Adult vs vps-35[D638N] Day 1 Adult	<0.0001	****
Wildtype Day 5 Adult vs vps-35[D638N] Day 5 Adult	0.0511	ns

3.8.2 *vps-35[D638N]* heterozygotes exhibit an impaired ciliation phenotype

Descriptive statistics and unpaired, two-tailed t-test P-values for wildtype mean normalised fluorescence intensities in day 5, 12 and 19 of adulthood.

Age (Days)	Genotype	Mean	Standard Deviation	Number	P Value	Significance
5	Wildtype	1.000	0.3010	28		
	vps-35[D638N] Heterozygote	0.6915	0.1591	22	<0.0001	****
	vps-35 deletion	0.8749	0.2101	5	0.6113	ns
12	Wildtype	1.000	0.1493	15		
	vps-35[D638N] Heterozygote	0.7115	0.2246	15	0.0004	***
19	Wildtype	1.000	0.1128	4		
	vps-35[D638N] Heterozygote	0.7514	0.2709	5	0.1158	ns

Descriptive statistics and One-way ANOVA for fluorescence intensity, with comparisons between day 5, 12 and 19 of adulthood

Genotype	**Age (days)**	**Mean**	**Standard Deviation**	**Number**
Wildtype	5	4532	1364	28
	12	4872	727.3	15
	19	2884	325.3	4
vps-35[D638N] heterozygotes	5	3134	721.1	22
	12	3467	1094	15
	19	2167	781.1	5

Comparison	**P Value**	**Significance**
Wildtype Day 5 Adult vs Wildtype Day 12 Adult	0.7417	ns
Wildtype Day 12 Adult vs Wildtype Day 19 Adult	<0.0001	****
vps-35[D638N] Day 5 vs vps-35[D638N] Day 12	0.7616	ns
vps-35[D638N] Day 12 vs vps-35[D638N] Day 19	0.0580	ns

3.8.3 *vps-35[D638N]* heterozygotes show reduced lipid accumulation as a marker for autophagy

Descriptive statistics and One-way ANOVA with Brown-Forsyth correction, P-values for wildtype mean normalised fluorescence intensities, in day 1 and day 5 of adulthood

Age (Days)	Genotype	Mean	Standard Deviation	Number	P Value	Significance
1	Wildtype	1.000	0.1098	5		
	vps-35[D638N] Heterozygote Unbalanced	0.6757	0.1367	28	0.0039	**
	vps-35[D638N] Heterozygote Balanced	0.7157	0.1300	37	0.0064	**
	vps-35 deletion	1.511	0.5397	7	0.1490	ns
	cat-2(n4547)	0.5416	0.08528	33	0.0010	**
5	Wildtype	1.000	0.1193	14		
	vps-35[D638N] Heterozygote Unbalanced	0.5758	0.1293	33	<0.0001	****
	vps-35[D638N] Heterozygote Balanced	0.4669	0.07284	36	<0.0001	****
	cat-2(n4547)	0.4825	0.1075	35	<0.0001	****

Descriptive statistics and One-way ANOVA for fluorescence intensity, with comparisons between day 1 and day 5 of adulthood

Genotype	Age (Days)	Mean	Standard Deviation	Number
Wildtype	1	2851	313.2	5
	5	5636	672.3	14
vps-35[D638N] Heterozygote Unbalanced	1	1927	389.9	28
	5	3245	728.5	33
vps-35[D638N] Heterozygote Balanced	1	2041	370.6	37
	5	2631	410.5	36
cat-2(n4547)	1	1544	243.2	33
	5	2719	605.6	35

Comparison	P Value	Significance
Wildtype Day 1 Adult vs Wildtype Day 5 Adult	0.3942	ns
vps-35[D638N] Day 1 Adult vs vps-35[D638N] Day 5 Adult Unbalanced	<0.0001	****
vps-35[D638N] Day 1 Adult vs vps-35[D638N] Day 5 Adult Balanced	0.0003	***
cat-2n(4547) Day 1 Adult vs cat-2n(4547) Day 5	<0.0001	****

Autophagic Marker and LRRK2 substrate SQSTM-1/p62

SQSTM1-p62 is a is an autophagosomal cargo receptor, upregulated in autophagy. Ubiquitinated substrates are recognised by SQSTM1-p62 and are incorporated into the autophagosome, leading to lysosomal fusion and cargo degradation. Thus, quantifying the concentration of SQSTM1-p62

present in mutant *C. elegans* lysates would be a powerful tool in evaluating autophagy between the *lrk-1* and *vps-35* mutant lines. This is especially pertinent, as SQST-p62 is a candidate substrate for human LRRK2 (Kalogeropulou *et al.,* 2018) and mutations in SQSTM-1/p62 have been associated with neurodegeneration in MND . Collaborators of the Kevei lab, Alexander Springhorn and Thorsten Hoppe (Institute for Genetics and CEAD research centre, University of Cologne, Germany) have developed a novel antibody detecting the C. elegans orthologue of SQSTM-1/p62, SQST-1. This has been shared with the Kevei laboratory and utilised for preliminary investigation.

SQST-1 is detectable in *C. elegans* lysates

Prior to investigation of *vps-35* or *lrk-1* mutants, the efficacy of this novel antibody was tested in *C. elegans*, following autophagic induction of wildtype through starvation, a highly evolutionarily conserved process. A higher intensity band at the expected size in the starved lysate demonstrated that SQST-p62 is a detectable autophagic marker in *C. elegans.*

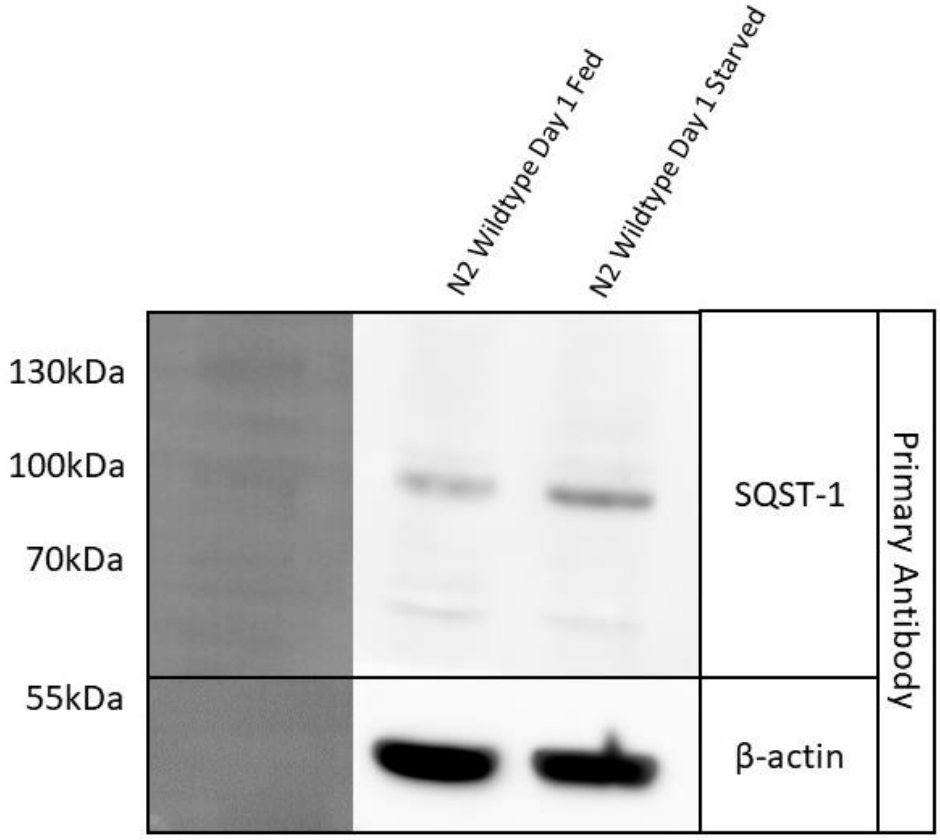

SQST-1 is detectable in C. elegans lysates

SQST-1 expected molecular weight is 68kDa, higher intensity band illustrated in starvation induced autophagy. β-actin control approximately 37kDa.

***vps-35[D638N]* may show reduced SQST-1 oligomerisation**

In *C. elegans,* molecular techniques such as semi-quantitative western blotting can be applied to study individual proteins in *C. elegans* lysates. We had encountered many challenges with this experiment, as multiple protein bands have been detected around the molecular weight of *C. elegans* p62 and our western blotting technique has been difficult to establish, requiring much troubleshooting and optimization. To overcome the challenge of multiple bands, a SQST-1 deletion mutant and a GFP tagged SQST-1 *C. elegans* line was ordered, to produce positive and negative control lysates. Utilizing these, the SQST-1 band at 68kDa has been established, utilizing

the deletion and GFP tagged protein. However, bands have been consistently observed at 125kDa, suggesting oligomerization. Oligomerization of SQSTM-1/p62 enables the selection of ubiquitinated cargo and membrane isolation during selective autophagy (Wurzer *et al.*, 2015) and is required for cargo targeting to the autophagosome (Itakura and Mizushima, 2011). However the PB1 domains which modulate oligomerization are not directly conserved in *C. elegans* (Donohue *et al.*, 2014) and little is known about the oligomerization process in this model.

Compared to wildtype, preliminary data suggests that *vps-35[D638N]* heterozygotes in day 5 of adulthood show modestly enhanced levels of 68kDa SQST-1, with a relative intensity of 0.49, compared to the wildtype 0.39. Interestingly, *vps-35[D638N]* show reduced levels of 125kDa SQST-1 bands, with an intensity of 0.45, compared to the wildtype 1.16. This data suggests that there could be reduced oligomerization in the *vps-35[D638N]* mutant compared to the wildtype, leading to reduced selection of ubiquitinated cargo to the autophagosome in autophagy. However, this data is preliminary and needs further replication in future studies.

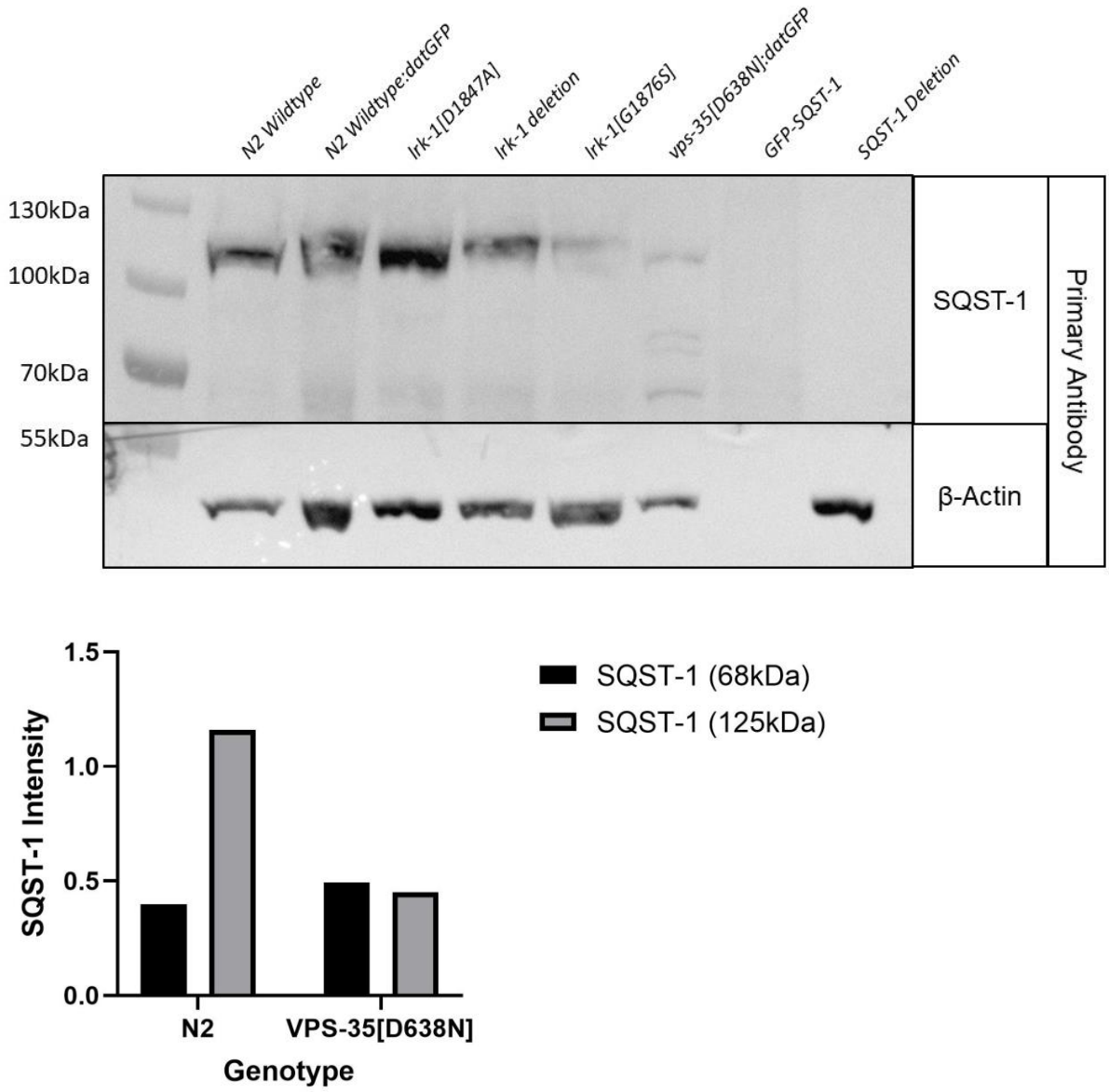

vps-35[D638N] heterozygotes may show reduced SQST-1 oligomerisation

SQST-1 intensity normalised against β-actin control per sample lane for preliminary quantification. The GFP-SQST-1 sample demonstrated no signal, likely due to long term -20oC storage and low sample volume for loading.

3.9 Visualisation of VPS-35[D638N] Dopaminergic Neurons *in vivo*

3.9.2.1 *vps-35[D638N]* heterozygotes show reduced CEP cell body fluorescence, not exacerbated by 5µM rotenone treatment

Descriptive statistics and One-way ANOVA with Brown-Forsyth correction, P-values.

Genotype	Treatment	Mean	Standard Deviation	Number
Wildtype:datGFP	Vehicle	3307	1444	35
	Rotenone	2190	834.5	34
vps-35[D638N]:datGFP	Vehicle	2079	920.5	25
	Rotenone	2098	810.0	31

Comparison	P-Value	Significance
Wildtype:datGFP Vehicle vs Wildtype:datGFP Rotenone	0.0011	**
vps-35[D638N]:datGFP Vehicle vs vps-35[D638N]:datGFP Rotenone	>0.9999	ns
Wildtype:datGFP Vehicle vs vps-35[D638N]:datGFP Vehicle	0.0004	***
Wildtype:datGFP Rotenone vs vps-35[D638N]:datGFP Rotenone	>0.9999	ns

3.9.2.2 *vps-35[D638N]* heterozygotes show impairments in CEP and ADE neuronal morphology, independent of 5µM rotenone treatment

Neuronal Subgroup	Genotype	Treatment	% Neurons in *C. elegans* Population Morphology					N
			Wildtype Appearance	Outgrowths	Branching	Blebbing	Degeneration	
CEP	Wildtype:GFP	Vehicle	88.57143	7.142857	2.142857	1.428571	0.714286	140
		Rotenone	81.61765	11.02941	3.731343	0.735294	2.941176	136
	VPS-35[D638N]:GFP	Vehicle	46	35	10	0	9	100
		Rotenone	38.70968	22.58065	16.12903	6.451613	16.12903	124
ADE	Wildtype:GFP	Vehicle	95.71429	1.428571	0	1.42857	1.428571	70
		Rotenone	69.11765	7.352941	1.470588	1.470588	20.58824	68
	VPS-35[D638N]:GFP	Vehicle	54	4	2	18	22	50
		Rotenone	40.32258	14.51613	1.612903	16.12903	27.41935	62

3.9.2.3 *vps-35[D638N]* heterozygotes show an increased number of impairments per *C. elegans*, irrespective of 5µM rotenone treatment

Type	Genotype	Treatment	% C. elegans in population with number of impairments							N
			0	1	2	3	4	5	6	
Total	Wildtype:GFP	Vehicle	68.57143	17.14286	11.42857	0	0	2.857143	0	35
		Rotenone	23.52941	32.35294	32.35294	8.823529	2.941176	0	0	34
	VPS-35[D638N]:GFP	Vehicle	0	4	32	36	12	12	4	25
		Rotenone	3.225806	6.451613	12.90323	25.80645	25.80645	3.225806	22.58065	31
Minor	Wildtype:GFP	Vehicle	71.42857	17.14286	11.42857	0	0	0	0	35
		Rotenone	50	26.47059	20.58824	2.941176	0	0	0	34

	VPS-35[D638N]:GFP	Vehicle	8	28	40	12	12	0	0	25
		Rotenone	25.80645	9.677419	25.80645	32.25806	3.225806	3.225806	0	31
Major	Wildtype:GFP	Vehicle	97.14286	0	0	0	0	2.857143	0	35
		Rotenone	55.88235	32.35294	8.823529	2.941176	0	0	0	34
	VPS-35[D638N]:GFP	Vehicle	32	40	12	12	4	0	0	25
		Rotenone	29.03226	29.03226	12.90323	9.677419	9.677419	3.225806	6.451613	31

3.9.2.4 The most prevalent neuropathology's in vps-35[D638N] are minor impairments in the CEP neurons and major impairments in the ADE neurons

Genotype	Treatment	Neuronal Subgroup	Type	% C. elegans in population with number of impairments					N
				0	1	2	3	4	
Wildtype:GFP	Vehicle	CEP	Minor	71.42857	20	8.571429	0	0	140
			Major	97.14286	0	0	2.857143	0	140
		ADE	Minor	97.14286	2.857143	0			70
			Major	97.14286	0	2.857143			70
	Rotenone	CEP	Minor	55.88235	29.41176	14.70588	0	0	136
			Major	88.23529	8.823529	2.941176	0	0	136
		ADE	Minor	82.35294	17.64706	0			68
			Major	58.82353	38.23529	2.941176			68
VPS-35[D638N]:GFP	Vehicle	CEP	Minor	12	28	36	16	8	100
			Major	84	0	12	4	0	100
		ADE	Minor	88	12	0			50
			Major	32	56	12			50
	Rotenone	CEP	Minor	29.03226	9.677419	45.16129	9.677419	6.451613	124
			Major	51.6129	22.58065	16.12903	3.225806		124
		ADE	Minor	70.96774	25.80645	3.225806			62
			Major	38.70968	35.48387	25.80645			62

3.9.3 Impairments in neuronal morphology in *vps-35[D638N]* heterozygotes are not exacerbated by 7.5 or 10μM rotenone

Following the successful treatment of *C. elegans* populations with 5μM rotenone, higher concentrations were tested to identify if there were any dose dependant responses and which concentration would be

optimal for further treatment. *C. elegans* were treated with 7.5 and 10µM of rotenone and displayed no exacerbations in CEP and ADE neuronal pathologies observed in 3.10.2.2. In *C. elegans* treated with 7.5µM rotenone, there was increased CEP neuronal degeneration in the wildtype compared to 5µM, however this was not reflected in the 10µM, suggesting the phenotype is not dose dependant, as shown in figure 46. Similarly, there is a similar proportion of CEP neuronal impairments following 7.5 and 10µM rotenone treatment of the *vps-35[D638N]* heterozygotes. Furthermore, 5µM rotenone treated wildtype *C. elegans* show the greatest proportion of degeneration, compared to 7.5 and 10µM treated lines, further highlighting the lack of dose dependency. This is also reflected in the *vps-35[D638N]* heterozygote lines.

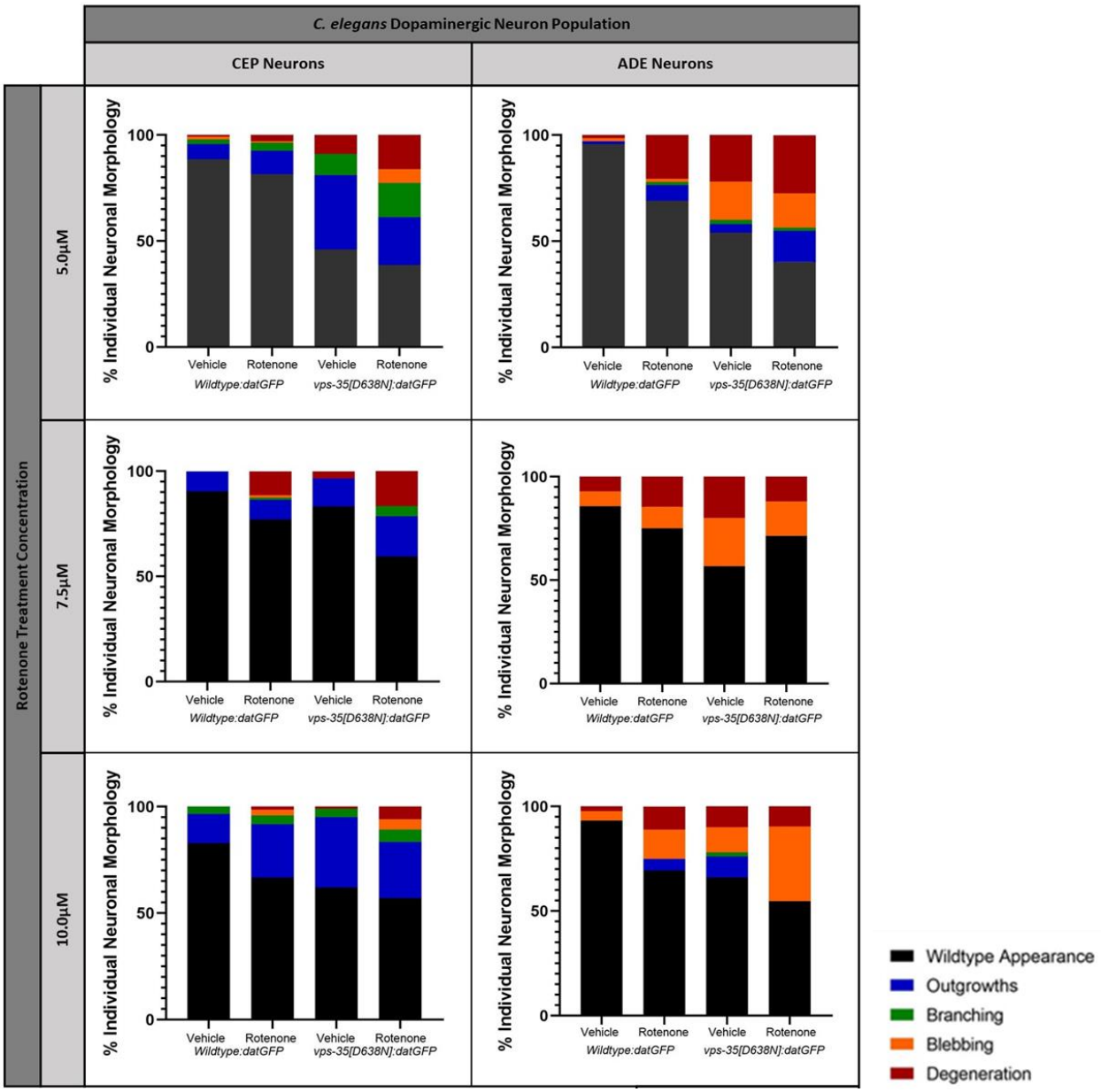

Tabulated values for 5uM treatment can be found in 3.9.2.

Neuronal Subgroup	Genotype	Treatment	% Neurons in *C. elegans* Population Morphology					N
			Wildtype Appearance	Outgrowths	Branching	Blebbing	Degeneration	
7.5μM Treatment								
CEP	Wildtype:GFP	Vehicle	90.47619	9.52380952	0	0	0	84
		Rotenone	77.08333	9.375	1.041667	1.041667	11.45833	60
	VPS-35[D638N]:GFP	Vehicle	83.33333	13.3333333	0	0	3.333333	96
		Rotenone	59.52381	19.047619	4.761905	0	16.66667	84
ADE	Wildtype:GFP	Vehicle	85.71429	0	0	7.142857	7.142857	42
		Rotenone	75	0	0	10.41667	14.58333	30
	VPS-35[D638N]:GFP	Vehicle	56.66667	0	0	23.33333	20	48
		Rotenone	71.42857	0	0	16.66667	11.90476	42
10μM Treatment								
CEP	Wildtype:GFP	Vehicle	82.95455	13.63636	3.409091	0	0	88
		Rotenone	66.66667	25	4.166667	2.777778	1.388889	100
	VPS-35[D638N]:GFP	Vehicle	62	33	4	0	1	72
		Rotenone	57.14286	26.19048	5.952381	4.761905	5.952381	84
ADE	Wildtype:GFP	Vehicle	93.18182	0	0	4.545455	2.272727	44
		Rotenone	69.44444	5.555556	0	13.88889	11.11111	50
	VPS-35[D638N]:GFP	Vehicle	66	10	2	12	10	36
		Rotenone	54.7619	0	0	35.71429	9.52381	42

Increased impairment number shown in vps-35[D638N] heterozygotes is not exacerbated by 7.5 or 10μM rotenone

As illustrated below, treatment with 7.5 and 10μM rotenone does not substantially increase the number of minor or major impairments in wildtype or *vps-35[D638N]* heterozygote *C. elegans* in a dose dependant manner. In terms of minor impairments, there is an increase in the number of impairments per wildtype *C. elegans* in 10μM rotenone treatment, with 2 or more impairments in 45% of the population, compared to 25% in the 5.0μM. However, there is not a dose dependant increase reflected in 7.5μM treatment, as only 12% are affected. Similarly, no dose dependent increase is shown in the vps-35[D638N] heterozygote.

Furthermore, there is no rotenone dose dependant increase in major impairments in either the wildtype, or vps-35[D638N] heterozygote. In the 7.5μM rotenone treated wildtype C. elegans, approximately 20% have 3-4 impairments, while this is not exhibited in the 10μM treated population. Furthermore, no dose dependent increase is shown in the vps-35[D638N] heterozygotes, in the 5.0μM rotenone treated population 25% have 4 or more impairments, while this is only exhibited in 10% of individuals in the 7.5 and 10μM rotenone treated populations.

Convergent with the minor and major impairments, there is an increase in total impairments for the wildtype C. elegans treated with 10μM rotenone compared to 5.0μM, however this is not reflected in the 7.5μM treatment and not dose dependent. Furthermore, this is reflected in the rotenone treated vps-35[D638N] heterozygote, further highlighting that there is not dose dependent neuropathology's.

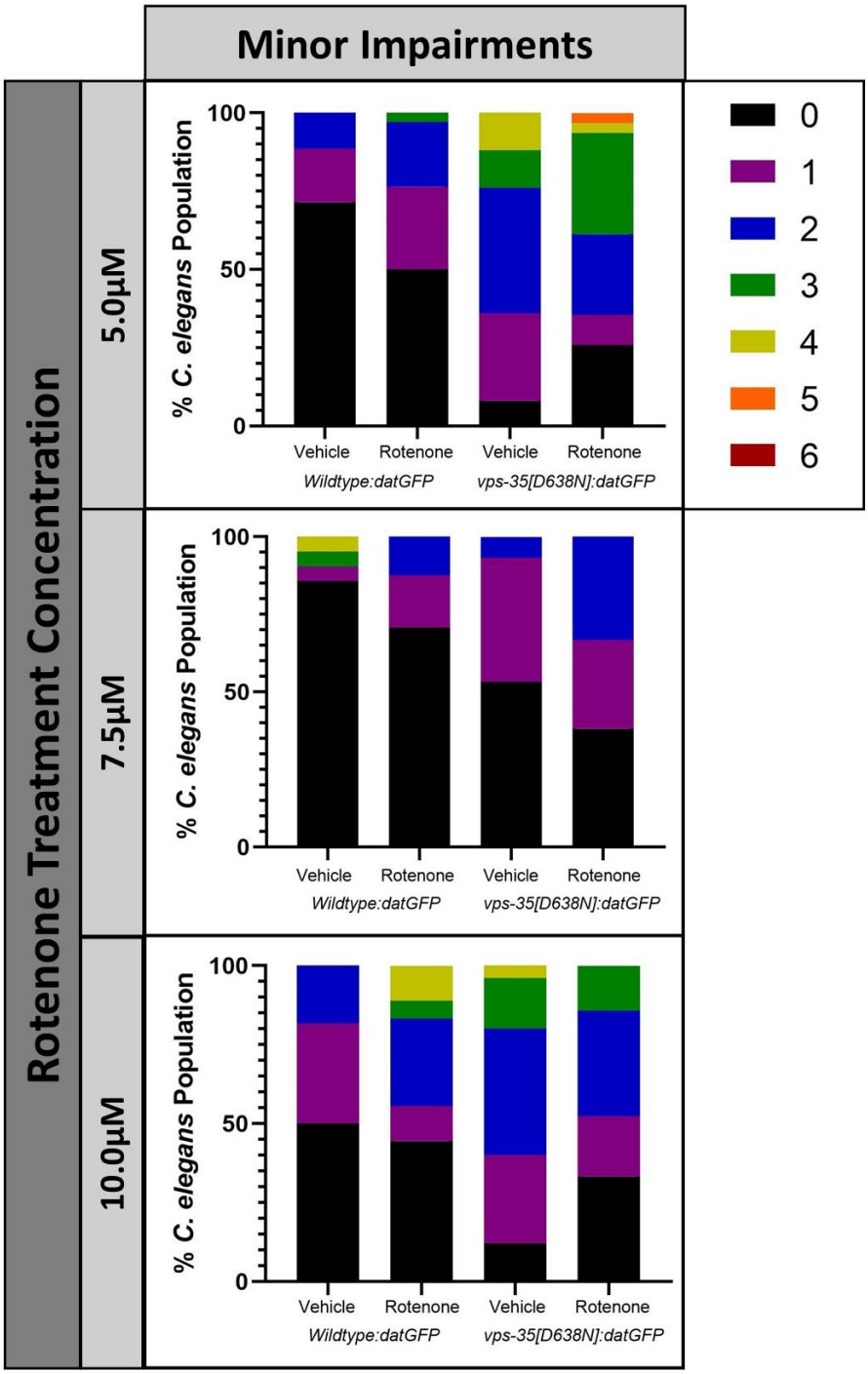
Minor Impairments
Rotenone Treatment Concentration
5.0µM
7.5µM
10.0µM
% C. elegans Population
100
50
0
Vehicle
Rotenone
Vehicle
Rotenone
Wildtype:datGFP
vps-35[D638N]:datGFP
0
1
2
3
4
5
6

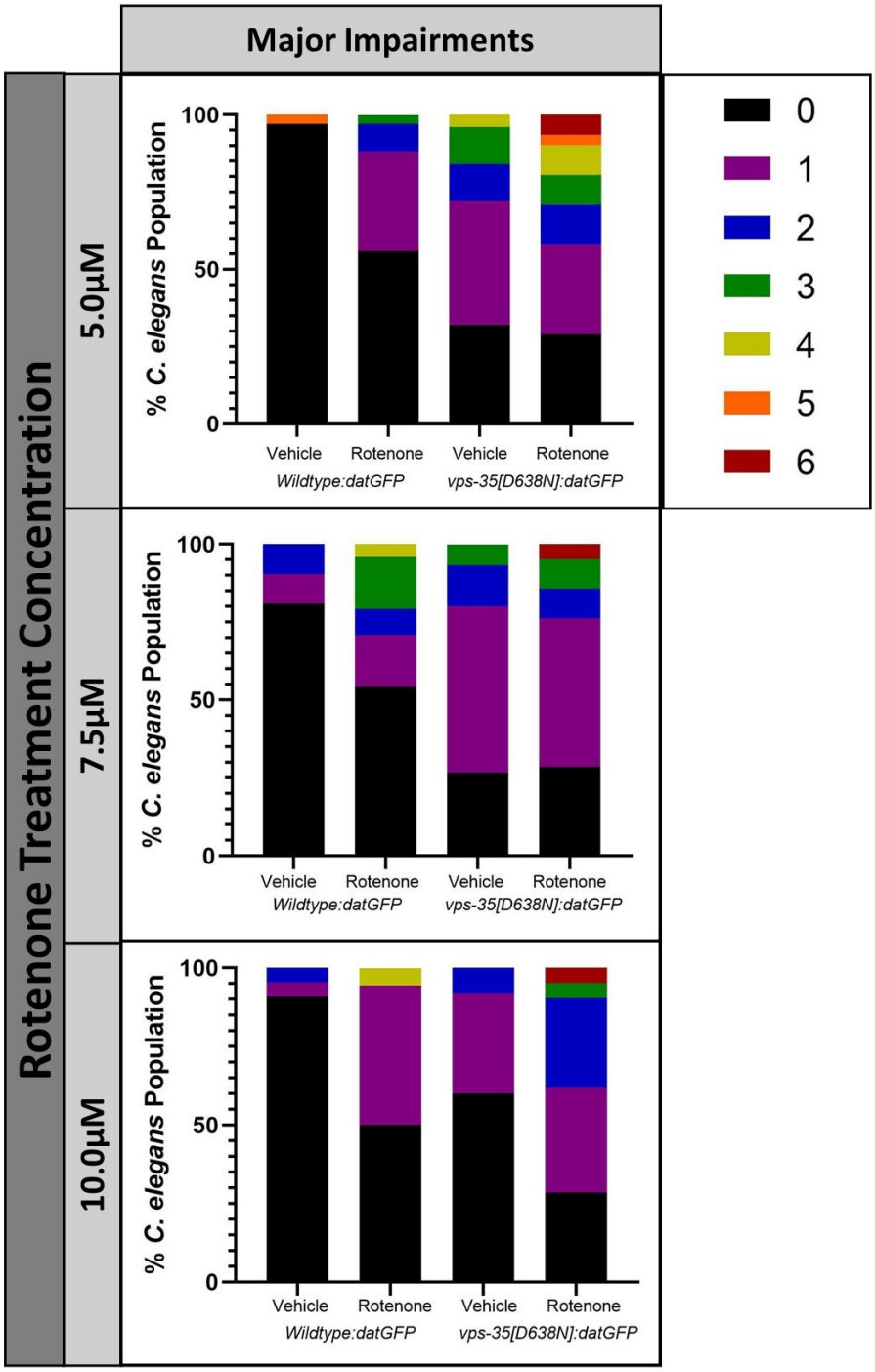
Major Impairments
Rotenone Treatment Concentration
5.0µM
7.5µM
10.0µM
% C. elegans Population
100
50
0
Vehicle
Rotenone
Vehicle
Rotenone
Wildtype:datGFP
vps-35[D638N]:datGFP
0
1
2
3
4
5
6

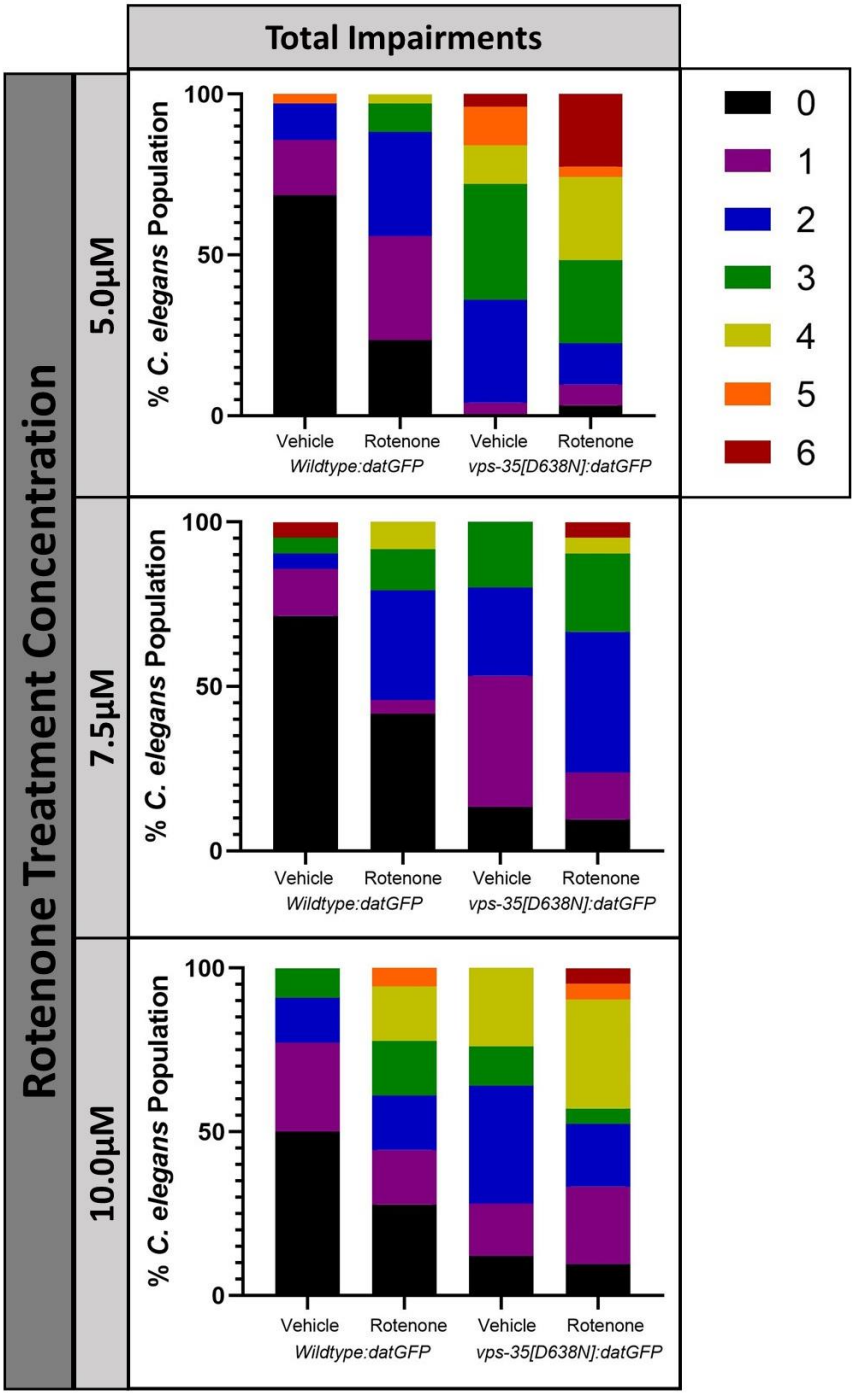
Total Impairments
Rotenone Treatment Concentration
5.0µM
7.5µM
10.0µM
% C. elegans Population
100
50
0
Vehicle
Rotenone
Vehicle
Rotenone
Wildtype:datGFP
vps-35[D638N]:datGFP
0
1
2
3
4
5
6

Tabulated values for 5uM treatment can be found in 3.9.2.

Type	Genotype	Treatment	% C. elegans in population with number of impairments							N
			0	1	2	3	4	5	6	
7.5μM Treatment										
Total	Wildtype:GFP	Vehicle	71.42857	14.28571	4.761905	4.761905	0	0	4.761905	21
		Rotenone	41.66667	4.166667	33.33333	12.5	8.333333	0	0	15
	VPS-35[D638N]:GFP	Vehicle	13.33333	40	26.66667	20	0	0	0	24
		Rotenone	9.52381	14.28571	42.85714	23.80952	4.761905	0	4.761905	21
Minor	Wildtype:GFP	Vehicle	85.71429	4.761905	0	4.761905	4.761905	0	0	21
		Rotenone	70.83333	16.66667	12.5	0	0	0	0	15
	VPS-35[D638N]:GFP	Vehicle	53.33333	40	6.666667	0	0	0	0	24
		Rotenone	38.09524	28.57143	33.33333	0	0	0	0	21
Major	Wildtype:GFP	Vehicle	80.95238	9.52381	9.52381	0	0	0	0	21
		Rotenone	54.16667	16.66667	8.333333	16.66667	4.166667	0	0	15
	VPS-35[D638N]:GFP	Vehicle	26.66667	53.33333	13.33333	6.666667	0	0	0	24
		Rotenone	28.57143	47.61905	9.52381	9.52381	0	0	4.761905	21
10μM Treatment										
Total	Wildtype:GFP	Vehicle	50	27.27273	13.63636	9.090909	0	0	0	22
		Rotenone	27.77778	16.66667	16.66667	16.66667	16.66667	5.555556	0	25
	VPS-35[D638N]:GFP	Vehicle	12	16	36	12	24	0	0	18
		Rotenone	9.52381	23.80952	19.04762	4.761905	33.33333	4.761905	4.761905	21
Minor	Wildtype:GFP	Vehicle	50	31.81818	18.18182	0	0	0	0	22
		Rotenone	44.44444	11.11111	27.77778	5.555556	11.11111	0	0	25
	VPS-35[D638N]:GFP	Vehicle	12	28	40	16	4	0	0	18
		Rotenone	33.33333	19.04762	33.33333	14.28571	0	0	0	21
Major	Wildtype:GFP	Vehicle	90.90909	4.545455	4.545455	0	0	0	0	22
		Rotenone	50	44.44444	0	0	5.555556	0	0	25
	VPS-35[D638N]:GFP	Vehicle	60	32	8	0	0	0	0	18
		Rotenone	28.57143	33.33333	28.57143	4.761905	0	0	4.761905	21

The most prevalent neuropathology's in vps-35[D638N] heterozygotes are not exacerbated by 7.5 or 10μM rotenone treatment

Furthermore, the most pertinent neuropathology's observed in both C. elegans genotypes have been contrasted following the three concentrations of rotenone treatment. In vehicle vps-35[D638N] heterozygotes, the most pertinent neuropathology's are minor impairments in the CEP neurons and major impairments in the ADE neurons. Following rotenone treatment, the vps-35[D638N] heterozygotes show an increase in major CEP neuronal impairments; however this is not dose dependant, with fewer C. elegans showing this following 10 and 7.5μM rotenone treatment compared to 5μM. Between 5 and 10μM rotenone treatment, there was a similar number of major impairments in the ADE neuron, but this is not as high in the 7.5μM treated C. elegans. In the wildtype, vehicle treated C. elegans, the most common neuropathology's are CEP minor impairments and ADE major impairments, but to a mech reduced extent compared to the vps-35[D638N] heterozygote. Following rotenone treatment, there is an increase in these impairments and an increase in major CEP neuronal impairments, however as with the vps-35[D638N], this is not in a dose dependant man

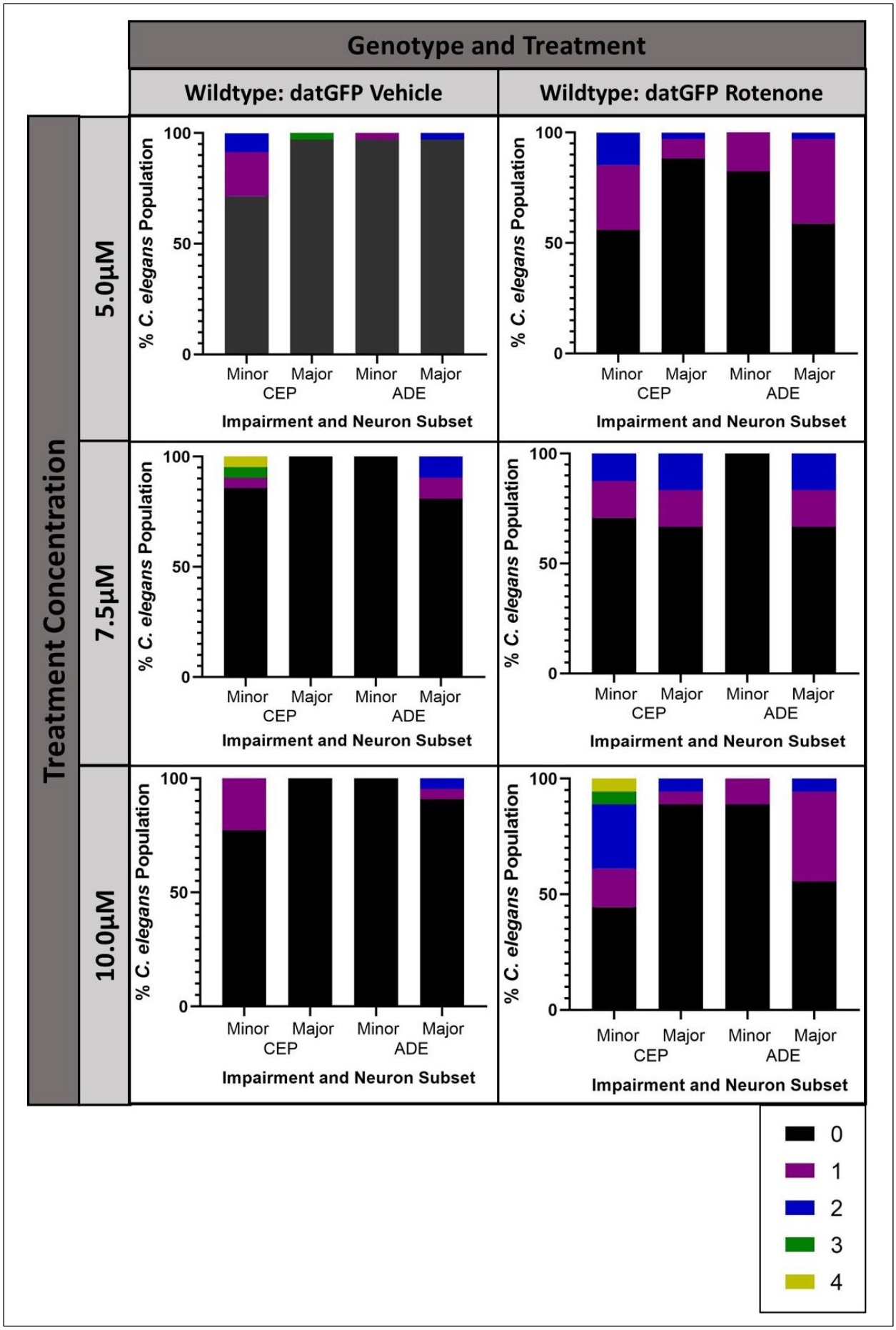
Genotype and Treatment
Wildtype: datGFP Vehicle
Wildtype: datGFP Rotenone
Treatment Concentration
5.0µM
7.5µM
10.0µM
% C. elegans Population
100
50
0
Minor
Major
Minor
Major
CEP
ADE
Impairment and Neuron Subset
0
1
2
3
4

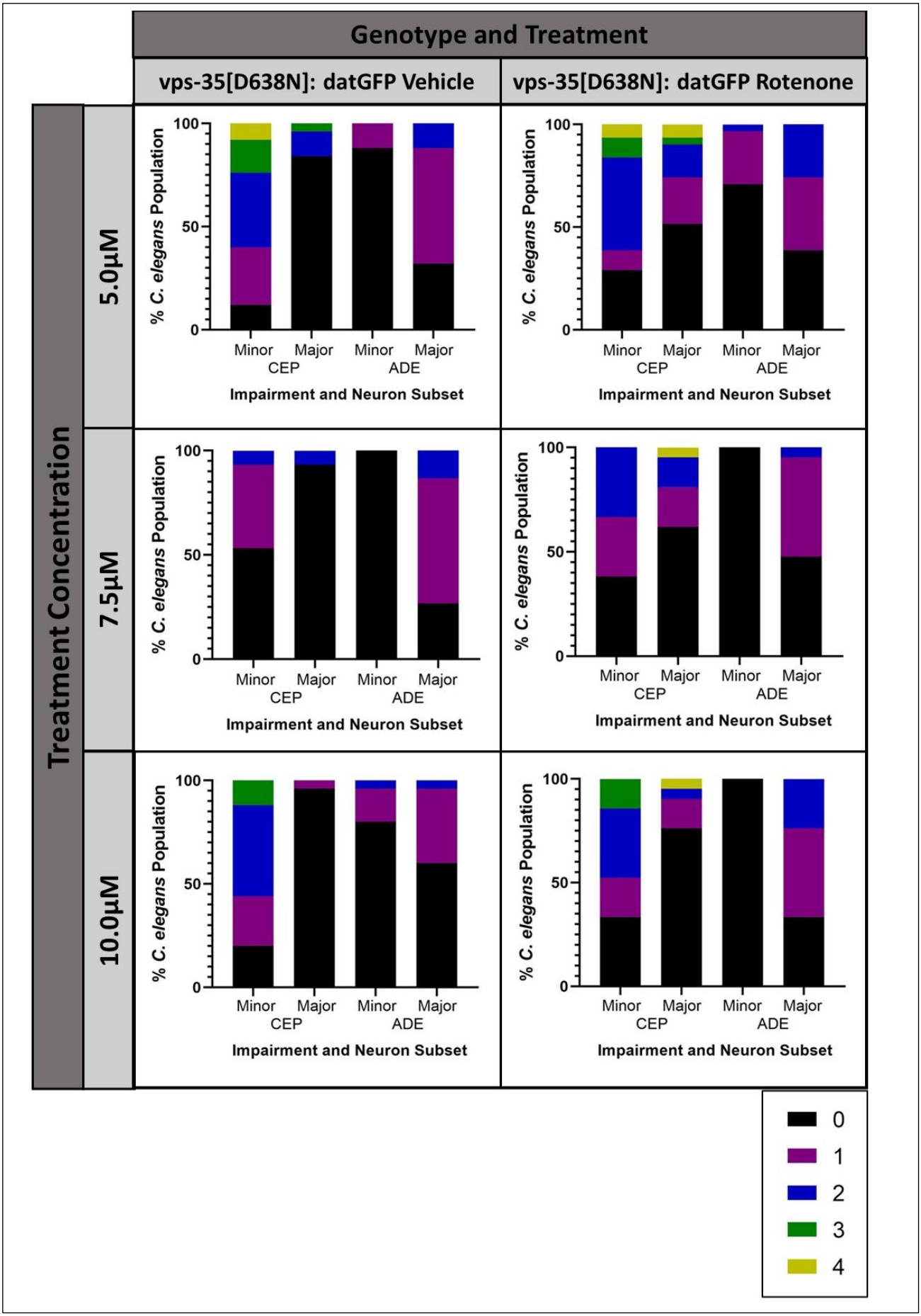
Genotype and Treatment
vps-35[D638N]: datGFP Vehicle
vps-35[D638N]: datGFP Rotenone
Treatment Concentration
5.0µM
7.5µM
10.0µM
% C. elegans Population
100
50
0
Minor
Major
Minor
Major
CEP
ADE
Impairment and Neuron Subset
0
1
2
3
4

Tabulated values for 5uM treatment can be found in 3.10.2.

Genotype	Treatment	Neuronal Subgroup	Type	% C. elegans in population with number of impairments					N
				0	1	2	3	4	
7.5μM Treatment									
Wildtype:GFP	Vehicle	CEP	Minor	85.71429	4.761905	0	4.761905	4.761905	84
			Major	100	0	0	0	0	84
		ADE	Minor	100	0	0			42
			Major	80.95238	9.52381	9.52381			42
	Rotenone	CEP	Minor	70.83333	16.66667	12.5	0	0	60
			Major	66.66667	16.66667	16.66667	0	0	60
		ADE	Minor	100	0	0			30
			Major	66.66667	16.66667	16.66667			30
VPS-35[D638N]:GFP	Vehicle	CEP	Minor	53.33333	40	6.666667	0	0	96
			Major	93.33333	0	6.666667	0	0	96
		ADE	Minor	100	0	0			48
			Major	26.66667	60	13.33333			48
	Rotenone	CEP	Minor	38.09524	28.57143	33.33333	0	0	84
			Major	61.90476	19.04762	14.28571	0	4.761905	84
		ADE	Minor	100	0	0			42
			Major	47.61905	47.61905	4.761905			42
10μM Treatment									
Wildtype:GFP	Vehicle	CEP	Minor	77.27273	22.72727	0	0	0	88
			Major	100	0	0	0	0	88
		ADE	Minor	100	0	0			44
			Major	90.90909	4.545455	4.545455			44
	Rotenone	CEP	Minor	44.44444	16.66667	27.77778	5.555556	5.555556	100
			Major	88.88889	5.555556	5.555556	0	0	100
		ADE	Minor	88.88889	11.11111	0			50
			Major	55.55556	38.88889	5.555556			50
VPS-35[D638N]:GFP	Vehicle	CEP	Minor	20	24	44	12	0	72
			Major	96	4	0	0	0	72
		ADE	Minor	80	16	4			36
			Major	60	36	4			36

	Rotenone	CEP	Minor	33.33333	19.04762	33.33333	14.28571	0	84
			Major	76.19048	14.28571	4.761905	0	4.761905	84
		ADE	Minor	100	0	0			42
			Major	33.33333	42.85714	23.80952			42

3.9.3.1 vps-35[D638N] heterozygotes show reduced fluorescence in the CEP cell bodies in day 15 and day 18 of adulthood

Descriptive statistics and unpaired two-tailed T-test with Welch's correction for unequal standard deviations, comparing fluorescence of age matched genotypes.

Age	Genotype	Mean	Standard Deviation	Number	P-Value	Significance
15	Wildtype:GFP	5695	1224	19		
	VPS-35[D638N]:GFP	3933	953.0	22	<0.0001	****
18	Wildtype:GFP	4924	978.4	14		
	VPS-35[D638N]:GFP	3136	1503	20	0.0002	***

3.9.3.2 *vps-35[D638N]* heterozygotes show enhanced degeneration and blebbing in the CEP and ADE neurons in day 15 and day 18 of adulthood

Neuronal Subgroup	Age	Genotype	% Neurons in *C. elegans* Population Morphology					N
			Wildtype Appearance	Outgrowths	Branching	Blebbing	Degeneration	
CEP	15	Wildtype:GFP	57.89474	38.15789	3.947368	0	0	76
		VPS-35[D638N]:GFP	26.13636	64.77273	0	0	9.090909	88
	18	Wildtype:GFP	30.35714	32.14286	7.142857	17.85714	12.5	56
		VPS-35[D638N]:GFP	12.5	17.5	6.25	27.5	36.25	80
ADE	15	Wildtype:GFP	81.57895	2.631579	2.631579	13.15789	0	38
		VPS-35[D638N]:GFP	45.45455	9.090909	0	38.63636	6.818182	44
	18	Wildtype:GFP	57.14286	0	0	32.14286	10.71429	28
		VPS-35[D638N]:GFP	10	0	5	37.5	47.5	40

3.9.3.3 vps-35[D638N] heterozygotes show substantially increased impairments per C. elegans in day 15 and day 18 of adulthood

Type	Age	Genotype	% C. elegans in population with number of impairments							N
			0	1	2	3	4	5	6	
Total	15	Wildtype:GFP	10.52632	21.05263	31.57895	26.31579	10.52632	0	0	19
		VPS-35[D638N]:GFP	0	4.545455	9.090909	18.18182	22.72727	36.36364	9.090909	22
	18	Wildtype:GFP	7.142857	0	14.28571	28.57143	14.28571	21.42857	14.28571	14
		VPS-35[D638N]:GFP	0	0	0	7.142857	7.142857	7.142857	78.57143	20
Minor	15	Wildtype:GFP	10.52632	26.31579	36.84211	26.31579	0	0	0	19

		VPS-35[D638N]:GFP	4.545455	4.545455	45.45455	18.18182	13.63636	9.090909	4.545455	22
	18	Wildtype:GFP	35.71429	0	42.85714	14.28571	7.142857	0	0	14
		VPS-35[D638N]:GFP	55	10	25	0	5	5	0	20
Major	15	Wildtype:GFP	73.68421	26.31579	0	0	0	0	0	19
		VPS-35[D638N]:GFP	22.72727	45.45455	18.18182	9.090909	4.545455	0	0	22
	18	Wildtype:GFP	21.42857	35.71429	7.142857	14.28571	7.142857	0	14.28571	14
		VPS-35[D638N]:GFP	0	25	5	5	5	5	55	20

3.9.3.4 vps-35[D638N] heterozygotes show a similar, but exacerbated neuropathology profile to wildtype in day 15 and day 18 of adulthood

Age	Genotype	Neuronal Subgroup	Type	% C. elegans in population with number of impairments					N
				0	1	2	3	4	
15	Wildtype:GFP	CEP	Minor	10.52632	26.31579	47.36842	15.78947	0	76
			Major	100	0	0	0	0	76
		ADE	Minor	89.47368	10.52632	0			38
			Major	73.68421	26.31579	0			38
	VPS-35[D638N]:GFP	CEP	Minor	4.545455	4.545455	45.45455	18.18182	27.27273	88
			Major	77.27273	9.090909	13.63636	0	0	88
		ADE	Minor	86.36364	9.090909	4.545455			44
			Major	27.27273	59.09091	13.63636			44
18	Wildtype:GFP	CEP	Minor	35.71429	0	42.85714	14.28571	7.142857	56
			Major	50	14.28571	14.28571	7.142857	14.28571	56
		ADE	Minor	100	0	0			38
			Major	28.57143	57.14286	14.28571			38
	VPS-35[D638N]:GFP	CEP	Minor	55	10	25	5	5	28
			Major	25	10	5	5	55	28
		ADE	Minor	90	10	0			40
			Major	0	30	70			40

Chapter IV: Results II
C. elegans LRK-1 as a model for human LRRK2 function

4.1 C. elegans LRK-1 shows conservation with human LRRK2 in silico

4.1.1. Sequence and domain conservation between human LRRK1 and LRRK2, with *C. elegans* LRK-1

ARM ANK LRR ROC COR Kinase WD40
PD Mutations PD risk genes Key Autophosphorylation sites Catalytic Ablations GTP/ATP binding
Anti-LRK-1 Sera Epitope
Emboss stretcher, Matrix: EBLOSUM62, Gap Penalty: 12, Extend Penalty: 2.

```
LRRK2              1 MASGSCQGCEEDEETLKKLIVRLNNVQEGKQIETLVQILEDLLVFTYSER     50
                     |...| .|.....:...:|    :|       ...:|::...::|
LRK-1              1 MDLSS-GGPSSSSDVASEL----DN-------SDAMQLVRQAVLF-----     33

EMBOSS_001        51 ASKLFQGKNIHVPLLIVLDSYMRVASVQQVGWSLLCKLIEVCPGTMQSLM    100
                        :|:.                      ||..|.:|.|..
EMBOSS_001        34 -------ENVE----------------------LLADLFKVNPWV-----     49

EMBOSS_001       101 GPQDVGNDWEVLGVHQLILKMLTVHNASVNLSVIGLKTLDLLLTSGKITL    150
                       |..:..|.....||..||..::    .|:|: |:|:...:.|
EMBOSS_001        50 --------WNRVDRHGRTPLMLAAHNGKLD----SLRTI-LMLSPNSLNL     86

EMBOSS_001       151 LILDEESDIFMLIFDAMHSFPANDEVQKLGCKALHVLFERVSEEQLTEFV    200
                     :                    ||.    |..|||:..|......:.|.|
EMBOSS_001        87 V---------------------NDR----GKTALHMAAESGETSIVLELV    111

EMBOSS_001       201 ENKDYMILLSALTNFKDEEEIVLHVLHCLHSLAIPCNNVEVLMSGNVRCY    250
                     |       |.:.....|.|.      ||...||....:.||
EMBOSS_001       112 E-------LGSDPMKSDNEG------HCALELAQMAGHNEV---------    139

EMBOSS_001       251 NIVVEAMKAFPMSERIQEVSCCLLHRLTLGNFFNILVLNEVHEFVVKAVQ    300
                       |..:.:.||:.|               ..|||.|..:.:.|
EMBOSS_001       140 --------AAKLIDAIQKES--------------EDLNEAHTMIISA--    164

EMBOSS_001       301 QYPENAALQISALSCLALLTETIF-LNQDLEEKNENQEN--DDEGEEDKL    347
                             |::...:.:: ::::...||.:::|.  :...|||:.
EMBOSS_001       165 --------------CISGSADVVYEISRRFMEKKQSREILFNGRNEEDET    200

EMBOSS_001       348 FWLEACYKALTWHRKNKHVQEAACWALNNLLMYQNSLHEKIGDEDGHFPA    397
                     ..|.||        .|.|::     .:.:||.::..|.:.      |  .
EMBOSS_001       201 ALLIAC--------TNGHIE-----IVRHLLQFEEHLLQS------H--V    229

EMBOSS_001       398 HREVMLSMLMHSSSKEVFQASANALSTLLEQNVNFRKILLSKGIHLNVLE    447
                     .::.::...:.|.:.||.|........|::...|.....|.........|
EMBOSS_001       230 SKDTVIHAAVSSQNVEVLQLCLEKFPQLVKSTNNEGSTCLHWAARCGSSE    279

EMBOSS_001       448 LMQKHIHSPEVAESGCKMLNHLFEGSNTSLDIMAAVVPKILTVMKRHETS    497
                     .:..             :||..|. |...::|.....|.....:..:|
EMBOSS_001       280 CVST------------ILNFPFP-SEFIIEIDTVGAPAYQLALDVNE--    313

EMBOSS_001       498 LPVQLEALRAILHFIVPGMPEESREDTEFHHKLNMVKKQCFKNDIHKLVL    547
                       |..|...|:...:..|..|..:..|:|         :|...|
EMBOSS_001       314 --VDGECRTAMYLAVAEGHLEVVKAMTDF---------KCTSID------    346
```

```
EMBOSS_001      548 AALNRFIGNPGIQKCGLKVISSIVHFPDALEMLSLEGAMDSVLHTLQMYP  597
                    |.|:|           |..|::....|....:|...
EMBOSS_001      347 ----------GRQRC-----------PFQLDVYCTRGRTPFMLAAF----  371

EMBOSS_001      598 DDQEIQCLGLSLIGYLITKKNVFIGTGHLLAKILVSSLYRFKDVAEIQTK  647
                     :|.:..:.|.|..          |....|...::.:.|   .|.|.:..
EMBOSS_001      372 -NQNLPLMTLLLDA----------GADVNLPLAVLDTEY---SVEEGRCI  407

EMBOSS_001      648 GFQTILAILKLSASFSKLLVHHSFDLVIFHQMSSNIMEQKDQQFLNLCCK  697
                    |...::..::           |..|.|.|.:........|.:.|.|
EMBOSS_001      408 GSGALVEAVR-----------SDGLHIVHFLLDRGALDTDNKALRL---  442

EMBOSS_001      698 CFAKVAMDDYLKNVMLERACDQNNSIMVECLLLLGADANQAKEGSSLI-C  746
                      |...::.|..|.|.|....:...:.   ....|..|.:.|.||: .
EMBOSS_001      443 --AAQGKNEKLIRVFLVRLVFADPEYKIN---KKNIDVGQIQVGQSLLPS  487

EMBOSS_001      747 QVCEKESSPKLVELLLNSGSREQDVRKALTISIGKGDSQIISLLLRRLAL  796
                    .:|..    |..:|..||.:.||     |........:..::..||...|
EMBOSS_001      488 SLCPS----KAAQLNWNSANLEQ-----LQSDWFVAAALHVNPRLRTTRL  528

EMBOSS_001      797 DVANNSICLGGFCIGKVEPSWLGPLFPDKTSNLRKQTNIASTLARMVIRY  846
                    .:|         .|.:|:.|                .|..:|...::  :
EMBOSS_001      529 SLA---------AITRVDLS----------------DNRLNTFPSIL--F  551

EMBOSS_001      847 QMKSAVEEGTASGSDGNFSEDVLSKFDEWTF-IPDSSMDSVFAQSDDLDS  895
                    ||.|.        ...|.:::.:.|.:..|: |..:|::.:..:::.|:.
EMBOSS_001      552 QMPSL--------RSLNLADNSIRKIEIPTYYISSTSLEILNLRNNQLEC  593

EMBOSS_001      896 EGSEG-SFLVKKKSNSISVGEFYRDAVLQRCSPNLQRHSNSLGPIFDHED  944
                    ...:. |.|.:.:...:|..|..:........|.|:..:.|...:.....
EMBOSS_001      594 IAIQFLSSLPQLQQLDVSKNELSQLPEYIWLCPALKELNASYNRLSTLPM  643

EMBOSS_001      945 LLKRKR-KILSSDDSLRSSKLQSHMRHSDSISSLASEREYITSLDLSANE  993
                    :.:..| :....::|..:...||..:.|:.|  :..:...:||     |.
EMBOSS_001      644 VARASRGERPRLNNSNNNFNTQSPTQESNPI--VVDDPPNVTS-----NP  686

EMBOSS_001      994 LRDIDALSQKCCISVHLEHLEKLELHQNALTSFPQQLCETLKSLTHLDLH 1043
                    ||..:...    .|::|..::...|       ||.....:..:||.::|.
EMBOSS_001      687 LRRQNVWQ----ASINLSKVDDDSL-------FPDFPVTSSNTLTTINLS  725

EMBOSS_001     1044 SNKFTSFPSYLLKMSC--IANLDVSRNDIGPSVVLDPTVKCPT-LKQFNL 1090
                    .|||.:|| :.|..:|  :..|::|.|.:   ..|.|....|. |:..:|
EMBOSS_001      726 FNKFHTFP-FCLACTCPRLLILNMSNNSM---TSLPPMACVPAHLRTLDL  771

EMBOSS_001     1091 SYNQLSFVPENLTDVVEKLEQLILEGNKISGICSPLRLKELKILNLSKNH 1140
                    |||              |:::..:|.:.:..:|..:........|.|..
EMBOSS_001      772 SYN-------------KIQESFIEASPLHVVCHAVPPTTSNGSMLPKRR  807

EMBOSS_001     1141 ISSLSENFLEACPKVESFSARMNFLAAMPFLPPSMTILKLSQNKFSCIPE 1190
                    .|...::...:...|.| ...::.......:.|.       :.:.||:.:
EMBOSS_001      808 NSPARQHRSRSKSAVRS-QRSLSVSRHHALIDPQ-------KEEESCVHK  849

EMBOSS_001     1191 AILNLPHLRSLDMSSNDIQYLPGPAHWKSLNLRELLFSHNQISILDLSEK 1240
                    ...:|..|::|.::.|.::                   .||:.:.:.|
EMBOSS_001      850 RHDSLEWLKTLQLAGNRLR--------------------SISVTNAASK  878

EMBOSS_001     1241 AYLWSRVEKLHLSHNKLKEIPPEIGCLENLTSLDVSYNLELRSFPNEMGK 1290
                    ..| ..:..:.:|.|||.:.||::..|..|:.|::|.|..::..|.:.|.
EMBOSS_001      879 VLL-PALNVMDISDNKLLQAPPDVARLTLLSMLNLSGNTAIKELPPDYGM  927

EMBOSS_001     1291 LSKIWDLPLDELHLNFDFKHI----GCKAKDIIRFLQQRLKKAVPYNRMK 1336
                    ||::|.|.|....|....:.:    .||..:|:.:|:..|::..|:.::
EMBOSS_001      928 LSRLWSLSLKGCSLKEPLESMVNVENCKTVEIVAYLKTILEESKTYHHLR  977

EMBOSS_001     1337 LMIVGNTGSGKTTLLQQLMKTK-KSDLGMQSATVGIDVKDWPIQIR---- 1381
                    |||:|:.|.||:.:...|.|.. :....:.|.|..|...:|..:.:
EMBOSS_001      978 LMILGSDGVGKSVIWDALCKEAVQKRQPIHSETGVIRQAEWKFEAKRSKG 1027

EMBOSS_001     1382 DKRKRDLVLNVWDFAGREEFYSTHPHFMTQRALYLAVYDLSKGQAEVDAM 1431
                    ||...:..:|.||.|:.|::|||.:|:::|:|.|.::.::.|...:..:
```

```
EMBOSS_001      1028 DKNLGPVGFSVIDFGGQREYHSTHQYFLSKRSLNLVLWKITDGDEALAQL 1077

EMBOSS_001      1432 KPWLFNIKARASSSPVILVGTHLDVSDEKQRK-------ACMSKITKELL 1474
                     ..||.||.|||.:|.||||||:||.......|       ....|:....:
EMBOSS_001      1078 DTWLVNIHARAPNSTVILVGTNLDQVASNSSKFGPGYIDIMEQKVRTRYM 1127

EMBOSS_001      1475 ----NKRGFPAIRDYHFVNATEESDALAKLRKTIINESLNFKIRDQLVVG 1520
                         :|.|.|.|.|...:|:|..:|..|.|. ||...:...:|..:...:.
EMBOSS_001      1128 VADADKSGLPRIVDVILINSTSRNDVKALLN-TIYRTAWEVRMGKERAME 1176

EMBOSS_001      1521 QLIPDCYVELEKI-----ILSERKNVPIEFPVI---DRKRLLQLVRENQL 1562
                     |.||..|:.|.|:     :...::..|....|.   :|.:...:.:..:.
EMBOSS_001      1177 QQIPSSYIALMKVTKELGVEFRKEGQPAVMTVEAYRERVKKRMISKFGRP 1226

EMBOSS_001      1563 QLDENELPHAVHFLNESGVLLHFQDPALQLSDLYFVEPKWLCKIMAQILT 1612
                     ..|:.|...|..||::.|.|:.|:|..|:  ||.||:|.||.:.:..::.
EMBOSS_001      1227 FRDDIEFYAACTFLHDCGELVRFEDATLR--DLIFVDPLWLAEFLTSVVI 1274

EMBOSS_001      1613 VKVEGCPKHPKGIISRRDVEKFL-SKKRKFPKNYMSQYFKLLEKFQIALP 1661
                     ::   .|..|.|::|...:.... |.|........:|...||.||::||.
EMBOSS_001      1275 LR---SPNLPAGLLSTDAINPHTRSFKSGALLMLKTQLLDLLHKFELALA 1321

EMBOSS_001      1662 IGEEYLLVPSSLSDHRPV-------------------IELPH-------- 1684
                     .....||:||.|.|...:                   :..|.
EMBOSS_001      1322 TQPRQLLIPSLLPDEYRLRSDFLASAVKIRMKMSQWNVRCPSPAGSPTKS 1371

EMBOSS_001      1685 ----------------------CENSEIIIRLYEMPYFPMGFWSRLINR 1711
                                           .::.:::.|:|.:.|.|.||||||:.|
EMBOSS_001      1372 PLRRTSPTDQNGVGSEDVMLQFTYDDDQLLRRIYALAYIPSGFWSRLVTR 1421

EMBOSS_001      1712 LLEI--------SPYMLSGRERA---------LRPNRMYWRQGIYLN--- 1741
                     ::..        |.:|.:..:||         .:...:.|:.||.|:
EMBOSS_001      1422 IVGDKNVCAAIESIFMTTSADRAKIADIATKHAKAEWVVWQTGIELHVKG 1471

EMBOSS_001      1742 ------------------------------------WS-----PEAYCLV 1750
                                                        |:     |....:|
EMBOSS_001      1472 HSLFTLKQFLPLAEVRDIDYSAIDMRAKDEQKRWRTWNQPSHRPIVEMVV 1521

EMBOSS_001      1751 GSEVLDNHPESFLKITVPSCRKG-CILLGQVVDHIDSLMEEWFPGL-LEI 1798
                     .|..:....:...|:::.:..:| ..||..:.|.:|:|:|:|:|.| ...
EMBOSS_001      1522 NSLSISAASQHGRKLSMKTDVEGRSRLLAMISDLLDTLLEDWYPALGTRF 1571

EMBOSS_001      1799 DICGEGETLLKKWALY-----------------------SFNDGE---- 1820
                     ....||:.|:.:.:.|.                      |.:|||
EMBOSS_001      1572 VHSSEGDLLVSRYVLCPQCVRDAERNGSRSRTSSSASHRRSQDDGELPIT 1621

EMBOSS_001      1821 --EHQK-----------------ILLDDLMKKAEEGDLLVNPDQPRLTI 1850
                       .|.|                .:::::.|....|.:.:..|....|.:
EMBOSS_001      1622 SSSHMKGSRTTGDISKCRGGVVHCFVIEECMLAGREYNWVECPSHGGLHM 1671

EMBOSS_001      1851 PISQIAPDLILADLPRNIMLNNDELEFEQAPEFLLGDGSFGSVYRAAYE- 1899
                       .::|||.:.||:...:.::.|:|:..:    :||.|:||.|:||...
EMBOSS_001      1672 --RELAPDTVFADIENALTIHPDQLKRSR----MLGRGAFGFVFRATVRQ 1715

EMBOSS_001      1900 --GE--EVAVKIFN----------------------KHTSLRLL----- 1917
                       ||  |||.|:..                     |..|:...
EMBOSS_001      1716 PNGELCEVAQKMLEPVDPGPGGRPSALAAYKAAADKWKRDSMEFACRAYC 1765

EMBOSS_001      1918 --RQELVVLCHLHHPSLISLLAAGIRPRMLVMELASKGSLDRLLQQDKAS 1965
                       ||||.:|..:.||::|.|:.....|..||:|||..|:|::||...:.:
EMBOSS_001      1766 TSRQELSLLSRMKHPNVIGLVGVCTFPLSLVVELAPLGALNQLLGSHRKA 1815

EMBOSS_001      1966 LTRTLQHRI---ALHVADGLRYLHSAMIIYRDLKPHNVLLFTL----YPN 2008
                     .|:.....|   |:.||..|.|||||.|||||||..|||.:..    .|.
EMBOSS_001      1816 GTKLSLGVIKESAVQVARALEYLHSAHIIYRDLKSENVLGWRFPAPFSPQ 1865

EMBOSS_001      2009 AAIIAKIADYGIAQYCCRMG-IKTSEGTPGFRAPEVAR--GNVIYNQQAD 2055
                     ..::.|:.||||:.....| .|...||.||.|||:.|  |...|.|:.|
EMBOSS_001      1866 TDVLLKLGDYGISRSVLPSGGAKGFGGTEGFMAPEIVRFNGEEEYTQKVD 1915

EMBOSS_001      2056 VYSFGLLLYDILTTGGRIVEGLKFPNEFDE----LEIQGKLPDPVKEYGC 2101
```

```
                .:|||:.||::||        ||||.|.:|    ..:.|..|..:.....
EMBOSS_001   1916 CFSFGMFLYELLT--------LKFPFESEEHVKERMLDGARPVLLPHELL   1957

EMBOSS_001   2102 APWPMVEKLIKQCLKENPQERPTSAQVFDILNSAEL-----VCLTRRILL   2146
                  .|.||::.|: .|...:|:.||:|:|:.....:.|.     ||.....|.
EMBOSS_001   1958 LPTPMLDLLV-HCWSAHPESRPSSSQLVGFCAAPEFTHLLDVCELGEALP   2006

EMBOSS_001   2147 PKNVIVECMV--ATHHNSRNASIWLGCGHTDRGQLSFLDLNTEGYTSEEV   2194
                  |..:.:..:.  ....:..|.:||          |..:.:..|.|....
EMBOSS_001   2007 PTQLMAVGITDEIDDPDDFEAQLWL----------SGREMVVMGCTQYGF   2046

EMBOSS_001   2195 ADSRILCLALVHLPVEK-ESWIVSGTQSGTLLVINTEDGKKRHT-LEKMT   2242
                  .|.:.:.|.....|.| ...:.|..:.|.:|.....:..|. |..:.
EMBOSS_001   2047 VDQKSIELPHRGKYVSKVRDSVWSCDECGQVTVYGISLHETGHLQLPSLN   2096

EMBOSS_001   2243 DSVTCLYCNSFSKQSKQKNFLLVGTADGKLAIFEDKTVKLKGAAPLKILN   2292
                  .:.:|.       .....|.:|:..:|.::       |.||.:...:.:
EMBOSS_001   2097 GTLICA-------PELISNDVLILISDKQI-------VLLKLSESNSVSH   2132

EMBOSS_001   2293 IGNVSTPLMCLSEST--NSTERNVMWGGCGTKIFSFSNDFTIQKLIETRT   2340
                  :|.:.:|...:.:.  |.:.|.: |.|.....|..:       |.:..
EMBOSS_001   2133 LGTIDSPYEIRTATFLGNGSTRQI-WAGHSEGRISIHH-------IASND   2174

EMBOSS_001   2341 SQLFSYAAF--SDSNIITVVVDTA----LYIAKQNSPVVEVWDKKTEKLC   2384
                  |..||.:.:  .|..|:..:|.:.    ::||.:.|..|::.:.:..::.
EMBOSS_001   2175 SFSFSSSLYLPDDKCIVRQLVGSKDAQKVWIALEKSSKVQMVEVEKRQVT   2224

EMBOSS_001   2385 GLIDCVHFLREVMVKENKESKHKMSYSGRVKTLC---LQKNTA--LWIGT   2429
                  |.:|    :|:||.........|..:.:....|   |::|..  |:|||
EMBOSS_001   2225 GSLD----IRKVMPGSETIHTIDMEMASQNYVTCIGLLERNDGDQLYIGT   2270

EMBOSS_001   2430 GGGHILLLDLSTRRLIRVIYNFCNSVRVMMTAQLGSL-------KNVMLV   2472
                  ..|.:::...:|.:.:.....|...:..:...:..|.       |...|.
EMBOSS_001   2271 SKGLLVIAHATTLQPLSACRPFEGDITSICILEEPSREEENTRGKATTLS   2320

EMBOSS_001   2473 -------LGYNRKNTEGT-----QKQKEIQSCLTVWDINLPHEVQNLEKH   2510
                        ||:.|:....|     .....:::.....:.:..:.::|...
EMBOSS_001   2321 TASSESGLGWVRERVSETVDRFRSSPATVETQGAALVVCIGRQFRSLSHR   2370

EMBOSS_001   2511 IEVRKELAE----KMRRTS--VE   2527
                  ....::||:    .:.||.  ..
EMBOSS_001   2371 FVAEEKLADVYSIAVWRTEEWAL   2393
```

4.3 Motility as a marker for Neuromuscular health

4.3.1 Crawling speed in selected novel lrk-1 CRISPR/Cas9 point mutants and transgenic human LRRK2 expressing C. elegans

Genotype	Age	Mean (mm/s)	Standard Deviation	Number
Wildtype	1	0.2026	0.05534	20
Wildtype	5	0.2275	0.04105	12
lrk-1[G1876S]	1	0.1643	0.04791	20
lrk-1[G1876S]	5	0.0760	0.04678	17
lrk-1[K988A]	1	0.2097	0.04190	20
lrk-1[K988A]	5	0.2384	0.09927	13
lrk-1[D1847A]	1	0.3111	0.06817	20
lrk-1[D1847A]	5	0.1195	0.04900	15
lrk-1(tm1898)	1	0.1590	0.05303	20
lrk-1(tm1898)	5	0.04675	0.03630	20
Hsa-LRRK2	1	0.2313	0.06469	20
Hsa-LRRK2	5	0.2139	0.07359	20
Hsa-LRRK2(G2019S)	1	0.1448	0.05894	20
Hsa-LRRK2(G2019S)	5	0.2188	0.02077	19

Comparison	**P-Value**	**Significance**
Genotype matched day 1 vs day 5		
Wildtype	0.6717	ns
lrk-1[G1876S]	<0.0001	****
lrk-1[K988A]	0.9244	ns
lrk-1[D1847A]	<0.0001	****
lrk-1(tm1898)	<0.0001	****
Hsa-LRRK2	0.9773	ns
Hsa-LRRK2(G2019S)	*	0.0345
Day 1 wildtype vs Day 1 Mutant		
lrk-1[G1876S]	0.0931	ns
lrk-1[K988A]	0.9839	ns
lrk-1[D1847A]	<0.0001	****
lrk-1(tm1898)	0.0579	ns
Hsa-LRRK2	0.4457	ns
Hsa-LRRK2(G2019S)	0.011	*
Day 5 wildtype vs Day 5 Mutant		
lrk-1[G1876S]	<0.0001	****
lrk-1[K988A]	0.9929	ns
lrk-1[D1847A]	<0.0001	****
lrk-1(tm1898)	<0.0001	****
Hsa-LRRK2	0.9360	ns
Hsa-LRRK2(G2019S)	0.9932	ns

4.3.2 Crawling Speed of LRK-1 'R1441C PD mutant' is not significantly different in dy 1 of adulthood, but impaired by day 5

Genotype	Age	Mean (mm/s)	Standard Deviation	Number
Wildtype	1	0.2387	0.1857	32
Wildtype	5	0.1291	0.07053	22
lrk-1[R1087C]	1	0.1550	0.1311	49
lrk-1[R1087C]	5	0.04741	0.02415	34
Comparison			**P-Value**	**Significance**
Day 1 Adult Wildtype vs Day 1Adult lrk-1[R1087C]			0.1174	ns
Day 5 Adult Wildtype vs Day 5 Adult			<0.0001	****
Day 1 Adult Wildtype vs Day 5 Wildtype			0.1096	ns
Day 1 Adult lrk-1[R1087C] vs Day 5 Adult lrk-1[R1087C]			0.1075	ns

4.3.3 Swimming as a marker of neuromuscular health

Genotype	Mean (mm/s)	Standard Deviation	Number
Wildtype	0.6563	0.1726	46
lrk-1[G1876S]	0.5094	0.1607	22
lrk-1[K988A]	0.4090	0.1623	47
lrk-1[D1847A]	0.6363	0.1307	37
lrk-1(tm1898)	0.6730	0.2269	22
Comparison		**P-Value**	**Significance**
lrk-1[G1876S]		0.0037	**
lrk-1[K988A]		<0.0001	****
lrk-1[D1847A]		0.9617	NS
lrk-1(tm1898)		0.9889	NS

4.4 LRK-1 and LRRK2 C. elegans mutant survival in response to oxidative stress

4.4.1 Novel LRK-1 point mutants and human LRRK2 expressing *C. elegans* show altered survival in response to oxidative stress

Time Elapsed (Days)	% Surviving C. elegans per genotype						
	Wildtype	lrk-1 [G1876S]	lrk-1 [K988A]	lrk-1 [D1847A]	lrk-1 (tm1898)	Hsa-LRRK2	Hsa-LRRK2 (G2019S)
0	100	100	100	100	100	100	100
1	100	100	100	100	100	100	100
2	90	90	87	99	69	96	89
3	87	88	84	97	64	95	86
4	83	86	83	96	63	95	84
7	81	85	82	96	62	91	82

Gehan-Breslow-Wilcoxon test, survival curve comparison between wildtype and selected mutant

Genotype	**P-value**	**Significance**
lrk-1[G1876S]	0.4143	ns
lrk-1[K988A]	0.8511	ns
lrk-1[D1847A]	<0.0001	****
lrk-1(tm1898)	0.001	**
Hsa-LRRK2	0.0001	***
Hsa-LRRK2(G2019S)	0.6883	ns

4.5. LRK-1 Parkinson's mutants show impaired dopaminergic phenotypes

4.5.1 Investigation of basal slowing phenotypes in established LRRK2 transgenic, *lrk-1* deletion and novel *lrk-1* CRISPR/Cas9 point mutants

Genotype	Age	Mean (% Slowing)	Standard Deviation	Number
Wildtype	1	83.84	12.74	20
Wildtype	5	43.52	39.25	12
lrk-1[G1876S]	1	31.23	35.46	20
lrk-1[G1876S]	5	-45.43	53.24	17
lrk-1[K988A]	1	62.04	18.79	20
lrk-1[K988A]	5	66.89	22.61	18
lrk-1[D1847A]	1	87.75	8.231	20
lrk-1[D1847A]	5	78.32	9.207	10
lrk-1(tm1898)	1	50.08	35.98	20
lrk-1(tm1898)	5	30.84	53.73	9
Hsa-LRRK2	1	74.31	18.26	20
Hsa-LRRK2	5	54.10	22.22	18
Hsa-LRRK2(G2019S)	1	65.98	33.84	20
Hsa-LRRK2(G2019S)	5	43.09	37.09	13

Comparison	**P-Value**	**Significance**
Genotype matched day 1 vs day 5		
Wildtype	0.304	*
lrk-1[G1876S]	0.0002	***
lrk-1[K988A]	0.9872	ns
lrk-1[D1847A]	0.0905	ns
lrk-1(tm1898)	0.9232	ns
Hsa-LRRK2	0.0307	*
Hsa-LRRK2(G2019S)	0.4399	ns
Day 1 wildtype vs Day 1 Mutant		
lrk-1[G1876S]	<0.0001	****
lrk-1[K988A]	0.0009	***
lrk-1[D1847A]	0.8159	ns
lrk-1(tm1898)	0.0035	**
Hsa-LRRK2	0.3169	ns
Hsa-LRRK2(G2019S)	0.1925	ns
Day 5 wildtype vs Day 5 Mutant		
lrk-1[G1876S]	0.0001	***
lrk-1[K988A]	0.3656	ns
lrk-1[D1847A]	0.0619	ns
lrk-1(tm1898)	0.9893	ns
Hsa-LRRK2	0.9447	ns
Hsa-LRRK2(G2019S)	>0.9999	ns

4.5.2 LRK-1 Parkinson's mutant R1441C equivalent shows an impaired basal slowing response in day 5 of adulthood

Genotype	**Age**	**Mean (mm/s)**	**Standard Deviation**	**Number**
Wildtype	1	63.63	16.09	20
Wildtype	5	60.54	23.87	18
lrk-1[R1087C]	1	58.65	40.17	28
lrk-1[R1087C]	5	-5.827	76.77	29
Comparison			**P-Value**	**Significance**
Day 1 Adult Wildtype vs Day 1Adult lrk-1[R1087C]			0.9589	ns
Day 5 Adult Wildtype vs Day 5 Adult lrk-1[R1087C]			0.0005	***
Day 1 Adult Wildtype vs Day 5 Wildtype			0.9829	ns
Day 1 Adult lrk-1[R1087C] vs Day 5 Adult lrk-1[R1087C]			0.001	**

4.6 Selected Cellular Phenotypes of LRRK2/LRK-1 mutants

4.6.1.1 Inference of mitochondrial function of selected LRK-1 mutants through TMRE staining

15-20 worms analysed per line. Quantified 6000-pixel area behind the pharynx. Hsa-LRRK2: *wlzls1[snb-1p::Hsa-LRRK2 + lin15*(+)]. Hsa-LRRK2(G2019S): . *wlzls3[snb-1p::Hsa-LRRK2(G2019S) + lin15(+)]*. Mean (M) and Standard Deviation (SD) indicated. Undertook one-way ANOVA, all genotypes compared with Wildtype. Welch's correction, accounting for differing SDs.

Genotype	Mean Normalised Fluorescence	Standard Deviation	Number	P-Value	Significance
Wildtype	1.0000	0.1218	20		
lrk-1[G1876S]	0.6800	0.2018	20	<0.0001	****
lrk-1[K988A]	0.7212	0.1901	18	<0.0001	****
lrk-1[D1847A]	2.0230	0.3040	20	<0.0001	****
lrk-1(tm1898)	0.8277	0.3388	20	2.188	ns
Hsa-LRRK2	0.8999	0.1634	20	0.1850	ns
Hsa-LRRK2(G2019S)	0.9399	0.4822	20	0.9942	ns

Selected LRK-1 'PD mutants' illustrate alterations in mitochondrial membrane potential

Following the characterisation of core *lrk-1* point mutants, preliminary investigation was undertaken into the mitochondrial membrane potential of alternative pathogenic PD consequent mutations in day 1 of adulthood. The *lrk-1[R1087C]* (LRRK2[R1441C]) mutant, located in the ROC domain, illustrated a significantly increased mitochondrial membrane potential compared to the wildtype. In contrast the *lrk-1[Y1409C]* (LRRK2[Y1699C]), located in the COR domain and the *lrk-1[I1877T]* (LRRK2[I2020T]), located in the kinase domain directly adjacent to the *lrk-1[G1876S]*, demonstrated a significantly reduced mitochondrial membrane potential compared to the wildtype. This is congruent with observations of the *lrk-1[G1876S]*, suggesting that PD mutations in the kinase and COR domain may reduce mitochondrial membrane potential and function, while mutations in the ROC domain may not illustrate this phenotype.

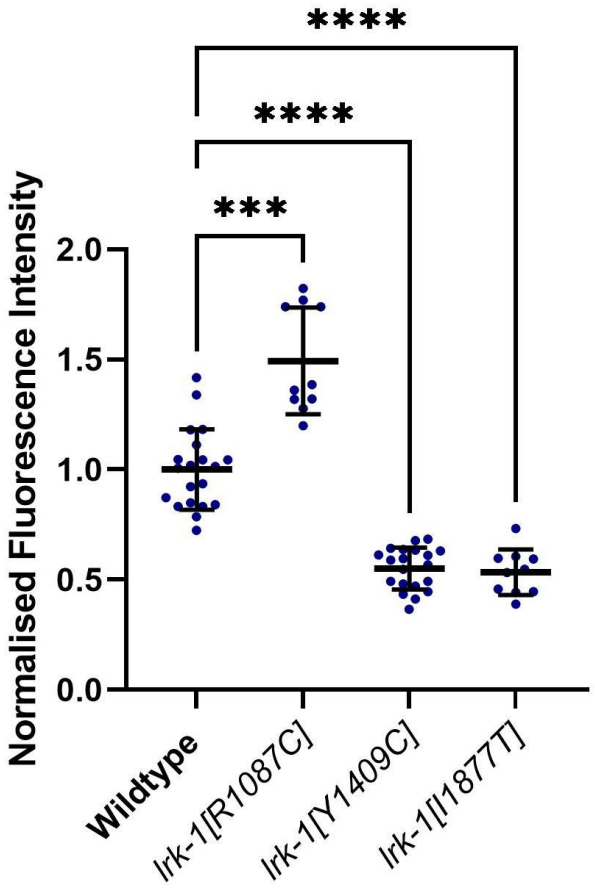

15-30 *C. elegans* were assayed per line at each developmental stage. Day 1 and Day 5 adults were from the same age-synchronised population. One way ANOVA with Brown-Forsythe and Welch Correction for unequal standard deviations undertaken. Full P values and descriptive statistics including mean, standard deviation and number can be found in the supplementary

Nomenclature on Graph	**Human orthologue and/or functionality**
lrk-1[R1087C]	LRRK2[R1441C], common PD point mutation, found in the GTPase domain, proposed 4-fold kinase hyperactive *in vitro*.
lrk-1[Y1409C]	LRRK2[Y1699C], PD point mutation found in intra-molecular ROC-COR interface. Alters LRRK2 dimerization.
lrk-1[I1877T]	LRRK2[I2020T], PD point mutation found in kinase domain. Stabilisises active state conformation, unclear increased kinase activity.

Genotype	**Mean Normalised Fluorescence**	**Standard Deviation**	**Number**	**P-Value**	**Significance**
Wildtype	1.000	0.1819	20		
lrk-1[R1087C]	1.493	0.242	10	0.0002	***
lrk-1[Y1409C]	0.5513	0.0948	20	<0.0001	****
lrk-1[I1877T]]	0.5343	0.1028	20	<0.0001	****

***lrk-1[G1876S]* may show reduced SQST-1 oligomerization**

SQSTM1-p62 is a is an autophagosomal cargo receptor, upregulated in autophagy. Ubiquitinated substrates are recognised by SQSTM1-p62 and are incorporated into the autophagosome, leading to lysosomal fusion and cargo degradation (Liu et al. 2016). Thus, quantifying the concentration of SQSTM1-p62 present in mutant *C. elegans* lysates would be a powerful tool in evaluating autophagy between the *lrk-1* and *vps-35* mutant lines. This is especially pertinent, as SQST-p62 is a proven substrate for human LRRK2 (Kalogeropulou *et al.*, 2018).

We have investigated SQST-1 levels in our selected *lrk-1* mutants through semi-quantitative Western blotting. There was a strong band at the expected molecular weight of SQST-1 at 68kDa and a second band at 125kDa, suggesting potential oligomerization. The *lrk-1[G1876S]* mutant did not show a reduced 68kDa SQST-1 band compared to the wildtype, but the 125kDa SQST-1 band was substantially lower than the wildtype, at an adjusted intensity of 0.51, compared to the wildtype 1.16, again a shared phenotype with our *vps-35[D638N]* heterozygote model. The lack of 125kDa SQST-1, suggests reduced oligomerization, a process integral in targeting of cargo to the autophagosome. The *lrk-1[D1847A]* kinase ablated and *lrk-1* deletion do not show a substantially different SQST-1 profile to the wildtype.

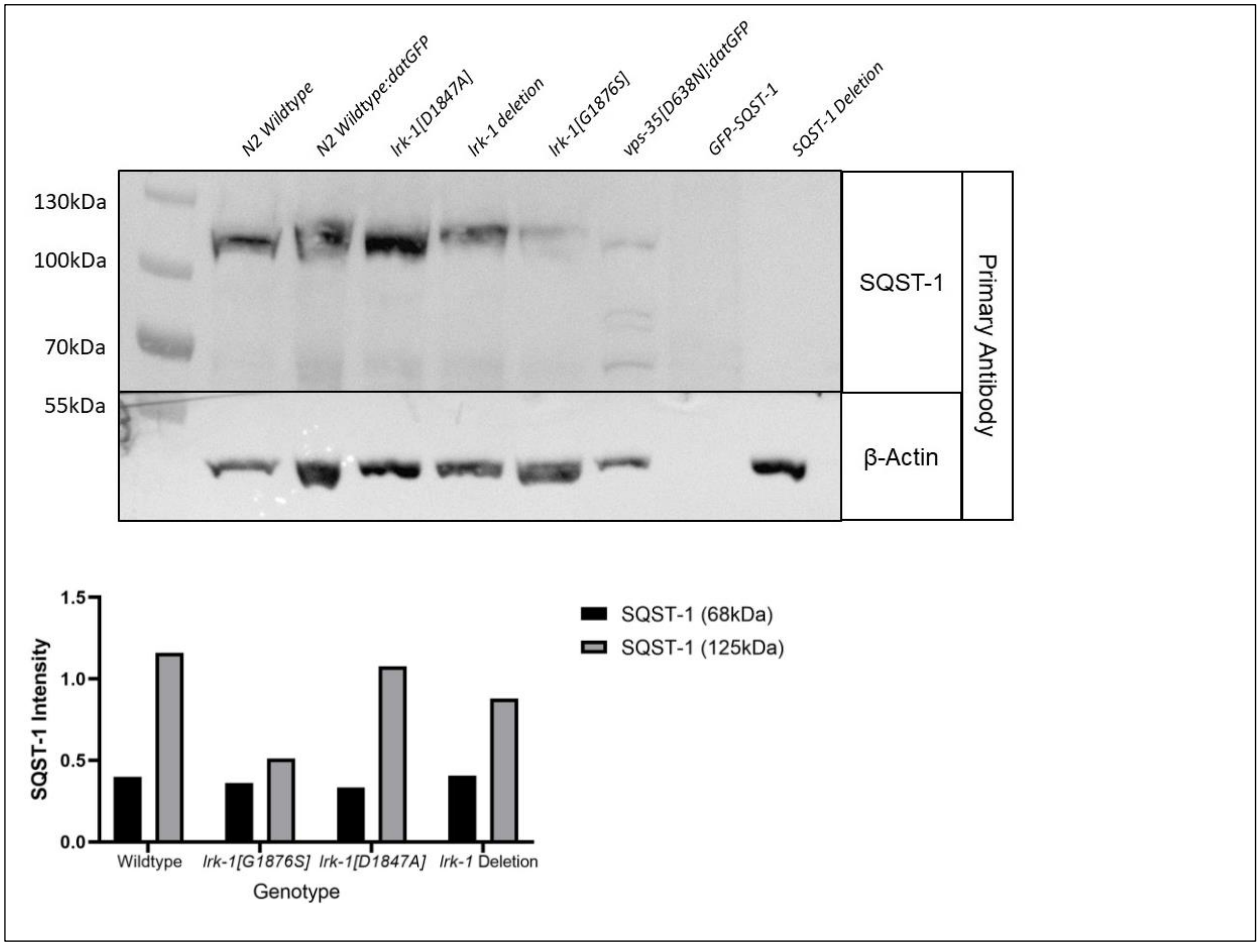

4.7 Treatment of selected LRK-1 point mutants with LRRK2 inhibitor Genentech 0877

4.7.1 1.0mM Genentech0877 leads to a significantly enhanced basal slowing phenotype in the LRK-1 G2019S equivalent

Genotype	**Treatment**	**Mean**	**Standard Deviation**	**Number**
Wildtype	Vehicle	83.02	16.17	15
Wildtype	Genentech0877	74.47	43.59	12
lrk-1[G1876S]	Vehicle	67.87	28.83	31
lrk-1[G1876S]	Genentech0877	84.72	8.68	35
lrk-1[D1847A]	Vehicle	66.59	26.73	18
lrk-1[D1847A]	Genentech0877	67.60	23.68	19
lrk-1[K988A]	Vehicle	68.83	13.84	19
lrk-1[K988A]	Genentech0877	57.96	24.41	19
Comparison			**P-value**	**Significance**
Wildtype Vehicle vs lrk-1[G1876S] Vehicle			0.1166	ns
Wildtype Vehicle vs lrk-1[D1847A] Vehicle			0.2265	ns
Wildtype Vehicle vs lrk-1[K988A] Vehicle			0.075	ns
Wildtype Vehicle vs. Wildtype Gen0877			0.9914	ns
lrk-1[G1876S] Vehicle vs lrk-1[G1876S] Gen0877			0.0181	*
lrk-1[D1847A] Vehicle vs lrk-1[D1847A] Gen0877			>0.999	ns
lrk-1[K988A] Vehicle vs lrk-1[K988A] Gen0877			0.5055	ns

0.2mM Genentech 0877 does not lead to alterations of dopaminergic phenotype in lrk-1[G1876S] mutants

C. elegans lines were incubated with 0.2mM of Genentech 0877 through development in liquid culture. In day 1 of adulthood, worms were assayed for basal slowing response. Control *lrk-1*(knu520[G1876S]), showed a reduced basal slowing response, which showed a modest, but non-significant, rescue following incubation with 0.2mM of inhibitor. This was not illustrated in the wildtype or knockout, basal slowing was impaired following incubation, suggesting off target effects in kinase inhibition. GTPase and Kinase ablated mutants do not show any significant effect of 0.2mM LRRK2 inhibitor treatment. There is a modest reduction in basal slowing, further suggesting off-target effects.

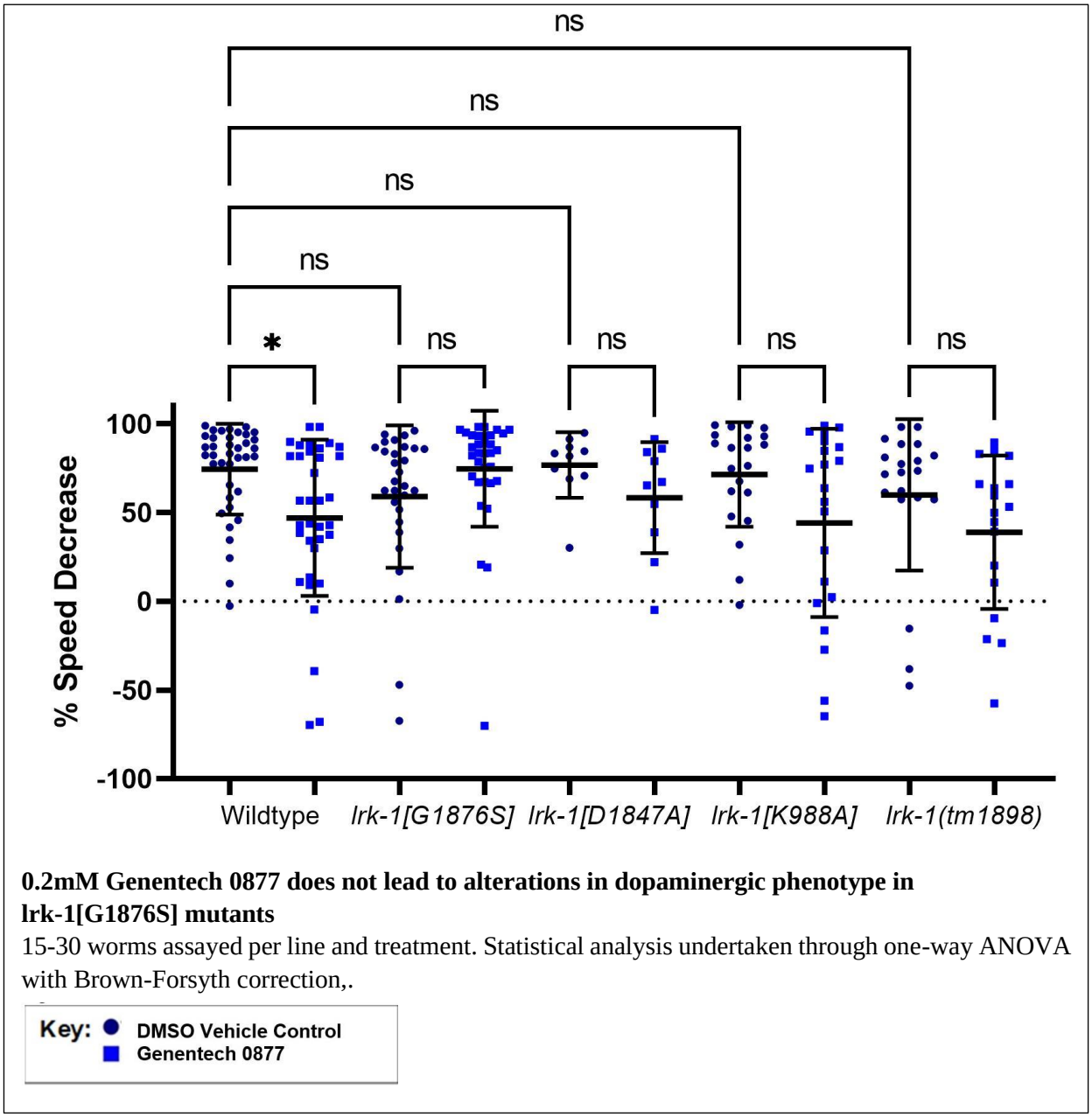

0.2mM Genentech 0877 does not lead to alterations in dopaminergic phenotype in lrk-1[G1876S] mutants

15-30 worms assayed per line and treatment. Statistical analysis undertaken through one-way ANOVA with Brown-Forsyth correction,.

Genotype	Treatment	Mean	Standard Deviation	Number
Wildtype	Vehicle	74.43	25.56	38
Wildtype	Genentech0877	46.99	43.96	35
lrk-1[G1876S]	Vehicle	58.97	40.08	29

lrk-1[G1876S]	Genentech0877	74.63	32.63	33
lrk-1[D1847A]	Vehicle	76.73	18.41	10
lrk-1[D1847A]	Genentech0877	58.35	31.23	10
lrk-1[K988A]	Vehicle	71.43	29.43	21
lrk-1[K988A]	Genentech0877	44.10	53.02	21
lrk-1(tm1898)	Vehicle	59.89	42.62	20
lrk-1(tm1898)	Genentech0877	38.88	43.18	18
Comparison			**P-value**	**Significance**
Wildtype Vehicle vs lrk-1[G1876S] Vehicle			0.4312	Ns
Wildtype Vehicle vs lrk-1[D1847A] Vehicle			>0.9999	Ns
Wildtype Vehicle vs lrk-1[K988A] Vehicle			0.9997	Ns
Wildtype Vehicle vs lrk-1(tm1898) Vehicle			0.**7096**	Ns
Wildtype Vehicle vs. Wildtype Gen0877			0.0148	*
lrk-1[G1876S] Vehicle vs lrk-1[G1876S] Gen0877			0.5096	Ns
lrk-1[D1847A] Vehicle vs lrk-1[D1847A] Gen0877			0.5743	Ns
lrk-1[K988A] Vehicle vs lrk-1[K988A] Gen0877			0.2749	ns
lrk-1(tm1898) Vehicle vs lrk-1(tm1898) Gen0877			0.6329	Ns

4.7.2 Administration through solid media treatment of a LRRK2 inhibitor to outcrossed LRK-1 lines demonstrate a rescued basal slowing response in *lrk-1[G1876S]*

Day 1

Genotype	**Treatment**	**Mean**	**Standard Deviation**	**Number**
Wildtype	Vehicle	84.53	7.238	22
Wildtype	Genentech0877	69.31	45.4	20
lrk-1[G1876S]	Vehicle	46.9	51.49	33
lrk-1[G1876S]	Genentech0877	78.05	22.57	17
lrk-1[D1847A]	Vehicle	90.79	11.17	18
lrk-1[D1847A]	Genentech0877	71.96	27.28	18
lrk-1(tm1898)	Vehicle	88.39	11.52	25
lrk-1(tm1898)	Genentech0877	76.94	31.94	27
Comparison			**P-value**	**Significance**
Wildtype Vehicle vs lrk-1[G1876S] Vehicle			0.0015	**
Wildtype Vehicle vs lrk-1[D1847A] Vehicle			0.2853	ns
Wildtype Vehicle vs lrk-1(tm1898) Vehicle			0.7152	ns
Wildtype Vehicle vs. Wildtype Gen0877			0.653	ns
lrk-1[G1876S] Vehicle vs lrk-1[G1876S] Gen0877			0.0321	*
lrk-1[D1847A] Vehicle vs lrk-1[D1847A] Gen0877			0.0801	ns
lrk-1(tm1898) Vehicle vs lrk-1(tm1898) Gen0877			0.4584	ns

Day 5

Genotype	**Treatment**	**Mean**	**Standard Deviation**	**Number**
Wildtype	Vehicle	75.51	38.21	16
Wildtype	Genentech0877	60.62	34.47	26
lrk-1[G1876S]	Vehicle	19.4	52.11	22
lrk-1[G1876S]	Genentech0877	24.83	44.32	21
lrk-1[D1847A]	Vehicle	35.95	46.08	20
lrk-1[D1847A]	Genentech0877	33.76	29.04	28

lrk-1(tm1898)	Vehicle	48.26	40.17	22
lrk-1(tm1898)	Genentech0877	51.62	29.71	24
Comparison			**P-value**	**Significance**
Wildtype Vehicle vs lrk-1[G1876S] Vehicle			0.0034	**
Wildtype Vehicle vs lrk-1[D1847A] Vehicle			0.0532	ns
Wildtype Vehicle vs lrk-1(tm1898) Vehicle			0.2433	ns
Wildtype Vehicle vs. Wildtype Gen0877			0.7901	ns
lrk-1[G1876S] Vehicle vs lrk-1[G1876S] Gen0877			0.9998	ns
lrk-1[D1847A] Vehicle vs lrk-1[D1847A] Gen0877			>0.9999	ns
lrk-1(tm1898) Vehicle vs lrk-1(tm1898) Gen0877			>0.9999	ns

4.7.3 LRK-1[G1876S] mutants show reduced lipid accumulation, rescued by LRRK2 inhibitor administration

Genotype	**Treatment**	**Mean**	**Standard Deviation**	**Number**
Wildtype	Vehicle	1.0000	0.3121	14
Wildtype	Genentech0877	0.8124	0.1909	25
lrk-1[G1876S]	Vehicle	0.5421	0.07146	35
lrk-1[G1876S]	Genentech0877	1.031	0.1829	32
lrk-1[D1847A]	Vehicle	1.105	0.1419	41
lrk-1[D1847A]	Genentech0877	1.158	0.1559	36
lrk-1(tm1898)	Vehicle	0.8049	0.1266	39
lrk-1(tm1898)	Genentech0877	0.8153	0.1342	27
Comparison			**P-value**	**Significance**
Wildtype Vehicle vs lrk-1[G1876S] Vehicle			<0.0001	****
Wildtype Vehicle vs lrk-1[D1847A] Vehicle			0.4806	ns
Wildtype Vehicle vs lrk-1(tm1898) Vehicle			0.1402	ns
Wildtype Vehicle vs. Wildtype Gen0877			0.3402	ns
lrk-1[G1876S] Vehicle vs lrk-1[G1876S] Gen0877			<0.0001	****
lrk-1[D1847A] Vehicle vs lrk-1[D1847A] Gen0877			>0.9999	ns
lrk-1(tm1898) Vehicle vs lrk-1(tm1898) Gen0877			>0.9999	ns

4.8.2 Newly developed 3xFLAG-LRK-1 is detectable in *C. elegans* lysates

Following the unsuccessful detection of LRK-1 utilising commercially available antibodies, a N-Terminal 3xFLAG tagged LRK-1 line was designed. CRISPR/Cas9 modification was outsourced to SunyBiotech.

DNA Coding Sequence- LRK-1 N-terminus and 3xFLAG

agaaaacatccaaaATGGATTATAAAGACGATGACGATAAGCGTGACTACAAGGACGACGACGACAAGCGTGAT
TACAAGGATGACGATGACAAGAGAGGAGGATCTGGAGGAGACCTCTCAAGTGGGGGTCCGTCATCTTCAAGCGA
TGTAGCTTCAGAATTGGATAATTCGGATGCAATGCAACTGGTTAGACAG

Amino Acid Translation

agaaaacatccaaaATGGATTATAAAGACGATGACGATAAGCGTGACTACAAGGACGACGACGA
M D Y K D D D D K R D Y K D D D D
CAAGCGTGATTACAAGGATGACGATGACAAGAGAGGAGGATCTGGAGGAGACCTCTCAAGTGGG
K R D Y K D D D D K R G G S G G D L S S G
GGTCCGTCATCTTCAAGCGATGTAGCTTCAGAATTGGATAATTCGGATGCAATGCAACTGGTT
G P S S S S S D V A S E L D N S D A M Q L
AGACAG
V R

3xFLAG LRK-1 DNA and protein sequences

lrk-1/LRK-1 genomic and protein sequence illustrated in blue, FLAG sequence shown in red. Flexible linker sequence shown in green, with LRK-1 start codon highlighted in yellow. Codon optimisation to C. elegans

4.8.3 Development of anti-LRK-1 sera

```
LRRK2          1751 GSEVLDNHPESFLKITVPSCRKG-CILLGQVVDHIDSLMEEWFPGL-LEI   1798
                    .|..:...:...|:::.:..:| ..||..:.|.:|:|:|:|:|.| ...
LRK-1          1522 NSLSISAASQHGRKLSMKTDVEGRSRLLAMISDLLDTLLEDWYPALGTRF   1571

LRRK2          1799 DICGEGETLLKKWALY----------------------SFNDGE----   1820
                    ....||:.|:.::.|.                        |.:|||
LRK-1          1572 VHSSEGDLLVSRYVLCPQCVRDAERNGSRSRTSSSASHRRSQDDGELPIT   1621

LRRK2          1821 --EHQK-----------------ILLDDLMKKAEEGDLLVNPDQPRLTI   1850
                      .|.|                 .:::::.|....|.:.:..|....|.:
LRK-1          1622 SSSHMKGSRTTGDISKCRGGVVHCFVIEECMLAGREYNWVECPSHGGLHM   1671

LRRK2          1851 PISQIAPDLILADLPRNIMLNNDELEFEQAPEFLLGDGSFGSVYRAAYE-   1899
                      .::|||.:.||:...:.::.|:|:..:    :||.|:||.|:||...
LRK-1          1672 --RELAPDTVFADIENALTIHPDQLKRSR----MLGRGAFGFVFRATVRQ   1715
```

Epitope: DDGELPITSSSHMKG

Anti-LRK-1 sera epitope of C. elegans LRK-1

Extract of sequence alignment between human LRRK2 and C. elegans LRK-1, with anti-LRK-1 epitope labelled. This region is not well conserved with human LRRK2. Sequence annotations are shown in the fourth row, kinase domain shown in orange, PD confirmed pathogenic mutations in red and PD risk mutations shown in turquoise.

4.8.4.1 Rb17 Sera shows most promise in LRK-1 detection in day 1 of adulthood

At the time of preliminary testing, it was unknown that LRK-1 is highly expressed in day 5 and day 10 of adulthood. For many western blotting approaches in C. elegans, day 1 of adulthood is used as standard and as a key timepoint frequently utilised in our experiments, this timepoint was employed for the preliminary testing sample lysates. Detection utilising the LRK-1 FLAG line had previously been shown in preliminary tests in day 1 of adulthood, as detailed in 4.8.3, hence this lysate was utilised as a positive control for LRK-1 presence and the *lrk-1* deletion model was employed as a negative control. Two sera were raised, Rb5 and Rb17, with pre-sera collected and supplied by the manufacturer prior to animal immunisation. The membrane incubated with Rb5 sera showed a promising band of around 260kDa, however there is a large area of unspecific detection in this region in the lrk-1 deletion model and this band is not reflected in the 3xFLAG-LRK-1 line. Furthermore, a similar size band is present in the wildtype and the 3xFLAG-LRK-1 samples on the membrane incubated in the pre-sera, further suggesting this may be unspecific. In addition, there is no FLAG detection in the 3xFLAG-LRK-1 sample, in the membrane incubated with the anti-FLAG antibody, illustrating that LRK-1 may not be present at this stage, despite earlier blots (shown in 4.8.3) and subsequent blots (shown in 4.8.4.2 and 4.8.5.1) illustrating that LRK-1 protein is expressed in day 1 of adulthood.

In the membrane incubated with the sera from Rb17, there are faint bands present around 266kDa, the expected molecular weight of LRK-1 in both the wildtype and 3xFLAG-LRK-1 samples, which are not present in the lrk-1 deletion. Furthermore, in the membrane incubated with Rb17 pre-sera these bands are not present, suggesting that there could be some LRK-1 detection. However, there is no 3xFLAG-LRK-1 detection in the membrane incubated with the anti-FLAG antibody. Concurrently, 3xFLAG-LRK-1 detection was under investigation at different stages of adulthood, later discussed in 4.8.5 and results were conflicting as to whether LRK-1-FLAG was

readily detectable at day 1 of adulthood. Between Rb5 and Rb17 sera, this data suggests that Rb17 sera is the most promising to further investigate.

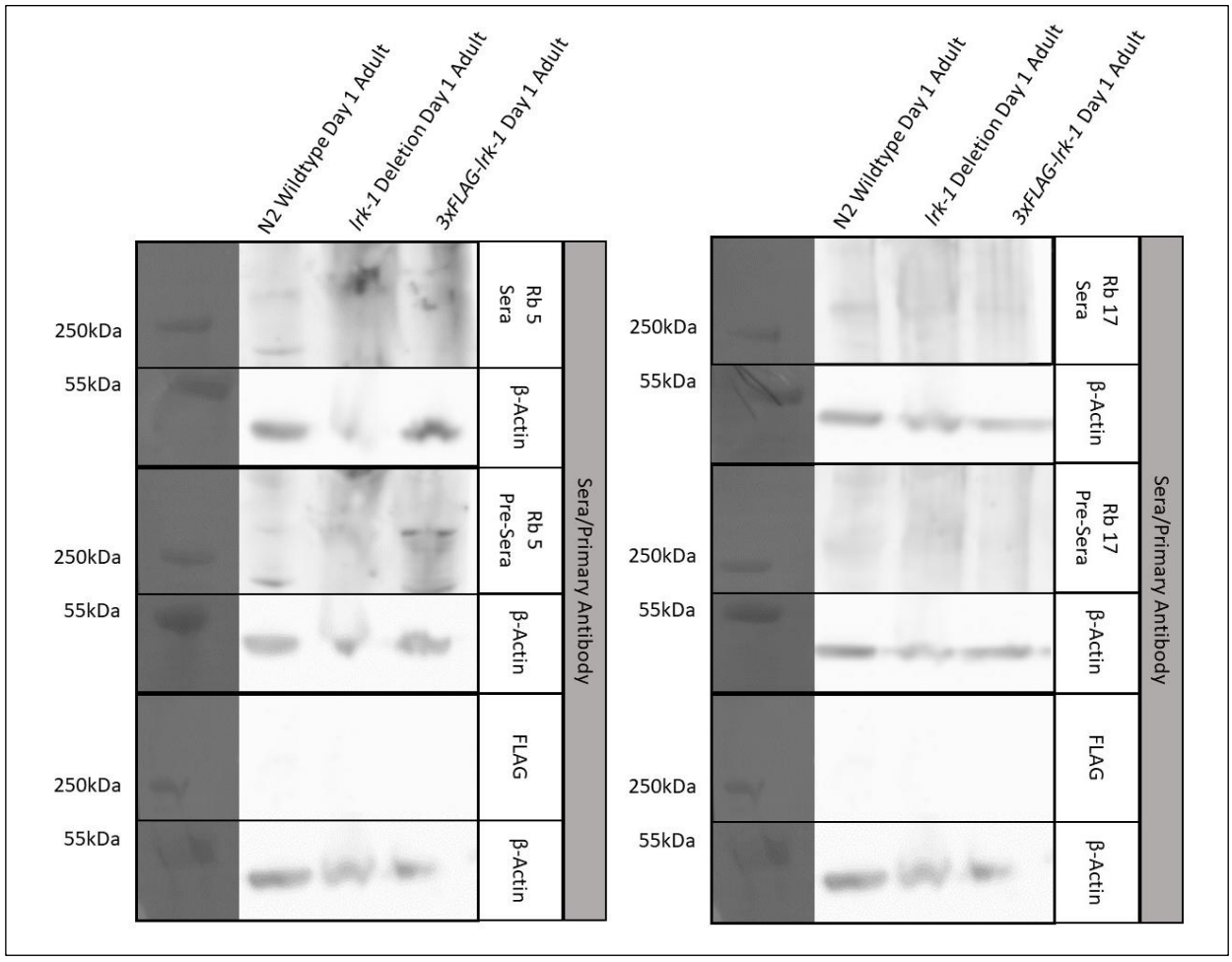

Testing of Rb17 sera through larval development

Following testing of both rabbit sera in day 1 adult C. elegans lysates, the sera from Rb17 was tested further in lysates collected at the larval stages of development, L1, L2/3 and L4, as mRNA expression data accessible on WormBase suggests that there is expression of LRK-1 at this stage at an RNA level. However, this has not been validated or characterised, so we sought to test this with our detectable 3xFLAG-LRK-1 line, the positive control in our sera testing. Furthermore, we wanted to test if the sera had any specific detection for LRK-1 at these developmental stages.

In L1, our lysates showed unspecific banding in the LRK-1 region of 266kDa in all three of our samples in both the anti-LRK-1 sera and the pre-sera, highlighting unspecific binding. Furthermore, a similar phenotype was shown on the membrane incubated with anti-FLAG antibody and detection was shown in all three samples at around 250kDa, a lower molecular weight than expected.

In contrast, at L2/3 the 3xFLAG-LRK-1 lysate is readily detectable when incubated with an anti-FLAG antibody, highlighting that LRK-1 is present at this developmental stage, coherent with the mRNA data available on WormBase. There are bands in the expected molecular weight of 266kDa most pertinently in the 3xFLAG-LRK-1 on the membrane incubated with the anti-LRK-1 sera, however these bands are also present in the lrk-1 deletion and on the membrane incubated with the pre-sera, further suggesting unspecific detection.

At L4 stage, there was insufficient N2 and lrk-1 deletion samples on the anti-LRK-1 sera incubated membrane, however no detection was shown in the 3xFLAG-LRK-1 sample. This is consistent in both the pre-sera incubated membrane and the anti-FLAG incubated membrane, suggesting that LRK-1 may not be as highly expressed at this stage as in L2/3.
Following these inconclusive experiments, the novel Rb17 anti-LRK-1 sera was tested against lysates from later stages in adulthood.

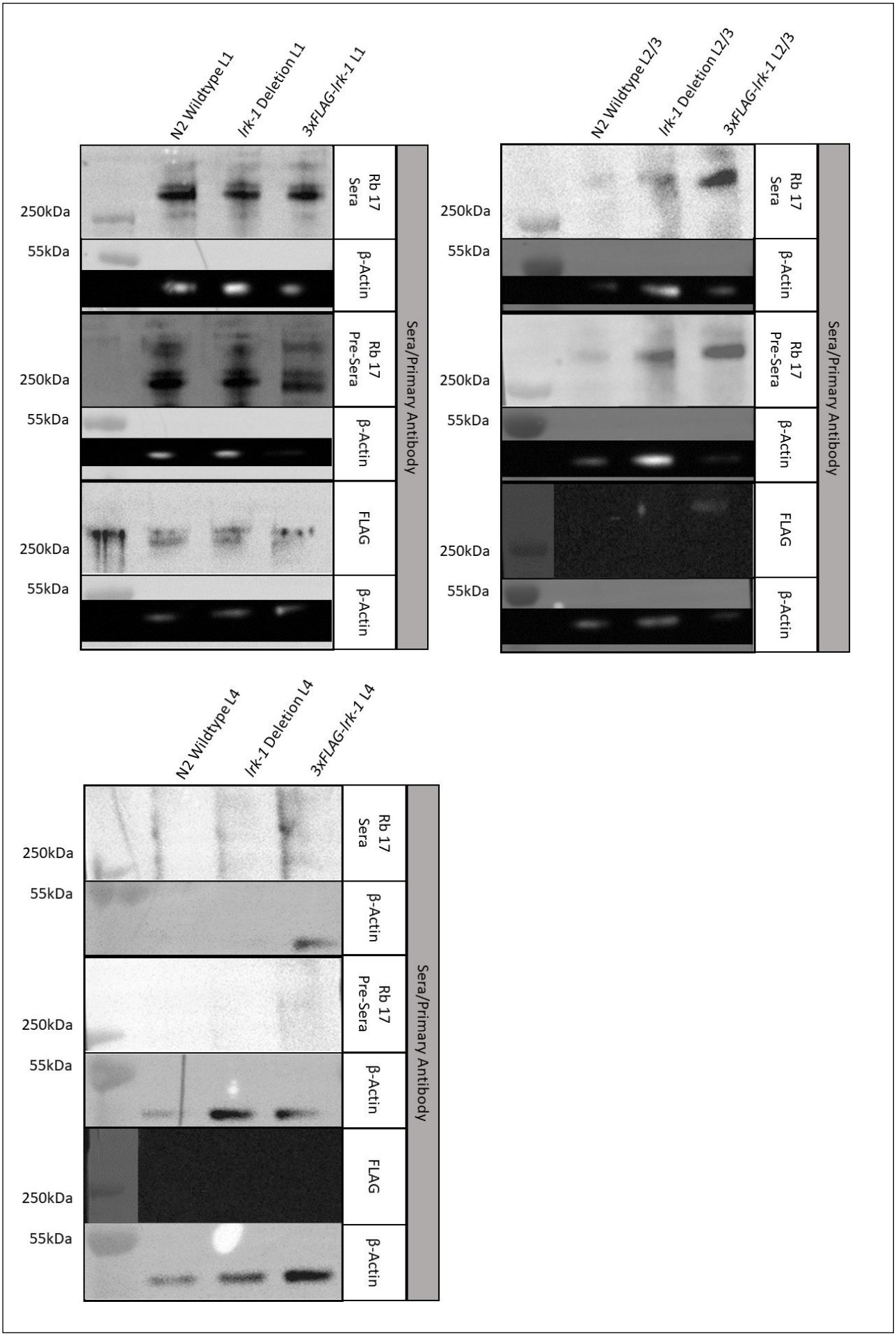
N2 Wildtype L2/3
Irk-1 Deletion L2/3
3xFLAG-Irk-1 L2/3
Sera/Primary Antibody
Rb 17 Sera
β-Actin
Rb 17 Pre-Sera
β-Actin
FLAG
β-Actin
250kDa
55kDa
250kDa
55kDa
250kDa
55kDa
N2 Wildtype L1
Irk-1 Deletion L1
3xFLAG-Irk-1 L1
Sera/Primary Antibody
Rb 17 Sera
β-Actin
Rb 17 Pre-Sera
β-Actin
FLAG
β-Actin
250kDa
55kDa
250kDa
55kDa
250kDa
55kDa
N2 Wildtype L4
Irk-1 Deletion L4
3xFLAG-Irk-1 L4
Sera/Primary Antibody
Rb 17 Sera
β-Actin
Rb 17 Pre-Sera
β-Actin
FLAG
β-Actin
250kDa
55kDa
250kDa
55kDa
250kDa
55kDa

Testing of Rb17 sera in day 5 and 10 of adulthood

Following the unsuccessful detection of LRK-1 during larval development utilising the Rb17 sera or the FLAG antibody, later stages of adulthood were tested for anti-LRK-1 sera specificity 3xFLAG-LRK-1 expression. Day 5 and day 10 of adulthood were selected, day 5 is a key experimental timepoint throughout this study and advanced signs of ageing can be illustrated in 10 day adult *C. elegans*.

In all three of our day 5 adult lysates on the membrane incubated with anti-LRK-1 Rb17 sera, there is unspecific detection in the LRK-1 expected region 266kDa. The lrk-1 deletion mutant was subsequently genotyped, to confirm that the population had the lrk-1 gene deleted, this showed that the gene deletion was present and therefore this population would not express LRK-1 protein. Furthermore, in the Rb17 pre-sera, this unspecific detection was present in the wildtype and lrk-1 deletion mutant, further illustrating unspecific detection of LRK-1 in the anti-LRK-1 sera. However, this was not the case for the 3xFLAG-LRK-1 sample incubated with the pre-sera, which showed no specific detection, but a band was present in the anti-LRK-1 sera. The membrane incubated with the anti-FLAG antibody illustrated that 3xFLAG-LRK-1 is present in day 5 of adulthood, in the expected region of 266kDa. This suggests that there could be some detection with the anti-LRK-1 sera in this genotype and it remains to be established whether addition if the 3xFLAG affects expression levels of LRK-1 compared to the wildtype.

In day 10 of adulthood, the 3xFLAG-LRK-1 sample is readily detectable with the Rb17 anti-LRK-1 sera and the anti-FLAG antibody. In the membrane incubated with pre-sera, there is unspecific detection in the wildtype and deletion samples, but no bands in the 3xFLAG sample. This is promising and suggests that the 3xFLAG mutant may be detectable with the novel LRK-1 sera, however further validation and purification would be needed.

This experiment inadvertently established, through membrane incubation with an anti-FLAG antibody in tandem, that LRK-1 is highly expressed in day 5 of adulthood and persists to day 10 of adulthood. This augments the relevance of LRK-1 as a model for LRRK2, ageing and PD, as expression is highest in ageing, suggesting a more prominent role at this timepoint. Subsequent blots were undertaken to replicate this experiment, as detailed in 4.8.5, with intermediate timepoints and three population replicates per life stage, in order to further understand LRK-1 expression throughout the adult lifespan. Furthermore, this sera testing highlighted that 3xLRK-1-FLAG in *C. elegans* was easily detectable and the method to be carried forward for future expression, localisation and interactome studies.

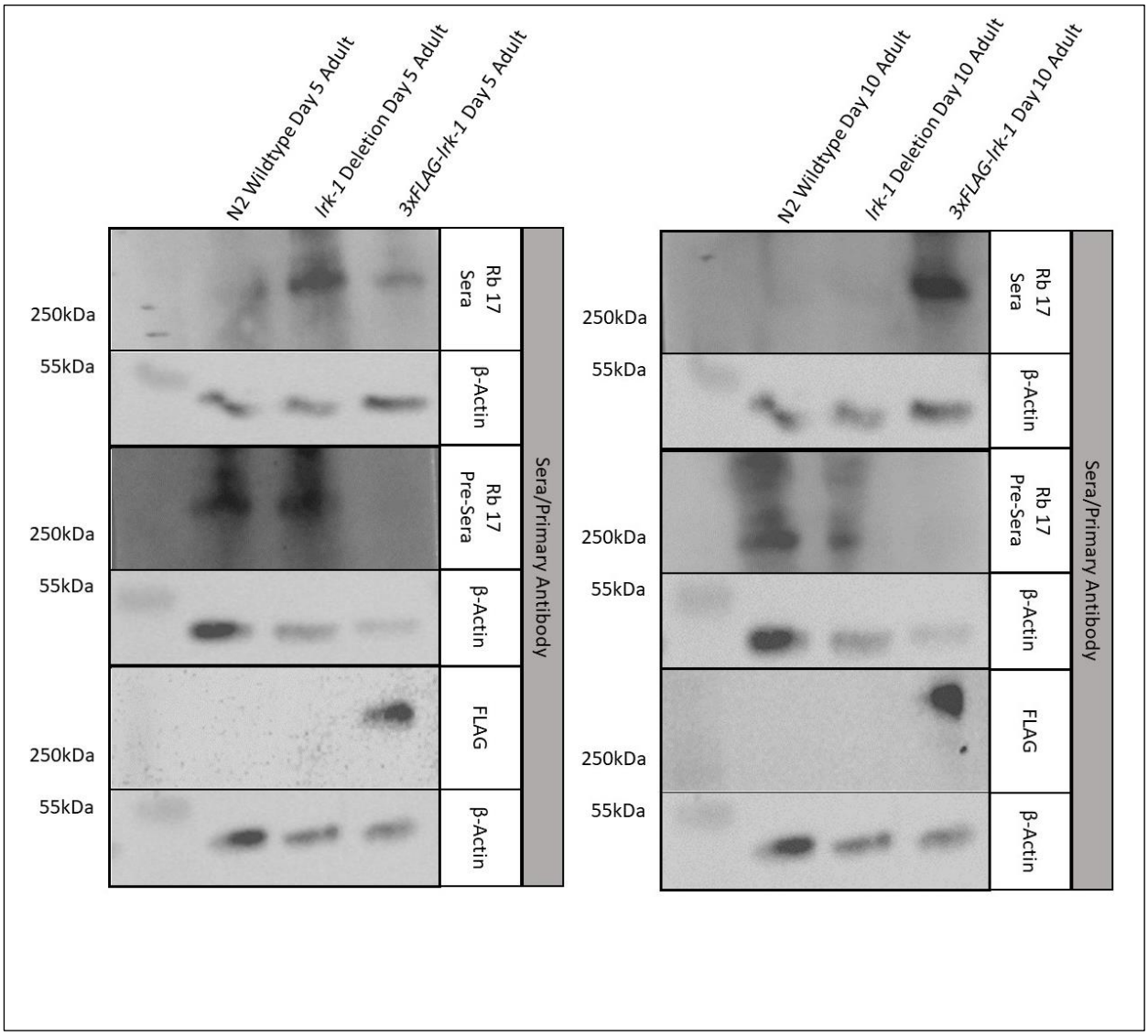
N2 Wildtype Day 10 Adult
Irk-1 Deletion Day 10 Adult
3xFLAG-Irk-1 Day 10 Adult
Sera/Primary Antibody
Rb 17 Sera
β-Actin
Rb 17 Pre-Sera
β-Actin
FLAG
β-Actin
250kDa
55kDa
250kDa
55kDa
250kDa
55kDa
N2 Wildtype Day 5 Adult
Irk-1 Deletion Day 5 Adult
3xFLAG-Irk-1 Day 5 Adult
Sera/Primary Antibody
Rb 17 Sera
β-Actin
Rb 17 Pre-Sera
β-Actin
FLAG
β-Actin
250kDa
55kDa
250kDa
55kDa
250kDa
55kDa

Chapter V: Results III
Modelling the VPS35/LRRK2 interplay in novel *C. elegans* models

5.2 The administration of a human LRRK2 inhibitor rescues *vps-35[D638N]* impaired dopaminergic function

5.2.1 Preliminary examination illustrates that administration of a LRRK2 inhibitor rescues the impaired basal slowing response of *vps-35[D638N]* Heterozygotes

Genotype	Treatment	Mean % (M)	Standard Deviation (SD)	Number (N)
Wildtype	Vehicle	82.44	12.23	21
	Genentech0877	70.78	48.13	18
vps-35[D638N] heterozygotes	Vehicle	58.89	37.69	22
	Genentech0877	83.57	9.417	21

Comparison	P Value	Significance
Wildtype Vehicle vs *vps-35[D638N]* heterozygote Vehicle	0.0100	*
Wildtype Vehicle vs Wildtype Gen0877	0.3296	ns
vps-35[D638N] heterozygote Vehicle vs *vps-35[D638N]* heterozygote Gen0877	0.0066	**

5.2.2 Administration of a LRRK2 inhibitor through solid media feeding rescues impairments in the basal slowing response in day 1 adult *vps-35[D638N]* heterozygotes

Day 1 Adult

Genotype	Treatment	Mean % (M)	Standard Deviation (SD)	Number (N)
Wildtype	Vehicle	68.29	17.44	28
	Genentech0877	57.39	28.75	25
vps-35[D638N] heterozygotes	Vehicle	49.72	36.87	38
	Genentech0877	69.08	23.69	35
cat-2(n4547)	Vehicle	-48.10	77.28	28
	Genentech0877	-59.74	79.91	19

Comparison	P Value	Significance
Wildtype Vehicle vs *vps-35[D638N]* heterozygote Vehicle	0.0422	*
Wildtype Vehicle vs *cat-2(n4547)* Vehicle	<0.0001	****
Wildtype Vehicle vs Wildtype Gen0877	0.4247	ns
vps-35[D638N] heterozygote Vehicle vs *vps-35[D638N]* heterozygote Gen0877	0.0443	*
Cat-2(n4547) Vehicle vs *cat-2(n4547)* Gen0877	0.9914	ns

Day 5 Adult

Genotype	Treatment	Mean % (M)	Standard Deviation (SD)	Number (N)
Wildtype	Vehicle	47.07	29.01	13
	Genentech0877	60.65	37.43	23

vps-35[D638N] heterozygotes	Vehicle	18.22	55.49	21
	Genentech0877	43.43	40.11	16
cat-2(n4547)	Vehicle	-0.5851	62.60	18
	Genentech0877	5.363	33.91	33

Comparison	**P Value**	**Significance**
Wildtype Vehicle vs *vps-35[D638N]* heterozygote Vehicle	0.2426	ns
Wildtype Vehicle vs *cat-2(n4547)* Vehicle	0.0427	*
Wildtype Vehicle vs Wildtype Gen0877	0.7226	ns
vps-35[D638N] heterozygote Vehicle vs *vps-35[D638N]* heterozygote Gen0877	0.4529	ns
Cat-2(n4547) Vehicle vs *cat-2(n4547)* Gen0877	0.9976	ns

5.2.3 The basal slowing response is not significantly impaired with ageing in vehicle and LRRK2 inhibitor treatment

Vehicle Treatment

Genotype	**Age**	**Mean % (M)**	**Standard Deviation (SD)**	**Number (N)**
Wildtype	Day 1	68.29	17.44	28
	Day 5	47.07	29.01	13
vps-35[D638N] heterozygotes	Day 1	49.72	36.87	38
	Day 5	18.22	55.49	21
cat-2(n4547)	Day 1	-48.10	77.28	28
	Day 5	-0.5851	62.60	18

Comparison	**P Value**	**Significance**
Wildtype Day 1 vs Wildtype Day 5	0.0754	ns
vps-35[D638N] heterozygote Day 1 vs *vps-35[D638N]* heterozygote Day 5	0.0765	ns
Cat-2(n4547) Day 1 vs *cat-2(n4547)* Day 5	0.0785	ns

Genentech0877 Treatment

Genotype	**Age**	**Mean % (M)**	**Standard Deviation (SD)**	**Number (N)**
Wildtype	Day 1	57.39	28.75	25
	Day 5	60.65	37.43	23
vps-35[D638N] heterozygotes	Day 1	69.08	23.69	35
	Day 5	43.43	40.11	16
cat-2(n4547)	Day 1	-59.74	79.91	19
	Day 5	5.363	33.91	33

Comparison	**P Value**	**Significance**
Wildtype Day 1 vs Wildtype Day 5	0.9816	ns
vps-35[D638N] heterozygote Day 1 vs *vps-35[D638N]* heterozygote Day 5	0.0785	ns
Cat-2(n4547) Day 1 vs *cat-2(n4547)* Day 5	0.0080	**

5.2.4 The crawling speeds of wildtype and vps-35[D638N] heterozygote C. elegans are significantly altered by Genentech0877 treatment

Day 1 Adult, crawling speed on unseeded NGM

Genotype	Treatment	Mean Speed (mm/s)	Standard Deviation (SD)	Number (N)
Wildtype	Vehicle	0.09843	0.01693	30
	Genentech0877	0.08496	0.02037	46
vps-35[D638N] heterozygotes	Vehicle	0.1004	0.02287	53
	Genentech0877	0.07457	0.02412	51
cat-2(n4547)	Vehicle	0.03118	0.01582	65
	Genentech0877	0.03130	0.01351	44

Comparison	P Value	Significance
Wildtype Vehicle vs *vps-35[D638N]* heterozygote Vehicle	0.9945	ns
Wildtype Vehicle vs *cat-2(n4547)* Vehicle	<0.0001	****
Wildtype Vehicle vs Wildtype Gen0877	0.0127	*
vps-35[D638N] heterozygote Vehicle vs *vps-35[D638N]* heterozygote Gen0877	<0.0001	****
Cat-2(n4547) Vehicle vs *cat-2(n4547)* Gen0877	>0.9999	ns

Day 1 Adult, crawling speed upon reaching *E. coli OP50*

Genotype	Treatment	Mean Speed (mm/s)	Standard Deviation (SD)	Number (N)
Wildtype	Vehicle	0.03121	0.01716	28
	Genentech0877	0.03620	0.02443	25
vps-35[D638N] heterozygotes	Vehicle	0.05050	0.03703	38
	Genentech0877	0.02306	0.01767	35
cat-2(n4547)	Vehicle	0.04618	0.02410	28
	Genentech0877	0.05000	0.02501	19

Comparison	P Value	Significance
Wildtype Vehicle vs *vps-35[D638N]* heterozygote Vehicle	*	0.0321
Wildtype Vehicle vs *cat-2(n4547)* Vehicle	*	0.0488
Wildtype Vehicle vs Wildtype Gen0877	ns	0.9165
vps-35[D638N] heterozygote Vehicle vs *vps-35[D638N]* heterozygote Gen0877	***	0.0007
Cat-2(n4547) Vehicle vs *cat-2(n4547)* Gen0877	ns	0.9893

Day 5 Adult, crawling speed on unseeded NGM

Genotype	Treatment	Mean Speed (mm/s)	Standard Deviation (SD)	Number (N)
Wildtype	Vehicle	0.07543	0.03409	21
	Genentech0877	0.07314	0.04650	21
vps-35[D638N] heterozygotes	Vehicle	0.08496	0.02979	26
	Genentech0877	0.05314	0.03498	44
cat-2(n4547)	Vehicle	0.04159	0.02847	34
	Genentech0877	0.05040	0.02804	64

Comparison	P Value	Significance
Wildtype Vehicle vs *vps-35[D638N]* heterozygote Vehicle	0.8450	ns
Wildtype Vehicle vs *cat-2(n4547)* Vehicle	0.0026	**
Wildtype Vehicle vs Wildtype Gen0877	>0.9999	ns
vps-35[D638N] heterozygote Vehicle vs *vps-35[D638N]* heterozygote Gen0877	0.0008	***
Cat-2(n4547) Vehicle vs *cat-2(n4547)* Gen0877	0.5412	ns

Day 5 Adult, crawling speed upon reaching *E. coli OP50*

Genotype	Treatment	Mean Speed (mm/s)	Standard Deviation (SD)	Number (N)
Wildtype	Vehicle	0.03992	0.02188	13
	Genentech0877	0.02878	0.02738	23
vps-35[D638N] heterozygotes	Vehicle	0.06948	0.04714	21
	Genentech0877	0.03006	0.02131	16
cat-2(n4547)	Vehicle	0.04183	0.02603	18
	Genentech0877	0.04770	0.01709	33

Comparison	P Value	Significance
Wildtype Vehicle vs *vps-35[D638N]* heterozygote Vehicle	ns	0.0900
Wildtype Vehicle vs *cat-2(n4547)* Vehicle	ns	0.9998
Wildtype Vehicle vs Wildtype Gen0877	ns	0.6370
vps-35[D638N] heterozygote Vehicle vs *vps-35[D638N]* heterozygote Gen0877	**	0.0097
Cat-2(n4547) Vehicle vs *cat-2(n4547)* Gen0877	ns	0.9113

5.2.5 The crawling speed is not altered in *vps-35[D638N]* heterozygotes between day 1 and day 5 in vehicle and Genentech0877 treated conditions

Vehicle, crawling speed on unseeded NGM

Genotype	Age	Mean % (M)	Standard Deviation (SD)	Number (N)
Wildtype	Day 1	0.09843	0.01693	30
	Day 5	0.07543	0.03409	21
vps-35[D638N] heterozygotes	Day 1	0.1004	0.02287	53
	Day 5	0.08496	0.02979	26
cat-2(n4547)	Day 1	0.03118	0.01582	65
	Day 5	0.04159	0.02847	34

Comparison	P Value	Significance
Wildtype Day 1 vs Wildtype Day 5	0.0240	*
vps-35[D638N] heterozygote Day 1 vs *vps-35[D638N]* heterozygote Day 5	0.0717	ns
Cat-2(n4547) Day 1 vs *cat-2(n4547)* Day 5	0.1523	ns

Vehicle, crawling speed upon reaching *E. coli OP50*

Genotype	Age	Mean % (M)	Standard Deviation (SD)	Number (N)
Wildtype	Day 1	0.03121	0.01716	28
	Day 5	0.03992	0.02188	13
vps-35[D638N] heterozygotes	Day 1	0.05050	0.03703	38
	Day 5	0.06948	0.04714	21
cat-2(n4547)	Day 1	0.04618	0.02410	28
	Day 5	0.04183	0.02603	18

Comparison	P Value	Significance
Wildtype Day 1 vs Wildtype Day 5	0.5142	ns
vps-35[D638N] heterozygote Day 1 vs *vps-35[D638N]* heterozygote Day 5	0.3142	ns
Cat-2(n4547) Day 1 vs *cat-2(n4547)* Day 5	0.9196	ns

Genentech0877, crawling speed on unseeded NGM

Genotype	Age	Mean % (M)	Standard Deviation (SD)	Number (N)
Wildtype	Day 1	0.08496	0.02037	46
	Day 5	0.07314	0.04650	21
vps-35[D638N] heterozygotes	Day 1	0.07457	0.02412	51
	Day 5	0.05314	0.03498	44
cat-2(n4547)	Day 1	0.03130	0.01351	44
	Day 5	0.05040	0.02804	64

Comparison	P Value	Significance
Wildtype Day 1 vs Wildtype Day 5	ns	0.6092
vps-35[D638N] heterozygote Day 1 vs *vps-35[D638N]* heterozygote Day 5	ns	0.3392
Cat-2(n4547) Day 1 vs *cat-2(n4547)* Day 5	****	<0.0001

Genentech0877, crawling speed upon reaching *E. coli OP50*

Genotype	Age	Mean % (M)	Standard Deviation (SD)	Number (N)
Wildtype	Day 1	0.03620	0.02443	25
	Day 5	0.02878	0.02738	23
vps-35[D638N] heterozygotes	Day 1	0.02306	0.01767	35
	Day 5	0.03006	0.02131	16
cat-2(n4547)	Day 1	0.05000	0.02501	19
	Day 5	0.04770	0.01709	33

Comparison	P Value	Significance
Wildtype Day 1 vs Wildtype Day 5	0.6925	ns
vps-35[D638N] heterozygote Day 1 vs *vps-35[D638N]* heterozygote Day 5	0.5885	ns
Cat-2(n4547) Day 1 vs *cat-2(n4547)* Day 5	0.9780	ns

5.3Administration of a LRRK2 inhibitor alleviates impairments in dopaminergic neuronal morphology in VPS-35[D638N]

5.3.1.1 LRRK2 inhibitor treatment improves the fluorescence intensity of vps-35[D638N] heterozygotes in day 1 of adulthood

Genotype	Treatment	Mean	Standard Deviation	Number
Wildtype:datGFP	Vehicle	3201	1140	28
	Genentech0877	2897	1038	23
vps-35[D638N]:datGFP	Vehicle	2719	795.9	28
	Genentech0877	4298	1484	28

Comparison	P-Value	Significance
Wildtype:datGFP Vehicle vs Wildtype:datGFP Gen0877	ns	0.7858
vps-35[D638N]:datGFP Vehicle vs vps-35[D638N]:datGFP Gen0877	****	<0.0001
Wildtype:datGFP Vehicle vs vps-35[D638N]:datGFP Vehicle	ns	0.2559
Wildtype:datGFP Gen0877 vs vps-35[D638N]:datGFP Gen0877	**	0.0010

5.3.1.2 Treatment with a LRRK2 inhibitor improves outgrowths in CEP neurons and blebbing in ADE neurons in the *vps-35[D638N]* heterozygotes in day 1 of adulthood

Neuronal Subgroup	Genotype	Treatment	% Neurons in *C. elegans* Population Morphology					N
			Wildtype Appearance	Outgrowths	Branching	Blebbing	Degeneration	
CEP	Wildtype:GFP	Vehicle	95.53571	1.785714	0	0	2.678571	112
		Gen0877	64.13043	8.695652	3.26087	4.347826	19.56522	92
	VPS-35[D638N]:GFP	Vehicle	69.64286	20.53571	8.928571	0	0.892857	112
		Gen0877	81.25	14.28571	4.464286	0	0	112
ADE	Wildtype:GFP	Vehicle	94.64286	0	0	0	5.357143	56
		Gen0877	60.86957	0	0	8.695652	30.43478	46
	VPS-35[D638N]:GFP	Vehicle	71.42857	0	0	16.07143	12.5	112
		Gen0877	91.07143	0	0	1.785714	7.142857	112

5.3.1.3 LRRK2 inhibitor treatment improves the number of impairments per *vps-35[D638N]* heterozygote in day 1 of adulthood

Type	Genotype	Treatment	% C. elegans in population with number of impairments							N
			0	1	2	3	4	5	6	
Total	Wildtype:GFP	Vehicle	85.71429	3.571429	7.142857	3.571429	0	0	0	28
		Gen0877	30.43478	13.04348	17.3913	17.3913	4.347826	0	17.3913	23
	VPS-35[D638N]:GFP	Vehicle	14.28571	17.85714	50	10.71429	7.142857	0	0	28
		Gen0877	39.28571	32.14286	25	3.571429	0	0	0	28
Minor	Wildtype:GFP	Vehicle	92.85714	7.142857	0	0	0	0	0	28

		Gen0877	69.56522	17.3913	8.695652	4.347826	0	0	0	23
	VPS-35[D638N]:GFP	Vehicle	17.85714	46.42857	35.71429	0	0	0	0	28
		Gen0877	50	28.57143	17.85714	3.571429	0	0	0	28
Major	Wildtype:GFP	Vehicle	89.28571	3.571429	3.571429	3.571429	0	0	0	28
		Gen0877	43.47826	21.73913	8.695652	4.347826	4.347826	0	17.3913	23
	VPS-35[D638N]:GFP	Vehicle	53.57143	35.71429	7.142857	3.571429	0	0	0	28
		Gen0877	82.14286	17.85714	0	0	0	0	0	28

5.3.1.4 Prevalence of major impairments in ADE neurons of *vps-35[D638N]* heterozygotes are reduced following LRRK2 inhibitor treatment in day 1 of adulthood

Genotype	Treatment	Neuronal Subgroup	Type	% C. elegans in population with number of impairments					N
				0	1	2	3	4	
Wildtype:GFP	Vehicle	CEP	Minor	92.85714	7.142857	0	0	0	112
			Major	96.42857	0	0	3.571429	0	112
		ADE	Minor	100	0	0			56
			Major	92.85714	3.571429	3.571429			56
	Gen0877	CEP	Minor	69.56522	17.3913	8.695652	4.347826	0	92
			Major	65.21739	13.04348	0	4.347826	17.3913	92
		ADE	Minor	100	0	0			46
			Major	52.17391	17.3913	30.43478			46
VPS-35[D638N]:GFP	Vehicle	CEP	Minor	17.85714	46.42857	35.71429	0	0	112
			Major	96.42857	3.571429	0	0	0	112
		ADE	Minor	100	0	0			56
			Major	53.57143	35.71429	10.71429			56
	Gen0877	CEP	Minor	50	28.57143	17.85714	3.571429	0	112
			Major	100	0	0	0	0	112
		ADE	Minor	100	0	0			56
			Major	82.14286	17.85714	0			56

5.3.2.1 LRRK2 inhibitor treatment reduces the fluorescence intensity of vps-35[D638N] heterozygotes in day 5 of adulthood

Genotype	Treatment	Mean	Standard Deviation	Number
Wildtype:datGFP	Vehicle	4414	1446	24
	Genentech0877	5353	1797	18
vps-35[D638N]:datGFP	Vehicle	3900	1240	24
	Genentech0877	2256	865.9	20

Comparison	P-Value	Significance
Wildtype:datGFP Vehicle vs Wildtype:datGFP Gen0877	ns	0.2709
vps-35[D638N]:datGFP Vehicle vs vps-35[D638N]:datGFP Gen0877	****	<0.0001
Wildtype:datGFP Vehicle vs vps-35[D638N]:datGFP Vehicle	ns	0.5673
Wildtype:datGFP Gen0877 vs vps-35[D638N]:datGFP Gen0877	****	<0.0001

5.3.2.2 Treatment with a LRRK2 inhibitor improves the dopaminergic impairments exhibited in vps-35[D638N] heterozygotes in day 5 of adulthood

Neuronal Subgroup	Genotype	Treatment	% Neurons in *C. elegans* Population Morphology					N
			Wildtype Appearance	Outgrowths	Branching	Blebbing	Degeneration	
CEP	Wildtype:GFP	Vehicle	83.33333	13.54167	1.041667	0	2.083333	96
		Gen0877	84.72222	9.722222	4.166667	0	1.388889	96
	VPS-35[D638N]:GFP	Vehicle	64.58333	23.95833	5.208333	0	6.25	72
		Gen0877	68.75	20	8.75	2.5	0	80
ADE	Wildtype:GFP	Vehicle	77.08333	0	0	20.83333	2.083333	48
		Gen0877	77.77778	5.555556	0	2.777778	13.88889	48
	VPS-35[D638N]:GFP	Vehicle	29.16667	8.333333	0	43.75	18.75	36
		Gen0877	65	5	0	25	5	40

5.3.2.3 LRRK2 inhibitor treatment improves the number of impairments in vps-35[D638N] heterozygotes in day 5 of adulthood

Type	Genotype	Treatment	% C. elegans in population with number of impairments							N
			0	1	2	3	4	5	6	
Total	Wildtype:GFP	Vehicle	45.83333	29.16667	4.166667	12.5	4.166667	4.166667	0	24
		Gen0877	44.44444	22.22222	22.22222	5.555556	5.555556	0	0	18
	VPS-35[D638N]:GFP	Vehicle	4.166667	16.66667	29.16667	20.83333	12.5	4.166667	12.5	24
		Gen0877	15	35	20	15	5	5	5	20
Minor	Wildtype:GFP	Vehicle	62.5	20.83333	12.5	4.166667	0	0	0	24
		Gen0877	50	33.33333	16.66667	0	0	0	0	18
	VPS-35[D638N]:GFP	Vehicle	41.66667	20.83333	16.66667	8.333333	8.333333	4.166667	0	24

		Gen0877	30	30	30	5	5	0	0	20
Major	Wildtype:GFP	Vehicle	62.5	29.16667	4.166667	0	4.166667	0	0	24
		Gen0877	66.66667	27.77778	5.555556	0	0	0	0	18
	VPS-35[D638N]:GFP	Vehicle	20.83333	25	37.5	16.66667	0	0	0	24
		Gen0877	50	40	5	0	0	0	0	20

5.3.2.4 Prevalence of major impairments in ADE neurons of vps-35[D638N] heterozygotes are reduced following LRRK2 inhibitor treatment in day 5 of adulthood

Genotype	Treatment	Neuronal Subgroup	Type	% C. elegans in population with number of impairments					N
				0	1	2	3	4	
Wildtype:GFP	Vehicle	CEP	Minor	62.5	20.83333	12.5	4.166667	0	96
			Major	95.83333	0	4.166667	0	0	96
		ADE	Minor	100	0	0			48
			Major	62.5	29.16667	8.333333			48
	Gen0877	CEP	Minor	55.55556	33.33333	11.11111	0	0	96
			Major	94.44444	5.555556	0	0	0	96
		ADE	Minor	88.88889	11.11111	0			48
			Major	66.66667	33.33333	0			48
VPS-35[D638N]:GFP	Vehicle	CEP	Minor	41.66667	25	16.66667	8.333333	8.333333	72
			Major	79.16667	16.66667	4.166667	0	0	72
		ADE	Minor	87.5	8.333333	4.166667			36
			Major	20.83333	33.33333	45.83333			36
	Gen0877	CEP	Minor	30	35	30	0	5	80
			Major	95	0	5	0	0	80
		ADE	Minor	90	10	0			40
			Major	50	40	10			40

5.4 Effect of LRRK2 inhibitor treatment upon selected vps-35[D638N] heterozygote cellular phenotypes

5.4.1 Treatment with LRRK2 inhibitor does not rescue impairments in vps-35[D638N] ciliation phenotypes

Genotype	Treatment	Mean	Standard Deviation	Number
Wildtype:datGFP	Vehicle	7561	1103	27
	Genentech0877	7774	980.3	33
vps-35[D638N]:datGFP	Vehicle	5360	916.5	12
	Genentech0877	5834	1344	22

Comparison	P-Value	Significance
Wildtype Vehicle vs Wildtype Gen0877	ns	0.8194
vps-35[D638N] Vehicle vs vps-35[D638N] Gen0877	ns	0.5415
Wildtype Vehicle vs vps-35[D638N] Vehicle	****	<0.0001

Treatment with LRRK2 inhibitor may alter SQST-1 levels in *vps-35[D638N]* heterozygotes

The effect of LRRK2 inhibition in VPS-35[D638N] heterozygotes, upon SQST-1 levels and oligomerisation, was investigated. This was studied in day 1 and day 5 of adulthood, in the dat1GFP expressing vps-35[D638N] heterozygote and wildtype. *C. elegans* populations had been treated overnight for 16 hours with Genentech0877 on solid media, prior to lysate preparation and were age matched and in parallel with the populations studied for neuronal morphology in 5.x.

In day 1 of adulthood, there is a similar proportion of SQST-1 oligomers for each mutant and treatment, for each there is an almost equal proportion of bands at 68kDa and 125kDa, as shown in figure x. The vehicle treated *vps-35[D638N]:dat1GFP* mutant shows a largely reduced SQST-1 band intensity, compared to the vehicle treated *wildtype:dat1GFP*. This is modestly improved in the *vps-35[D638N]:dat1GFP* treated with Genentech 0877, with a higher SQST-1 intensity at both 68 and 125kDa. In contrast, the inhibitor treated wildtype line exhibited reduced SQST-1 intensity, compared to the vehicle. This data suggests that the *vps-35[D638N]:dat1GFP* mutant does show reduced SQST-1, suggesting impaired autophagy, which can be modestly improved through inhibitor treatment. Whereas in the wildtype, inhibitor treatment may lead to impaired autophagy.

An altogether different picture is shown in day 5 of adulthood, in which the vehicle treated *vps-35[D638N]:dat1GFP* population shows an increased intensity of SQST-1 compared to the wildtype and notably, there is a higher proportion of 68kDa SQST-1, compared to 125kDa in all samples. Furthermore, by day 5 of adulthood there are multiple p62 bands, for each sample, suggesting SQST-1 targeting and an altered autophagic state compared to day 1. Following LRRK2 inhibitor treatment, SQST-1 intensity increases for both *wildtype:dat1GFP* and *vps-35[D638N]:dat1GFP* mutation carriers, with the intensity highest in *vps-35[D638N]:dat1GFP*, but the proportional increase compared between each genotypes inhibitor and vehicle is proportional. This suggests that with ageing, treatment of a LRRK2 inhibitor may promote autophagy related processes, but not SQST-1 oligomerization, which is integral in autophagosome targeting of ubiquitinated cargos.

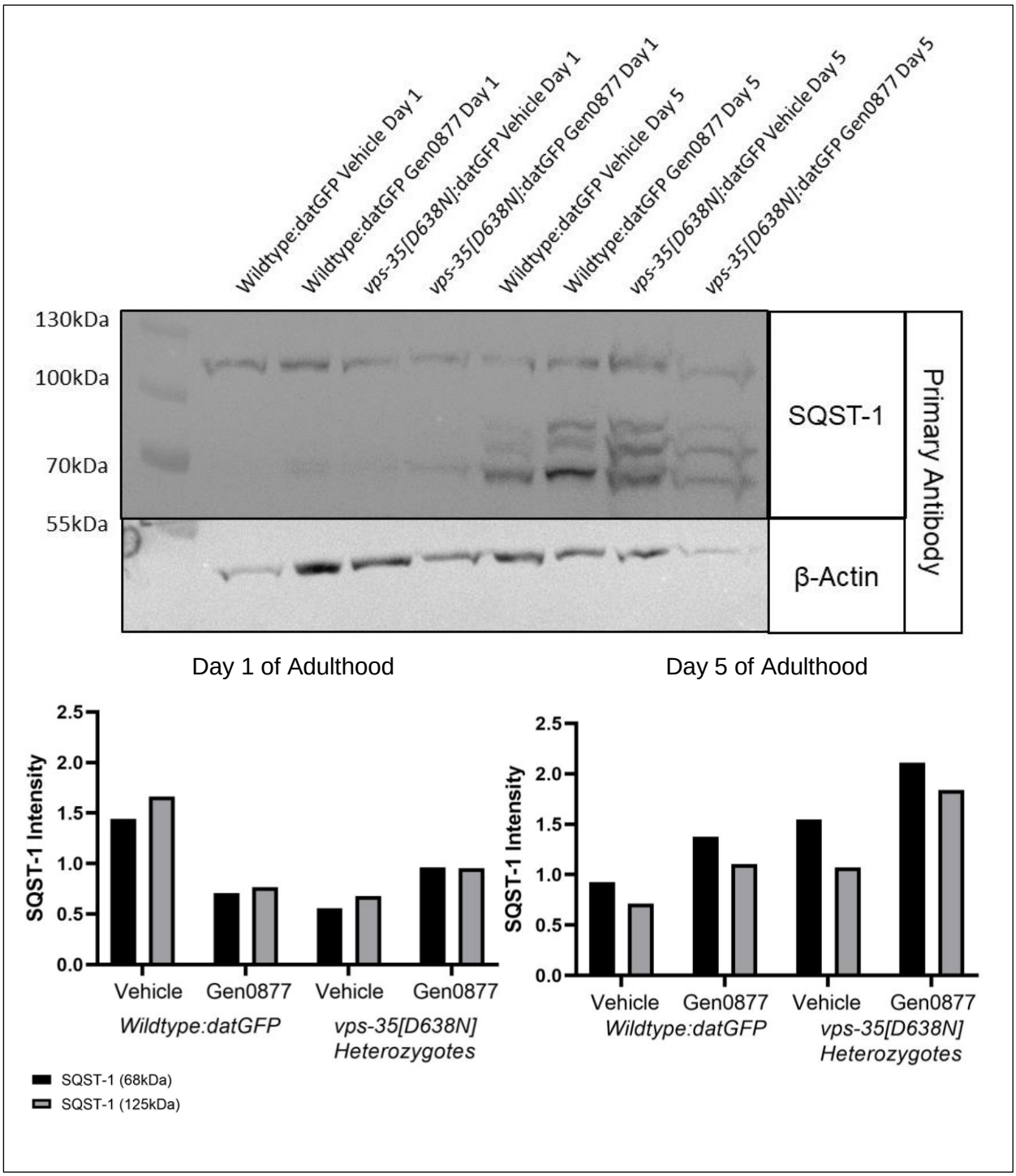
Wildtype:datGFP Vehicle Day 1
Wildtype:datGFP Gen0877 Day 1
vps-35[D638N]:datGFP Vehicle Day 1
vps-35[D638N]:datGFP Gen0877 Day 1
Wildtype:datGFP Vehicle Day 5
Wildtype:datGFP Gen0877 Day 5
vps-35[D638N]:datGFP Vehicle Day 5
vps-35[D638N]:datGFP Gen0877 Day 5
130kDa
100kDa
70kDa
55kDa
SQST-1
β-Actin
Primary Antibody
Day 1 of Adulthood
Day 5 of Adulthood
SQST-1 Intensity
2.5
2.0
1.5
1.0
0.5
0.0
Vehicle
Gen0877
Vehicle
Gen0877
Wildtype:datGFP
vps-35[D638N] Heterozygotes
SQST-1 (68kDa)
SQST-1 (125kDa)

5.6 *vps-35[D638N]* heterozygotes with homozygous *lrk-1[D1847A]* genetic kinase ablation show improved basal slowing responses

5.6.1 *vps-35[D638N]* heterozygotes with homozygous *lrk-1[D1847A]* kinase ablation show a significantly improved basal slowing response in day 1 of adulthood

Genotype	Replicate	Mean % slowing	SD	N
Wildtype	**1**	84.17	10.31	18
	2	83.57	13.86	22
	3	87.59	6.422	26
Genotype Descriptive Statistics		86.00	6.665	26
vps-35[D638N]	**1**	48.51	65.06	36
	2	81.06	12.46	18
	3	56.53	58.24	32
Genotype Descriptive Statistics		61.86	33.20	36
lrk-1[D1847A]	**1**	89.14	10.56	23
	2	87.94	7.540	15
	3	93.17	7.090	22
Genotype Descriptive Statistics		90.64	4.913	23
vps-35[D638N]; lrk-1[D1847A]	**1**	83.94	20.82	31
	2	87.19	8.892	19
	3	86.17	8.372	22
Genotype Descriptive Statistics		84.08	18.07	31

Comparison	P Value	Significance
Wildtype vs. VPS-35[D638N]	***	0.0008
Wildtype vs. LRK-1[D1847A]	*	0.0437
Wildtype vs. VPS-35[D638N]:LRK-1[D1847A]	ns	0.9942
VPS-35[D638N] vs. LRK-1[D1847A]	****	<0.0001
VPS-35[D638N] vs. VPS-35[D638N]:LRK-1[D1847A]	**	0.0061
LRK-1[D1847A] vs. VPS-35[D638N]:LRK-1[D1847A]	ns	0.3072

5.6.2 *vps-35[D638N]* heterozygotes with homozygous *lrk-1[D1847A]* kinase ablation do not show significantly different crawling speeds in day 1 of adulthood

Genotype	Condition	Replicate	Mean (mm/s)	SD	N
Wildtype	NGM	1	0.06176	0.03452	38
		2	0.1057	0.03524	30
		3	0.08617	0.03508	46
	Genotype Descriptive Statistics		0.08567	0.02842	46
	E. coli OP50 NGM	1	0.009778	0.006367	18
		2	0.01736	0.01465	22
		3	0.01069	0.005534	26
	Genotype Descriptive Statistics		0.01215	0.006148	26
vps-35[D638N]	NGM	1	0.07186	0.02651	36
		2	0.09356	0.03109	39

		3	0.07060	0.03649	43
	Genotype Descriptive Statistics		0.07779	0.02180	43
	E. coli OP50 NGM	1	0.03700	0.04675	36
		2	0.01772	0.01166	18
		3	0.03069	0.04112	32
	Genotype Descriptive Statistics		0.02790	0.02407	36
lrk-1[D1847A]	NGM	1	0.08929	0.03903	35
		2	0.1039	0.03202	41
		3	0.08650	0.03021	40
	Genotype Descriptive Statistics		0.09435	0.02339	41
	E. coli OP50 NGM	1	0.009696	0.009426	23
		2	0.01253	0.007836	15
		3	0.005909	0.006133	22
	Genotype Descriptive Statistics		0.008674	0.004588	23
vps-35[D638N]; lrk-1[D1847A]	NGM	1	0.08474	0.02427	38
		2	0.09571	0.02818	31
		3	0.07888	0.02822	24
	Genotype Descriptive Statistics		0.08468	0.01547	38
	E. coli OP50 NGM	1	0.01361	0.01764	31
		2	0.01226	0.008510	19
		3	0.01091	0.006604	22
	Genotype Descriptive Statistics		0.01358	0.01533	31

Comparison	**P Value**	**Significance**
NGM		
Wildtype vs. VPS-35[D638N]	ns	0.6008
Wildtype vs. LRK-1[D1847A]	ns	0.5351
Wildtype vs. VPS-35[D638N]:LRK-1[D1847A]	ns	>0.9999
VPS-35[D638N] vs. LRK-1[D1847A]	**	0.0073
VPS-35[D638N] vs. VPS-35[D638N]:LRK-1[D1847A]	ns	0.4699
LRK-1[D1847A] vs. VPS-35[D638N]:LRK-1[D1847A]	ns	0.1768
E. coli OP50 NGM		
Wildtype vs. VPS-35[D638N]	**	0.0032
Wildtype vs. LRK-1[D1847A]	ns	0.1556
Wildtype vs. VPS-35[D638N]:LRK-1[D1847A]	ns	0.9974
VPS-35[D638N] vs. LRK-1[D1847A]	***	0.0002
VPS-35[D638N] vs. VPS-35[D638N]:LRK-1[D1847A]	*	0.0270
LRK-1[D1847A] vs. VPS-35[D638N]:LRK-1[D1847A]	ns	0.4575

5.6.3 *vps-35[D638N]* heterozygotes with homozygous *lrk-1[D1847A]* kinase ablation show a significantly improved basal slowing response in day 5 of adulthood

Genotype	**Replicate**	**Mean % Slowing**	**SD**	**N**
Wildtype	**1**	42.23	46.07	12
	2	77.85	25.87	17
	3	37.57	65.83	12
Genotype Descriptive Statistics				
vps-35[D638N]	**1**	55.63	20.30	10
	2	8.236	54.03	26

	3	43.23	25.38	30
Genotype Descriptive Statistics				
lrk-1[D1847A]	**1**	79.79	20.38	19
	2	54.67	38.28	7
	3	60.86	25.37	11
Genotype Descriptive Statistics				
vps-35[D638N]; lrk-1[D1847A]	**1**	58.37	34.28	11
	2	64.05	19.83	12
	3	44.51	37.45	12
Genotype Descriptive Statistics				

Comparison	**Significance**	**P-Value**
Wildtype vs. VPS-35[D638N]	*	0.0186
Wildtype vs. LRK-1[D1847A]	ns	0.9242
Wildtype vs. VPS-35[D638N]:LRK-1[D1847A]	ns	0.9391
VPS-35[D638N] vs. LRK-1[D1847A]	****	<0.0001
VPS-35[D638N] vs. VPS-35[D638N]:LRK-1[D1847A]	*	0.0295
LRK-1[D1847A] vs. VPS-35[D638N]:LRK-1[D1847A]	ns	0.1602

5.6.4 *vps-35[D638N]* heterozygotes with homozygous *lrk-1[D1847A]* kinase ablation do not show significantly different crawling speeds from wildtype in day 5 of adulthood

Genotype	**Condition**	**Replicate**	**Mean (mm/s)**	**SD**	**N**
Wildtype	NGM	1	0.08525	0.04330	12
		2	0.07276	0.04647	33
		3	0.06741	0.03858	34
	Genotype Descriptive Statistics		0.07028	0.03120	34
	E. coli OP50 NGM	1	0.04925	0.03928	12
		2	0.01612	0.01882	17
		3	0.04208	0.04438	12
	Genotype Descriptive Statistics		0.02773	0.02460	17
vps-35[D638N]	NGM	1	0.2008	0.05888	18
		2	0.07578	0.04812	27
		3	0.1986	0.06991	34
	Genotype Descriptive Statistics		0.1620	0.05110	34
	E. coli OP50 NGM	1	0.08910	0.04077	10
		2	0.06954	0.04094	26
		3	0.1127	0.05039	30
	Genotype Descriptive Statistics		0.09337	0.03903	30
lrk-1[D1847A]	NGM	1	0.08618	0.03621	22
		2	0.06429	0.03462	21
		3	0.08812	0.06020	17
	Genotype Descriptive Statistics		0.07918	0.02766	22
	E. coli OP50 NGM	1	0.01742	0.01757	19
		2	0.02914	0.02461	7
		3	0.04091	0.02651	11
	Genotype Descriptive Statistics		0.02439	0.01965	19
vps-35[D638N]; lrk-1[D1847A]	NGM	1	0.09892	0.04187	24
		2	0.08160	0.04955	25

		3	0.06323	0.04459	13
	Genotype Descriptive Statistics		0.08628	0.02990	25
	E. coli OP50 NGM	1	0.04118	0.03391	11
		2	0.02933	0.01618	12
		3	0.03508	0.02368	12
	Genotype Descriptive Statistics		0.03556	0.01431	12
Nested Comparison. One-way ANOVA, Brown-Forsyth & Welch				**Significance**	**P-Value**
NGM					
Wildtype vs. VPS-35[D638N]				****	<0.0001
Wildtype vs. LRK-1[D1847A]				ns	0.8375
Wildtype vs. VPS-35[D638N]:LRK-1[D1847A]				ns	0.2647
VPS-35[D638N] vs. LRK-1[D1847A]				****	<0.0001
VPS-35[D638N] vs. VPS-35[D638N]:LRK-1[D1847A]				****	<0.0001
LRK-1[D1847A] vs. VPS-35[D638N]:LRK-1[D1847A]				ns	0.9497
E. coli OP50 NGM					
Wildtype vs. VPS-35[D638N]				****	<0.0001
Wildtype vs. LRK-1[D1847A]				ns	0.9981
Wildtype vs. VPS-35[D638N]:LRK-1[D1847A]				ns	0.8557
VPS-35[D638N] vs. LRK-1[D1847A]				****	<0.0001
VPS-35[D638N] vs. VPS-35[D638N]:LRK-1[D1847A]				****	<0.0001
LRK-1[D1847A] vs. VPS-35[D638N]:LRK-1[D1847A]				ns	0.3714

5.7 Dopaminergic Neuronal Morphology of VPS-35[D638N] Heterozygotes with homozygous LRK-1[D1847A] mutation

5.7.1 The vps-35[D638N]:lrk-1[D1847A] double mutants show improved CEP and ADE neuropathology's in day 1 of adulthood

Mean Neuronal Morphology

Neuronal Subgroup	Genotype	% Neurons in *C. elegans* Population Morphology					N
		Wildtype Appearance	Outgrowths	Branching	Blebbing	Degeneration	
CEP	Wildtype	91.2454333333	5.6532366666	3.101343333	0	0	216
	vps-35[D638N]	68.7247443333	21.30051111	8.838384444	0	1.1363633333	196
	lrk-1[D1847A]	94.8798	3.9583333333	1.16186	0	0	196
	vps-35[D638N]; lrk-1[D1847A]	92.0600333333	6.7198433333	1.220133333	0	0	256
ADE	Wildtype	93.083	0	0	2.115383333	4.801586666	108
	vps-35[D638N]	82.8282866666	0	0	12.27273766	4.898977666	98
	lrk-1[D1847A]	98.9583333333	0	0	0	1.041666666	98
	vps-35[D638N]; lrk-1[D1847A]	99.2424333333	0	0	0.757576666	0	128

Replicate Values

When the three replicates for each genotype are contrasted, there is consistency in the neuropathology's shown, with a similar profile to the mean for that genotype, as shown in figure 92. The *vps-35[D638N]* heterozygote shows consistently increased outgrowths and branching in the CEP neurons compared to the wildtype, in all three replicates, while the *lrk-1[D1847A]* consistently shows the reverse phenotype. In the *vps-35[D638N]:lrk-1[D1847A]* double mutant, between 5 and 10% of the CEP neurons in the population show outgrowths or branching. This is lower than all three of the *vps-35[D638N]* replicates, but higher than the *lrk-1[D1847A]* populations, suggesting that LRK-1 kinase activity may not account for all *vps-35[D638N]* neuropathology and additional mechanisms may be in action.

In the ADE neurons a similar consistency is shown in the three replicates for each genotype. In the vps-35[D638N] heterozygote, between 33-36% of ADE neurons show major impairments, such as blebbing or degeneration in each population, while in the wildtype this ranges from 5-15%. Furthermore, the lrk-1[D1847A] mutant shows no major impairments in the ADE neurons in two populations and <5% in one population, which is consistent with the novel vps-35[D638N]:lrk-1[D1847A] double mutant, further demonstrating that vps-35[D638N] mutation may act through LRK-1 kinase hyperactivation.

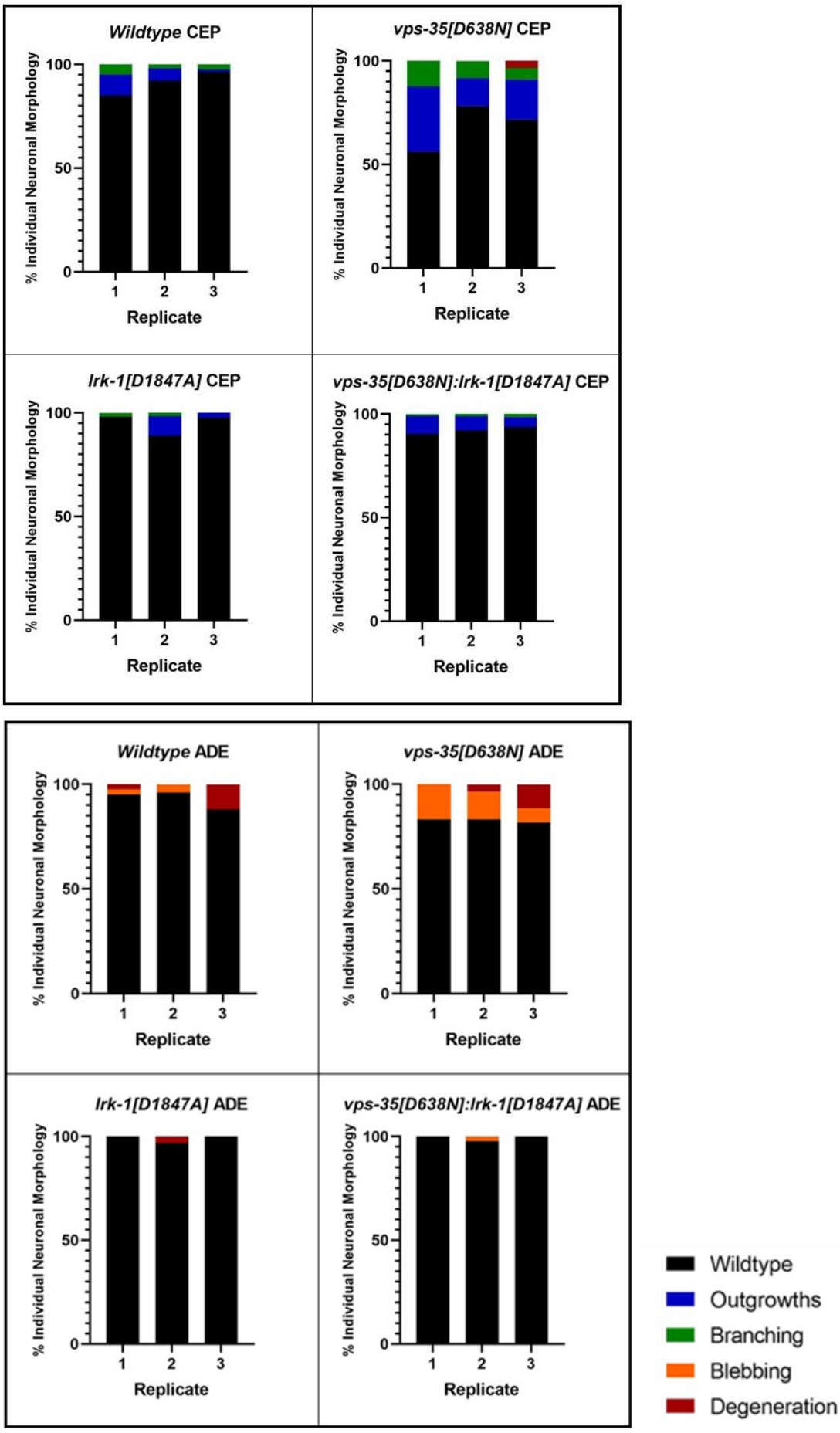

Replicates of double mutant CEP and ADE neuropathology's

Neuronal Subgroup	Replicate	% Neurons in *C. elegans* Population Morphology					N
		Wildtype Appearance	Outgrowths	Branching	Blebbing	Degeneration	
Wildtype							
CEP	1	85	10	5	0	0	80
	2	92.3077	5.76923	1.92308	0	0	52
	3	96.4286	1.19048	2.38095	0	0	84
ADE	1	95	0	0	2.5	2.5	40
	2	96.1538	0	0	3.84615	0	26
	3	88.0952	0	0	0	11.90476	42
vps-35[D638N]							
CEP	1	56.25	31.25	12.5	0	0	48
	2	78.333333	13.33333333	8.333333333	0	0	60
	3	71.5909	19.3182	5.68182	0	3.40909	88
ADE	1	83.33333	0	0	16.6667	0	24
	2	83.33333	0	0	13.333333	3.333333	30
	3	81.8182	0	0	6.81818	11.3636	44
lrk-1[D1847A]							
CEP	1	98.0769	0	1.92308	0	0	52
	2	89.0625	9.375	1.5625	0	0	64
	3	97.5	2.5	0	0	0	80
ADE	1	100	0	0	0	0	26
	2	96.875	0	0	0	3.125	32
	3	100	0	0	0	0	40
vps-35[D638N]; lrk-1[D1847A]							
CEP	1	90.3846	8.65385	0.96154	0	0	104
	2	92.0455	6.81818	1.13636	0	0	88
	3	93.75	4.6875	1.5625	0	0	64
ADE	1	100	0	0	0	0	52
	2	97.7273	0	0	2.27273	0	44
	3	100	0	0	0	0	32

5.7.2 The *vps-35[D638N]:lrk-1[D1847A]* double mutant shows a reduced minor, major and total impairment number per *C. elegans* than *vps-35[D638N]* heterozygotes in day 1 of adulthood

Mean Impairment number per genotype

Type	Genotype	% C. elegans in population with number of impairments							N
		0	1	2	3	4	5	6	
Total	Wildtype	66.72773	20.86690	9.23077	3.174603	0	0	0	54
	vps-35[D638N]	18.28283	34.49496	25.05053	16.61616	2.777776	2.777776	0	49
	lrk-1[D1847A]	79.51923	18.39743	2.083333	0	0	0	0	49
	vps-35[D638N]; lrk-1[D1847A]	74.88346	19.75526	2.564103	2.7972	0	0	0	64

Minor	Wildtype	74.21246	16.55676	9.23077	0	0	0	0	54
	vps-35[D638N]	25.05053	41.9697	23.13132	7.070716	2.777777	0	0	49
	lrk-1[D1847A]	81.60256	16.31410	2.083333	0	0	0	0	49
	vps-35[D638N]; lrk-1[D1847A]	74.88346	19.75526	4.079253	1.28205	0	0	0	64
Major	Wildtype	89.34066	7.484736	3.174603 3333333 3	0	0	0	0	54
	vps-35[D638N]	65.6566	31.3131	1.51515	1.51515	0	0	0	49
	lrk-1[D1847A]	97.91666	2.083333 3333333 3	0	0	0	0	0	49
	vps-35[D638N]; lrk-1[D1847A]	98.48483	1.51515	0	0	0	0	0	64

Replicates Values

When the three replicates for each genotype are studied further in terms of minor impairments, there are varying degrees of similarity across the three replicates in each genotype. There is variability in the wildtype, with 40% of the population showing one or more minor impairment in population 1, with only 15% illustrating this in population 3. The *vps-35[D638N]* heterozygote shows greater consistency, with between 15-30% of each population showing no minor impairments, highlighting the prevalence of impairments in this group, however the extent varies, as in population 1 25% show three or more impairments, which is not illustrated in populations 2 and 3. In two of the *lrk-1[D1847A]* kinase ablated mutant populations, 10% of individuals show one impairment, while in one population this is exhibited by 35% of the population, with a further 5% showing two impairments. The *vps-35[D638N]:lrk-1[D1847A]* double mutant shows a more consistent profile, with one or more impairment shown in approximately 25% of the population for all three populations. This is a substantially smaller proportion of the population than the *vps-35[D638N]* heterozygote, implicating LRK-1 kinase hyperactivation in toxicity.

The major impairments illustrated across the three replicates for each genotype show a greater consistency than minor impairments. In the wildtype approximately 10% of individuals show one or more major impairment, while in the *vps-35[D638N]* 35% show one or more impairment, consistent with prior studies. In both the *lrk-1[D1847A]* and *vps-35[D638N]:lrk-1[D1847A]* populations, two populations show no major impairments, with the remaining population showing one impairment in 5% of individuals. This consistent phenotype highlights further the protective effect of genetic LRK-1 kinase ablation upon *vps-35[D638N]* pathogenicity.

In terms of total impairments per *C. elegans*, there is some inconsistency between replicates within genotypes, yet the profile for each genotype appears distinct. In the wildtype, between 25-50% of the population show one or more impairments. In the *vps-35[D638N]*, this figure is between 75-80% of the population, highlighting the substantial perturbations induced by this mutation. In the *lrk-1[D1847A]* populations two show one impairment, while the remaining population 2 shows thus in 45% of individuals, accounted for by the prevalence of minor impairments in this specific population. The *vps-35[D638N]:lrk-1[D1847A]* population illustrates impairments in one or more neuron in approximately 25% of individuals across all three replicates, further highlighting the improvements illustrated compared to the *vps-35[D638N]* heterozygote.

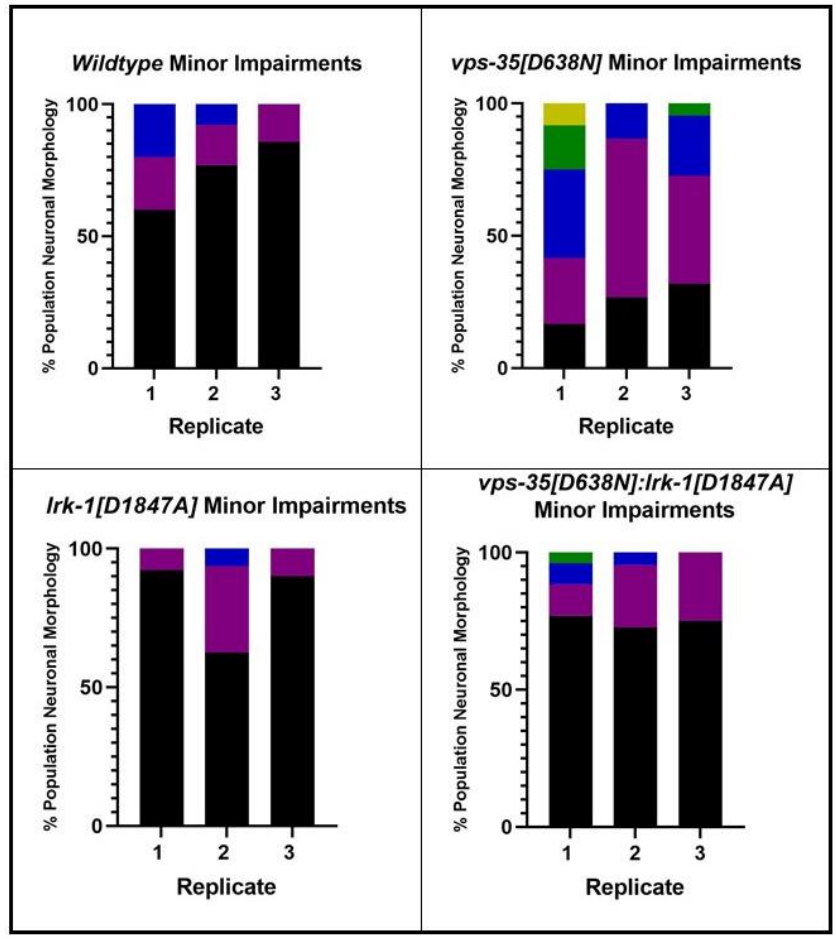
Wildtype Minor Impairments
vps-35[D638N] Minor Impairments
lrk-1[D1847A] Minor Impairments
vps-35[D638N]:lrk-1[D1847A] Minor Impairments
% Population Neuronal Morphology
100
50
0
1
2
3
Replicate

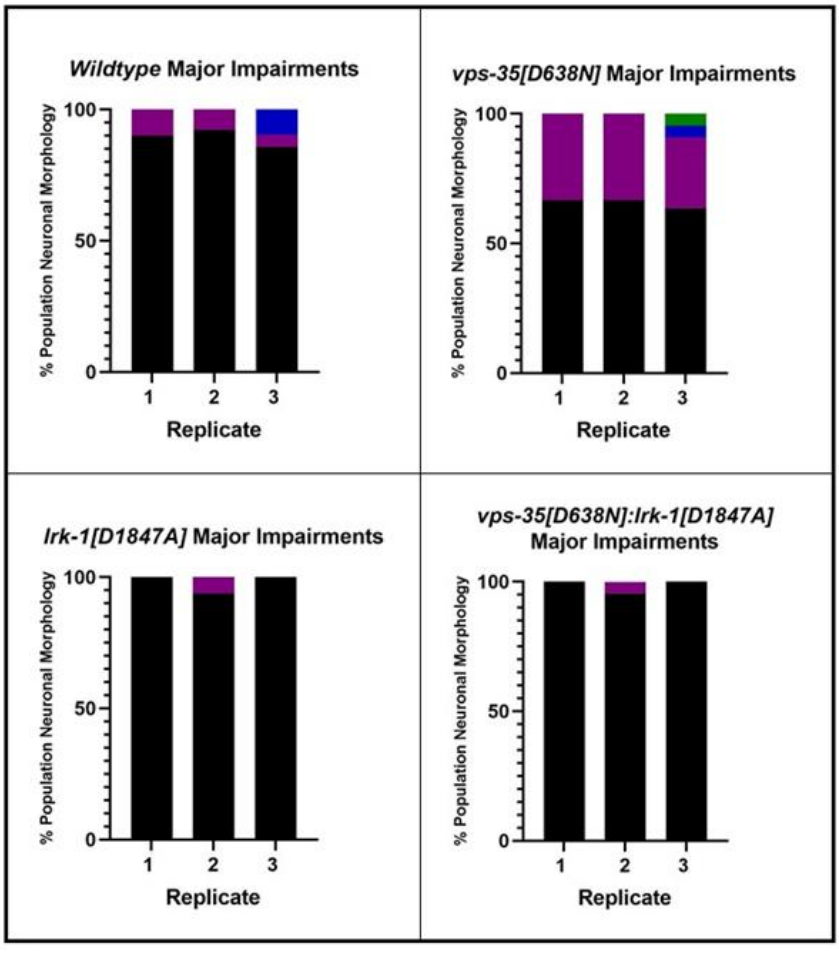
Wildtype Major Impairments
vps-35[D638N] Major Impairments
lrk-1[D1847A] Major Impairments
vps-35[D638N]:lrk-1[D1847A] Major Impairments
% Population Neuronal Morphology
100
50
0
1
2
3
Replicate


0
1
2
3
4

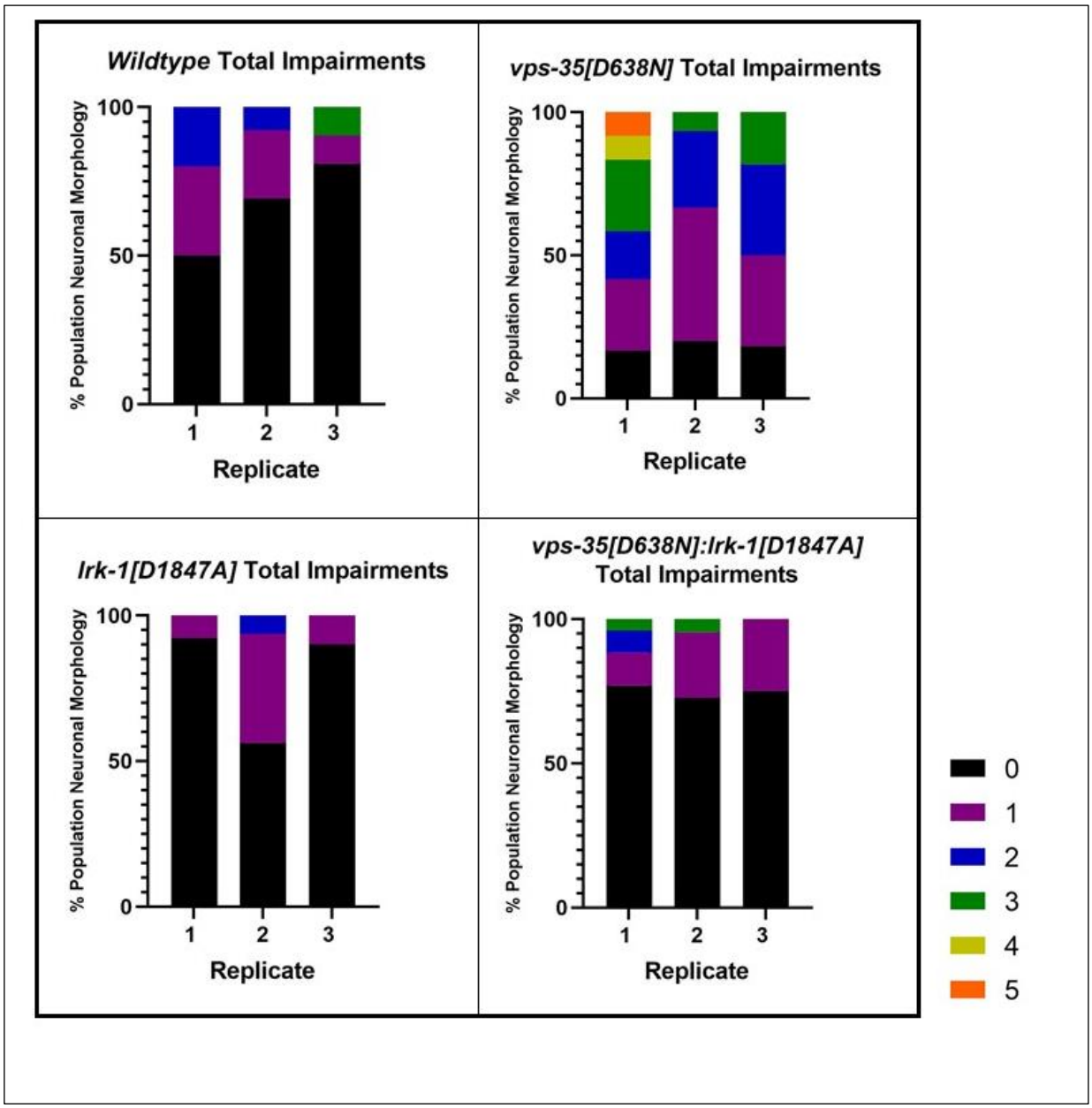
Wildtype Total Impairments
% Population Neuronal Morphology
100
50
0
1
2
3
Replicate
vps-35[D638N] Total Impairments
% Population Neuronal Morphology
100
50
0
1
2
3
Replicate
Irk-1[D1847A] Total Impairments
% Population Neuronal Morphology
100
50
0
1
2
3
Replicate
vps-35[D638N]:Irk-1[D1847A] Total Impairments
% Population Neuronal Morphology
100
50
0
1
2
3
Replicate
0
1
2
3
4
5

Type	Replicate	% C. elegans in population with number of impairments							N
		0	1	2	3	4	5	6	
Wildtype									
Total	1	50	30	20	0	0	0	0	20
	2	69.2308	23.0769	7.69231	0	0	0	0	13
	3	80.9524	9.52381	0	9.52381	0	0	0	21
Minor	1	60	20	20	0	0	0	0	20
	2	76.9231	15.3846	7.69231	0	0	0	0	13
	3	85.7143	14.2857	0	0	0	0	0	21
Major	1	90	10	0	0	0	0	0	20
	2	92.3077	7.69231	0	0	0	0	0	13
	3	85.7143	4.7619	9.52381	0	0	0	0	21
vps-35[D638N]									
Total	1	16.6667	25	16.6667	25	8.33333	8.33333	0	12
	2	20	46.6667	26.6667	6.6667	0	0	0	15
	3	18.1818	31.8182	31.8182	18.1818	0	0	0	22
Minor	1	16.6667	25	33.33333	16.6667	8.333333	0	0	12
	2	26.6667	60	13.33333	0	0	0	0	15
	3	31.8182	40.9091	22.7273	4.54545	0	0	0	22
Major	1	66.6667	33.3333	0	0	0	0	0	12
	2	66.6667	33.3333	0	0	0	0	0	15
	3	63.6364	27.2727	4.54545	4.54545	0	0	0	22
lrk-1[D1847A]									
16Total	1	92.3077	7.69231	0	0	0	0	0	13
	2	56.25	37.5	6.25	0	0	0	0	16
	3	90	10	0	0	0	0	0	20
Minor	1	92.3077	7.69231	0	0	0	0	0	13
	2	62.5	31.25	6.25	0	0	0	0	16
	3	90	10	0	0	0	0	0	20
Major	1	100	0	0	0	0	0	0	13
	2	93.75	6.25	0	0	0	0	0	16
	3	100	0	0	0	0	0	0	20
vps-35[D638N]; lrk-1[D1847A]									
Total	1	76.9231	11.5385	7.69231	3.84615	0	0	0	26
	2	72.7273	22.7273	0	4.54545	0	0	0	22
	3	75	25	0	0	0	0	0	16
Minor	1	76.9231	11.5385	7.69231	3.84615	0	0	0	26
	2	72.7273	22.7273	4.54545	0	0	0	0	22
	3	75	25	0	0	0	0	0	16
Major	1	100	0	0	0	0	0	0	26
	2	95.4545	4.54545	0	0	0	0	0	22
	3	100	0	0	0	0	0	0	16

5.7.3 The *vps-35[D638N]:lrk-1[D1847A]* double mutant shows a similar individual neuropathology profile to the wildtype and *lrk-1[D1847A]* in day 1 of adulthood

Mean Impairment number per genotype

Genotype	Neuronal Subset	Type	% C. elegans in population with number of impairments					N
			0	1	2	3	4	
Wildtype	CEP	Minor	74.2124566666667	16.5567766666667	9.23076933333333	0	0	216
		Major	100	0	0	0	0	216
	ADE	Minor	100	0	0	0	0	108
		Major	89.34066	7.48473766666667	3.17460333333333	0	0	108
vps-35[D638N]	CEP	Minor	25.0505066666667	41.9696966666667	23.13131	7.07070833333333	2.77777766666667	196
		Major	100	0	0	0	0	196
	ADE	Minor	96.9696966666667	1.51515166666667	1.51515166666667	0	0	98
		Major	65.6565666666667	34.3434333333333	0	0	0	98
lrk-1[D1847A]	CEP	Minor	81.6025666666667	16.3141033333333	2.08333333333333	0	0	196
		Major	100	0	0	0	0	196
	ADE	Minor	100	0	0	0	0	98
		Major	97.9166666666667	2.08333333333333	0	0	0	98
vps-35[D638N]; lrk-1[D1847A]	CEP	Minor	74.88345	19.7552433333333	4.07925433333333	1.28205133333333	0	256
		Major	100	0	0	0	0	256
	ADE	Minor	100	0	0	0	0	128
		Major	98.4848333333333	1.51515	0	0	0	128

Replicate Values

Between replicates for each genotype, there is consistency in the pathology profile. In the wildtype, the most prevalent pathology for all three replicates are minor impairments in the CEP neurons, followed by major impairments in the ADE neurons. These pathologies are exhibited to a greater extent in the *vps-35[D638N]* heterozygote, with minor CEP impairments the most prevalent, followed by major ADE impairments in all three replicates. In the *lrk-1[D1847A]* mutant line, there is less consistency, in population 1 and 3 the only pathology shown are minor impairments in the CEP neurons, while in population 2 this is the most prevalent pathology, but major impairments in the ADE neurons are shown in <10% of the population, however overall, this

genotype shows greater neuroprotection than the wildtype. Similarly, the *vps-35[D638N]:lrk-1[D1847A]* double mutant demonstrated minor CEP impairments as the most prevalent pathology, affecting approximately 25% of individuals in each replicate population, however in one population <5% show major impairments in the ADE neurons. Overall, the *vps-35[D638N]:lrk-1[D1847A]* double mutant shows a higher prevalence of minor CEP neuron impairments than the *lrk-1[D1847A]*, suggesting the rescue is incomplete and additional mechanisms may be perturbed by vps-35[D638N], although LRK-1 kinase hyperactivation is likely to be a key player.

Wildtype

Replicate	Neuronal Subset	Type	% C. elegans in population with number of impairments					N
			0	1	2	3	4	
1	CEP	Minor	60	20	20	0	0	80
		Major	100	0	0	0	0	80
	ADE	Minor	100	0	0	0	0	40
		Major	90	10	0	0	0	40
2	CEP	Minor	76.92308	15.38462	7.692308	0	0	52
		Major	100	0	0	0	0	52
	ADE	Minor	100	0	0	0	0	26
		Major	92.30769	7.692308	0	0	0	26
3	CEP	Minor	85.71429	14.28571	0	0	0	84
		Major	100	0	0	0	0	84
	ADE	Minor	100	0	0	0	0	42
		Major	85.71429	4.761905	9.52381	0	0	42

vps-35[D638N]

Replicate	Neuronal Subset	Type	% C. elegans in population with number of impairments					N
			0	1	2	3	4	
1	CEP	Minor	16.66667	25	33.33333	16.66667	8.333333	48
		Major	100	0	0	0	0	48
	ADE	Minor	100	0	0	0	0	24

		Major	66.66667	33.33333	0	0	0	24
2	CEP	Minor	26.66667	60	13.33333	0	0	60
		Major	100	0	0	0	0	60
	ADE	Minor	100	0	0	0	0	30
		Major	66.66667	33.33333	0	0	0	30
3	CEP	Minor	31.81818	40.90909	22.72727	4.545455	0	88
		Major	100	0	0	0	0	88
	ADE	Minor	90.90909	4.545455	4.545455	0	0	44
		Major	63.63636	36.36364	0	0	0	44

lrk-1[D1847A]

Replicate	**Neuronal Subset**	**Type**	**% C. elegans in population with number of impairments**					**N**
			0	**1**	**2**	**3**	**4**	
1	CEP	Minor	92.3077	7.69231	0	0	0	52
		Major	100	0	0	0	0	52
	ADE	Minor	100	0	0	0	0	26
		Major	100	0	0	0	0	26
2	CEP	Minor	62.5	31.25	6.25	0	0	64
		Major	100	0	0	0	0	64
	ADE	Minor	100	0	0	0	0	32
		Major	93.75	6.25	0	0	0	32
3	CEP	Minor	90	10	0	0	0	80
		Major	100	0	0	0	0	80
	ADE	Minor	100	0	0	0	0	40
		Major	100	0	0	0	0	40

vps-35[D638N];lrk-1[D1847A]

Replicate	Neuronal Subset	Type	% C. elegans in population with number of impairments					N
			0	1	2	3	4	
1	CEP	Minor	76.92308	11.53846	7.692308	3.846154	0	104
		Major	100	0	0	0	0	104
	ADE	Minor	100	0	0	0	0	52
		Major	100	0	0	0	0	52
2	CEP	Minor	72.72727	22.72727	4.54545	0	0	88
		Major	100	0	0	0	0	88
	ADE	Minor	100	0	0	0	0	44
		Major	95.4545	4.54545	0	0	0	44
3	CEP	Minor	75	25	0	0	0	64
		Major	100	0	0	0	0	64
	ADE	Minor	100	0	0	0	0	32
		Major	100	0	0	0	0	32

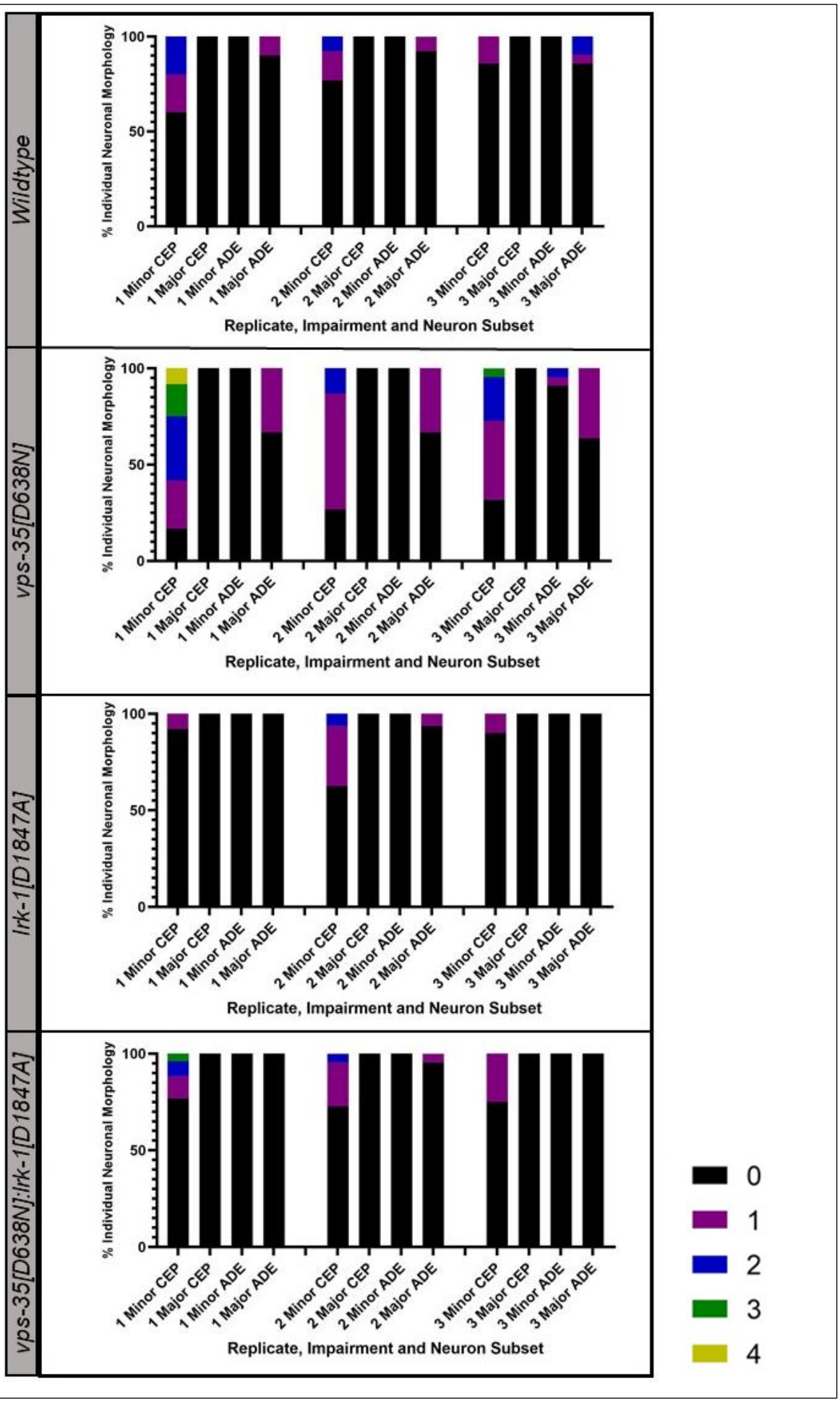
Wildtype
vps-35[D638N]
lrk-1[D1847A]
vps-35[D638N];lrk-1[D1847A]
% Individual Neuronal Morphology
100
50
0
1 Minor CEP
1 Major CEP
1 Minor ADE
1 Major ADE
2 Minor CEP
2 Major CEP
2 Minor ADE
2 Major ADE
3 Minor CEP
3 Major CEP
3 Minor ADE
3 Major ADE
Replicate, Impairment and Neuron Subset
0
1
2
3
4

Appendix Bibliography

Donohue, E. *et al.* (2014) 'Induction of Covalently Crosslinked p62 Oligomers with Reduced Binding to Polyubiquitinated Proteins by the Autophagy Inhibitor Verteporfin', *PLOS ONE*. Public Library of Science, 9(12), p. e114964. doi: 10.1371/JOURNAL.PONE.0114964.

Itakura, E. and Mizushima, N. (2011) 'p62 targeting to the autophagosome formation site requires self-oligomerization but not LC3 binding', *The Journal of Cell Biology*. The Rockefeller University Press, 192(1), p. 17. doi: 10.1083/JCB.201009067.

Kalogeropulou, A. F. *et al.* (2018) 'P62/SQSTM1 is a novel leucine-rich repeat kinase 2 (LRRK2) substrate that enhances neuronal toxicity', *Biochemical Journal*, 475(7), pp. 1271 LP – 1293. doi: 10.1042/BCJ20170699.

Liu, W. J. *et al.* (2016) 'P62 Links the Autophagy Pathway and the Ubiqutin-Proteasome System Upon Ubiquitinated Protein Degradation', *Cellular and Molecular Biology Letters*. Cellular & Molecular Biology Letters, 21(1), pp. 1–14. doi: 10.1186/s11658-016-0031-z.

Wurzer, B. *et al.* (2015) 'Oligomerization of p62 allows for selection of ubiquitinated cargo and isolation membrane during selective autophagy', *eLife*. eLife Sciences Publications Ltd, 4(September 2015). doi: 10.7554/ELIFE.08941.